

**Early Mesozoic stratigraphy, sedimentology and structure of the
Gharian area, north-western Libya**

by

Emhemed Alfandi

A thesis submitted to Plymouth University
in partial fulfilment for the degree of

DOCTOR OF PHILOSOPHY

School of Geography, Earth and Environment Sciences
Faculty of Science and Technology

2012

Abstract

Early Mesozoic stratigraphy, sedimentology and structure of the Gharian area, north-western Libya

Emhemed Alfandi

The Gharian area is used as a case study to examine the sedimentary succession, structural evolution and timing of sedimentary and structural events during basin development in the Early Mesozoic. These sediments (Kurrush, Al Aziza and Abu Shaybah Formations) are examined in order to provide palaeoenvironmental and palaeogeographic reconstructions for the study area. The formations are described using facies analysis. The Kurrush is probably deposited in delta plain environment. A complete section (140 m) has been logged and seven facies from the Al Aziza Formation represent a shallow shelf platform area (inner ramp: an intertidal-subtidal carbonate flat to shelf lagoonal environment), which was deposited during the opening of the Early Triassic Neo-Tethys Ocean. Eleven localities from the Abu Shaybah Formation have been investigated with a cumulative thickness of 125 m. Ten facies from the Abu Shaybah Formation represent deposition in a shallow marine environment as part of low gradient continental margin, succeeded by sand deposition in braided and meandering fluvial systems. Regional tectonic activity, regional relative sea-level fluctuations and climatic conditions led to control of the sedimentary megasequences (266 m coarsening upward and fining upward megasequence). A magnetostratigraphic analysis was undertaken in the above units as their depositional age is poorly constrained and currently based on limited fossil evidence. Most of these samples convey a weak but stable remanent magnetization. The Al Aziza Formation yielded a primary remanence that has suffered a substantial post-acquisition clockwise rotation ($\sim 50^\circ$). Restoration of the rotation about a simple vertical axis would place the pole on the APW path at an appropriate point in time. The palaeomagnetic data from the studied formations yield a distinct series of polarity zones that provide clear local and regional correlation and are readily tied to a recently compiled global magnetostratigraphic time scale. The Al Aziza Formation at Gharian is latest Ladinian in age, whilst the Abu Shaybah Formation is earliest Carnian in age. The Abu Shaybah Formation at Gharian suggests that the stratigraphic equivalence with the Aziza Formation at Azizyah and Kaf Bates (Jafarah Plain). The study established that the Gharian area is the expression of major normal faults (NNE-SSW, WNW to ESE, NW to NNW and NE-SE) in a system of half-grabens which formed as part of the African extensional margin on the southern Tethyan margin in Latest Early Cretaceous.

Contents

| | |
|----------------------------|----------|
| Abstract | i |
| List of Contents | ii-vii |
| List of Figures and Tables | viii-xix |
| Acknowledgments | xx |
| Author's Declaration | xxi |

Chapter 1: Introduction

| | |
|--|----|
| 1.1 Introduction | 1 |
| 1.2 Aim and objectives of study | 4 |
| 1.3 General tectonic history | 4 |
| 1.4 The Jabel Nafusah | 10 |
| 1.4.1 Physical setting of the immediate study area | 10 |
| 1.4.2 Stratigraphy of the Gharian area | 13 |

Chapter 2: Techniques: Strategy, Data Collection and Presentation

| | |
|---|----|
| 2.1 Introduction | 15 |
| 2.2 Research strategy | 15 |
| 2.3 Field work and presentation | 16 |
| 2.4 Field techniques | 17 |
| 2.4.1 Graphic sedimentary logs | 18 |
| 2.5 Palaeocurrent analysis | 22 |
| 2.6 Field facies and stratigraphic analysis | 23 |
| 2.6.1 Facies and facies associations | 23 |
| 2.7 Geological mapping | 25 |
| 2.7.1 Structural data | 25 |
| 2.8 Laboratory methodology | 26 |
| 2.8.1 Petrographic analysis | 26 |

| | |
|----------------------------|----|
| 2.8.2 X-ray diffraction | 26 |
| 2.9 Palaeomagnetic methods | 27 |
| 2.9.1 Introduction | 27 |
| 2.9.2 Sample collection | 27 |
| 2.9.3 Sample preparation | 30 |

Chapter 3: Stratigraphic Framework

| | |
|--|----|
| 3.1 Introduction | 31 |
| 3.2 Stratigraphic outline of Libya | 31 |
| 3.3 Mesozoic rocks of Northern Libya | 35 |
| 3.4 Geological setting of the Gharian area | 37 |
| 3.4.1 Introduction | 37 |
| 3.4.2 Stratigraphic succession of the Gharian area | 39 |
| 3.4.3 Proposed new stratigraphic nomenclature | 41 |
| 3.5 Mesozoic succession of the Gharian area | 42 |
| 3.5.1 Kurrush Formation | 42 |
| 3.5.2 Al Aziza Formation | 45 |
| 3.5.3 Abu Shaybah Formation | 46 |
| 3.5.4 Abu Ghaylan Formation | 47 |
| 3.5.5 Kiklah Formation | 48 |
| 3.5.6 Sidi as Sid Formation | 49 |
| 3.5.7 Nalut Formation | 50 |
| 3.5.8 Qasr Tigrinnah Formation | 51 |

Chapter 4: Early Mesozoic Sedimentary Processes and Environments

| | | |
|-------|---|-----|
| 4.1 | Introduction | 52 |
| 4.2 | Kurrush Formation | 52 |
| 4.2.1 | Introduction | 52 |
| 4.2.2 | Sedimentary characteristics of the Kurrush Fm | 55 |
| 4.2.3 | Environment interpretation | 65 |
| 4.2.4 | Palaeogeography of the Kurrush Formation | 66 |
| 4.3 | Al Aziza Formation | 67 |
| 4.3.1 | Introduction | 67 |
| 4.4 | Sedimentary facies of the Al Aziza Formation | 67 |
| 4.4.1 | Introduction | 67 |
| 4.4.2 | Facies (F-BD): Burrowed and laminated micrites | 69 |
| 4.4.3 | Facies (F-PE): Peloids micrite | 75 |
| 4.4.4 | Facies (F-AB): Algal biolithites | 77 |
| 4.4.5 | Facies (F-MS): Mudstone | 79 |
| 4.4.6 | Facies (F-AD): Argillaceous biomicrities | 79 |
| 4.4.7 | Facies (F-CL): Cherty limestone | 80 |
| 4.4.8 | Facies (F- PL): Phosphate facies | 83 |
| 4.5 | Facies association and deposition environment | 86 |
| 4.6 | Palaeogeography of the Al Aziza Formation | 88 |
| 4.7 | Abu Shaybah Formation | 92 |
| 4.7.1 | Introduction | 92 |
| 4.8 | Facies and sedimentary processes of the Abu Shaybah Formation | 96 |
| 4.8.1 | Facies (F-SD): Symmetrically rippled siltstone and andstone | 96 |
| 4.8.2 | Facies (F-BS): Bioturbated fine grained sandstone | 107 |
| 4.8.3 | Facies (F-MS): Massive fine to medium sandstone | 109 |
| 4.8.4 | Facies (F –VC): Sandstone with vug carbonate | 110 |

| | |
|---|-----|
| 4.8.5 Facies (F-SR): Medium sandstone with rootlets | 112 |
| 4.8.6 Facies (F-TS): Trough cross-bedded medium to coarse sandstone | 119 |
| 4.8.7 Facies (F-PS): Tabular cross bedded medium sandstone | 123 |
| 4.8.8 Facies (F-CS): Medium sand with calcretes | 130 |
| 4.8.9 Facies (F-MS): Red mudstone | 131 |
| 4.8.10 Facies (F-GS): Green clay stone | 133 |
| 4.9 Facies association and depositional environment | 135 |
| 4.9.1 Shallow marine facies association | 135 |
| 4.9.2 Braided river facies association | 145 |
| 4.9.3 Meandering river facies association | 158 |
| 4.10 Palaeogeography of the Abu Shaybah Formation | 163 |
| 4.11 Driving mechanisms for environmental change | 165 |
| 4.12 Conclusions | 179 |

Chapter 5: Principles of Palaeomagnetism

| | |
|---|-----|
| 5.1 Introduction | 181 |
| 5.2 The geomagnetic field acquisition of magnetisation | 183 |
| 5.3 Magnetic minerals | 185 |
| 5.4 Demagnetisation | 187 |
| 5.4.1 Measurements process | 190 |
| 5.5 Presentation of the directional data | 191 |
| 5.6 Statistical analysis | 192 |
| 5.7 Fold test | 193 |
| 5.8 Palaeomagnetic reference poles and reference directions | 194 |
| 5.9 Magnetostratigraphy overview | 195 |

Chapter 6: Palaeomagnetism of the Mesozoic Units of the Gharian Area

| | | |
|-----|---|-----|
| 6.1 | Introduction | 198 |
| 6.2 | Previous research | 198 |
| 6.3 | Palaeomagnetic sampling localities | 204 |
| 6.4 | Results | 207 |
| | 6.4.1 Initial NRM | 207 |
| | 6.4.2 Demagnetization | 207 |
| | 6.4.3 Demagnetization of samples of the Al Aziza Formation | 208 |
| | 6.4.4 Interpretation of the isolated components in the Al Aziza Formation | 218 |
| | 6.4.5 Demagnetization behaviour of samples of the Abu Shaybah FM | 222 |
| | 6.4.6 Interpretation of the isolated component in the Abu Shaybah FM | 227 |
| 6.5 | Other samples | 231 |
| 6.6 | Pole positions and geological interpretation of results | 232 |
| 6.7 | Magnetostratigraphic Al Aziza and Abu Shaybah Formations | 238 |
| | 6.7.1 Correlation with published literature | 241 |
| 6.8 | Conclusions | 245 |

Chapter 7: Structural Evolution of the Gharian Area

| | | |
|-----|--|-----|
| 7.1 | Introduction | 246 |
| 7.2 | Regional context and literature with respect to structural development of the Gharian area | 247 |
| 7.3 | Key field observations | 260 |
| | 7.3.1 Al Azizyah Fault | 260 |
| | 7.3.2 Structural analysis of faults around the Gharian area | 263 |
| | 7.3.3 The Jabel Nafusah faults in cross-section | 277 |
| | 7.3.4 The Hun Graben faults in cross section | 285 |
| 7.4 | The interaction between topography, stratigraphy and structure | 291 |

| | | |
|-----|----------------------------------|-----|
| 7.5 | Structural control of intrusions | 300 |
| 7.6 | Structural synthesis | 305 |
| 7.7 | Summary and conclusions | 312 |

Chapter 8: Synthesis and Conclusions

| | | |
|-----|---|-----|
| 8.1 | Introduction | 315 |
| 8.2 | Geological history of the Gharian | 315 |
| | 8.2.1 Kurrush Formation | 315 |
| | 8.2.2 Al Aziza Formation | 317 |
| | 8.2.3 Abu Shaybah Formation | 318 |
| | 8.2.4 Palaeogeography of the Early Mesozoic | 319 |
| | 8.2.5 Depositional controls during the Triassic | 322 |
| 8.3 | Conclusions | 324 |

| | | |
|--|------------------|-----|
| | Reference | 327 |
|--|------------------|-----|

| | | |
|------------|--|-----|
| Appendix 1 | X-Ray diffraction | 359 |
| Appendix 2 | Sedimentary log from east and west of the Wadi Gabel section | 363 |
| Appendix 3 | Sample orientation utilised both sun and magnetic compass | 364 |
| Appendix 4 | Geological map of the Gharian area | 374 |

List of Figures and Tables

Figures

Chapter 1: Introduction

| | | |
|------------|--|----|
| Figure 1.1 | The Earth at the Permian-Triassic boundary. | 2 |
| Figure 1.2 | Sketch map showing major structural trends of NW Africa. | 5 |
| Figure 1.3 | The major structural and tectonic feature of Libya. | 8 |
| Figure 1.4 | Map of Libya showing the uplifted basins and adjacent regions. | 9 |
| Figure 1.5 | DEM map showing the location of Jabel Nafusah escarpment. | 11 |
| Figure 1.6 | Map showing the topography of Libya and the change in elevation. | 12 |

Chapter 2: Techniques: Strategy, Data Collection and Presentation

| | | |
|------------|---|----|
| Figure 2.1 | Map showing the sections of Kurrush, Al Aziza and Abu Shaybah Formations. | 18 |
| Figure 2.2 | Key to sedimentary logs used throughout this study. | 19 |
| Figure 2.3 | The distribution of sand bedforms plotted in the field of current velocity and sediment grain size. | 20 |
| Figure 2.4 | Middle to Late Trassic magnetic polarity time scale (from magnetostratigraphy). | 28 |
| Figure 2.5 | Collecting oriented paleomagnetic samples in the sandstone rocks of the Abu Shaybah Formation using orientation tool. | 30 |

Chapter 3: Stratigraphic Framework

| | | |
|------------|---|----|
| Figure 3.1 | Geological map of Libya. | 33 |
| Figure 3.2 | Map of Libya, showing the basins boundaries and names of places discussed in the text. | 34 |
| Figure 3.3 | Photograph showing a general view of the area within formations names and igneous rocks are exposed in the central of the area. | 38 |
| Figure 3.4 | Photograph and sketch cross section through the Gharian area. | 40 |
| Figure 3.5 | Geological map of the Gharian area, formation names on the map are referred to in the text. | 44 |

| | | |
|---|--|----|
| Figure 3.6 | Map showing the location of Jabel Nafusah escarpment, names and village referred to within the text. | 48 |
| Chapter 4: Early Mesozoic Sedimentary Processes and Environments | | |
| Figure 4.1 | DEM map showing the location of the Gharian are and the Ras Mazul dome. | 53 |
| Figure 4.2 | Simplified sedimentary log from Well A1-38 showing lithology of the Kurrush Formation. | 54 |
| Figure 4.3 | Map showing the outcrop of facies the Kurrush Formation. | 56 |
| Figure 4.4 | Field photo imagery of the Wadi Abu Shaybah showing the dominant Al Aziza Formation overlying a small exposure of Kurrush Formation. | 57 |
| Figure 4.5 | Sedimentary features from the Kurrush Formation. | 61 |
| Figure 4.6 | Thin sections of the Kurrush Formation. | 62 |
| Figure 4.7 | Palaeogeographic reconstruction of the Kurrush Formation during the Early Triassic. | 66 |
| Figure 4.8 | Location map of the Al Aziza Formation at the Gharian area and Jafarah Plain. | 68 |
| Figure 4.9 | Log of the Al Aziza Formation at location at the Gharian area. | 71 |
| Figure 4.10 | Sedimentary long from the Jafarah Plain. | 73 |
| Figure 4.11 | View of the Gharian area, showing the type section of Al Aziza Formation. | 74 |
| Figure 4.12 | Photomicrograph of the peloids under cross-polarised light. | 76 |
| Figure 4.13 | Surface of domal algal bolithite in the field and under cross-polars. | 78 |
| Figure 4.14 | View of the Ras Lefa section, showing the type section of Al Aziza Formation. | 81 |
| Figure 4.15 | Examples of cherty limestone of facies (F-CL). | 82 |
| Figure 4.16 | Geological map showing location of the Gharian phosphorite. | 84 |
| Figure 4.17 | Photograph of facies (F-PL) showing the exposure along the Wadi Gabel. | 85 |
| Figure 4.18 | Depositional model of the Al Aziza Formation. | 88 |
| Figure 4.19 | Terminology used for marine depositional environments throughout this study. | 88 |
| Figure 4.20 | Map is showing the Late Triassic palaeographic map and tectonic evolution of southern margin of the Tethys Ocean. | 90 |
| Figure 4.21 | Isopach map of the Carboniferous, Permian and Triassic succession, NW Libya. | 91 |
| Figure 4.22 | DEM map showing the location of the Jabel Nafusah. | 92 |
| Figure 4.23 | Map of the Gharian area showing the outcrop of the Abu Shaybah Formation. | 94 |

| | | |
|-------------|--|-----|
| Figure 4.24 | Main measured section through the Abu Shaybah Formation exposed in Wadi Abu Shaybah. | 95 |
| Figure 4.25 | Principal localities of facies the Lower unit of the Abu Shaybah Formation. | 97 |
| Figure 4.26 | Examples of sedimentary structures observed in Facies (F-SD). | 100 |
| Figure 4.27 | Sedimentary structures observed in the Facies (F-SD). | 101 |
| Figure 4.28 | Fossils material of Lower unit of the Abu Shaybah Formation. | 102 |
| Figure 4.29 | Thin sections of Lower unit of the Abu Shaybah Formation. | 103 |
| Figure 4.30 | Thin sections of Lower unit of the Abu Shaybah Formation. | 104 |
| Figure 4.31 | Sedimentary structures and fossils are observed in lower unit of the Abu Shaybah. | 109 |
| Figure 4.32 | Sandstone with vug carbonates facies (F-VC). | 111 |
| Figure 4.33 | Map showing the outcrop of facies of the Middle and Upper unit of the Abu Shaybah Formation. | 113 |
| Figure 4.34 | Field photo of typical outcrop of Facies (F-SR). | 115 |
| Figure 4.35 | Root traces in the Abu Shaybah Formation. | 116 |
| Figure 4.36 | Photomicrographs of typical textures seen in the rootlets within the facies (F-SR). | 117 |
| Figure 4.37 | Photomicrographs of typical textures seen in the rootlets within the facies (F-SR). | 118 |
| Figure 4.38 | Cross bedded coarse sandstone, Middle unit of Abu Shaybah Formation. | 120 |
| Figure 4.39 | Thin sections of the Abu Shaybah typical samples for facies (F-TS). | 121 |
| Figure 4.40 | Palaeocurrents measured from Abu Shaybah Formation. | 122 |
| Figure 4.41 | Sedimentary structures observed in the Facies (F-PS). | 126 |
| Figure 4.42 | Photograph the geometry/ organisation of trough beds in channel forms | 127 |
| Figure 4.43 | Field photographs of the Abu Shaybah Formation. | 128 |
| Figure 4.44 | Photo micrograph of samples (AB- 35 and AB-9) under cross polarized. | 129 |
| Figure 4.45 | Principal localities of facies the Upper of the Abu Shaybah | 132 |

| | | |
|-------------|---|-----|
| | Formation. | |
| Figure 4.46 | General view of facies (F-MS) exposed in Abu Ghaylan section. | 134 |
| Figure 4.47 | Composite log of the Abu Shaybah Formation showing three facies associations. | 136 |
| Figure 4.48 | Field photo imagery of the Abu Rashada road section. | 138 |
| Figure 4.49 | Sedimentary log from the Abu Rashada section. | 139 |
| Figure 4.50 | Field photograph showing an east looking perspective into the central part of Wadi Gabel. | 140 |
| Figure 4.51 | Sedimentary log from east west of the Wadi Gabel section. | 141 |
| Figure 4.52 | A sedimentary facies model of the lower unit of the Abu Shaybah Formation. | 144 |
| Figure 4.53 | Field photo imagery of the Kabted Jamel section. | 147 |
| Figure 4.54 | Sedimentary logs from the Kabted Jamel section north west of Wadi Abu Shaybah. | 148 |
| Figure 4.55 | Field photo imagery of the Palm Tree section. | 150 |
| Figure 4.56 | Field photo imagery of the upper part of Palm tree section. | 151 |
| Figure 4.57 | Sedimentary Logs from the Palm Tree section north west of Wadi Abu- Shaybah. | 152 |
| Figure 4.58 | Terminology used to describe of sandstone body geometry. | 153 |
| Figure 4.59 | Field sketch of the braided river system showing stacked channel bars exposed in the mid part of the Abu Shaybah Formation. | 154 |
| Figure 4.60 | Composite log illustrating the low sinuosity braided river facies. Association. | 157 |
| Figure 4.61 | Architectural model for sand-bed braided river. | 157 |
| Figure 4.62 | Field photograph showing an east looking perspective into the west part of Wadi Abu Shaybah. | 159 |
| Figure 4.63 | Long showing the Upper Unit of the Abu Shaybah Formation measured along northwest of Kaf Kalaya section. | 161 |
| Figure 4.64 | Main morphological features of a meandering river. | 162 |
| Figure 4.65 | Palaeogeographic reconstruction of the Abu Shaybah Formation | 164 |

during the Triassic.

| | | |
|-------------|--|-----|
| Figure 4.66 | Typical vertical mag-a-sequences through the Kurrush, Al Aziza and Abu Shaybah Formations. | 167 |
| Figure 4.67 | Chronostratigraphic chart and inferred eustatic sea level for the Triassic. | 176 |

Chapter 5: Principles of Palaeomagnetism

| | | |
|------------|---|-----|
| Figure 5.1 | Description of the direction of the magnetic field. | 184 |
| Figure 5.2 | Ternary phase diagram of iron and Titanium oxides showing the solid solution series and the dashed lines with arrows indicate the direction of increasing oxidation. | 186 |
| Figure 5.3 | Principle of progressive demagnetization. Specimens with two components are shown by arrows on the right hand side whilst histograms are shown on the left hand side. | 188 |
| Figure 5.4 | Principle of the direction of the magnetic field. | 191 |
| Figure 5.5 | Example of ChRM direction that pass that pass fold test. | 193 |
| Figure 5.6 | Africa paleomagnetic poles for Upper Carboniferous (Cu) to lower Jurassic (Jl) compared to pole from Triassic palaeomagnetic data (Italy). | 197 |

Chapter 6: Palaeomagnetism of the Mesozoic Units of the Gharian Area

| | | |
|------------|---|-----|
| Figure 6.1 | The location of the Al Aziza and Kaf Bates quarries with respect to Gharian, the study area Al Zawia superimposed on a DEM showing the Jafrah Plain and Jabel Nafusah uplift. | 199 |
| Figure 6.2 | Showing isolated components for specimens denoted as A, B and Ch on equal area projections for both sampled localities (Muttoni et al., 2001). | 200 |
| Figure 6.3 | Magnetostratigraphy across the Anisian-Ladinian-Carnian boundary (Muttoni et al., 2000; Hounslow and Muttoni, 2010). | 203 |
| Figure 6.4 | Location map of the palaeomagnetically sampled sections in the | 205 |

Gharian area.

| | | |
|-------------|---|-----|
| Figure 6.5 | Composite log of Al Aziza section sampled in two overlapping section AZ1 and AZ2 for paleomagnetic analysis. | 206 |
| Figure 6.6a | Examples of samples which yielded only A components either in the initial demagnetisation steps only after which they became unstable. | 213 |
| Figure 6.6b | Examples of samples which yielded C only or A with C components and all samples are projected in situ. | 214 |
| Figure 6.6c | Examples of samples which yielded C only or A with C components and all samples are projected in situ. | 215 |
| Figure 6.7 | Orthogonal projections showing the behaviour of samples from the Al Aziza Formation during thermal demagnetization. | 216 |
| Figure 6.8 | Examples of samples which yielded B only or A with B components and all samples are projected in situ. | 217 |
| Figure 6.9 | Equal area projections before (in situ) and after bedding tilt correction of the “A”, “B” and “C” component directions from Al Aziza Formation. | 220 |
| Figure 6.10 | Statistic fold tests for the B and C component from the Al Aziza Formation. | 221 |
| Figure 6.11 | Equal area stereographic and orthogonal projections showing the behaviour of samples from the Abu Shaybah Formation during thermal demagnetization. | 225 |
| Figure 6.12 | Orthogonal projections showing the behaviour of samples from the Abu Shaybah Formation during thermal demagnetization. | 226 |
| Figure 6.13 | Equal area projections before (in situ) and after bedding tilt correction of the “D”, “E” and “F” component directions from Abu Shaybah Formation. | 229 |
| Figure 6.14 | Statistic fold tests for the E and F component from the Abu Shaybah Formation. | 230 |
| Figure 6.15 | Equal area stereographic and Orthogonal projections showing the behaviour of samples from the Kurrush Formation during thermal demagnetization. | 231 |
| Figure 6.16 | The Early Permian to Pliocene AWP path for Africa and Adria. | 234 |
| Figure 6.17 | Magnetostratigraphy of the Al Aziza Formation in the Gharian area. | 239 |

| | | |
|-------------|--|-----|
| Figure 6.18 | Magnetostrigraphy of the Abu Shaybah Formation in the Gharian area area. | 240 |
| Figure 6.19 | Summary correlation of the known magnetostratigraphy of the Al Aziza and Abu Shaybah Formations in Northern Libya. | 243 |
| Figure 6.20 | Synoptic stratigraphic and facies correlation for the Al Aziza and Abu Shaybah Formations in Northern Libya. | 244 |

Chapter 7: Structural Evolution of the Gharian Area

| | | |
|------------|---|-----|
| Figure 7.1 | Regional DEM (A) and outline geological map (B) of the Jabel Nafusah in NW Libya and Tunisia (from Bodin et al., 2010). | 248 |
| Figure 7.2 | Geological map of the Central and Eastern Jabel Nafusah and adjacent Jafarah plain (from Saadi et al., 2009). | 250 |
| Figure 7.3 | Geological map of the Gharian area (enclosure Map 2). Modified from Gray 1971 supplemented by recent mapping and extended by interpretation of Google Earth images. | 252 |
| Figure 7.4 | Illustrative cross-sections of the Jafarah Plain and the Jabel Nafusah escarpment from borehole data at the western end of the escarpment (see Fig. 7.1 for approximate location) based primarily on well depths only. A is from Klett 2002 (after Boote et al., 1998 and others) and B from Letouzey et al., (2005). | 256 |
| Figure 7.5 | Illustrative cross-sections through Gharian from Pizzi et al., 1999. | 257 |
| Figure 7.6 | Sketch map of the distribution of Aziza limestone north of the Jabel Nafusah and illustrative calculation of the displacement at the Jabel Nafusah were it assumed to be a single simple normal fault. | 262 |
| Figure 7.7 | Stereonet projection of all faults recording during the fieldwork presented as A) planes and B) contoured poles to planes. | 266 |
| Figure 7.8 | Stereonets of poles and planes for a) A group and b) B group faults. | 267 |
| Figure 7.9 | Group A faults displaying minor normal displacement in the form of mini horsts and grabens (Locality 7 Trak al hamer). B Karstic fill and open voids in Group A faults (Locality 1 Old Gharian-Tripoli Highway). | 269 |

| | | |
|-------------|---|-----|
| Figure 7.10 | Google Earth image showing Group B orientated faults traversing the Wadi Guasim-Abu Ghaylan topographic plateau, where they show little or no displacement but are readily picked out by the growth of low shrubby vegetation associated with them. | 270 |
| Figure 7.11 | Horst and graben type structures with associated minor displacement of Group B normal faults, Wadi Jabil. | 271 |
| Figure 7.12 | The fault population after removal of the A and B groups plotted as (a) planes and (b) contoured poles to planes. | 273 |
| Figure 7.13 | Stereonet of the remaining faults separated into a) a NW-NNW group 'The Hun Graben' faults and b) an NE – ENE 'Jabel Nafusah' group. | 274 |
| Figure 7.14 | Hun Graben faults showing significant drag of their hanging walls a) Wadi Jabel and b) Wadi Ghan. | 275 |
| Figure 7.15 | Jabel Nafusah faults showing a) significant offset of the Abu-Shaybah-Abu Ghaylan boundary on the Kabted Jamel road section and b) an unbreached anticline overlying JN faults in Wadi Gabel. | 275 |
| Figure 7.16 | Geological map of the Nafusah area centred on Gharian showing lineaments from DEMs and geological maps as rose diagrams for individual stratigraphic units. | 276 |
| Figure 7.17 | NW-SE cross section through Gharian. | 278 |
| Figure 7.18 | The Gharian rollover showing Al Aziza Fm. in the core of the structure immediately north of Gharian viewed looking East | 279 |
| Figure 7.19 | A ~30m wide brecciated fault zone closest to Gharian. Given the location, the substantial width and the proximity to very shallowly southward dipping strata in the footwall (some 35m to right of the photograph) this fault zone is thought to be the master fault in the system. | 280 |
| Figure 7.20 | Highly cusped fault affecting the Aziza formation in the Wadi Abu Shaybah. Gharian, to the south, is at the top of the image. | 282 |
| Figure 7.21 | Possible relay ramp in the main escarpment immediately northeast of Gharian town, viewed from old Wadi Gabel road | 283 |
| Figure 7.22 | Large rollover structure adjacent to the Lenita fault of the Bremer Basin, Australia (http://www.pesa.com.au/publications/pesa_news/feb_06/pesane_ws_8026.html accessed 28/11/2011). The seismic image shows the Lenita fault on the right with a rollover anticline and | 284 |

| | | |
|-------------|--|-----|
| | synclinal crestal collapses with similar geometries to that seen at Gharian. Growth sedimentation post dates the main part of the section and really occurs in the uppermost part of the section. | |
| Figure 7.23 | SW-NE section across the NW trending Hun Graben Faults. | 286 |
| Figure 7.24 | Interaction of the Aziza rollover anticline with the NW trending faults/monoclines. | 287 |
| Figure 7.25 | E-W cross section of the Hun Graben and Sirt basin showing the effect of NW trending faults (from Abadi et al., 2008). | 289 |
| Figure 7.26 | Summary of the major NW structures in the Gharian area. | 290 |
| Figure 7.27 | SRTM derived DEM image (http://www.geomapapp.org & Ryan et al., 2009) of northern Libya showing the parallelism of the Wadi Ghan and Hun Graben rifts. | 290 |
| Figure 7.28 | Tectonic map of Libya (from Abadi et al., 2008) to emphasise the scale of the NW-SE trending Hun Graben-Sirt Basin system in northern central Libya. | 291 |
| Figure 7.29 | A) Google Earth image and B) sketch of the main geomorphology of Gharian. | 295 |
| Figure 7.30 | Differential erosion and its interplay with the main structures. | 299 |
| Figure 7.31 | A) Location of igneous intrusions around Gharian from the 1:25,000 scale geological maps. B) Their interpretation as being located at the intersection of NW-SE Hun Graben faults and NW-SE Jabel Nafusah faults. | 302 |
| Figure 7.32 | Regional map showing the distribution of the main volcanic fields in northern Libya and inset their setting in northern Africa and Arabia as a whole (Farahat et al., 2006). | 303 |
| Figure 7.33 | Nafusah escarpment north of the village of Abu Ghaylan viewed from the old Gharian-Tripoli highway looking across the new highway. On the right hand side of the image the Jafarah plain is visible in the distance. K marks the Kiklah formation displaced by two major normal faults of the JN system and forming a broad, low amplitude anticline between them. The red arrows mark the position of the JN faults one being concealed in a major valley. The Kiklah formation is also offset by NW trending faults of the Hun Graben system in the foreground | 306 |
| Figure 7.34 | Horst block system, road section. | 307 |
| Figure 7.35 | NW–SE regional schematic cross section showing the setting of the Nafusah Horst block in relation to the Jafarah Plain, the | 308 |

| | | |
|--------------------|---|-----|
| | Nafusah Escarpment and the Gharian horst. | |
| Figure 7.36 | Seismic reflection profile and interpretation across the Jafarah fault system in southern Tunisia (from Gabtni et al., 2009). | 308 |
| Figure 7.37a and b | Subsidence and fault history of the Hun Graben and Sirt basin (from Abadi et al., 2009). | 310 |
| Figure 7.38 | Synoptic tectonostratigraphic column for the Jabel Nafusah and wider area (modified from Abadi et al., 2009). | 313 |
| Figure 7.39 | Modern geotectonic setting of the north African coast. The sharp northward deflection of the Maghebrides fold and thrust belt, through Sicily and into Italy, around the remains of the Ionian oceanic plate immediately north of Libya has meant that tectonic inversion of this part of the Tethyan margin is relatively limited. | 314 |

Chapter 8: Synthesis and Conclusions

| | | |
|------------|--|-----|
| Figure 8.1 | Palaeoenvironment model during the Early Mesozoic Kurrush, Al Aziza and Abu Shaybah Formations times, showing the overall of depositional facies. | 320 |
| Figure 8.2 | Triassic palaeographic reconstructions of palaeotethys and Neotethys at the northern Gondwana region (after Stampfi and Borel, 2002a and Makhoul, 2006). | 321 |

Tables

Chapter 1

| | | |
|-----------|--|----|
| Table 1.1 | Plate tectonic summary showing the main plate tectonic events which have shaped the development of North Africa, the reflection of these events can be observed in the structural history of Libya and adjacent areas (Schandelmeier and Reynolds, 1997; Badalini et al., 2002). | 3 |
| Table 1.2 | The Mesozoic succession of Jabel Nafusah, showing the stratigraphic variation from west to east. | 14 |

Chapter 3

| | | |
|-----------|--|----|
| Table 3.1 | Lithostratigraphic nomenclatures for Mesozoic rocks of Libya and adjacent areas. | 36 |
|-----------|--|----|

| | | |
|-----------|---|----|
| Table 3.2 | Proposed stratigraphic nomenclatures of Mesozoic rocks of the Gharian area and it come from transliteration and combination of the Italian and French schools of thought. | 41 |
|-----------|---|----|

Chapter 4

| | | |
|-----------|---|----|
| Table 4.1 | Summary characteristics of the Kurrush Formation in the Gharian area. | 59 |
|-----------|---|----|

| | | |
|-----------|---|----|
| Table 4.2 | Summary characteristics of the Al Aziza Formation in the Gharian area and Ras Lefa section. | 70 |
|-----------|---|----|

| | | |
|-----------|--|----|
| Table 4.3 | Summary of the main facies characteristics of the Abu Shaybah Formation in the Gharian area. | 98 |
|-----------|--|----|

| | | |
|-----------|---|-----|
| Table 4.4 | Summary characteristics of the key humidity-aridity palaeoclimate for the Gharian area. | 174 |
|-----------|---|-----|

Chapter 5

| | | |
|-----------|---|-----|
| Table 5.1 | Summary of different types of natural remanent magnetization. | 183 |
|-----------|---|-----|

Chapter 6

| | | |
|-----------|--|-----|
| Table 6.1 | The results of Muttoni et al., (2001). | 201 |
|-----------|--|-----|

| | | |
|-----------|--|-----|
| Table 6.2 | Summary of the palaeomagnetic sampling localities in the Gharian area. | 207 |
|-----------|--|-----|

| | | |
|-----------|---|-----|
| Table 6.3 | The isolated components from samples during thermal demagnetisation Straw Yellow = Present Day A component, Brown = B component and Green = the Ch component. | 211 |
|-----------|---|-----|

| | | |
|-----------|---|-----|
| Table 6.4 | Palaeomagnetic direction from the Al Aziza Formation. | 221 |
|-----------|---|-----|

| | | |
|-----------|--|-----|
| Table 6.5 | The isolated components from samples during thermal demagnetisation for Abu Shaybah Formation. Straw Yellow = Present Day A component, Brown = B component and Green = the Ch component. | 224 |
|-----------|--|-----|

| | | |
|-----------|---|-----|
| Table 6.6 | Palaeomagnetic direction from the Abu Shaybah Formation | 228 |
| Table 6.7 | Palaeomagnetic poles from the Al Aziza and Abu Shaybah Formations. | 233 |
| Table 6.8 | Middle – late Triassic palaeomagnetic from the Southern Alps and Africa. | 235 |
| Table 6.9 | Early Permian to Pliocene mean paleomagnetic poles for West Gondwana and Adria apparent polar wander paths. | 236 |

Chapter 7

| | | |
|-----------|---|-----|
| Table 7.1 | Locations of traverses undertaken primarily to collect structural data on faults. | 264 |
| Table 7.2 | Cross cutting relations data. | 268 |
| Table 7.2 | The Stratigraphic units and their topographic expressions. | 293 |

Chapter 8

| | | |
|-----------|--|-----|
| Table 8.1 | Plate tectonic summary showing the main plate tectonic events which have shaped the development of North Africa, the reflection of these events can be observed in the structural and sedimentological history of Jabel Nafusah and adjacent areas (modified from Boot et al., 1998; Vail, 1991; Hallett, 2002). | 316 |
|-----------|--|-----|

Acknowledgements

I am grateful to Almighty Allah, who bestowed me with ability to successfully complete this research work and present my thesis. This thesis was born within framework of cooperation between the University of Al Zawia in Libya and University of Plymouth in UK.

The successful completion of my PhD thesis would not have been possible without the efficient assistance, support and cooperation of a great number of people and organization. I would like to express my sincere gratefulness for their contribution and support.

In the first place, I am sincerely grateful to my supervisors, Dr's Martin Stokes, Graeme Taylor, Sarah Boulton and Salem Sharata for their help, clear guidance and inspiration. They have been nicest guys to work with them over the last few years. They always have a positive attitude when encountering problems and have been on my side the whole time and cheering me up and giving me the strength to continue my study.

I would also like to thank the support from fellow postgraduate students and the help I have received from several members of staff in the Department of Earth Sciences in the University of Plymouth.

I am grateful to the University of, Al Zawia for their financial support during the field work. I would like to thanks the members of the geological department of the University of Al Zawia and they were always inspiring and helpful, especially in arranging facilities in Libya during the fieldwork.

I wish to thanks my father, mother, sisters and brothers in Libya, who suffered from my years of absence, for their patience and support.

Finally, I would like to express my deep gratitude to my wife for her encouragement, support and understanding during all these years of my study.

AUTHOR'S DECLARATION

At no time during the registration for the degree of Doctor of Philosophy has the author been registered for any other University award without prior agreement of the Graduate Committee.

This study was financed with the aid of Faculty Development programme of Higher Education commission, Libya, University of Al Zawia.

Word count of main body of thesis: 53628

Signed: Emhemed

Date: 12/1/ 2012

Chapter 1: Introduction

1.1 Introduction

Since at least Late Carboniferous times the geology of the North African-Arabian margin was principally affected by the evolution of the ocean lying directly to its north, first the Tethys and later the Neo-Tethys Ocean. During the Mesozoic–Tertiary period the tectonic evolution of the region was also linked to a combination of the opening of the Atlantic Ocean and the dynamics of the African-Eurasian convergence events that led to the break-up of the supercontinent Pangaea and subsequently Gondwana, the southern part of Pangaea. This sequence of events commenced in the Late Carboniferous with the development of the Tethys Ocean. By Permian-Triassic times there had developed a narrow Neo-Tethys Ocean whose southern margin includes the northern margin of Libya (Fig. 1.1). In the Triassic a major continental rift system developed within Gondwana (Sengor, 1979; Sengor, 1984; Sengor, 1985; Guiraud, 1998; Ziegler et al., 2001). Rifting in one form or another has therefore affected the North African margin from the Permian onwards, likely propagating westward from the north-eastern Arabian margin to Morocco during the Permian and Triassic (Guiraud, 1989) (Table 1.1). Subsequently the Mesozoic-Cenozoic structural history of North Africa can be divided into three successive rifting events that correspond with the development of the Equatorial, South and North Atlantic Ocean and with the associated opening and subsequent closure of the Tethyan Basin (Glover, 1999).

Early Mesozoic deposits have been reported from different areas lying along the south Tethyan strandline on the North African margin and the Arabian sub-plate including Tunisia, Egypt, Jordan, Morocco and Libya (Bishop, 1975; Makhlouf, 2006). However, and critical to this thesis, it is not yet clear how and to what extent sedimentation patterns of NW Libya were controlled by local versus regional tectonic events and how

these interacted with global sea level changes. To investigate this question and to better understand the geodynamic processes in the NW Libya region, sedimentary facies analysis and magnetostratigraphic analysis of Triassic and Jurassic formations in the Gharian area of north-western Libya have been carried out. During the course of this work it also became apparent that a better understanding of the key structures of the region was also required and hence the structure of the Jabel Nafusah in the Gharian area has also been investigated.

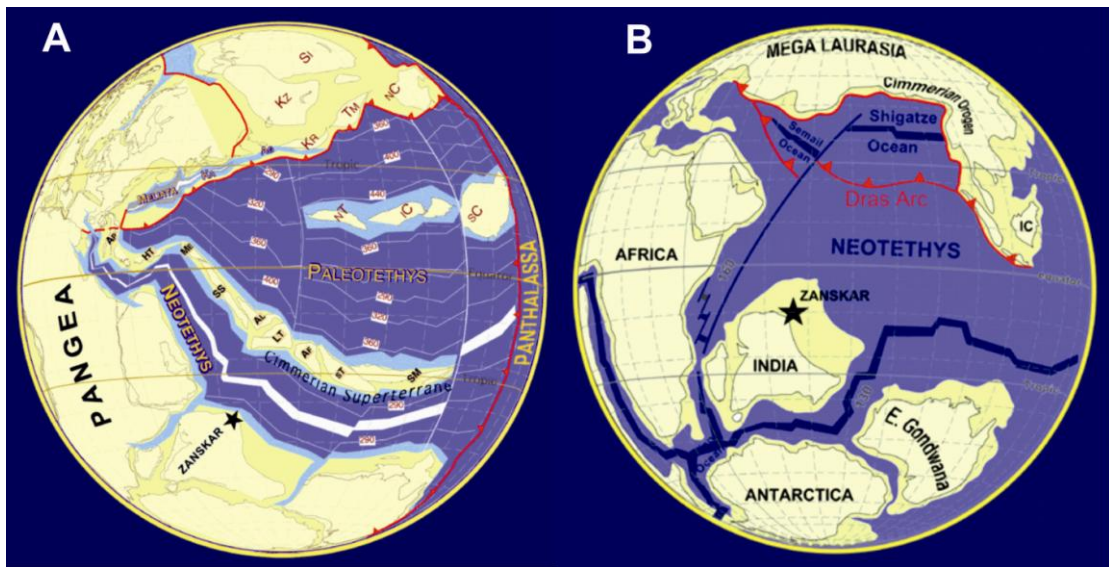


Figure 1.1 A: The Earth at the Permian-Triassic boundary. The opening of the Neotethys separates the Cimmeridion Superterrane from Gondwana. **B:** The Earth in the Cretaceous. The Cimmeridion Superterrane has accreted to Mega Laurasia, the oceanic crust of the Neotethys is subducted to the north along the Dras volcanic arc, the Shigatze Ocean opens as a consequence of back-arc spreading, and India is separated from Africa (from Stampfli and Borel, 2002).

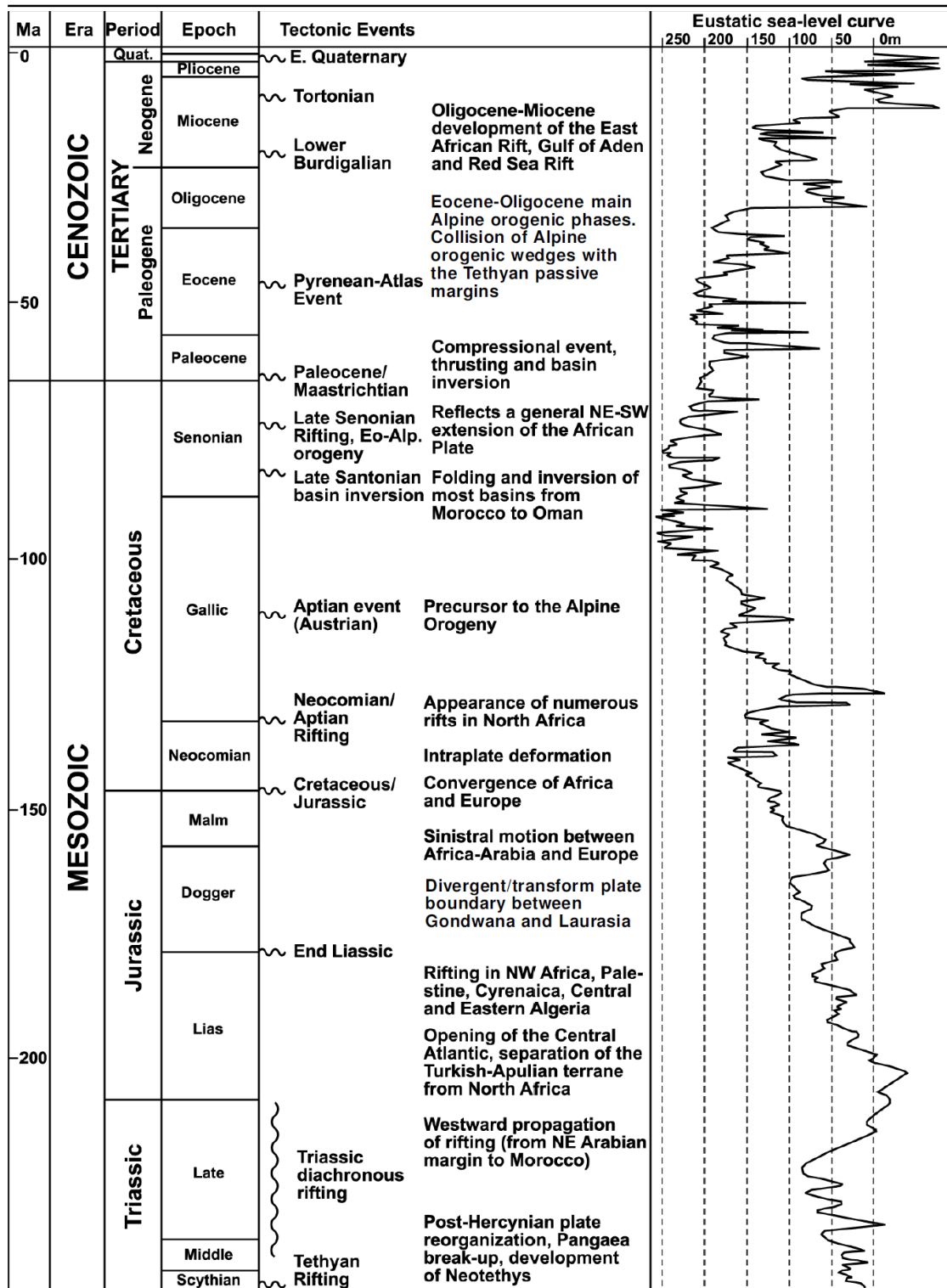


Table 1.1 Plate tectonic summary showing the main tectonic events which have shaped the development of North Africa, the reflection of these events can be observed in the structural history of Libya and adjacent areas (Schandelmeier and Reynolds, 1997; Badalini et al., 2002).

1.2 Aims of the study

The aim of this thesis is to study the Early Mesozoic geological history of the Jabel Nafusah region of north-central Libya, specifically in the Gharian area. The main objectives of this study are therefore to:

1. To describe and interpret the sedimentary processes and palaeoenvironments of the
 - a. Kurrush Formation
 - b. Al Aziza Formation
 - c. Abu Shaybah Formation
2. To assess the relative importance of tectonics, climate, sea-level and internal mechanisms as seen through variation in depositional style in this area during the Early Mesozoic.
3. To undertake a magnetostratigraphic study of the above units in order to help assess their age and determine the paleoposition of the studied area during the relevant geological time period.
4. To describe and quantify the geological structure of the Jabel Nafusah region, specifically in Gharian as it has affected the key units of interest.
5. To map the main structural elements of the region and Mesozoic sedimentary succession in the Gharian area.

1.3 General tectonic history

Since the late 1960s, much scientific data has been generated on the tectonic evolution of the Mediterranean basin. However, most of the data dealt with the northern, and to a certain extent, the southwestern continental margins. In comparison, little work has been undertaken on the tectonic evolution of the southern margin (including Libya) of the central Mediterranean basin.

The major structural and tectonic features of NW Africa have been discussed by many geologists (e.g; Conant and Goudarzi, 1967; Klitzsch, 1970; 1971; Desio, 1971; El Hinnawy and Cheshitev, 1975; Goudarzi, 1980; Vail, 1991; Tawadros, 2001 and Gabtni et al., 2009). Klitzsch (1970; 1971) first indicated that the basins in NW Africa evolved as a result of a diagonally-intersecting system of uplifts during the Phanerozoic. He also indicated that these uplifts represent a weak suture zone of Pan-African origin that was later reactivated during the Early Caledonian tectonic phase. Therefore, this appears to be the source of an often repeated idea that the uplift is part of an essentially E-W trending ‘Nafusah arch’ including recently published papers (Saadi et al., 2008; 2009), this concept is considered in more detail in Chapter 7. North western Libya and southern Tunisia are situated at the eastern flank of the south Atlas fold belt adjacent to the Saharan flexure or lineament (Fig. 1.2). This lineament system bifurcates near the Gulf of Gabes where it appears to underlie the Pelagian platform in the offshore and Jafarah Basin to the south on land (Anketell, 1996). According to Anketel and Ghellali (1991) and Gabtni (2009) the southern branch represents the line of the Hercynian Jafarah axis, which is dominated by basement structural features in northwest Libya and southern Tunisia.

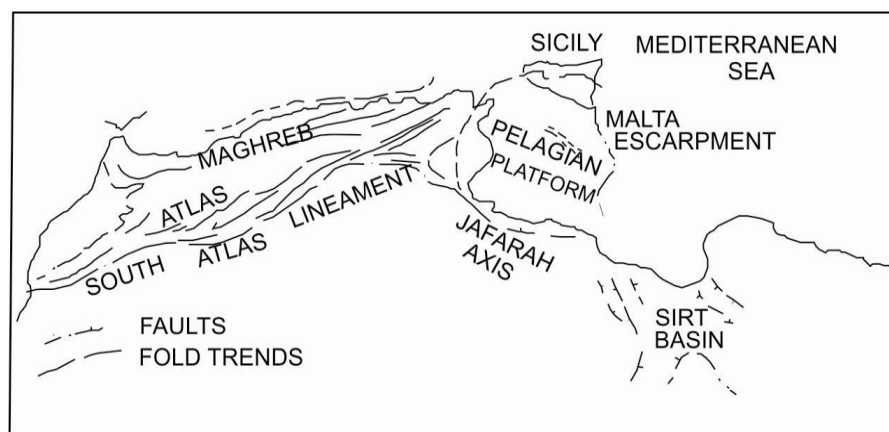


Figure 1.2 Sketch map showing major structural trends of NW Africa (modified from Anketell and Ghellali, 1991).

Libya is broadly divisible into two major geologic regions (Fig. 1.3). The southern part of Libya is dominated by a series of intracratonic and mainly Paleozoic basins separated by Precambrian crystalline basement highs (traditionally referred to as 'arches' in the literature). In the north and west lies the Al Hamra or Ghadamis Basin (Fig. 1.3), of which the northern part was uplifted during Hercynian folding, then subsided and partially reactivated during early Mesozoic rifting. This is separated by the Al Gargaf arch from the Murzuq Basin in the south west, which is in turn separated by the Tibesti crystalline basement massif from the Al Kufra Basin in the southeast (Klitzsch, 1970; Goudarzi, 1980).

The northern part of the country is situated on the tectonically more active subsiding margin that has been formed by rifting and opening of the Neotethys ocean basin, at the northern continental margin of Gondwana (Goudarzi, 1980; Gumati and Nairn, 1991; Abadi, 2008). This includes, from west to east, the Jafarah Basin (also known as the Tripolitania Basin), the extensive Sirt Basin, and Benghazi Basin which extends far to the south and finally the Cyrenaica Platform (Fig.1.3). Based on Anketell and Ghellali, (1991), there are three major fault zones present in the Jafarah region (Coastal fault zone, Al Azizyah fault zone and Wadi Ghan fault zone). These zones follow two main trends, E-W and NW-SE. In all the zones the component faults are most commonly exhibit dip-slip normal motion with the amount of throw varying from a few meters to several hundred meters.

Superimposed on Precambrian basement uplifts, Palaeozoic and Mesozoic basins are a series of large volcanic fields and their intrusive equivalents (Fig. 1.4). Age wise these span much of the Tertiary period with age dates mainly concentrating in the range 50 to 5 Ma. In the study area this is represented by a series of basic intrusions although located only some 30 km southwest of the field area lies the northernmost edge of the most northerly plateau basalt field.

There is limited geological research on the immediate Gharian area undertaken by Gray, (1971) (see Chapter 7). Therefore, it is important to compare the basins of NW Libya with the Gharian area to allow an overall understanding of the tectonic development. For example, the Sirt Basin is a major intracratonic rift system on the north central African plate (Abedi et al., 2008) and comprises numerous horst and graben complexes that began to develop in the Early Cretaceous time (Abedi et al., 2008). It is very important to determine whether these Early Cretaceous units have a clear developmental relationship with the half-graben system observed in the Gharian area (see Chapter 7). Earlier work on the Jabel Nafusah region was not supported by detailed structural data from the Gharian area and therefore this is the first work to present detailed surface geology data to improve the structural knowledge of the Gharian area.

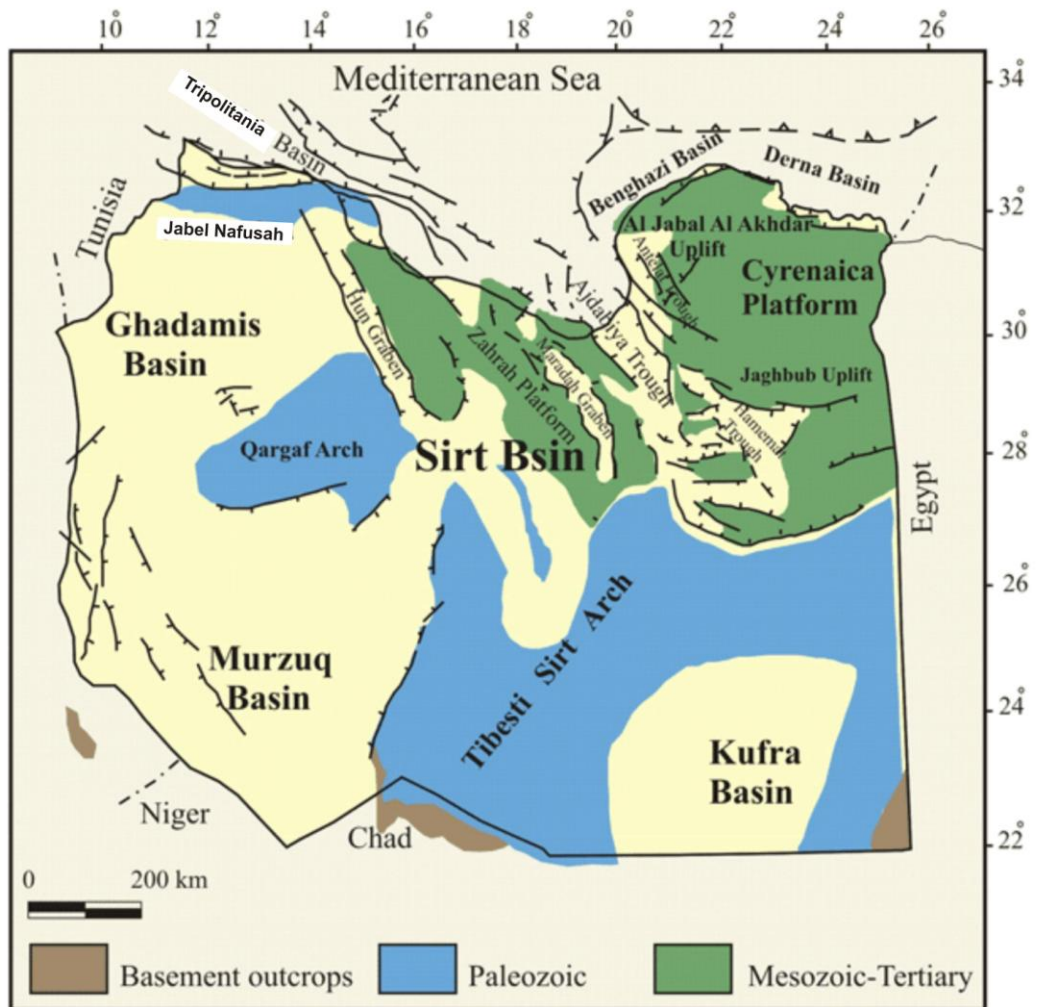


Figure 1.3 The major structural and tectonic feature of Libya (modified from Hassan, 2009).

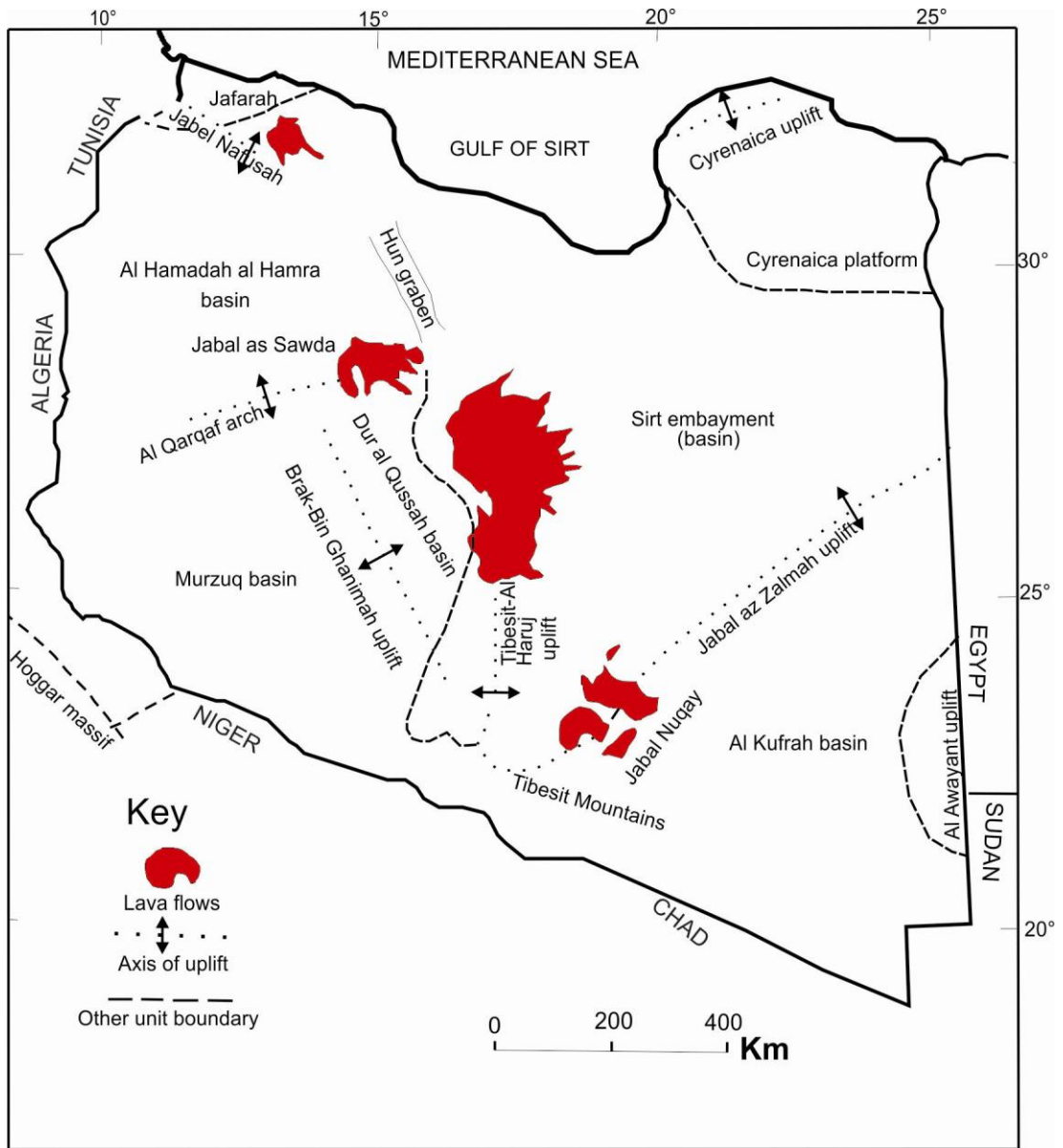


Figure 1.4 Map of Libya showing the uplifted, basins and adjacent regions (modified from Goudarzi, 1980).

1.4 The Jabel Nafusah

The Jabel Nafusah escarpment (or Nafusah mountains) is some 400 km long, extending from the coast in the east (near the town of Trahunah) to the Tunisian border in the west (Fig. 1.5) where it continues westward before turning sharply northward within Tunisia itself. Within Libya it is a major east–west escarpment that rises up to 800 m above the plain that lies to the north and is viewed as separating the Ghadamis Basin to the south from the Jafarah Basin to the north (Fig. 1.6). The Nafusah escarpment is one of the most prominent morphological features in north-western Libya (Miller et al., 1971; Giraudi, 2005) and is considered in more detail in Chapter 7. Furthermore, the Jabel Nafusah can be divided into three areas based primarily on the geographic location and nature of the escarpment (Fatmi et al., 1978):

1. Kiklah-Nalut area (western Jabel)
2. Gharian area (central Jabel)
3. Trahunah area (eastern Jabel)

1.4.1 Physical setting of the immediate study area

The area involved in this study, around the regionally important town of Gharian, is situated in the central part of the Jabel Nafusah escarpment, some 70 km south the Mediterranean coast with Wadi Ghan to the east, and 56 km from Kiklah to the west (Fig. 1.5). The Gharian area is bounded by the Ghadamis Basin in the south and the Jafarah Basin to the north (Fig. 1.6).

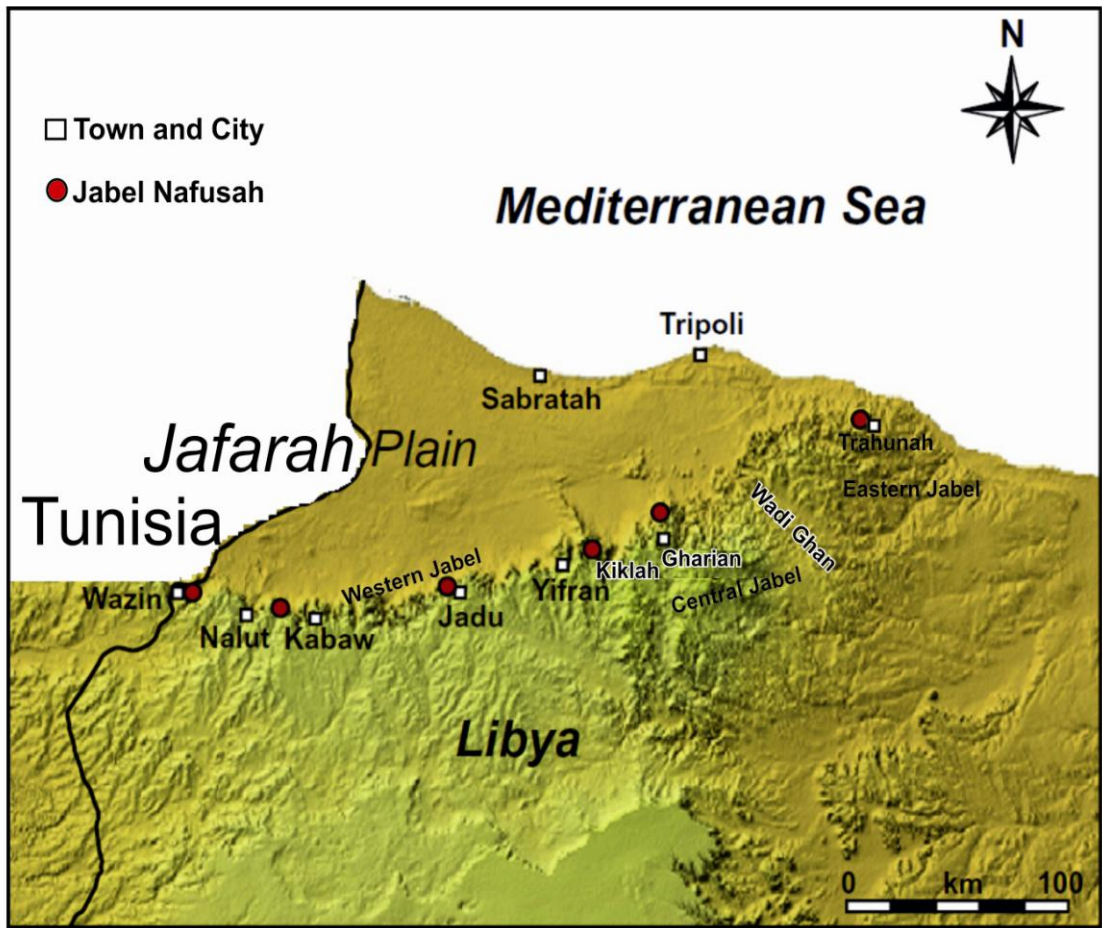


Figure 1.5 DEM map showing the location of Jabel Nafusah escarpment, names and town referred to within the text (modified from Bodin et al., 2010).

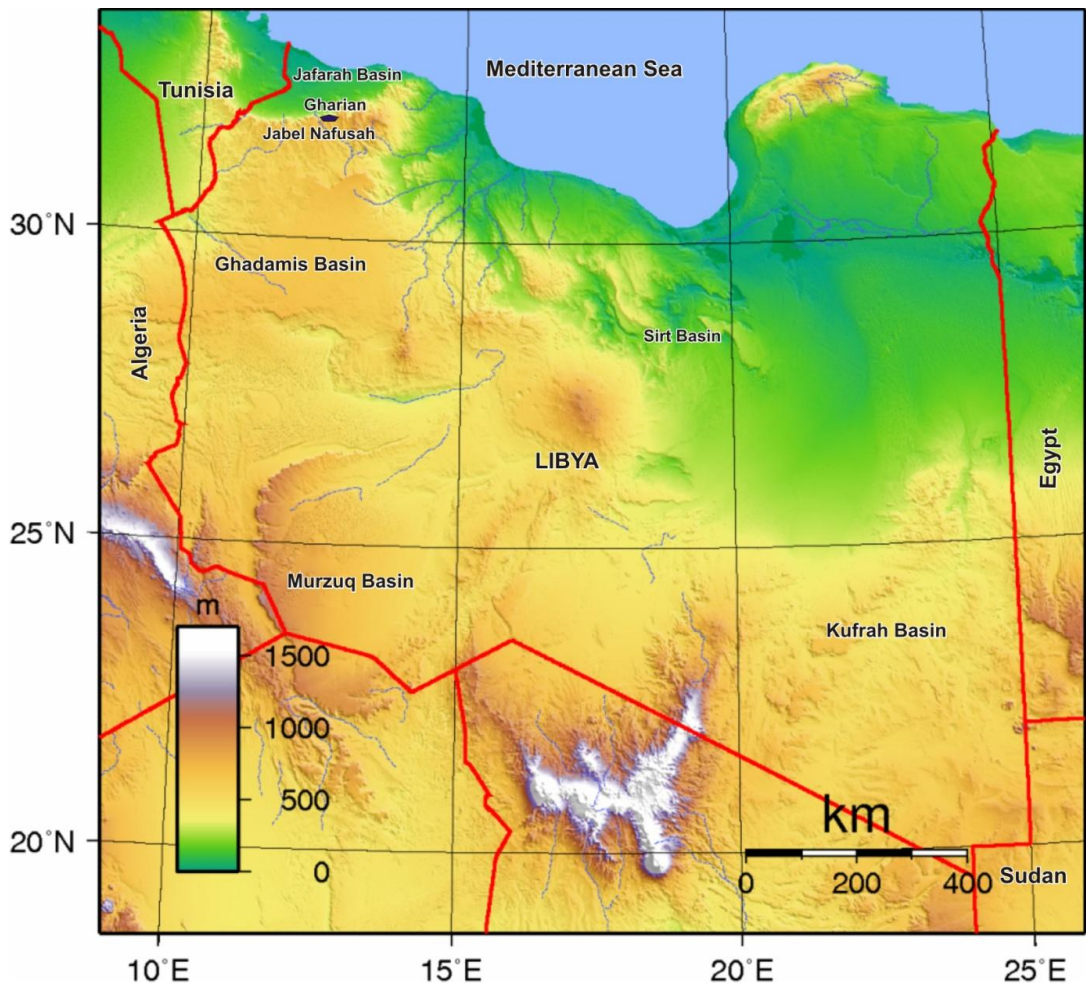


Figure 1.6 Map showing the topography of Libya and the location of Jabel Nafusah between two basins (Jafarah and Ghadamis Basins) (modified from Sadalmelik, 2007).

1.4.2 Stratigraphy of the Gharian area

The sedimentary rocks of the Gharian area consist of clastics and carbonate rocks, which reveal the depositional environment and the subsequent tectonic history (Table 1.2). The oldest rocks, of Triassic age, outcrop in the central part of the Jabal Nafusah (Gharian area). There are two significant exposures in the study area; the first of these is located near town of Aziziyah (Al Aziza Formation) in an isolated hillock nearly 42 km south of Tripoli; and the second is located to the east and west of the Tripoli-Gharian highway. The escarpment is capped by upper Cretaceous carbonates (Sidi as Sid and Nalut Formations; for more details see Chapter 3). Christie (1966) and Assertor and Benelli (1971) reported their stratigraphic studies of NW Libya, aimed primarily at hydrogeology, which included stratigraphic measured sections from the Gharian. However, their interpretation was based upon limited field work and restricted spatial coverage. Furthermore, the ages of formations are poorly constrained due to very limited fossil evidence (Swire and Gashgesh, 2000); this is considered in more detail in Chapter 6. To understand the geological history of any area, we need palaeoenvironmental and palaeogeographic reconstructions. These allow us to investigate the influence of water and sediment supply on the preservation of sedimentary systems within a given geodynamic context. The Early Mesozoic of the Gharian area has provided excellent exposure and is considered in more detail in Chapter 4 where a palaeogeographic model is developed.

| Geologic time | | | WESTERN JABAL NAFUSAH | | | CENTRAL JABAL NAFUSAH | | | EASTERN JABAL NAFUSAH | | | |
|--|--------|--------|--------------------------|-------|-----------|------------------------|-------|-----------|------------------------|-------|-----------|--------|
| | | | NALUT-YAFARIN-KIKLAH SEC | | | GHARIAN -MIZA SECTIONS | | | TARHUNA-GEZZAR SECTION | | | |
| CENOZOIC | SYSTEM | SERIES | STAGE | GROUP | FORMATION | MEMBER | GROUP | FORMATION | MEMBER | GROUP | FORMATION | MEMBER |
| | | | | | | | | | | | | |
| CRETACEOUS | | | | | | | | | | | | |
| UPPER | | | | | | | | | | | | |
| MAESTRICHTIAN | | | | | | | | | | | | |
| MONTIAN | | | | | | | | | | | | |
| DANIAN | | | | | | | | | | | | |
| CAMPAIAN | | | | | | | | | | | | |
| SANTONIAN | | | | | | | | | | | | |
| CONIACIAN | | | | | | | | | | | | |
| TURONIAN | | | | | | | | | | | | |
| CENOMAIAN | | | | | | | | | | | | |
| ALBIAN | | | | | | | | | | | | |
| APTIAN | | | | | | | | | | | | |
| NEOCOMIAN | | | | | | | | | | | | |
| TITHONIAN | | | | | | | | | | | | |
| KIMMERIDGIAN | | | | | | | | | | | | |
| OXFORDIAN | | | | | | | | | | | | |
| CALLOVIAN | | | | | | | | | | | | |
| BATHONIAN | | | | | | | | | | | | |
| BAJOCIAN | | | | | | | | | | | | |
| TOARCIAN | | | | | | | | | | | | |
| PLIENSBACHIAN | | | | | | | | | | | | |
| SINEMURINA | | | | | | | | | | | | |
| HETTANGIAN | | | | | | | | | | | | |
| RHAETIAN | | | | | | | | | | | | |
| NORIAN | | | | | | | | | | | | |
| CARNIAN | | | | | | | | | | | | |
| LADINIAN | | | | | | | | | | | | |
| ANISIAN | | | | | | | | | | | | |
| SCYTHIAN | | | | | | | | | | | | |
| NOT EXPOSED | | | | | | | | | | | | |
| JURASSIC | | | | | | | | | | | | |
| UPPER | | | | | | | | | | | | |
| TIGI GROUP | | | | | | | | | | | | |
| SHAKSHUK FORMATION | | | | | | | | | | | | |
| CHAME AU MORT FM. | | | | | | | | | | | | |
| TAKBAL FORMATION | | | | | | | | | | | | |
| ABREGHS FORMATION | | | | | | | | | | | | |
| BUEN NIRAN MBR | | | | | | | | | | | | |
| MAHMEL FORMATION | | | | | | | | | | | | |
| UPPER | | | | | | | | | | | | |
| MIDDLE | | | | | | | | | | | | |
| LOWER | | | | | | | | | | | | |
| BIR AL GHANAMI GROUP | | | | | | | | | | | | |
| KIKLAH FORMATION | | | | | | | | | | | | |
| SIDI AS SID FM. | | | | | | | | | | | | |
| YAFRIN MBR | | | | | | | | | | | | |
| AIN TOBI MBR | | | | | | | | | | | | |
| NALUT FORMATION | | | | | | | | | | | | |
| QASR TIGIRINNAH FM | | | | | | | | | | | | |
| MIZDAH FORMATION | | | | | | | | | | | | |
| THALA MEMBER | | | | | | | | | | | | |
| MAZUZAH MEMBER | | | | | | | | | | | | |
| ZMAM FORMATION | | | | | | | | | | | | |
| HAD LS | | | | | | | | | | | | |
| TAR MEMBER | | | | | | | | | | | | |
| SUCCESSION PRESENT ON THE SOUTH BANI WALID AREA | | | | | | | | | | | | |
| OVERLAIN TOWARDS THE NORTH BY MIOCENE AL-KHUMS FM. | | | | | | | | | | | | |
| CENTRAL JABAL NAFUSAH | | | | | | | | | | | | |
| EASTERN JABAL NAFUSAH | | | | | | | | | | | | |
| GHARIAN -MIZA SECTIONS | | | | | | | | | | | | |
| TARHUNA-GEZZAR SECTION | | | | | | | | | | | | |
| UPPER | | | | | | | | | | | | |
| NALUT FORMATION | | | | | | | | | | | | |
| SIDI AS SID FORMATION | | | | | | | | | | | | |
| YAFRIN MBR | | | | | | | | | | | | |
| AIN TOBI MBR | | | | | | | | | | | | |
| KIKLAH FORMATION | | | | | | | | | | | | |
| ABU GHAYLAN FORMATION | | | | | | | | | | | | |
| ABU SHAYBAH FORMATION | | | | | | | | | | | | |
| ABU SHAYBAH FORMSTION | | | | | | | | | | | | |
| BASE | | | | | | | | | | | | |
| NOT EXPOSED | | | | | | | | | | | | |
| AL AZIZA FORMATION | | | | | | | | | | | | |
| KURRUSH FORMATION | | | | | | | | | | | | |

Table 1.2 The Mesozoic succession of Jabel Nafusah, showing the stratigraphic variation from west to east (modified from the Industrial Research Centre, 1975).

Chapter 2: Techniques, Strategy, Data Collection and Presentation

2.1 Introduction

This chapter describes the strategy and the main techniques applied in sedimentological, structural geology and palaeomagnetic studies used throughout this research. This chapter is organised into four sections. The first part explains the research strategy of data collection used within this thesis. Both the field work and data presentation are explained in the second part, whilst part three is based on the facies sedimentary and stratigraphic analysis. The final section elaborates on laboratory analysis and the palaeomagnetism study. The field localities are described in the relevant results chapters (Chapter 4 and 6) for ease of reference.

2.2 Research Strategy

In order to reconstruct the Triassic palaeoenvironmental history of the Gharian area and to meet the objectives of this study (Chapter 1), a scientific methodology was applied to show how ancient environments and environmental changes could be reconstructed by describing and interpreting natural phenomena to provide a scientific explanation. To understand an area under study should involve the generation and testing of hypotheses or theories. Reading (1986) proposed a scientific methodology using three stages of interpretation to understand the occurrence of ancient sequences. The first stage is to develop initial working hypotheses whilst the next stage is the development of a palaeogeographical or local model and the final stage is to produce a realistic interpretation or actual facies model.

For this study, working hypotheses were constructed during collection of sedimentary, stratigraphic and structural data from numerous key sections. A sedimentary facies approach was used to describe and interpret sedimentary data (outlined in section 2.6) allowing reconstruction of depositional processes and environment. Data were collected from a number of key sections (Fig. 2.1) which then enabled localised palaeogeographic models to be made for the stratigraphic formations under study. Further discussion of the techniques applied in structural geology and palaeomagnetism (section 2.7.1 and 2.9).

2.3 Field Work and Presentation

The purpose of the fieldwork was to collect a comprehensive field data set from key locations throughout the study area. Sample description, photographs and structural measurements were recorded (see Chapter 4). The data and samples used in this study were collected during five field seasons; two extensive field mapping seasons were conducted during the autumn of 2008 and spring of 2009. Sedimentary data were collected over two main field seasons whilst one fieldtrip was undertaken to collect samples for palaeomagnetic analyses.

1. Geological Map

These maps served as a basic source of stratigraphic, lithologic and structure geological information in the Gharian area. The 1:25,000 scale geological maps were obtained from Gray, (1971) and Industrial Research Centre (IRC, 1975) of Libya (The Geological Survey of Libya).

2. Topography Map

Topographic maps are the most widely used maps. These depict the surface morphology by showing variety of elevations (contour lines) and landforms. For this study the geological map of the Gharian area is constructed on a topographic base map (1:50,000 scale topographic map sheet numbers 3/1989) of the Industrial Research Centre of Libya).

3. Aerial Photographs

Aerial photography was the first type of remote sensing and still plays an important tool in geologic applications. Since the 1950s, black and white aerial photography has been used for Earth surface mapping and still counts for 99% of all topographic mapping (Miller et al., 1961).

Aerial photography served as a source of knowledge about the general geologic features such as rock types, topography, drainage patterns and structural elements. The black and white aerial photographs on the scale 1:50,000 were obtained from the Libyan government.

2.4 Field Techniques

Standard geological fieldwork techniques as outlined in McClay (1987) and Tucker (1982, 2003) were applied in measuring and describing the field sections. Reading of grid reference defining data collection sites or field localities use UTM coordinate, derived from a Global Positioning System (GPS) and also from field cross-referencing with topographic maps (Longitude and Latitude). The field localities are described in the relevant results chapters. Observations in the field included measuring vertical sections, preparing graphic logs showing lithology, sedimentary structures, fossils and interpreted facies changes. The samples were collected and numbered relating to the

locations and the rocks units. All field observations were recorded in a field notebook. Photographs and field sketches were taken for several purposes and were developed during the fieldwork (see result chapters).

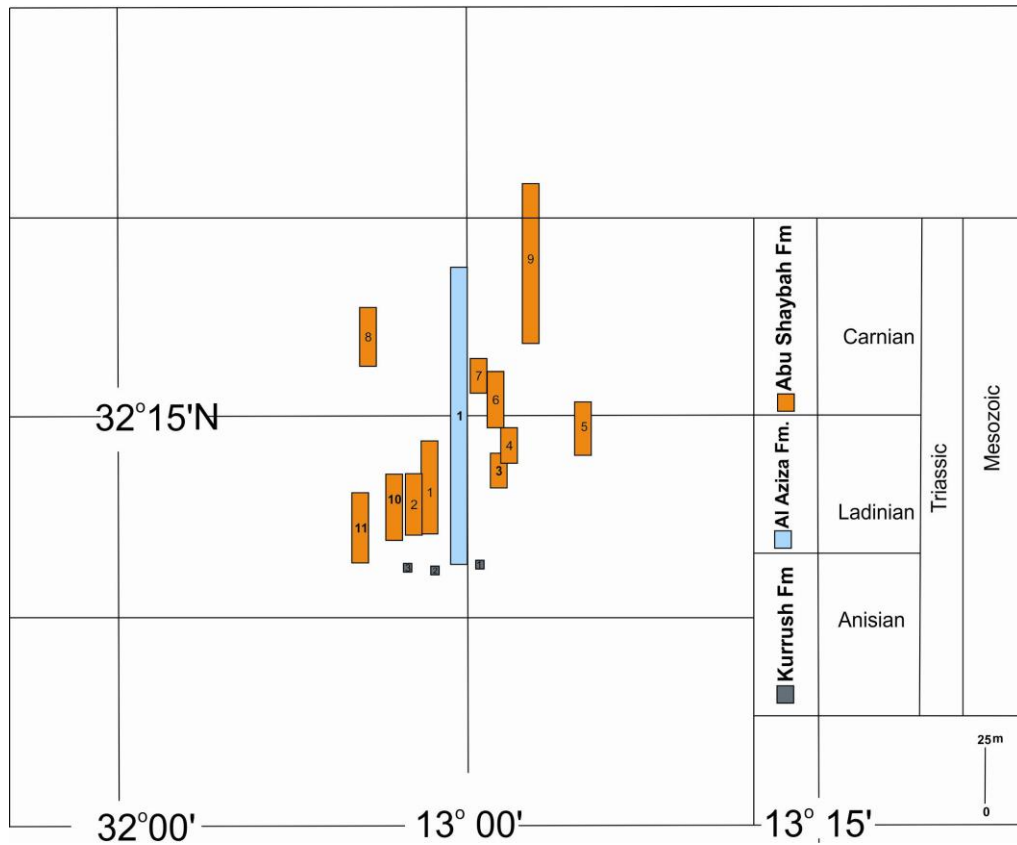


Figure 2.1 Map showing the sections of Kurrush, Al Aziza and Abu Shaybah Formations.

2.4.1 Graphic Sedimentary Logs

A sedimentary log is a graphical method for representing data collection from sedimentary rocks. There are many different formats to represent the data collection; however, in this study, the format presented by Tucker (1982, 1996) was followed.

The standard technique for collecting field data from sedimentary rocks is to prepare a graphic log of the succession. The vertical scale for the logs measured in this study is 1 cm to 1 m. The vertical logs were drawn up using CorelDraw X4 and the standard log

symbols used throughout this study are shown in Figure. 2.2. Features which are recorded on the log include lithology, unit thickness, textures, colour, sedimentary structures (e.g. cross-beds, ripples etc.), palaeocurrent measurements and the nature of bed contacts.

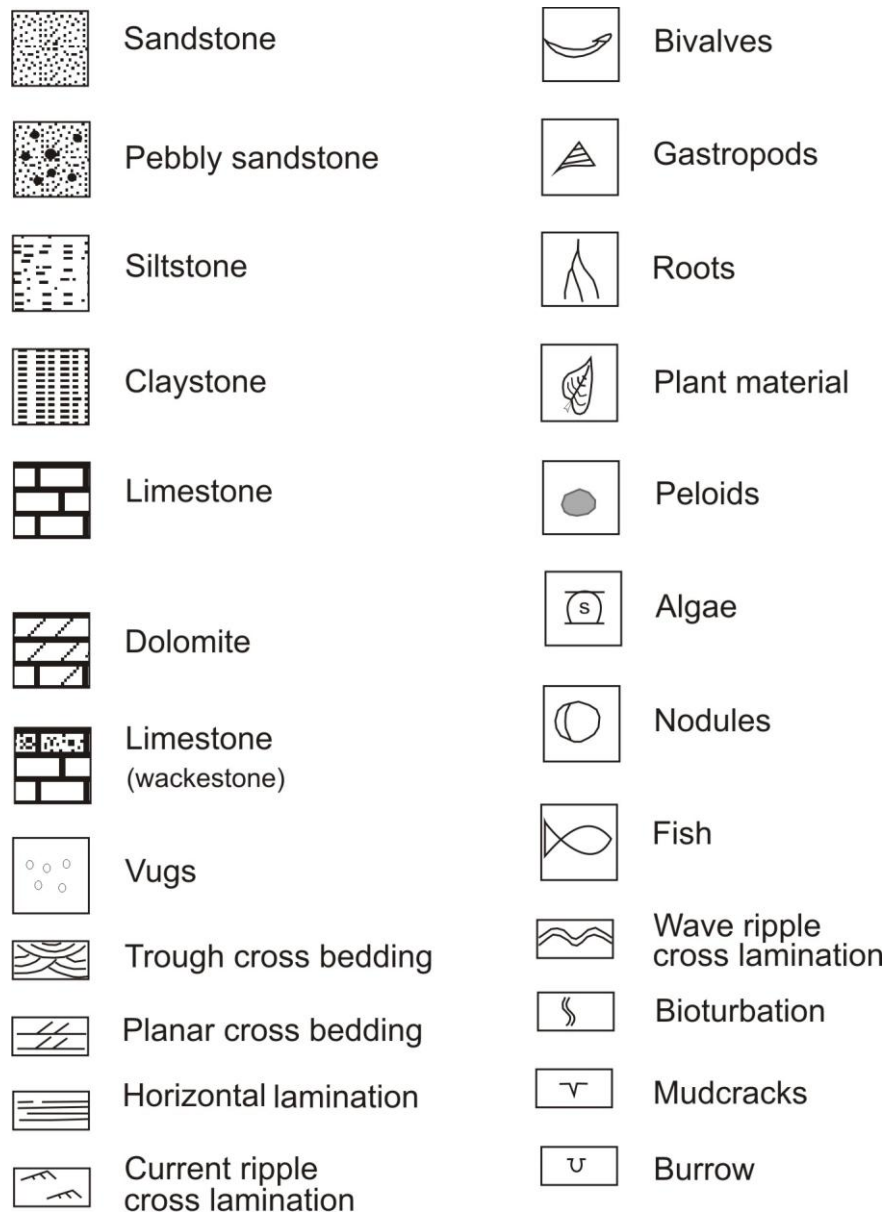


Figure 2.2 Key to sedimentary logs used throughout this study.

1. Lithology

Studying the lithology of the sedimentary facies can give insights into weathering, transport process, deposition and environment (Selley, 1985). The grain distribution of clastic sediments provides a relative measure of the energy of the transporting medium and the energy of the basin of deposition. For example, coarse grain size gives some indication of the flow power at time of deposition (Fig. 2.3).

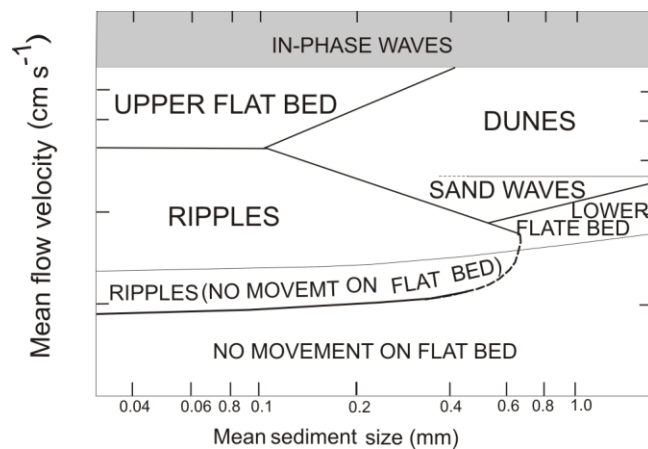


Figure 2.3 The distribution of sand bedforms plotted in the field of current velocity and sediment grain size (source Harms et al., 1975).

2. Texture

Textural characteristics includes the sorting of a sediments and roundness of grains. On the graphic log, the grain-size was recorded by using the Udden–Wentworth classification (after Tucker, 2001) where the horizontal scale, showing clay, silt and sand, which is divided into fine, medium, coarse and very coarse etc. The limestones were classified in the field using Dunham’s classification scheme (Dunham 1962; Tucker and Wright, 1990).

3. Unit Thickness

The sedimentary units were measured in the field using a metric tape measure and Abney level. The Abney level was used where the rocks have a high angle and the outcrop surface is oblique to the bedding and also used to log large gaps in section exposure or parts of section where lithological uniformity was observed.

4. Colour

Studying the colour of sedimentary facies is vital in the description of many sedimentary rocks. The primary colour is original colour of rocks whilst the secondary colour is produced during the weathering. Thus both the fresh rock and weathered rock surfaces were recorded in the field notebook and colours were assigned to rock using the standard notation from a Munsell rock colour chart (Rock Colour Chart, 2009), for example 5YR 5/6 – light brown and noted next to relevant part of the field log.

5. Sedimentary Structures

Sedimentary structures are formed during and after deposition (Knut, 1989). Preserved sedimentary structures, which form during deposition, reflect the condition of the flow, climate and the quantity of sediment discharge. Lamination and cross-bedding, which are formed by sedimentary bedform migration, are good parameters to interpret the sedimentary facies (Collinson and Thompson, 1989; Allen, 1968; Knut, 1989).

Moreover, sediments that appear without lamination and bedding (massive) may reflect very rapid deposition and/or intense bioturbation that collectively destroy the primary sedimentary structures. On the graphic logs the sedimentary structures were recorded in separate columns.

6. Fossils and Trace Fossils

Traces of living organisms within sediments or on sediment surfaces are useful parameters to interpret the depositional environment (Reineck and Singh, 1975). There are two important types of fossils that can be used in environmental analysis. These are micro-fossils and trace fossils. The skeletal parts of benthic organisms are preserved in the rock as fossils such as shells, teeth and fish scales. Bioturbation structures are traces produced by manner of living animals in the bed. Trace fossils include: 1) footprint, tracks and burrows, 2) rasping, borings and etchings in rigid substrates, 3) faecal pellets, However, some geologists include 4) plant root penetration structures (e.g. Richter, 1936; Bromely, 1996). There are many different groups of microfossils that can be used in environmental interpretation (foraminifera, ostracods etc.). The study and classification of fossils and trace fossils can provide important information about the environment.

2.5 Palaeocurrent Analysis

Palaeocurrent analysis has been measured to establish transport directions of sediment transport. Selley (1985) stated that the palaeocurrent analysis of a facies involves the following steps:

- 1- Measurement of the orientation of significant sedimentary structures in the field (e.g. cross-bedding dip direction);
- 2- Preparation of a regional palaeocurrent map;
- 3- Integration of the palaeocurrent map with other lines of facies analysis to determine environment and palaeogeography.

During the fieldwork in the Gharian area, readings of cross-bedding were collected from eight stations within the map area. Cross-bedding is one of the most widely used palaeocurrent indicators (Collinson and Thompson, 1989). Palaeocurrent measurements were taken on thin to medium bedded planar–tabular cross-beds. In general, palaeocurrent data obtained from tectonically tilted units were corrected for dip. The readings of the cross-bedding and bedding of tilted beds were plotted onto rose diagrams and corrected to represent the real directions of the palaeocurrent. Information from these stations and map from them is incorporated into Chapter 4.

2.6 Field Facies and Stratigraphic Analysis

The description of outcrops was made based on colour, texture, contacts, bedding and sedimentary structures. Then, detailed descriptions for each outcrop were carried out using standard fieldwork techniques. Hammer, hand lens, notebook, compass, a small bottle of HCl, and camera were used in the work.

Based on lateral variation of the outcrops, geometry, lithology, sedimentary structure, thickness and bedding, facies were identified and interpretations made. The data obtained were transferred onto vertical section using symbols commonly used in logging.

2.6.1 Facies and Facies Associations

Facies has many definitions (see Selley, 1976; Selley, 1985; Reading, 1986; Walker, 1992), this study uses a definition as is outlined by Walker (1992, p.2), who defined the facies ‘as a body of rocks characterized by a particular combination of lithology, physical and biological structures that bestow an aspect different from the bodies of rocks above, below and laterally adjacent’. This means that the facies must display different aspects to be recognized from the adjacent rocks. Within a sedimentary rock

these aspects are lithology, sedimentary structures, fossils, geometry, change in grain size and change laterally.

Sedimentary facies are a product of the primary sedimentary process and post-depositional modification. The characteristics of each facies can reflect the dominant environment conditions during the period of deposition. The facies can be defined on many different scales based upon the objectives of the study, the time available in the field, and the abundance of physical and biological structures in the rocks.

Each facies which has specific depositional process can be combined together into facies associations. A facies association is a grouping of facies that are genetically or environmentally related. The association provides additional evidence, which makes environmental interpretation easier than treating each facies in isolation (Reading, 1986). Thus, the data presented within this research identifies facies and facies associations which correspond to marine to continental environments of deposition. Chapter 4 examines the phases of marine and continental environment within the Gharian area. For these marine and continental deposits, many sedimentary facies have been identified with each facies being defined on the basis of discrete sets of sedimentary characteristics with each facies being assigned a name and code such as '*Symmetrically rippled siltstone and fine sandstone facies (F-Sd)*'. The facies are then grouped into facies associations based upon their occurrence with other facies which relate to a specific environment of deposition.

2.7 Geological Mapping

Field mapping was conducted during the autumn of 2008 and spring of 2009 with aid of Google Earth software (version 2010), Gray's (1971) map and 1: 50,000 scale topographic maps with 20 m contour intervals. Geological boundaries were located by comparison with 1:50.000 scale aerial photographs, compass techniques and GPS. An area of about 42 km² was geologically mapped on a 1:50,000 scale, from east of Qosam village to the west of Ras Tunat village. The field localities are described in the relevant result chapter (7). The map was completed using iterative processes of air photo interpretation, Landsat images, and field mapping. The map presented within this thesis has been redrawn using Corel DAW X4 and map and result of geological mapping are discussed in Chapter 7.

2.7.1 Structural Data

Fault plane orientation was measured by strike-dip and dip-dip direction methods outlined in McClay (1987). For each fault measured in the field, the following features were noted: (a) the attitude of the plane, (b) the stratigraphic units that were displaced, (c) whenever possible, the relative order of movement and type of kinematic indicator (if present). Structural data were grouped and plotted on Schmidt stereographic projection using the StereoNet programme.

2.8 Laboratory Methodology

2.8.1 Petrographic Analysis

Sedimentary petrology was used to further identify the type of mineral province across the area and contributes information about grain size, roundness and bedding characteristics. Forty-two samples of sediments were selected for thin section. These samples consisted of very fine to coarse sandstone and carbonates. Thin sections were cut by the Department of Geology, University of Plymouth whilst other were cut by the Department of Geology of Tripoli (Oil Research Centre in Tripoli).

Optical mineralogy was carried out by studying the optical characteristics of the observed minerals. The minerals composition, grain-size, shape, sorting, texture and packing of the sandstone samples were analyzed. These parameters were used to classify the sandstone according to Pettijohn's classification (1987).

A point counter is a tool connected to a petrographic microscope and was used to determine the percentage of each component in the study sample. Information from them is incorporated into Chapter 4.

2.8.2 X-Ray Diffraction

This technique was used to further identify the type of clay minerals in the samples. X-Ray diffraction (XRD), which is another analytical tool used to complement thin-section petrography. XRD provides the most efficient tool for determination of clay minerals in mud rocks and sandstone (Tucker, 1988). This technique is based on the characteristic reflection of X-rays by crystal lattice planes within minerals. Each mineral has diagnostic X-ray pattern with known peak location and intensities.

Fine-grained samples from Abu Shaybah Formation were used in X-ray diffraction (XRD) to help determine their provenance. Therefore six samples of sandstone and clay

were selected to determine the type of minerals (Fig. 26). XRD can determine the type and approximate abundance of minerals in a powdered rock sample therefore six samples were powdered and tested and the results of the X-Ray analysis are discussed in Chapter 4 and figures are shown in Appendix 1.

2.9 Palaeomagnetic Methods

2.9.1 Introduction

The primary objective in any magnetostratigraphic study is to collect orientated samples as frequently as possible from as long a continuous section as possible. The Global Polarity Time Scale (see Figure. 2.4) resembles a barcode in that it is presented as a series of black (normal) and white (reverse) coded polarity intervals (Muttoni et al., 2000). Matching the studied section to this timescale essentially relies upon being able to recognise the variation in duration of each polarity interval both in the section and the timescale. Hence, the needs for detailed sampling over as long an interval as possible. However, given that sediments do not accumulate at constant rates in most sedimentary environments even this approach has limitations. A total of 234 oriented cores distributed over 9 sections have been collected during this study. Samples were collected from Kurrush, Al Aziza, Abu Shaybah and Abu Ghaylan Formations. The type sections of these formations lie between Wadi Abu Shaybah and Gharian it self (GR 312972 3562969).

2.9.2 Sample Collection

Field sampling for paleomagnetic analysis was carried out using a portable water-cooled drill to take 25 mm diameter cores, up to 100 mm long, from which 25 mm cylindrical specimens were subsequently cut. Sampling was accompanied by detailed sedimentary field logging of the section. As far as possible one core from each bed

observed in the field was collected, however in practice sample spacing was dictated by the robustness and suitability of the material to coring. The field localities are described in the relevant results Chapter.

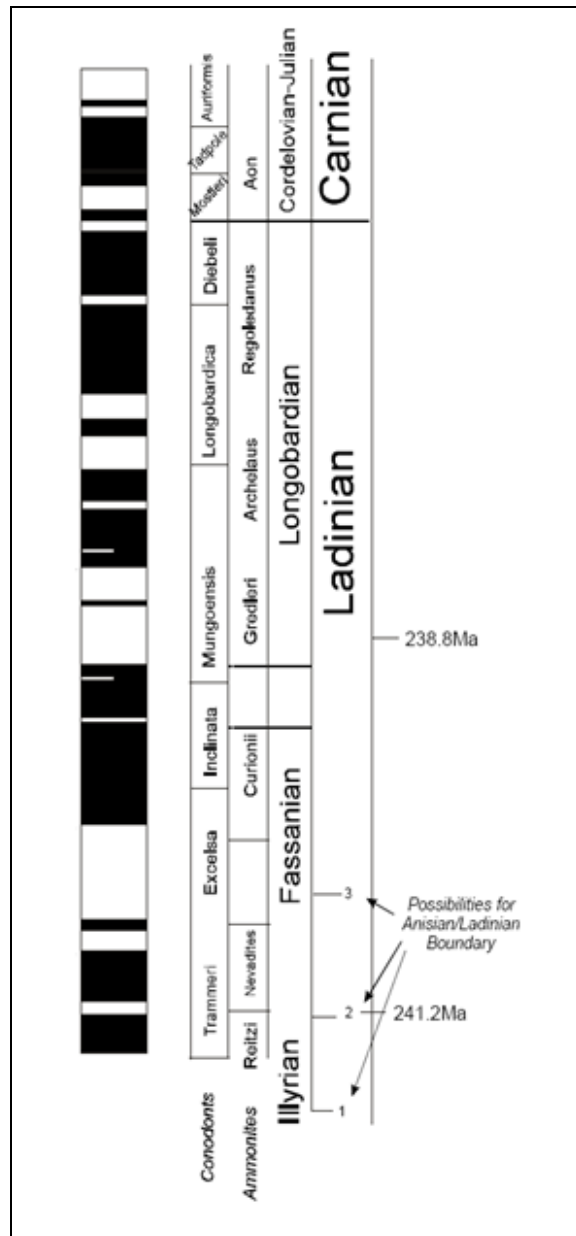


Figure 2.4 Middle to Late Triassic magnetic polarity time scale (from magnetostratigraphy). Normal polarity chrons are shown in black while reversed polarity are white (from Muttoni et al., 2000).

The sampling spacing for each section is shown in Chapter 6. On average the spacing was 0.5- 1 m in the Al Aziza Formation sections and 1- 2 m in the Abu Shaybah sections. The sampling in the Abu Shaybah sections is markedly worse than that of the Al Aziza as both the sandstones and mudstones often proved to be very friable.

Sample orientation utilised both sun and magnetic compass bearings using a specially designed ASC Scientific Sun Compass (Fig. 2.5). Thus, samples were oriented before being removed from the outcrop. The up-core orientation was marked on the samples and all samples were given descriptive code numbers. For example **AR1.1** corresponds to the Abu Shaybah Formation and **R** related to Abu Rashada Road section while **AZ1.1** corresponds to Al Aziza Formation and **Z1** related to the SE section in Wadi Abu Shaybah (see Tables in Appendix 3). Moreover, for each section or part of a section the dip and strike of bedding was measured (see Tables in Appendix 3). All field orientation data were recorded in the field and later sun sight data processed with the Palaeomagnetic tools (PMAG software). Sun sight data were found to be on average 3° clockwise of the magnetic data, which is slightly greater (c.f. 1.75°) than the theoretical declination variation for northern Libya as calculated using the national geophysical data Centre (NGDC) calculator (see Table 4.2 in the Appendix 3). Any data collected by magnetic compass alone (no sun visible at the time of collection) were corrected for this declination anomaly.

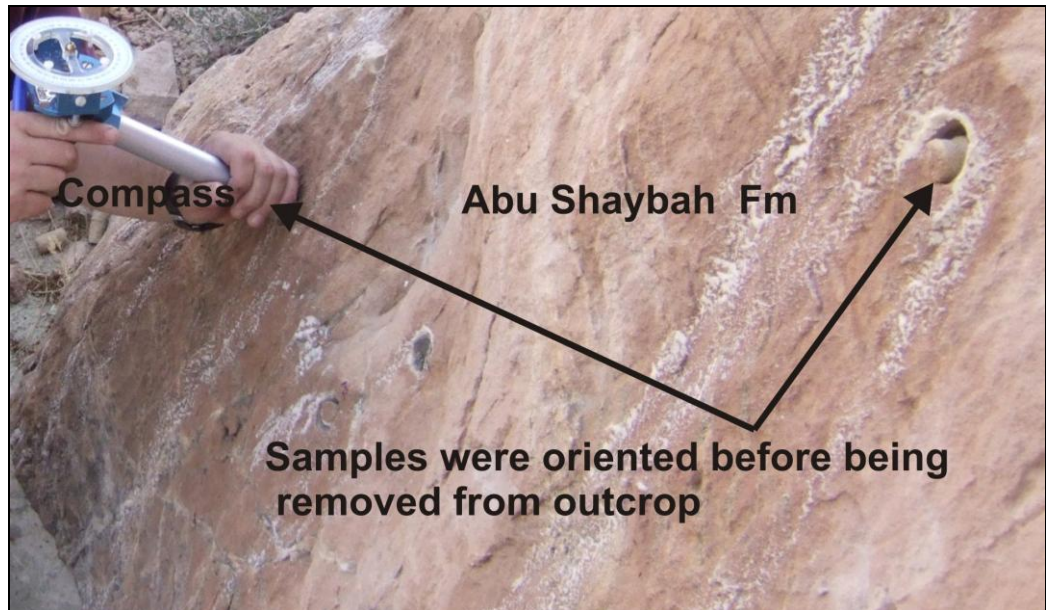


Figure 2.5: Collecting oriented paleomagnetic samples in the sandstone rocks of the Abu Shaybah Formation using orientation tool. This tool uses a magnetic compass, a sun compass, and an inclinometer to orient the samples.

2.9.3 Sample Preparation

The principal objective of palaeomagnetic laboratory procedures is to examine the stability of the magnetism of the rock. Therefore, the samples were returned for slicing into standard sized cylinders (2.5 x 2.2 cm) and then marked with a code number for each sample.

Chapter 3: Stratigraphic Framework

3.1 Introduction

Research examining the stratigraphy of the Gharian area has been subjected to numerous different hypotheses. So far, no comprehensive study of field data that would enable a regional analysis of stratigraphy of the Gharian area has been conducted. This is probably because oil exploration was the main incentive in the region (e.g. Dardour et al., 2004; Alikalefa, 2005; Gabtni et al., 2006; Abadi et al., 2008). The stratigraphic and lithologic characteristics of the Gharian area are considered in this chapter and Chapter 4 where they provide a palaeogeographic hypothesis to be formulated. This chapter begins with a brief overview of the stratigraphy of Libya while the second part of this chapter outlines the stratigraphy for the Early Mesozoic rocks of the Gharian area to provide a framework for sedimentological and structural studies throughout this thesis.

3.2 Stratigraphic Outline of Libya

i) Introduction

The Gharian area is bordered to north and south by a series of units composed of Mesozoic, Paleozoic and older basement (Fig. 3.1). Due to their importance in provenance studies within this study the following section provides a brief introduction to stratigraphy of the Libyan Platform.

ii) Brief Overview of the Stratigraphy of Libya

The stratigraphy of the Libyan Platform has been studied by many authors (Conant and Goudarzi, 1967; Desio, 1971; Klitzsch, 1970, 1971; El Hinnawy and Cheshitev, 1975; Goudarzi, 1980; Tawadros, 2001). Palaeozoic rocks cover a wide area across the North African Platform located between the Atlantic coast in the west, the Arabian Peninsula in the east, the late Precambrian Pan-African shield in the south and the Mediterranean coast in the north. Precambrian crystalline rocks are exposed in south-central Libya (Fig. 3.1), west of Jabel Eghi, Tibesti area, in the south-eastern part near the border with Sudan and Egypt, at Jabel Al Hasawinah north of Brak (Fig. 3.2), and north of Waw an Namus (Beagi and Perski, 1996; Carr, 2002).

The Palaeozoic outcrops in the North African Platform are restricted to the southern part of the platform in areas around the massifs of the Pan-African shield (Fig. 3.2). These areas include the Ghadamis, Al Kufra, and Murzuk Basins (Fig. 3.2). Deposition of the late Palaeozoic rocks was dominated by accumulation of clastic and carbonate facies of Hebila and Waitiah Formations.

During the Cambro-Ordovician, up to 1000 m of quartzite sandstone was deposited throughout northern Libya (Anketell, 1996). During the latest Early Devonian shales and sandstone rocks were deposited throughout North Africa. In addition, parts of western Libya and eastern Algeria were affected by significant periods of Middle and Late Devonian tectonic activity and erosion. However, the Late Silurian to Early Devonian in central North Africa (western Libya, eastern Algeria) is characterised by large scale uplift in the Murzuq Basin, Garagaf arches, and Ghadamis Basin (Lottaroli et al., 2009; Tawadros, 2006).

According to Haq et al., (1987) and Swire and Gashgesh 2004, during the Mesozoic the palaeogeography of North Africa can be divided into three facies belts, an open-marine

belt to north, a shallow marine carbonate belt in the middle and a continental belt to the south. These facies belts are exposed in Tunisia and in western Libya.

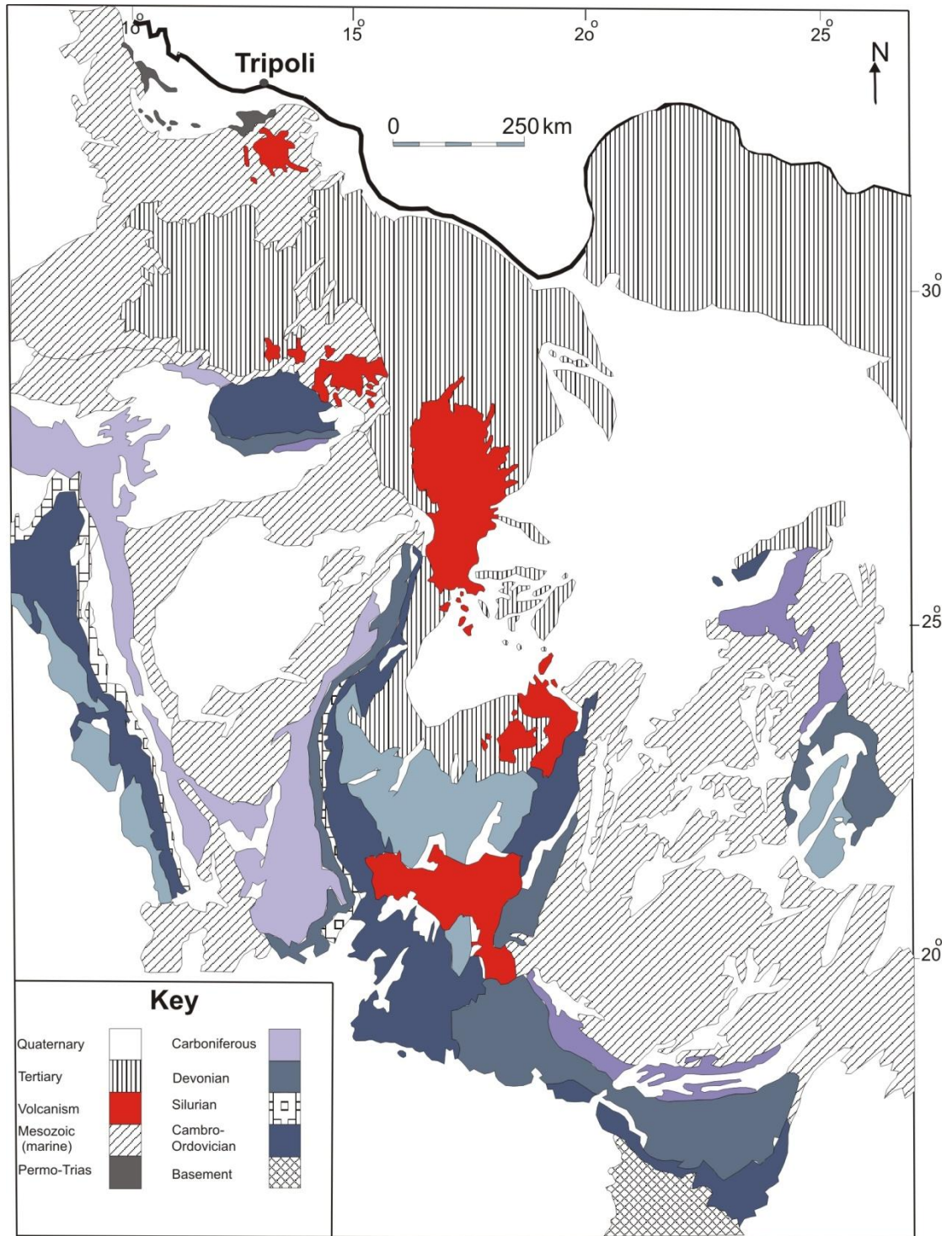


Figure 3.1 Simplified geological map of Libya (modified from Bellini and Massa, 1980).

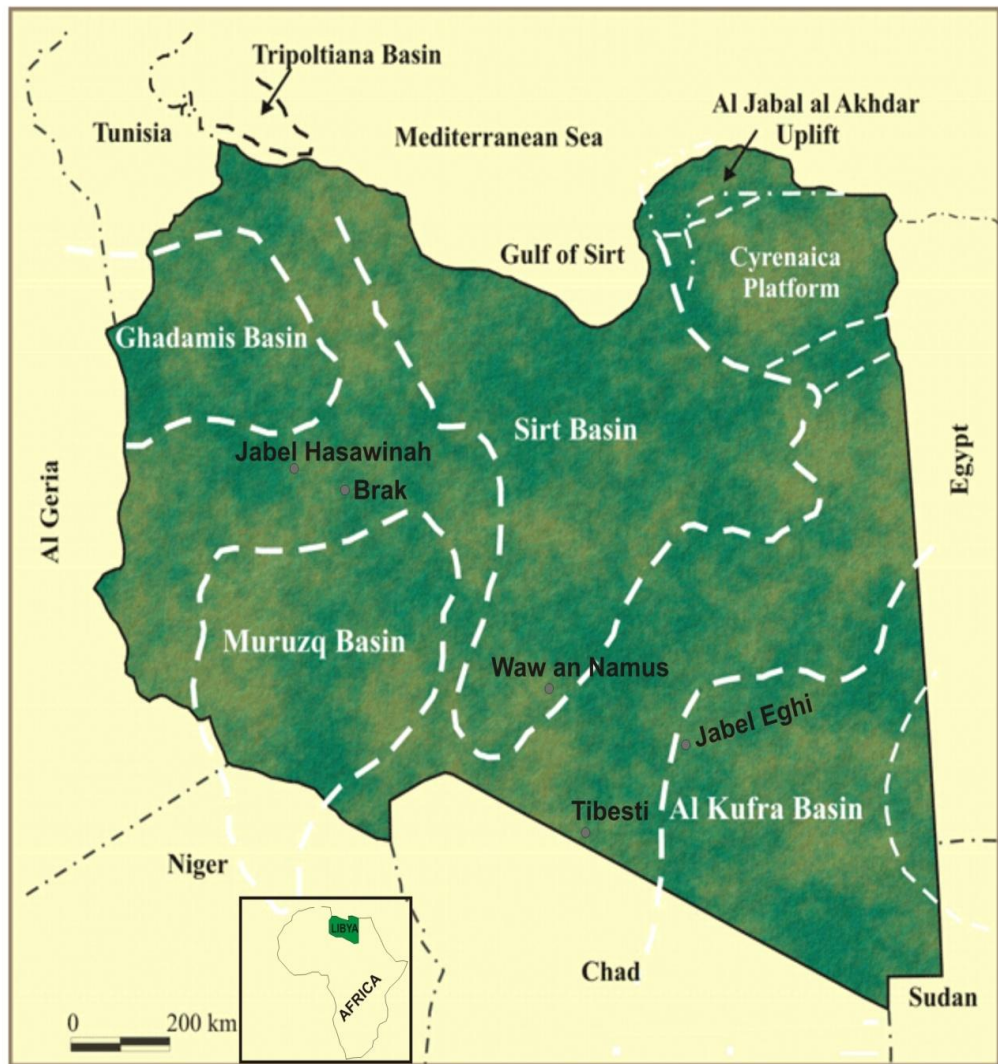


Figure 3.2 Map of Libya, showing the basins boundaries and names of places discussed in the text (Modified from Hassan, 2009).

3.3 Mesozoic Rocks of Northern Libya

Mesozoic strata outcrop in northern Libya and south-eastern Tunisia (Table 3.1) where an almost complete sequence from Triassic to Cretaceous is known, one of the few areas in the whole African continent. In northwest Libya, Mesozoic rocks are exposed along the Jabel Nafusah escarpment for a distance of some 400 km. They also occur in the subsurface of the Jafarah plains, the Gharian area and the northern Ghadamis Basin, extending westwards into Tunisia (Bishop, 1975). Furthermore, Early Cretaceous regional uplift along the north edge of the Africa platform is reflected in the deposition of a continental sequence of sandstones and pebble conglomerates in the Gharian area (Tawadros, 2001). Swire and Gashgash (2004) point out that deposition of the Mesozoic rocks has been influenced by extensional events in Jafarah basin in NW Libya, particularly during the Triassic and Jurassic.

During the Late Cretaceous most of NW Libya was covered by the Neotethys Ocean. At this time a carbonate platform existed in NW Libya. By the end of the Cretaceous the sequence was deformed into an anticline trending NW-SE. This movement was followed by faulting and doming accompanied by syntectonic magmatic activities, which are represented in the area by extrusive and intrusive volcanic rocks (Bausch, 1978; Farahat et al., 2006).

According to Guiraud (1998) volcanic activity resumed again in post-Eocene times, situated outside the zone of Cretaceous rifting on the western side of the Sirt Basin. These volcanics are believed to have been emplaced concurrent with movement along deep seated fractures (major basement fault zones) possibly related to the Alpine Orogeny (Goudarzi, 1980).

| PERIOD/STAGE | | NW LIBYA | | LIBYA CONTINENTAL Equivalents | | | TUNISIA | | |
|--------------|---------------|-------------|----------|---------------------------------------|------------|-------------------------------------|-------------------------------|---------------------|-------------|
| CRETACEOUS | ALBIAN | KLAH | | CONTINENTAL INTERCALAIRE = MESSAK | NUBIAN | DJOUA | L.FAHDENE | | |
| | APTIAN | | | | | | GAFSA | SERJ | SIDI KHALIF |
| | BARREMIAN | | | | | | BOUDINAR | | |
| | HAUTERIVIAN | KABAW | | | | | ASFER | | |
| | VALANGINIAN | SHAKSUK | | | | | FOUM TATAHOUINE TECHOUT | | |
| | BERRIASIAN | | | | | | ARACHAOUA | | |
| TITHONIAN | MESTAOUA | | | | | | | | |
| JURASSIC | KIMMERIDGIAN | SHAKSUK | | CONTINENTAL POST TASSILIEN = TILÉMSIN | TAOURATINE | ZMILET HABER | | | |
| | OXFORDIAN | | | | | KHASHM AS AZRZUR TAKBAL | | LOWER EVAPORITES | |
| | CALLOVIAN | | | | | BIR AL GHANAM | ABREGHS | | |
| | BATHONIAN | | | | | | BU EN NIRAN | | |
| | BAJOCIAN | | | | | | | | |
| | AALENIAN | ABU SHAYBAH | | | | JABAL REHACH | | | |
| | TOARCIAN | AL AZIZA | | | | | | | |
| | PLIENSBACHIAN | | | | | | | | |
| | SINEMURIAN | KURRUSH | | | | ZARZAITINE | | KIRCHAOU | |
| | HETTANGIAN | | | | | | | AL GUIDR | |
| | TRIASSIC | RHAETIAN | AL AZIZA | | | ZARZAITINE | | JABAL REHACH | |
| NORIAN | | | | | | | | | |
| CARNIAN | | | | | | | | | |
| LADINIAN | | KURRUSH | | ZARZAITINE | | | | KIRCHAOU | |
| ANISIAN | | | | | | | | AL GUIDR | |
| SCYTHIAN | | KURRUSH | | ZARZAITINE | | | | KIRCHAOU | |
| | AL GUIDR | | | | | UNNAMED CONTINENTAL SANDSTONE | | | |

Table 3.1 Lithostratigraphic nomenclatures for Mesozoic rocks of Libya and adjacent areas (source Hallett, 2002).

The northern edge of the Jafarah Basin in NW Libya was subjected to marine, and shallow marine sedimentation in the Miocene, characterised by siltstones interbedded with sandstone, gypsum, limestone and dolomite. The Jafarah Basin acted as a continental basin receiving gravels and sandy silt, eroded from the uplifted escarpment region and southern interior (Swire and Gashges, 2004).

3.4 Geological Setting of the Gharian Area

3.4.1 Introduction

This section is concerned with the general stratigraphic succession of the Gharian area (Fig. 3.3), as part of geologic history of NW Libya. Most of the information has been obtained from Stratigraphic Lexicon of Libya by the Industrial Research Centre (IRC) Tripoli, the Petroleum Geology of Libya and by field mapping.

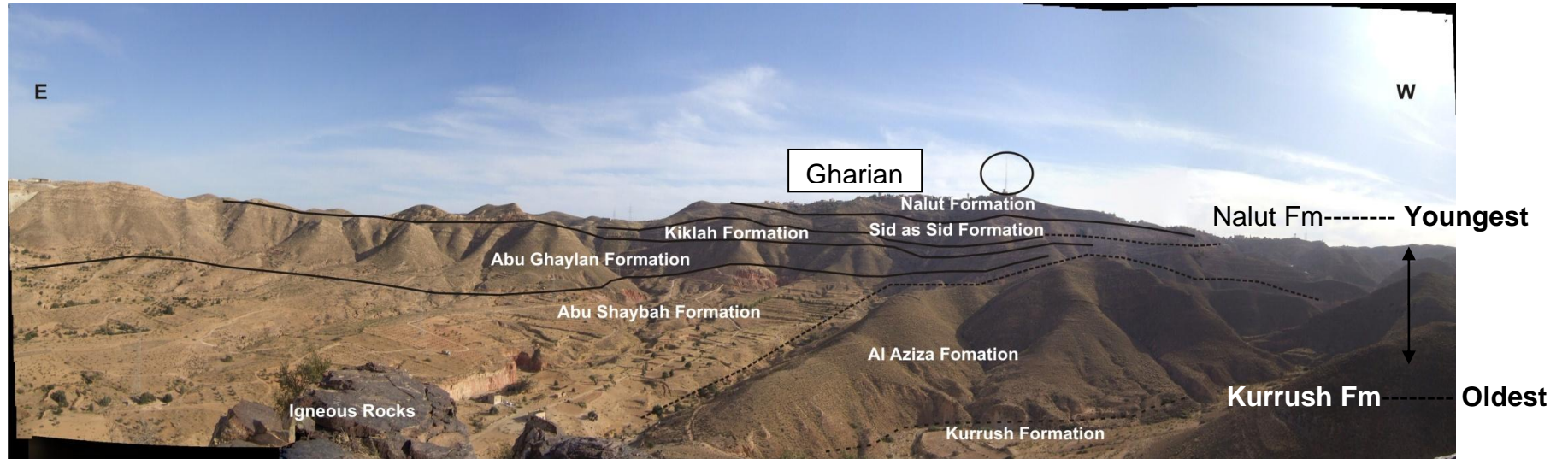


Figure 3.3 Photograph showing a general view of the Gharian area within formations names and igneous rocks are exposed in the central of the area. Telecommunication mast for scale circled at the top.

3.4.2 Stratigraphic Succession of the Gharian Area

Early geological mapping of NW Libya was undertaken by Parona, (1914); Desio et al., (1963); Christie (1966); Desio (1971); El Hinnawy and Cheshitev (1975); Banerjee (1980); Hammuda et al., (1985) who collectively worked on stratigraphic studies in the Jabel Nafusah.

In 1975, the Industrial Research Centre (IRC) of Libya set about the task of systematically mapping the whole of northern and western Libya at scale of 1:250,000. One of these maps covers the Gharian area (Map reference NI 33-13 R; Tarabulus, 1975).

The Triassic-Early Cretaceous succession in the Gharian area consists of the Middle Triassic Kurrush Formation, and Late Triassic Al Aziza, Abu Shaybah, Abu Ghaylan and Kiklah Formations, followed by the Late Cretaceous Sidi as Sid, Nalut and Qasr Tigrinnah Formations (Fig. 3.4). This sequence is considered to be exposed as a result of the Aziza Fault Zone (Miocene age) and then later by the doming of these sediments by the intrusion of phonolitic and trachytic type magma during the Tertiary (Gray, 1971).

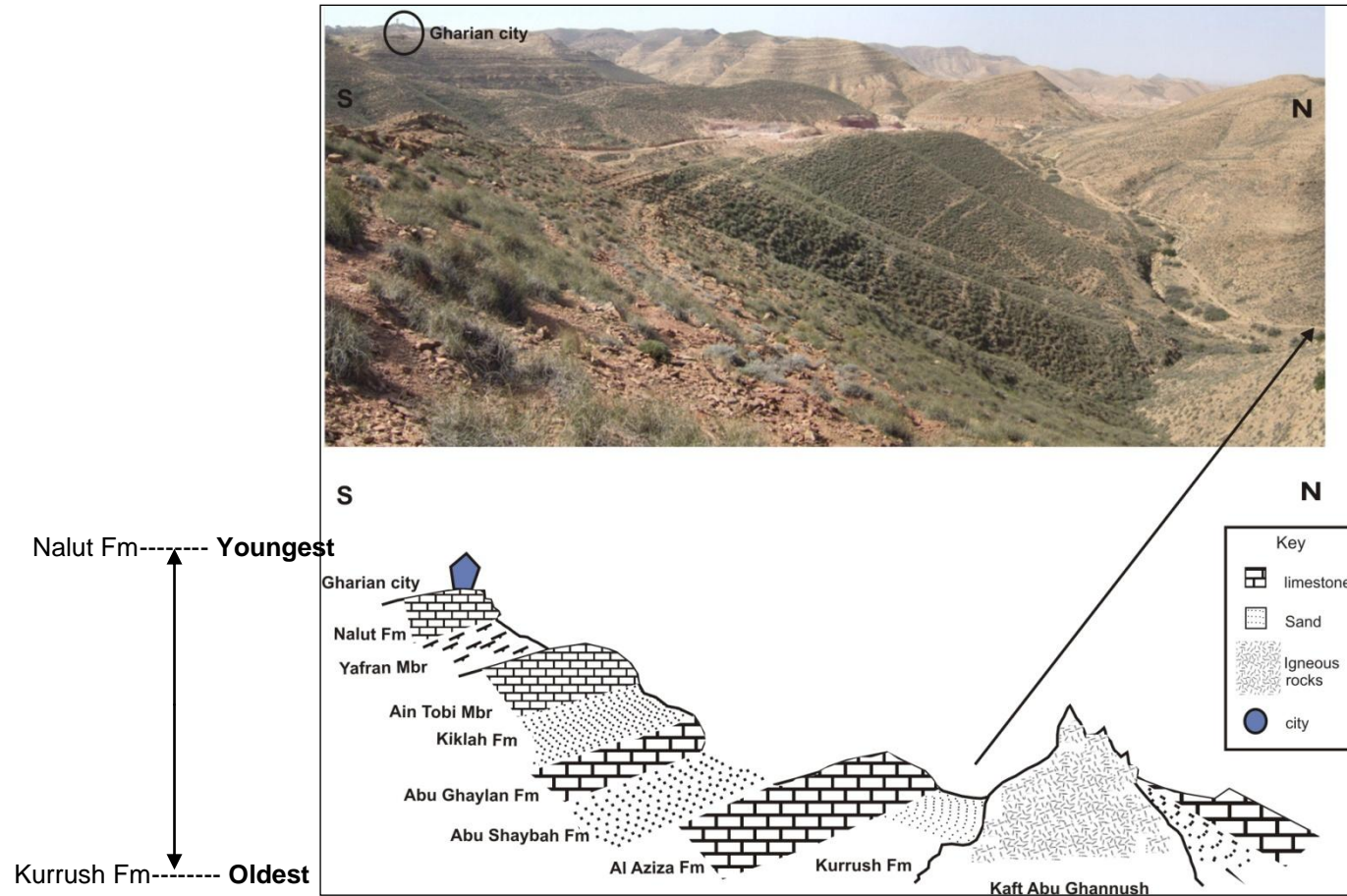


Figure 3.4 Photograph and sketch cross section through the Gharian area: From bottom to top: Kaft Abu Ghannush Tertiary phonolite, Kurrush Formation at the centre of the dome and Wadi Abu Shaybah running throughout, Al Aziza Formation overlain by the Abu Shaybah Formation, followed by the Abu Ghaylan, Kiklah, Sidi as Sid (Ain Tobi and Yarfran Mbrs), and Nalut Formations.

3.4.3 Proposed New Stratigraphic Nomenclature

During the early 1960s two schools (Italian and French) of thought studied the Mesozoic stratigraphy of the Gharian area. This resulted in controversies on the nomenclature and placement placing of geological boundaries creating some confusion in literature. Therefore, in order to avoid confusion in this study a new scheme will be used derived from the transliteration and combination of the Italian and French schools of thought (Table 3.2). The new stratigraphy will be formally defined using ISC (International Stratigraphic Commission) guide lines.

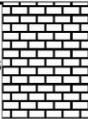
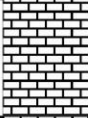
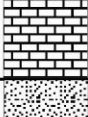
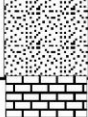

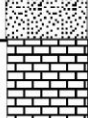
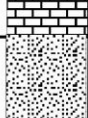

| Authors | Formation | Age | Lithology | This study |
|--|------------------------------------|---------------------------------|--|--------------------------|
| Christe (1966) Desio et al (1963) | Gasr Tigrinna | Cenomanian | Carbonates  | Qasr Tigrinnah Formation |
| Christie (1966) Desio (1963) | Garian Nalut | Cenomanian | Carbonates  | Nalut Formation |
| Christie (1966) | Sid al sidi | Late Cretaceous | Carbonates  | Sidi as sid Formation |
| Christie (1960) Desio et al (1963) | Chicla Kiklah | Early Cretaceous | Sandstone  | Kiklah Formation |
| Desio et al (1963) Christie (1966) | Abu Gheilan Abu Ghylian | Late Triassic to Jurassic | Carbonates  | Abu Ghaylan Formation |
| Christie (1955) Christie (1966) Desio et al (1963) | Bu Sceba Abu Shybah | Late Triassic | Sandstone  | Abu Shaybah Formation |
| Parona (1914) Desio et al (1963) | Al Azizyah Aziza Azizah | Middle Triassic | Carbonates  | Al Aziza Formation |
| Desio (1963) Christie (1966) Magnier et al (1963) | Ras Hamia Currusc Boutoniere | Lower Triassic | Sandstone  | Kurrush Formation |

Table 3.2 Proposed stratigraphic nomenclatures of Mesozoic rocks of the Gharian area derived from transliteration and combination of the Italian and French schools of thought.

3.5 Mesozoic Succession of the Gharian Area

An almost complete Triassic succession is present in the Gharian region of the Jabel Nafusah. Stratigraphic units include the Kurrush, Al Aziza and the Abu Shaybah Formations (Fig. 3.5). The age of the latter may be as old as late Triassic. Macrofossils that are typically used for biostratigraphical age control purposes are lacking from these formations in the study area and the Jabel Nafusah region in general. Swire and Gashgesh (2000) also proposed that biostratigraphical control of the age of these formations in the Jafarah plain is limited because both fossil abundances and diversities are very low. Thus, it is important to determine the age of the formations by using magnetostratigraphy as outlined in Chapter 6.

3.5.1 Kurrush Formation

Name and type location: Previously known as Ras Hamia Formation and was first named by Christie (1966). The formation has also been referred previously to as the Ras Boutoniere and Currusc Formation (e.g. Desio et al., 1960; Magnier et al., 1963; Hammuda et al., 1985). The formation is exposed in only four places in the Jabel Nafusah region and all exposures are at, or near, the centres of small domes. Two exposures are just to the north of Gharian town and two are just to the east of Wadi Ghan (Tawadros, 2001). However, little attention was given to sedimentological detail of the mapped lithostratigraphic units in the Gharian area. The Kurrush Formation is also correlative, in part to the Kirchaou Formation of southern Tunisia (Busson, 1967) which is transitional from marine clastics to marine carbonates. The spelling of Kurrush Formation was changed by the Industrial Research Centre (IRC) for use on the new 1:250,000 geological maps (El Hinnaway and Cheshitev, 1975).

Lithology and variation: The Kurrush Formation is represented by green and red, sandy shales with sandstone intercalations, and occasional dolomitic limestones. In southern Tunisia it is represented by silts, red shale and sandstones which show different types of cross-bedding (Dridi, 1998).

Lower and upper boundaries: The lower contact is not exposed in the Gharian area (Banerjee, 1980). The upper contact with the Al Aziza Formation is transitional from marine clastic to marine carbonates.

Thickness and lateral extent: The formation is restricted in extent, as it is only exposed on two hill bottom of anticline and just to south of Gharian town. The maximum thickness of the formation in the Jabel Nafusah is 34 m (Desio et al., 1963).

Dating evidence: The age of this formation in the Jafarah basin is Middle Triassic (Anisian- Fassanian). It is based on the highest occurrences of the miospore taxa *Cristianisporites triangulates*, *Stellapollenites thirgtii* and Polysacoid pollen (Swire and Gashgesh, 2000). The Myophoria have been reported from Kurrush Formation surface exposures (Hammuda et al., 1985). However, there seems to be disagreement that the Kurrush Formation at its surface exposures is of Middle Triassic age, this is because no one has recorded any fossils in the Gharian area (Hammuda et al., 1985).

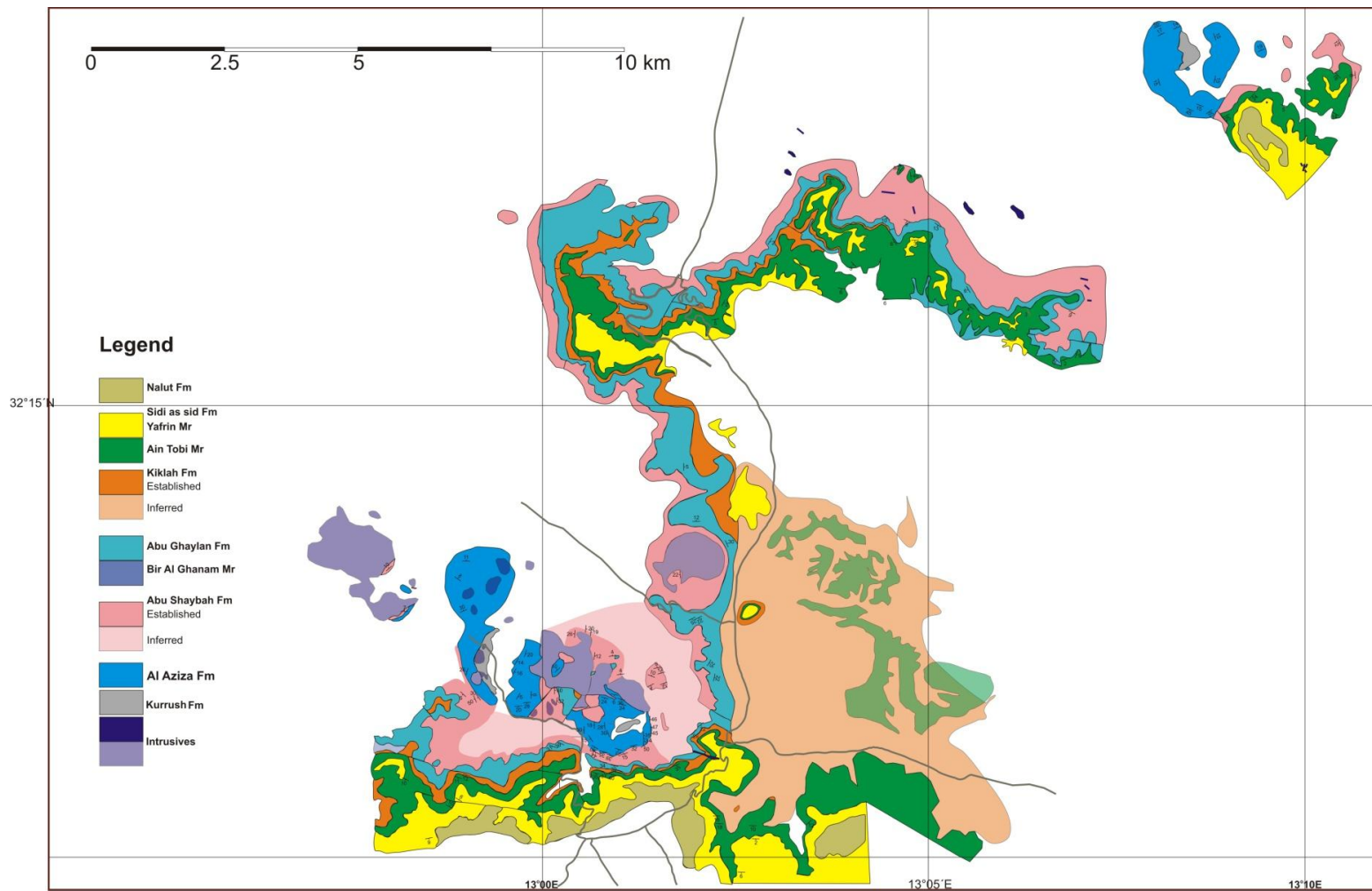


Figure 3.5 Geological map of the Gharian area, formation names on the map are referred to in the text (modified from Gray, 1971 supplemented by recent mapping and extended by interpretation of Google Earth).

3.5.2 Al Aziza Formation

Name and type location: The formation was initially studied by Parona (1914), who identified the outcrop of carbonate rocks in Al Aziza village in NW Libya. Christie, (1966) regarded this outcrop as the type section of the formation, naming it the Al Aziza Formation.

Lithology and variation: The formation consists of dark grey dolomite and dolomitic limestone with interbedded clay and chert (Assereto and Benelli, 1971).

Lower and upper boundaries: The lower boundary contact with Kurrush Formation is conformable whilst the upper an erosive contact with overlying the Abu Shaybah Formation is unconformable (Hammuda et al., 1985).

Thickness and lateral extent: The thickness of Al Aziza Formation varies from about 60 m in the south to 650 m in northward near the Mediterranean coast line (Hammuda et al., 1985). The outcrops of the Al Aziza Formation in the Gharian area are offset by fault systems that complicate the problem of quantifying accurate thickness.

Dating evidence: A middle Triassic age has been proposed based upon on two palynological samples that were collected from the Jafrah Basin (Muttoni et al., 2001).

3.5.3 Abu Shaybah Formation

Name and type locality: Christie (1966) first described the Abu Shaybah Formation. The type section was located in the Wadi Abu Shaybah in the Gharian area (Fig. 3.6).

Lithology and Variation: The formation consists of sandstone, siltstone and mudstone. The formation can be divided into two parts; the lower part of the formation consists of red siltstone with carbonate cement and sandy dolomites and the upper part consists mainly of poorly cemented white or rose-coloured sandstone alternating with clay and siltstone (e.g. Asserto and Benelli, 1971; Fatmi et al., 1978; Banerjerr, 1980).

Lower and upper boundaries: the lower boundary is sharp and unconformable with Al Aziza Formation whilst the upper is also unconformable with Abu Ghaylan Formation. Furthermore the upper unconformable boundary is specially visible along Jabel Nafusah scarp between Wadi Ghan and Ar Rabita (El Hinnawy and Chechitev, 1975; Banerjee, 1980).

Thicknes and lateral extent: The formation is confined in distribution to the central and east of Jabel Nafusah region. Moreover, the Abu Shaybah was reported in the subsurface from water well near Bir al Ghanam (Christie, 1966). This formation has a thickness of 110 m (Hammud et al., 1985).

Dating evidence: None. However, Burollet (1960) and Hecht et al., (1964) assigned this formation to the Late Triassic. Desio et al., (1960) assigned this formation to Norian (Late Triassic) and El Hinnaway and Chesitev, 1975) assigned to the Carnian. Christie (1955) and Desio et al., (1963) alternatively assigned the formation to Late and Early Jurassic, respectively. Thus, age of the Abu Shaybah Formation is based upon the

relative stratigraphic position of the Abu Ghaylan above and Al Aziza Formations below.

3.5.4 Abu Ghaylan Formation

Name and location: The Abu Ghaylan Formation was originally proposed by Christie (1955), who introduced (Bu Ghaylan Limestone) as a stratigraphic term, named after the village of Abu Ghaylan at 23° 16'N:13° 02' E. Subsequent revisions of the stratigraphy have been outlined by Desio (1963); and El Hinnawy and Heshitev (1975). The Abu Ghaylan Formation is limited to the Jabel Nafusah escarpment in the Gharian area from Ar Rabitah village to Wadi Ghan.

Lithology: The Abu Ghaylan Formation consists of white to light brown limestone and dolomitic limestone.

Lower and upper boundaries: The formation conformably overlies the Abu Shaybah Formation and is unconformably overlain by the Kiklah Sandstone.

Thickness: The total thickness of the formation is variously given as 55 m by Christie (1966) and Asserto and Benelli (1971).

Dating evidence: No diagnostic fossils have been reported except for some small poorly preserved bivalves. Its relative stratigraphic position suggests an Early Jurassic age (Desio, 1971).

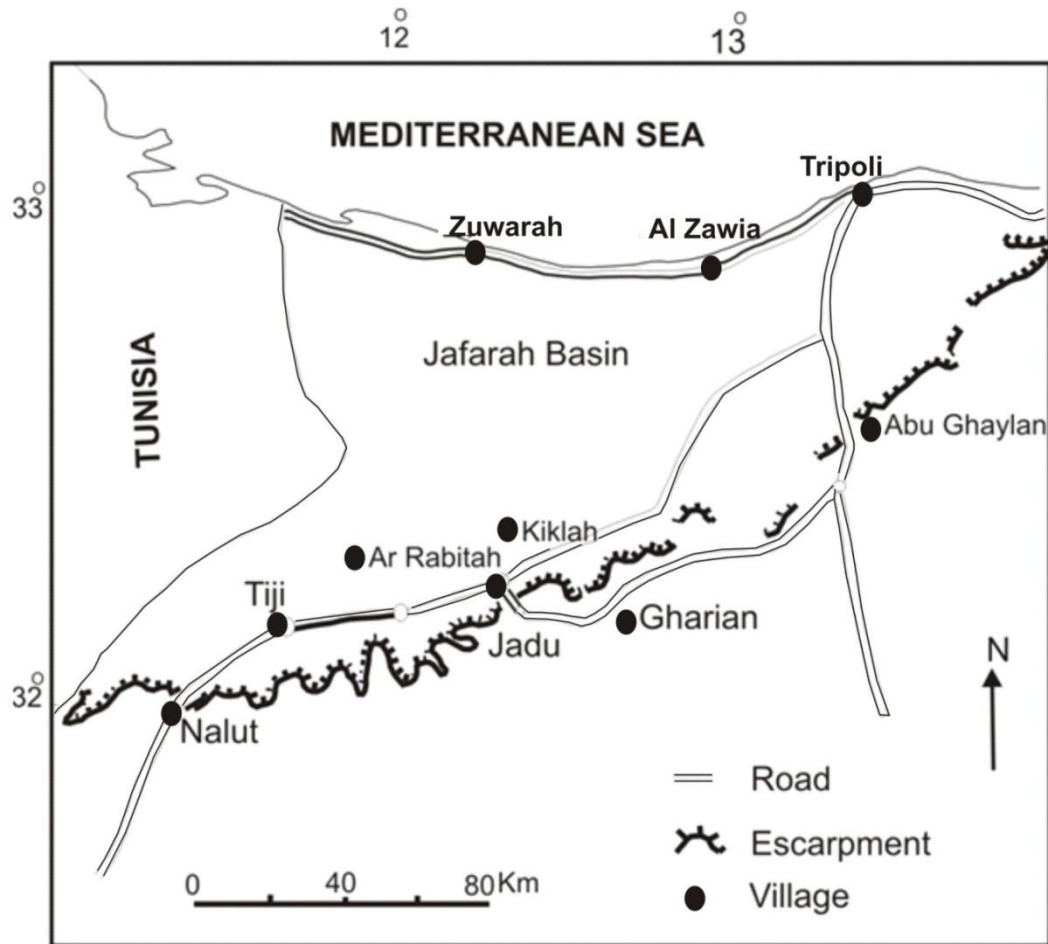


Figure 3.6 Map showing the location of Jabal Nafusah escarpment, names and village referred to within the text.

3.5.5 Kiklah Formation

Name and location: The Kiklah Formation is named after the Kiklah village (Christie, 1966). The Kiklah Formation has a wide regional distribution from the Tunisian border to Rus at Tahuna village in the east approximately 3 km west of Abu Ghaylan (Fig. 3.6).

Lithology and Variation: The formation is divided into Ar Rajban, Shaksuk and Khashm az Zarzur members. The Ar Rajban member consists of red and yellow-grey, medium to coarse grained, cross-bedded sandstone interbedded with pebble conglomerate (Banerjerr, 1980; Bodin et al., 2010). The Shaksuk Member is dominantly

composed of fine *clastics* with sandstone. The Khashm as consists of clays with minor sandstone interbeds.

Lower and upper boundaries: The upper contact with the Sidi as Sid Formation is unconformable and the lower boundary of the Kiklah Formation is unconformable with Abu Ghaylan Formation.

Thickness: The thickness of the formation in Gharian area is 10-60 m (El-Zouki, 1980).

Dating evidence: From paleontological evidence and stratigraphical position El Hinnawy and Heshitev, (1975) determined the age as between the Bathonian and Oxfordian-Kimmeridgian. Novovic (1977b) reported spores and pollen from the upper part of the Kiklah Fm dating formation to the Late Bathonian-Callovian.

3.5.6 Sidi as Sid Formation

Name and location: The formation is named after the Sidi as Sid village (Ar Rabitah) (Fig. 3.6). The major outcrops of the Sidi as Sid Formation are located in the Gharian area (Desio, 1963).

Lithology and Variation: The formation was divided into two members: the Ain Tobi Member and the Yafrin Member (Christie, 1966; Hallett, 2002). The Ain Tobi Member consists of grey to white limestones and dolomite whilst the Yafrin Member consists of gypsum.

Lower and upper boundaries: The lower contact is unconformable with Early Cretaceous Kiklah Formation. The upper contact of the Sadi as Sid Formation with the Nalut Formation is conformable (Fatmi et al., 1980; Banerjee, 1988).

Thickness: The type section for Ain Tobi is located on the Tripoli to Gharian highway, with an exposed thickness of 80-170 m.

Dating evidence: The age of the Sidi as Sid Formation was assigned as the Late Cretaceous- Cenomanian on the basis of lithostratigraphic position and fossil evidence (*Hedbergella sp.* and *Globo truncana sp.*) (Christie, 1966; Desio et al., 1963; Banerjee, 1988).

3.5.7 Nalut Formation

Name and location: The formation is named after Nault village (Fig. 3.6) and the term Nalut Formation was introduced by El-Hinnawy and Cheshitev (1975). The formation is widely distributed along the Jabel Nafusah from the town of Misrath to the Tunisian border.

Lithology: The Nalut Formation consists of grey crystalline dolomitic limestone with chert bands.

Lower and upper boundaries: The upper contact with the Qasr Tigrinnah Formation and the lower contact with Sidi as Sid Formation are conformable.

Thickness: The thickness in the Gharian area is about 50 m, decreasing westwards to about 30-40 m in the Nalut area.

Age: Desio et al., (1963) reported forminifera and he assigned a Cenomanian age. A more recent study (Novovic, 1997) found two macrofossils *Gryphostrea cf. canaliculata* Soweby and *Cardium cf. productum* Sowerby; and one micro-fossils

Psudorhapydionina dubia De Casto which is known from the shallow water Cenomanian-Turonian deposits of Italy.

3.5.8 Qasr Tigrinnah Formation

Name and Location: The formation is named after the Berber fort of Qasr Tigrinnah. The Qasr Tigrinnah Formation extends over a wide area from Soffegin to the Tunisian border (Desio et al., 1963) (Fig. 3.6).

Lithology: The formation consists of soft marls with red, pink, and yellow bands of limestone, and white, chalky limestone at the top.

Lower and upper boundaries: The Qasr Tigrinnah Formation conformably overlies the Nalut Formation and underlies the Mizdah Formation.

Thickness: The thickness of the formation is 87 m.

Age: Desio (1963) reported gastropods, bivalves and echinoids from upper unit of Qasr Tigrinnah to which he assigned a Cenomanian age.

Chapter 4: Early Mesozoic Sedimentary Processes and Environments

4.1 Introduction

This chapter examines patterns of continental and marine sedimentation within the Gharian area. These Early Mesozoic sedimentation phases are examined in order to provide insights into palaeoenvironmental and palaeogeographic variability for the study area, which has been considered as part of northern Gondwana in the Palaeozoic and as part of the southern Tethyan basin in the Mesozoic (Boot et al., 1998; Swire and Gashghesh, 2004; Makhoul, 2006). Sedimentary successions are considered in ascending stratigraphic order from the Kurrush Formation, Al Aziza Formation through to the Abu Shaybah Formation.

The continental and marine depositional environments of the Mesozoic formations have been established using qualitative and semi-quantitative sedimentary and related data. These data were collected from key localities in the Gharian area in order to illustrate the depositional characteristics and their relative spatial and temporal variations within the stratigraphic units. This allows for palaeogeographic models to be constructed for the study area and discussion in terms of environmental driving mechanisms (e.g. tectonics, climate etc.).

4.2 Kurrush Formation

4.2.1 Introduction

The Kurrush Formation is the oldest formation in the Gharian area. The term Kurrush Formation was first applied by Christie (1966) based upon exposures in the Gharian area and the Ras al Mazul Dome region (Fig. 4.1). The Kurrush Formation is considered to be correlative in part to the Kirkauo Formation of southern Tunisia (Busson, 1967).

The surface exposures of the Kurrush Formation are quite limited in Libya. Within the Gharian area, exposures of the Kurrush Formation reveal red and brown, fine grain sandstones with yellow and green clay beds. However, much of the stratigraphic and sedimentological information about the Kurrush Formation comes from subsurface oil well data sets (e.g. Hammuda et al., 1985: Fig. 4.2). Well A1-38 has been designated as a reference section for the subsurface area in the north of Libya (Hammuda et al., 1985). The lower contact of the Kurrush Formation with underlying the Al Guidr Formation occurs only in the subsurface in well A1-38 (Fig. 4.2). The Kurrush Formation in A1-38 consists of 581 m of sandstone with textures from fine to coarse-grained, grey and varicoloured shales along with subordinate dolomities (Hammuda et al., 1985). The base of the formation in well A1-38 consists of grey to brownish grey shales with interbedded white to grey occasionally dolomitic limestones. These are known as ‘Myophoria beds’ due to the presence of the Triassic bivalve *Myophoria* (Fig. 4.2) (Hammuda et al., 1985).

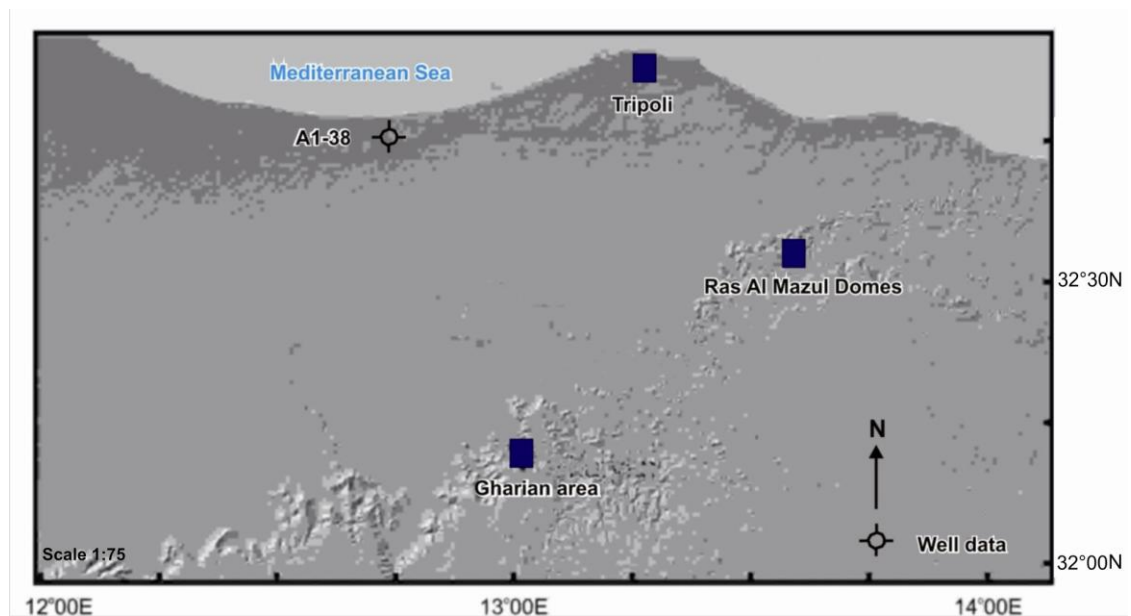


Figure 4.1 DEM map showing 1) the location of the Gharian area and the Ras Mazul dome region and 2) the subsurface A1-38 oil well location for the Kurrush Formation.

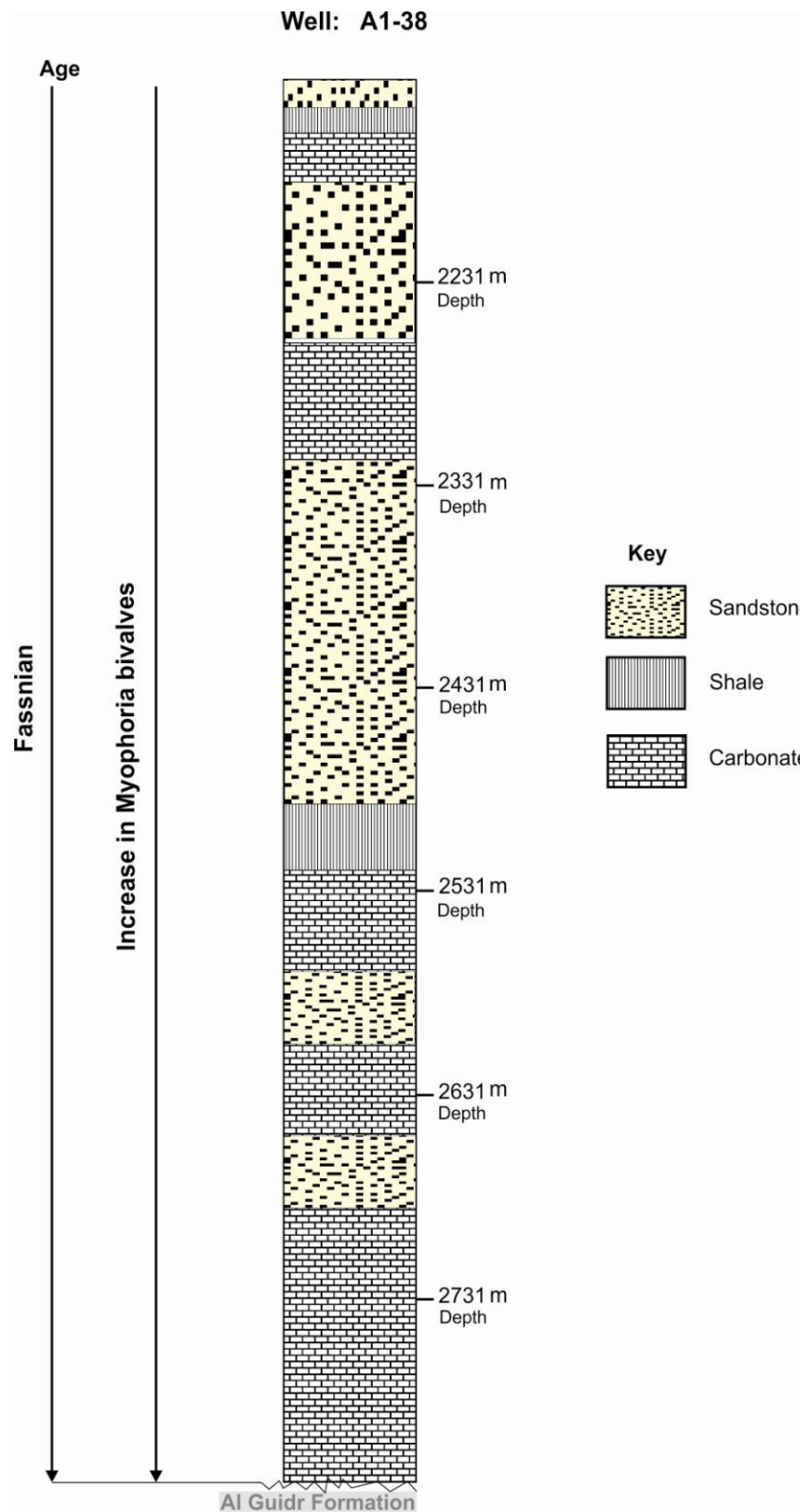


Figure 4.2 Simplified sedimentary log from well A1-38 showing the sub-surface lithologies of the Kurrush Formation and contact of the basal *Myophoria* carbonate beds with the underlying Al Guidr Formation (modified from Hammuda et al., 1985).

4.2.2 Sedimentary characteristics of the Kurrush Formation

The field investigations of the Kurrush Formation reveal that the deposits are composed of sandstone, siltstone and claystone. An incomplete section of the Kurrush Formation was logged and described from the Wadi Abu Shaybah area (Fig. 4.3). The Kurrush Formation is also exposed to the north in the Jafarah plain at the Ras Lefa section. This section was also analysed as it clearly shows the contact between the Al Aziza and Kurrush Formations. It also provides an opportunity to compare facies and environments between basin margin and more basinal settings.

For the purpose of this study, the Kurrush Formation is not described using a full facies analysis approach as adopted later in this chapter. This is due to poor exposure, lack of clear stratigraphic bounding contacts and limited section thickness. The limited exposure means a full environmental interpretation is challenging and therefore depositional environments are only tentatively assigned. The main techniques employed for analysis of the Kurrush Formation are field stratigraphy, field description and petrographic analysis.

1. Field stratigraphy

In the Gharian area exposures of the lower contact of the Kurrush Formation are not observed. Only the upper contact between the Kurrush and the overlying Al Aziza Formation is visible. This contact appears to be gradational and conformable (Fig. 4.4). Small outcrops occur on the east and west side of the Wadi Abu Shaybah and west of the Abu Rashada road (Fig. 4.3).

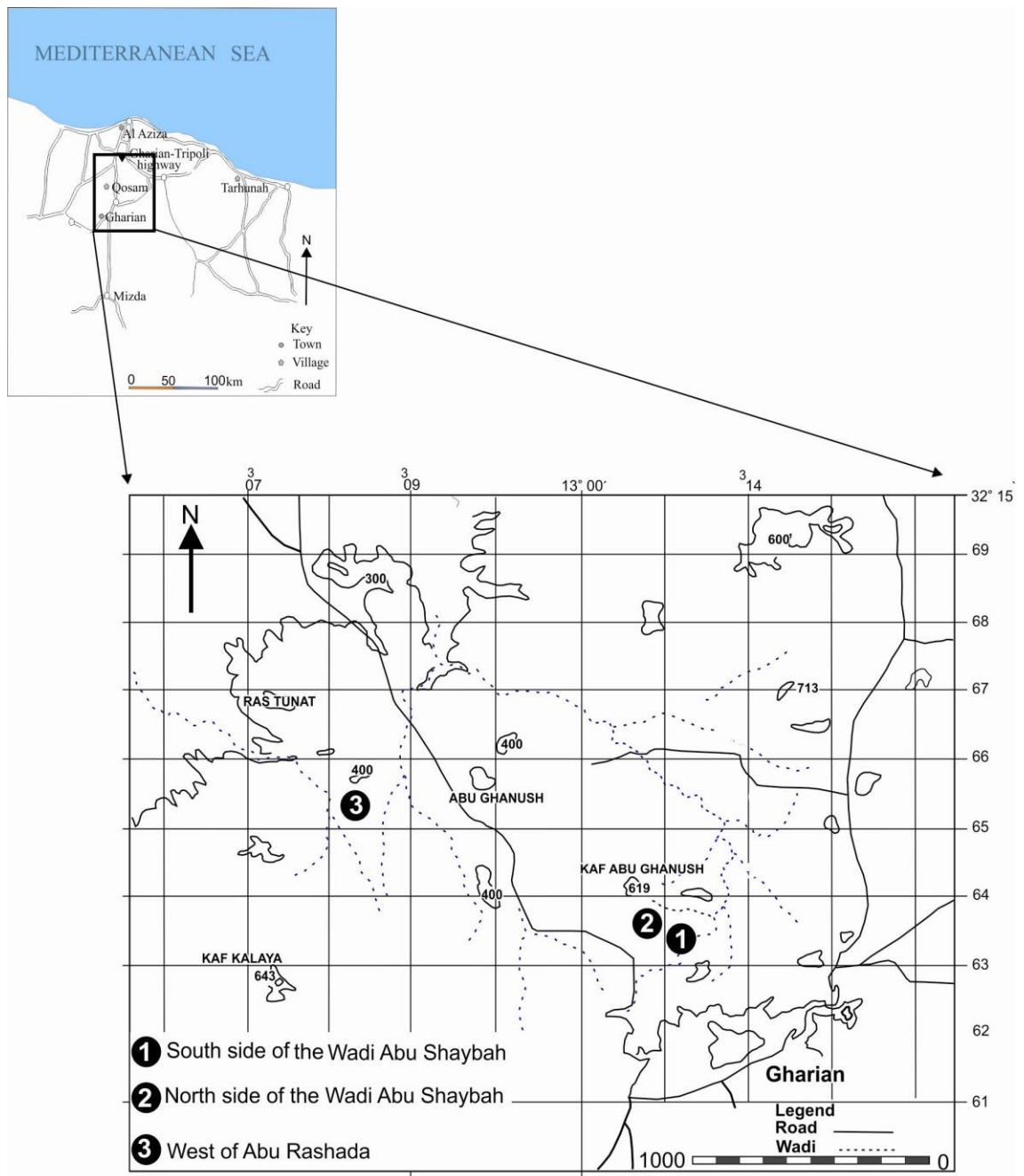


Figure 4.3 Map showing the outcrop of facies the Kurrush Formation. Numbers indicate position of locations discussed in the text.

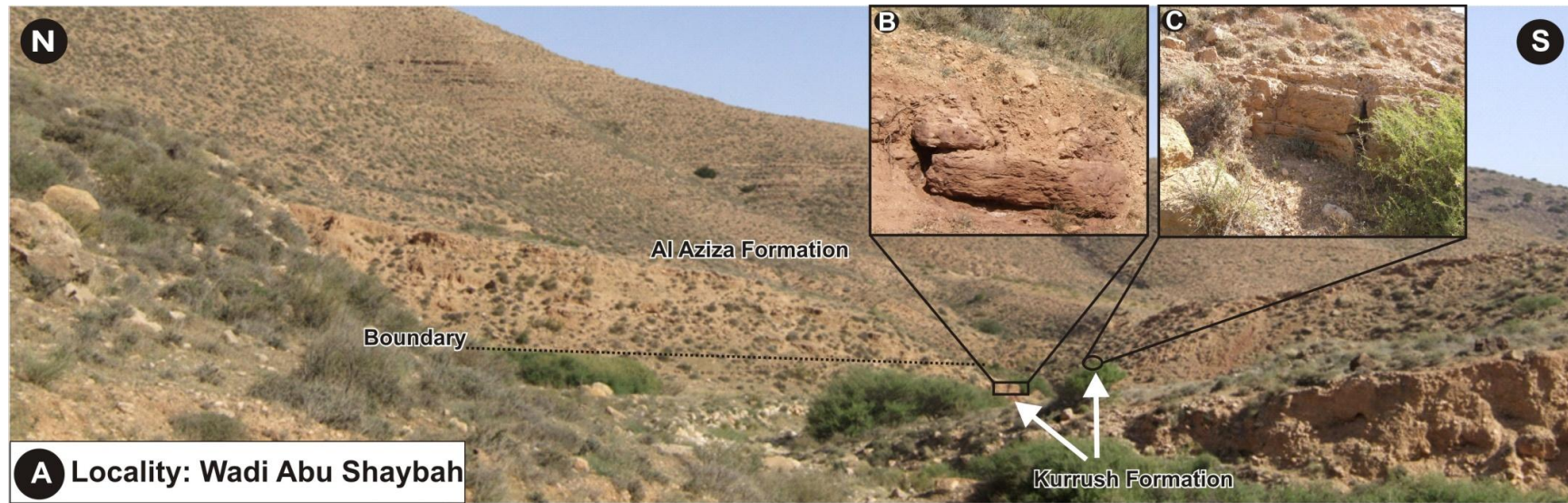


Figure 4.4 A: Field imagery of Wadi Abu Shaybah showing the dominant Al Aziza Formation overlying a small exposure of Kurrush Formation (white arrows) in the base of the valley. **B:** North side of the Wadi Abu Shaybah showing reddish micaceous sandstone facies (F-SR). The measured thickness of reddish micaceous sandstone facies is ca. 1.10 m. **C:** South side showing the Kurrush Formation with the overlying Al Aziza Formation. The measured thickness of south side is < 1 m.

2. Field description of the Kurrush Formation

Exposures from three localities are used to describe the main sedimentary characteristics of the Kurrush Formation (Fig. 4.4). These characteristics are summarised in Table 4.1.

a) South of the Wadi Abu Shaybah

This section is exposed in the area south of the Wadi Abu Shaybah (● Fig. 4.3), located approximately 2.5 km to north of Gharian town (GPS 0342853/3253042). It shows the contact with the overlying Al Aziza Formation. Here, the Kurrush Formation is characterised by facies (F-YS). F-YS is dominated by pale yellowish orange (10YR 8/6) fine-grained sandstones with minor dolomitic beds. This facies is capped by dolomitic limestone facies of the Al Aziza Formation. The maximum measured thickness of the yellow sandstone facies (F-YS) is *ca.* 0.90 m. The sandstones are massive, lack sedimentary structures and are lacking fossils and bioturbation structures.

b) North of the Wadi Abu Shaybah

This section is exposed along the north side of the Wadi Abu Shaybah ● (Fig. 4.3) (GR. 0312845/3561991). The main characteristics of the section are illustrated in field photographs (Fig. 4.5A and Fig. 4.5E) and a graphic log (Fig. 4.5F). The log was recorded from the northern side of the Wadi Abu Shaybah and is characterised by reddish micaceous sandstone facies (F-SR). The maximum measured thickness of facies (F-SR) is *ca.* 1.10 m. The facies comprises moderate red coloured (10R 4/6), very fine to fine grained sandstone that displays symmetrical ripples. These have an average wavelength of 1 cm and crest height < 1 cm (Fig. 4.5E). Some of the cross laminations have a north westerly palaeoflow direction (Fig. 4.5F), although limited palaeocurrent analyses (n = 5) were conducted due to the poor quality of the sedimentary structures. Fossils and bioturbation were not observed in this facies.

| Lithology | | Description | | | | |
|-----------|--|------------------------|---------------------------------|--------------------------------------|------------------------|---------|
| | | Thickness (maximum) | Grain size (Wentworth scale) | Colour (Munsell colour chart) | Sedimentary structures | Fossils |
| 1 | Reddish sandstone (F-SR) | 1.10 m | Very fine sand | 10R 4/6 Moderate reddish brown | Symmetrically rippled | None |
| 2 | Yellow sandstone (F-YS) | 0.90 m | Very fine sand | 10YR 8/6 Pale yellowish orange | None | None |
| 3 | Light brown sandstone (F-LS) | 1.20 m | Fine sand | 5YR 5/6 Light brown | Cross-laminated | None |
| 4 | Pale yellowish orange (10YR 8/6) mudstone | 0.6 m | Mud | 10YR 8/6 Pale yellowish orange | None | None |

Table 4.1 Summary characteristics of the Kurrush Formation in the Gharian area.

c) West of the Abu Rashada Road

This outcrop is exposed in the northwest of the study area along the Abu Rashada road ⑤ (Fig. 4.3), located approximately 1.5 km south of Kaf Kalaya (GR. 0310177/3564359). The main characteristics of the section are illustrated in some field photographs (Fig. 4.5C and Fig. 4.5D). This section is affected by Tertiary basaltic volcanism. The outcrop is dominated by light brown (5YR 5/6) fine-grained sandstones with minor clay lenses. The maximum measured thickness of light brown sandstone (F-LS) is *ca.* 1.20 m (Fig. 4.5C). This consists of fine grained sandstone and green silty claystone that displays fine parallel lamination. The average thickness of the parallel laminations is approximately 1 mm (Fig. 4.2D).

d) Ras Lefa Section

This outcrop is exposed in the Jafarah Plain at the Ras Lefa section, located approximately 21 km to north of Gharian town. The maximum measured thickness of facies (F-MS) is *ca* (Fig. 4.5 B). 0.6m. The section shows the contact between the Al Aziza and Kurrush Formations. The Kurrush Formation is characterised by facies (F-MS). F-MS is dominated by pale yellowish orange (10YR 8/6) mud and siltstone. This facies is capped by dolomitic limestone facies of the Al Aziza Formation. Fossils and bioturbation were not observed in this facies.

Petrographic analysis reveals that the sandstone comprises quartz and mica grains that are angular to sub angular in shape with moderate sorting (Fig. 4.6). Quartz makes up approximately 92% of the grains. The quartz occurs as both mono-crystalline and polycrystalline forms (Fig. 4.6), but most of sandstone samples are dominated by polycrystalline quartz. Mica (muscovite) is also present and represents about 5% of total components. Feldspars are very rare (< 1% e.g. Sample K002 in Fig. 4.6). Rock

fragments are also present and represent about 2% of total components. Furthermore, proportions (5-10%) of clay matrix were observed in the studied samples (Fig. 4.6).

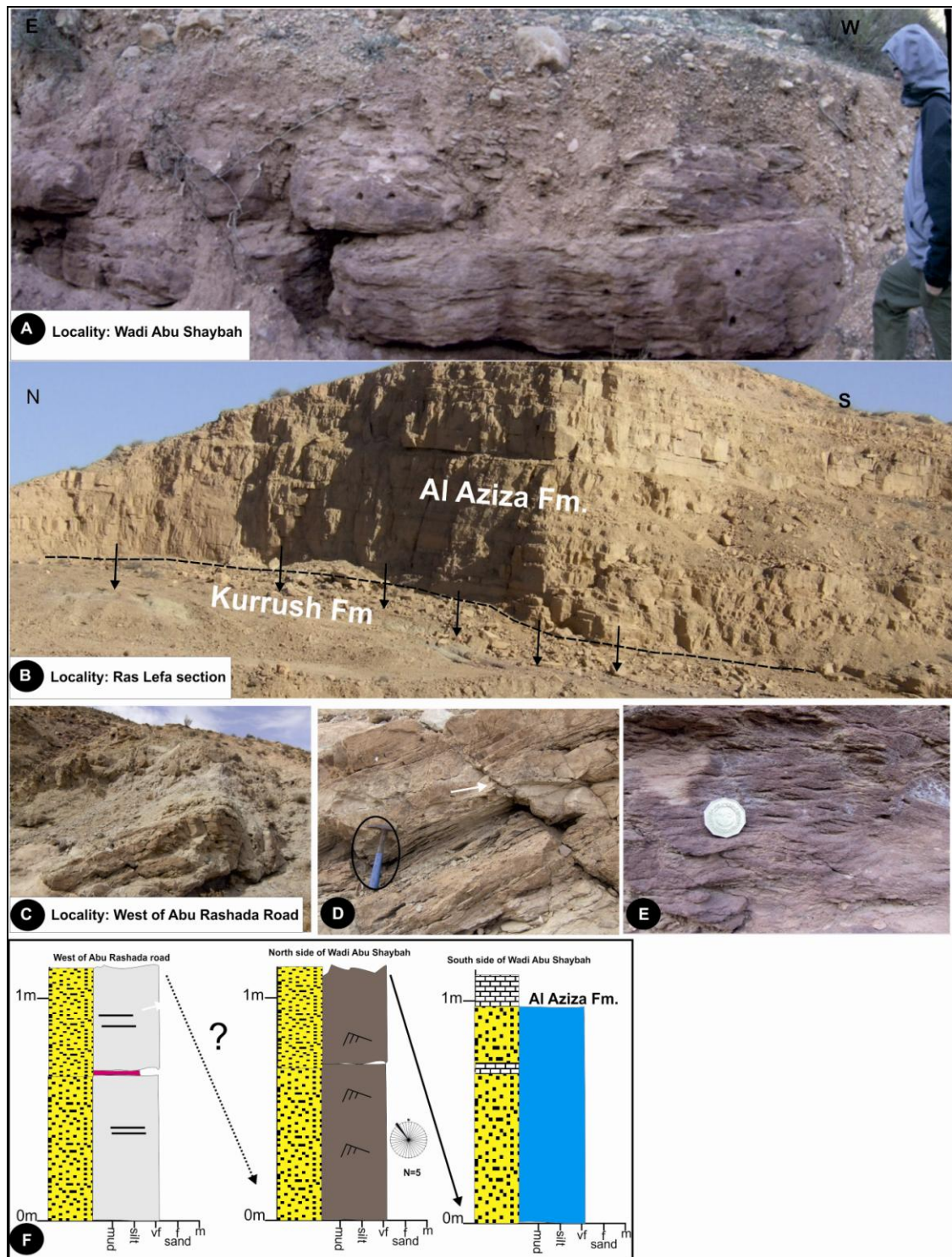


Figure 4.5 A: General view of Reddish sandstone (F-SR) exposed in Wadi Abu Shaybah, person's height = 1.82 m. B: View of the Ras Lefa section showing the Kurrush Formation with the overlying Al Aziza Formation. C: General view of light brown sandstone (F-LS) exposed in west of Abu Rashada road (Fig. 4.1). D: Parallel lamination exposed in the Kurrush Formation (west of Abu Rashada road in Fig. 4.1). Hammer circled for scale. Fault has NW trend (white arrow). E: View of symmetrical ripples in the Kurrush Formation (1) (Fig. 4.1) (coin = 2.5 cm diameter) F: Sedimentary logs from the north and south of Wadi Abu Shaybah and west of Abu Rashada locations.

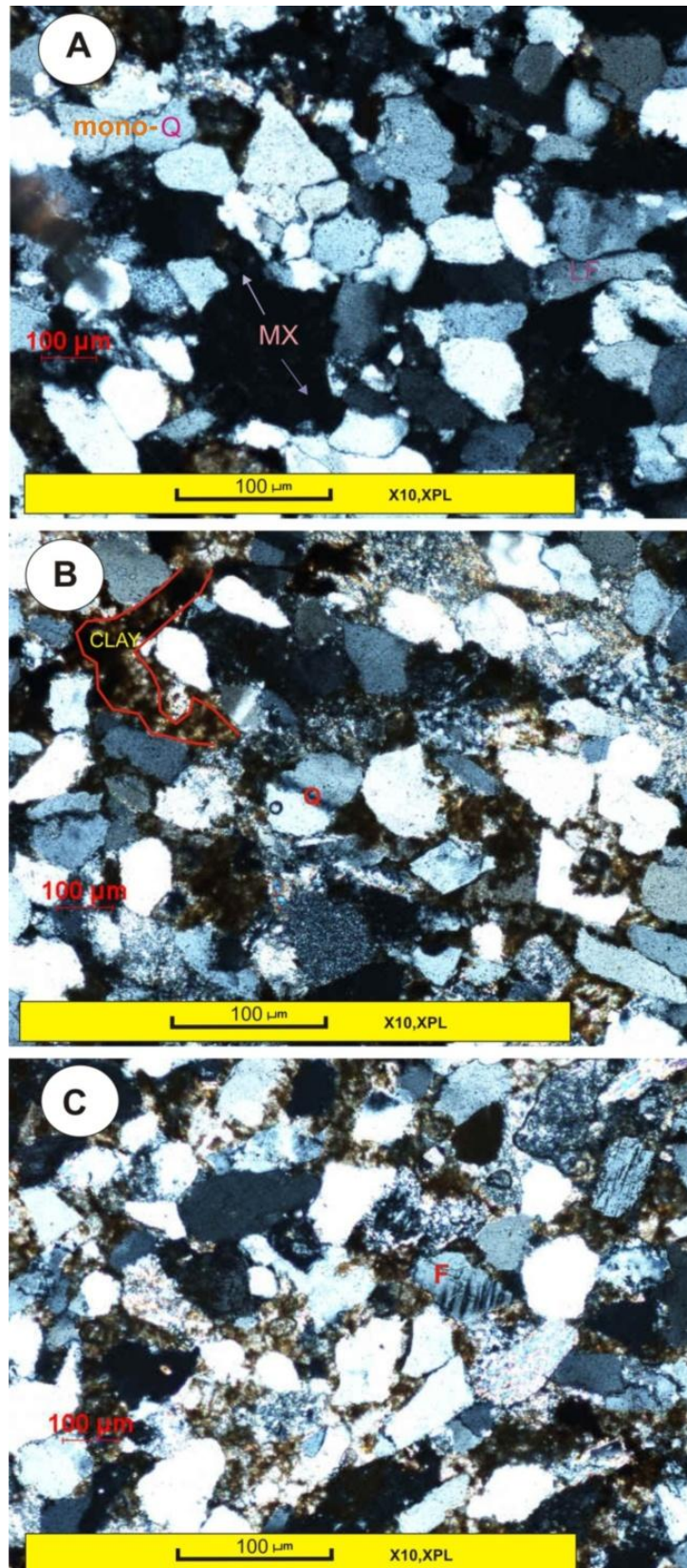


Figure 4.6 Thin sections of the Kurrush Formation from west of the Abu Rashada road. **A:** Microphotograph of sample **K001** taken under crossed polars illustrate moderate sorted. **B** and **C:** Microphotographs for sample **K002** and **K003** taken under crossed polars, illustrating clay and feldspar crystal at the right top of the view (**C**).

3) Interpretation

i) South of the Wadi Abu Shaybah

The fine grain size indicates a relatively low energy depositional process. A general lack of internal structures within beds suggests that either: 1) primary sedimentary structures may have been completely destroyed during deposition; 2) extensive bioturbation of sediment has occurred, which has destroyed any evidence for lamination or cross-bedding; or 3) surface intensive weathering.

ii) North of the Wadi Abu Shaybah

The fine-grain size of the sandstone suggests deposition under low energy deposition, whilst the cross-laminations indicate the presence of ripple bed forms (e.g. Harms et al., 1975; Boggs, 1995; Collinson et al., 2006). Symmetrical ripple marks which trend N-W in this facies suggest wave activity related to the oscillatory patterns of water movement close to the water-sediment interface. Moreover, the reddish colour of the very fine sandstone suggests that the facies formed under well-drained oxidation conditions (Loughnan et al. 1964; Turner, 1980). Alternatively, the red colour may be due to erosion of pre-existing red-beds or sediment that was deposited and modified under desert conditions (e.g. Van Houten, 1948; Krynine, 1948, 1950; Loughnan et al., 1964; Turner, 1980).

iii) West of Abu Rashada Road

The fine-grain size of the sandstone facies (F-LS) and the presence of laminations can be interpreted in two ways: 1) settling from suspension or 2) by current flows in upper flow regime where sedimentary beds such as ripples or dune are destroyed. The parallel lamination and absence of fining upwards between lamination suggests current flow in the upper regime (e.g. Allen, 1965; Collinson et al, 2006).

The dominant mineral present in the thin sections is quartz. Based upon Pettijohn's classification (1987) these are interpreted as quartz arenites (Fig. 4.6). This suggests that materials are being sourced from distance, possibly from Palaeozoic and older quartzites or quartz rich metamorphic rocks (see Chapter 3, Section, 3.2) that are exposed immediately to the south of the Gharian area. Alternatively, the quartz may be sourced from further to the south in the Ghadamis basin (Chapter 1, Fig. 1.3). Lower sea level during Kurrush Formation times may have enabled fluvial systems to incise and expand their catchment areas into more distant parts of the Gondwanan cratonic landmass. Moreover, the low percentages of feldspars indicate that these minerals were transported over a great distance to the area. The weathering of feldspars can form kaolinite, but it is not present in this section. Muscovites are present in some thin sections (5%) and are likely to originate from metamorphic rocks from outside the basin.

iv) Ras Lefa Section

Due to the fine-grained nature and uniformity of this sediment it is interpreted as having been deposited from sediment low energy conditions. Facies characteristics suggest post-depositional modification has destroyed any sedimentary structures (Selley, 1976). The yellowish orange colour of the fine grained suggests pedogensts.

4.2.3 Environment Interpretation

The textural characteristics observed in the southern part of Kurrush Formation show an overall fine-grain size indicative of a relatively low energy environment. The occurrence of minor dolomitic beds within these sediments could suggest a shallow marine shelf setting. However, the lack of sedimentary structures makes palaeogeographic reconstruction difficult. The oil well data from the Jafarah basin which includes the presence of the *Myophoria* bivalve (Hammuda et al., 1985) provides clearer evidence for a marine setting (Gao et al., 2009).

The mud facies of the Kurrush Formation from the Jafarah Plain is interpreted as a flood plain environment. Deposition of mud usually occurs under low energy conditions with low flow velocity. However, the sedimentological characteristics of the red sandstone in the Wadi Abu Shaybah indicate deposition within a continental environment.

Textural characteristics show an overall fine grain size reflecting low energy depositional environment. Evidence from thin sections further supports a continental environment for Northern Wadi Abu Shaybah and West of Abu Rashada road, which the sediment possibly derived locally from quartzites or quartz rich metamorphic rocks.

The presence of small-scale symmetrical ripples is typical of elements of shallow water waves. However, it is not possible to be more precise about whether the environment is continental (e.g. lacustrine) or marine (e.g. tidal etc.). Siltstones often relate to fluvial environments with over bank flooding or low energy parts of a deltaic system (Heward, 1978; Walker, 1992). Furthermore, delta plain settings often include low energy environments such as tidal flats and swamps.

The upper part of the Kurrush Formation contact with Al Aziza Formation is transitional from marine clastics to marine carbonates. Therefore, the Kurrush is probably deposited in a marginal continental environment, possibly a delta plain setting, with facies changes possibly reflecting localised sea level oscillations.

4.2.4 Palaeogeography of the Kurrush Formation

In the Jafarah Basin sub-surface record (A1-38) a marine incursion is indicated by the presence of dolomitic limestone and the bivalve *Myophoria* (Hammuda et al., 1985; Swire and Gashgash, 2000). The upper part of the Kurrush Formation outcrops in the Gharian area of Jabel Nafusah region where it is represented by micaceous red sandstones. Textural characteristics show an overall fine grain size reflecting low energy depositional environment. Evidence for continental environments is based on 1) grain size; 2) colour; 3) palaeocurrent trend and the absence of fossils. Figure 4.7 shows that the Kurrush Formation is dominantly marine environment in the Jafarah Plain and becomes marginal marine in the Gharian area.

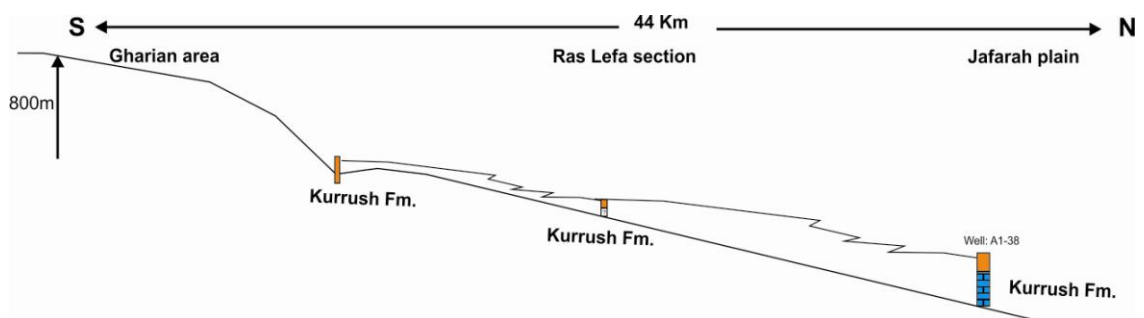


Figure 4.7 Sketch diagram to show palaeogeographic reconstruction of the Kurrush Formation during the Early Triassic.

4.3 Al Aziza Formation

4.3.1 Introduction

The name of the Al Aziza Formation was formally introduced by Christie (1966) for the Late Triassic. The exposures of the Al Aziza Formation are mainly restricted to the Jabel Nafusah escarpment and small hills on the southern Jafarah plain (Desio et al., 1963; Hammuda et al., 1985). A complete section is located in the central Jabel Nafusah region (Gharian area) and Ras Mazul domes. Burolet (1963); Desio et al., (1963) and Busson (1970) also reported the Al Aziza Formation in subsurface oil wells of the Jafarah Plain and near the Tunisian border. The formation is on average 140 m thick but a thickness up to 200 m is inferred from wells (Banerjee, 1980). The Gharian sections expose the entire Al Aziza Formation with observable contacts with underlying Kurrush and overlying Abu Shaybah Formations. The exposures on the Jafarah Plain exhibit only the lower part of the Al Aziza Formation, with a clear contact with the underlying Kurrush Formation. Collectively, the Al Aziza Formation consists of limestone, partially dolomitized in places, and dolomite with narrow bands of chert. These sediments in the Gharian area were interpreted by Assereto and Benelli (1971) as a continental margin sequence.

4.4 Sedimentary Facies of the Al Aziza Formation

4.4.1 Introduction

This section involves the study of sedimentary facies of the Al Aziza Formation in the Jafarah plain and Gharian area (Fig. 4.8). A complete section of the Al Aziza Formation has been logged and described in the Gharian area where the base with underlying Kurrush Formation and top of the formation with the overlying Abu Shaybah Formation is best exposed (Fig. 4.9). In addition, the basal part section was

also logged in the Jafarah plain (Ras Lefa section) (Fig. 4.10) where the contact with the underlying Kurrush Formation is observed.

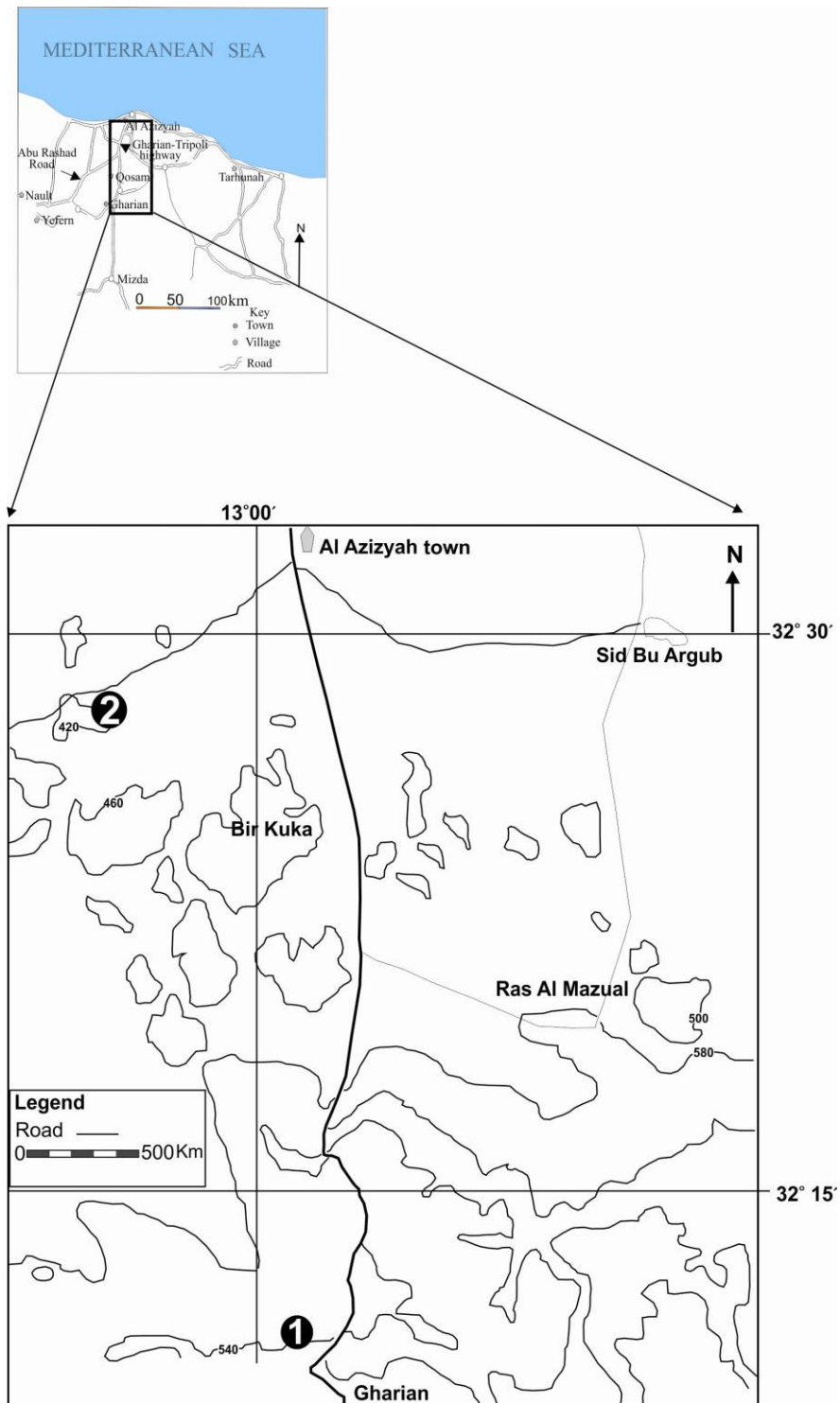


Figure 4.8 Location map of the Al Aziza Formation in the Gharian area and Jafarah Plain. ❶ and ❷ correspond to the localities referred to within the text.

The field observations and petrographic analysis of two outcrops of the Al Aziza Formation has enabled seven carbonate facies to be identified on the basis of their sedimentary structures, grain size and faunal content (Table. 4.2). The facies were grouped into a single facies association.

4.4.2 Facies (F-BD): Burrowed and laminated micrites and dolomites

i) Description

This facies was recorded at localities ❶ and ❷ within the Gharian and Ras Lefa sections (Fig. 4.8). The maximum measured thickness of facies F-BD is *ca.* 15 m. This facies is distributed through the lower and middle part of the Gharian section ❶, whilst it is rare in the Ras Lefa section ❷. This facies consists of grayish black (N2), very fine-grained limestone. Sedimentary structures are rare but very fine parallel lamination and tube-like structures were observed. Bedding surfaces exhibit a high density of tube structures, these are *ca.* 0.2 to 0.6 mm long and <1 mm wide. The tube structures (Fig. 4.11B) are horizontal with no branching system, and are usually more or less isolated from each other. However, in some cases they form concentrations in specific beds, as in the Al Aziza section (Fig. 4.11 B). This facies is known locally as Al Aziza stone and is commonly used as a decorative building stone.

Petrographically, this facies consists mainly of dense dolomite (Fig. 4.11C). Fragments of body fossils are also present and these include ostracods. However, the poor preservation of fragments of body fossils prevents a more detailed classification. The main petrographic characteristics of the Al Aziza Formation are dolomitization of the precursor calcite; therefore, the dolomite consists mainly of dolomicrite. Individual dolomite crystals are 10-80 µm across, however most are close 60 µm in size.

| Facies code and name | | Description | | | | | Section | |
|----------------------|---|---------------------|------------------------------|--|------------------------------|---------------|---------|----------|
| | | Thickness (Maximum) | Grain size (Wentworth scale) | Colour (Munsell colour chart) | Sedimentary structures | Fossils | Gharian | Ras Lefa |
| 1 | Facies (F-BD): Burrowed and laminated micrites and dolomites | 15 m | Very fine | N2 Grayish black | Very fine lamination | Trace fossils | ✓ | ✓ |
| 2 | Facies (F-PE): Peloidal limestone | 10 m | Silt to fine | 5Y 8/4 Grayish yellow | None | | ✓ | ✗ |
| 3 | Facies(F-AB): Algal biolithites | 22 m | Fine | 5Y 8/4 Grayish yellow | Very fine cross-lamination | gastropods | ✓ | ✗ |
| 4 | Facies (F-MS): Mudstone | 2 m | Mud | 10 YR 8/6 Pale yellow orange mudstone | None | None | ✓ | ✓ |
| 5 | Facies (F-AD) Argillaceous biomicrities and dolomitized biomicrities | 14 m | Very fine | 5Y 7/2 Yellowish gray | None | Bivalves | ✓ | ✓ |
| 6 | Facies (F-CL): Cherty limestone | 35 m | Very fine to fine | 10 YR 6/2 pale yellowish brown | Cross-lamination and nodules | None | ✓ | ✗ |
| 7 | Facies (F-PL): Phosphate facies | 12 m | Fine | 5Y 8/4 Grayish yellow | Cross-lamination | None | ✓ | ✗ |

Table 4.2 Summary characteristics of the Al Aziza Formation in the Gharian area and Ras Lefa section.

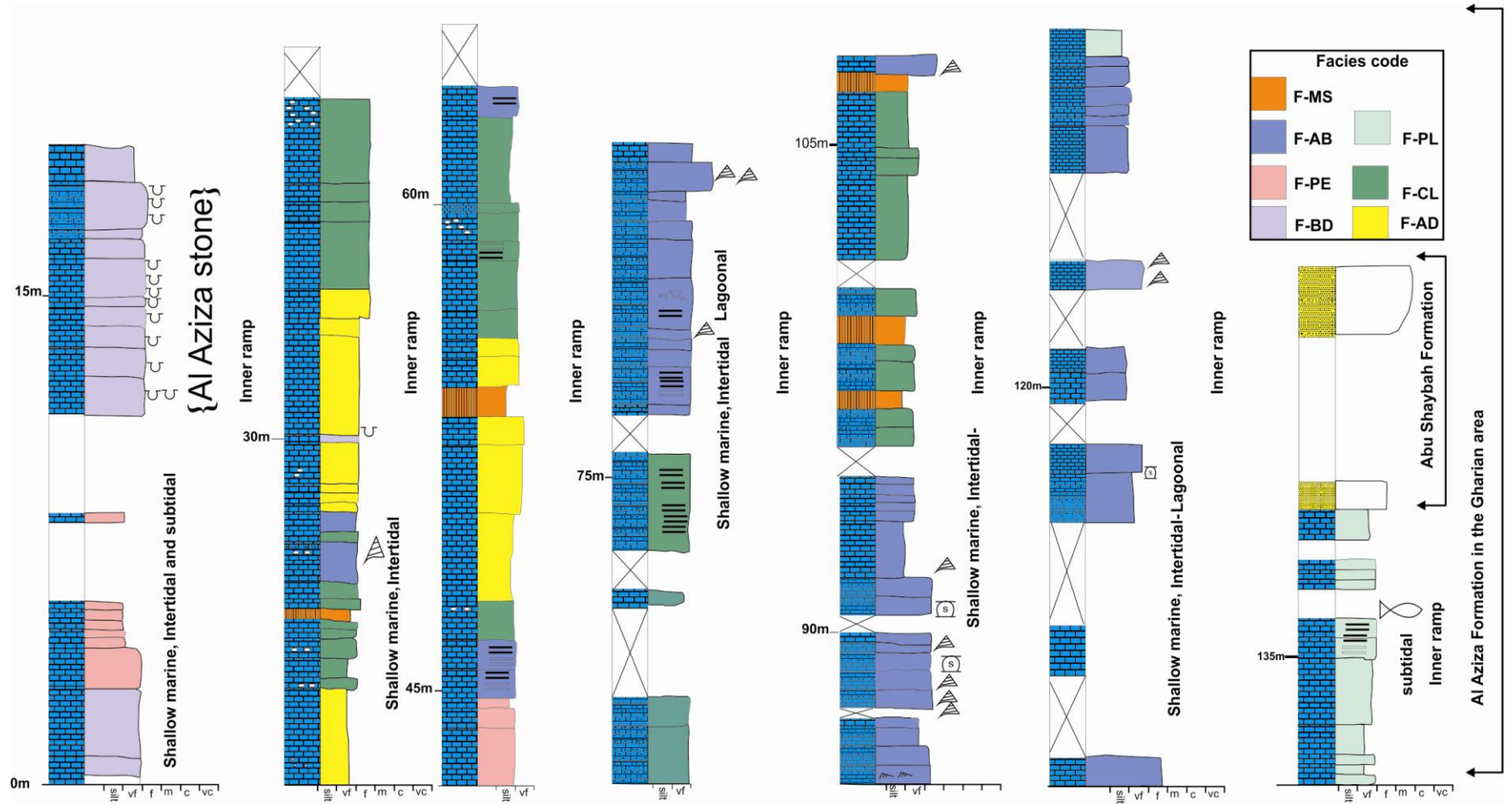


Figure 4.9 Log of the Al Aziza Formation at location 1 (Fig. 4.2) (GR 0312805/3562881). For key to symbols see Chapter two (Fig. 2.1).

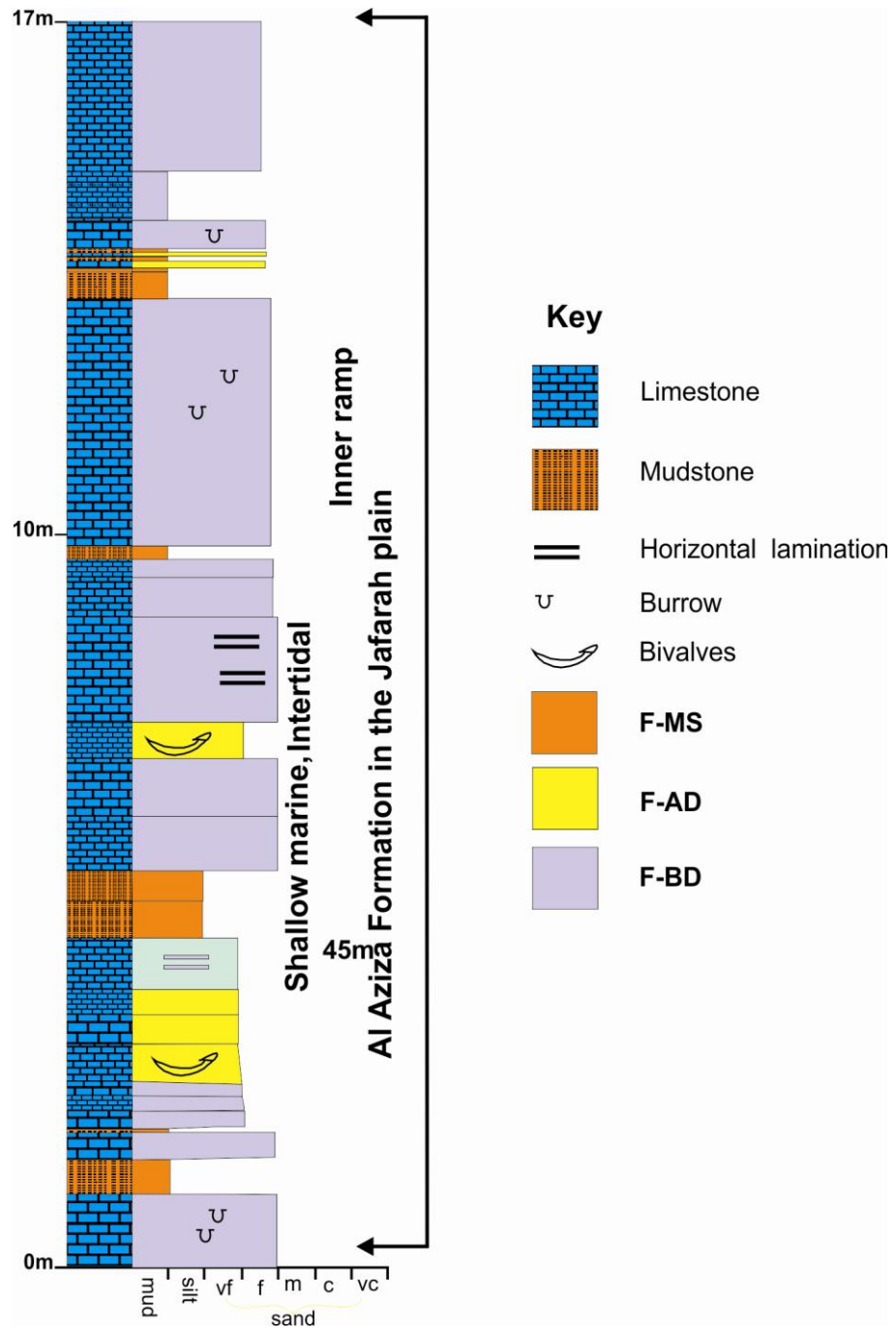


Figure 4.10 Sedimentary log from the Jafarah Plain (Ras Lefa section ②) (Fig. 4.6).

ii) Interpretation

The very fine grain size and the presence of laminations suggest either current flow in the upper regime or settling from suspension (e.g. Harms, 1975; Collinson et al., 2006). Depositional processes leading to the presence of laminations suggests settling-out of grains from suspension (Flugel, 2004).

The tube-like structures are trace fossils (e.g. Selley, 1976; Bromley, 1996; Retallack, 2001), and most likely to represent burrows, as most root traces taper, branch downward and are very irregular in width. These bioturbation structures are infaunal feeding burrows classified as *Skolithos*, which normally occur within the nearshore zone (Collinson and Thompson, 1989; Bromley, 1990; Flugel, 2004). The finer-grained and burrowed sediment suggests that the sediment was deposited in less turbulent conditions largely below wave base. Although ostracods have been identified there fossils do not allow an estimation of palaeodepth as ostracods occupy a wide range of environments (Selley, 1985).

Further evidence of the shallow water depth of this facies is provided by high density of burrows (Tucker and Wright, 1990). As Flugel (2004) proposed that burrows are the most common features observed in shelf limestone and occurs in carbonates both in intertidal and subtidal settings, inner shelf/ inner ramp environment. The fossil component of the limestone may have been deposited either in situ or transported during stages of erosion by current or waves.

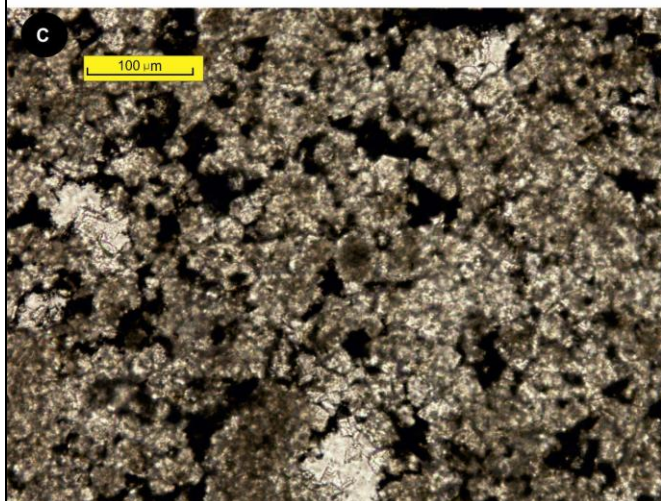


Figure 4.11 A: View of the Gharian area, showing the type section of Al Aziza section (●), person's height = 1.82 m (GR 0312805/3562881).

B: Bedding surfaces exhibiting density burrowed micritic limestone (Al Aziza Stone).

C: Photomicrograph of the dolomite under cross-under crossed-polars.

4.4.3 Facies (F-PE): Peloidal micrite

i) Description

This facies is only recorded in the Gharian section ① (Fig. 4.8). This facies is rare in the field sections examined and the maximum measured thickness of facies F-PE is ca. 10 m. The facies comprises grayish-yellow coloured (5Y 8/4), silt to fine-grained limestone that displays small to medium-scale parallel laminations. This facies is represented by 4 thin sections (Fig. 4.12). Petrographic analysis reveals that the facies is composed of rounded to sub-rounded peloids that have an average diameter of 200-300 μm that lack internal structures (Fig. 4.12). The facies is also characterized by sparry-filled holes developed within the micrite, with the spar comprising different crystal sizes.

ii) Interpretation

Peloids are generally of diverse origins. Some that have regular outlines and are well sorted are regarded as faecal pellets (Flügel, 2004), whilst those that exhibit a range of different shapes and sizes are believed to be mainly micritized skeletal fragments. Most faecal pellets are homogeneous and can occasionally exhibit a peripheral rim in transmitted light, which is caused by the high content of organic matter or iron (Flügel, 2004). The cement is mostly sparite; however, in some cases it is microsparite. The rocks of this microfacies are classified as pelsparite according to Folk (1959) and grainstone according to Dunham (1962). The predominance of lime mud as a matrix along with peloids suggests a subtidal setting and the presence of parallel lamination suggest deposition above fair-weather wave base (FWWB) in an inner ramp setting (Tucker, 1985; Sinclair et al., 1998). Peloids result from the boring and rasping of mud by various organisms (Reading, 1996). This facies was probably deposited in a shallow water depth with low to moderate energy conditions, with mudstones suggesting

deposition very close to the shoreline (Tucker and Wright, 1990; Flugel, 2004). This facies has been previously identified as oosparites by Asserto and Benelli (1971), but samples taken in this study do not support their interpretation. This may be due to either: 1) lateral facies changes or 2) Asserto and Benelli (1971) misinterpreted the samples they collected.

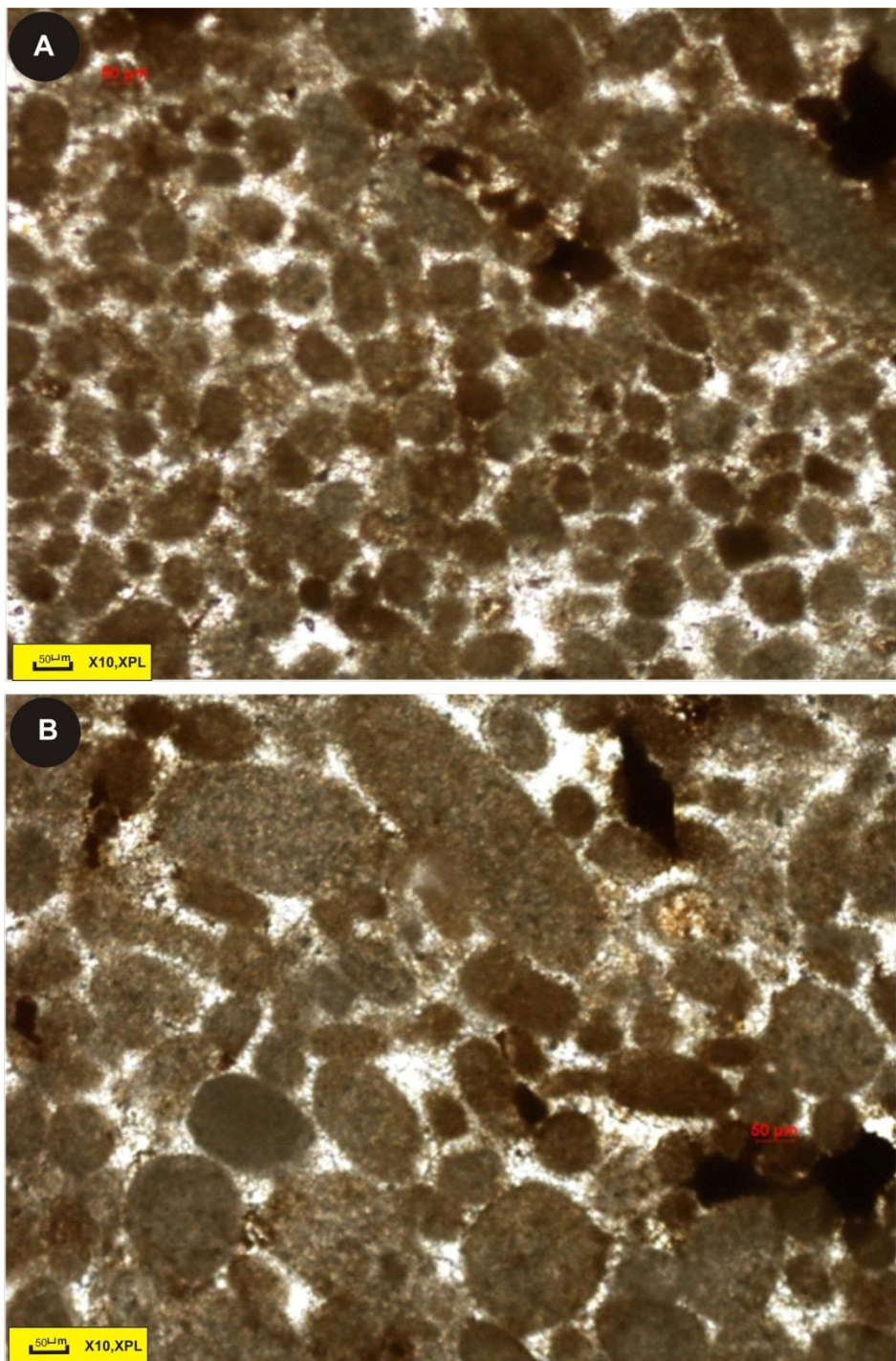


Figure 4.12 A and B): Photomicrograph of the peloids under crossed-polars (FOV= 10x PPL). Locality: Gharian section.

4.4.4 Facies (F-AB): Algal biolithites

i) Description

This facies occurs at locality ① (Fig. 4.8). It is widespread in the Gharian section, mainly in the middle and upper parts of the section, the facies is rare in the Jafarah section. The maximum measured thickness of facies F-AB is *ca.* 22 m and consists of grayish yellow (5Y 8/4), medium-bedded limestone with bed thickness of average 10 to 30 cm. The lower unit of this facies displays very fine cross-lamination (average ~ 1 mm in thickness). The facies contains algae, gastropods, and also drusy calcite filled vugs. The algae range from 8-25 cm thick. In the lower part of the Gharian section, brecciated algae (Fig. 4.13B) is observed interbedded with clayey biomicrites. No bioturbation was observed in this facies. This microfacies is represented by two thin sections. Petrographically, these rocks comprise 0.2-1.5 mm thick laminae of dense micrite. Rare, well preserved green algae (dasyclad) can also be observed (Fig. 4.13C).

ii) Interpretation

The lamination and fine grain size of this facies indicate deposition out of suspension in a low energy environment. The fine scale of the laminations further suggests low energy deposition (e.g. Collinson and Thompson 1989; Selley, 1985; Flugel, 2004). Disrupted laminations in this facies suggest an exposure index of 50% (lower intertidal zone, inner shelf/ inner ramp environment) based on Reading's exposure index scheme (Reading, 1996). Using the classification scheme of Logan et al., (1964) and Tucker, (1982) based on the morphology of algal mats (Fig. 4.13A), these algal forms can be classified as laterally-linked hemispheroid (LLH) stromatolites. The presences of green algae reflect shallow water (lagoonal setting) of normal salinity under oxygenated conditions in the photic zone (Fig. 4.20 in section 4.5.1) (Wray, 1978; Tucker, 1985). The lime mud matrix reflects low energy conditions (Rohl et al., 1992). Furthermore, microbial mats

can form domal structures or stromatolites, those with a relief of more than a few centimetres also appear to have formed in lower intertidal or subtidal zone, inner shelf/ inner ramp environment (Monty, 1966; Monty, 1976; Hagan and Logan, 1974; Ozkan, 2009). The breccias are of solution collapse origin (Pomomi-papaioammou and Karakiltios, 2002). Some samples exhibit vugs completely infilled with calcite and may have developed due to the release of gases from the algae (Khalaf and Gaber, 2008).

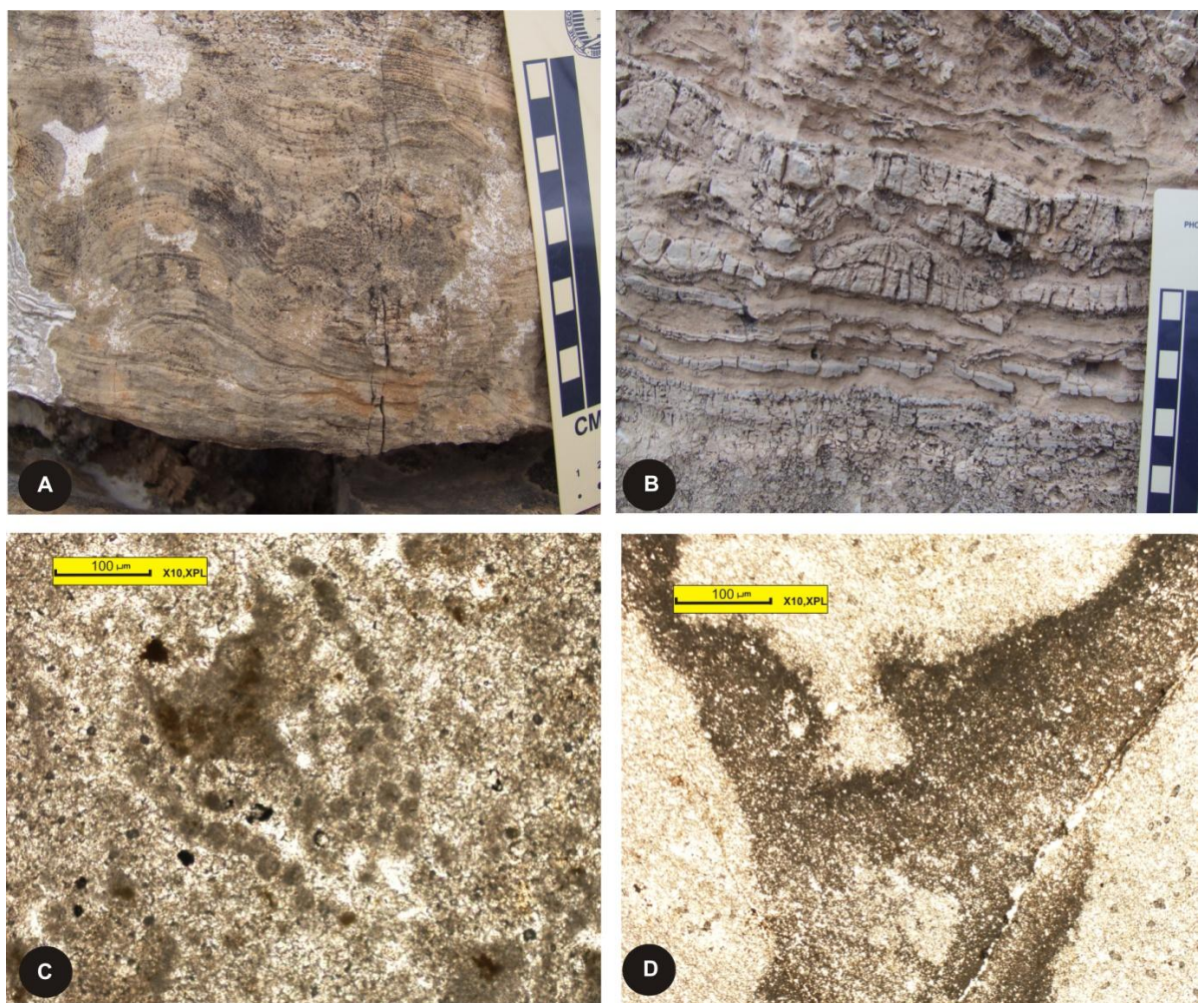


Figure 4.13 **A:** Surface of domal algal bolithite in the field. **B:** the brecciation algal of the F-AB facies. **C:** the green algae under crossed polars. **D:** brecciated limestone (FOV= 10x PPL). Locality: Gharian area.

4.4.5 Facies (F-MS): Mudstone

i) Description

The F-MS facies was observed at locations ❶ and ❷ (Fig. 4.8) where it has a maximum thickness of *ca.* 2 m. It is distributed through the lower and middle part of the Gharian section, where it is interbedded with marl, and also occurs throughout the lower part of the Ras Lefa section (Fig. 4.14A). The facies consists of pale yellow orange (10 YR 8/6) mudstone. No sedimentary structures and fossils were observed in this facies.

ii) Interpretation

Due to the fine-grained nature and uniformity of this sediment it is interpreted as having been deposited from sediment suspended within the water column. The mudstone could represent the suspension fall-out sedimentation during normal (fair weather) conditions (Flügel, 2004). Facies characteristics suggest post-depositional modification has destroyed any primary sedimentary structures, either by bioturbation or post-depositional compaction and diagenesis. Similar facies are to be found in the offshore sequences of western Libya (Mriheel and Alhnaish, 1995).

4.4.6 Facies (F-AD): Argillaceous Biomicrities and Dolomitized Biomicrities

i) Description

This facies was observed at locations ❶ and ❷ (Fig. 4.8). The maximum measured thickness of facies F-AD is *ca.* 14 m. This facies is distributed through the lower and middle part of the Wadi Abu Shaybah section, whilst it is rare in the Ras Lefa section. The facies consists of yellowish gray (5Y 7/2), very fine-grained limestone and occasional marl horizons. The facies is highly fossiliferous, especially on bedding plane surfaces (Figs. 4.14B and C). Rare casts of bivalves are preserved but these are small (1 to 2.1 cm diameter) (Fig. 4.14C) and fragmented.

ii) Interpretation

The fine grain-size of the carbonates can be interpreted as settling from suspension or by current flows in upper flow regime where sedimentary such as ripples are destroyed. The facies is rich in fragmented bivalves and this is indicative of a marine setting. However, the poor preservation of the fossil material (Fig. 4.13B and Fig. 4.14C) prevents a more detailed classification.

4.4.7 Facies (F-CL): Cherty limestone

i) Description

This facies occurs at locality ① (Fig. 4.8). The maximum measured thickness of facies F-CL is *ca.* 35 m. It is distributed through the middle and upper parts of the Gharian section. This facies displays cross-lamination and chert (Fig. 4.15). The average thickness of cross lamination is approximately ≥ 2 mm. Chert in this facies can be divided by morphology into two types: 1) the chert occurs as discontinuous, lenses, nodules, and 2) thin continuous irregular layers. The chert nodules and lenses range from a few cm's to 8 cm in diameter. Some chert nodules contain carbonate within their centres resulting in a hollow morphology. The colour of chert nodules varies from pale yellowish brown (10 YR 6/2) on the outside to dusky yellow (10 YR 2/2) inside. The irregular chert horizons are 2-22 cm wide, parallel to bedding and typically occur in sets of 4 or 8 layers that can comprise 10% of the bed.

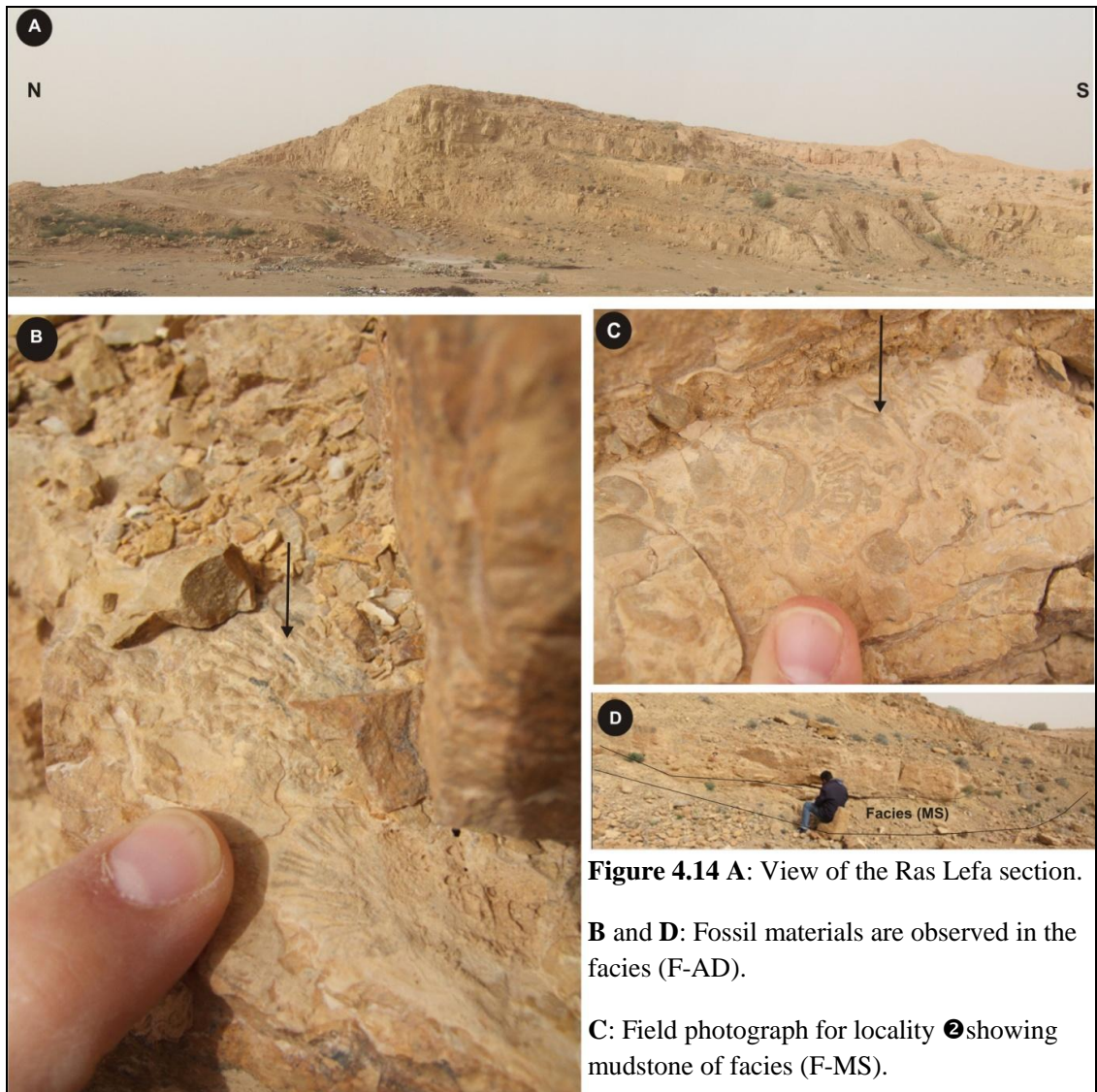


Figure 4.14 A: View of the Ras Lefa section.
B and D: Fossil materials are observed in the facies (F-AD).
C: Field photograph for locality 2 showing mudstone of facies (F-MS).

ii) Interpretation

The parallel laminations suggest settling from suspension or upper flow regime conditions on the upper of the bedform (e.g. Selley, 1985; Collinson and Thompson, 1989). Chert is a general term for a siliceous sedimentary rock of chemical, biochemical or biogenic origin (Dolbier et al., 2010). The bands of chert were either deposited by primary sedimentation or from diagenetic processes. Almost all the chert nodules in this facies suggest diagenetic formation by the replacement of another mineral by sea water rich in silica (Tucker and Wright 1990; Boggs, 1995; Nichols, 1999). The variety of chert nodules and lenses in the Al Aziza Formation could be late diagenetic features, because the edges of some chert nodules cross-cut bedding

(Lehrmann et al., 2003; Pope, 2004). Furthermore, the cherty facies indicates this area received abundant dissolved silica throughout the Triassic period. The source of silica for many chert nodules was probably derived mainly from the dissolution of sponge spicules (Tucker, 1982). The abundance of chert in this facies could indicate high productivity and upwelling.



4.4.8 Facies (F-PL): Phosphate Facies

i) Description

This facies is recorded at location ❶ (Fig. 4.8) and only occurs at the top of the Al Aziza Formation (Fig. 4.16) with observable contacts with overlying Abu Shaybah Formation. The maximum measured thickness of facies F-PL is ca. 12 m and it forms laterally discontinuous lens shaped bodies. The facies is comprised of grayish yellow (5Y 8/4) coloured, very fine to fine-grained sandstone that exhibits very fine cross-lamination. Phosphate elements such as bone fragments and clasts of phosphatic material that have variable morphologies (Fig. 4.17 A & B) make up a large proportion of this facies. Most of the clasts are characterised by rounded to sub-rounded shapes that are up to 30 cm diameter in the layers.

This facies is represented by 4 thin sections. Petrographic study reveals that this sediment consists of phosphate clasts and angular to sub-rounded grains of quartz with a micrite matrix. The bone fragments are elongated (Fig. 4.17D) and infilled in some samples with microsparite.

ii) Interpretation

The fine-grain size of the sandstone and the presence of laminations can be interpreted in two ways: 1) settling from suspension or 2) by current flows in upper flow regime where sedimentary bedforms such as ripples or dunes are destroyed. Therefore, the fine grain-size of the sandstone and parallel lamination in this facies suggests current flows in the upper regime (e.g. Collinson and Thompson, 1989; Collinson et al., 2006). The yellowish colour of the sandstone unit suggests that ferric or limonites are present in the facies. Furthermore, the presence of the quartz seems to be either the result of silicification processes, which accompanied the dolomitization of calcite, or more likely these are detrital quartz grains.

Phosphates occur in the geological record from the Precambrian (Archaean) to the Recent (Muller, 1978; Shemesh et al., 1983). The source of the sedimentary phosphate is microbial breakdown of buried organic matter and redox-driven phosphate desorption from iron and manganese oxyhydroxides (Follmi, 1996; Saltzman, 2003). Furthermore, organic phosphates are concentrated in higher organisms and maybe related to fishes which have phosphate contents in their bone and teeth (Shemesh et al., 1983; Follmi, 1996). Thus, the presence of phosphate as part of facies F-PL suggests an area with a high content or input of organic material. The fragmented nature of the phosphatic material (Fig. 17D, E) suggests that it is a reworked (Flügel, 2004) and redeposited phosphate connection (RPC) and black rounded lithoclasts (phosphatic clasts, PC). Reworking requires higher energy flows and thus provides additional support of upper flow regime conditions. The presence of quartz indicates a terrigenous influx into the area. Angular to sub-rounded grains of quartz normally occur in a near shore, inner shelf/ inner ramp environment. Therefore, these criteria indicate that this facies was deposited on inner ramp near shore area (Sinclair et al., 1998).

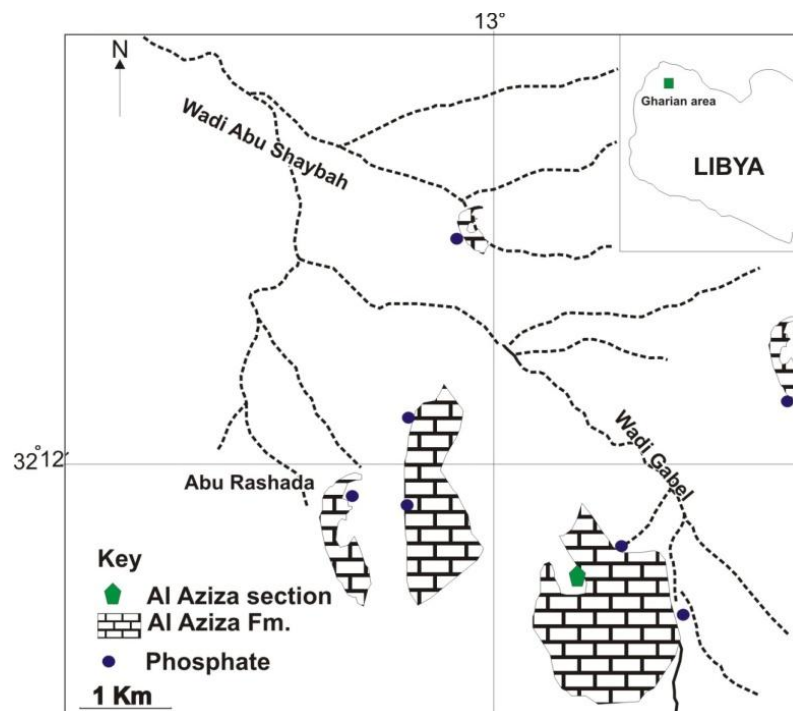


Figure 4.16 Map showing location of the Gharian phosphorite distribution (modified after Lagha, 1977).



Figure 4.17 A: Photograph of facies F-PL showing the exposure along the Wadi Gabel, view to the south. **B and C:** Field image of phosphate remains in facies F-PL (coin = 2cm).

D and E Photomicrograph of phosphate under crossed polars (Sample Lgt 35 and 36) (FOV = 10x PPL).

4.5 Facies Association and Depositional Environment

i) Introduction

The facies of Al Aziza Formation can be grouped into one facies association based on the seven observed facies. The proposed facies association scheme is presented in Figure 4.18.

ii) Shallow Marine Facies Association

The sedimentological and palaeontological features of the Al Aziza Formation are characteristic of a shallow marine carbonate facies association, resulting from deposition along an intertidal-subtidal carbonate flat to shelf lagoonal environment (Fig. 4.18). The facies are dominated by mudstone and fine-grained limestones, suggesting that sedimentation probably occurred mostly within the inner ramp setting (Fig. 4.19). Burchette and Wright (1992) subdivided ramp settings based on the degree of wave and storm action or activity with reference to the depositional processes (Fig. 4.19). The inner area of the carbonate ramp is characterized by the presence of a low-energy protected environment such as a lagoon (e.g. Sinclair et al., 1998; Badenas et al., 2010), where peloids, burrows and green algae can all be observed. Furthermore, the inner ramp in Al Aziza Formation is characterized by detrital quartz accompanied by phosphatic material suggesting organic and terrigenous influxes into the sandy shore face region of the inner ramp setting (Fig. 4.19).

Evidence from sedimentary structures and palaeontological remains further supports inner ramp. A common feature of tidal carbonates is fine-scale lamination. Many ancient peritidal limestones exhibit a lamination consisting of millimeters micrite or dolomiticrite (Reading, 1996; Flugel, 2004). As already mentioned in the facies F-AB some planar lamination produced by the sediment activity of mats of microbial and

microbial mats–laminations are common criteria of ancient tidal carbonates. More specifically, Desyclad algae are common in the Tethyan Middle and Late Triassic shallow marine carbonates (Varol et al., 1988; Rohl, 1992; Flugel, 2004).

The predominance of lime mud as a matrix along with peloids indicates a subtidal setting with sedimentation occurring below fair-weather wave conditions. The occurrence of burrowed micrites (Flugel, 2004) also reflects a shallow marine shelf setting (intertidal to very shallow subtidal). Peloids indicate a more restricted environment (intrashelf lagoon) as compared with the marl/limestone (Al-Ghamdi, 2006). The abundance of chert and phosphate in these subtidal facies could indicate they formed within a region of strong upwelling (Pope, 2004). The distinctive sediments of inner ramp are carbonate sands (Facies F-PL) formed in the agitated shallow subtidal shoreface zone (above fair weather wave conditions) and low intertidal zone.

The textural uniformity of the shallow marine facies association observed the Al Aziza Formation is similar to facies patterns observed from Mesozoic outcrops in South Tunisia and the United Arab Emirates (Marzouk and Youssef, 2008; Alsharhan, 1993).

Figure 4.18 Depositional model of the Al Aziza Formation (modified after Alyagoubi, 2007).

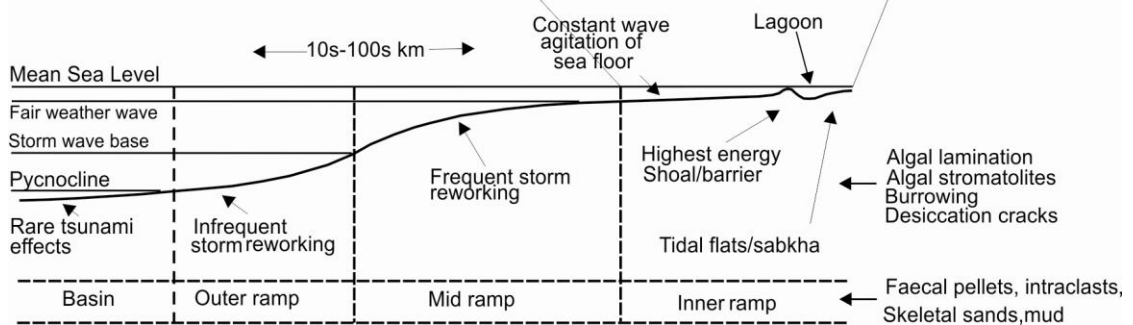
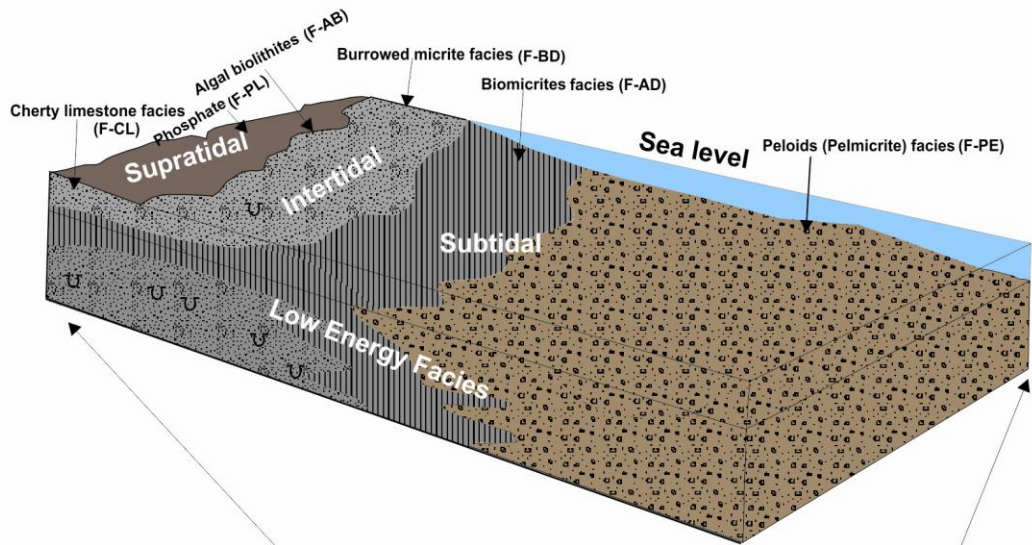


Figure 4.19 Terminology used for marine depositional environments throughout this study (modified from Burchette and Wright, 1992).

4.6 Palaeogeography of the Al Aziza Formation

The Al Aziza Formation is diagrammatically represented by two sedimentary logs (Figs. 4.9 and 4.10) and a depositional model diagram (Fig.4.18). Collectively, these show relative spatial and temporal patterns of sedimentation. These are considered accordingly.

Initial deposition was characterised by a series of shelf muds, wave rippled and carbonates deposited within a low energy marine inner ramp in the Gharian area (Fig. 4.19), with marine conditions becoming more prevalent towards the Jafarah basin. During the late Triassic a broad and deep Tethys Ocean (palaeo-Tethys) existed in the northeast of the study area (Fig. 4.20). Carbonate facies are found along the margins of the Tethys and along areas of future rifting (Biju-Duval et al., 1977). The palaeogeography during the Triassic time was controlled by two processes: 1) rifting and 2) sea level fluctuations (see Chapter 1, Table 1.1). The Triassic was generally a time of a low sea level and the Tethys covered only small area in NW Libya (Haq et al., 1987). This study proposes a depositional model for the Al Aziza Formation comprising of a low energy, inner ramp setting, from intertidal-subtidal carbonate flat to shelf-lagoon palaeoenvironment, based upon field observation (section 4.4).

With reference to the facies analysis (Figs. 4.9 and 4.10), deposition of the Al Aziza Formation represents a relative rise in eustatic sea level and a marine transgression onto the northern Gondwana continental margin. The Al Aziza Formation extends over the entire study area and an isopach map (Swire and Gashgesh, 2004) (Fig. 4.21) indicates thinning over the Al Azizyah fault system southwards from the Jafarah Plain into the Gharian area and across the Ghadamis Basin further south. At this time, the deposition of carbonates facies continued in NW Libya and across Tunisia. However, continental conditions and sediment also continued to exist in the inner areas of Africa (Swire and Gashgesh, 2000 and 2004). This carbonate deposition indicates a maximum transgression, which in turn, probably corresponds to the maximum extensional phase during Late Triassic time.

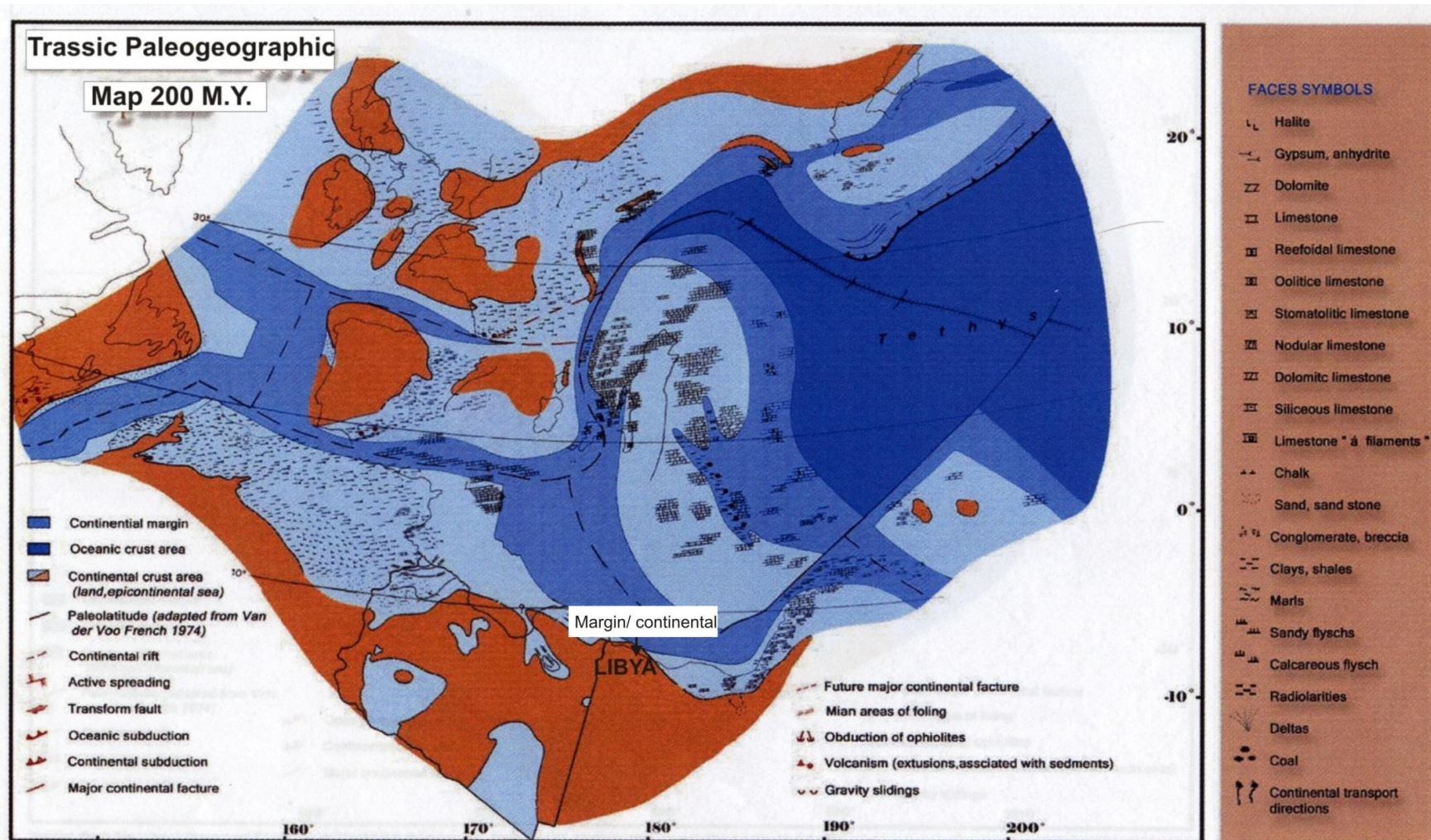


Figure 4.20 Map showing Late Triassic palaeogeography map and tectonic configuration of the southern margin of the Tethys Ocean (El Makrouk, 2004; Biju-Duval et al., 1977).

4.7 Abu Shaybah Formation

4.7.1 Introduction

The Abu Shaybah Formation is exposed along the base of the Jabel Nafusah escarpment from Ar Rabth Gharbiyah village in the west to a point north of Trahunah town in the east (Fig. 4.22). Further west, the Abu Shaybah Formation is reported in the subsurface from a water well near Bir Al Ghanam town and also near the town of Giado (Burollet, 1963; Banerjee, 1980) (Fig. 4.22). The Abu Shaybah Formation in the Gharian area is stratigraphically positioned between the marine Al Aziza Formation below and the marine Abu Ghaylan Formation above. The term ‘Abu Shaybah sandstone’ was first applied by Christie (1966) based upon exposure in the Gharian area. The Abu Shaybah Formation has been studied by Assertor and Benelli (1971) who divided the formation into two units, the lower part was assigned to the upper Triassic whilst the upper part to the lower Jurassic age (see Chapter 3).

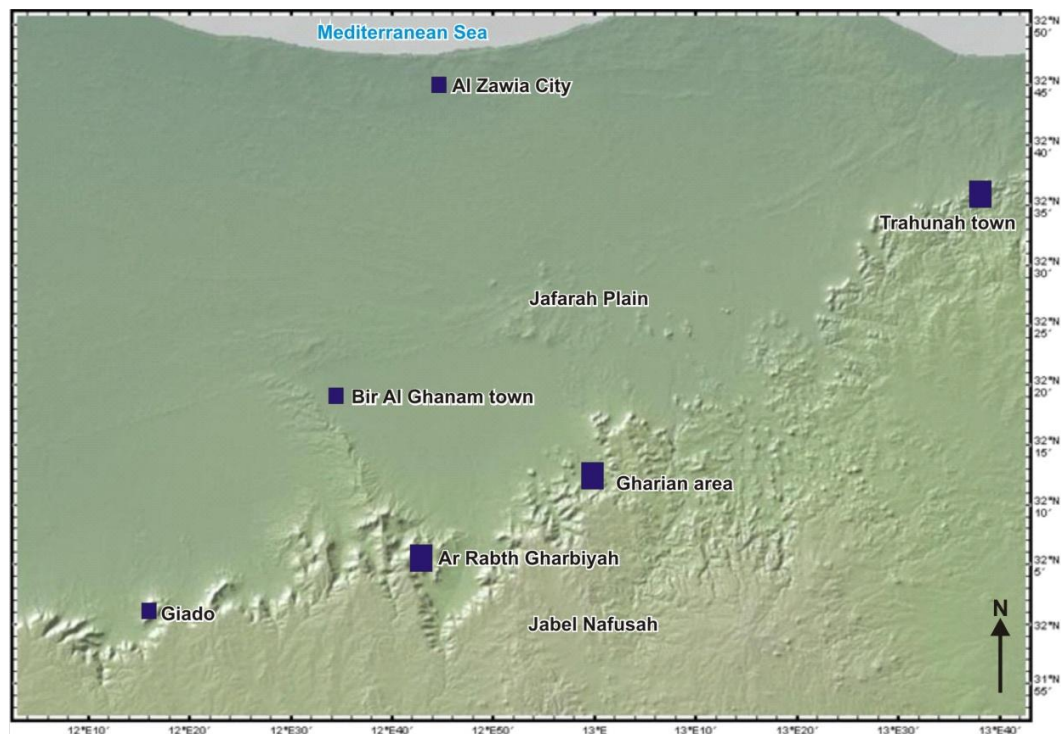


Figure 4.22 DEM map showing the location of the Jabel Nafusah and key villages and towns referred to within the context of the Abu Shaybah Formation.

The Abu Shaybah Formation consists principally of red to yellow, fine to coarse-grained, cross-bedded sandstones, alternating with green and red clays and rare pebble conglomerates. The lower member was interpreted by Assertor and Benelli (1971) as having been deposited in shallow water, neritic, to low inter-tidal or shallow sub-tidal environment while, the upper member was interpreted to have been deposited in a range of arid continental alluvial and coastal/lagoonal settings. Makhlouf (2003; 2006) has used the Abu Shaybah Formation as correlation along the strike between Libya and Jordan. However, these interpretations were based upon very little fieldwork with a limited spatial coverage.

By contrast, in this study, stratigraphically the facies and facies associations are distributed between three units: 1) a lower unit, exposed at Abu Rashada (Wadi Abu Shaybah) and Wadi Gabel, and 2) a middle unit, exposed at the Kabted Jamel section west of the Tripoli-Gharian highway and 3) an upper unit, that is exposed in the Abu Ghaylan area and also west of Abu Rashada road (Fig. 4.23).

A complete 125 m thick section of the Abu Shaybah Formation has been logged and described from the Gharian area in Wadi Abu Shaybah where the base and top of the formation are best exposed (Fig. 4.24). The logged sections and the subsequent facies analysis have been used to describe and interpret the sedimentary processes and environments (section 4.8) and changes in palaeogeography (section 4.9).

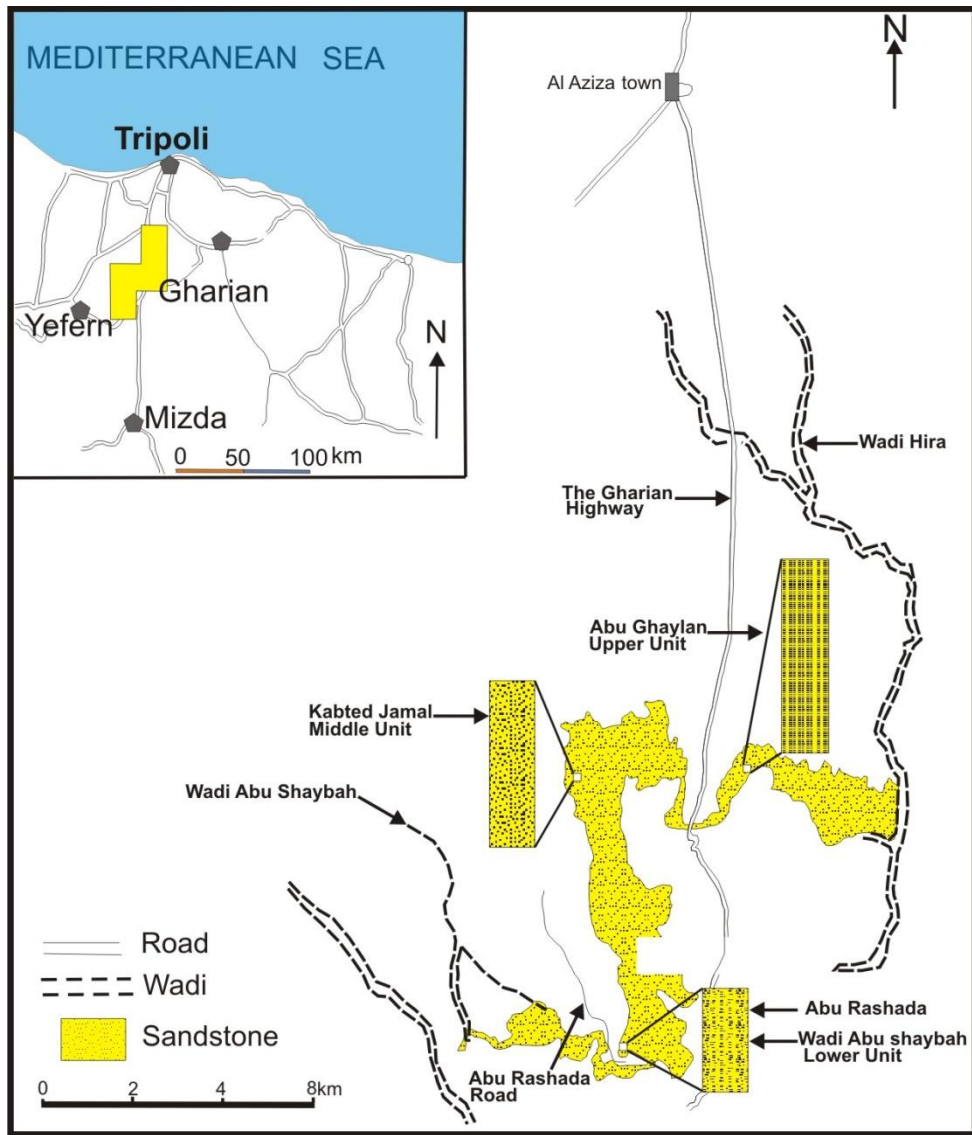


Figure 4.23 Map of the Gharian area showing the outcrop of the Abu Shaybah Formation, its three component units and their type localities as used in this study (modified after Desio et al., 1963).

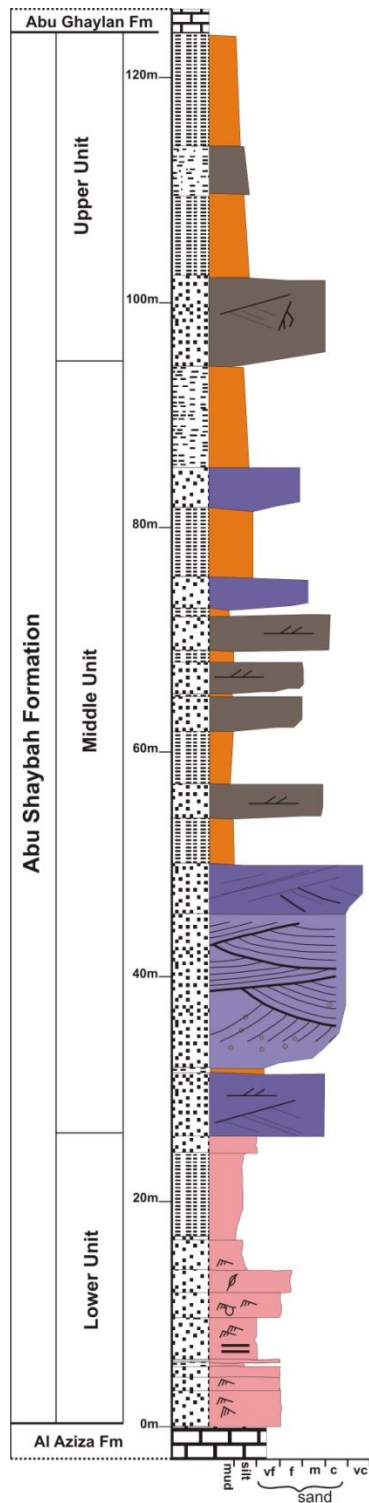


Figure 4.24 Main measured section through the Abu Shaybah Formation exposed in Wadi Abu Shaybah (Fig. 4.25), Gharian area. For key to symbols see Chapter two (Fig. 2.1).

4.8 Facies and Sedimentary Processes of the Abu Shaybah Formation

The field observation and petrographic analysis of eleven outcrops of the Abu Shaybah Formation allowed ten facies to be identified on the basis of the following characteristics: lithology, sedimentary structures, textural features and faunal content. These facies characteristics are summarised within Table 4.3 and are described fully below.

4.8.1 Facies F-SD: Symmetrically Rippled Siltstone and Fine Sandstone

i) Field description

Symmetrically rippled siltstone and fine sandstone is the most commonly occurring facies in the Lower unit. The facies is present in three sections (Wadi Gabel, west of Abu Rashada road and east of Abu Rashada road (Fig. 4.25). The type section for this facies (F-SD) is located to the east and west of the Abu Rashada road (Fig. 4.25). Facies F-SD consists of moderate red (5R 5/4) and grayish yellow (5Y/8/4) coloured, fine-grained sandstone and siltstone. The maximum measured thickness of facies (F-SD) is *ca.* 22 m.

This facies displays cross-lamination (Fig. 4.26A) and symmetrical ripples.

Symmetrical ripples were exposed on bedding plane surfaces. Ripple crests have been observed during the field observation and then analysed for palaeocurrent purposes (Fig. 4.26A and B). Generally, most ripple marks trend E-W. However, a minority of the ripples have a north-south direction (2%). The average thickness of cross-lamination is approximately 2 cm. Tube-like structures are observed within the facies F-SD, exposed on the tops of bedding plane surfaces (Fig. 4.26C). The tube-like structures have a length of *ca.* 0.9 mm and width of < 0.2 mm. These structures are filled with silt and fine sandstone. The tube-like structures possess no branching systems and are infilled with siltstone.

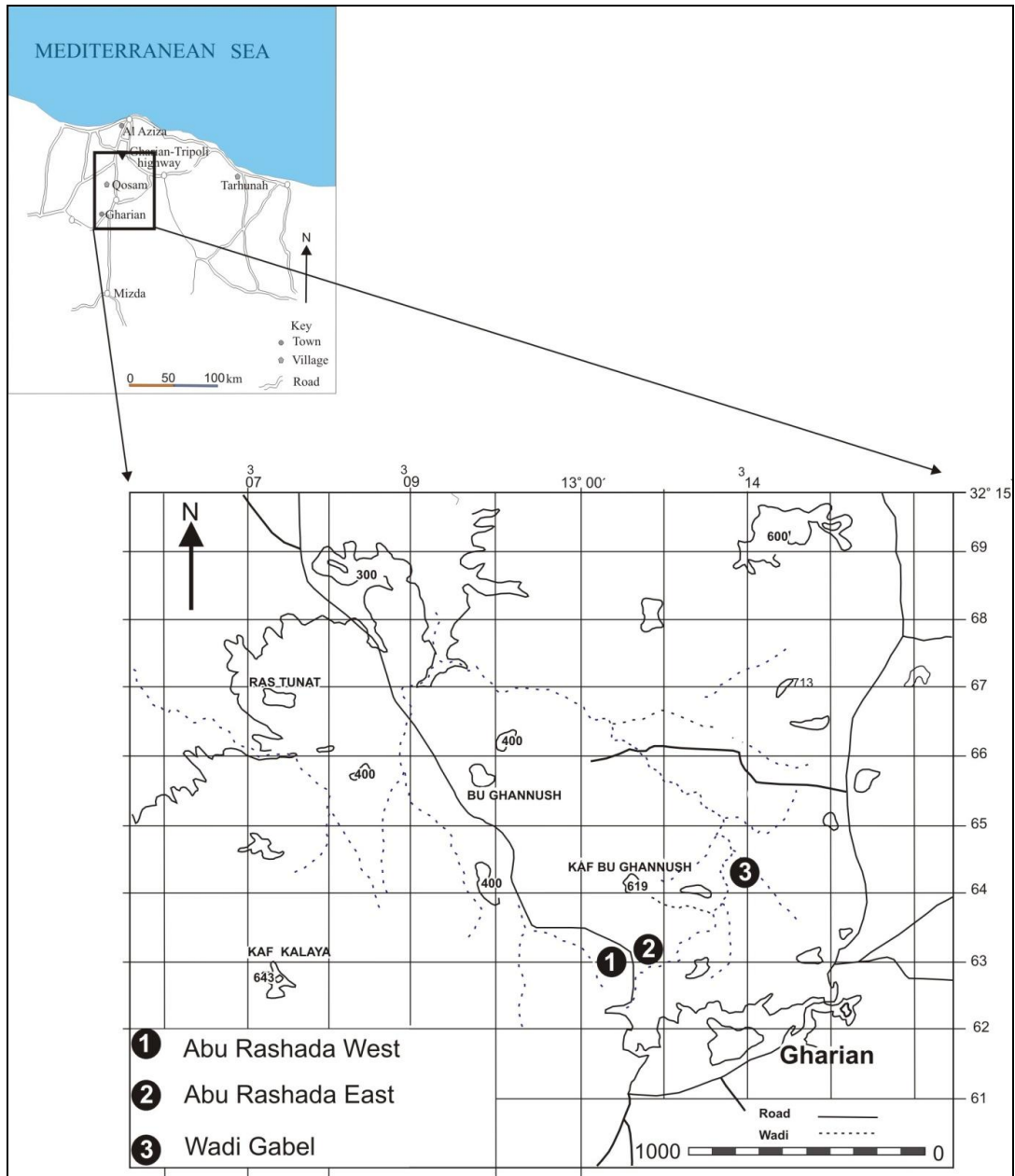


Figure 4.25 Principal localities of facies of the lower unit of the Abu Shaybah Formation. Numbers indicate position of locations discussed in the text.

| Facies code and name | | Description | | | | |
|----------------------|---|---------------------|------------------------------|-----------------------------------|--|--|
| | | Thickness (maximum) | Grain size (Wentworth scale) | Colour (Munsell colour chart) | Sedimentary structures | Fossils and trace fossils |
| 1 | Facies (F-SD): Symmetrically rippled silt stone and fine sandstone | 22 m | Silt to fine sand | 5R 5/4 Moderate red | Symmetrically rippled (2-10 cm thick). Desiccation cracks | Bivalves fragments, burrows |
| 2 | Facies (F-SB): Biotruncated fine grained sandstone | 2.50 m | Fine sand | 5Y 8/4 Moderate orange pink | Structureless | Bioturbation is common. Bivalves fragment |
| 3 | Facies (F-MS): Massive fine to medium sandstone | 2 m | Fine to medium | 5Y 8/4 Grayish yellow | Structureless | None |
| 4 | Facies (F-VC): Sandstone with vug carbonate | 2 m | Fine sand | 10YR 8/6 Pale yellowish orange | Structureless | None |
| 5 | Facies (F-SR): Medium sandstone with rootlets | 10 m | Medium sand | 10 YR 8/2 Very pale orange | Trough cross bedded, The troughs are generally 0.2-0.8 m in width and 0.1-10 cm in height. | Root traces |
| 6 | Facies (F-TS): Trough cross bedded medium to coarse sandstone | 15 m | Medium to coarse sand | 5R 6/6 Light red | Trough cross bedded, The troughs are generally 0.6-5 m in width and 0.1-50 cm in height | None |
| 7 | Facies (F-PS): Tabular cross bedded medium sandstone alternating with pebbles | 18 m | Medium | N9 White | Tabular cross bedded (12 cm in width while 8 cm in height) | None |
| 8 | Facies (F-CS): Medium sand with calcrete | 8 m | Fine to medium sand | 10YR 8/2 Very pale orange | Nodule calcrete | None |
| 9 | Facies (F-MS): Red mudstone | 28 m | Mud | 10 R Moderate reddish brown | Structureless | None |
| 10 | Facies (F-GS): Green mudstone | 14 m | Mud | 10GY 5/2 Grayish green | Structureless | None |

Table 4.3 Summary of the main facies characteristics of the Abu Shaybah Formation in the Gharian area.

In plan view, large polygonal shapes are observed at location ❶ (Fig. 4.25). These polygonal shapes are 3 to 4 cm wide on the surface and up to 0.3 cm deep (Fig. 4.27). These are mostly filled with very fine sand grain and separated from each other by mud. Additionally, some edges of the polygons have been removed (Fig. 4.27B).

Within the sediment, rare casts of fossil shells bivalves are possibly preserved (Fig. 4.28B and C). The casts are small and fragmented. The casts have a diameter of approximately 1.2 to 2.1 cm. They display a 5YR 6/4 light brown colouration and a series of concentric rings/ribs.

Moreover, in plan view, small rectangular shape is observed at location ❷ (Fig. 4.25). This rectangular shape has a diameter of approximately 1.2 cm and a length of 2 to 4.5 cm. It displays 5YR 6/10 pale brown, with rounded ridges and liner ribs (Fig. 4.28A).

ii) Petrographic Description

This facies is represented by five thin sections. Petrographic study reveals that the sandstone comprises fine quartz grains that are angular to sub angular in shape, moderately sorted, with proportions of lithic fragments (Fig. 4.29 and 4.30). Quartz makes up the greatest proportion of the total component (97.2%). Rock fragments are also present and represent about 2.8% of total components. Feldspar comprises < 1% of the grains.

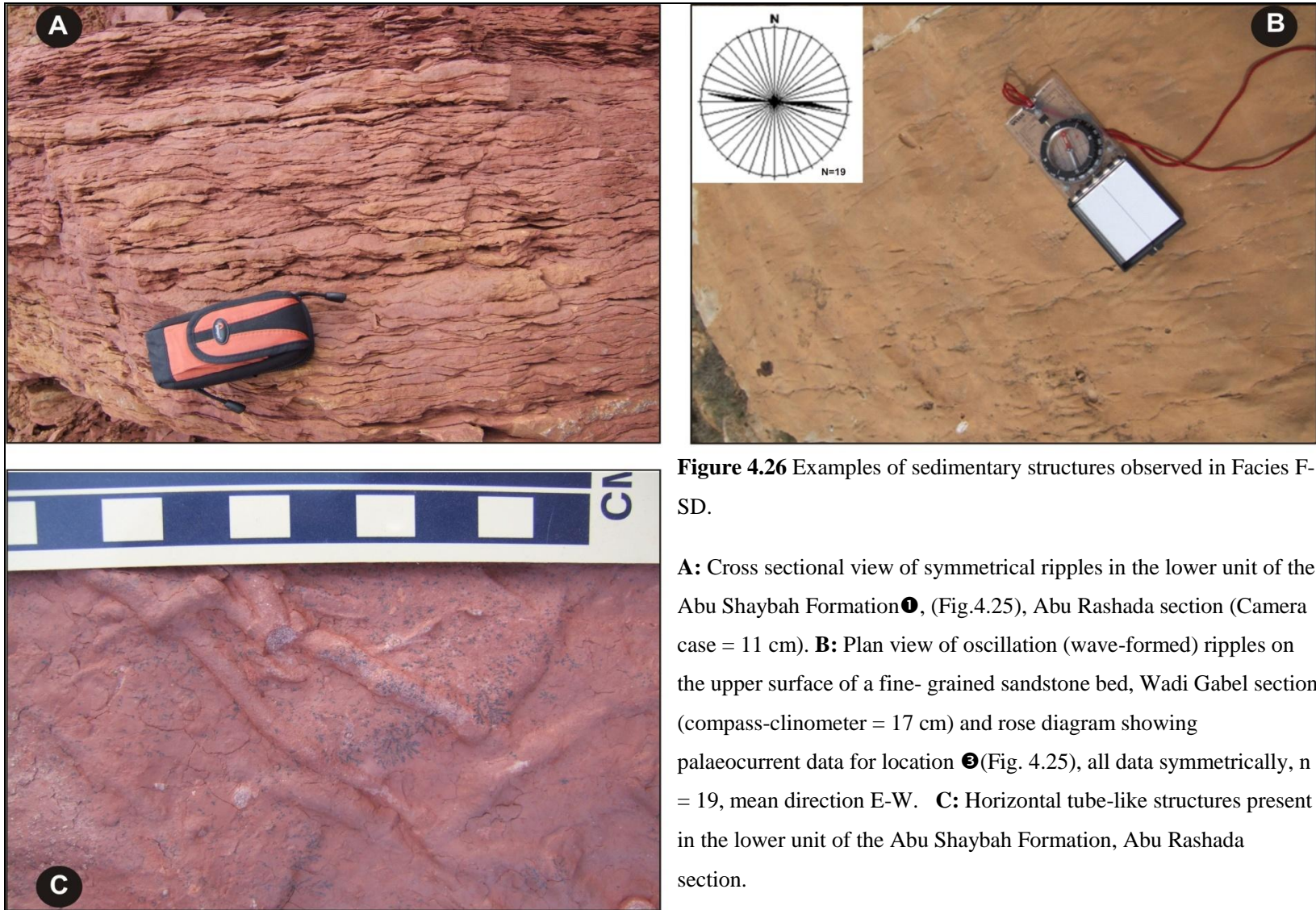


Figure 4.26 Examples of sedimentary structures observed in Facies F-SD.

A: Cross sectional view of symmetrical ripples in the lower unit of the Abu Shaybah Formation ❶, (Fig.4.25), Abu Rashada section (Camera case = 11 cm). **B:** Plan view of oscillation (wave-formed) ripples on the upper surface of a fine- grained sandstone bed, Wadi Gabel section (compass-clinometer = 17 cm) and rose diagram showing palaeocurrent data for location ❸ (Fig. 4.25), all data symmetrically, n = 19, mean direction E-W. **C:** Horizontal tube-like structures present in the lower unit of the Abu Shaybah Formation, Abu Rashada section.



Figure 4.27 Sedimentary features from the facies F-SD. **A and B:** Examples of desiccation cracks exposed on bedding surfaces in the lower unit of Abu Shaybah Formation, Wadi Abu Shaybah section (Pencil = 17 cm long and camera bag = 11 cm long).

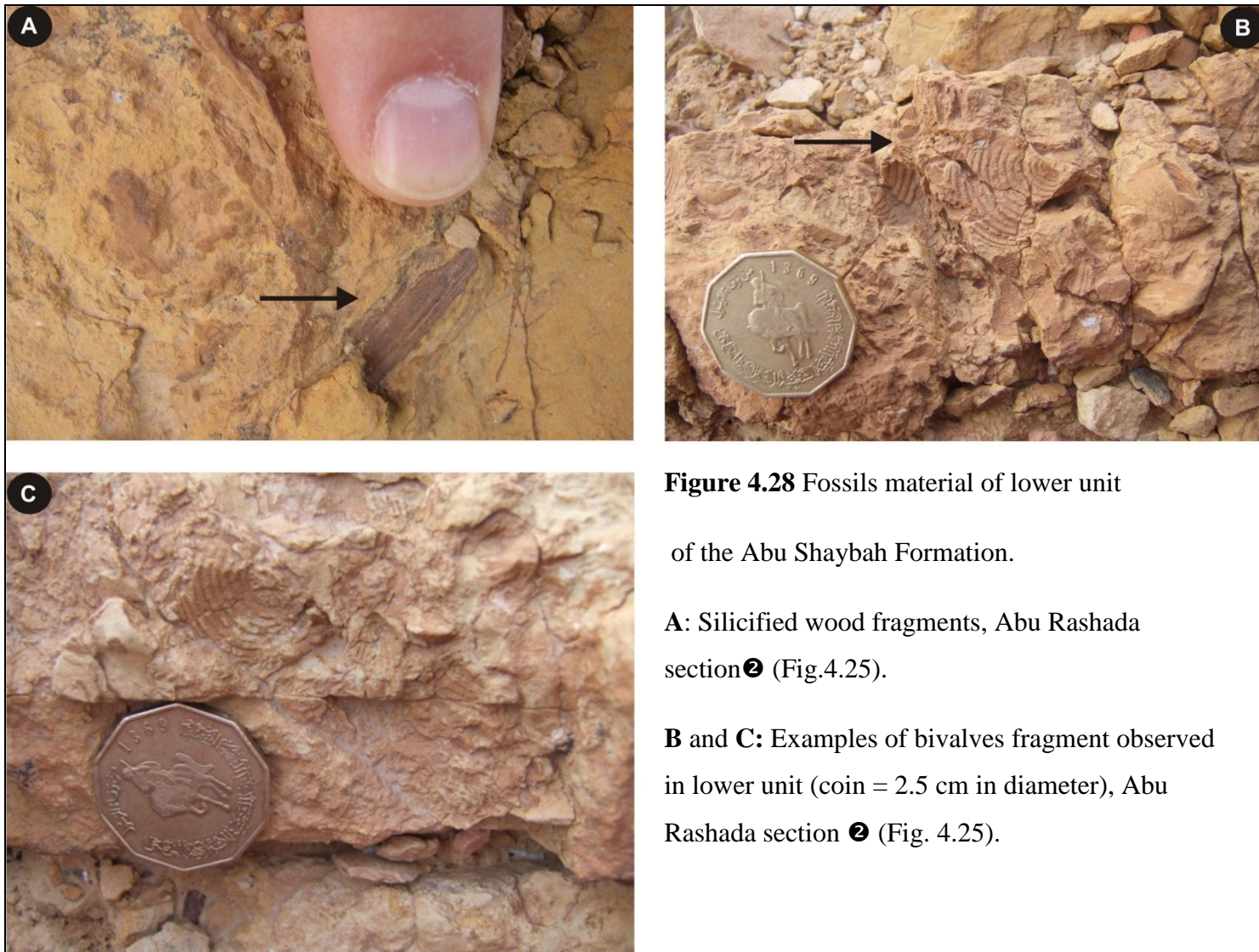


Figure 4.28 Fossils material of lower unit of the Abu Shaybah Formation.

A: Silicified wood fragments, Abu Rashada section ② (Fig.4.25).

B and C: Examples of bivalves fragment observed in lower unit (coin = 2.5 cm in diameter), Abu Rashada section ② (Fig. 4.25).

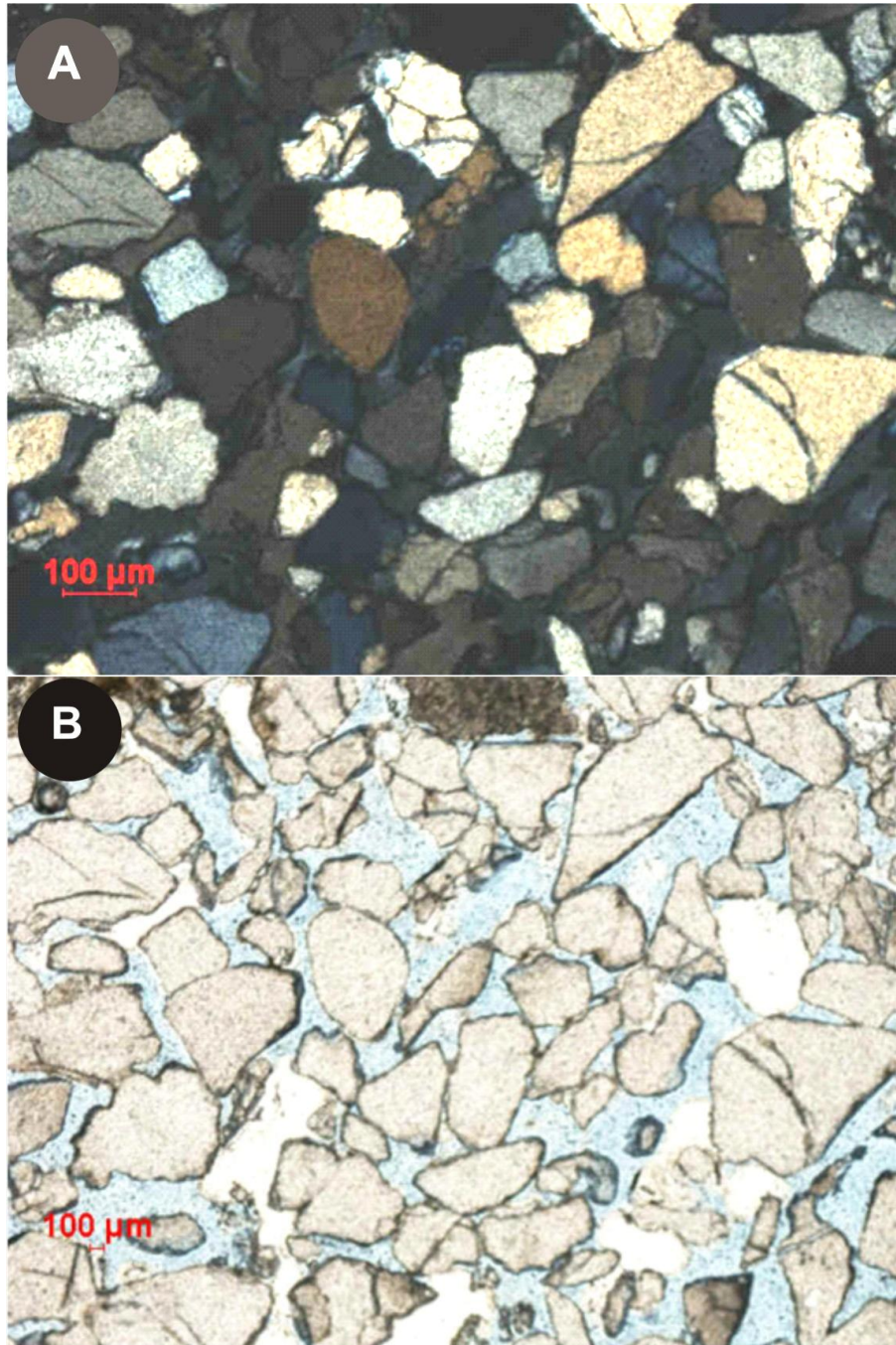


Figure 4.29: Thin section imagery of lower unit of the Abu Shaybah Formation. **A:** Photo micrograph under polars, illustrating moderately well sorted sandstone of sample (AB-30). **B:** Show the textures under plane-polarized light (FOV = x 10 PPL).

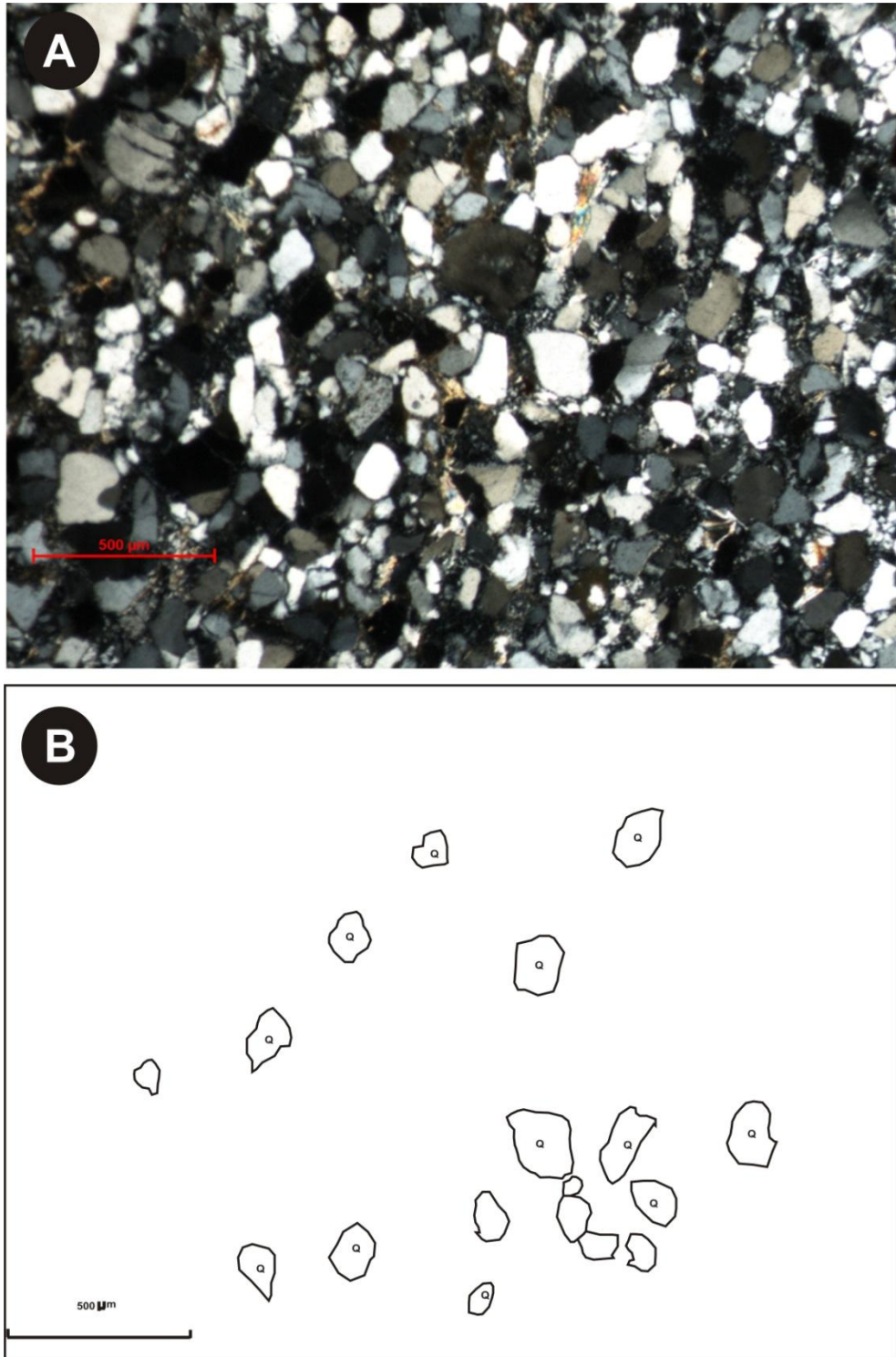


Figure 4.30 Thin sections of lower unit of the Abu Shaybah Formation. **A:** Photo micrograph under cross-polarized light illustrating moderately well sorted sandstone of sample (AB-31). **B:** Shape of grains of the lower unit of Abu Shaybah Formation.

iii) Interpretation

The fine grain size of the sandstone (Fig. 4.29 and 4.30) suggests a low energy sedimentary process, whilst the cross laminations indicate the presence of ripple bed forms. Ripples typically form in shallow water < 1 m depth at flow velocities ranging from 0.2 to 1.0 m/s (see Fig. 2.2) (e.g. Allen, 1965; Harms et al., 1975; Collinson et al., 2006). Symmetrical ripple marks which trend E-W in this facies and are composed of fine-grained sand suggest wave activity related to the oscillatory patterns of water movement close to the water-sediment interface (Allen, 1968). The small scale of the symmetrical ripples together with the fine sandstone-siltstone alternation (Fig. 4.26A) have probably been formed by wind driven waves in relatively short-lived periods of shallow water (a few centimetres) (Harms et al., 1975; Allen, 1968).

The red colouration of facies F-SD may be due to following mechanisms: 1) sub-aerial oxidation of detritus at the depositional site (Turner, 1980); 2) development after burial by the introduction of ferruginous cement; 3) reworking of pre-existing red-bed siliciclastic sedimentary rocks; 4) that the red colour may be due to erosion and re-deposition of red soil sediment (Van Houten, 1948; Krynine, 1948, 1950; Loughnan et al., 1964). The red colour could also suggest post depositional modification with sediments once deposited being characterised by well-drained oxidized conditions with Fe rich ground water movements (Turner, 1980; Nielsen, 2005).

The tube-like structures are trace fossils (e.g. Selley 1985; Retallack, 2001). The trace fossils found in this unit could be burrows because most root traces taper and branch downward and are very irregular in width. Trace fossils always appear in situ and cannot be reworked like other fossils. Burrows are formed in soft sediments and can be found commonly in marine deposits (e.g. Selley, 1976; Boggs, 1987; Bromley, 1996;

Hasiotis, 2004). The tube form is typical of *Skolithos*, an assemblage dominated by simple forms of vertical burrows (Seilacher, 1967; Bromley, 1996). *Skolithos* tend to relate to suspension feeders that normally occupy nearshore zones (Seilacher, 1967; Bromley, 1996; Donovan, 2009). Trace fossil assemblages are influenced by numerous of factors including: 1) the strength of the current, 2) the rate at which sediment is being deposited, 3) oxygen levels in the water, 4) turbidity, which is the amount of fine suspended sediment in the water (Pemberton, et al., 1992).

The example shown in Figure 4.28 suggests possibly two different types of organism. The bivalves are indicative of a marine setting, commonly occurring within a shelf zone (Grill and Zuschin, 2001), whilst the small rectangular shape (Fig. 4.28A) is silicified wood, which is resistant to erosion could suggest transported over long distances (Schoning and Bandel, 2004). Remnants of plant debris suggest supply from a terrestrial setting. Furthermore, Selley (1985) and Voneynatten et al., (1993) proposed that silicified wood indicates current movement. The poor preservation of these silicified wood fragments and bivalves prohibits a more detailed classification.

The polygons are desiccation cracks (Plummer and Gostin 1981; Weinberger, 1999). In plan view, the observed desiccation cracks (Fig. 4.27) can be sub-divided into orthogonal and non-orthogonal systems on the basis of the desiccation crack angles (Lachenbruch, 1962). Desiccation crack formation is influenced by numerous of factors including; 1) rate of initial drying, 2) subaerial exposure time, 3) depth of the water and, 4) direction of surface drainage (Plummer and Gostin, 1981).

The absence of some of the edges of the desiccation cracks (Fig. 4.27B) suggests a preservation issue such as removal by subsequent water current activity. The mud cracks are probably related to the presence of very shallow water depth and also

indicative of periods of partial subaerial exposure (e.g. Allen, 1970; Miall, 1984; Flugel, 2004).

The textural characteristics (size, shape etc) of the very fine sand grains suggest subaqueous grain transport. This is because very fine sand is more easily transported and sorted by water and fine sediments are found in a low energy sedimentary process (e.g. Tucker, 1982; Allen, 1977; Pye, 1994; Selley, 2000).

4.8.2 Facies F-BS: Bioturbated Fine Grained Sandstone

i) Field Description

Facies F-SB is best exposed at localities ❶ and ❷ within the central and northwest part of Wadi Gabel (Fig. 4.25). This facies is generally poorly exposed and comprises fine to very fine-grained sandstone organised into beds up to *ca* 2.50 m thick. The sandstone colour is moderate orange pink (5R 5/4). The lower contacts are sharp to gradational, whilst the upper contacts are sharp and erosive. The sandstone beds appear massive (structure-less) in some cases; however, irregular horizontal bedding is common. The facies possesses a common mottled-like colouration (orange-pink), with mottles arranged into vertical to sub-horizontal orientation (Fig. 4.31A). The mottles are often surrounded by a halo of stronger red colouration commonly occur, particularly with thicker units (Fig. 4.31A).

Very rare moulds of fossil shells are present. The moulds are small (diameter = ≤ 1 cm; length = 0.8 cm) and fragmented. They display a 5 YR 6/4 light brown colouration and also a series of concentric rings and ribs (Fig. 4.31B). These moulds are rounded and angular in shape and are similar to features found within facies (F-SD). These types of

features have only been observed within a limited number of exposures along Wadi Gabel.

ii) Interpretation

Due to the fine-grained nature and uniformity of this sediment it is interpreted as having been deposited from low energy conditions. The mottling can be interpreted as bioturbation or soil development (Holmes, 1995). Although field observation did not unequivocally identify evidence for rootlets in this facies. In this case the extensive degree of mottling appears to have occurred following several depositional events and thus, could relate to water table fluctuations (Arndorff, 1993; Holmes, 1995). The presence of beds containing burrows (infaunal feeding and /or dwelling activity) suggests that deposition took place in very shallow water (Abdul Aziz et al., 2003). The strong bioturbation suggests slow sedimentation and little physical reworking whilst the overlying structureless sandstone within the facies suggests that unit formed by strong currents. Moreover, extensive bioturbation may be responsible for the massive nature of the fine sandstone unit having destroyed any bedding of sedimentary structures (e.g. Klein et al, 1963).

The moulds of fossils shells within this facies are shell fragments of bivalves. The poor preservation of the bivalves fragments prevents a more detailed classification. The shape of some of the bivalves fragments (Fig. 4.31B) suggests transported by water. The fine to very fine-grained sandstone and bioturbation probably relates to the presence of shallow water (Bromley, 1990; Hasiotis, 2004; Hertweck et al., 2007).

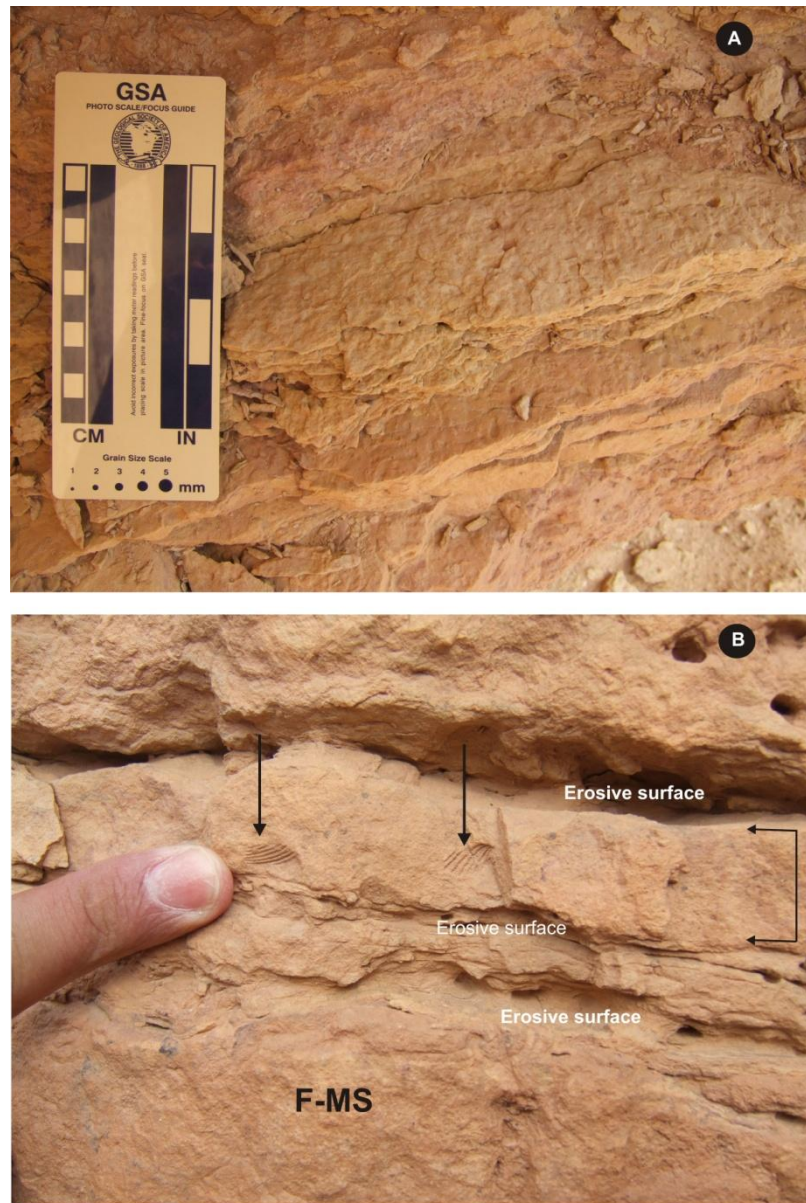


Figure 4.31 Sedimentary structures and fossils are observed in the lower unit of the Abu Shaybah Formation. **A:** Extensively bioturbated fine sandstone facies (F-BS); **B:** Species of bivalves in facies (F-BS) (black arrows).

4.8.3 Facies F-MS: Massive Fine to Medium Sandstone

i) Field Description

This facies occurs at locality ② and ③ (Fig. 4.25). Facies (F-MS) consists of grayish yellow (5Y 8/4), fine to medium grained sandstone. The maximum thickness of Facies F-MS is *ca.* 2 m. The contacts between this facies and all other facies are sharp.

Moreover, this facies can be divided into sub-facies based on grain size and thickness.

At Wadi Gabel the sandstone facies is capped by a weathered surface, whilst at two other sections (Wadi Gabel and Abu Rashada) it is capped by a clay facies (F-GS). The sandstone is massive with no visible sedimentary structures.

ii) Interpretation

The massive sandstone suggests that sediment is deposited from suspension or from highly concentrated sediment dispersions during sediment gravity flows (e.g. Boggs, 1987; Collinson and Thompson, 1989). The sandstones were probably deposited under low energy conditions and the absence of any sedimentary structures in the facies is interpreted to be a product of weathering rather than an indication of truly massive sandstone, which are typical the product of turbidity or gravity flows (Walker, 1984). Furthermore, the lack sedimentary structures within the facies suggests that 1) a bed may be massive due to diagenesis, or 2) that primary sedimentary structures may have been completely destroyed during deposition, 3) a bed may be massive due to extensive bioturbation and 4) intensive weathering (Selley, 1976).

4.8.4 Facies F-VC: Sandstone with bioturbated and Vuggy Carbonate

i) Field Description

This facies was observed only at location ⑤ (Fig. 4.25) (west and east of the Wadi Gabel section). It consists of pale yellowish orange (10YR 8/6) fine grained-sandstone with small holes in the top surface (Fig. 4.32). The holes have diameter of approximately 1.1 to 3.4 cm. This facies contains no visible sedimentary structures. The maximum measured thickness of Facies F-VC is *ca* 0.50 m. The holes are commonly filled with white (N9) dolomite and /or light brown (5YR 6/4) calcite, with minor mounts of quartz. This facies was used as a marker horizon between two sections in the

Wadi Gabel (see Fig. 1 in Appendix 2). At the eastern end of the Wadi Gabel section the facies is capped by very fine sand stone and silt facies (F-SD).

ii) Interpretation

The fine grained sand in this facies suggests that deposition occurred under lower energy whilst the absence of any sedimentary structures suggests limestone and dolomites have been extensively recrystallized (Selley, 1976). The pale yellowish orange can be interpreted as bioturbation or soil development. The holes infilled with calcite / dolomite / quartz are interpreted as vugs. Vug development is not often addressed in sandstone research. Vugs can be related to presence of water, with a tectonically and topographically driven fluid being the most likely alternative to explain the calcite dissolution and recrystallisation (Vandeginste et al., 2006). Furthermore, cements in the vugs are probably precipitated from warm saline groundwater. However, this facies is situated in the northeast of the Wadi Gabel, 0.5 km south from igneous intrusion (see Chapter 3, Fig. 3.6). Therefore, the vugs could be due to fluid migration linked to the igneous intrusion.

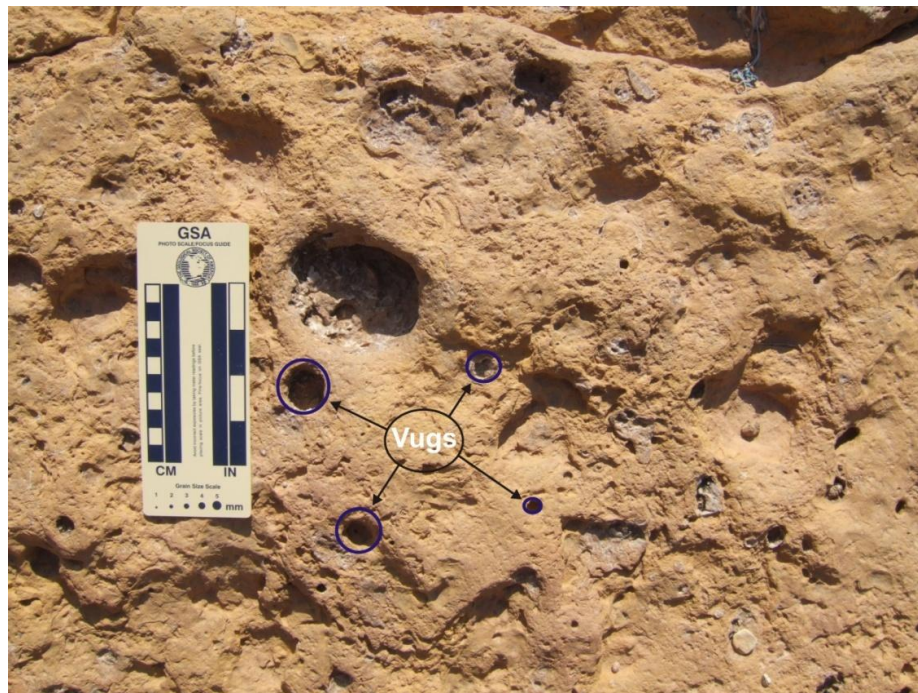


Figure 4.32 Sandstone with vug carbonate facies (F-VC) is observed in the lower unit of the Abu Shaybah Formation.

4.8.5 Facies F-SR: Medium Sandstone with Rootlets

i) Field Description

Facies F-SR is observed at localities ⑥ and ⑦ (Fig. 4.33). The facies consists of very pale orange (10 YR 8/2) coloured, fine to medium grained sandstone that is poorly cemented (Fig 4.33A). The maximum thickness of facies (F-SR) is *ca.* 8 m. The most common structures are trough cross-bedding and various vertical tube-like structures (Fig. 4.34B). In section, the trough cross-bedded foresets are organised into sets up to 8 cm thick (Fig. 4.34C). The trough-cross bedding was not observed in plan view.

There are three types of tube-like structures observed in this facies. The vertical tubes in Figure 4.35A are finger-like and branch down from a single column. The single column diameter is approximately 5.2 cm and length is 8 cm on the surface and the individual fingers are 2.2 cm wide and 3 cm long. The second type of vertical tube observed in Figure 4.35B is a single column 11 cm long and 3 cm wide with no branching structures. Several sub-horizontal (most common) to vertical tubes are also observed (Fig. 4.35C). The length of these horizontal tubes is in the range of 1 to 4.5 cm. Overall, these tube-like structures are a uniform colour of ranging from moderate orange pink (10 R 7/4) to pale yellowish orange (10 YR 8/6).

ii) Petrographic Description

Petrographic analysis reveals that vertical tube structures consist of carbonaceous mudstone. There is also fine to medium-grained quartz present within those thin sections (Fig. 4.36 and 4.37). Quartz is sub-angular to sub-rounded and is less abundant than the mud.

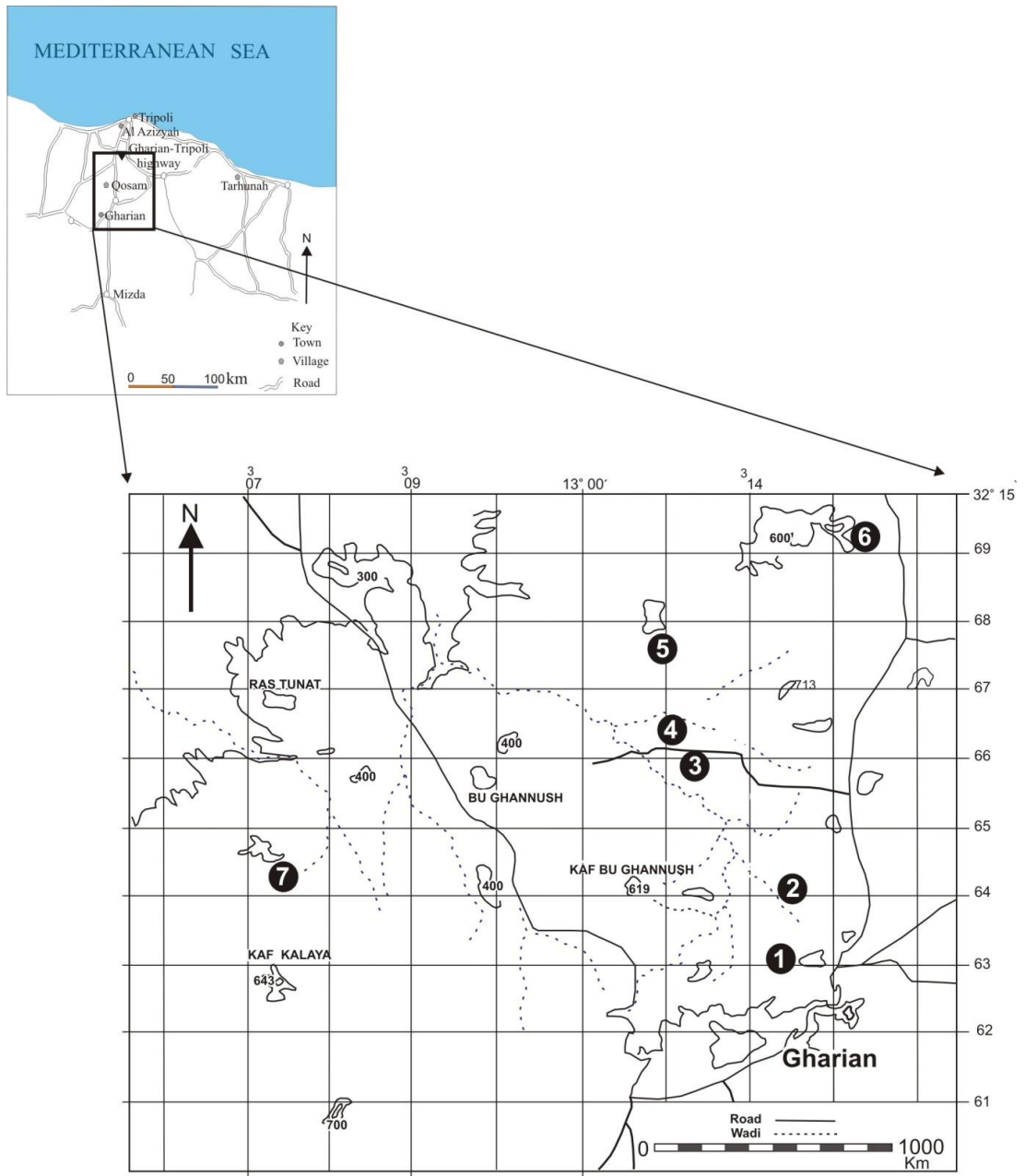


Figure 4.33 Map showing the outcrop of facies of the middle and upper unit of the Abu Shaybah Formation. Numbers indicate position of locations discussed in the text.

Moreover, all tube-like structures have been filled by moderate orange pink (10 R 7/4) sandstone of the same size as that surrounding the casts. Some casts also contain a narrow core of calcite (Fig. 4.36 and 4.37).

ii) Interpretation

The grain size of this facies indicates medium energy deposition whilst the trough cross-bedding suggest unidirectional sediment transport as dune-scale bed forms. The orientations of trough cross bedding indicates deposition by currents flowing towards the northwest (Fig. 4.38). However, a scatter of palaeoflow directions is also present, especially in the upper parts of sections where this facies is observed (Fig. 4.40).

The tube-like structures in the facies are interpreted as roots. Root systems of plants disrupt the internal structures of beds and root traces are preserved either as carbonaceous films or as casts (Tucker, 1982; Bridge, 2003; Reading, 1996). Retallack (2001) has classified similar root systems to those found in the field area as rhizoconcretions. The rhizoconcretions can form in several ways: 1) the root dies and the hole is filled with other materials such as calcium carbonate and iron oxyhydrates; 2) rhizconcretions also from by biologically mediated roots. Furthermore, roots could also alter the local chemical microenvironment, with gleying associated with anaerobic decay of root material after burial below the water table (Retallack, 1988).

A low percentage of rootlets in this facies could indicate that the roots formed under semi-arid to arid conditions, facies suggesting an area with sparse vegetation (Schmid et al., 2006). Equally, limited occurrence could reflect a preservation issue. The rootlets may relate to palaeosol formation being formed when the basin was active (Kearsey, 2009). In addition, the reddish colour of these drained root indicates their formation occur under well drained oxidizing conditions.

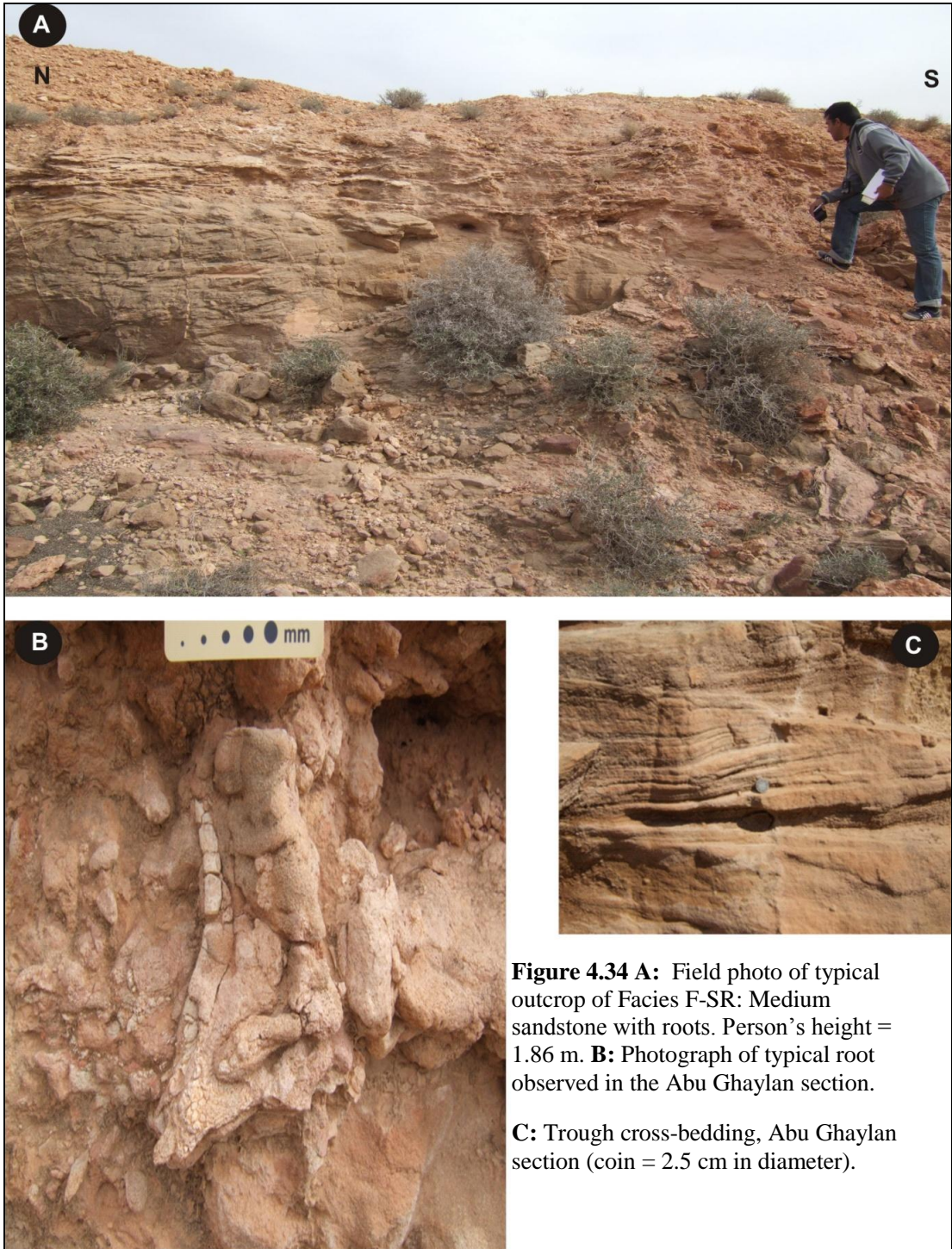


Figure 4.34 A: Field photo of typical outcrop of Facies F-SR: Medium sandstone with roots. Person's height = 1.86 m. **B:** Photograph of typical root observed in the Abu Ghaylan section.

C: Trough cross-bedding, Abu Ghaylan section (coin = 2.5 cm in diameter).

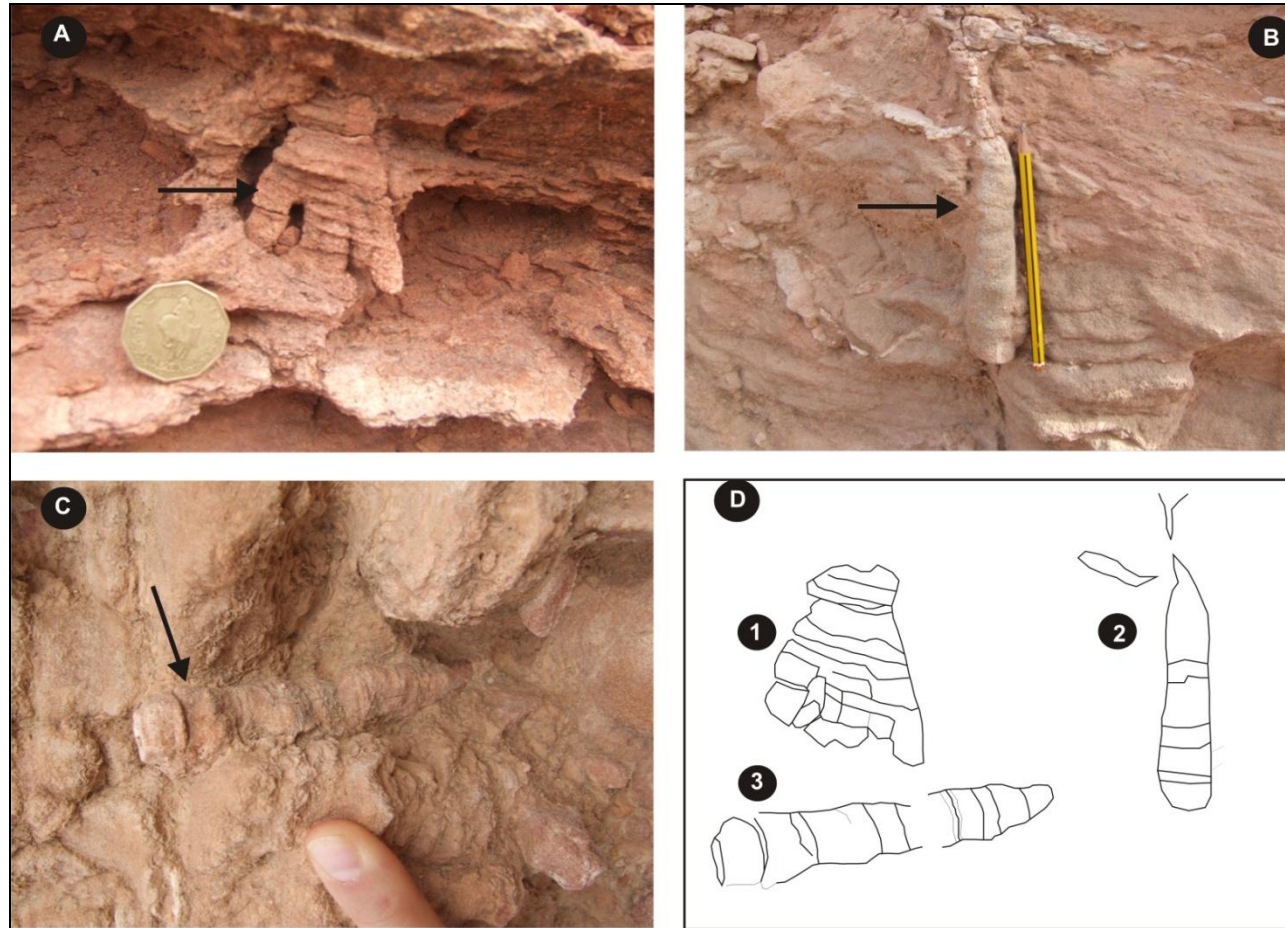


Figure 4.35 Root traces in the Abu Shaybah Formation. **A:** Root are branching (coin = 2.5 cm in diameter).
B: Vertical root (pen = 17 cm long). **C:** Sub- horizontal root found in the middle unit of Abu Shaybah Formation.
D: Sketches of three types of roots.

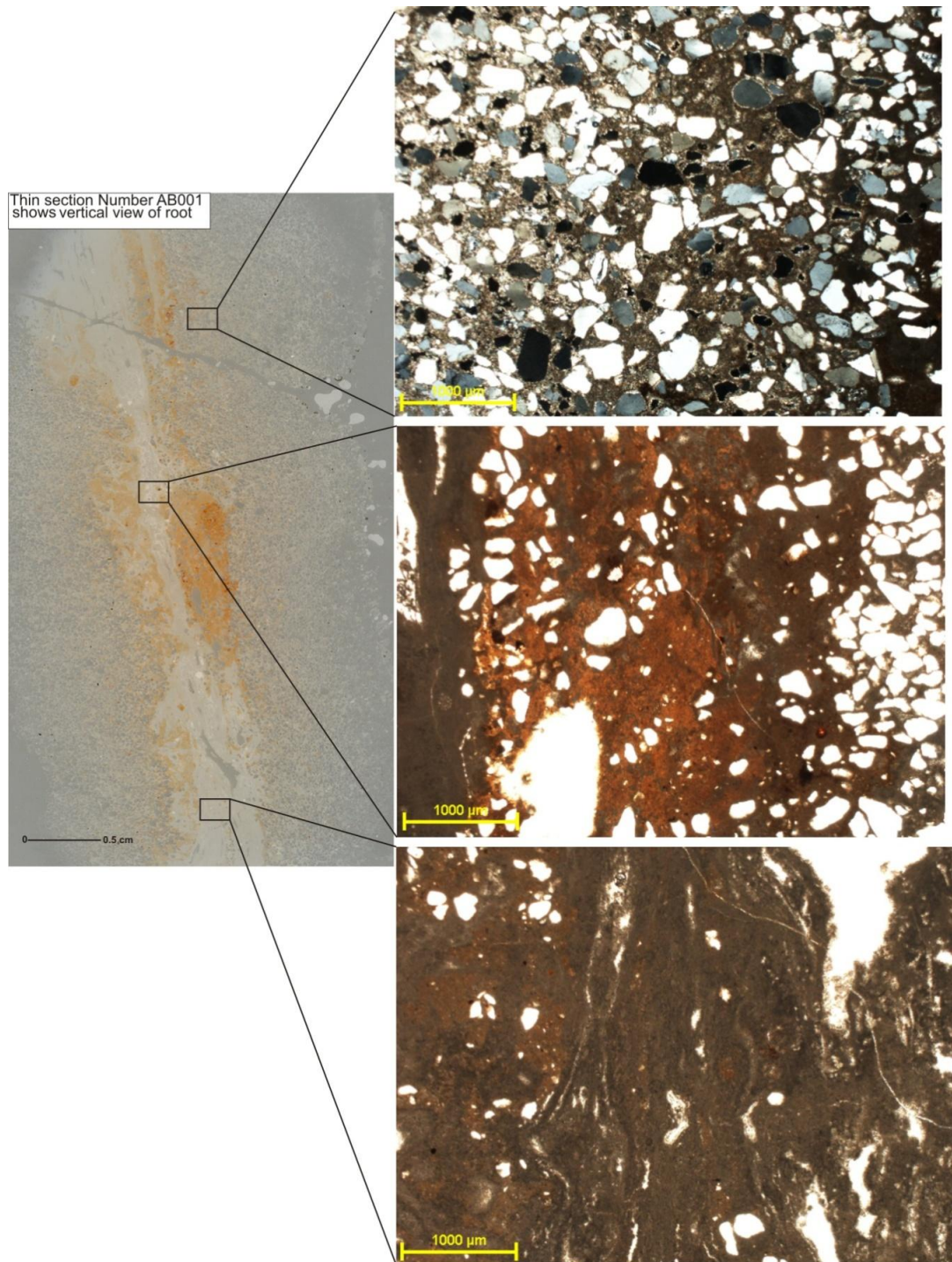


Figure 4.36 Vertical view of root from facies (F-SR) under cross polarized and thin section consists of dark area of mottled clays and iron oxides and quartz grains (FOV = x 10 XPL).

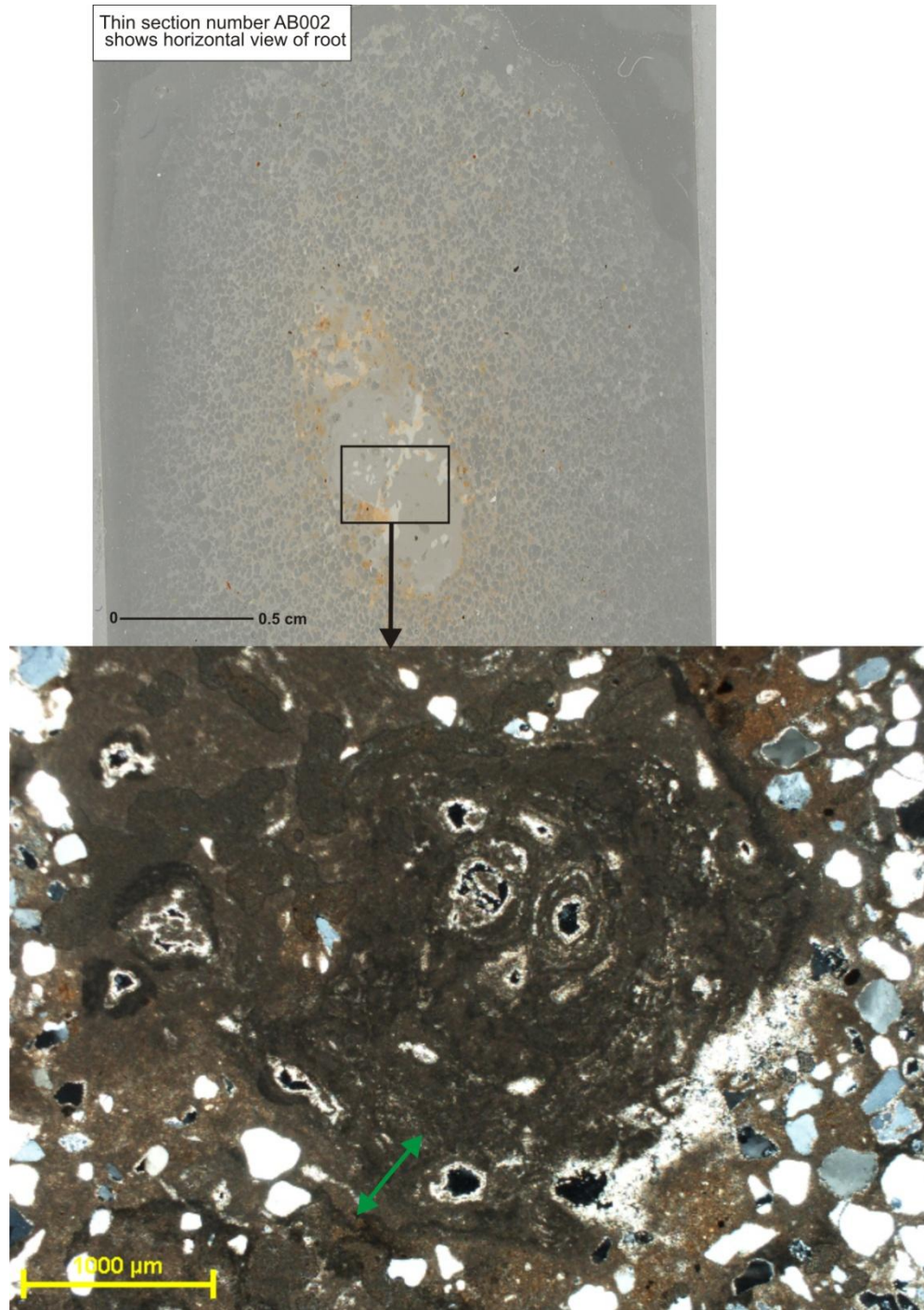


Figure 4.37 Horizontal view of root from facies (F-SR) under cross polarized and thin section consists of dark area of mottled clays (see arrow) and iron oxides and quartz grains (FOV = x 10 XPL).

4.8.6 Facies F-TS: Trough Cross-Bedded Medium to Coarse Sandstone

i) Field Description

Facies F-TS is well represented by thick beds (2 m) composed of one, few or many beds. This facies is the most commonly occurring facies in the middle unit of the Abu Shaybah Formation (see section 4.9.2, Fig. 4.54) and it is present in every single section exception four sections. This facies occurs at locality ④ Kabted Jamel section (Fig. 4.33), where it forms a poorly cemented unit up to 12 m in thickness. The facies comprises light red (5 R 6/6) coloured medium to coarse grained sandstone that displays trough cross bedding (Fig. 4.38A and B).

The sandstone is dominated by trough cross-stratification with set thickness of 0.45 m and sets also can be traced laterally to the limit of palm tree section (≤ 35 m). The trough cross bedding can also be observed in plan view, exposed on eroded bedding plane surfaces (Fig. 4.38B). The tops of curved foresets can be observed forming distinct adjacent sets that range from 0.6 m to 0.95 m wide and several metres long. Palaeocurrent measurements obtained from trough axes show a general transport direction towards the northwest (Fig. 4.40). Some sandstone in this facies has spheroidal structures. The spheroidal structures have a diameter of approximately 0.1 to 2 cm (Fig. 4.38 E and D), and colour is N9 white on fresh surfaces whilst 10R 6/6 moderate reddish orange where weathered and very fine to fine grained sandstone. No fossils or bioturbation were observed in this facies.

ii) Petrographic Description

This facies is represented by five thin sections. Petrographic analysis revealed well sorted, clast-supported sub-angular to sub-rounded quartz grains (Fig. 4.39). This facies is composed almost entirely of quartz grains that make up approximately 96% of the

grain composition components. Quartz grains are present in both mono and polycrystalline forms and silica cement consists of quartz. Rock fragments comprise less than 4% of the grains.

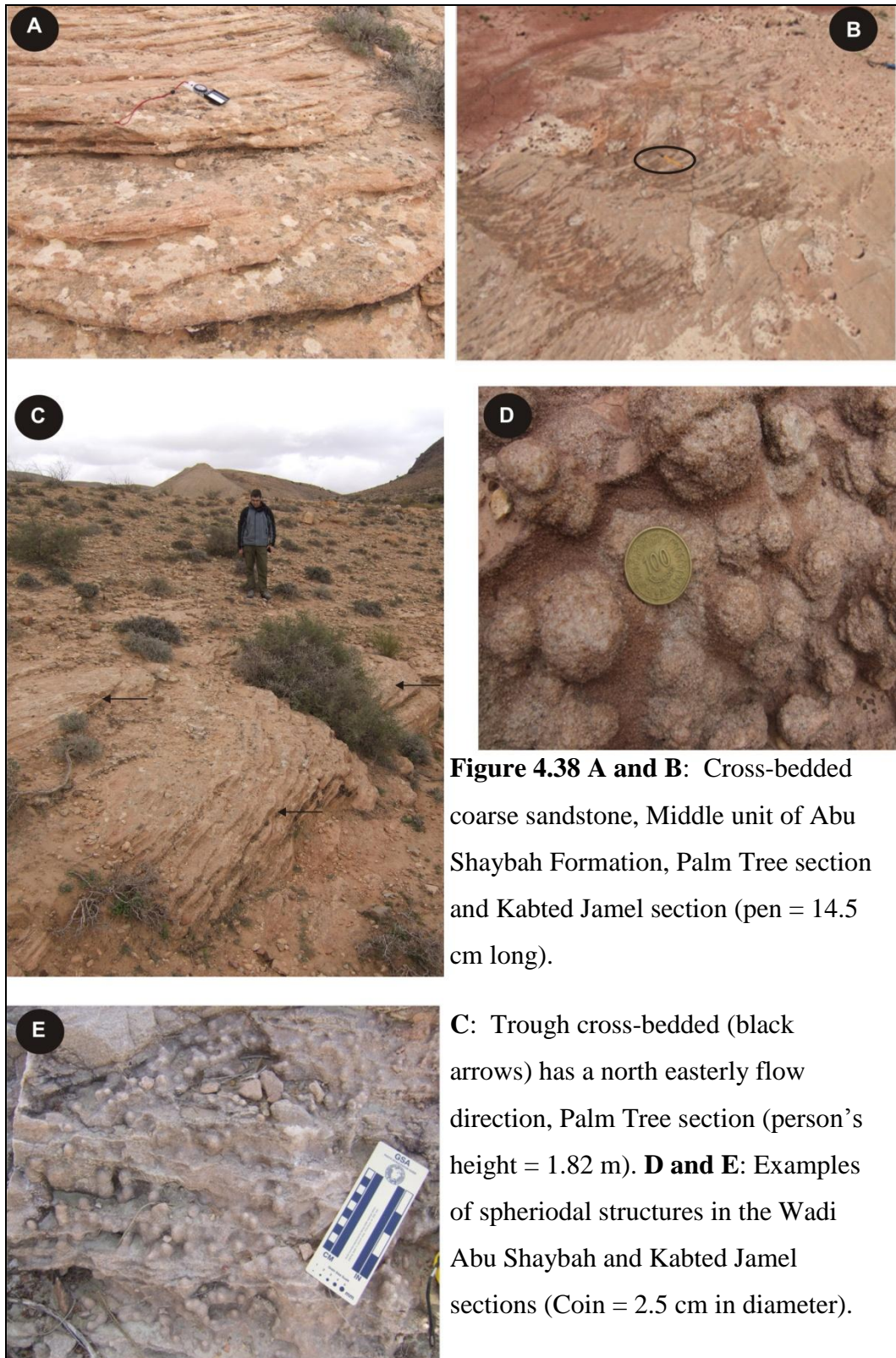


Figure 4.38 A and B: Cross-bedded coarse sandstone, Middle unit of Abu Shaybah Formation, Palm Tree section and Kabted Jamel section (pen = 14.5 cm long).

C: Trough cross-bedded (black arrows) has a north easterly flow direction, Palm Tree section (person's height = 1.82 m). **D and E:** Examples of spheroidal structures in the Wadi Abu Shaybah and Kabted Jamel sections (Coin = 2.5 cm in diameter).

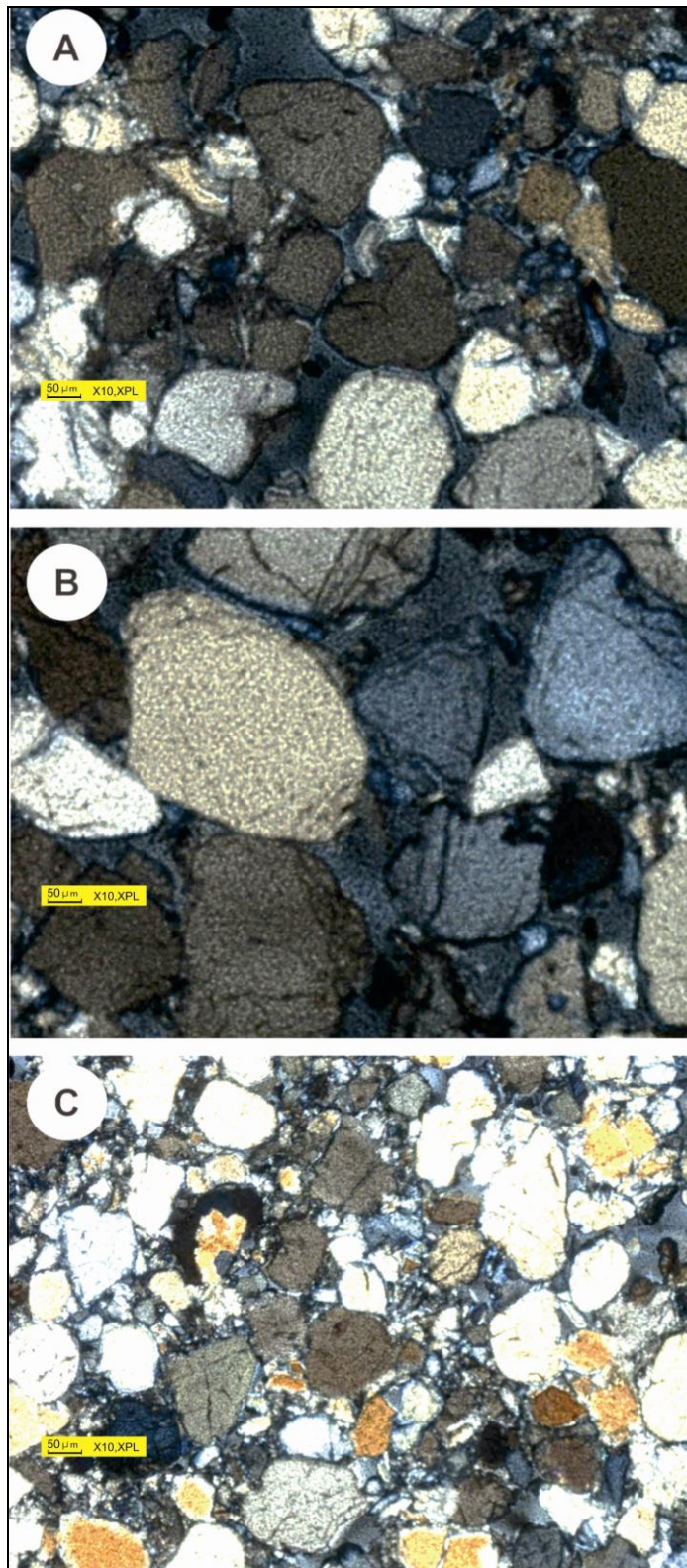


Figure 4.39 Thin sections of the Abu Shaybah Formation from for facies (F-TS). **A, B** and **C**: Photomicrographs of samples (AB-31, AB-32 and AB-33) taken under crossed polarized showing that facies (F-PS) consists of quartz arenite (FOV = X 10 XPL).

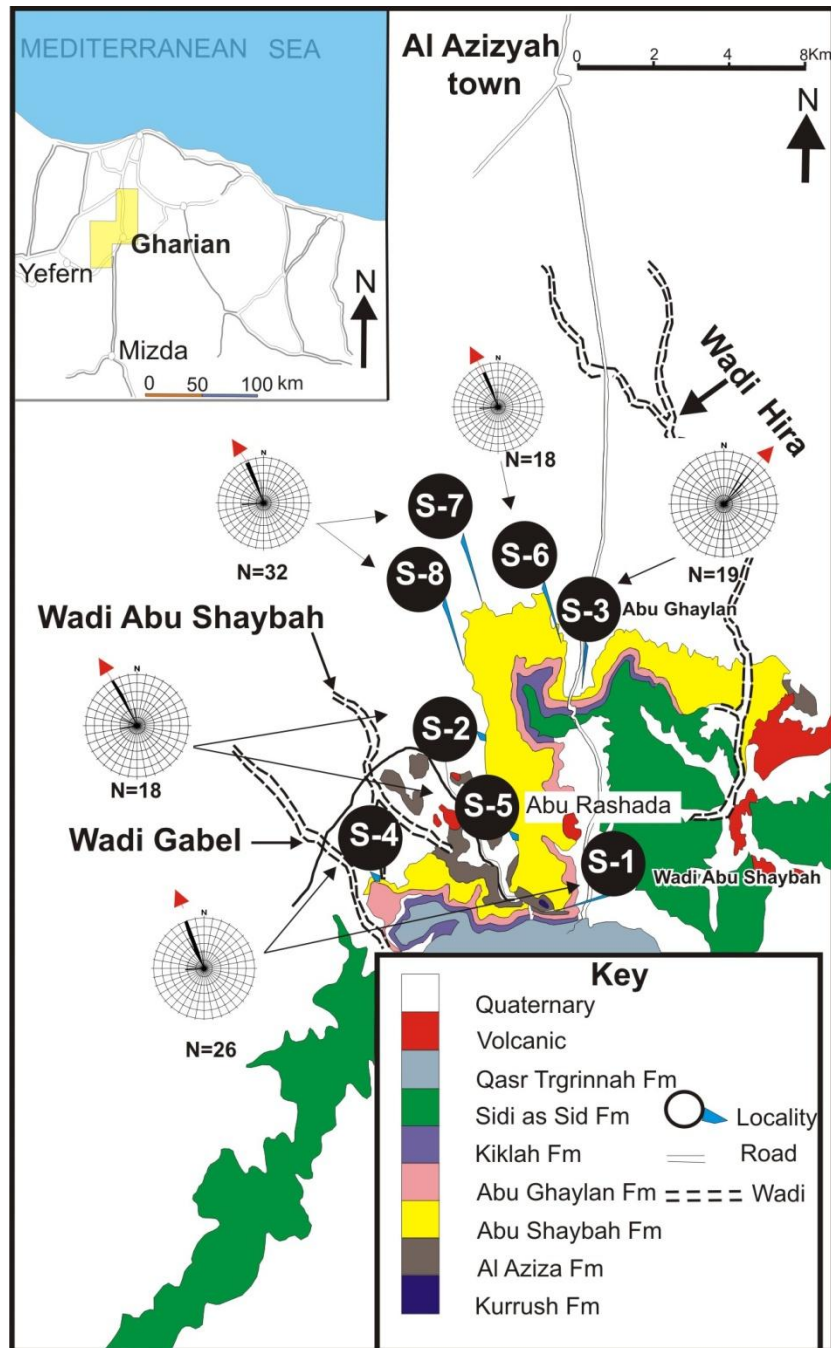


Figure 4.40 Palaeocurrents measured from Abu Shaybah Formation, location numbers and the numbers of data points are given for eight stations. All palaeocurrent measurements were derived from cross-bedding.

ii) Interpretation

The trough cross-bedding suggests unidirectional sediment transport as dune-scale bed forms. Moreover, the thickness of the trough sets suggests a minimum average flow depth, thus the depth of the flow regime must exceed the maximum thickness of trough set and flow level is several times the height of sand dunes (Harms, et al., 1975). The textural characteristics of the sand grains (size, sorting, shape etc) suggest subaqueous grain transport (Allen, 1970). The organisation of the sandstone into stacked and laterally adjacent sets of trough cross beds suggests infilling of a large channel-like feature by subaqueous dunes, within a low-sinuosity river (Miall, 1977; Simpson, et al., 2008). The coarse grain sizes of trough cross-beds from the upper part of the unit suggest sediment supply by upper flow regime conditions (Fielding, 2006). Cross bedding axis orientation indicate a dominant north-westerly flow direction. A minor north easterly flow direction is also present, especially in the upper part of this facies at Palm Tree section (Fig. 4.40 S-3).

The spheroidal structures (Fig. 4.38 D and E) suggests that the sandstones have on orbicular weathering surface, formed by differential erosion around more intensely cemented nuclei (Asserto and Benelli, 1971). The rate of spheroidal weathering is related to the mechanical properties of rocks (Fletcher et al., 2006).

4.8.7 Facies F-PS: Tabular Cross-Bedded Medium Sandstone alternating with Pebble

i) Field Description

Facies F-PS has been observed at localities ③, ④ and ⑤ (Fig. 4.33). The measured thickness of this facies is in ranges from 2 to 18 m (Fig. 4.41). Facies F-PS consists mainly of fine to medium grained sandstone, alternating with pebbly sandstone. The

colour is white N9 on fresh surfaces and very pale orange (10YR 8/2) where it is weathered. The quartz pebbles are in range of 2 to 3 cm in diameter and are grayish orange pink (10R 8/2) to moderate orange pink (10R 7/2). Many of these pebbles are very rounded or subrounded in shape. The pebbles are of quartz composition and have distinct polished surfaces (Fig .4.41 B). Cross bedding is the main sedimentary structure in this facies. In cross-section, the tabular cross beds are arranged into sets up to 0.60 m thick (Fig. 4.41C) with an average of 1 m.

Typical channel sand bodies are up to 0.80 m thick and tens of meters in lateral extent (Fig. 4.42A), are observed in the Kabted Jamel section ④ (Fig. 4.33). The channels are in-filled by cross-bedded fine to medium-grained sandstones bounded by erosive bases. Each channel is separated by mudstones facies. The tops of the channels are flat to slightly irregular. Within a channel sandstone body, the beds of sandstone are usually 0.60 to 1 m and fining-upwards grain size can be observed in this facies (Fig. 4.43A).

ii) Petrographic Description

This facies is represented by five thin sections. Petrographic study of the sandstone reveals poorly-to-moderately sorted, clast-supported sub-angular to sub-rounded quartz grains (Fig. 4.44). Most of the sandstone samples are dominated by quartz grains. Quartz makes up approximately 97 % of the grains. The quartz occurs as both monocrystalline and polycrystalline from. Feldspar is not common in the sandstone of the facies (F-PS) and represents about 1 %. Rock fragments comprise less than 2% of the grains.

ii) Interpretation

The textural characteristics of the sandstone grains (size, sorting, shape, etc) suggest high energy subaqueous grain transport, whilst moderately sorted quartz arenites with minor amounts of pebbly suggests deposition with a high energy. Pebbles with polished surfaces suggest reworked and transported by the fluvial system (Rodriguez-Lopes, et al., 2010).

Small to medium tabular sets of cross-bedding are produced by either straight-crested, dunes, bars and chute bars (Collinson and Thompson, 1989). The orientation of cross bedding indicates a dominant north-westerly flow. The channel probably records the transverse to linguoid bar of a stream (Fig. 4.42B); this is supported by medium-scale trough cross- stratification and medium grained sandstone, alternating with pebbly sandstone (Allen, 1965). Friend et al., (1979) have classified similar types of channel to those found in the field area as ribbon channels (Fig. 4.42B). The ribbon characterized by an abundance of linguoid bar and dune deposits (planar and trough stratification).

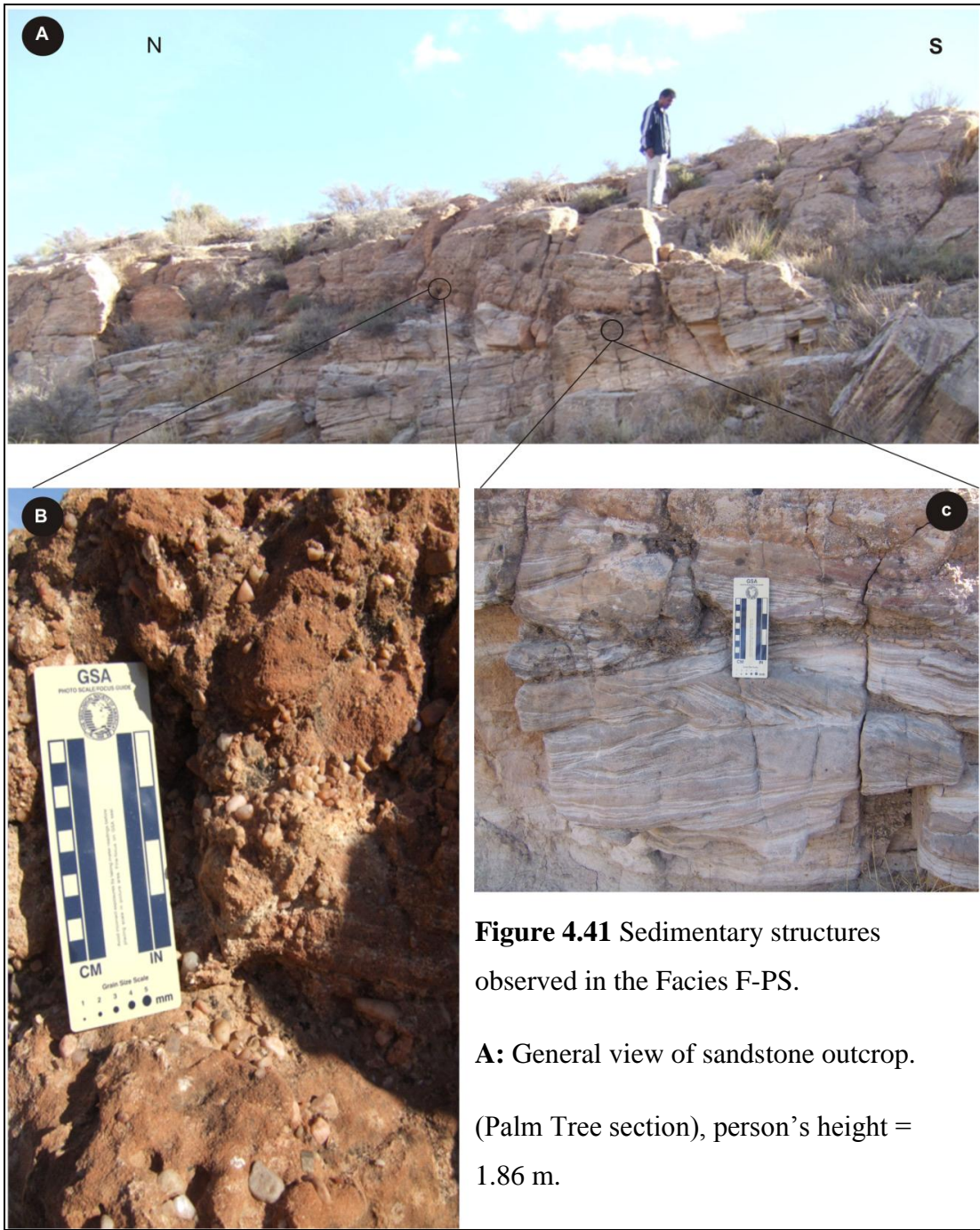


Figure 4.41 Sedimentary structures observed in the Facies F-PS.

A: General view of sandstone outcrop. (Palm Tree section), person's height = 1.86 m.



Figure 4.42 A: Photograph the geometry/ organisation of trough beds in channel forms. Hammer for scale (circled).

B: Field sketch of location ④ showing stacked channel features exposed in the Kabted Jamel section. GR 0313687/3565659.



Figure 4.43 Field photographs of the Abu Shaybah Formation showing (A) close up photo for fining-upward grain size (pen = 14.5 cm) from facies F-PS, (B) close up photo for calcretes in Facies F-CS, exposed in Wadi Gabel.

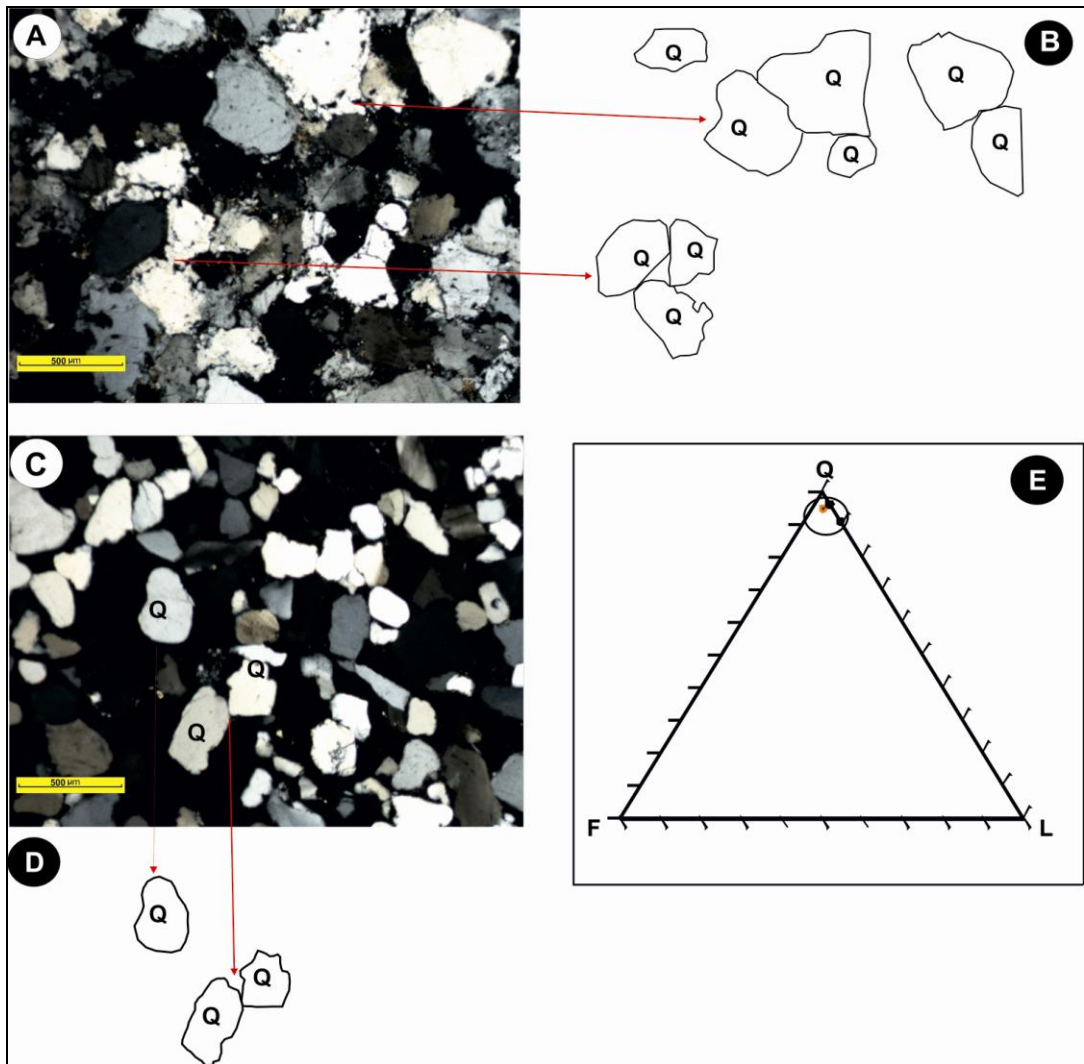


Figure 4.44 A and C: Photomicrograph of samples (AB-3 and AB-9) under cross polarized showing the quartz arenites of facies F-PS. B and D: Shape of the grains. E: Point-counting results.

4.8.8 Facies F-CS: Medium Sand with Calcretes

i) Field Description

This facies was identified at localities ❶ and ❷ in Wadi Abu Shaybah (Fig. 4.33) and is restricted to the middle unit of the Abu Shaybah Formation. The maximum measured thickness of facies F-CS is around 8 m (Fig. 4.43). This facies consists mainly of very pale orange (10YR 8/2) coloured, fine to medium grained sandstone, that are cemented by calcium carbonate. The nodules in Figure 4.43B are 1 to 4 cm in diameter interbedded with sandstone. The nodule consists of medium to coarse-grained quartz and rare pebbles.

ii) Interpretation

The nodules are interpreted as calcrete nodules. Calcrete is a sedimentary rock with a variety of forms from powdery to nodular to highly indurated (Wright and Tucker, 1991). Calcrete is an accumulation of predominantly calcium carbonate and it can form in three main ways; 1) as vadose or pedogenic minerals relatively close to the sediment surface, 2) as phreatic or groundwater minerals formed around the water table, 3) or a combination of both (Wright, 1994; Khadkikar et al., 1998; Alonso-Zarza, 2003; Schmid et al., 2006). The nodules in Figure 4.43 B are interpreted as stage II developments based on the Machette (1985) classification. Calcretes are widespread in modern semi-arid climates, particularly in tropical and sub-tropical latitudes such as Africa (Hay et al., 1978). Arid climates are suitable for calcretes; however, sub-humid climate are more suitable for palustrine carbonates (Alonso-Zarza, 2003). Thus, the calcrete observed within this facies suggests vertical movement of water through the sediment and probably the sediment surface is exposed with little or no sedimentation for period of time (Collinson and Thompson, 2006). Furthermore, the occurrence of calcrete within the siliciclastic sediments is evidence for a low sedimentation rate in the basin (Khalaf and Gaber, 2008).

4.8.9 Facies F-MS: Red Mudstone

i) Field Description

This facies F-MS was identified at localities ❶, ❷ and ❸ (Fig. 4.45). The facies varies in thickness from 2 to 28 m (Fig. 4.46). Laminated clay layers are 0.1 to 0.3 m thick alternating with siltstone layers up to 0.2 m thick (Fig. 4.46C). Small scale iron concretions and dark yellowish orange (10YR 6/6) coloured iron staining are common. The facies consists of two types of lithologies, green claystone and 5R 4/6 moderate red mudstone (Fig. 4.46A). The green claystone are very compact 8-12 cm bedded. This facies lacks any primary sedimentary structures. This facies is overlain by the Abu Ghaylan Formation (Fig. 4.46A). No fossils or bioturbation were observed in this facies. X-ray diffraction analysis reveals that the red mudstone is composed of kaolinite and quartz (sample AB = 22, Appendix 1).

i) Interpretation

The deposition of mud typically occurs under low energy conditions. The dark yellowish colour suggests the occurrence of weathering processes. The laminated mud could result from over bank suspension fallout during water inundation (Hillier et al., 2007). Laminations are due to grain size changes. On the other hand the absence of lamination in some sections may be due to abundance of clay-size particles or due to rapid deposition and lack of platy grains. Kaolinite suggests that in *situ* weathering processes under hot and humid conditions or sourcing of sediment from an area dominated by hot humid weathering processes (Key et al., 2008).

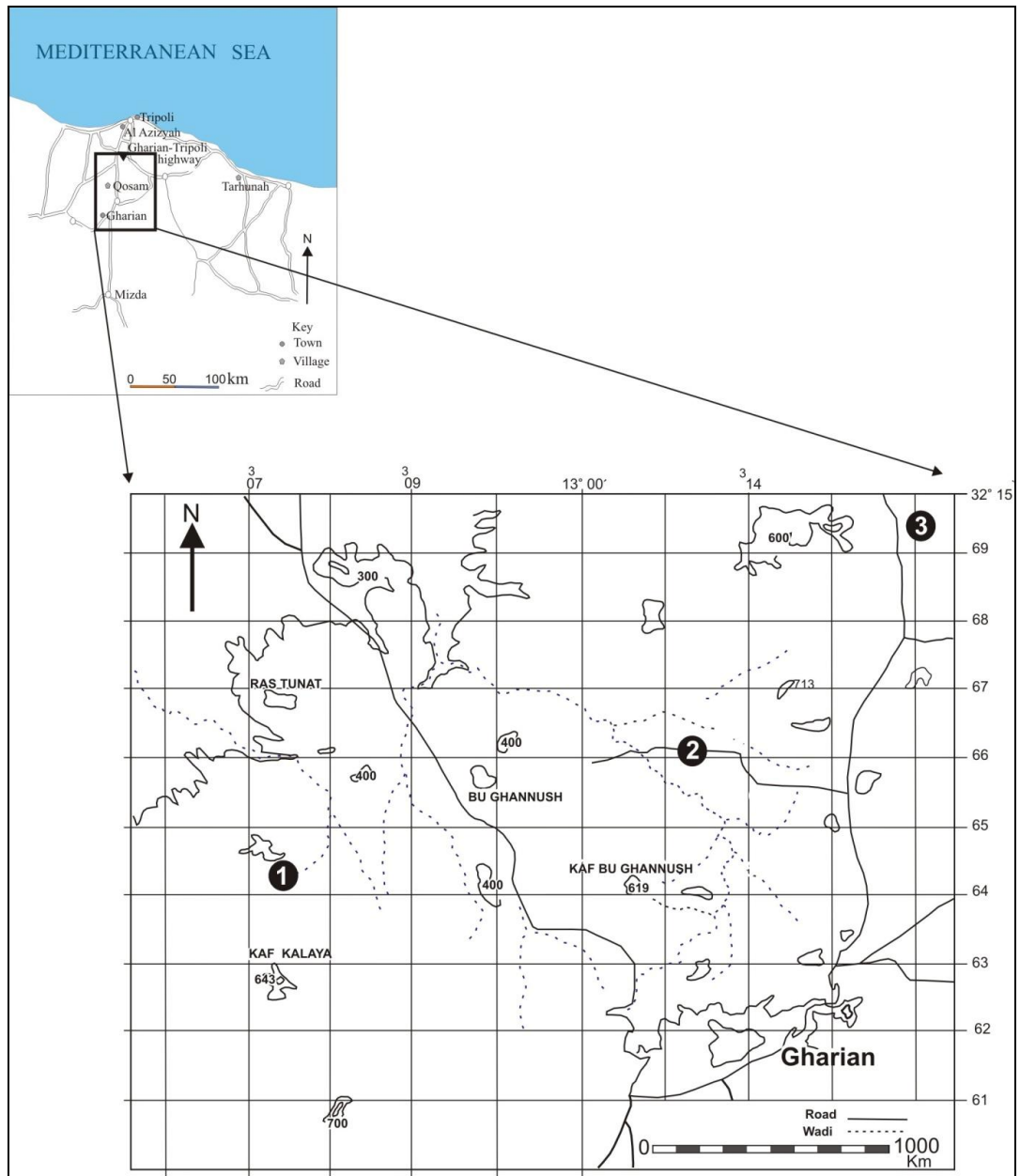


Figure 4.45 Principal localities of facies the upper unit of the Abu Shaybah Formation. Numbers indicate locations described in the text.

4.8.10 Facies F-GS: Green Claystone

i) Field Description

Facies F-GS was observed at localities ❶ and ❷ (Fig. 4.45). The facies consists of interbedded muddy, grayish green (10GY 5/2) siltstone and silty mudstone. Clay units are generally a few centimetres to several meters thick and have a massive appearance in the Kabted Jamel section ❷ (Fig. 4.46B). The maximum measured thickness of facies F-GS is *ca.* 14 m. Clay is the main component whilst the fine siltstone makes up a minor proportion of the facies. In some locations the clay appears to be massive and lacking in sedimentary structures. Two samples were used for X-ray analysis and revealed that this mudstone is composed of quartz (e.g. sample AB-23 and AB-24, Appendix 1).

ii) Interpretation

The clays and silts were either deposited by settling from suspension (Catuneanu et al., 2006) or from current activity. This is usually achieved when a flow carrying a load of suspended sediment slows down on entering quieter water (e.g. Turner, 1980; Collinson et al., 2006). Thus, silty mud stone formed at low velocities below the lower flow regime (Hubert et al., 1982). The massive nature of the facies suggests post-depositional modification that has destroyed any primary sedimentary structures, either by pedoturbation / bioturbation or post-depositional compaction and diagenesis. Moreover, the absence of lamination within the mud unit may be due the uniformity of the clay size or due to rapid deposition of suspended sediments and lack of platy grains (Collinson and Thompson, 1982).

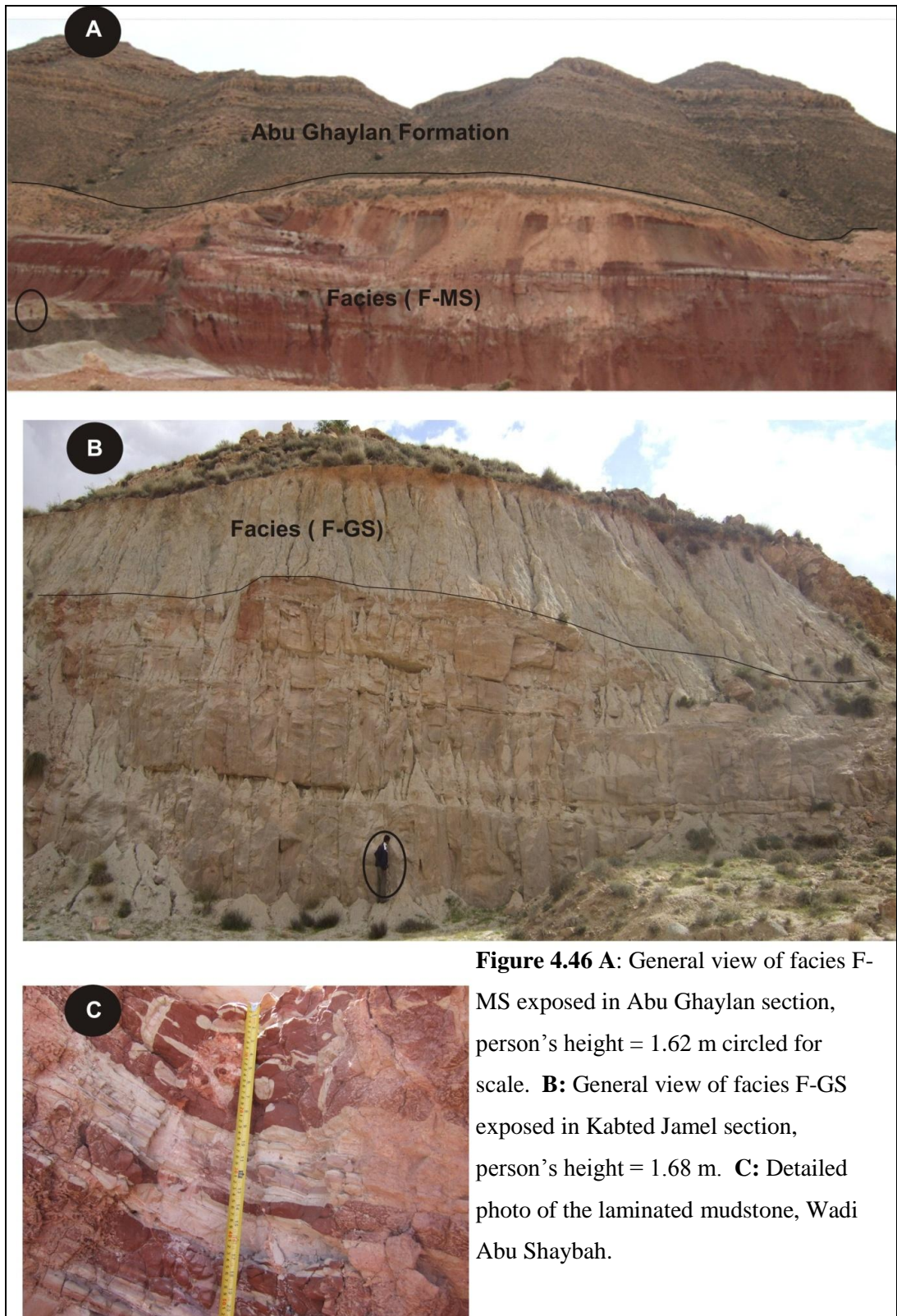


Figure 4.46 **A:** General view of facies F-MS exposed in Abu Ghaylan section, person's height = 1.62 m circled for scale. **B:** General view of facies F-GS exposed in Kabted Jamel section, person's height = 1.68 m. **C:** Detailed photo of the laminated mudstone, Wadi Abu Shaybah.

4.9 Facies Associations and Depositional Environment

The ten facies observed within the Abu Shaybah Formation can be grouped into three facies associations. These are illustrated in a composite graphic sedimentary log (Fig. 4.47). The facies associations were assigned from a number of key localities in the Gharian area in order to illustrate the characteristics and variation within the stratigraphic units. In turn, grouping of the data from key localities allowed for a localised palaeogeographic model to be constructed (section 4.9.4). Details of the three facies associations are explained accordingly.

4.9.1 Shallow Marine Facies Association

i) Introduction

The shallow marine facies association is restricted to the base and lower part of the Abu Shaybah Formation (Fig. 4.25) where up to 30 m in thickness of sediments are well exposed in the area along the Abu Rashada road and the Wadi Gabel (Fig. 4.25). The association comprises four siltstone and sandstone facies: (F-SD, F-SB, F-MS and F-VC). These are exposed primarily along the Abu Rashada road. The lower part of the facies association is less extensive, whereas the upper part of the facies association can be observed over a much wider area.

Exposures from two localities are used to describe the sedimentary characteristics of the shallow marine facies association. This is reasoned as follows: 1) the Abu Rashada section, shows the contact with the underlying Al Aziza Formation; 2) the main sedimentary structures evidence is derived from exposure of the Abu Rashada section, and 3) the Wadi Gabel section shows the sandstone with carbonate vugs facies (F-VC) as well as clearly displaying sedimentary structures such as ripple marks and parallel lamination. The following text provides details about the type localities of the shallow marine facies association and their main sedimentological and palaeontological features.

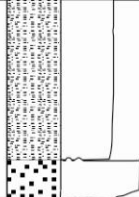
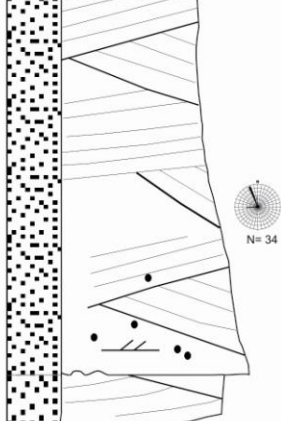
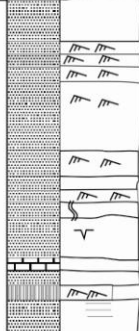
| Unit | Thickness (m) | Log | Facies and code | Facies Association |
|-------------|---------------|--|--|--------------------|
| Upper Unit | 22-30m |  | Red mudstone, green claystone and trough bedded sandstone (F-MS, F-GS and F-SR) | Meandering river |
| Middle Unit | 40-60m |  | Sandstone medium to coarse grained with pebbly, trough, tabular bedded sandstone (F-TS and F-PS) | Braided river |
| Lower Unit | 20-30m |  | Silt stone- sandstone and sandy carbonate (F-SD,F-SB,F-MS and F-VC) | Shallow marine |

Figure 4.47 Composite log of the Abu Shaybah Formation showing three facies associations: 1) Shallow marine facies association, 2) Braided river facies association and 3) Meandering river facies association.

a) Abu Rashada section

The Abu Rashada road section is the main type locality for the shallow marine facies association (Fig. 4.25), located approximately 2 km to the southwest of Gharian town.

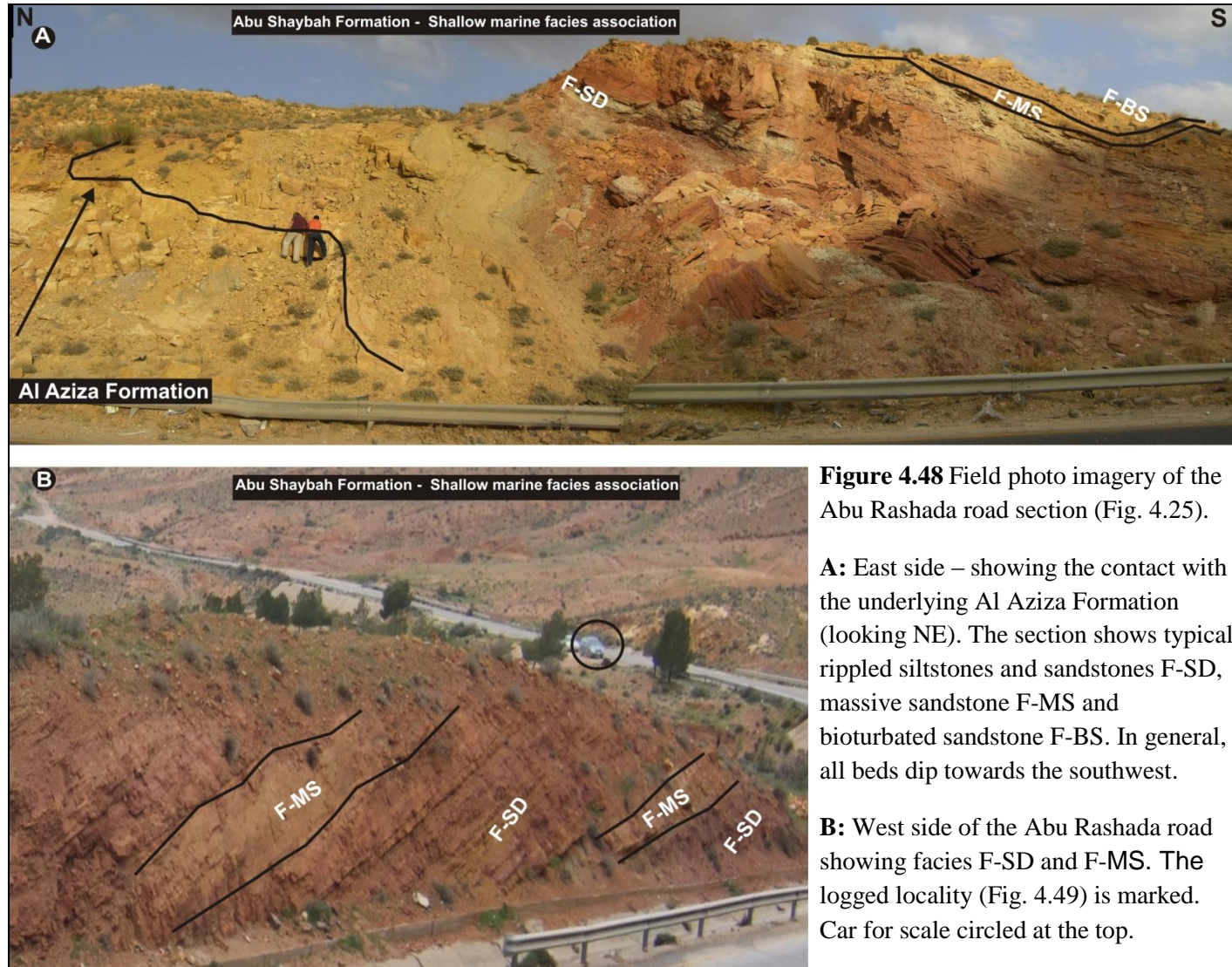
It shows the contact with the underlying Al Aziza Formation and the dominant sedimentary characteristics of the shallow marine facies association. The main characteristics of Abu Rashada road section are illustrated in field photographs (Fig. 4.48) and a graphic sedimentary log (Fig. 4.49). The sedimentary log was recorded from the east and west side of Abu Rashada section and is characterised by thinly interbedded

red and yellow coloured siltstones and fine grained sandstones deposited by facies (F-SD, F-BS and F-MS). Sedimentary structures are typically dominated by cross-lamination and symmetric ripples exposed on bedding plane surfaces.

The facies association contains rare fossil content, particularly casts of small bivalve shell fragments. Biogenic structures are features of bioturbation probably representing simple dwelling structures. Their simplicity and occurrence within fine grained sediment corresponds to a *Skolithos* assemblage. Furthermore, desiccation cracks are common features found within the Abu Rashada section.

b) Wadi Gabel section

The second type locality is located in the central part of Wadi Gabel (Fig. 4.25), where it forms a sequence up to 15 m in thickness. The Wadi Gabel section is illustrated in Figure 4.50 and in a graphic sedimentary log (Fig. 4.51). The log is dominated by interbedded fine grained sandstones and siltstones (85%) with minor dolomitic beds. The log comprises four siltstone and sandstone facies (F-SD, F-SB, F-MS and F-VC). This outcrop shows internal sedimentary structures such as ripple marks and parallel lamination and also shows the sandstone with carbonate vug facies (F –VC) which are not observed at the Abu Rashada section. Bedding plane surfaces are intensely bioturbated and also contain rare casts of fossil bivalves (Section 4.5).



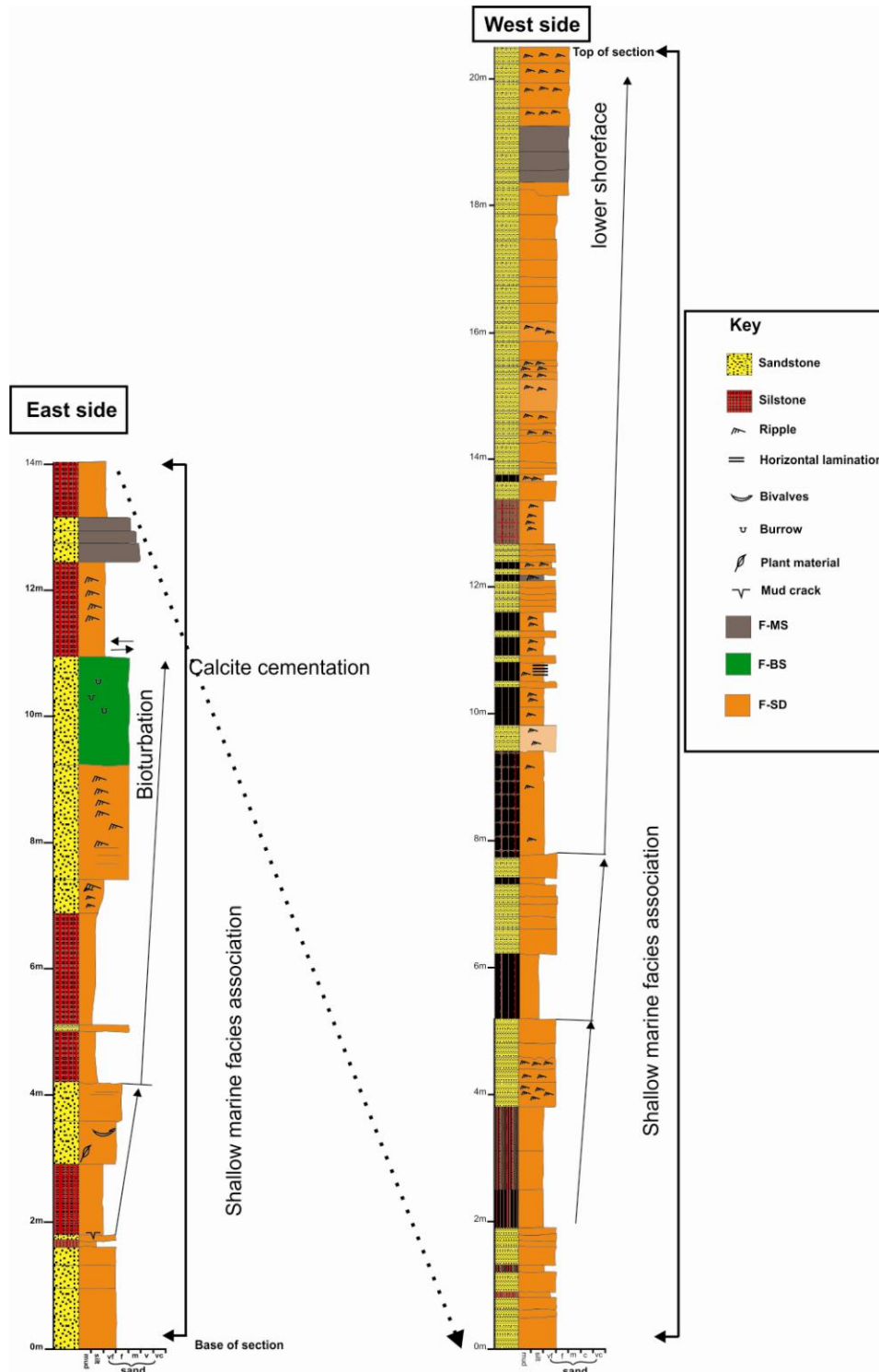


Figure 4.49 Sedimentary log from the Abu Rashada section (Location ❶ and ❷, Fig. 4.25), west of Wadi Abu Shaybah. The section shows the Lower Unit of the Abu Shaybah Formation and west side overlying of east side. The logs are dominated by fine grained sandstones (53%) and siltstones (43%). The sediments correspond to a shallow marine environment. For facies codes see Table 4.3.

Abu Shaybah Formation - Shallow marine facies association



Figure 4.50 Field photograph showing an east looking perspective into the central part of Wadi Gabel. The section shows the rippled siltstone and fine sandstone (F-SD) in the base of the section overlain by the bioturbated sandstone (F-BS). Beds dip towards the northeast. Person's height = 1.86 m.



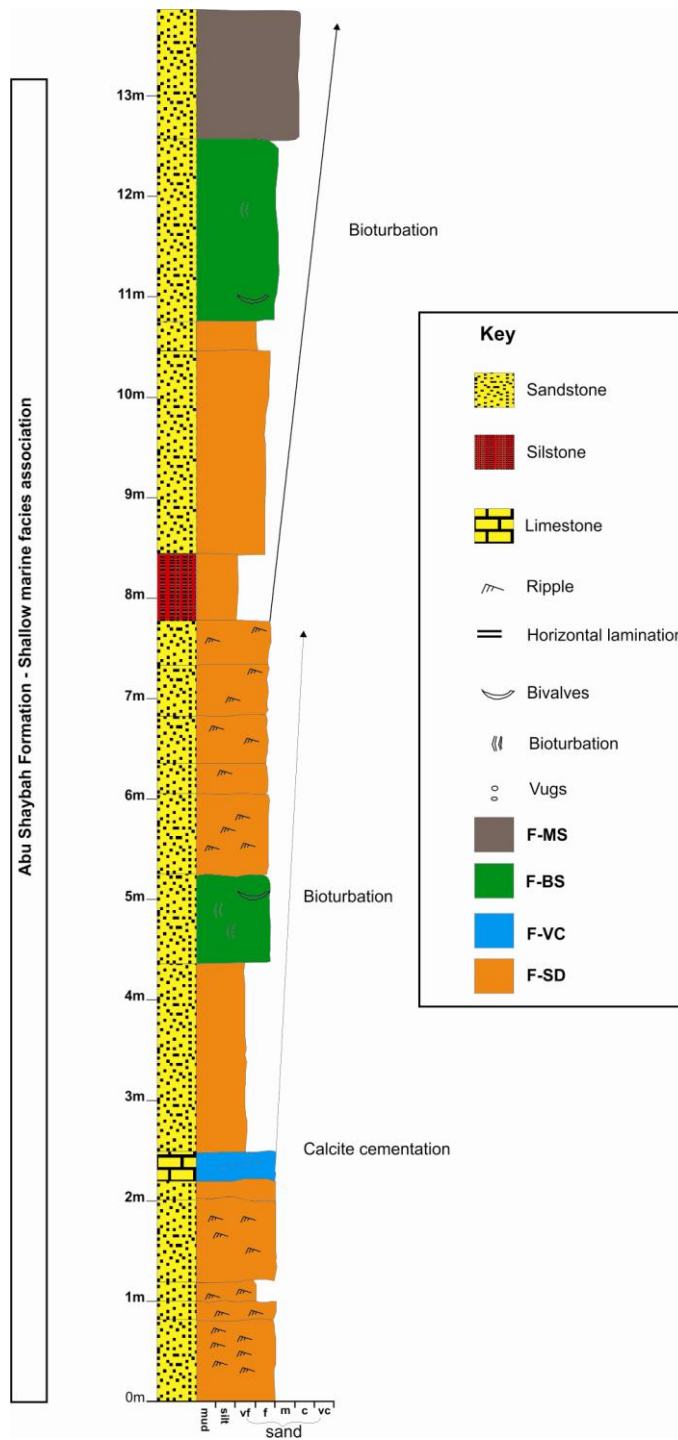


Figure 4.51 Sedimentary log from east of the Wadi Gabel section (Locality ③ in Fig. 4.25), where the shallow marine facies association is exposed. For facies codes see Table 4.3.

ii) Interpretation

The sedimentological and palaeontological characteristics of the lower part of the Abu Shaybah Formation correspond to deposition within nearshore zone in shallow marine setting. The siltstones and sandstones facies (F-SD) dominate the shallow marine facies association. Evidence for a shallow marine setting is based on 1) the grain size; 2) sedimentary structures that indicate wave ripples; 3) palaeontological evidence from marine fossils shells and bioturbation structures.

The siltstones and sandstones were probably deposited as fairweather background sedimentation within nearshore zone in shallow marine setting. The dominance of rippled sandstone and siltstones suggests a shallow water setting dominated by wave current activity (Leeder, 1999). Wave action is inferred from the presence of symmetrical ripples produced by current oscillations. Symmetrical ripples with an average wavelength of 3 cm and crest highest of 1 cm (Fig. 4.26), and cross lamination suggests a shallow water setting (Harms et al., 1975) (Section 4.7.1). Surface waves depends on the ratio of wave depth wavelength $d \div \lambda_o$ that subscript denoting that the wavelength is measured or calculated from deep water (Allen, 1971). Therefore, if $d \div \lambda_o$ is small, the wave is called a shallow water whilst if $d \div \lambda_o$ is large, the wave is called deep-water and can be explained as follows:

- 1) $d \div \lambda_o \geq 0.5$ = deep water;
- 2) $0.05 < d \div \lambda_o < 0.5$ = intermediate water;
- 3) $d \div \lambda_o \leq 0.05$ = shallow water.

Therefore, it is clear that symmetrical ripples with an average wavelength of 3 cm suggest shallow water waves and therefore probably a nearshore shallow marine setting. Changes in grain size reflect either fluctuations in current strength or changes in sediment supply (Fig. 4.52). Massive sandstone and bioturbated facies occur in a near

shore / inner ramp environment (Fig. 4.19), that were probably deposited above wave base (storm and fair weather) (Hildebrandt and Egenhoff, 2007). Evidence from palaeontological remains further supports a shallow water setting for this facies association. The presences of bivalve moulds (Fig.4.28B and C) are indicative of shallow water setting in a marine environment (e.g. Komatsu et al., 2004; Damborenea and Lanes, 2007). Bivalves appear to have been either in situ or transported during stages of erosion by current or waves (Straaten, 1954).

The occurrence of a *Skolithos* trace fossil assemblage within these sediments further supports a shallow marine shelf setting (Donovan, 2009). *Skolithos* are characteristic of suspension feeders and normally occur in shallow water environment where detrital food is kept in suspension by wave action (Seilacher, 1967; Allen Gurrán, 1985; Bromley, 1990).

The small remnants of plant debris (Fig. 4.28A) suggests sediment supply from a terrestrial setting in close proximity to the shallow marine setting, although within such a setting it is possible for current reworking of plant material to occur. The wood content in marine sediments is obviously an indicator of nearshore setting (Voneynatten, 1993). Moreover, the wood was most probably transported to the marine setting by river inputs from the nearby land.

The presence of desiccation cracks suggests periodic sub-aerial exposure during deposition (Youri and Gilles, 2008). Furthermore, desiccation cracks suggest a change in water depth, flow direction and intensity (Plummer and Gostin, 1981).

This study proposes a depositional model for the lower unit of the Abu Shaybah Formation comprising of a low energy, based upon field observation (section 4.8). The shallow marine features include upwards-coarsening show an upwards gradation from mudstone to sandstone and an associated in current and wave generated structures.

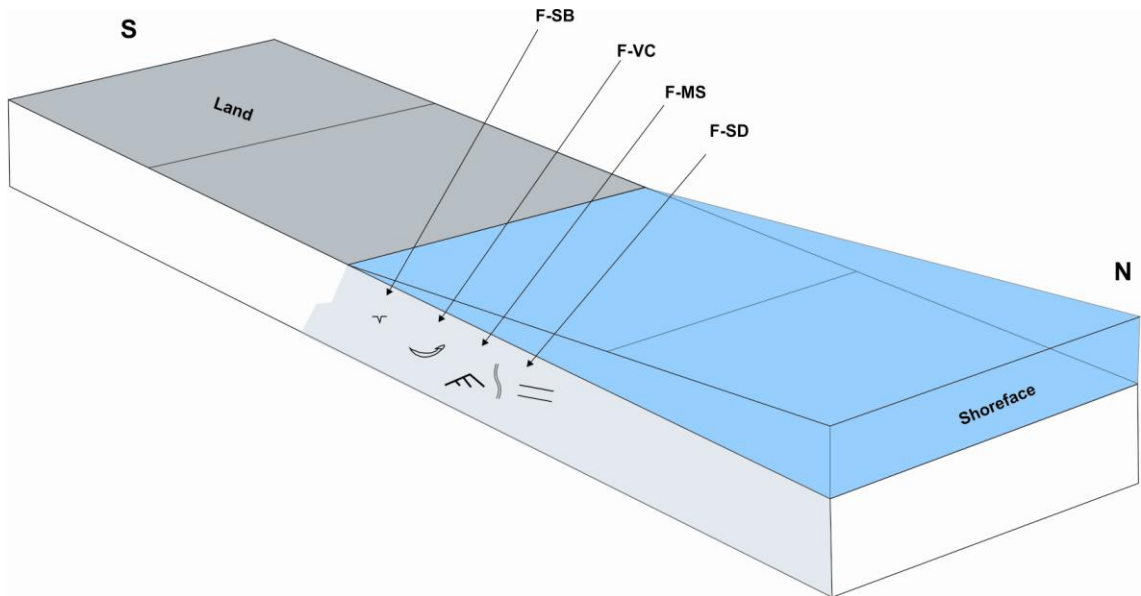


Figure 4.52 A sedimentary facies model of lower unit of the Abu Shaybah Formation. For facies codes see Table 4.3.

4.9.2 Braided River Facies Association

i) Introduction

The low sinuosity braided river facies association occurs in the middle part of the Abu Shaybah Formation (Fig. 4.33), and is well preserved in outcrops throughout the study area. The maximum measured thickness of the low sinuosity braided river facies association facies association is *ca.* 40-60 m. The association comprises three sandstone facies (F-TS, F-PS and F-CS). Exposures from two localities (Kabted Jamel and Palm Tree) are used to describe the main geometric and sedimentary characteristics. This is reasoned as follows: the Kabted Jamel section shows sandstone facies organised into channel and sheet-like forms. These sand bodies however, lack clarity of internal sedimentary structures composition, therefore the Palm Tree section shows the best exposure for internal sedimentary structures characterised by tabular and trough cross-strata. The following text describes the two type localities.

a) Kabted Jamel section

The type locality for the low sinuosity braided river facies association is located in the area along the old road of Kabted Jamel to the town of Qasam (Fig. 4.33). The maximum measured thickness of Kabted Jamel section is *ca.* 20 m that can be traced laterally over 50 m. The basal part of the section is characterised by a 15 m thickness of medium to coarse-grained sandstone that occur within a series of ill defined beds up to 2m in thickness corresponding to Facies (F-PS). Claystone and siltstone of facies (F-GS) occur mainly within the upper parts of the section, forming a unit up to 4 m thick that can be traced laterally over several metres.

An exposure at the Kabted Jamel section is shown in Figure 4.53 whilst a sedimentary log through this section shows the principle facies characteristics and palaeocurrent

directions (Fig. 4.54). The sedimentary facies are diverse being dominated by medium to coarse-grained sandstones, interbedded with sheet and channel fill pebbly sandstones. The channel size reduces upwards in the Kabted Jamel section (Fig. 4.53). Therefore, in the Kabted Jamel section, moving away from the thicker part of channel body there is a concurrent decrease in bedform height, bed thickness, scour depth and an increase in mudstone facies F-GS.

The sheet-like bodies display a wide and high variation in dimensions. Individual sandstone bodies are generally 1 to 2.5 m thick and they extend laterally for tens of meters. The bodies have sharp contacts with mudstone facies.

Single sandstone bodies are typically dominated by medium to coarse-grained sandstone but small pebble-sized are present in the lower stories. Each sandstone body is separated by mudstones (several centimetres thick). The internal structures of the channels are tabular cross-stratification (small and medium scale) and trough cross-strata indicate paleoflow towards the NW (Fig. 4.40).

b) Palm Tree section

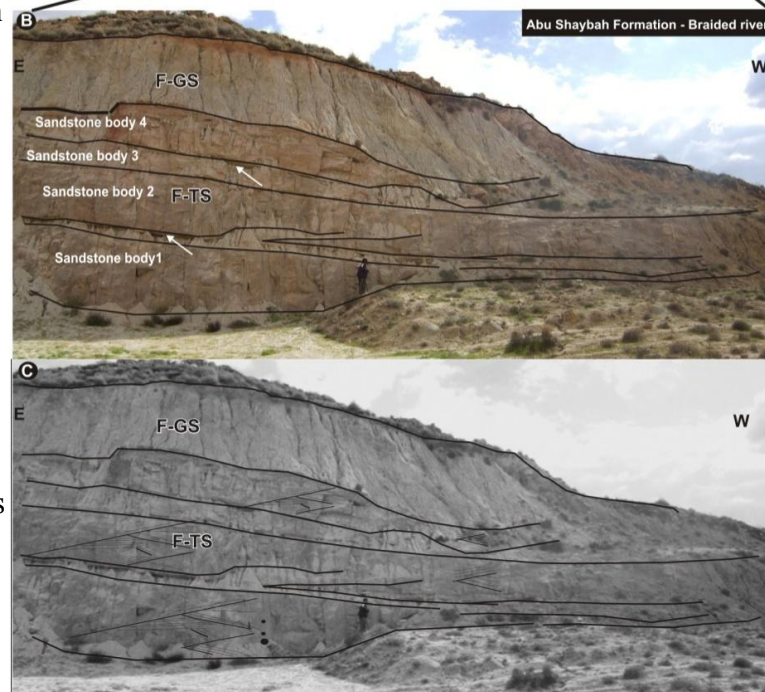
The Palm Tree section is located in the northwestern region of the Gharian area (Fig. 4.33) where it forms a sequence up to 6 m in thickness that can be traced laterally over 30 m (Fig. 4.55). The Palm Tree section is characterised by facies F-TS, F-PS and F-MS. The base of the Palm Tree section is typically defined by red mud to siltstone whilst upper part of the section is characterised by a 5 m thickness of medium to coarse-grained sandstone.



Figure 4.53 A: Overview of main section.

B: Field photo imagery of the Kabted Jamel section (Fig. 4.31) and erosion surface between sandstone body 1, sandstone body 2, sandstone body 3 and sandstone body 4 is marked by white arrows.

C: Field sketch section shows a series of cross-bedded channel fills pebbly sandstone and dominated northwesterly transport direction of braided river (person's height = 1.52 m). For facies codes see Table 4.3.



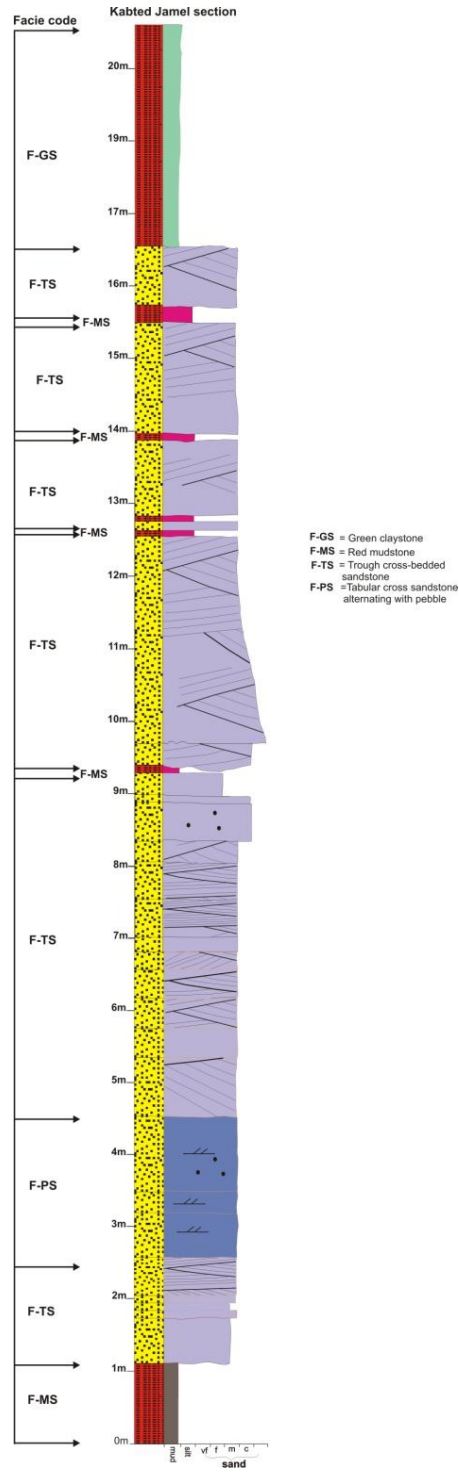


Figure 4.54 Sedimentary log from the Kabted Jamel section (NW of Wadi Abu Shaybah), where the low sinuosity braided river facies association is exposed. For key to symbols see Chapter Two (Fig. 2.1) and for facies code see Table 4.3.

An exposure at the Palm Tree section is shown in Figure 4.55 whilst a sedimentary log through the Palm Tree section demonstrates the principle facies, red mud to siltstone, sandstones bodies, sedimentary structures and palaeocurrent directions is shown in Figure 4.56. The Palm Tree section comprises two sand bodies and these bodies on average are more than 30 m wide and 1.5 to 3 m thick (Fig. 4.55).

- **Sand body I**

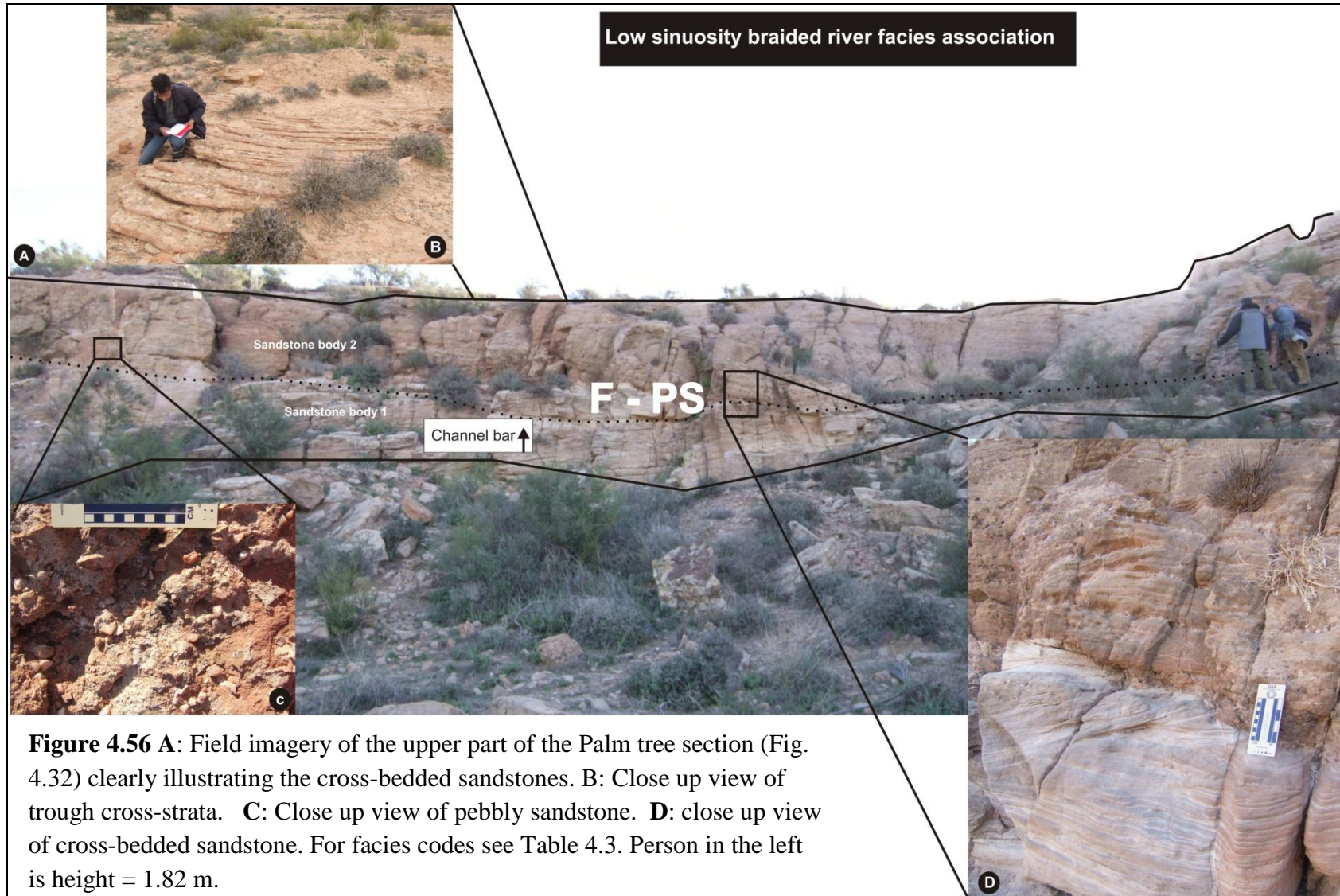
The sand body I (2 m thick and 28 m wide) is dominated by the medium to fine grained sandstone (F-PS) with minor amounts of pebbly sandstone (Fig. 4.56). The internal sedimentary structures are characterised by tabular cross-strata (≤ 1 m thick). This sand body shows an overall thinning upwards trend in set thickness of cross-strata and a weak fining upwards trends in grain size and sedimentary structures.

- **Sand body II**

The sand body II is characterised by facies F-TS. The sand sheet body (3 m thick and 30 m wide) is characterised by moderately sorted quartz arenites with minor amounts of pebbly sandstone. The internal sedimentary structures show trough cross strata (see section 4.5 for a full description), which an overall thinning upwards trend in set thickness of trough cross stratification. Pebbles are very rounded or subrounded in shape with polished surfaces (section 4.7.7). Palaeocurrents indicate a dominant transport direction towards the northwest (Fig. 4.40). However, minor north easterly flow directions are also present, especially in the upper part of this facies at the Palm Tree section (Fig. 4.40 S-3).



Figure 4.55 Field imagery of the Palm Tree section (Fig. 4.32). The section is dominated by siltstones and medium to coarse grained sandstones. This out crop shows internal sedimentary structures such as tabular and troughs cross strata cross-cut by a Tertiary dike (black line and arrow).



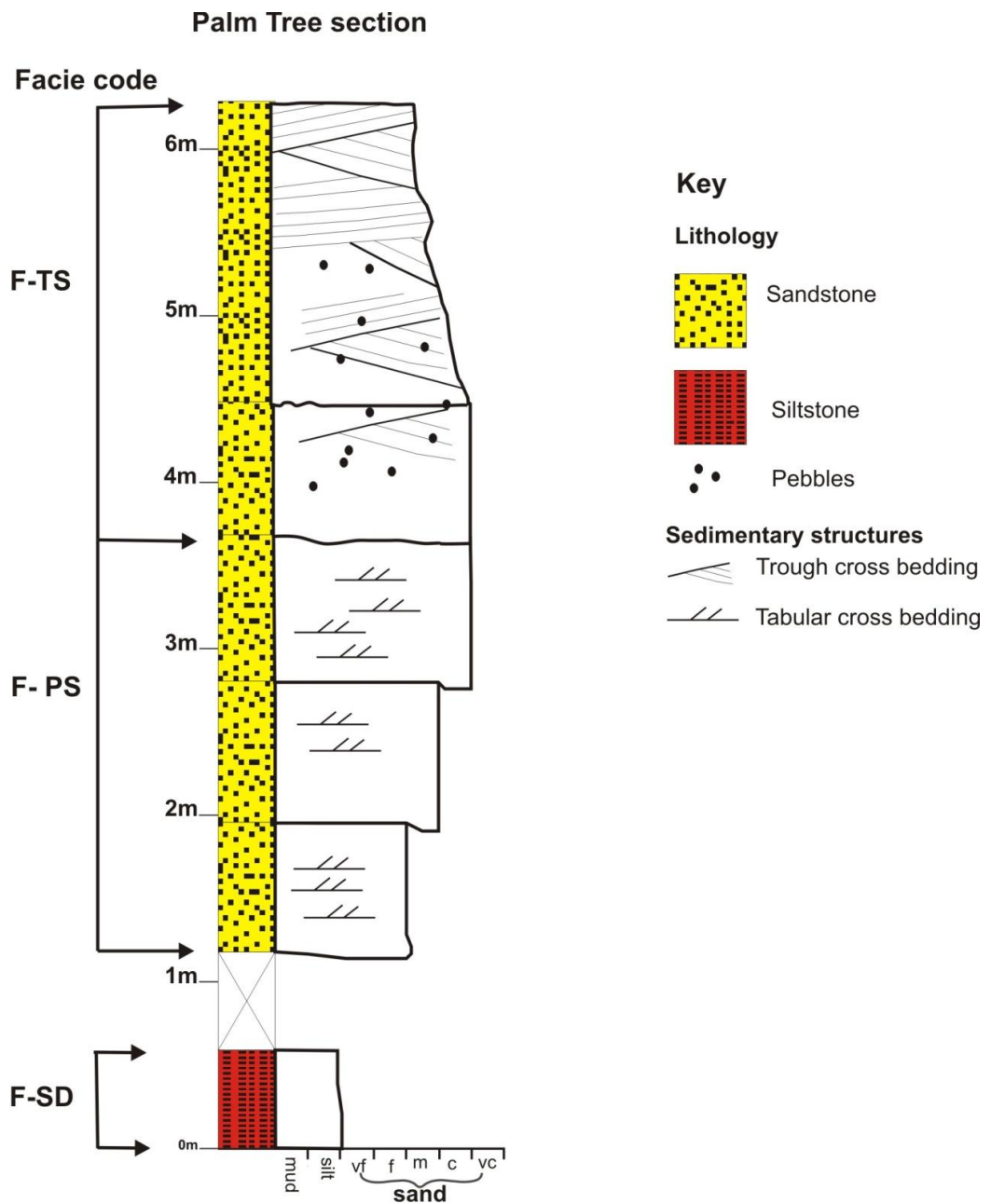


Figure 4.57 Sedimentary log from the Palm Tree section (NW of Wadi Abu Shaybah), where the fluvial facies association is exposed. The positions of the main facies referred to within the text are outlined and Figure (4.32). For facies codes see Table 4.3.

i) Interpretation

The facies association of the middle unit of the Abu Shaybah Formation is interpreted as a braided river environment. Evidence for the braided river system is based on 1) sandbody geometry; 2) grain size; 3) sedimentary structures; 4) palaeocurrent trend, and the absence of fossils. The braided river environment comprises a suite of widely recognized components. A set of bedforms, such as dunes is typically organized into bars and bedload sheets, lies with channels (Gibling, 2006). Miall (1977) divided bars into three main bar types: longitudinal, comprising crudely bedded gravel sheets; transverse to linguoid, consisting of sand or gravel and formed by downstream avalanche-face progradation and point or side bars.

Using the classification scheme of Friend et al., (1979) based on the geometry of the sandstone bodies (Fig. 4.53), these sandstone bodies forms can be classified as ribbon bodies. Friend et al., (1979) proposed that a cross-section width (w) to depth of 15:1 in the central body only (Fig. 4. 58), to distinguish sheet sandstone bodies (w : h greater than 15) from ribbon sandstone bodies (w : h less than 15). Ribbon bodies are typically characterized by an abundance of linguoid bar and dune deposits characterized by trough cross stratification.

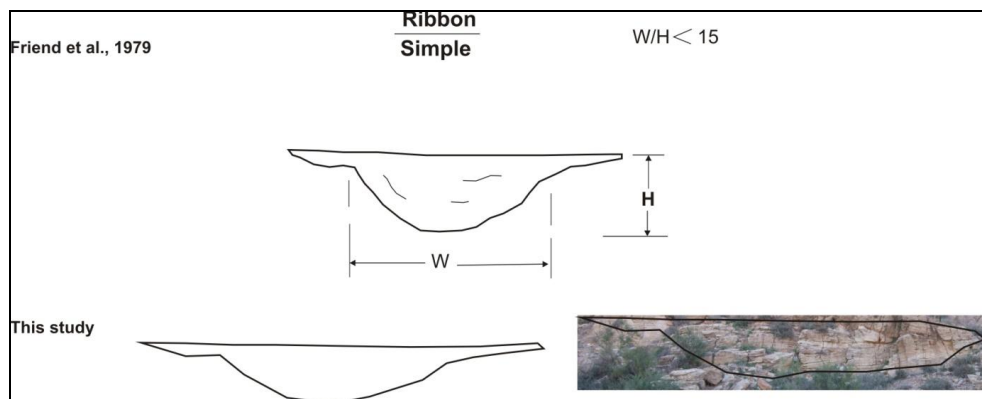


Figure 4.58 Terminology used to describe aspect of sandstone body geometry.

The nature of the ribbon bodies which commonly fine upwards from basal erosion surface that overlain medium to coarse-grained sandstones with little or no preserved fine-grained sandstones represent bedload deposits (Collinson, 1996). The fining-upward sequence of medium to coarse-grained, medium to small-scale trough cross bed sandstone could have been deposited as channel bar or channel fill sands (Fig. 4.59).

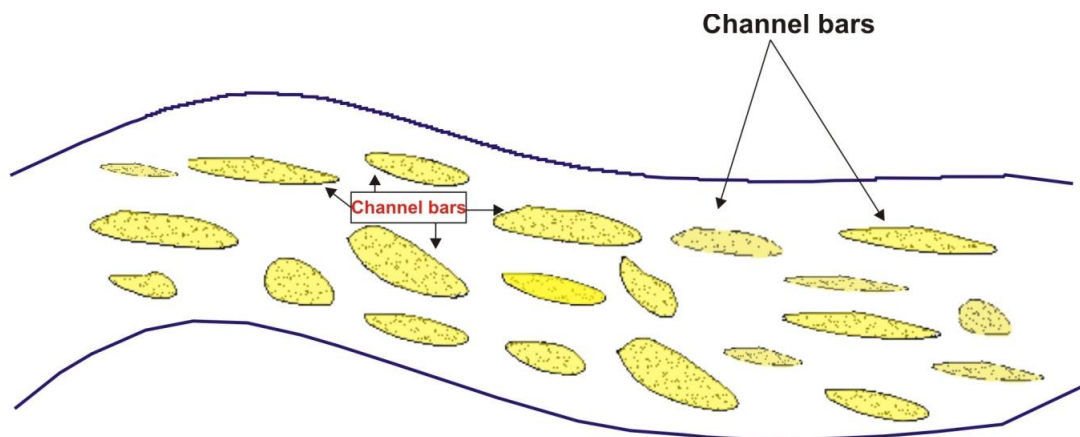


Figure 4.59 Field sketch of the braided river system showing stacked channel bars exposed in the mid part of the Abu Shaybah Formation.

Channel deposits contain channel lag and linguoid bar deposits. Hein and Walker (1977) and Nichols (2009) proposed that transverse and linguoid bars have a higher relief and generate well-defined cross-stratification dipping downstream. The channel lag occurs at the base of channel facies (F-TS) and linguoid bar was deposited over the channel lag (Fig. 4.60). Trough and tabular cross bedded sandstones, usually in set 45-90 cm thick, are the principle facies (F-TP and F-PS) of the bar sequence within a braided channel system. The occurrence of trough cross-bedded sandstone on top of tabular cross-bedded sandstone may be reflecting shallowing water (Harms et al., 1975). Decimetre-scale trough and tabular cross stratification is well observed from outcrops and both suggest formed by the migration of sinuous and straight-crested dunes (Plint,

1983). The presence of relatively (smaller and medium) trough cross-strata and gradual upward transition to mudstone facies (F-GS) suggests gradual abandonment of the channel system (Fig. 4.60). The presence of thin beds of mudstone beds between the ribbon bodies suggests flood plain.

The channels appears to be low sinuosity because palaeocurrent directions have not changed through middle section of the Abu Shaybah Formation. The orientation of the trough stratification shows a remarkably uniform trend to the northwest, indicating a southerly source area region. The main mineral present in the majority of the samples is composed of quartz (section 4.7.6 and 4.7.7). Quartz grains are present as both monocrystalline and polycrystalline forms. These suggest that material is being sourced from elsewhere, possibly from lithologic quartzites exposed to the south in the Al Kafrah basin, or further away from the Tibesti massif. The Tibesti massif consists of Precambrian granites, granodiorites and covered by low rank metamorphic rock which is overlain by a thick sequence of Palaeozoic clastic rock (Baegi and Perski, 1996; Turner, 1980). These would have formed the cratonic interior of the Gondwanan continental land mass during Abu Shaybah Formation times. Alternatively, the quartz may be sourced from igneous rocks; heavy minerals are observed from some thin sections. Thus, both medium and coarse, rounded quartz grains suggest subaqueous grain transport over a long distance of hundreds of kilometres or further.

Braided rivers are subjected to rapid fluctuations in flow velocity causing sediment to be deposited mainly in the form of channel bars as represented by facies F-PS and F-TS. The sand bars consist of medium to coarse-grained and pebbly medium stratified sandstone (Fig. 4.56) and then becoming fine to medium-grained sandstone with cross-bedded attributed to high stage deposition within transverse bars (Smith, 1970;

Bourquin et al., 2010). The coarseness suggests that deposition as bed load by a river that has strong and turbulent flow regimes, whilst the finer material (silt and clay) tends to be transported through the system.

Pebbles with polished surfaces suggest that clasts are reworked during transport by the fluvial system (Rodriguez-Lopes, et al., 2010). The presence of calcrete suggests soil formation between active channels and after bar abandonment. The nodules in Figure 4.43 are interpreted as stage II (Machette, 1985). The degree of reddening and carbonate within carbonate soils can be used for identifying chronosequences with fluvial terraces (Maher and Harvey, 2008). Hence, calcrete within the facies (F-CS) reflects short period of time. The ribbon bodies and the dominance of sand in the middle part of the Kabted Jamel section suggest deposition within a high-gradient bed load-dominated low-sinuosity channels (Schumm, 1972).

The channel size reduces both laterally and vertically (Fig. 4.53) and this reduction may be due to change flow regime. In sandy braided rivers the braid bars comprise a complex of subaqueous dunes over the bar surface (Fig. 4.61). A modern analogy for the braided river facies association could be similar to the braided Platte River. These features include bars represent cross-bedded strata and the finer material (silt and clay) transported across the bar surfaces to the slip face (Smith, 1970).

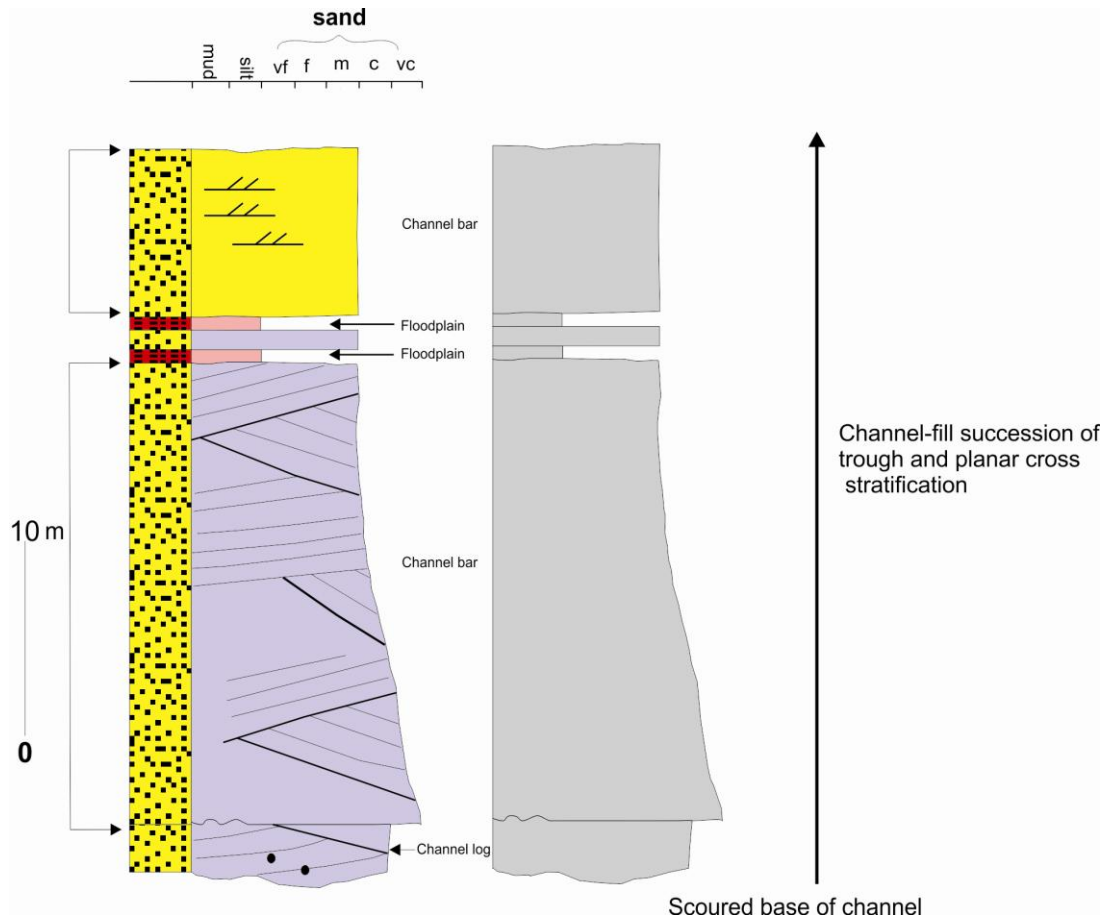


Figure 4.60 Composite log illustrating the low sinuosity braided river facies association. The rock units and structures that compose the Middle unit of Abu Shaybah Formation represent sandy braided river.

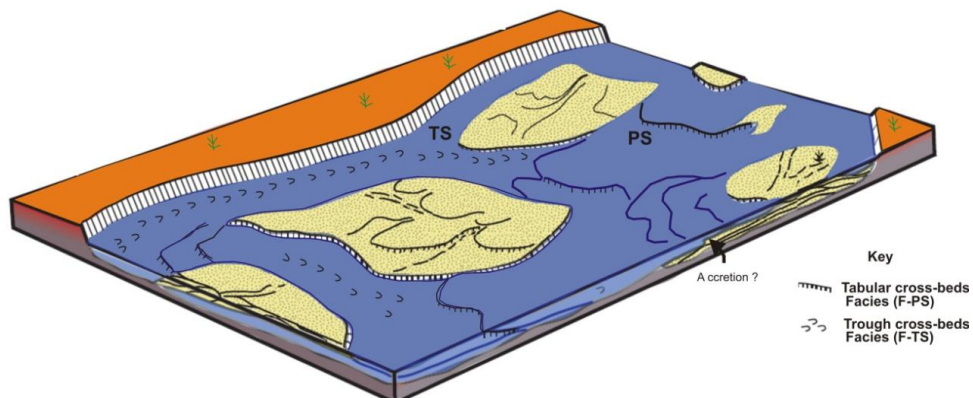


Figure 4.61 Facies model for the low sinuosity sand-bed braided river (modified after Miall, 1996; Ryan, 2008).

4.9.3 Meandering River Facies Association

i) Introduction

The meandering river facies association is restricted to the upper part of the Abu Shaybah Formation. This facies association is 30 m in thick in its type locality, northwest of Kaf Kalaya (Fig. 4.45). The association comprises three sandstone, siltstone and claystone facies: F-SR, MS and F-GS. Exposure from Kaf Kalaya is used to describe the main geometric and sedimentary characteristics. This is reasoned as follows: the Kaf Kalaya section shows lithology, assemblages of sedimentary structures and sediment body architectures.

ii) Kaf Kalaya

The maximum measured thickness of the Kaf Kalaya section is *ca.* 32m that can be traced laterally over 19 m. The Kaf Kalaya section shows the contact with the overlying Abu Ghaylan Formation and the dominant sedimentary characteristics of the higher sinuosity meandering river facies association.

The main characteristic of the Kaf Kalaya section is illustrated in field photography (Fig. 4.62) and a graphic sedimentary log (Fig. 4.63). The Kaf Kalaya section is represented by sandstone beds that have a sheet-like geometry and thick bedded mudstones (MS and F-GS; 0.5 to 6m thick) that are interbedded with fine to medium-grained sandstone (F-SR, 0.5 to 1.0 m thick). A series of fining-upwards successions are observed, characterised by trough cross-bedded sandstones (Fig. 4.63) at the base with mudstones at the top. The basal contact of the sandstone with the red mudstone is erosional and concave upward (Fig. 4.62) but in the some cases it may be flat or wavy. It is also characterised by the presence of lateral accretion surfaces, palaeosols and burrowed sandstone. This outcrop shows internal sedimentary structures such as cross

lamination and trough cross bedding. Both massive mudstone and laminated mudstone are found mainly in the lower and middle part of the outcrop.

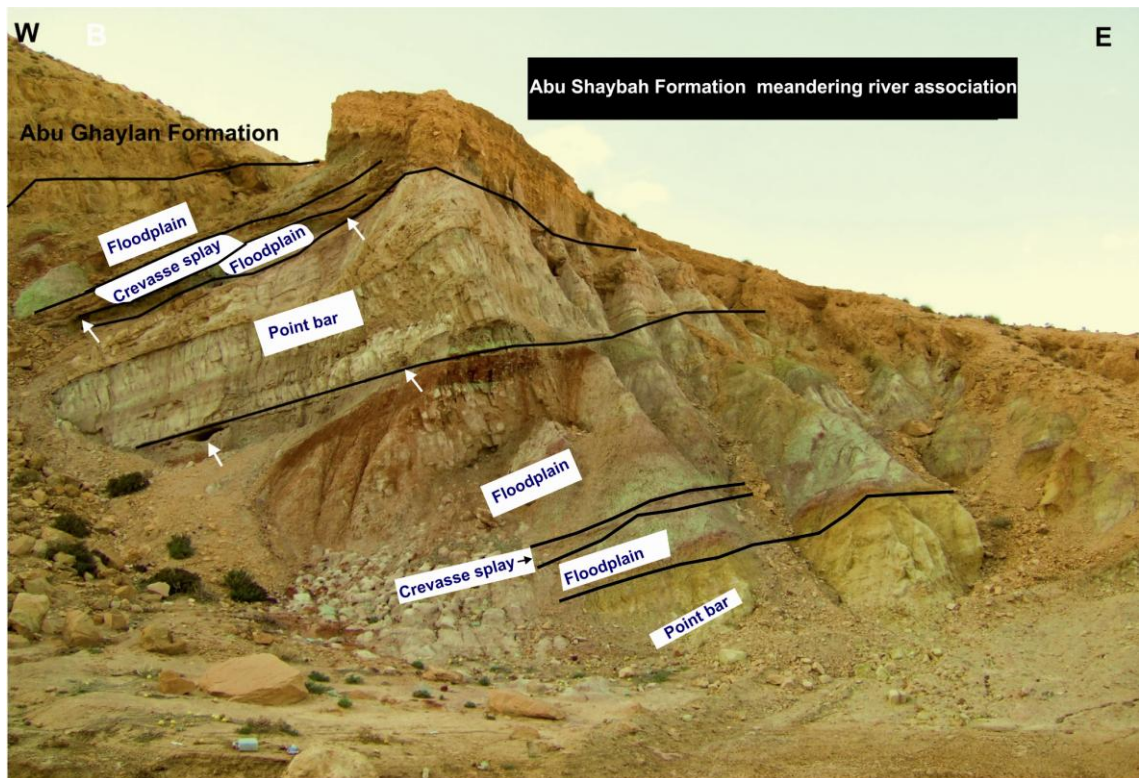


Figure 4.62 Field photograph showing an east looking perspective into the west part of Wadi Abu Shaybah and sketch of locality ❶ in Figure. 4.45 showing units and features exposed within this location (Northwest of Kaf Kalaya). Erosion surface between the sand bodies and mudstone are marked by white arrows.

i) Interpretation

The facies association of the upper unit of the Abu Shaybah Formation is interpreted as a meandering river. Evidence for the meandering river system is based on the lithology, assemblages of sedimentary structures and sediment body architectures. The meandering river comprises a suite of widely recognized components such as channel cut into muds, a series sandstone lateral accretion surface depicted by cross-beds that build from a channel margin, a thick wedge of floodplain sediments and crevasse splay. These recognized components correspond to the facies F-SR, F-MS and F-GS (Fig. 4.64).

This facies association is thought to be product of a fine-grained meandering river due to presence of burrows and thick bedded mudstone facies (Ireland, et al., 1978; Nichols, 2009). Red and green colours may be derived from a high haematite and chlorite content of the cement (Michalzik, 2003). The red mudstone suggests pervasive oxidation of overbank mudstone in a well- drained and well-aerated setting (Ghosh et al., 2006). Mudstone facies (MS and F-GS) and the lateral accretionary architectures of sandstone are interpreted as having been deposited from high sinuosity meandering river system (Fig. 4.64).

Fining-up from coarser at the base to finer succession at the top within cross-beds (Fig. 4.63) are interpreted as point bar. Cross-beds and sandstone facies (F-SR) interbedded within mudstone facies (F-MS) suggest crevasse splay deposits (Olsen and Larsen, 1993; Ulak, 2009). MjØs et al., (1993) proposed that the individual crevasse splay sandstone units are often rooted in the upper part and this can be observed from the Kaf Kalaya section (Fig. 4.63).

The erosional base of facies (F-SR, F-MS and F-GS) comprising the small fining-upward cycles (≤ 1 m thick) suggests an abrupt incision by strong currents into the flood-plain deposits. The interbedded laminated mudstones and fine grained sandstones are interpreted to be representative of floodplain areas. Massive mudstone is interpreted having been deposited within-channel, muddy bars or floodplain. Their structureless nature suggests thorough bioturbation (Hillier et al., 2007; Wolela, 2008).

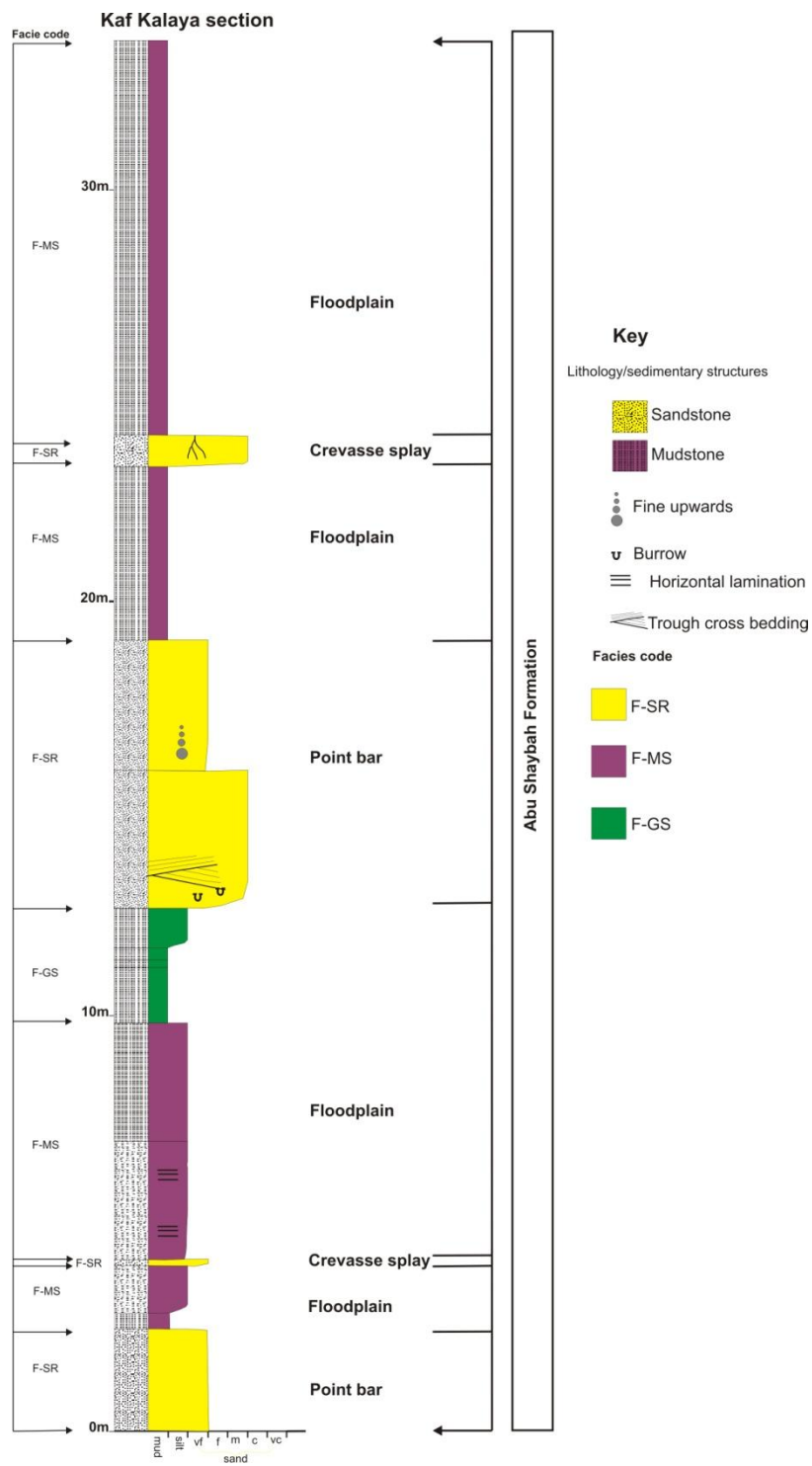


Figure 4.63 Log showing the Upper Unit of the Abu Shaybah Formation at the Kaf Kalaya section. Number seven in Figure 4.33 shows the location where the log was measured. For facies codes see Table 4.3.

Figure 4.63 shows vertical section through a point bar deposit identified at the Kaf Kalaya section illustrating a gradation from coarse material at the base to finer sediments (mud) in the upper of the section. Therefore, the occurrence of the mudstone at the top of the fining-upward succession represents deposition occurring in calm and stagnant conditions (Nakajim, 1982; Ulak, 2009). The high proportion of the mudstone suggests that this period of deposition at least was dominated by a muddy river system (Hillier et al., 2007). The clear presence of palaeosols (F-SR) suggests the presence of extensive flood plain areas adjacent to the main meandering sand channel regions (Ward, et al., 2000; Michalzik, 2003; Ulak, 2009). Burrowed siltstone is interpreted as overbank deposited that developed during flood event or during on early stage of channel avulsion (Labourdette and Jones, 2007).

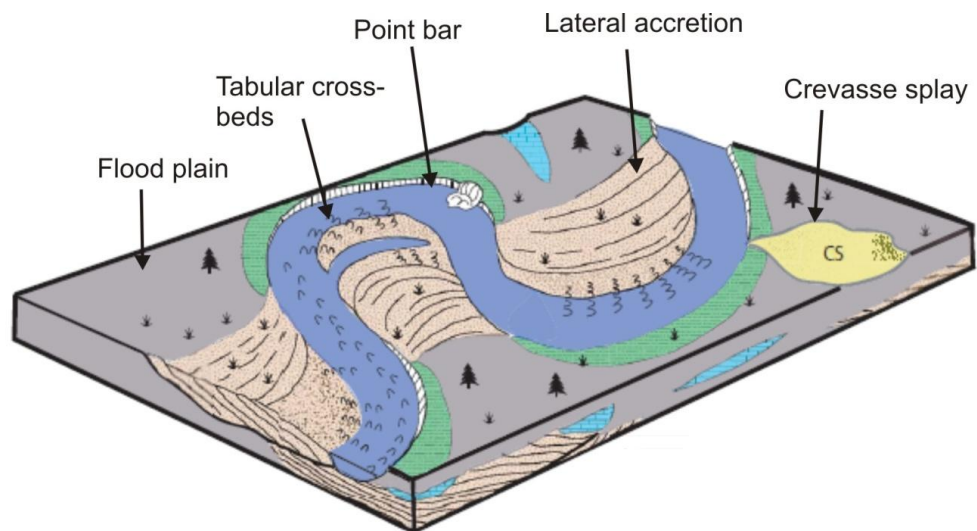


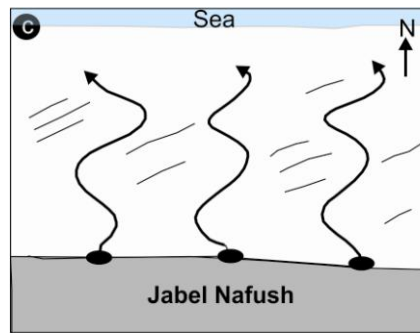
Figure 4.64 Main morphological features of a meandering river (modified after Miall, 1996; Ryan, 2008).

Further evidence for a meandering river system is derived from the wide scatter of palaeoflow directions. This could be due to: 1) changes in the flow strength in the river; 2) non-deposition on the point bar or non-deposition due to climate change from humid to dry. This typically occurs where streams carry a high relative quantity of silt and clay which is easy to transport. The sandstone and mudstone facies were deposited as point bars and over bank sediments.

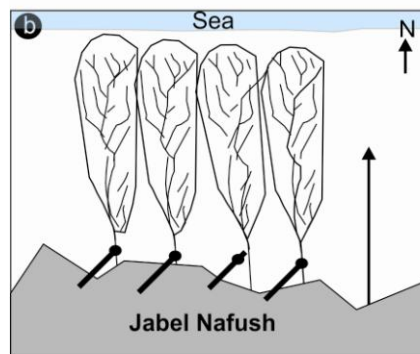
4.10 Palaeogeography of the Abu Shaybah Formation

The upper Al Aziza Formation contact with Abu Shaybah Formation is transitional from marine carbonates to clastic and boundary is conformable. Three facies association from Abu Shaybah Formation are diagrammatically represented by three sedimentary logs and deposition diagrams (see section 4.9). The shallow marine association forms the lowermost sedimentary units of the Abu Shaybah Formation (Fig. 4.65). The sea partially retreats northwards from the Tethyan margin (Libya), the sea level falls and it only remains shallow environment.

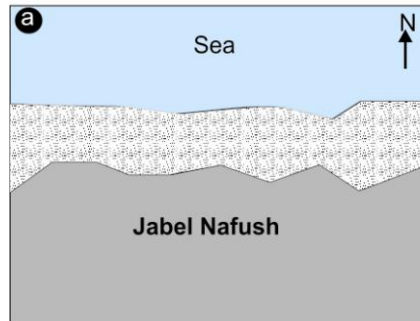
Initial deposition of the lower unit of the Abu Shaybah Formation ended by emergence and establishment of continental conditions (Fig. 4.65). Subsequent changes in the palaeographic setting of the area under study, as integrated part of southern Tethyan basin, and consequent changes in the paleoclimate during the Late Triassic resulted in drastic changes in sedimentary facies from shallow marine to the braid river system and higher sinuosity meandering of the Abu Shaybah Formation. In southern Tunisia outcrop the stratigraphical equivalent of the Abu Shaybah Formation is recognised as the Messaoudi Formation (Dridi, 1998; Swire and Gashgesh, 2000).



Late Triassic fluvial sedimentation continued with a higher sinuosity meandering river



A sea-level fall- deposition of the fluvial system (low sinuosity braided-river)



Early Triassic- Sea-level rise. Deposition of early Abu Shaybah slice

Figure 4.65 Palaeogeographic reconstruction of the Abu Shaybah Formation during the Triassic: a) shallow marine coastal setting, followed by establishment of continental conditions (b-c), characterized by drainage network development that evolves from a braided (b) to a meandering river system (c).

4.11 Driving Mechanisms for Environmental Change

i) Introduction

Spatial and temporal changes in sedimentation can be clarified from the sedimentary sequence. Sequences will fine or coarsen upwards at a range of different scales. The identification of sequences is considered to be a standard methodology for the analysis of genetically related packages of sediment deposited during a particular period in the basin history (Miall, 1996; Nichols, 1999). Sequences are generated by a variety of causes including external (allocyclic) factors such as local to continental-scale tectonics, eustatic sea-level changes and climatic changes (Miall, 1996), as well as the internal (autocyclic) dynamics of a specific sedimentary system. In order to understand the mechanisms driving environmental change, this section identifies sequence patterns within the field area and then discusses these in terms of external and internal driving mechanisms. The sequence patterns are considered primarily using graphic sedimentary log and related data.

Sequences occur at a range of scales and are classified accordingly:

- Sequence = single bed or series of related beds up to 10 m thickness;
- Megasequence = arrangements of related beds and sequences of 10 – 100 m thickness.

Sequences or megasequences that fine upwards correspond to a location where a depositional environment becomes increasingly distal through time (Heward, 1978; Miall, 1996). In contrast, coarsening upwards correspond to a location where a depositional environment becomes increasingly proximal through time (Heward, 1978; Miall, 1996).

There is a relationship between spatial and temporal scales when considering sequence changes and their relationship to driving mechanism. For example, autocyclic factors are typically related to short term (local changes) in environmental behaviour and are characterised by smaller ‘sequence’ scale patterns (0-10 m). Autocyclic behaviour includes sedimentary processes such as channel meandering, avulsion etc. which tend to be reflected on smaller sequence scales (Heward, 1978; Miall, 1996; Bridge, 2003). In contrast, allocyclic factors are related to longer term (regional changes) in environmental behaviour and these are normally reflected within mega-sequence scales (10s-100s m). Allocyclic factors include:

- 1) climate changes which can affect the rates of sediment supply and transport;
- 2) changes in sea level, which controls the space available for erosion and sedimentation as well as acting as a base level for continental sedimentary systems;
- 3) tectonics which also governs the space available for erosion and sedimentation as well as acting as a base level for continental sedimentary systems.

Figure 4.66 shows a composite graphic sedimentary log compiled for all locations in the study area encompassing the Kurrush-Aziza-Abu Shaybah (K-A-AS) Formations. Two megasequences can be identified from this log:

- 1) A coarsening upward megasequence of 170 m thickness characterises the lower to mid parts of the sedimentary succession. This comprises the sandstones, siltstones and mudstones of the Kurrush, carbonates of the Aziza and the sandstones, siltstones and mudstones of the lower unit of the Abu Shaybah Formation. Followed by:

- 2) A fining upward megasequence of 96 m thickness comprising mudstone, siltstone, and sandstone of middle and upper parts of the Abu Shaybah Formation.

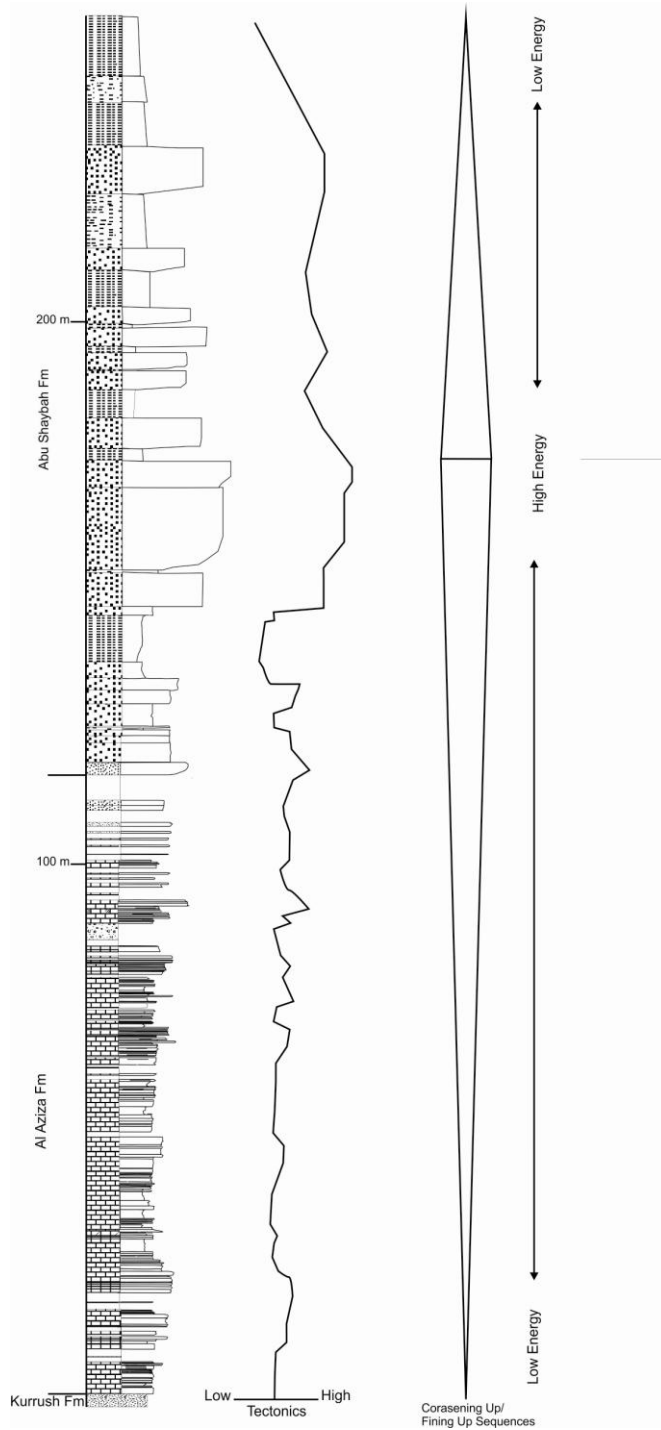


Figure 4.66 Coarsening and fining mega-sequences identified from the Kurrush, Al Aziza and Abu Shaybah Formations (K-A-AS).

ii) Tectonic controls on megasequence patterns

The fining and coarsening upwards megasequence patterns observed in Figure 4.66 could be related to changes in tectonic activity. Tectonic activity can be considered as a sedimentary response to active tectonic processes such as faulting and fault related uplift / subsidence patterns. The coarsening and then fining upwards megasequence could be considered as an increase followed by a decrease in tectonic activity. To explore this pattern aspects of the structural geology (presented in detail in Chapter 7) are briefly reviewed.

An increase in tectonic activity to produce the initial coarsening upwards megasequence could be generated by fault related activity. Extensional faults have been observed within the study area (Chapter 7) but these cross-cut all of the studied stratigraphic formations. Cross-sections through the study area do not significantly demonstrate thickening or thinning of stratigraphic units between fault structures. Collectively, these observations suggest that syn-tectonic sedimentation did not occur (at least in the study area) and that faulting occurred after sedimentation of the K-A-AS Formations. The literature that reviews Mesozoic tectonic activity in the broader region (e.g. Desio et al., 1963; Boot et al., 1998; Swire and Gashghesh, 2000) suggests that active rifting was taking place during sedimentation of the K-A-AS Formations. This tectonic activity appears to be focussed along major E-W fault structures that form part of the Aziziyah fault system immediately to the north of the study area (Chapter 7). Sub-surface datasets from which cross-sections have been compiled show significant thickening of K-A-AS and equivalent strata to the north of the Aziziyah Fault system (Pizzi et al., 1999; Klett, 2002; Letouzey et al., 2005). Clearly, the study area occupies a rift flank / broad footwall region and such areas commonly undergo uplift during rifting (Steckler et al., 1988). Thus, although there is no direct evidence for fault activity within the local study

area it is possible that the initial coarsening upwards megasequence could be a function of the broader regional scale rifting process characterised by relative uplift and tilting towards the south into, across and beyond the Aziziyah fault zone. The uplift and tilting would certainly drive a lowering of base-level, which in turn could manifest itself in a drop of sea-level (see below). This would support a change from marine to continental conditions as observed in the conformable transition between the Al Aziza and Abu Shaybah Formations and thus, progressive coarsening upwards.

It is possible that uplift may have occurred much further to the south of the study area in the continental interior of the Gondwanan landmass. Large (modern) continental landmasses are commonly subjected to neotectonic activity, normally in relation to mantle processes whereby uplift is generated by rising plumes associated with hot spots (Farahat et al., 2006). Such activity can express itself in the creation of topography with significant (km-scale) relief. This in turn would create upland areas that can be subjected to erosion, the products of which would be transported and deposited into continental margin areas. The facies and provenance of the Abu Shaybah fluvial sandstones which form the uppermost part of the coarsening upwards megasequence suggests the establishment of a large fluvial system sourcing its sediment from a distant continental interior. Whether the source of this sediment is from an uplifting continental interior is difficult to prove, but given the patterns observed in modern landmasses it is certainly a valid explanation that may warrant future exploration with more data.

The overlying fining upwards megasequence could equally be explained by a reduction in tectonic activity, either associated with the Aziziyah Fault system to the north or uplift within the continental interior. A reduction of activity along the Aziziyah Fault could correspond to a rising of base-level and a reduction of gradient, resulting in a

change from braided to meandering fluvial style as observed in the upper to mid parts of the Abu Shaybah Formation. Equally, a reduction in uplift or even a switching off of tectonics in the continental interior could leave an upland region to simply be eroded, with lower rates of sediment supply to the continental margin and thus the creation of a fining upwards in the study area succession.

Changes in tectonic activity may have influenced local / regional relative sea-level fluctuations. Within the study area tectonic activity appears to be relatively quiescent over the studied time interval (Mid-Late Triassic). The main areas of active tectonics are instead associated with the main Aziziyah fault to the north or possibly inland to the south within the continental interior. Whilst tectonic activity may have slightly modified topographic gradients within the study area (e.g. to produce a braided river: Schumm, 1977), tectonic related changes in local topography appear to be minimal and can easily be explained by changes in sediment supply (see below). Instead, the area appears to have remained as a relatively low gradient plain-like feature during K-A-AS times and as such tectonically driven relative sea level changes are unlikely or are difficult unravel from climate change driving mechanisms.

iii) Climatic controls on megasequence patterns

Climate is the weather conditions of a specified region averaged over a long time interval such as decades, years, seasons, months, or specific dates of a year (Winstanley, 1990). Climate factors include temperature, atmospheric pressure, precipitation, humidity and wind, all of which are influenced by latitude and position relative to land and sea (Winstanley, 1990). Climate controls the degree of rainfall, temperature variability, vegetation types, weathering rates and water discharge that in turn influence sediment supply (Bull, 1991). On a global basis, climate is organised into a series of

zones whereby sedimentary processes and the depositional setting reflect the dominant temperature, precipitation and related characteristics.

The coarsening and fining upwards megasequence patterns observed in Figure 4.66 could be related to changes in climate. To consider this relationship the following climate-related points are considered:

1. Indicators of climate and climate change
2. Climate-related changes in sediment supply
3. Climate-related controls on sea level
4. Tectonic controls on climate change

1. Indicators of climate and climate change

Direct evidence for local climate is provided from palaeosols, palaeontological evidence, sedimentary structures / features and clay mineralogy (Table 4.4). The coarsening upwards megasequence suggests a relatively arid climate, based upon the Al Aziza Formation which comprises lagoonal-like coastal conditions with stromatolites and the basal Abu Shaybah Formation containing desiccation cracks (Paik and Lee, 1998). The fining upwards megasequence appears to record a change from arid to humid conditions on the basis of changes in palaeosol and clay mineralogy. Poorly developed soils with evidence for carbonate accumulation and calcrete development are found in the lower part of the fining upwards megasequence. Within the upper part of the fining upwards megasequence, the soils become better developed showing oxidation, some mottling and an absence of calcrete. Kaolinite is present throughout the fining upwards megasequence but increases substantially with the development of a meandering river system. Kaolinite is an indicator of chemical weathering of acid igneous rocks, typically

under humid to tropical conditions (Dill et al., 1997; Ruffell et al., 2002). The source of kaolinite is not considered to be local and is likely to be derived from the continental interior where igneous rocks are located. The meandering river system in the upper part of the Abu Shaybah Formation is carrying the kaolinite in suspension and then depositing it in substantial flood plain areas where soil formation, with variable drainage, occurs.

Collectively, evidence for specific climatic conditions from the sedimentary succession within the study area appears to suggest climatic change. The majority of the sedimentary succession is characterised by relatively arid conditions. The arid conditions are maintained into the lower part of the fining upwards succession but evidence for a more humid climate begins to appear and become progressively more dominant in the uppermost part of the fining upwards megasequence. A return to arid conditions occurs in the overlying Abu Ghaylan Formation. This is especially clear on a regional scale where thick evaporate sequences are found along strike to the west in Tunisia (Marzouk and Youssef, 2008).

2. Climate related changes in sediment supply and flood regime

Climate controls source area weathering rates and the processes to transport the sediment away from the sites of weathering. The changes in grain size and the changes in environment recorded in the coarsening and fining upwards megasequences observed in the field area suggests that climatic changes may have altered weathering rates and sediment transport processes (Allen and Allen, 1990).

The coarsening upwards would correspond to a progressive increase in sediment supply. This would require a climate change to increase the landmass weathering regime to

create progressively more coarse sediment. It would also require an increase in flood discharge to transport the material away from the site of weathering. This pattern can only be clearly linked to the topmost part of the coarsening upwards megasequence where there is a transition from shallow marine to continental conditions and establishment of the low sinuosity braided river in the Abu Shaybah Formation. In contrast, the fining upwards megasequence would correspond to a progressive reduction in coarse sediment supply (Reading, 1996). The middle and upper parts of the Abu Shaybah Formation record this by a transition in fluvial style from braided (dominance of cross-bedded sandstones) to meandering (channel sandstones encased within thick muds). Whether the flood regime changed during the fining upwards megasequence remains unclear. The amount of water carried by the fluvial system may have remained similar throughout the Abu Shaybah Formation but the change from a braided to a meandering pattern may simply reflect sediment supply / availability (braided = dominance of coarse bedload sediment, meandering = dominance of suspended sediment, Schumm, 1972).

The presence of kaolinite in the fining upwards megasequence appears to be an indicator that the climate in the study area has changed from more arid to more humid conditions (Ruffell et al., 2002). However, a humid climate would have been required at source to weather igneous bedrock in order to create the kaolinite. This appears to have happened at some considerable distance within the continental interior to the south. Therefore it is highly likely that the local climate has remained relatively arid throughout the studied time interval and that the fining upwards megasequence and its dominant kaolinite mudstone composition are reflecting distant, but within catchment climate variability and changes in regional sediment supply.

| Factors | Indicator | Observation | Interpreted | Literature |
|---|----------------------------------|---|--|--|
| According to palaeomagnetic time frame work | Regional (Tectonic and Climatic) | During Triassic time | Northern Libya moved northward over the period of Pangea and crossed the boundary between the humid equatorial and the arid condition in the Late Triassic | This study and Muttoni et al., (2001). |
| Wood debris | Locally | Facies (F-SD) | May suggest climatic evolution to more humid condition | Marzouk and Youssef, (2008). |
| Xerophytic elements | Locally | Kurrush Fm | Humid condition | Kilani-Mazraoui et al., (1990). |
| Carbonates | Locally | Al Aziza Formation | Reflect somewhat semi-arid conditions | Marzouk and Youssef, (2008). |
| Desiccation cracks and vugs carbonate | Locally | Facies (F-SD) Facies (F-VC) | Arid climatic period | Paik and Lee, (1998). |
| Mud | Regional | Facies (F-MS) Facies (F-GS) | A more humid regime leads to persistent mud-rich systems through more intense chemical weathering, the development of soils and presence of vegetation | Tucker, (2003). |
| Calcrete nodules | Locally | Facies (F-CS) | Sub-humid and arid environment | Alonsozarza (2003) |
| Kaolinite | Locally | Facies (F-MS) | Sub-humid and arid environment | Ruffell et al., (2002). |
| Rootlets | Locally | Facies (F-SR) | Arid and semi-arid conditions | Schmid et al., (2006). |
| The mud facies grades laterally westward into evaporate | Locally | Facies (F-MS) Facies (F-GS) | Dry climate | This study |
| Changes in fluvial style | Locally | Upper facies of the Abu Shaybah Fm | Response to variable sediment accommodation space development | Paredes et al., (2007). |
| Upward-coarsening | Locally | Kurrush, Al Aziza and lower of the Abu Shaybah Fm | Climatically driven changes in either water or sedimentary supply | Schumm, (1972). |
| Fining upward | Locally | Abu Shaybah Fm | Interpreted as migration and avulsion of the fluvial channels | Frostick and Reid, (1987). |

Table 4.4 Summary characteristics of the key humidity-aridity palaeoclimate for the Gharian area.

3. Climate-related sea-level change

Sea level will provide accommodation space for sediment deposition and act as a base level for fluvial systems. Global sea levels will commonly reflect the extent of polar ice coverage, with cooler (icehouse) periods marked by lower sea-levels and warmer (greenhouse) periods marked by higher sea levels. The Triassic is a transitional period of marking the onset and establishment of a dominant Mesozoic greenhouse period, after the icehouse conditions of the Permian and Late Palaeozoic (Ezaki, 2009).

A climate-related change in sea level would require a sea-level lowering to occur to produce the initial coarsening upwards megasequence followed by a sea level rise to produce the fining upwards megasequence. These patterns would need to be associated with climatic cooling followed by a warming. The global sea level curves compiled by Haq et al., (1987); Hardenbol et al., (1998); Haq and Al Qahtani, (2005) are closely linked to major climate and tectonic changes. For the Triassic, the sea level data (Fig. 4.67) reveals a series of short term fluctuations that are superimposed onto a longer term rising sea level trend. Precise comparison of the study area stratigraphy and the component coarsening and fining upwards megasequences with the Haq sea level curves requires a robust age control. In this study age control has been established using magnetostratigraphy, and this, together with its tectonic and climatic implications, is detailed in chapter 6. However, the magnetostratigraphy from this study and from existing stratigraphic schemes (Chapter 6, Fig 6.17 and 6.18) suggests that the K-A-AS formations span the Middle (Ladinian) to Late (Carnian) Triassic. Whilst the general Triassic sea level trend is of a relative rise in global sea-level, the Ladinian to Carnian coincides with a shorter term fluctuation when sea-level falls and then rises. Such a fall and rise in sea level could correspond to the observed coarsening upwards and fining megasequences. These megasequences document a withdrawal of marine conditions

(Al Aziza and lower Abu Shaybah), establishment of continental conditions and a change in fluvial style (braided to meandering: middle to upper AS Fm).

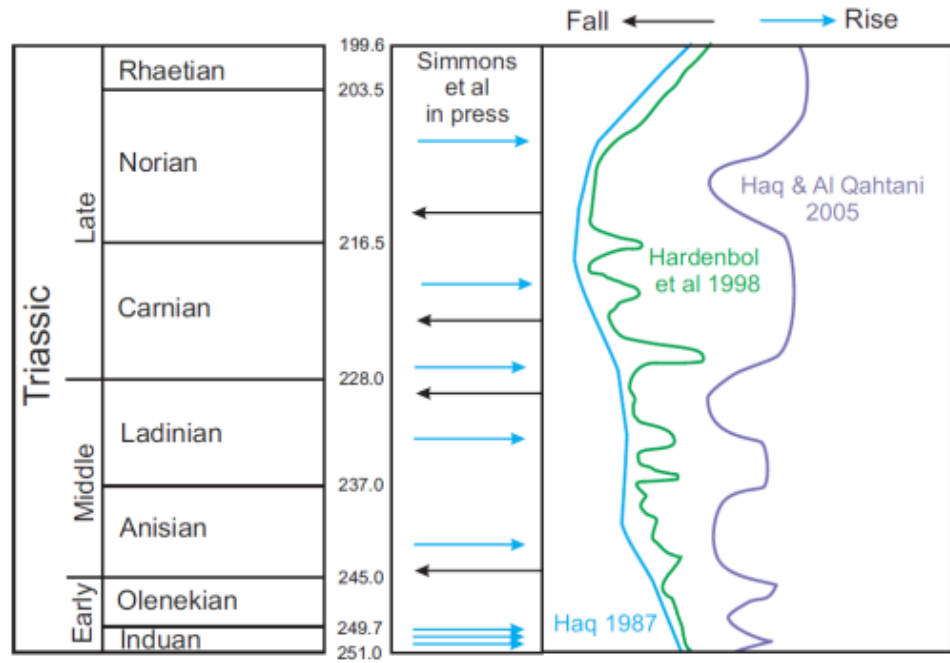


Figure 4.67 Triassic sea-level curves (source Haq et al., 1987; Hardenbol et al., 1996 and Haq and Al Qahtani, 2005).

4. Tectonic controls on climate change

Given that the sedimentary succession in the study area spans the Middle to Late Triassic (Ladinian-Carnian), a period of ~5Ma, it is possible that plate motion could have moved the landmass through different climate zones and thus could account for a climate change. This is a commonly observed phenomenon throughout geological time whereby lateral and vertical plate motions have impacted upon atmospheric and oceanic circulation patterns that in turn have driven regional or even global climatic changes (Pratt, 2000). Evidence for lateral plate motion during the Triassic can be derived from the results of palaeomagnetic studies of the region (Muttoni et al, 2001; Chapter 6). The research suggests that the study area occupied an equatorial location but moved progressively northwards through time. This may have been sufficient to alter the broader regional climatic setting by moving the study area through different climate zones. The evidence for local climatic conditions in the study area (facies, vegetation, soils, clay mineralogy etc.) suggests a dominance of relatively arid conditions throughout the coarsening upwards megasequence. In the overlying fining upwards megasequence the climate appears to become more humid due to the presence of the kaolinite. However, this change to a relatively humid climate may be a localised and short lived occurrence or reflect distant climate changes in other parts of a large catchment area (see previous climate change related variations in sediment supply and flood regime discussion). This observation is based upon the return to arid environmental conditions in the overlying Abu Ghaylan Formation and its laterally equivalent unit to the west, the Bir al Ghanam Formation. In particular, the Bir al Ghanam Formation is characterised by thick gypsum carbonate successions deposited in a continuously sinking show, mostly closed, sedimentary basin varying between lagoonal (gypsum facies) to open marine environment (carbonate facies) (Banerjee, 1980).

Although there may have been a localised change from arid to more humid conditions both within the study area and during the Middle-Late Triassic time interval of study, the regional setting appears to have been consistently arid but with minor climatic changes.

iv) Autocyclic

Although the above lines of evidence support the allocyclic influence of tectonic and climatic, it cannot be totally discount autocyclic as an influence on sedimentation.

Controls on channel meandering and avulsion are considered to be related to autocyclic processes. The fining upwards sequence may reach a thickness of about 8 m (Fig.6.66).

This fining upwards sequence (meandering facies association, Fig. 6.66) could result from lateral autocyclic and avulsion of fluvial system (Allen and Allen, 1990). The fining-upwards sequence would correspond to a progressive reduction in coarse sediment supply and could be due to an increase in generation of accommodation space. This suggests a climatic control which influences the bedload transport capacity of the depositing fluvial system. The presence of kaolinite in the fining upwards sequence is a further indicator that the climate in the study area has controlled the sediment supply and flood regime. It is possible that autocyclic factors are changes in position of the fluvial channels, either by sudden shift mechanisms (avulsion) or by continuous lateral migration. Therefore, it is apparent that the short term autocyclic for fining upwards sequence was governed by allocyclic climatic or tectonic factors.

4.12 Conclusions

A sedimentary succession of more than 250 m thick, span the Middle to Late Triassic is widely distributed in the Gharian area. The sedimentary facies and depositional systems were analysed to provide palaeoenvironmental and palaeogeographic reconstruction for the study area. For the purpose of this study, the Kurrush Formation is not described using fully developed facies analysis as adopted in Al Aziza and Abu Shaybah formations and this is due to poor exposure of facies. The Kurrush is probably deposited in continental to nearshore environments. Seven depositional facies and one facies association from the Al Aziza Formation represents a shallow shelf platform area, which was located in the opening of the Early Triassic Neo-Tethys Ocean. A sedimentary analysis of the Abu Shaybah Formation allows the recognition of ten facies (symmetrically rippled siltstone and fine sandstone, bioturbated fine grained sandstone, massive fine to medium sandstone, sandstone with vug carbonate, medium sandstone with rootlets, trough cross bedded medium to coarse sandstone, tabular cross bedded medium sandstone alternating with pebbles, medium sand with calcrete, red mudstone and green mudstone), then grouped into three facies associations (shallow marine and low to a high energy sand fluvial). It is suggested that the coarsening and fining upwards megasequence patterns can be explained by autocyclic and allocyclic mechanisms which is driving palaeogeographic and environmental changes. A number of important conclusions drawn from autocyclic and allocyclic mechanisms can be summarised as follows:

1. The study indicates that allocyclic control due to local tectonics was not significant but a possible allocyclic control mechanism resulted from regional tectonics.

2. A possible allocyclic controlling mechanism could involve climatic conditions.
3. There is a possibility that climate in the Gharian area was linked to the regional climatic setting by moving the study area to the north during the Early Mesozoic.
4. The presence of kaolinite in the fining upwards megasequence appears to be an indicator that the climate in the study area has changed from more arid to more humid conditions
5. A possible short term fluctuations in SL (SL curves) driving transgression (K-A), regression (AS) and transgression (AG).
6. The fining upwards sequence could result from lateral autocyclic and avulsion of the fluvial system.

Chapter 5: Principles of Palaeomagnetism

5.1 Introduction

This chapter outlines the concept of palaeomagnetic study and how it has been used within this geological study for dating purposes. In addition to identifying the age of the formations, via magnetostratigraphy, the data may better our understanding of the structural development and tectonic history of the area. The main part of the chapter deals with the specific methods, equipment and analytical methods used throughout this research. The second part of the chapter presents a review of magnetostratigraphy.

5.2 The Geomagnetic Field Acquisition of Magnetisation

One of the major objectives of this research is the investigation of age control and plate tectonic movement in the central of Jabel Nafusah region (Gharian area). Changes of the geomagnetic field and the geomagnetic poles observed at the Earth's surface occur on time scales ranging from milliseconds to a few million years. According to Butler (1992) there are two types of changes influencing the geomagnetic field on geological time scales. The first type of changes are much slower with periods of years to million of years and is called no-dipole while the second types change the dipole field with longer periods and it is called dipole. Both the dipole and the no-dipole field are generally affected by secular variation (Merrill and McElhinny, 1983). The dipole field's current intensity is decreasing at rate of approximately 5% per century. At this rate, the field should disappear entirely in approximately 2000 years (Kono, 2006). The best way of describing the geomagnetic field directional changes is simply to plot different magnetic elements such as declination or inclination (defined in Fig. 5.1). Declination (D) is the angle between the magnetic field and geographic north counted clockwise from north, whilst inclination (I) is angle measured in the vertical plane and ranges from -90 to +90.

Rocks often carry a weak but measurable permanent (remanent) magnetism that provides information both on the nature of the past geomagnetic fields and on the position of the rocks at the time of remanence acquisition. In general, igneous and sedimentary rocks are capable of recording the direction of the geomagnetic field and in some cases an intensity proportional to the intensity of the geomagnetic field.

In fact the Earth's magnetic field changes direction intensity and even polarity, when viewed over sufficiently long time spans (Kirsschvink, 1980). This variation is often referred to as paleosecular variation over shorter time periods (directional changes) and the global polarity timescale (polarity changes) over longer periods. Palaeomagnetic studies in general either; 1) exploit this variation in the form of detailed continuous sampling of sedimentary sections (or lava piles) to document these changes and use them as stratigraphic marker tools for correlation purposes, or 2) aim to average out the variation by sufficient sampling usually in the context of regional tectonic studies.

The Natural Magnetization (NRM) of rocks usually relates to two or more episodes in the geological history of the samples. First, a primary magnetization which is related to the ancient field at the time of formation (Tarling, 1971), typically cooling (Thermoremanent Magnetisation - TRM) in igneous rocks or deposition (Depositional Remanent Magnetisation - DRM) and/or immediate post deposition (Post Depositional Remanent Magnetisation - PDRM) in sedimentary (Table 5.1). Any subsequent magnetisation is referred to as a secondary magnetisation and could be acquired at any time up and until measurement in the magnetometer. The natural remanent magnetization (NRM) is the total remanence in rocks before any demagnetization has been carried out (Van der Voo, 1993). The prime function of demagnetisation and the analysis of the demagnetisation (see below) data is to isolate and recover the directions of any and all magnetisation directions and relate these to the timing of magnetisation acquisition.

Having isolated a remanence direction and established its age, usually by a variety of field tests and comparisons to other data, this direction can then be converted to a pole position and compared to others from the same plate and other tectonic plates adjusted for subsequent motion.

| Type of remanent magnetization | Acronym | Description | Type of rocks |
|--|----------------|--|------------------------------|
| Natural Remanent Magnetization | NRM | Sum of all remanences | All rocks |
| Thermoremanent Magnetization | TRM | Magnetization acquired when minerals cool from above the Curie temperatures of their magnetic minerals. | Igneous or metamorphic rocks |
| Depositional Remanent Magnetization | DRM | Magnetization during the depositional process | Sedimentary rocks |
| Post Depositional Remanent Magnetization | pDRM | Magnetization acquired when magnetic grains in sediment are allowed to re-orient themselves in an existing field | Sedimentary rocks |
| Chemical Remanent Magnetization | CRM | Magnetization acquired when chemical changes affect the magnetic minerals | All rocks |

Table 5.1 Summary of different types of natural remanent magnetization (NRM) (combined from Tarling, 1971 and Van der Voo, 1993).

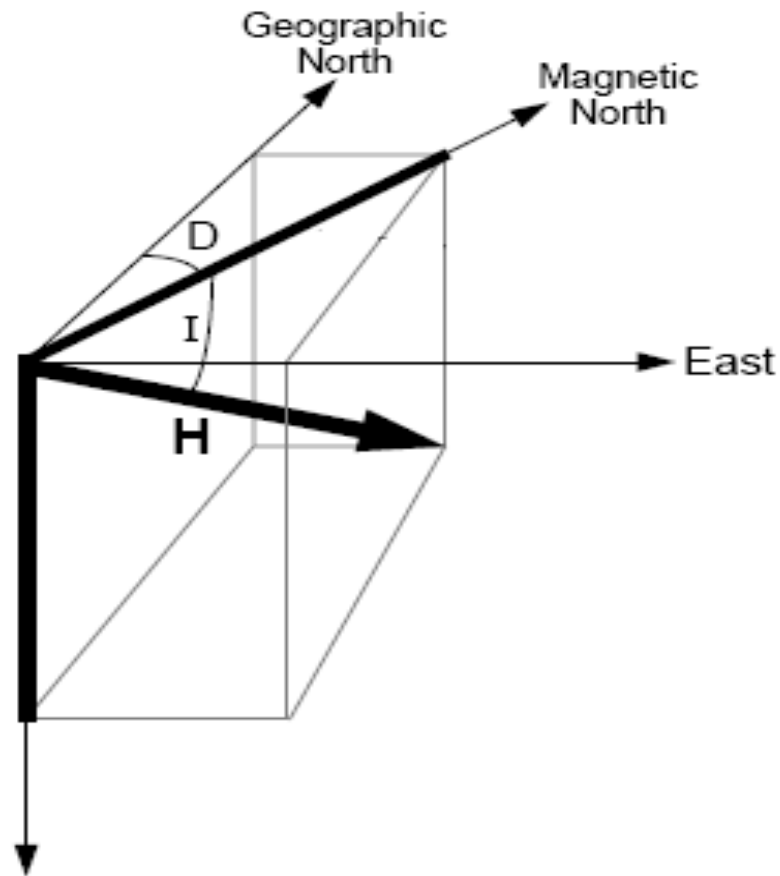


Figure 5.1 Description of the direction of the magnetic field. The total field vector **H** can be divided into a horizontal and vertical component. Inclination, **I**, is the angle measured in vertical plane with range from -90 to +90. Declination, **D**, is the azimuthal angle between the horizontal component of **H** and geographic north; the component of the Earth's magnetic field in the geographic north direction is $\mathbf{H} \cos \mathbf{I} \cos \mathbf{D}$; the east component is $\mathbf{H} \cos \mathbf{I} \sin \mathbf{D}$ (modified from Butler, 1992).

5.3 Magnetic Minerals

Minerals that retain a remanence that can be of any use in palaeomagnetism are very few. However, they are contained in a wide variety of rocks and almost all of them as accessory minerals. The major magnetic minerals responsible for the magnetization can be divided into two solid solution series (Fig. 5.2). The first group is known as the ulvöspinel-magnetite series (Titanomagnetites) ($\text{Fe}_2\text{TiO}_4\text{-Fe}_3\text{O}_4$) with an inverse spinel structure (Tarling, 1971). Magnetite is a dark black, mineral and is very important in palaeomagnetism as the carrier of Natural Remanent Magnetism (NRM). Magnetite (Fe_3O_4) is common in most igneous, some metamorphic and sedimentary rocks. The Curie temperature of magnetite is 570°C . Oxidation of titanomagnetites can take place either at high temperature during cooling of the igneous rocks. Moreover, titanomagnetites can appear as primary minerals in igneous rocks.

The second group of magnetic minerals are known as the ilmenite-hematite series (Titanohematites) (Fig. 5.2) ($\text{FeTiO}_3\text{-Fe}_2\text{O}_3$) and have a Curie temperature of 680°C and are extremely important as the carrier of natural remanent magnetization NRM in a wide range of sedimentary, igneous and metamorphic rocks (Butler, 1992). In sediments, it occurs as black grains or as yellow –brown through orange to red and purple pigments.

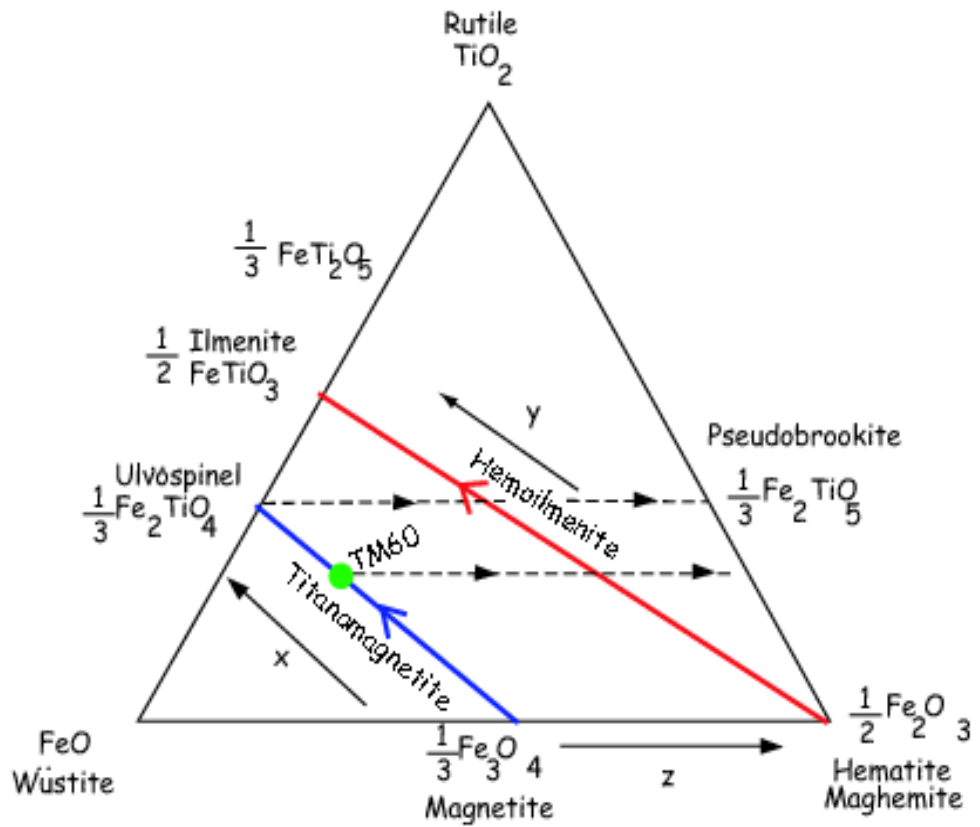


Figure 5.2 Ternary phase diagram of iron and Titanium oxides showing the solid solution series and the dashed lines with arrows indicate the direction of increasing oxidation (Modified from Butler, 1992).

5.4 Demagnetisation

In order to reveal the magnetic history of a rock, samples are progressively demagnetised to isolate all the possible components which it acquired since it was formed (Fig.5.3). There are two laboratory techniques that are available to remove secondary components of magnetisation (Butler, 1992; Tauxe, 2007).

The first technique is known as thermal demagnetisation and is a stepwise procedure in which sample is progressively heated to below the Curie temperature and cooled again to room temperature, and then it is measured. During the heating, the grains with laboratory unblocking temperatures less than Curie temperature will become superparamagnetic and lose their magnetisation (Butler, 1992; Tauxe, 2007). Between these temperatures the grain behaves in paramagnetic behaviour and can acquire a magnetisation. However, this will quickly decay to zero and the grain needs to have a short relaxation time. This relaxation time is a few hundred seconds to hold a stable primary magnetisation. All grains with unblocking temperatures below the high applied temperature at each thermal demagnetisation step will be NRM removed from the specimens.

The general procedure in thermal demagnetisation is to sequentially demagnetize a specimen at progressively higher temperatures, measuring NRM following each demagnetization. The principle of progressive demagnetization is shown in Figure 5.3. Specimens that have two components of magnetization are shown by arrows (Fig. 5.3) whilst discrete coercivities are plotted as histograms (Fig. 5.3). The NRM is the sum of both magnetic components and Figure 5.3 is a summary of possible outcomes:

- a) The two magnetic components are completely separated;
- b) The two magnetic components are partially overlapped;
- c) The magnetic components are completely overlapped;

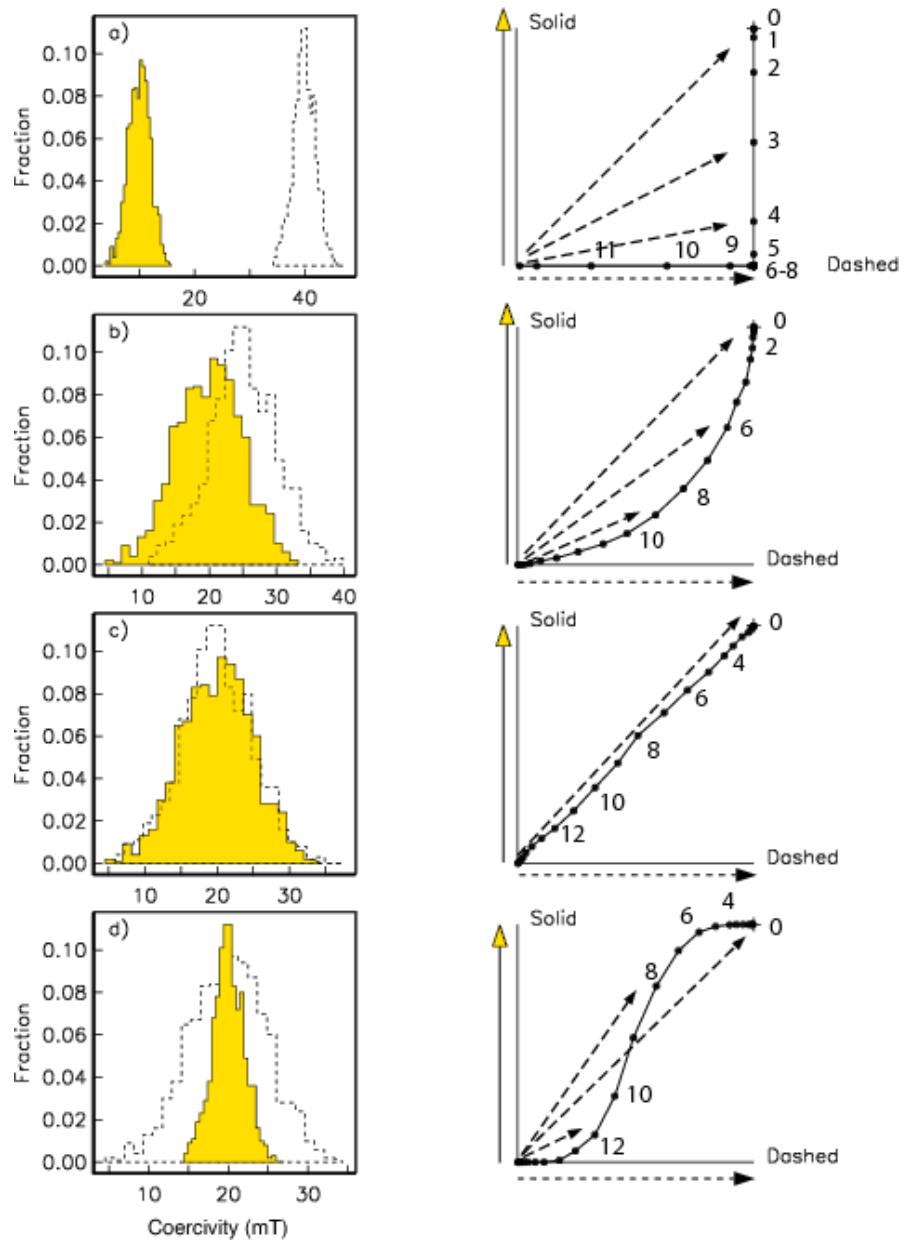


Figure 5.3 Principle of progressive demagnetization. Specimens with two components are shown by arrows on the right hand side whilst histograms are shown on the left hand side (Tauxe, 2007).

d) One distribution envelopes the other.

The second technique of demagnetisation is Alternating Field (AF). In this stepwise procedure samples are placed in alternating field and increased to peak value and then slowly down into zero. All grains with unblocking coercive force below the peak AF will track the field direction. To demagnetise the samples, the amplitude of the AF is reduced by a small amount during each alternating cycle and this field decay to low intensity (zero) with time (Butler, 1992).

The sample is orientated around two axes during Alternating Field (AF) decay to present all axes of the samples to the demagnetiser and this is allowing demagnetisation in a single stage. Therefore alternating field (AF) peak value allows preferential removal of the component with a lower unblocking temperature. A number of samples from Kurrush, Al Aziza, Abu Shaybah and Abu Ghaylan formations were subjected to Alternating Field (AF) demagnetization, however this was found to be less effective in most cases.

For this study, all the specimens were fully and subsequently subjected to thermal demagnetisation. Therefore, choice of thermal demagnetisation techniques for run all samples was based on the behaviour of the samples. This is because magnetization did change in both direction and intensity through the treatment by using thermal demagnetisation. In palaeomagnetism the change in the magnetization, observed during demagnetisation, is usually presented by means of a Zijderveld diagram in which the projections of the data into two orthogonal planes are plotted at each demagnetization step.

5.4.1 Measurements Process

To recover the characteristic remanent magnetization 'ChRM' from the total NRM, specimens are progressively demagnetised to remove secondary component of magnetization. The measurement process can be divided into three major steps:

- 1) The natural remanent magnetization (NRM) of individual samples was measured in terms of the intensity of magnetization (in mA/m).
- 2) Pilot samples from the Kurrush, Al Aziza and Abu Shaybah Formations were selected for testing of stability of the magnetization first against an AF applied stepwise.
- 3) Each sample was thermally demagnetization in a magnetically shielded oven. Typically 12 specimens were demagnetised at a time and each had a 2 cm gap from its neighbour to reduce magnetic interference between the specimens. This is achieved by a long process since it involved 18 demagnetization steps per sample. These steps were 100,120,150, 200, 250, 300, 350, 400, 440, 480, 520, 540, 560, 580, 600, 620, 640, and 660 °C. For each step the specimen was placed in the centre of the oven and heated and cooled back to room temperature in a magnetic field free space.

Moreover, the length of time that a specimen needed to be held at the elevated temperature was initially 20 minutes and got longer with higher temperatures.

Magnetization of the sample was then measured at room temperature after each temperature step with long a Molspin magnetometer and then the procedure is repeated again at successively higher temperatures. In fact the weakest specimen intensities were repeat measured more than twice. These steps were continued until the magnetism of the samples become unstable or too weak to measure with higher temperatures of the samples were 660 °C.

5.5 Presentation of the Directional Data

The magnetic measurements are also displayed as declination and inclination and displayed in a Schmidt equal area stereographic projection. The declination is counted clockwise from north and the inclination (angle measured in vertical plane with range from -90 to +90. Positive inclination is plotted in the lower hemisphere and negative are plotted in the upper hemisphere (Fig. 5.4). Data are displayed on both stereographic projections and a Zijderfeld diagrams and both also show declination and inclination data the Zijderfeld diagram shows changes in intensity of magnetization.

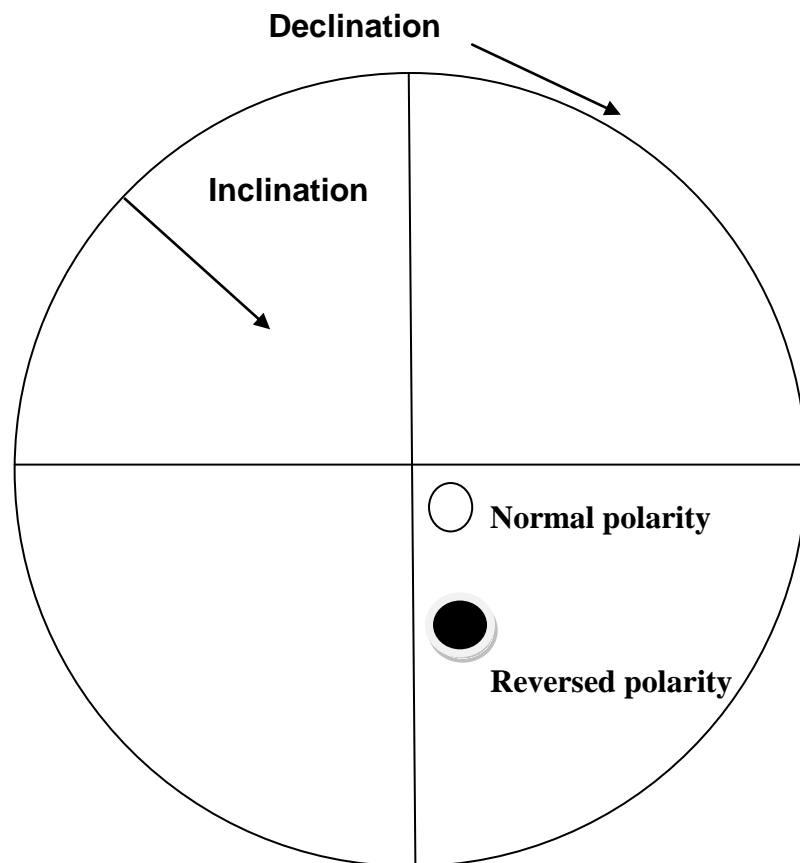


Figure 5.4 Principle of the direction of the magnetic field. The solid dot is of reversed polarity and the hollow circle is of normal polarity.

5.6 Statistical Analysis

The direction of magnetisation and the pole position are analysed using a statistical model developed by the British statistician (Fisher, 1953) to define the distribution of points on a sphere, and is widely used in palaeomagnetic research. Distribution of point on unit sphere will be distribution with probability density function p (Butler, 1992), given by:

$$P_{dA}(\theta) = \frac{K}{4\pi \sinh(K)} \exp(K \cos \theta) \quad (1)$$

Where θ is the angle between the direction of specimen and true mean direction and K is precision parameter. The notation $P_{dA}(\theta)$ is used to emphasize and is a probability per unit angular area. The precision parameter K is a measure of the concentration of the individual data points around the mean direction and can be estimated as:

$$k = \frac{N - 1}{N - R} \quad (2)$$

Where N is the number of direction unit vectors and R is the resultant length of their vectorial sum. The 95% confidence angle and $\alpha 95$ define the accuracy of the mean direction and is the radius of a circle on the surface of sphere. A small value of $\alpha 95$ indicates convergent direction. Small values of $\alpha 95$ indicate reliable mean direction. If the $K = 0$ then directions are random but if the value of K is high they cluster tightly around the mean direction.

5.7 Fold Test

The fold test or bedding-tilt test is most practical field test for assessing the stability and age of palaeomagnetic directions (Butler, 1992). The fold test can also provide crucial information about the timing of acquisition of component of ChRM and folding can be evaluated. The ChRM directions are said to pass the fold test if the direction of remanence from sites or samples around a fold become closely grouped after unfolding it can be suggested that magnetization was acquired prior to the development of the fold (Fig. 5.5). Fail the fold test if the ChRM directions become widely dispersed after the correction and this suggested that magnetization was acquired after the folding.

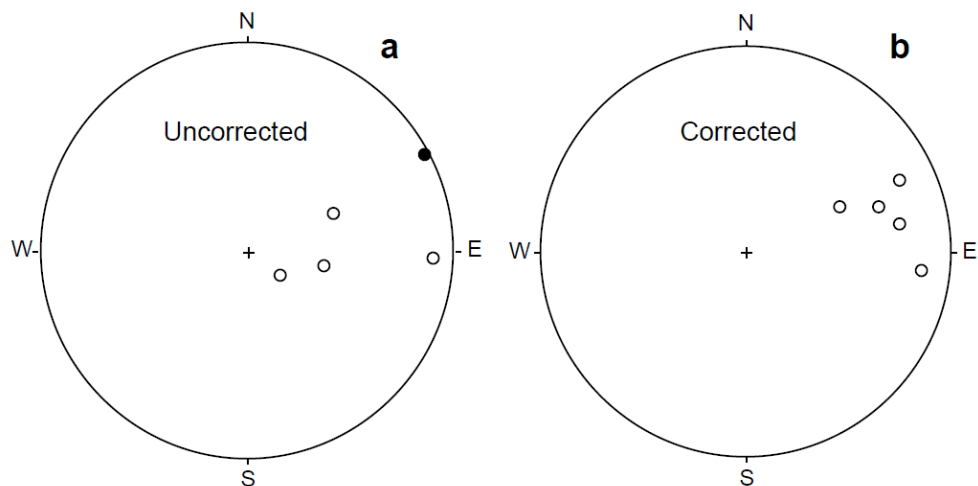


Figure 5.5 Example of ChRM direction that pass that pass fold test. (a) ChRM direction before bedding tilt correction. (b) ChRM direction after bedding tilt correction (Butler, 1992). .

5.8 Palaeomagnetic Reference Poles and Reference Directions

Palaeomagnetic data could be used to determine the palaeolatitude at which rock were magnetized. A reference paleopole is recorded to represent the direction of the magnetic field at specific age. Palaeolatitude determinations are based on the average of the observed directions related to a direction acquired in a dipolar geomagnetic field.

Palaeomagnetic pole position does not coincide with the present geographic pole, but lie on a path which gradually leads way from the present pole same age of the rocks considered.

In order to allow comparison of the pole with the reference poles is by construction of paths. Paths are called apparent polar wander position (APWPs) as the observed movement of the palaeomagnetic pole position reflection the actual drift of continental blocks relative to the geomagnetic pole. Hence determination of the apparent polar wander (APW) paths of major cartons is one of the main objectives pursued by the paleomagnetic community (Besse and Courtillot, 1991). To determine the APWP a best fit path is fitted through the data points (Fig. 5.6) this is normally done by applying time window to the data (Irving and Irving, 1982).

The precision of path varies from continent to continent and this due to; 1) the quantity and quality of paleomagnetic data; 2) depends on geologic age. As the rocks in this area under study are Mesozoic in age, thus apparent polar wander position (APWPs) covering this time scale is considered. A review of Permo –Triassic palaeomagnetic data for Libya and other continents which could be used as reference for the Libya data. The paucity of Permo –Triassic palaeomagnetic data from Africa and other continents results in poor definition of the late Permian to late Triassic of the African APWP.

Moreover, there are numerous Early Permian to Early Jurassic paleopoles from North America and Europe which delineate polar wander path, but Early Permian and the Late Triassic/Early Jurassic the polar wander path (APWP) for the west Gondwana is

too poorly defined (Muttoni et al., 1996). Besse and Courtillot (1991) proposed that four criteria need to meet by an individual pole to pass the reliability criteria. These criteria are following as

1. Mean direction are based on six sites per pole and six samples per site;
2. Directions have 95% confidence interval less than 15° for Mesozoic;
3. Directions are based on successful thermal demagnetisation or AF;
4. Maximum dating uncertainty of 15 Ma.

A pole position was calculated for each of the formations involved in the present study therefore that reliability of these data can be compared with one another and also with other Mesozoic pole positions and palaeolatitude for the Africa and Southern Alps (section 6.5).

5.9 Magnetostratigraphy Overview

Magnetostratigraphy is a chronostratigraphic method used to date both sedimentary and volcanic sections. Magnetic polarity is called normal (N) if the field directions are parallel to the present dipole polarity and reversed (R) if opposite (Muttoni et al., 2010). Rocks have the same age but from widely separated collecting localities were found to have the same polarity.

The characteristic remanent magnetization ('ChRM') direction for samples was used to compute the Virtual geomagnetic pole (VGP) latitude for each stratigraphic horizon. Therefore, the Virtual geomagnetic pole (VGP) could be used for magnetostratigraphy investigation. These palaeomagnetic data are plotted against stratigraphic position. Hence these data are then used to define a magnetic polarity zonation for the

stratigraphic section. Magnetic polarity zone is the corresponding interval in a stratigraphic outcrop deposited during the polarity chors.

Magnetostratigraphic studies represent an important method for correlation purposes since they deal with global synchronous events such as inversions of the magnetic field. Hence recognition of the characteristic magnetic polarity and subsequent correlation with the Global magnetic polarity time scale may provide an additional key in the determination of the age.

There are there factors can be used to correlation magnetic polarity zone to the sequence of magnetic polarity chrons of the GPTS (Butler, 1992) and these are:

1. The quality of palaeomagnetic data used to define the polarity for each samples;
2. Stratigraphic coverage of sites used to define the magnetic polarity zones;
3. Matching between the pattern of magnetic polarity zone and the GPTS.

However, equivocal correlation (Muttoni et al., 2004) may appear from; 1) presence of localized remagnetization; 2) age model uncertainties; 3) incomplete recovery of the magnetic polarity zone; 4) differing patterns of distortion of the polarity patterns due to variations of sediment accumulation rate.

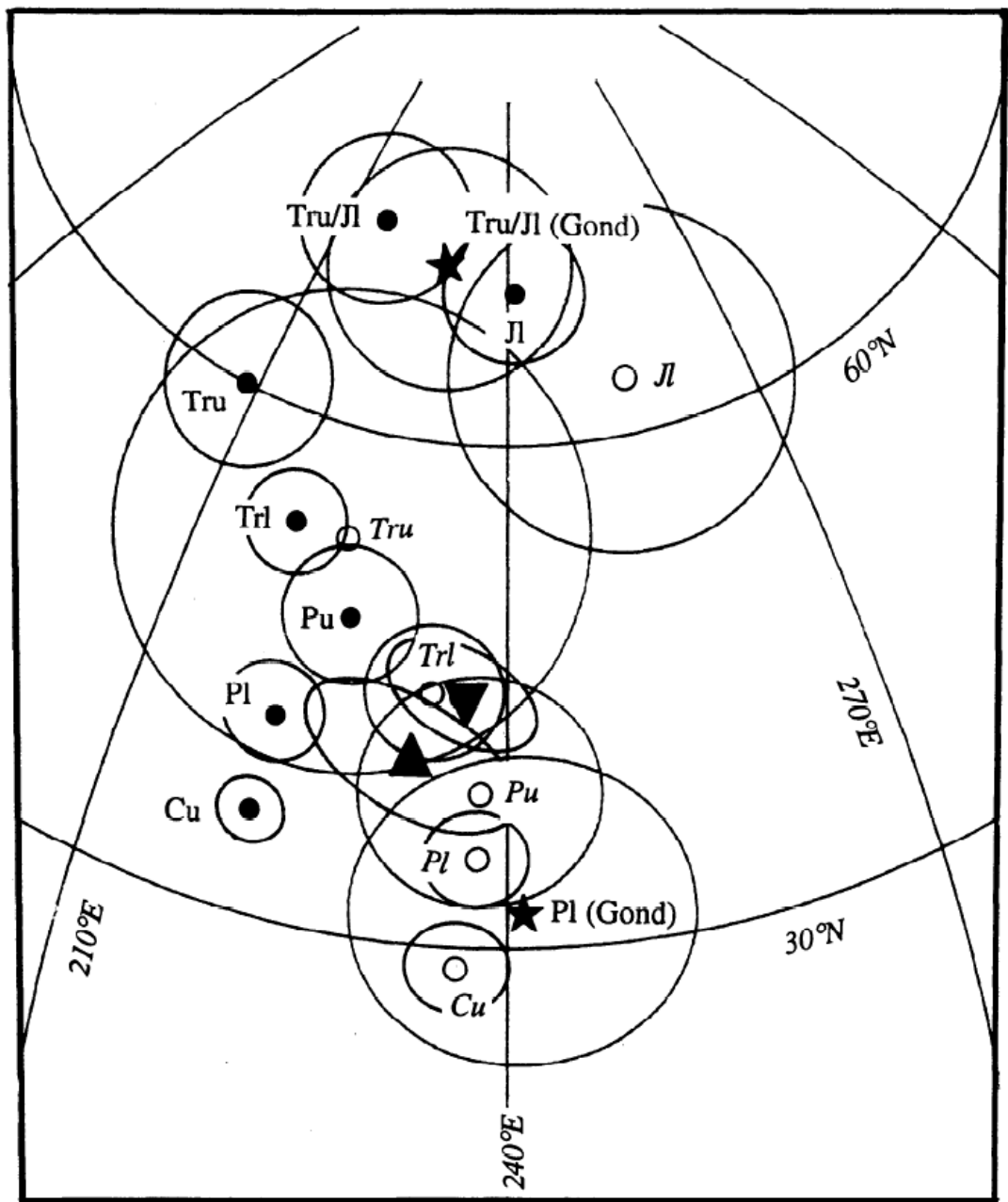


Figure 5.6 Africa paleomagnetic poles for Upper Carboniferous (Cu) to lower Jurassic (Jl) compared to pole from Triassic pelomagnetic data (Italy) (Channell and Doglioni., 1994). Solid circles North American poles (Van der Voor, 1993) related to African coordinates.

Chapter 6: Palaeomagnetism of the Mesozoic Units of the Gharian Area

6.1 Introduction and Rationale for the Study

The primary target for this study was the Al Aziza and Abu Shaybah Formations as their age of deposition is poorly constrained based on very limited fossil evidence (as discussed in Chapter 3). Type sections of both formations lie between Wadi Abu Shaybah and Gharian itself (GR. 0312972 3562969). Given that they are supposedly of Ladinian and Carnian age they should both exhibit multiple polarities based on the current understanding of the Geomagnetic Polarity Timescale (Hounslow and Muttoni, 2010). In addition, limited sampling of the Kurrush and Abu Ghaylan formations stratigraphically immediately below and above our primary section have been carried out.

6.2 Previous Research

The Aziza Formation has been palaeomagnetically studied previously. The first study, based on a section in Al Azizyah town itself (Fig. 6.1) failed to isolate any useful information due to limited demagnetisation and lack of a sufficiently sensitive magnetometer (Martin, et al. 1991). A more recent study (Muttoni et al., 2001) sampled the Aziza Formation at quarries (Fig. 6.1) again in Al Azizyah (32.5°N, 13.2°E) and also at Kaf Bates (32.4°N, 13.1°E). They measured the NRM of all specimens using a squid cryogenic magnetometer (at ETH Zurich) and all samples, bar a small number used for AF pilot studies, were stepwise thermally demagnetized in 20 steps up to a maximum temperature of 670 °C in a magnetically shielded oven.

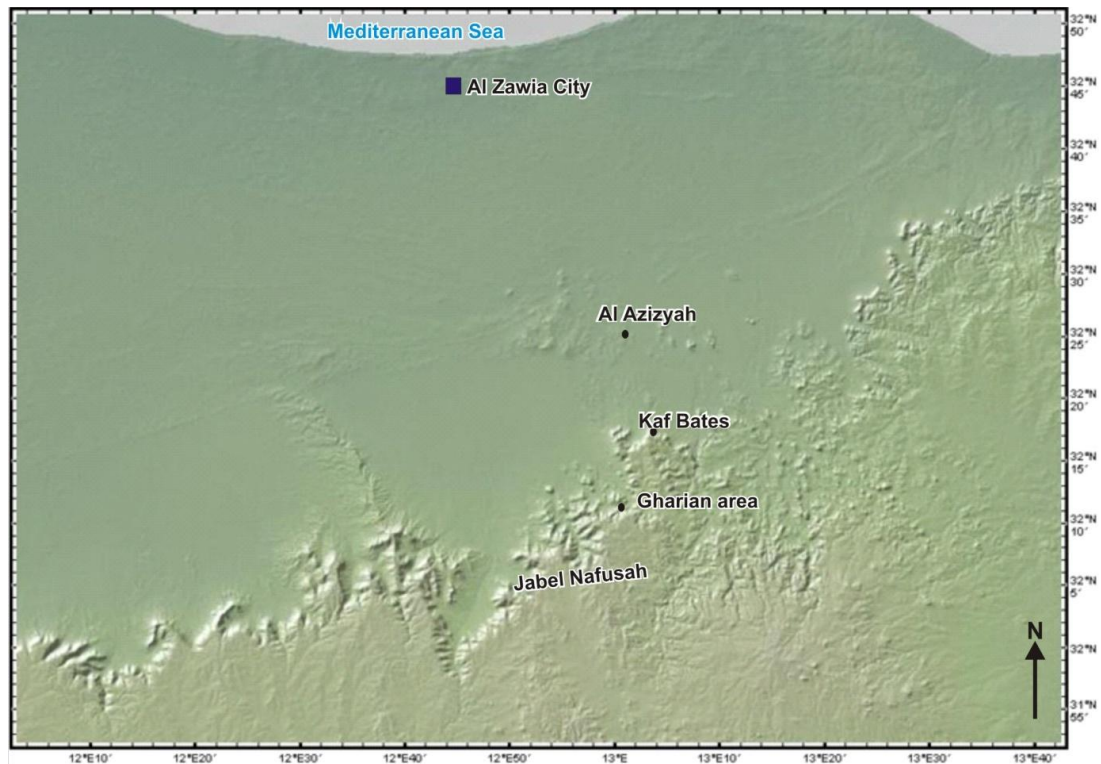


Figure 6.1 The location of the Al Azizyah and Kaf Bates quarries with respect to the Gharian study area and Al Zawia superimposed on a DEM showing the Jafrah plain and Jabel Nafusah uplift.

The Muttoni et al. (2001) study revealed three apparently distinct components (Fig. 6.2 and Table 6.1) as follows:

“A” - a component isolated between room temperature and 200°C and present in 58% and 70% of samples at Al Azizyah and Kaf Bates respectively. Based on its low unblocking temperature, northerly declination, and positive inclination this component was interpreted as being acquired in the Present Day field direction.

“B” - a NW (SE) with positively (negatively) inclined dual polarity direction which was typically isolated between 200 and 500°C but occasionally persisted up to a maximum

of 670°C. The “B” component pole was considered to be an Early Jurassic overprint being comparable to other palaeopoles from Africa and Adria of that age.

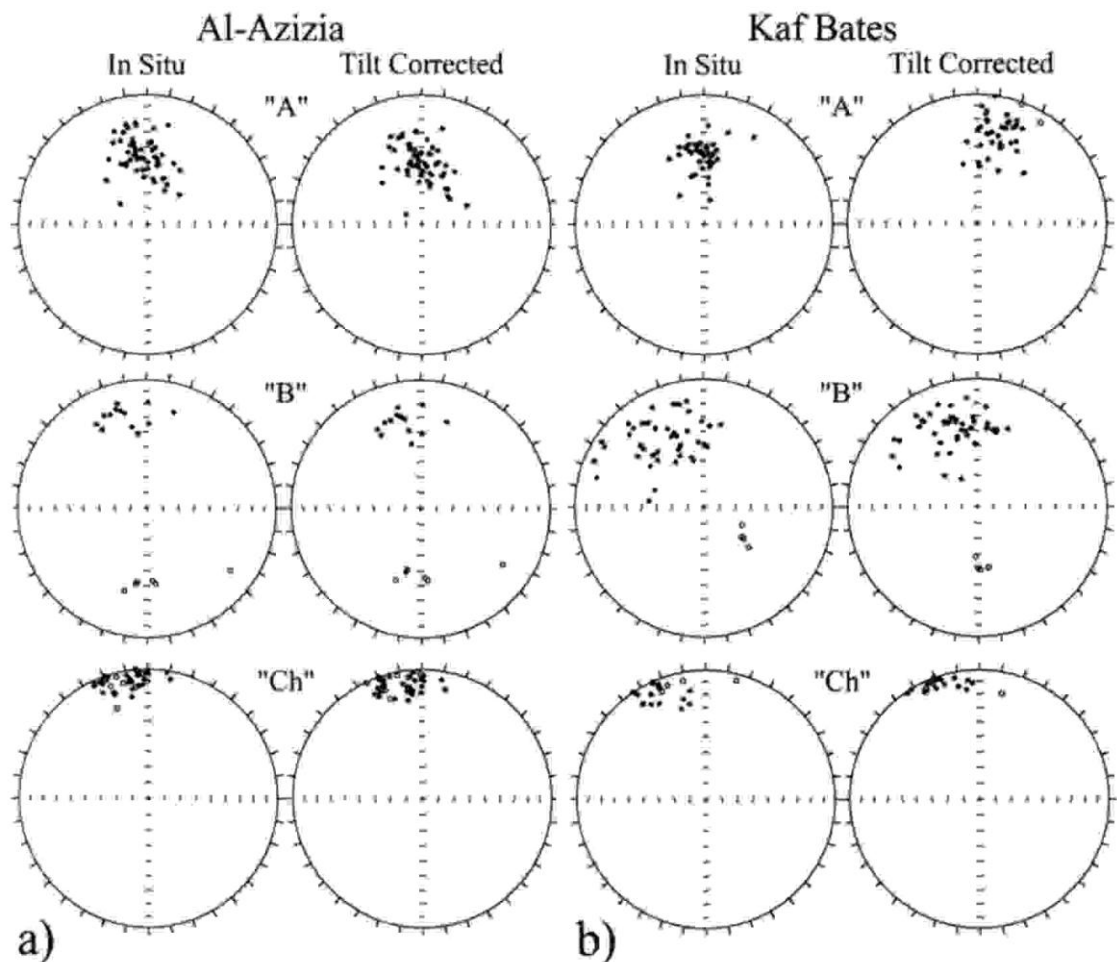


Figure 6.2 showing their isolated components for specimens denoted as A, B and Ch on equal area projections for both sampled localities (Muttoni et al., 2001). Filled (open) circles represent positive (negative) inclinations.

| Comp | %Normal | n/N | In Situ | | | | Tilt Corrected | | | |
|-------------------|---------|---------|---------|------|----|----------------|----------------|------|----|----------------|
| | | | Dec | Inc | k | α 95 | Dec | Inc | k | α 95 |
| Al Azizia A | 100 | 058/109 | 355.5 | 45.6 | 26 | 3.7 | 000.1 | 50.4 | 25 | 3.8 |
| Kaf Bates A | 100 | 039/068 | 358.6 | 45.6 | 36 | 3.9 | 012.7 | 28.1 | 22 | 5.0 |
| Al Azizia 'B' | 68 | 019/109 | 349.2 | 30.8 | 22 | 7.3 | 350.7 | 35.9 | 21 | 7.4 |
| Kaf Bates 'B' | 91 | 046/068 | 327.7 | 38.9 | 12 | 6.4 | 343.6 | 36.9 | 17 | 5.3 |
| Al Azizia 'Ch' | 100 | 040/109 | 349.0 | 1.5 | 35 | 3.9 | 349.5 | 6.9 | 36 | 3.8 |
| Kaf Bates 'Ch' | 100 | 020/068 | 339.0 | 7.9 | 25 | 6.7 | 341.7 | 2.7 | 36 | 5.5 |

Table 6.1 Results of Muttoni et al., (2001). The abbreviations are: Comp is the magnetization component; % Normal: percentage of samples bearing normal polarity; n: the number of samples used to calculate the mean; N: total number of samples; Dec., Inc: declination and inclination; K: Fisher precision parameter; α 95: the precision parameter and cone of 95% confidence of standard Fisher statistics.

“ChRM” – the characteristic component they defined as being NW directed with a shallow positive inclination (Normal polarity) and found in samples with either only an A component or with A and B components. It was always isolated at temperatures below 550°C. The “ChRM” component was interpreted as being primary in origin by Muttoni et al., (2001), because, in tilt corrected coordinates, it yielded a pole consistent with Early-Middle Triassic poles from the southern Alps. While they do not state that the data pass a fold test they do imply it. The age of the pole was further refined to latest Ladinian to earliest Carnian age based on limited findings from two palynological samples from the section studied for paleomagnetism.

The lower sample yielded a Ladinian/Carnian assemblage and the upper an earliest Carnian. The shallow inclination of the 'ChRM' component indicates that it was acquired at low paleolatitudes in the northern hemisphere consistent with the known palaeogeography of the region (Muttoni et al., 2001). However, Hounslow and Muttoni (2010) recently defined the Ladinian-Carnian stage boundary as being coincident with a reverse to normal polarity change such that the lowermost Carnian is of normal polarity (Fig. 6.3). The absence of reversed samples in the Aziza Formation study suggests that the sampled strata are probably of early Carnian age and that the section in Al Azizyah does not in fact include the boundary itself as a consequence of the limited thickness (~25 m) of strata actually sampled (see Muttoni et al., 2001).

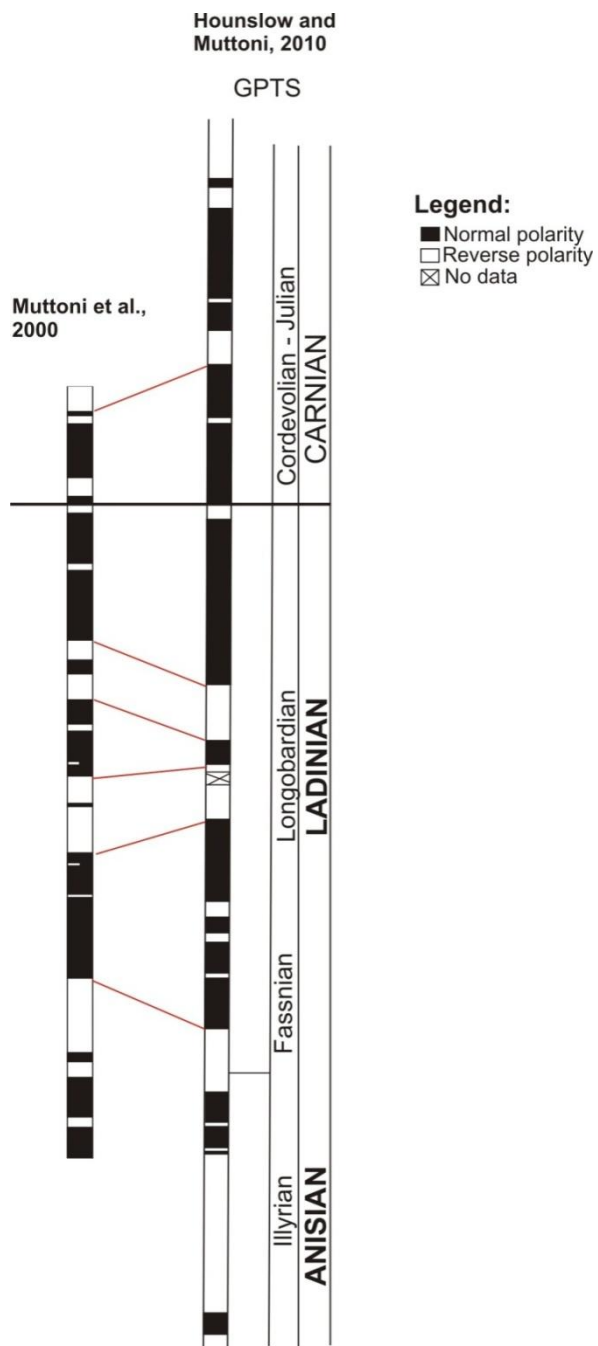


Figure 6.3 Magnetostratigraphy across the Anisian-Ladinian-Carnian boundary (Muttoni et al., 2000; Hounslow and Muttoni, 2010).

6.3 Palaeomagnetic Sampling Localities

The samples for this palaeomagnetic study were collected from the central Jabel Nafusah in the Gharian area (Fig. 6. 4 and Table 6.2). The Kurrush Formation was sampled in Wadi Abu Shaybah in two small sections a short distance apart (KU1 and KU2; Table 6.2, Fig. 6.4).

The Al Aziza Formation was sampled in two (stratigraphically) overlapping section (AZ1 and AZ2) in Wadi Abu Shaybah (Fig. 6.5 & Table. 6.2). The Al Aziza Formation has a total thickness of 140 m and comprises limestones, dolomitic limestones, siltstones, and claystone (see Chapter 4, section 4.4). Samples were selected based on the quality of exposure and the outcrops capacity to produce viable samples (i.e. well consolidated material) when drilled. Hence, few siltstones and claystones were collected due to their friable to very friable state in most cases.

The Abu Shaybah section has a total thickness of 125 m and comprises mainly sandstones and siltstones (see Chapter 4, Fig. 4.24). It was sampled at 4 sites where fresh faces were exposed, these are: Wadi Gabel (WG) stream section; Abu Rashada (AR) road section; Kabted Jamal (KC) quarry section and Trak AL Hamer (ER) road section both just NW of Qasam village (Fig. 6.4 and Table 6.2). Limited sampling of the Abu Ghaylan Formation (AG) was carried out in a stream section stratigraphically and topographically immediately above the Abu Shaybah Formation and the main sampled Al Aziza (AZ1) section where it is in apparent continuity with the Abu Shaybah unit below (Fig. 6.4).

In total nine sections were sampled yielding a total of 234 oriented samples (Table 6.2). Detailed sedimentary logging accompanied or preceded all of the magnetostratigraphic sampling in the Gharian area (Fig. 4.24 & Fig. 6.5).

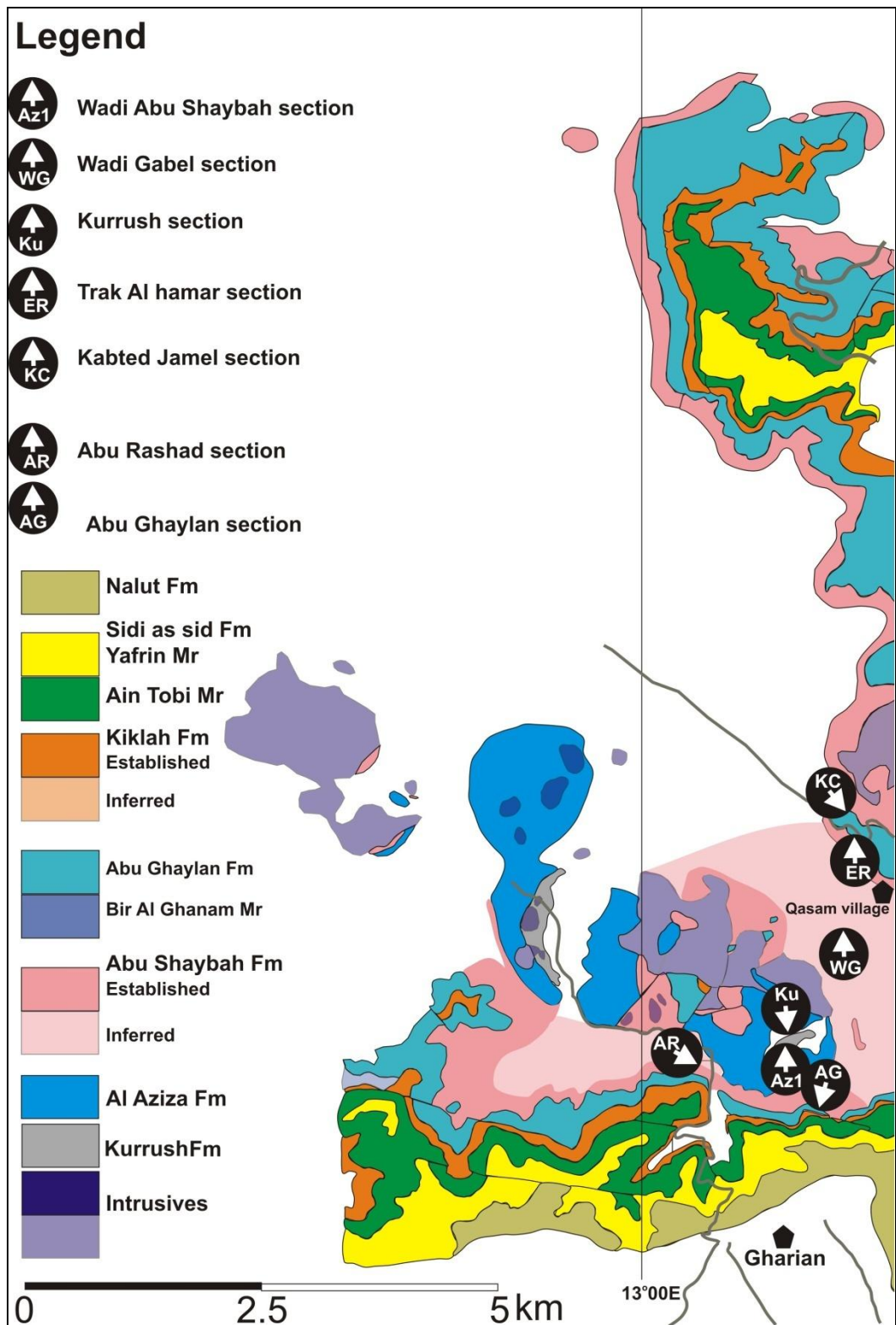


Figure 6.4 Location map of the palaeomagnetically sampled sections in the Gharian area. Ku is the Kurrush Formation and AZ1, AZ2 the Al Aziza Formation. Both are located in Wadi Abu Shaybah. The Abu Shaybah formation was sampled at AR (Abu Rashada road) WG (Wadi Gabel) ER (Trak Al Hamar road) and KC (Kabted Jamel). The Abu Ghaylan Formation (AG) was sampled in an extension of the longest AZ1 section.

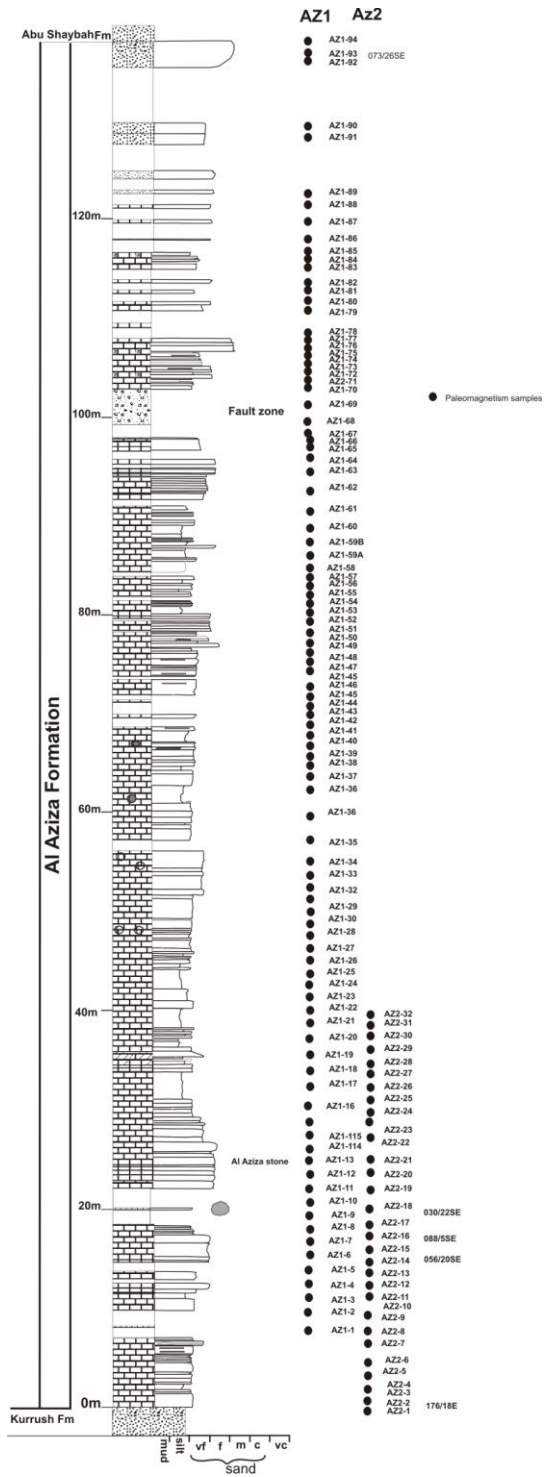


Figure 6.5 Composite log of Al Aziza section sampled in two overlapping sections AZ1 and AZ2 for palaeomagnetic analysis.

| Formation | Locality | Total Number of samples | Code | RG | Lithology |
|-------------|--|-------------------------|------|-----------------|-----------|
| Kurrush | Wadi Abu Shaybah in two sections | 4 | KU1 | 0312853 3563042 | Sandstone |
| | | 2 | KU2 | 0312845 3561991 | |
| Al Aziza | Wadi Abu Shaybah in two section | 94 | AZ1 | 0312972 3562969 | Carbonate |
| | | 32 | AZ2 | 0312805 3562881 | |
| Abu-Shaybah | Abu Rashada Kabted Jamel Wadi Gabel Trak Al hamer | 32 | AR1 | 0312181 3562806 | Sandstone |
| | | 21 | KC1 | 0313397 3566003 | |
| | | 19 | WG1 | 0313537 3564033 | |
| | | 19 | ER1 | 0313687 3565659 | |
| Abu-Ghaylan | Wadi Gabel | 11 | AG1 | 0313070 3562335 | Carbonate |

Table 6.2 Summary of the palaeomagnetic sampling localities in the Gharian area.

6.4 Results

6.4.1 Initial NRM

Measurement of the total NRM intensity before demagnetization revealed that many samples, in all formations, were extremely weak ($\leq 0.5 \times 10^{-5} \text{ Am}^{-3}$) and therefore at or below the ‘background’ sensitivity of the magnetometer used and therefore demagnetization was not practicable. This was particularly the case for samples from the Kurrush, Abu Shaybah and Abu Ghaylan formations. In other cases the NRM was reduced to this level after only a few demagnetization steps. However, the majority of the Aziza Formation samples although found to be weak in terms of intensity did yield usable demagnetization data.

6.4.2 Demagnetization

Pilot samples from all formations were subjected to stepwise applied AF demagnetisation. These pilot samples all behaved in a similar manner whereby the magnetization did not show significant directional changes and only limited decay of the magnetisation intensity throughout the treatment. This suggested that hematite may have been a significant carrier of remanence and hence it was decided that thermal demagnetisation, although considerably slower in operational terms, had the potential to

yield better results. Consequently for the main study, all samples were subjected to progressive stepwise thermal demagnetization up to a maximum of 660 °C in 18 steps. Thermal demagnetisation was therefore undertaken using the ‘Shaw’ MMTD1 oven using appropriate ramp, hold and decay times. Demagnetization results were plotted on orthogonal diagrams (Zijderveld, 1967) and stereographic projections as discussed Chapter 5 (section 5.5).

6.4.3 Demagnetization of Samples of the Al Aziza Formation

The demagnetisation behaviour of the Al Aziza Formation samples was found to be highly variable (see Table 6.3 for an overview of the components isolated in each sample and with respect to their unblocking temperatures). Some 15% of samples yielded no useful information either being too weak or completely unstable to demagnetisation. A further 20% of samples yielded only a northerly directed, moderately inclined positive directions, referred to as a the “A” component hereafter, during the first few steps of demagnetisation after which they failed to yield any further useful information (Fig. 6.6 a, Table 6.3). Exceptionally this “A” component was found to persist throughout the temperature range and even, apparently, to temperatures as high as 580-600°C (e.g. sample AZ1-77 and AZ1-88 in Fig. 6.6 a).

The great majority of samples exhibit multi-component behaviour yielding interpretable data indicating at least two and often three (or more) apparent components of magnetisation. The most common initial behaviour of these multi-component samples is to yield an “A” component isolated at or below temperatures of 150°C as the first component isolated (Table 6.3 see Figures 6.6 a,b and c). Although not investigated in detail two other behaviours at low temperatures demagnetisation steps were also observed which typically preceded or replaced the “A” component. In a few samples the

first, low temperature component, was randomly orientated and is therefore believed to be the result of post sampling, viscous acquisition in the laboratory field; a second and even rarer occurrence was of the recovery of very steep directions close to the long (Z) axis of the sample which may have been the result of drilling induced remanence. Both of these magnetisations are forms of Viscous Remanence Magnetisations commonly observed in many palaeomagnetic studies (Weaver et al., 2002; Yu and Tauxe, 2006; De Kock et al., 2009).

In terms of actually resolvable directions, two-component behaviour was more common than three component (Table 6.3); although overlap of these two higher temperature components is such that many samples showed partial curved or spurious linear trajectories on Zijderveld diagrams (indicative of overlap) and that could not be fully resolved (e.g. Sample AZ1-47, AZ1-54 and AZ1-89 in Fig. 6.7 and for more details see section 5.4 in Chapter 5, Fig. 5.3). For further directional statistical analysis only the most clearly resolved of directions were used and the use of great circle analysis (McFadden and McElhinny, 1988) was deliberately limited.

The most commonly isolated higher temperature component is of dual polarity and lies in the SW quadrant with shallow inclinations or its antipode. This component, referred to as the “C” component, was generally isolated between temperatures of 200 to 250°C and 540°C occasionally persisting to above the Curie Temperature of magnetite at 578°C suggesting that it could be carried both by titanomagnetite and hematite carriers (e.g. sample AZ1-33, AZ1-78 and AZ1-94 in Fig. 6.7). The broad range of unblocking temperatures, resistance to AF demagnetisation previously noted yet typical peak unblocking temperatures in the 500-540°C range tend to suggest the presence of small (single domain, hence the high resistance to AF demagnetisation) but possibly variably

Ti rich titanomagnetites (hence the wide range of unblocking temperatures) as the main remanence carrier within absence of large (multi-domain) titanomagnetites which would have been indicated by intensity decay during AF demagnetisation. The hematite fraction when present (as indicated by stable direction in excess of magnetite T_c 578°C (e.g. AZ1-33, AZ1-78 and AZ1-94 in Fig. 6.7) always was found to carry the same component of magnetisation as the titanomagnetite suggesting it formed/deposited/magnetised at, or very nearly, the same time as the titanomagnetite.

A second intermediate to high temperature component was isolated in about 25% of the samples (Table 6.3 and Fig. 6.8). If present with the “C” component it was always isolated at lower temperatures (e.g. samples AZ1-10 and AZ1-94 in Fig. 6.6c and 6.7) but when present on its own again persisted to high temperatures after removal of the “A” component (Fig. 6.8 samples 53 and 91). Directionally it is dominantly of normal polarity, NW directed and of moderate positive inclination. Being intermediate in terms of the unblocking temperatures in samples when all three components were found to co-exist it is referred to as the “B” component.

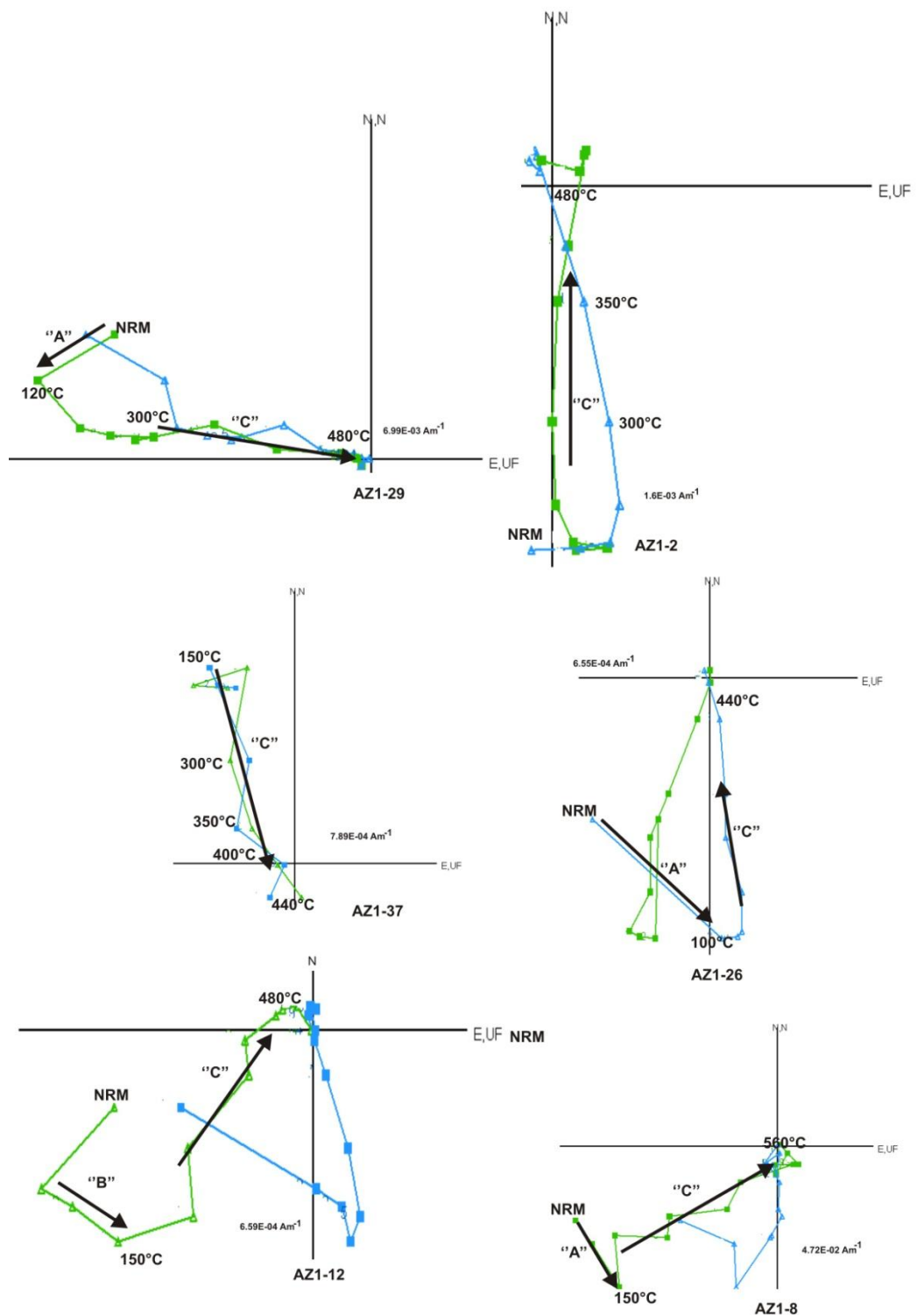


Figure 6.6b Example of samples which yielded C only or A with C components and all samples are projected in situ. Zijderveld diagrams show vector projections on the horizontal (green) and (vertical) plane in (blue).

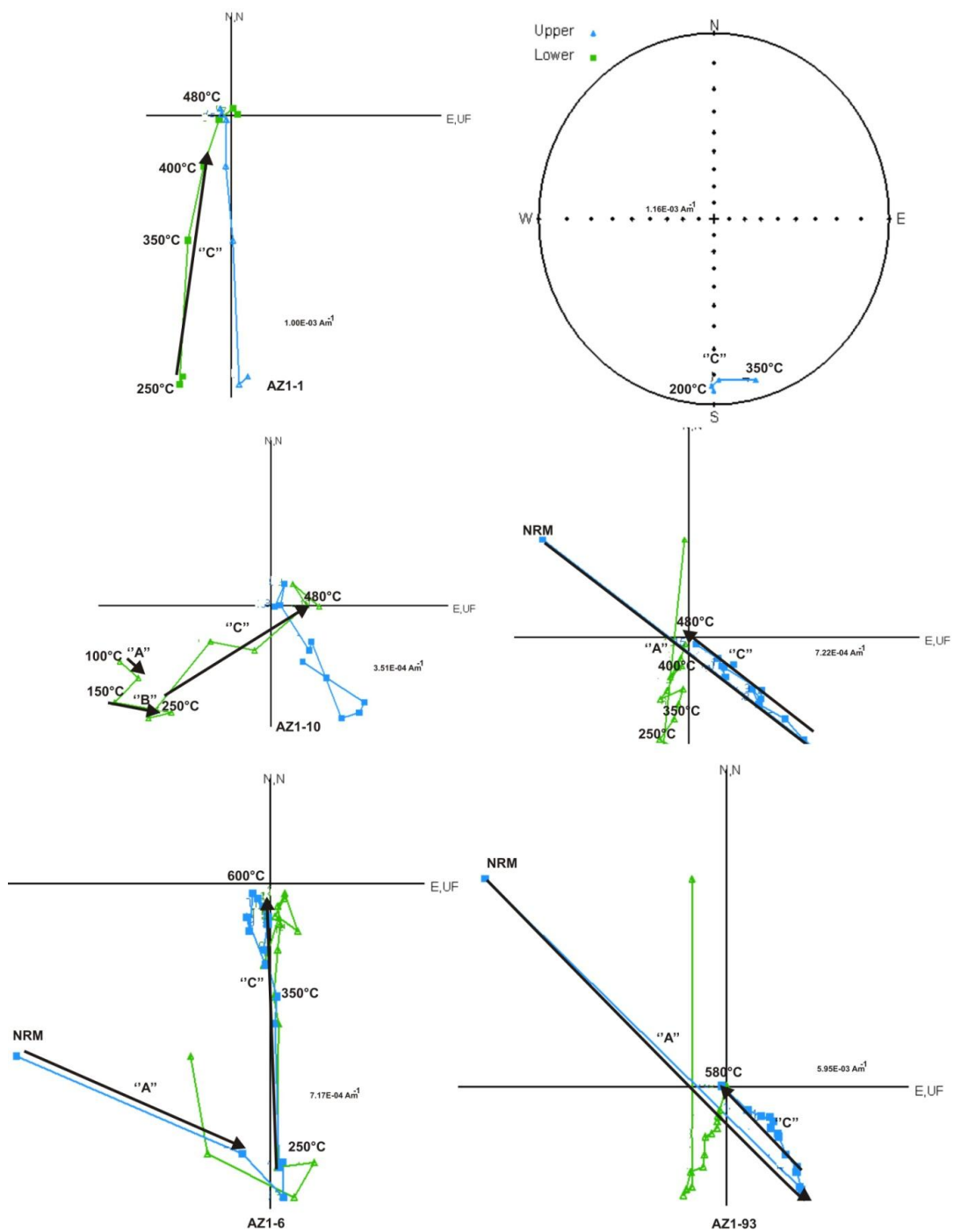


Figure 6.6c Example of samples which yielded C only or A with C components and all samples are projected in situ. Zijderveld diagrams show vector projections on the horizontal (green) and (vertical) plane in (blue). Stereonet projections show blue as positive (green) as negative inclinations.

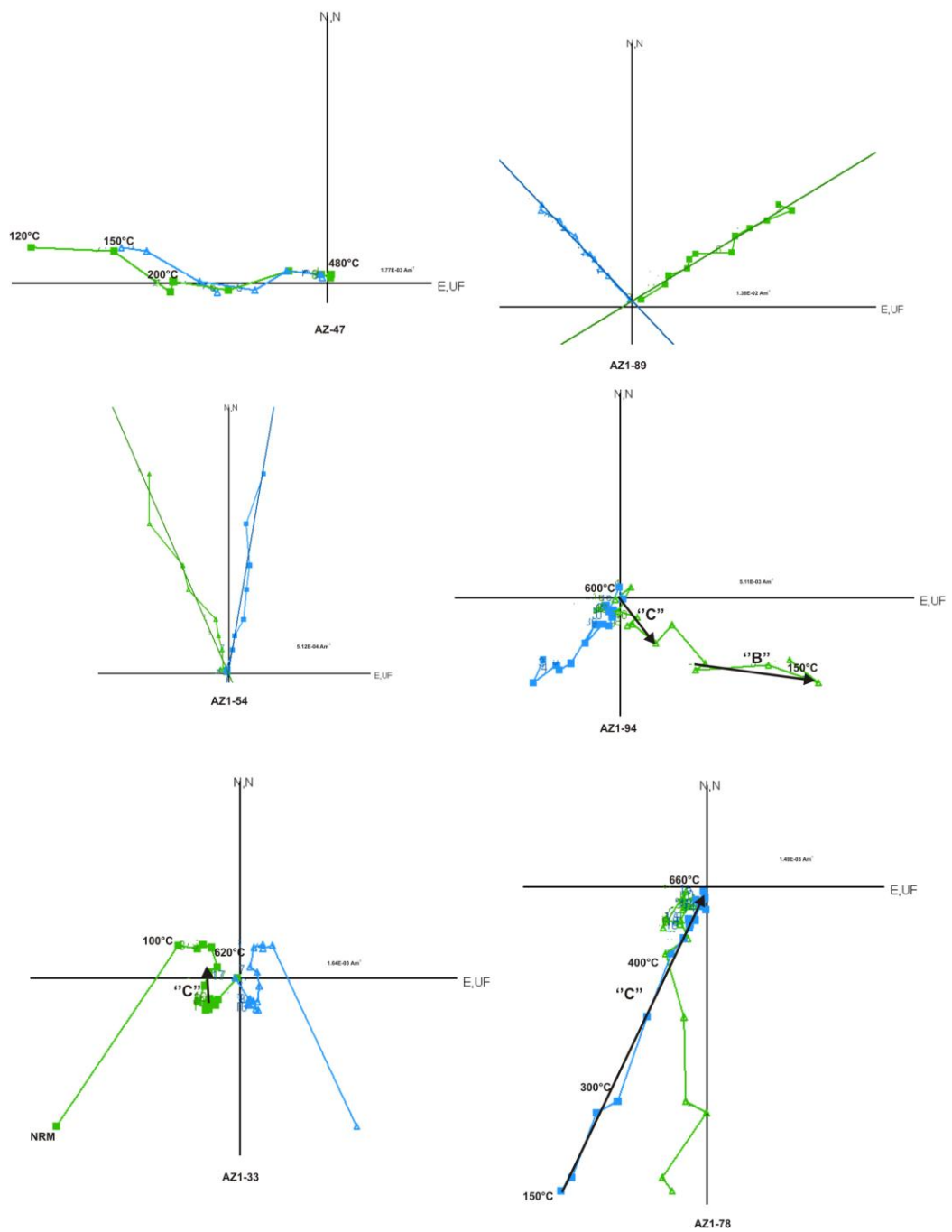


Figure 6.7 Orthogonal projections showing the behaviour of samples from the Al Aziza Formation during thermal demagnetization. Samples referred to within the text. All samples are projected in situ. Zijdeveld diagrams show vector projections on the horizontal (green) and (vertical) plane in (blue). Stereonet projections show blue as positive (green) as negative inclinations.

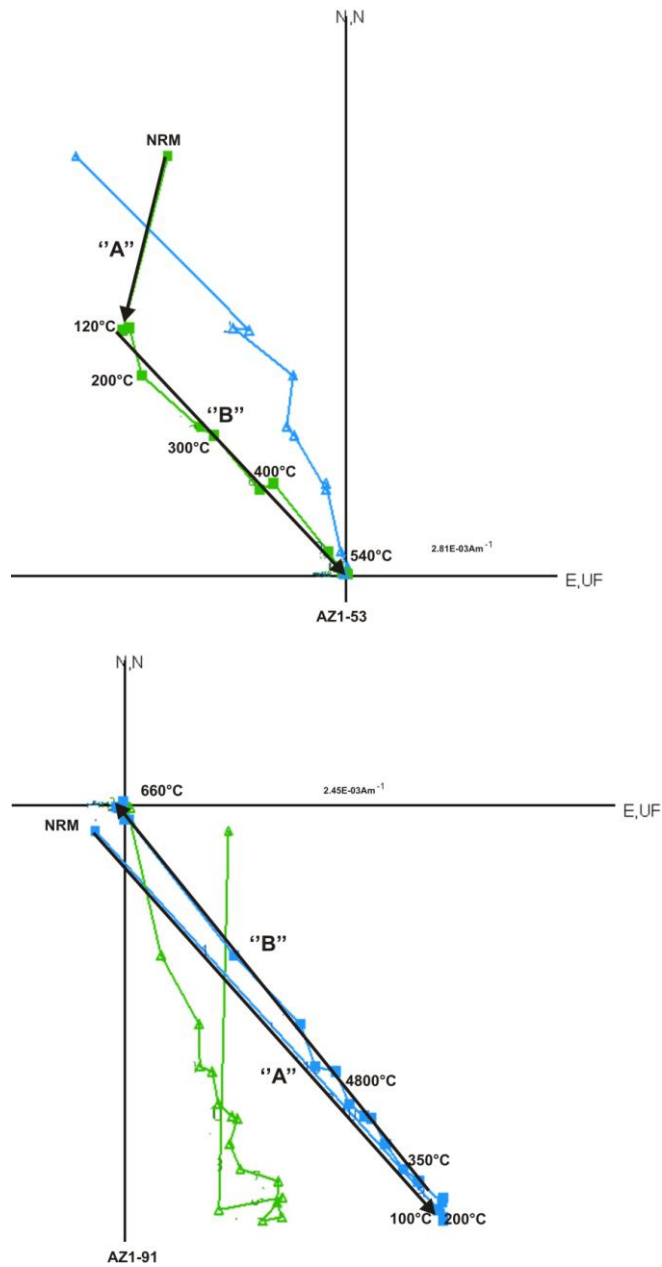


Figure 6.8 Examples of samples which yielded B only or A with B components and all samples are projected in situ. Zijderveld diagrams show vector projections on the horizontal (green) and (vertical) plane in (blue). Stereonet projections show blue as positive (green) as negative inclinations.

6.4.4 Interpretation of the Isolated Components in the Al Aziza Formation

The isolated components are shown in terms of stereographic projections of their distributions in Figure 6.9 and their statistical analysis in Table 6.4.

The “A” component – The mean direction for this component is Declination = 359.1, Inclination = 47.8; it is highly clustered in *in situ* coordinates for the 82 samples in which it was isolated and becomes more dispersed when *tilt corrected*. Directionally it is statistically indistinguishable from the Present Day Field direction (Dec. = 344.5°, Inc. = 60° - calculated using the online calculator available from the NOAA National Geophysical Data Center and using the latest version, 11, of the International Geomagnetic Reference Formula) for the area (<http://www.ngdc.noaa.gov/geomagmodels/struts/calcIGRFWMM>). This component is therefore a Present Day remanence.

The “B” Component – The *in situ* mean direction of the “B” component is calculated at Dec.= 320.7 Inc.= 19.4 ($k=8.2$ and $\alpha_{95}=8.4$ for $n=32$ samples) and is rather ill defined overall. The distribution of isolated directions is notably elongate in terms of its declination spread encompassing an arc of almost 90° (Fig. 6.9) which leads to the relatively low statistical parameters given the number of samples involved (Table 6.4). Such distributions are generally held to be due to three possibilities: 1) poor tectonic control; 2) inadequate/insufficient demagnetisation; or 3) incomplete separation of components due to overlap. The factors 1 and 2 have been fully addressed during fieldwork and laboratory studies and believe that overlap (see previous discussion of unblocking temperatures in section 6.4.3.) is the primary cause of this distribution. Despite careful data selection the distribution, it can be argued, lies along great circle arcs which would encompass the Present Day direction and the C direction so the B component directions may be contaminated by overlap with one or both of these other components. Nevertheless the mean direction needs to be further considered. It changes

directionally little upon tilt correction due to the relatively small and consistent dips from the sampled section and their orientation with respect to the direction. Owing to the limited range of tectonic correction available the fold test is not a particularly strong tool for determining the primary or secondary nature of the magnetisations in this setting. Nevertheless for the B Component it yields a negative result (Table 6.4, Fig. 6.9) which is apparently statistically valid (due to the relatively high number of individual samples used) and despite the distribution. It is interesting to note that the recovery of this component was not systematic throughout the sampled sections but rather that it occurs in stratigraphically controlled clusters whereby successive or nearly successive samples exhibit this component (see Table 6.3). This tends to suggest that there may be a lithological control on the acquisition of the B component, perhaps as a function of porosity and permeability, but this is not discernible from our field logging alone and is beyond the scope of our petrological studies.

The “C” Component – The isolated “C” components from the Al Aziza Formation are shown in Figure 6.9 and the fold test in Figure 6.10. Like the B component it shows quite a wide distribution but unlike the B component it is not ‘strung’ in that declination and inclination show a similar range of variation (i.e. it is, as expected, a circular Fisherian like distribution) and the variation is thought to reflect natural palaeosecular variation. It is dominantly but not exclusively of reversed polarity (82.5:17.5 %). For a combination of reasons i.e. being generally the highest temperature component when all three (A-C) are present, its mixed polarity and with a mean direction that shows a statistically significant improvement upon tilt correction this the “C” Component is interpreted to be the **Characteristic Remanent Magnetisation (ChRM)** for the formation i.e. the oldest component present and expected to be of primary age i.e. at or close to deposition.

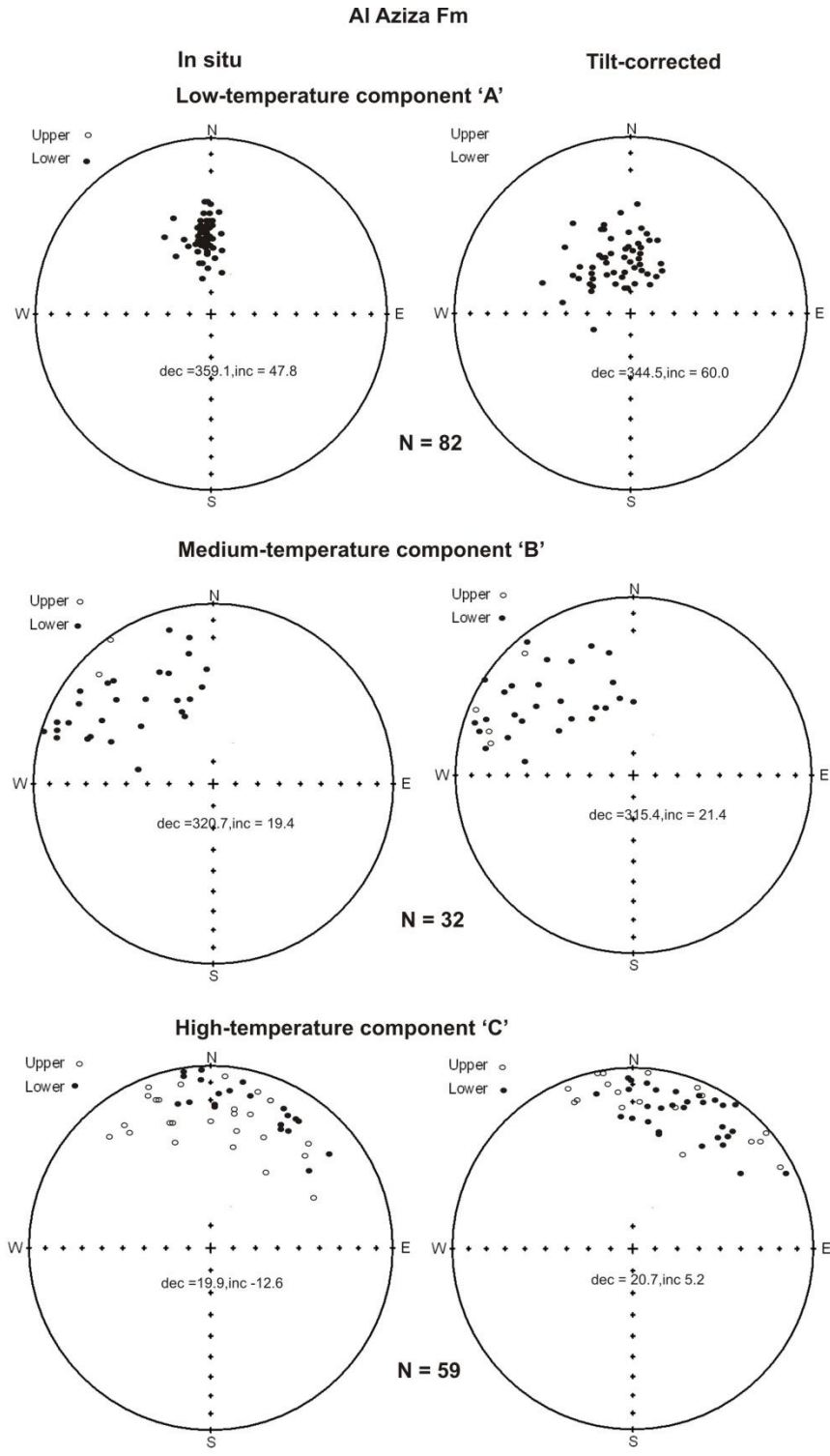


Figure 6.9 Equal area projections before (in situ) and after bedding tilt correction of the “A”, “B” and “C” component directions from Al Aziza Formation Closed (open) symbols are on the upper (lower) hemisphere.

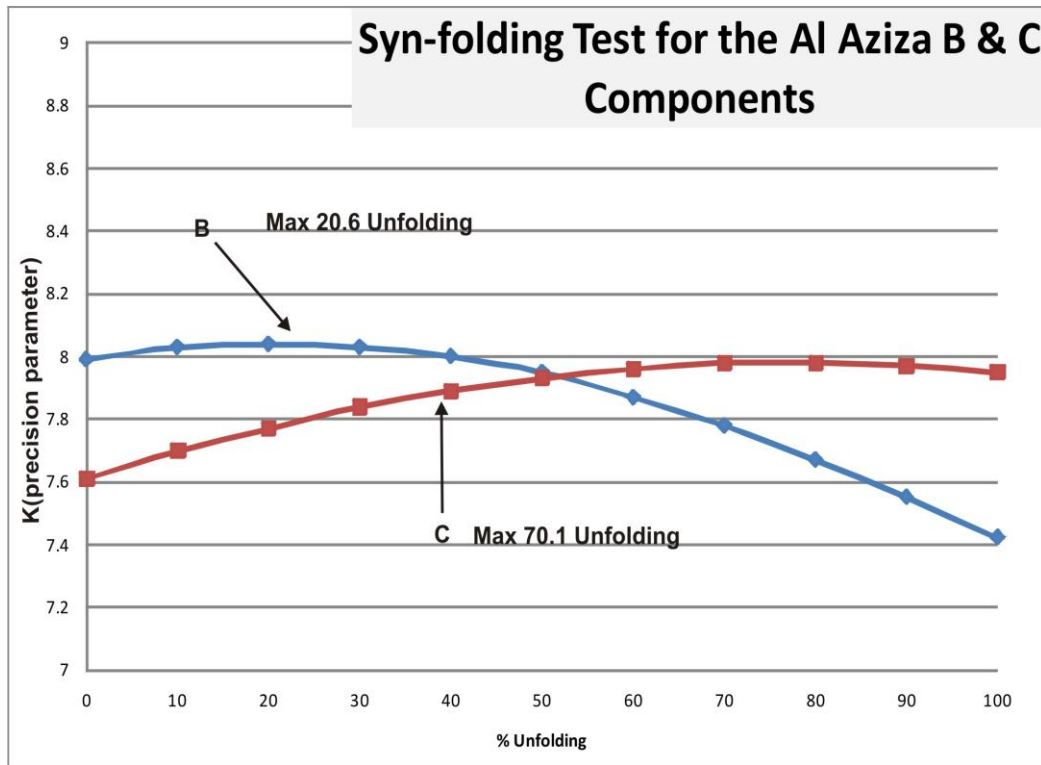


Figure 6.10 Statistic fold tests for the B and C component from the Al Aziza Formation.

| Comp | n/N | %N | %R | In Situ | | | | Tilt Corrected | | | |
|---------------|--------|------|------|---------|-------|------|---------------|----------------|------|-----|---------------|
| | | | | Dec | Inc | k | α_{95} | Dec | Inc | k | α_{95} |
| Al Aziza 'A' | 82/126 | 100 | 0 | 359.1 | 47.8 | 31.0 | 2.8 | 344.5 | 60.0 | 14 | 4.1 |
| Al Aziza 'B' | 32/126 | 81.5 | 18.5 | 320.7 | 19.4 | 8.2 | 8.4 | 315.4 | 21.4 | 7.7 | 8.7 |
| Al Aziza 'Ch' | 59/126 | 17.5 | 82.5 | 19.9 | -12.6 | 8 | 6.3 | 20.7 | 5.2 | 8.6 | 6.0 |

Table 6.4 Palaeomagnetic direction from the Al Aziza Formation, the abbreviation are: Comp is the magnetization component; n: the number of samples used to calculate the mean; N: total number of samples; % N: percentage of samples bearing normal polarity; % R: percentage of samples bearing reverse polarity; Dec and Inc the declination and inclination; k: Fisher precision parameter; α_{95} : the cone of 95% confidence of standard Fisher statistics.

6.4.5 Demagnetization Behaviour of Samples of the Abu Shaybah Formation

The behaviour of samples during thermal demagnetisation treatment was again divided into three main classes, i.e. Type A, B and C (see Table 6.5 for an overview of the components isolated in each sample and with respect to their unblocking temperatures).

A-Type behaviour, some samples were unstable to thermal demagnetization treatment and / or extremely weak and failed to yield useful information. The great majority of samples yielded only a northerly directed, moderately positively inclined directions (B-type behaviour; e.g. Sample WG1-4 in Fig. 6.11), referred to as a low unblocking temperature component "D". This "D" component was isolated normally between room temperatures and 150 °C as the first component isolated or much more rarely persisted up to as high as 580-600°C (Table 6.5).

Some of the samples exhibited multi-component behaviour yielding interpretable data indicating at least two or more components of magnetization (C-type behaviour; e.g. Sample AR1-17 and AR1-24 in Fig. 6.11, 6.12) which in some cases are overlapping (e.g. Sample AR1-18 in Fig. 6.12). The most common initial behaviour of these multi-component samples carries a well defined low blocking temperature component 'D'.

The most commonly isolated higher temperature component was defined as being NW directed with a shallow positive inclination. This component, referred to as the "F" component was generally isolated between temperatures of 150 to 300 and 540 °C (e.g. Sample KC1-15 and ER1-9 in Fig. 6.11). In some samples, the "F" component was found to persist to maximum unblocking temperatures of 660 °C, indicating the presence of both titanomagnetite and hematite as main magnetic carries (e.g. Sample KC1-15 in Fig. 6.11).

A second intermediate to high temperature component was isolated in about 14% of the samples (Table 6.5 and e.g. Sample AR1-17 in Fig. 6.12). If present with the “F” component it was always isolated at lower temperatures (Table 6.5) but when present on its own again persisted to high temperatures after removal of the “D” component (e.g. Sample samples AR1-2 in Fig. 6.12). This component is defined as being NW (SE) directed with a shallow positive (negative) inclination. This ‘E’ component exhibiting both polarities (normal and reverse) was determined between 150°C and 350°C. The “E” component is defined based on its intermediate unblocking temperature.

| Sample | Unblocking Temperature | | | | | | | | | | | | | | | | | | | |
|--------|------------------------|--------|--------|--------|--------|--------|--------|--------|--------|--------|--------|--------|--------|--------|--------|--------|--------|--------|--------|--------|
| | NRM | 100 | 120 | 150 | 200 | 250 | 300 | 350 | 400 | 440 | 480 | 520 | 540 | 560 | 580 | 600 | 620 | 640 | 660 | |
| KC1-1 | Yellow | Yellow | | | | | | | Green | Green | | | | | | | | | | |
| KC1-3 | | | | | | | | | | | | Green | Green | Green | | | | | | |
| KC1-4 | Yellow | Yellow | | | | | | | | | | | | | | | | | | |
| KC1-7 | | | | | | | | | Green | Green | Green | Green | Green | Green | | | | | | |
| KC1-9 | Yellow | Yellow | | | | | | | | | | | | | | | | | | |
| KC1-11 | | | | | | | | | Green | Green | Green | Green | Green | | | | | | | |
| KC1-12 | | | | | | | | | Green | Green | Green | Green | Green | Green | | | | | | |
| KC1-14 | | | | | | | | Green | Green | Green | Green | Green | Green | Green | | | | | | |
| KC1-15 | | | Green | Green | Green | Green | Green | Green | Green | Green | Green | Green | Green | Green | Green | Green | Green | Green | Green | Green |
| KC1-16 | | | | Brown | Brown | Brown | Brown | Brown | Brown | Brown | Brown | Brown | Brown | Brown | Brown | Brown | Brown | Brown | Brown | Brown |
| KC1-17 | | | | | | | | | Green | Green | | | | | | | | | | |
| KC1-18 | Yellow | Yellow | | | | | | Green | Green | Green | Green | Green | Green | Green | | | | | | |
| KC1-20 | Yellow | Yellow | | | | | | | | | | | | | | | | | | |
| AR1-1 | | | | | | | | | | | Green | Green | Green | Green | Green | Green | Green | Green | Green | Green |
| AR1-2 | | | Brown | Brown | Brown | Brown | Brown | Brown | Brown | Brown | Brown | Brown | Brown | Brown | Brown | Brown | Brown | Brown | Brown | Brown |
| AR1-5 | | Brown | Brown | Brown | Brown | Brown | Brown | Brown | Brown | Brown | Brown | Brown | Brown | Brown | Brown | Brown | Brown | Brown | Brown | Brown |
| AR1-6 | | Brown | Brown | Brown | Brown | Brown | Brown | Brown | Brown | Brown | Brown | Brown | Brown | Brown | Brown | Brown | Brown | Brown | Brown | Brown |
| AR1-7 | | | | | Brown | Brown | Brown | Brown | Brown | Brown | Brown | Brown | Brown | Brown | Brown | Brown | Brown | Brown | Brown | Brown |
| AR1-10 | Yellow | Yellow | Yellow | Yellow | Yellow | Yellow | | | | | | | | | | | | | | |
| AR1-13 | | | | | | | Brown | Brown | Brown | Brown | Brown | Brown | Brown | Brown | Brown | Brown | Brown | Brown | Brown | Brown |
| AR1-14 | Yellow | Yellow | | | | | Brown | Brown | Brown | Brown | Brown | Brown | Brown | Brown | Brown | Brown | Brown | Brown | Brown | Brown |
| AR1-16 | | | Green | Green | Green | Green | Green | Green | Green | Green | Green | Green | Green | Green | Green | Green | Green | Green | Green | Green |
| AR1-17 | Yellow | Yellow | Yellow | | | | Brown | Brown | Brown | Brown | Brown | Brown | Brown | Brown | Brown | Brown | Brown | Brown | Brown | Brown |
| AR1-19 | Yellow | Yellow | Yellow | | | | Brown | Brown | Brown | Brown | Brown | Brown | Brown | Brown | Brown | Brown | Brown | Brown | Brown | Brown |
| AR1-24 | Yellow | Yellow | Yellow | | | | Green | Green | Green | Green | Green | Green | Green | Green | Green | Green | Green | Green | Green | Green |
| ER1-1 | | | | | | | | | | | | Green | Green | Green | | | | | | |
| ER1-2 | | | | | | | | | | | | | | | | | | | | |
| ER1-3 | | | Yellow | Yellow | Yellow | | | | | | | | | | | | | | | |
| ER1-5 | | | | | | | Brown | Brown | Brown | Brown | Brown | Brown | Brown | Brown | Brown | Brown | Brown | Brown | Brown | Brown |
| ER1-6 | | | | | | | | | | | | | | | | | | | | |
| ER1-7 | Yellow | Yellow | | | | | Brown | Brown | Brown | Brown | Brown | Brown | Brown | Brown | Brown | Brown | Brown | Brown | Brown | Brown |
| ER1-8 | | Yellow | Yellow | Yellow | Yellow | | | | | | | | | | | | | | | |
| ER1-9 | | | | Green | Green | Green | Green | Green | Green | Green | Green | Green | Green | Green | Green | Green | Green | Green | Green | Green |
| ER1-11 | Yellow | Yellow | Yellow | | | | Brown | Brown | Brown | Brown | Brown | Brown | Brown | Brown | Brown | Brown | Brown | Brown | Brown | Brown |
| ER1-13 | Yellow | Yellow | Yellow | | | | Green | Green | Green | Green | Green | Green | Green | Green | | | | | | |
| ER1-14 | Yellow | Yellow | | | | | | | | | | | | | | | | | | |
| ER1-15 | Yellow | Yellow | Yellow | | | | | | | | | | | | | | | | | |
| ER1-16 | | | | Green | Green | Green | Green | Green | Green | | | | | | | | | | | |
| ER1-18 | | | | Yellow | Yellow | Yellow | | | | | | | | | | | | | | |
| ER1-19 | | | | | | | | | | | | | | | | | | | | |
| WG1-1 | Yellow | Yellow | | | | | | | | | | | | | | | | | | |
| WG1-2 | Yellow | Yellow | | | | | | | | | | | | | | | | | | |
| WG1-3 | Yellow | Yellow | | | | | | | | | | | | | | | | | | |
| WG1-6 | | | Yellow | Yellow | Yellow | Yellow | Yellow | Yellow | Yellow | Yellow | Yellow | Yellow | Yellow | Yellow | Yellow | Yellow | Yellow | Yellow | Yellow | Yellow |
| WG1-7 | | | Yellow | Yellow | Yellow | Yellow | Yellow | Yellow | Yellow | Yellow | Yellow | Yellow | Yellow | Yellow | Yellow | Yellow | Yellow | Yellow | Yellow | Yellow |
| W1-9 | | | | Yellow | Yellow | Yellow | Yellow | Yellow | Yellow | Yellow | Yellow | Yellow | Yellow | Yellow | Yellow | Yellow | Yellow | Yellow | Yellow | Yellow |
| WG1-18 | Yellow | Yellow | | | | | | | | | | | | | | | | | | |
| WG1-19 | Yellow | Yellow | | | | | | | | | | | | | | | | | | |

Table 6.5 The isolated components from samples during thermal demagnetisation for Abu Shaybah Formation. Straw Yellow =Present Day ‘A’ Component, Brown = ‘B’ component and Green = the ‘Ch’ component.

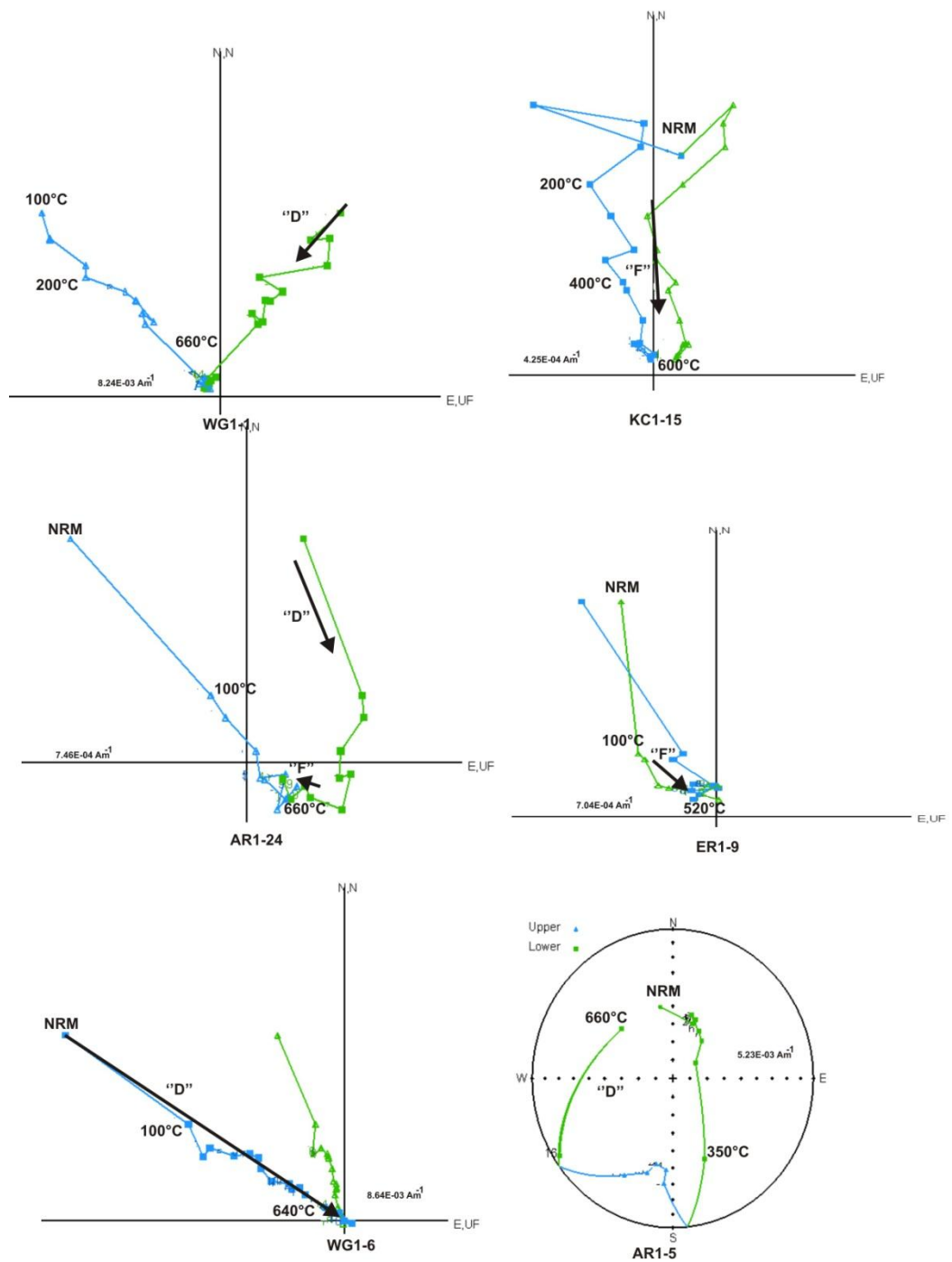


Figure 6.11 Equal area stereographic and Orthogonal projections showing the behaviour of samples from the Abu Shaybah Formation during thermal demagnetization. Samples referred to within the text. All samples are projected in situ. Zijderveld diagrams show vector projections on the horizontal (green) and (vertical) plane in (blue). Stereonet projections show blue as positive (green) as negative inclinations.

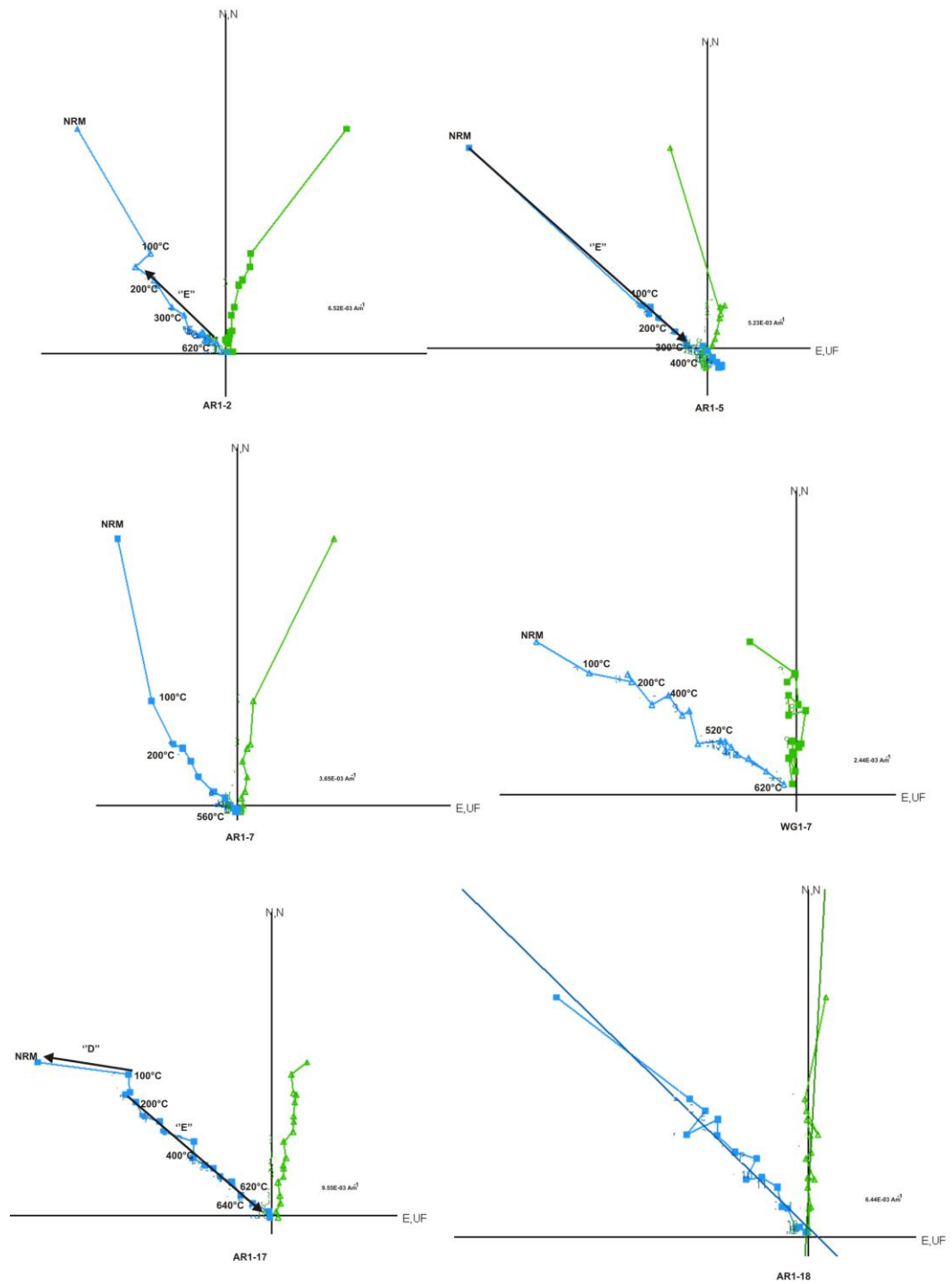


Figure 6.12 Orthogonal projections showing the behaviour of samples from the Abu Shaybah Formation during thermal demagnetization. Samples referred to within the text. All samples are projected in situ. Zijderveld diagrams show vector projections on the horizontal (green) and (vertical) plane in (blue). Stereonet projections show blue as positive (green) as negative inclinations.

6.4.6 Interpretation of the Isolated Components in the Abu Shaybah Formation

The isolated components are shown in terms of stereographic projections of their distributions in Figure 6.13 and their statistical analysis in Table 6.6.

The “D” component- The mean direction of the low-temperature component ‘D’ from the Abu Shaybah Formation has Declination = 1.9, Inclination = 49.5. Comparing the statistical parameters for the mean before and after tilt-correction (Table 6.6), shows it to be slightly better grouped in *in situ* coordinates which suggest post-tilting acquisition of this component of remanent magnetization. This component ‘D’ is interpreted as a present day remanence.

The “E” Component- The mean direction for this component is Declination = 344.9, Inclination = 44.3; it is widely scattered in *in situ* coordinates for the 13 samples in which it was isolated and becomes more highly clustered when tilt corrected (Table 6.6). It is clearly that some of these directions are still grouping around the Present Day Field direction before tilt adjustment, (Fig 6.13) and hence there may be a degree of contamination of the mean. There is no definite explanation for this origin of this component. However as previously noted, grouping of the mean direction for the ‘D’ component improves upon tilt correction, suggesting that magnetisation was acquired prior to the tilting of the strata in Abu Shaybah Formation. Therefore the mean direction needs to be further considered.

The “F” Component – The isolated “F” components from the Abu Shaybah Formation are shown in Figure 6.13 and the fold test for this data in Figure 6.14. It is dominantly but not exclusively of normal polarity (79%). The grouping of this high-temperature component improves slightly after-correction (Table 6.6) although the improvement is not significant statistically, it does suggest that acquisition of remanent magnetization took place prior to tilting, probably during or shortly after deposition. Therefore it is

assumed that high-temperature component represents the **Characteristic Remanent Magnetisation (ChRM)** for the formation i.e. the oldest component present and expected to be of primary age.

| Comp | n/N | %N | %R | In Situ | | | | Tilt Corrected | | | |
|-----------------|-------|-----|----|---------|------|------|-------------|----------------|------|------|-------------|
| | | | | Dec | Inc | k | α 95 | Dec | Inc | k | α 95 |
| Abu Shaybah 'D' | 33/91 | 100 | 0 | 1.9 | 49.5 | 13 | 6.8 | 347.9 | 58.8 | 9.1 | 8.3 |
| Abu Shaybah 'E' | 13/91 | 60 | 50 | 344.9 | 44.3 | 13.5 | 11.2 | 315.5 | 50.3 | 35.4 | 6.8 |
| Abu Shaybah 'F' | 17/91 | 79 | 21 | 349 | 7.6 | 12.3 | 10.3 | 348.8 | 13.5 | 14.5 | 9.4 |

Table 6.6 Palaeomagnetic direction from the Abu Shaybah Formation, the abbreviation are: Comp is the magnetization component; n: the number of samples used to calculate the mean; N: total number of samples; % N: percentage of samples bearing normal polarity; % R: percentage of samples bearing reverse polarity; Dec and Inc the declination and inclination; k: Fisher precision parameter; α 95: the cone of 95% confidence of standard Fisher statistics.

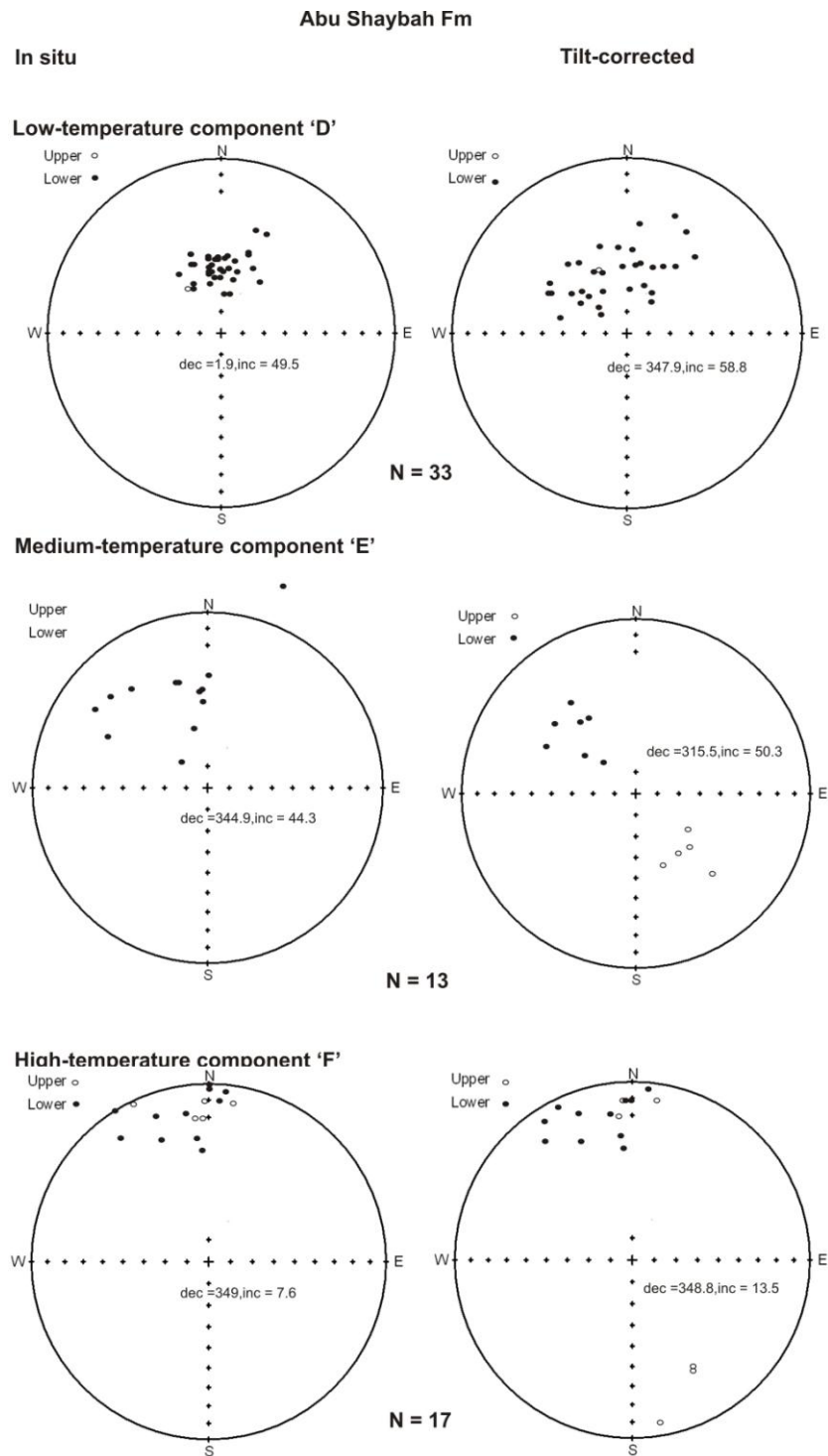


Figure 6.13 Equal area projections before (in situ) and after bedding tilt correction of the “D”, “E” and “F” component directions from Abu Shaybah Formation. Closed (open) symbols are on the upper (lower) hemisphere.

Syn-folding test for Abu Shaybah E&F component

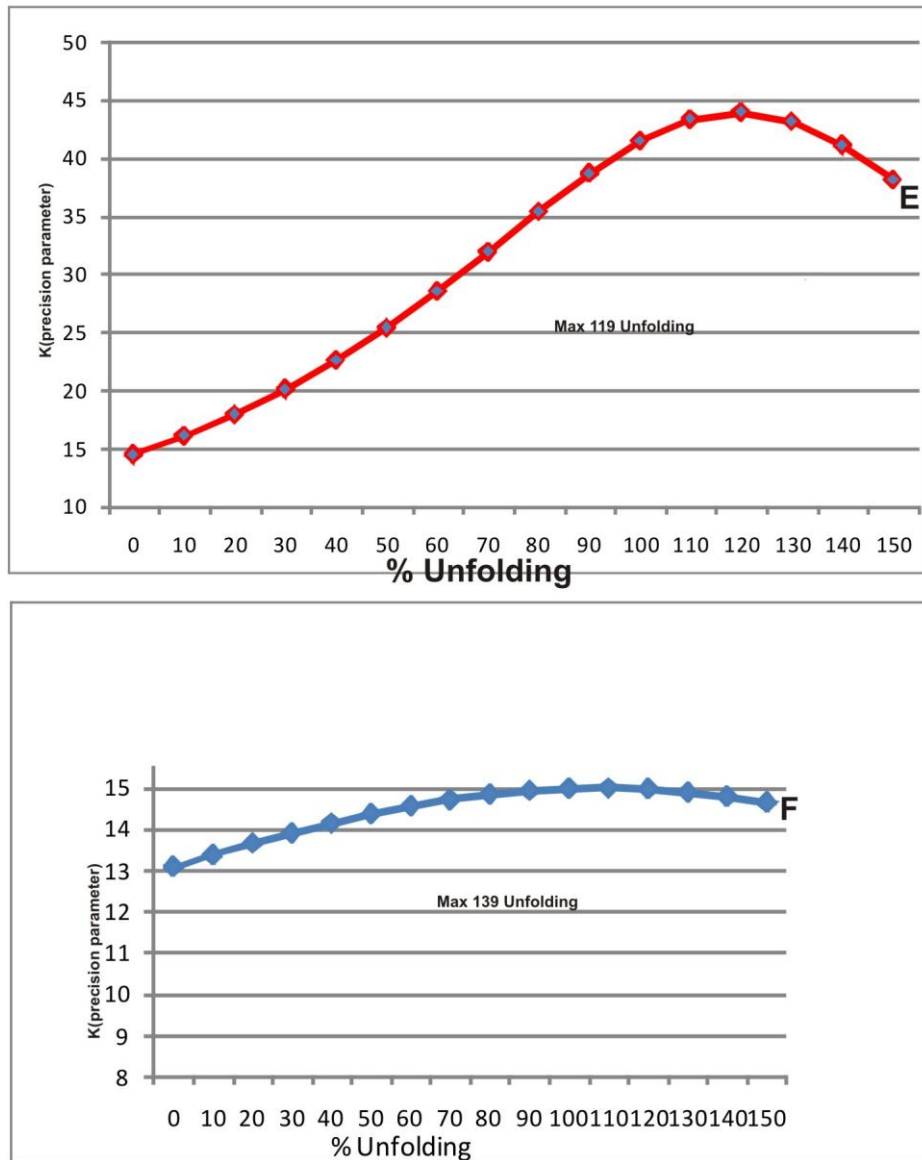


Figure 6.14 Statistic fold tests for the E and F component from the Abu Shaybah Formation.

6.5 Other Samples

Most samples from the Kurrush Formation were unstable to demagnetisation (e.g. KU1-2 in Fig. 6.15) and only 2 yielded poorly resolved components (KU2-2 in Fig. 6.15).

Given the very limited data available from this unit it is not further discussed. Likewise the limestones of the Abu Ghaylan failed to yield useful information and these too are not further discussed.

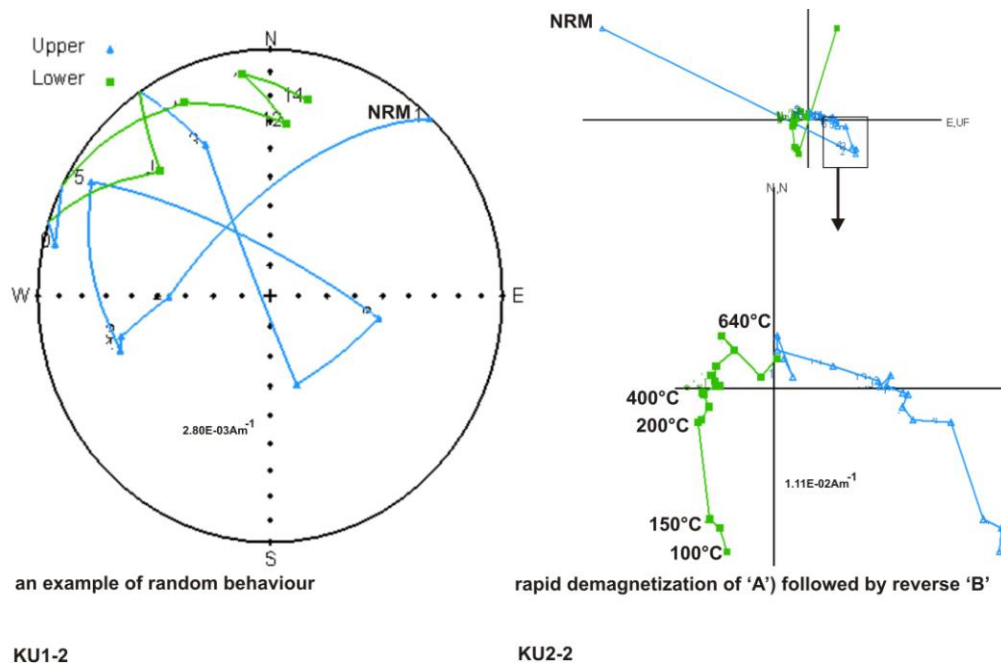


Figure 6.15 Equal area stereographic and Orthogonal projections showing the behaviour of samples from the Kurrush Formation during thermal demagnetization. All samples are projected in situ. Zijderveld diagrams show vector projections on the horizontal (green) and (vertical) plane in (blue). Stereonet projections show blue as positive (green) as negative inclinations.

6.6 Pole Positions and Geological Interpretation of Results

As with the previous study of the Aziza Formation (Muttoni et al., 2001) a low temperature component was readily isolated in this study for both the Aziza and Abu Shaybah formations. Its characteristics and directions are consistent with it being a Present Day field direction.

Overall behaviour of the B and E and C and F components in both formations of this study are very similar to that found by Muttoni et al. (2001) in their study. What does differ significantly are the isolated directions and their consequent pole positions (Table 6.7).

The arguments have been made for the C and F components being older than the corresponding B and E components based on unblocking temperatures when they co-exist and their response to untilting but it is now important to consider their pole positions.

The intermediate ‘‘B’’ direction of the Al Aziza Formation which grouped best in *in situ* coordinates (Table 6.4) yields a palaeomagnetic pole (Long. 259.4 °E, Lat. 48.3° N, Table 6.7, Fig. 6.16) which coincides with mid Cretaceous palaeomagnetic poles from Africa and Adria (the Southern Alps) (Table. 6.8). Given its demagnetisation characteristics and pole positions this component is interpreted as the product of a remagnetization event of Early to mid Cretaceous age (Table 6.9). During the Early Cretaceous, accelerated rifting affected much of the African-Arabian Craton, as evidenced by the development of rifts in Yemen and Somalia (Guiraud and Maurin, 1992; Ziegler et al., 2001). The Early Cretaceous is the period of the opening of the south and equatorial Atlantic during the Barremian and Albian respectively. More locally this Early Cretaceous rifting resulted in the formation of relatively small E-W trending troughs such as Hameimat Trough in the south-eastern part of

| In Situ | | | | Tilt Corrected | | |
|-----------------|---------|--------|----------|----------------|--------|----------|
| Comp | Long. E | Lat. N | dp/dm | Long. E | Lat. N | dp/dm |
| Al Aziza 'A' | 207.2 | 86.8 | 3.7/2.4 | 322.9 | 74.7 | 6.2/4.7 |
| Al Aziza 'B' | 259.4 | 48.3 | 8.8/4.6 | 265.0 | 44.8 | 9.3/4.9 |
| Al Aziza 'C' | 163.1 | 47.2 | 6.4/3.3 | 155.3 | 54.7 | 6/3 |
| Abu Shaybah 'D' | 184 | 87.7 | 9/46 | 324 | 77.6 | 12.4/9.2 |
| Abu Shaybah 'E' | 262.4 | 75.2 | 14.1/8.8 | 293.7 | 52.3 | 9.1/6.1 |
| Abu Shaybah 'F' | 215.4 | 60 | 10.4/5.2 | 217.9 | 62.8 | 9.6/4.9 |

Table 6.7 Palaeomagnetic poles from the Al Aziza and Abu Shaybah Formations, the abbreviations are; Long and Lat are longitude and latitude of the palaeomagnetic poles; dp/dm the axes of the confidence oval about the palaeomagnetic pole.

the Sirt Basin in Libya (Abadi et al., 2008). Although Muttoni et al. (2001) interpreted their B components poles (numbered 1 and 2 on Fig. 6.16) as being consistent with an early Jurassic overprint age they fall into an area of ambiguity such that they could also be of Late Cretaceous to earliest Tertiary age. As will be discussed in Chapter 7 the younger remagnetisation age (Late Cretaceous –earliest Tertiary) is preferred for tectonic reasons.

The “C” component or ‘ChRM’ from Al Aziza section yields a pole, after tilt-correction (where grouping is best; Table 6.4) that lies at Long 155.4° E, Lat.58.8° N (Table 6.7) which is latitudinally distant from the known APW path (Fig 6.16).

Although there is no definitive explanation for the origin of this pole, it would appear to be the consequence of a locally important vertical axis tectonic clockwise rotation.

Locally rotation occurs in the Al Aziz section due to curving of the fault plane and could reflect an original listric type of geometry for this fault (As will be discussed in chapter 7). However, the Al Aziz section needs to be sampled further in different locations at the Gharian area. Restoration of some 50° clockwise rotation would bring the pole position back to the APWP path at a time that just precedes the 233Ma pole which is Early Carnian in age and into overlap with the Muttoni et al. (2001) poles from Al Azizyah and Kaf Bates (marked by open and filled stars respectively).

Muttoni et al. 2001
Adria- W . Africa APWP

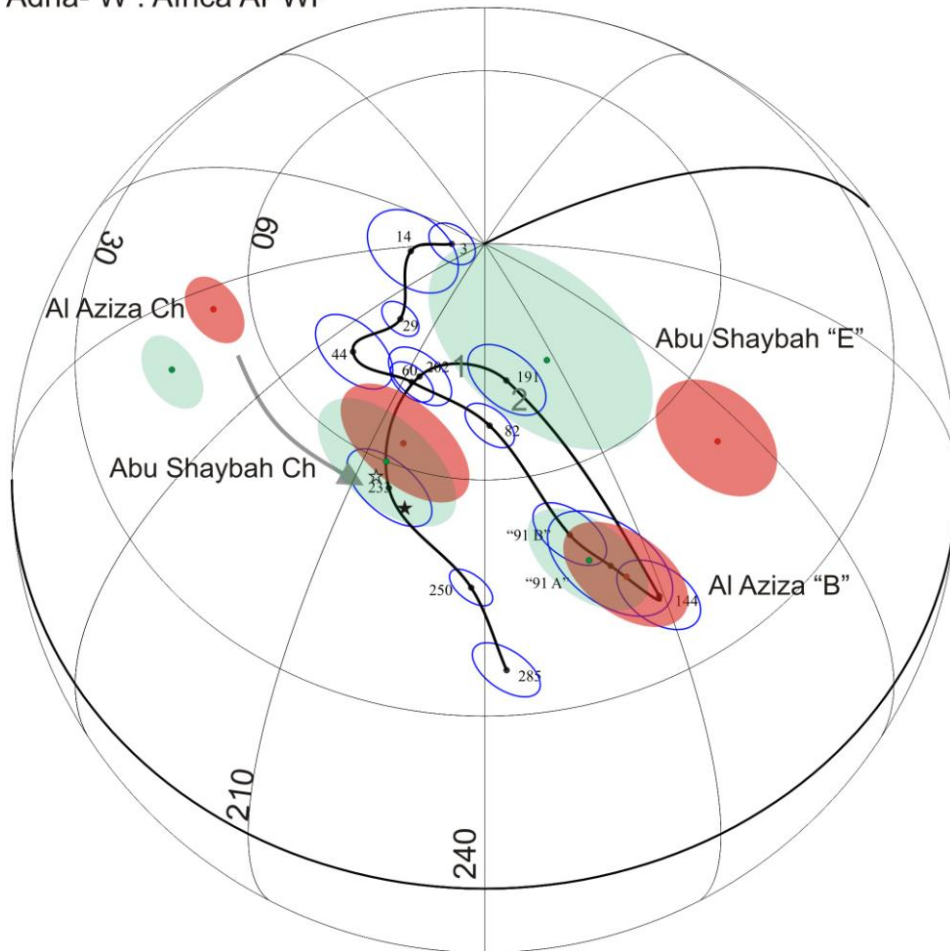


Figure 6.16 The Early Permian to Pliocene AWP path for Africa and Adria from Muttoni et al., (2001) with ages shown in My, note the slight ambiguity about the mid Cretaceous (91 My) pole position. The poles and their associated errors for the components isolated in this study are shown as green *in situ* and orange *tilt corrected* filled ovals. See text for discussion.

Table 6.8 Middle – late Triassic palaeomagnetic from the Southern Alps and Africa.

| Rock unit | locality | coordinates | <u>In situ</u> | | <u>Tilt-corrected</u> | | | | <u>Reference</u> |
|--------------------|---------------|-------------|----------------|------|-----------------------|-------|------|----------|-------------------------|
| | | | Long. | Lat. | dp/dm | long | Lat | dp/dm | |
| Buchenstein | Belvedere | 46.4/12 | 284.7 | 69.3 | 10.9/8.4 | 217.4 | 52.3 | 7.8/4.1 | Brack and Muttoni, 2000 |
| Buchenstein | Pedracas | 46.6/11.9 | 197.4 | 24.7 | 13.7/7.8 | 223.2 | 68.4 | 15.3/9.8 | Brack and Muttoni, 2000 |
| Val Sabbia | Lambardy | 45.8/10 | 209.6 | 56.5 | 22.6/12.2 | 215 | 56.6 | 14.1/7.7 | Muttoni et al., 1996 |
| Edivetur Fm | Bulgaria | 43.6/22.7 | 115.4 | 73.1 | 12.8/9.6 | 132.4 | 53.8 | 5.9/3.6 | Muttoni et al., 2000 |
| Buchenstein | Frostschnbach | 46.6/11.8 | 211 | 56 | 03/06 | 211 | 64 | 04/07 | Muttoni et al., 1997 |
| Al Aziza Fm | Libya | 32.5/13.2 | 213.5 | 56.6 | 2.0/3.9 | 214.1 | 59.3 | 1.9/3.9 | Muttoni et al., 2001 |
| Kaf Bates | Libya | 32.4/13.1 | 232.2 | 55.4 | 3.4/6.7 | 225.8 | 54.5 | 2.8/5.5 | Muttoni et al., 2001 |
| Agouim | Morocco | 31.1/7.4 | 258 | 67 | 4.0/2.4 | 245 | 66 | 3.8/2.1 | Knight et al., 2004 |
| Ait Qurir | Morocco | 31.4/7.4 | 261.5 | 42 | 3.4/1.8 | 292 | 64 | 4.5/3.0 | Knight et al., 2004 |

| Age | Age _(Ma) | Lat. °N | Long. °E | K | A95 | N | Locality | Reference |
|----------|---------------------|---------|----------|-----|---------|-----|-------------------------|--|
| eP | 285 | 36.2 | 243.3 | 77 | 4.8 | 13* | AF,SAP | Muttoni et al.,1996 |
| IP/e Tr | 250 | 46.8 | 237.6 | 317 | 3.1 | 8* | SAP | Muttoni et al.,1996 |
| mTr/eTrl | 233 | 57.1 | 218.1 | 67 | 6.3 | 9* | AF,SAP | Muttoni et al.,2001 |
| lTr/eJ | 202 | 71.1 | 214.8 | 458 | 4.3 | 4* | AF | Muttoni et al.,1996 |
| eJ | 191 | 72.0 | 248.5 | 108 | 4.7 | 10* | AF | Van der Voo, 1993 |
| iJ/ek | 144 | 40.8 | 269.2 | 125 | 6.0 | 6* | AF,NAM,SAP, G,U | Channell, 1996 Fossen and Kent, 1993 Hargraves, 1989 |
| mK | 99 | 46.8 | 262.9 | 42 | 4.9/8.1 | 12* | AP | Marton and Nardi, 1994 |
| IK | 82 | 66.6 | 241.5 | 71 | 3.2 | 29* | AF,SAM,SAP,IS G,IB,U | Channell, 1996 Van der Voo, 1993 |
| Pa | 60 | 70.1 | 213.0 | | 2.4/4.4 | | AF | Schneider and Kent, 1990 |
| E | 44 | 69.0 | 189.0 | | 5.8 | | AF | Tauxe et al.,1983 |
| O | 29 | 75.9 | 193.0 | | 2.0/4.4 | | AF | Schneider and Kent, 1990 |
| M | 14 | 81.0 | 154.0 | | 5.6 | | AF | Tauxe et al.,1983 |
| P | 3 | 86.0 | 149.0 | | 2.6 | | AF | Tauxe et al.,1983 |

Table 6.9 Early Permian to Pliocene mean paleomagnetic poles for West Gondwana and Adria apparent polar wander paths. , the abbreviations are; ep= Early Permian, IP/eTr = Late Permian/Early Triassic, mTr/eTrl = Middle Triassic/early Late Triassic, lTr/eJ = Late Triassic /Early Jurassic, ej= Early Jurassic, lJ/ek=Late Jurassic/Early Cretaceous, mK= Middle Cretaceous, IK= Late Cretaceous, Pa= Paleocene, E=Eocene, O=Oligocene, M= Miocene , P= Pliocene.Long and Lat are longitude and latitude of paleomagnetic poles; K = precision parameter; A95 = radius of cone of 95% confidence about the pole. N: number of overall mean (*) or site mean (~) directions used to calculate the paleopole. AF = Africa, SAM = South America, NAM = North America, SAP = South Alps, IS = Istria, G = Gargano, AP = Apulia, IB = Iblei, U = NW Umbria (Muttoni et al., 2001).

The timing of the rotation is therefore constrained to be post Early Triassic (Ladinian-Carnian), the oldest possible age of the magnetisation and prior to the mid Cretaceous “B” Component pole which does fall on the APW path.

The ‘ChRM’ magnetization component “F” from the Abu Shaybah formation yields, after tilt-correction (Table 6.6) a palaeomagnetic pole that lies at Long. 217.9 E, Lat. 62.8 N (Table 6.7). This pole is consistent with Middle to Early Late Triassic palaeomagnetic poles from the APW path (Table 6.8 and Fig. 6.16) and into overlap with the poles from the Al Aziza and Kaf Bates sections of the Al Aziza Formation by Mutton et al., (2001). This might appear to imply that the tectonic rotation observed in the Al Aziza Gharian section of this study can be tightly constrained in terms of timing of rotation to be of latest Ladinian-earliest Carnian age however, as will be discussed in chapter 7, the sample localities contributing to the Abu Shaybah Formation may actually come from a significantly different structural tectonic block than that of the Al Aziza formation and hence this pole is not believed to be a true temporal constraint on the rotation.

The intermediate “E” component of the Abu Shaybah Formation yields, after tilt-correction, (Table 6.6) a palaeomagnetic pole that lies at Long. 293.7 °E, Lat. 53.3° N (Table 6.7 and Fig. 6.16). This pole does not coincide with the expected APW path. However, it is not possible to explain the pole position as being caused by tectonic rotation as for this to be the case then the ChRM component would also be displaced. The safest explanation is that this is a poorly constrained component that is in part a function of poor separation of a Present Day and Cretaceous (?) overprint.

6.7 Magnetostratigraphic Al Aziza and Abu Shaybah Formations

Regardless of the net tectonic rotation and the timing of that rotation the Al Aziza section in the Gharian area should still produce a recognisable magnetostratigraphic signal if the isolated components, as argued in section 6.4.4, are in fact primary characteristic remanences acquired at or shortly after the time of deposition.

The virtual geomagnetic pole (VGP) was calculated for each ChRM direction identified after correction for bedding tilt and the pole latitude plotted against stratigraphic height for both formations (Fig. 6.17 and 6.18). The pole latitudes should cluster around the mean pole latitude and its reverse, polarities normally being accepted as being within 30° of the mean pole latitude, with those further away considered to be intermediate. Each specimen was assigned a quality value of 1 to 4 (excellent - poor based on the specimen α_{95} , comparable to the procedure used by Hounslow et al., (2008).

The Al Aziza section yielded a mix of normal and reverse polarities but is predominantly of reversed magnetic polarity. There are 4 isolated normal VGP latitudes between 30 and 80 m but none are from specimens of the highest quality suggesting that at best these may represent very short lived normal events if true. In contrast between 90-100 m in the section were 5 high quality data points of normal polarity and 1 of reversed suggesting that this is truly a short lived normal polarity chron.

The stratigraphically younger Abu Shaybah section (Fig. 6.18) is in contrast to the Al Aziza very incomplete but with the exception of 3 isolated reversed specimens is of normal polarity.

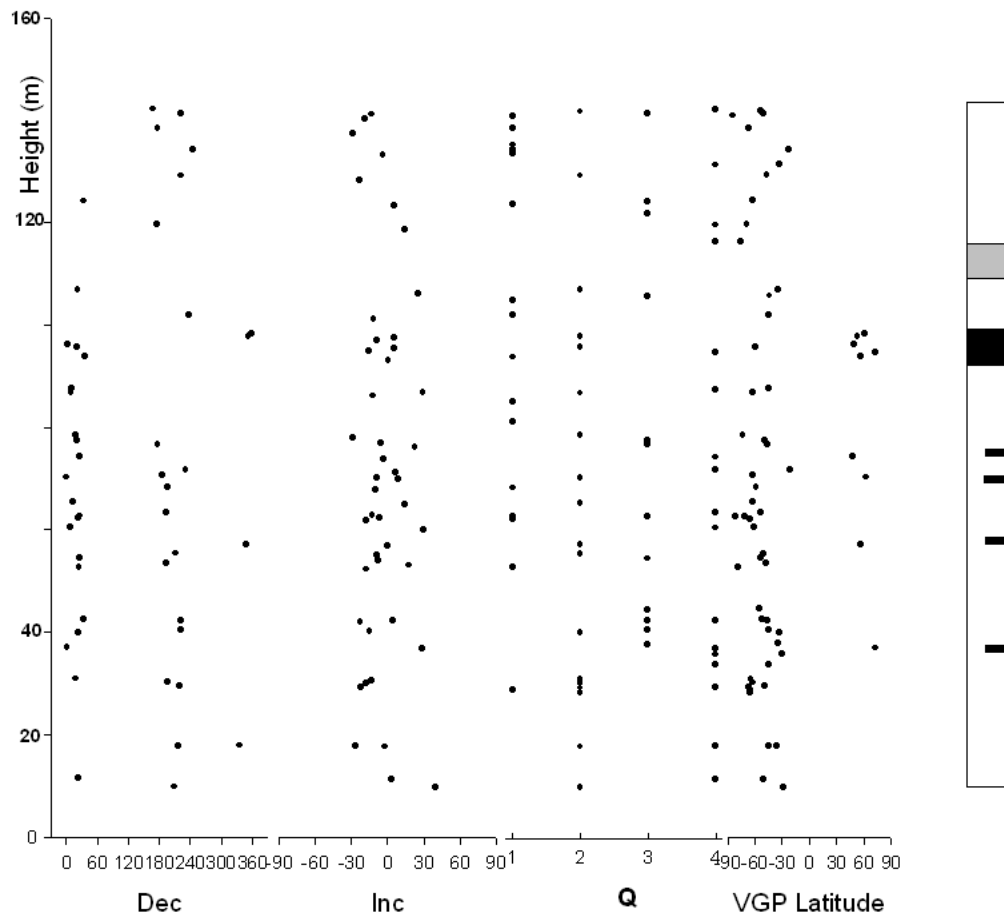


Figure 6.17 Magnetostratigraphy of the Al Aziza Formation in the Gharian area. Left to right: declinations and inclination: Q the quality factors (1 = excellent and 4= poor). The GVP latitude calculated for the measured declination and inclination. The polarity zonation is shown magnetic polarity: black – normal, white- reverse, and grey-uncertain.

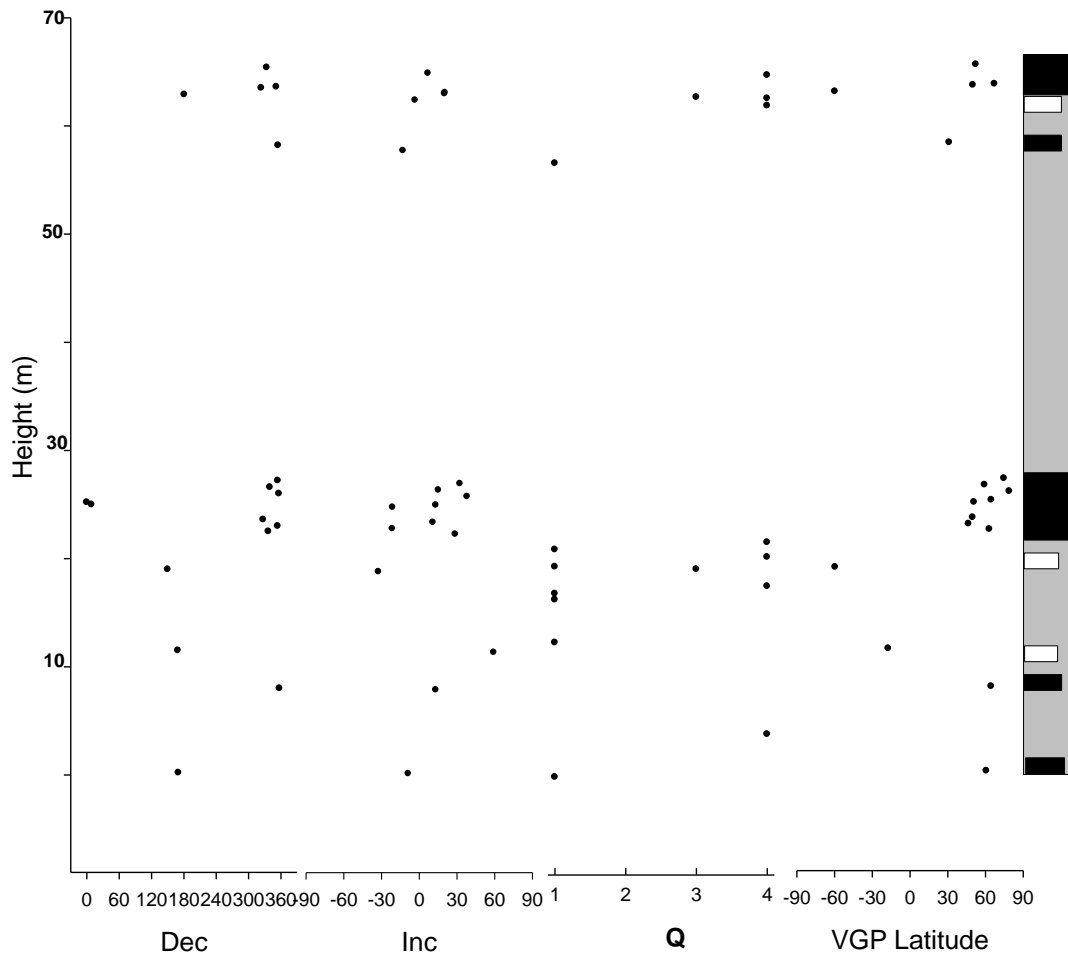


Figure 6.18 Magnetostratigraphy of the Abu Shaybah Formation in the Gharian area. Left to right: declinations and inclination: Q the quality factors (1 = excellent and 4= poor). The GVP latitude calculated for the measured declination and inclination. The polarity zonation is shown magnetic polarity: black – normal, white- reverse, and grey- uncertain.

6.7.1 Correlation with the Published Literature

A magnetostratigraphic correlation is usually accomplished by matching polarity patterns of the sampled section(s) with the established and settled Global Polarity Timescale (GPTS), where if possible, biostratigraphic data are also incorporated. As noted previously the Aziza and Abu Shaybah formations are believed to be of Middle to Early Late Triassic age. The most generally accepted GPTS is that of Gradstein et al., (2004) but all aspects of the Triassic timescale have recently been extensively reviewed and revised (see Lucas, 2010). This work includes a revision of the magnetostratigraphic timescale (Hounslow and Muttoni, 2010) in relation to other forms of correlation and supported by radiometrically dated calibration points and is believed to be the most authoritative current version of the GPTS for this time period and hence is adopted herein.

In their study of the Al Aziza Formation Muttoni et al. (2001) carried out limited palynological study of two samples from their Al Azizyah section and, based on the limited recovery of material, assigned the lower sample to Ladinian age and the upper, with a better preserved and more diverse flora, as belonging to the Secatus-Vigens phase of earliest Carnian age hence suggesting the section covered the Ladinian-Carnian boundary. In the recent review of the Triassic timescale Kürschner and Waldemaar (2010) indicate the C. Secatus pollen zone to be of very latest Ladinian to Carnian age.

In order to assess the reliability of the Libyan Triassic palaeomagnetic data in a consistent framework data from both the Muttoni et al. (2001) study and this one are plotted (Figure 6.19) against the new Triassic Timescale (Lucas 2010; Hounslow and Muttoni 2010). Given the known, but limited, biostratigraphy from the Aziza Formation at Al Azizyah town and the normal polarity of that section this would be consistent with the Aziza Formation having an Early Carnian age but does not actually contain the

Ladinian-Carnian boundary itself a minor modification from the conclusion of Muttoni et al., (2001). As defined by Hounslow and Muttoni (2010) this period is part of their first polarity chron for the Upper Triassic (UT1) which is dominantly Normal in polarity (Fig. 6.19).

The polarity recovered herein from the Aziza section, is as predominantly reversed, indicating that there is no direct correlation between this section and that in Al Azizyah itself but must correlate with the longer, but inadequately sampled, section at Kaf Bates (Muttoni et al., 2001). It is therefore suggested that Gharian section (Fig. 6.19) of the Al Aziza Formation predates that at Azizyah and is probably best correlated in part or with all of the upper Middle Triassic chrons MT11 and MT 12 (Hounslow and Muttoni, 2010) which are predominantly reversed in character. The dominantly normal polarity of the overlying Abu Shaybah Formation at Gharian suggests that it may be the stratigraphic equivalent of the Aziza Formation at Azizyah and Kaf Bates but without further constraints this is a tenuous correlation at best. However the carbonate and clastic facies present in the three areas are consistent with transgressive and regressive shorelines (Aziza has marginal marine and lagoonal facies carbonates with abundant evidence of Xerophytic pollens – Muttoni et al., 2001) which could readily be reconciled with a lateral equivalence of the lagoonal facies Aziza Formation carbonates at Al Azizyah with shoreline to fluvial clastic facies of the Abu Shaybah Formation at Gharian (see Chapter 4) indicating diachronous deposition of the facies in the area (Fig. 6.20). Such a model would imply a gross northward movement of the shoreline during this period.

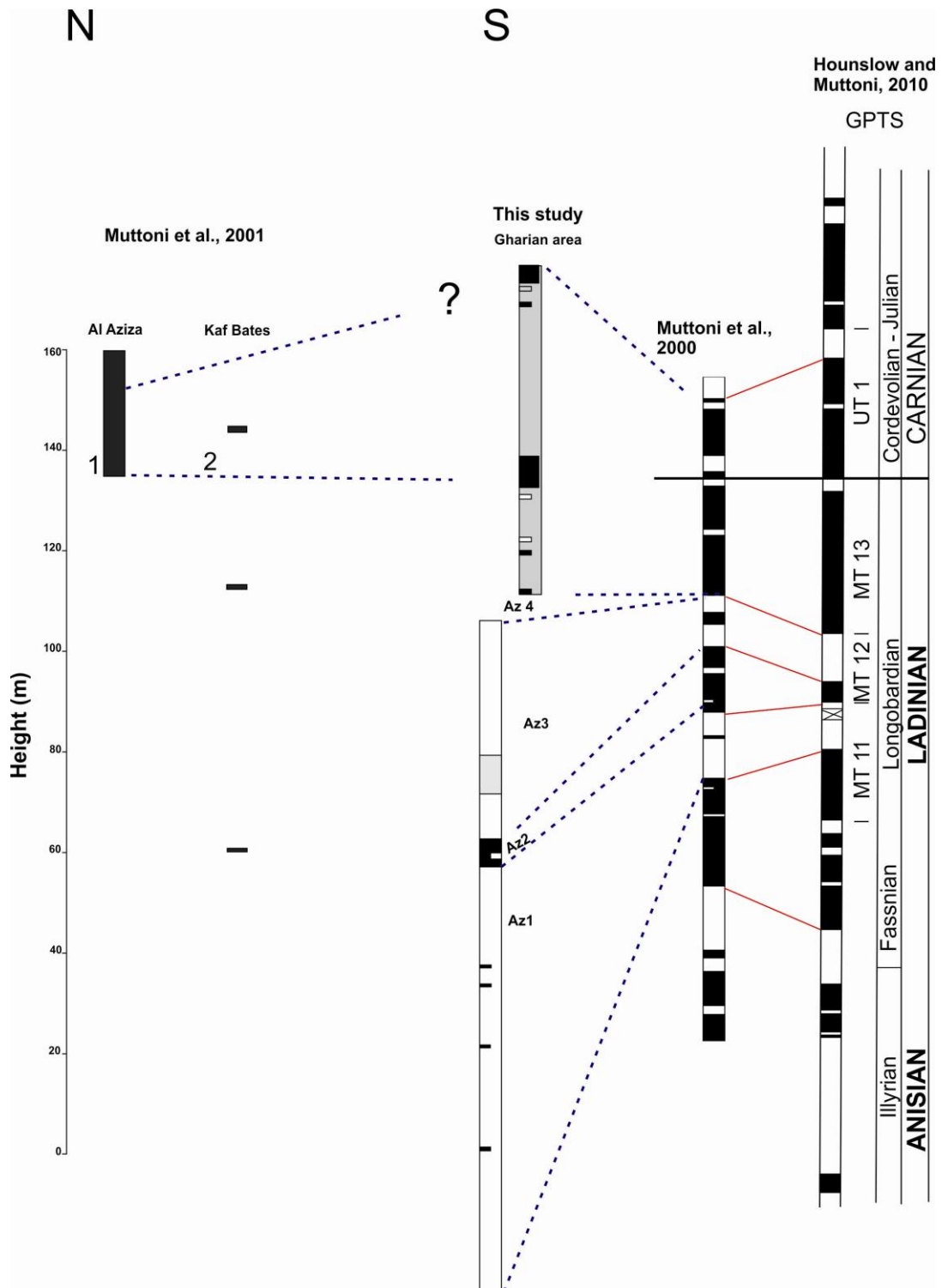


Figure 6.19 Summary correlation of the known magnetostratigraphy of the Al Aziza and Abu Shaybah Formations in Northern Libya (Timescale after Muttoni et al., 2001; Hounslow and Muttoni, 2010).

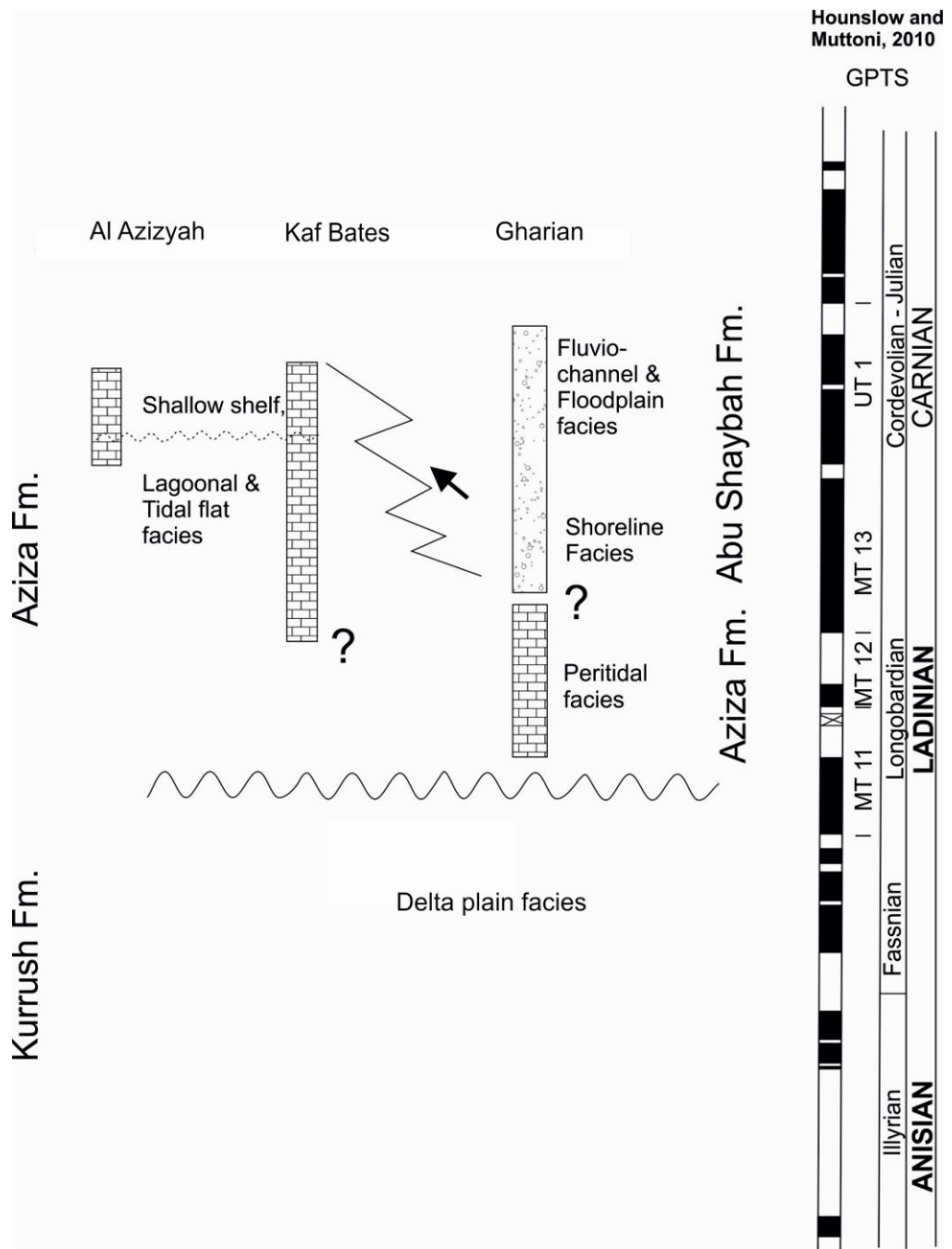


Figure 6.20 Synoptic stratigraphic and facies correlation for the Al Aziza and Abu Shaybah Formations in Northern Libya.

6.8 Conclusions

Palaeomagnetic study of the Triassic rocks from the Gharian area was restricted in scope, yet the results provide some significant insights into the area. The main conclusions from this chapter can be summarised as:

- 1- Magnetisations were found to be generally weak and multi-component in nature.
- 2- The Al Aziza Formation has yielded what is believed to be a primary remanence that has suffered a substantial post acquisition clockwise rotation ($\sim 50^\circ$).
Restoration of the rotation about a simple vertical axis would place the pole on the APW path at an appropriate point in time. This unit also carried an intermediate component which is believed to be in the form of an overprint acquired in mid Cretaceous times.
- 3- The Abu Shaybah Formation also yielded a primary component little different from those observed in the Al Aziza formation at Al Azizyah and Kaf Bates and is readily assigned a middle Triassic age based on its pole position being in agreement with the known APW path.
- 4- Taken together the data from this study and that of Mutton et al.(2001) is consistent with the carbonates of the Aziza Formation being diachronous in age and in part the lateral equivalent of the overlying clastic Abu Shaybah Formation and suggest a northward migration of the shoreline during the latest Ladinian to earliest Carnian time period.

Chapter 7: Structural Evolution of the Gharian Area

7.1 Introduction

It was not the intention of this project to undertake a full structural analysis of the region. But it became obvious during the course of the study that the current structural understanding of the area, as a whole, contains inconsistencies and misconceptions. To better understand the geological evolution of the immediate Gharian area a limited structural investigation has therefore been undertaken.

This primarily consisted of the “ground truthing” of Gray’s (1971) map of the Gharian area, supplemented by extensive use of Google Earth to interpret, extend and investigate parts of Gray’s map (see Map 1 in Appendix 4). This was coupled with the detailed collection of structural data from faults from key locations within the immediate vicinity of Gharian itself and the field assessment of the Landsat interpretation of lineaments reported by Saadi et al., (2009).

It was felt necessary, given the scale of the structures involved, to extend reconnaissance fieldwork some 25 km NE-SW along strike of the Jabel Nafusah escarpment from Wadi Ghan in the northeast to some 10 km west of Gharian with still further but rather more limited reconnaissance east toward the town of Tarhunnah and west as far as Kiklah.

This work has allowed slight modifications of Gray’s map but more importantly provides, what is believed to be, a more coherent understanding of the structural and geomorphological evolution and expression of the area in light of modern geological concepts as will be outlined in this chapter.

7.2 Regional Context and Literature Review with Respect to Structural Development of the Gharian Area

Two recently published papers bear directly on the geology of the area and are briefly outlined below before the established literature is discussed. Bodin et al. (2010) clarify and correlate the Jurassic to Cretaceous stratigraphic succession along the entire length of the Jabel Nafusah escarpment from Tunisia to Libya and assess the tectonic and regional significance of unconformities.

This study included the measurement of the stratigraphic succession from Gharian. Their regional DEM and geological map spanning Tunisia and Libya are shown as Figure 7.1A and B respectively. The DEM (Fig. 7.1a) clearly shows the escarpment as a major tectonic feature of the regional geomorphology and the map emphasises its direct control on the pattern of geological outcrop (Fig. 7.1b). They identify three major unconformities: a major Upper Jurassic to Lower Cretaceous (uppermost Kimmeridgian to uppermost Hauterivean) hiatus, and two shorter late Lower Cretaceous (Late Aptian and Middle Albian) unconformities.

In the Gharian area the first and second are represented by the stratigraphic gap between the Abu Ghaylan and Kiklah formations. The second above the Kiklah formations and below the overlying Sidi as Sid Formation (see Chapter 3). There has been much past discussion regarding tectonic versus sea level controls on these unconformities (see Bodin et al., 2010 for the broader discussion). More locally there has been debate about the form and extent of the Kiklah and Abu Ghaylan formations between Gharian, Wadi Ghan and eastward to Trahunah (Fatmi and Sbeta, 1991) where one or both formations can be absent so merging all the unconformities together. In terms of the strong parallelism of the outcrop of all the units above and below these unconformities in the field around Gharian and east to Wadi Ghan there is very limited,

if any, angular discrepancy visible, except in the immediate vicinity of one or possibly two faults.

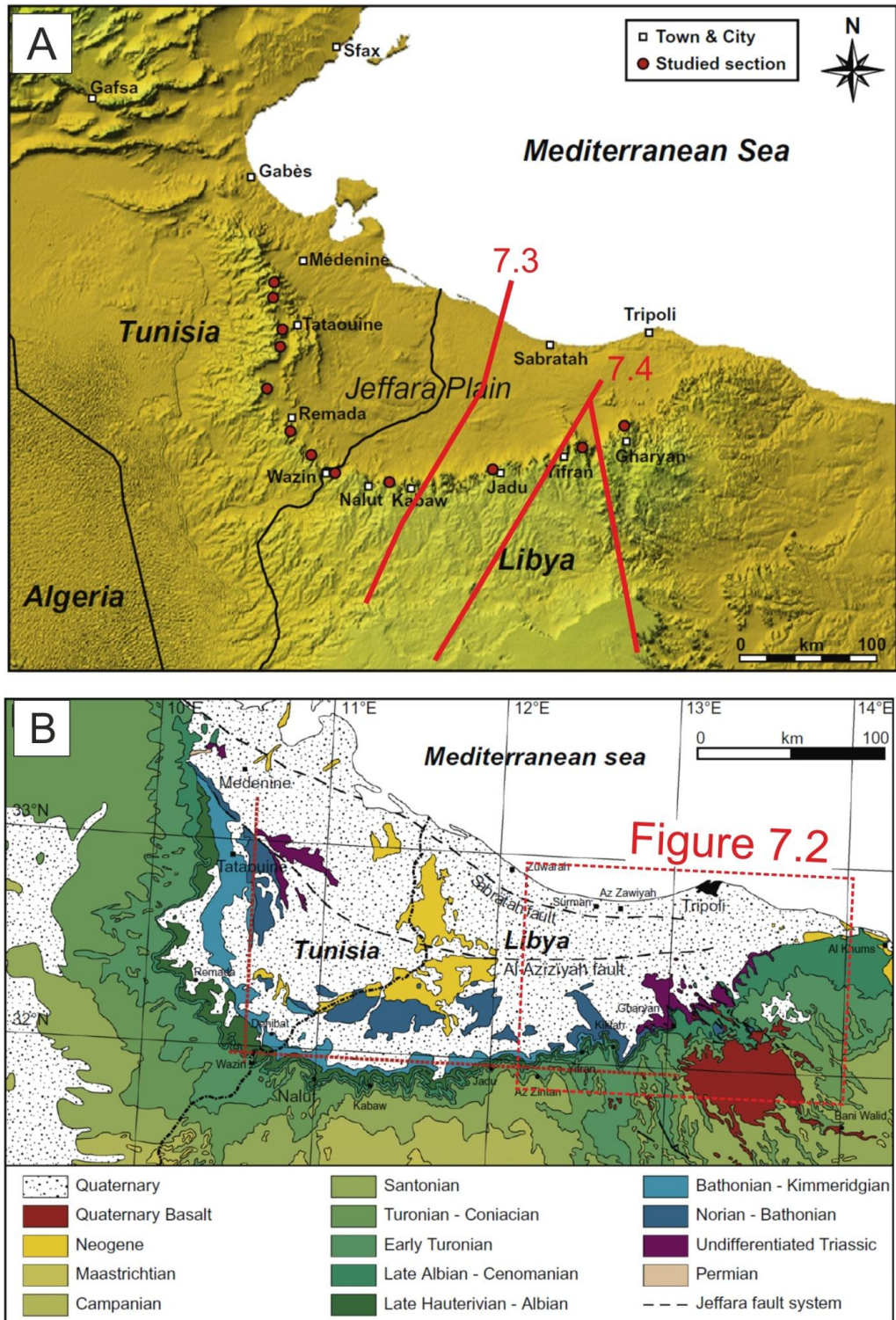


Figure 7.1 Regional DEM (A) and outline geological map (B) of the Jabel Nafusah in NW Libya and Tunisia (from Bodin et al., 2010).

This suggests that significant localised tectonics was not an important factor in their creation rather that these unconformities are a function of much longer wavelength topographic and or sea-level changes leading to non-deposition at large regional scales. Locally at least, where the Kiklah Formation thickness varies it is quite strongly controlled by facies variations and normally in relation to pre-existing topography (i.e., it is notably thicker in valley fills).

In the Hun Graben and Sirt Basin in central northern Libya the Albian and Aptian unconformities and subsidence rates are in part linked to variations in Atlantic rifting and changes in Tethyan dynamics during the Early Cretaceous (Abadi et al., 2008 and Table 7.1). In the Gharian area exposure is such (and the level of detail that could be achieved in the limited time available for structural studies) that nowhere was there a simple means of measuring outcrop thickness across known faults.

Therefore, it is impossible to determine whether the Early Cretaceous units present (i.e., Sidi as Sid and Nalut formations, have any clear growth relationships to observable faults. In short all of our fault observations appear to post-date the creation of the unconformities and deposition of the strata although we cannot rule out their initiation at an earlier tectonic stage.

In a second recent study, Saadi et al (2009) focussed upon the Central and Eastern Jabel Nafusah and Jafarah plain, which includes Gharian, and integrated existing geological maps, DEM, Landsat and aeromagnetic data (Fig. 7.2). This paper emphasises the interpretation of lineaments and faults and this is considered later in the chapter. In terms of explanation of the Jabel Nafusah escarpment itself this paper merely offers the two rather old but most commonly repeated explanations that it is either an old marine cliff or the retreating scarp of the Azizyah Fault.

They do however, emphasise the importance of NW-SE faults and NE-SW faults noting the former's long strike lengths and apparently significant throws. However, their discussion of the structures in terms of their evolution is far from clear as in their conclusions they first suggest that Hercynian and then Caledonian orogenic movements were responsible for imparting strong controls on the area, but offer no rationale for this and there is, consequently, no clear explanation of the Jabel Nafusah escarpment itself.

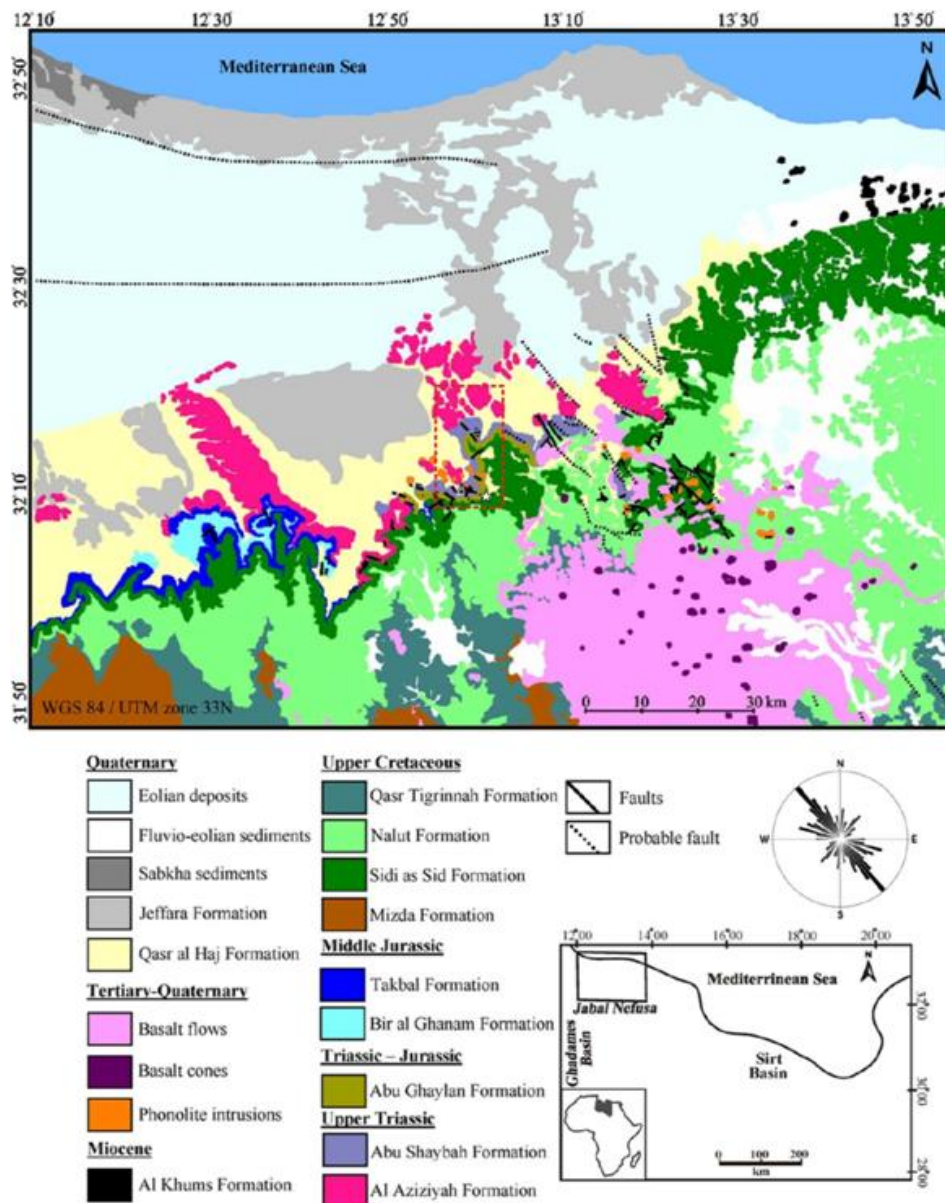


Figure 7.2 Geological map of the Central and Eastern Jabel Nafusah and adjacent Jafarah plain (from Saadi et al., 2009).

Prior to these two regional papers the literature on the immediate Gharian area (Fig. 7.3) (and indeed the wider Jabel Nafusah and Jafarah plain) is both sparse and dated.

The literature prior to 1991 is summarised in Anketell and Ghellali (1991) in their regional interpretation of the then existent information and is briefly summarised below in terms of three broad areas.

i) The Gharian area

Lipparini (1940) interpreted the gross structure of the region as a NW–SE trending anticline whose axial trace lies west of Gharian. This major fold is paralleled by a number of NW-SE faults which he deduced served as the loci for volcanic intrusion and extrusion. These he believed to be cut by E-W to ENE-WSW faults (trending parallel to the Jabel Nafusah escarpment) which was a critical point in the understanding of the structural development of the region.

In contrast to Lipparini (1940), Desio et al (1963) considered the major structure of the region to be an “ellipsoid trending ENE-WSW from Al Khums to the Tunisian Border” with associated major faults paralleling it. In part at least this appears to be the source of an often repeated idea that the Jabel Nafusah uplift is part of an essentially E-W trending ‘Nafusah arch’ which is referred to in more recent works. The use of the term arch in older North African literature is, at best, loosely defined and appears to cover any uplift but in particular basement cored uplifts of Precambrian basement, e.g. Gargaf arch (see Chapter 1, Fig .1.3). In the case of the Jabel Nafusah basement type rocks have never been encountered although low grade metamorphosed Lower Palaeozoic sediments are known in the west from deep exploration boreholes.

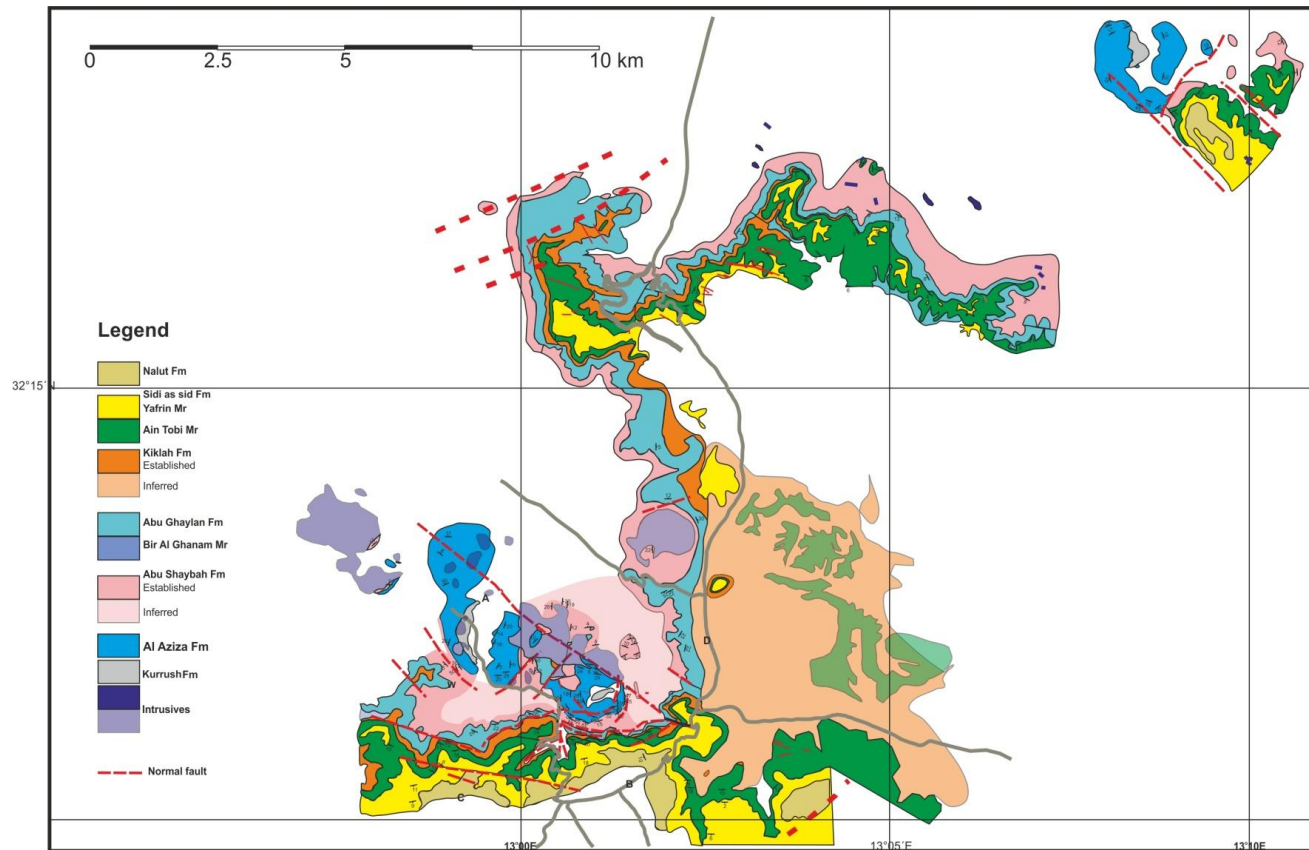


Figure 7.3 Geological map of the Gharian area (enclosure Map 2) Modified from Gray (1971) supplemented by recent mapping and extended by interpretation of Google Earth image.

Christie (1966) reported his stratigraphic studies of the area, aimed primarily at hydrogeology, and in particular gives stratigraphic measured sections from the Gharian. However, in terms of structure, he merely reports some significant (up to 200 m of displacement but crucially of unreported sense) NW trending faults in Wadi Ghan and links these NW structures spatially to small igneous domes.

A key development in understanding the structure of the area was the work of Gray (1971) who published for the first time a detailed map (compiled at 1:25,000 scale; see Fig. 7.3) and supported this with the description of key field observations and cross sections. Critically he notes that the presence of igneous intrusions is linked to the presence of faults and that ‘arching’ of the sediments by the exposed intrusives cannot be demonstrated.

Furthermore, some of the intrusives show remarkably little disturbance of the enclosing beds (Gray 1971, p 315). In his discussion he also notes that the flat lying floors and roofs of some of the intrusives are observed and elsewhere that exposed marginal contacts of intrusion follow contours and goes on to describe the intrusions as sills or having sill like characteristics in several places and finally refers to the intrusions as laccoliths.

He however went on to conclude that “most of the doming of the beds was caused by deeper seated intrusives not now exposed (Gray, 1971 p 315). This sowed the seed that the ‘Gharian Dome’ was a function of an intrusion and since then the concept has persisted in the literature (e.g. Tawadros, 2001; Hallett, 2002).

Equally as important Gray also discussed the presence of faults in some detail and broadly describes them in terms of three groups as follows;

- The most common strike between 280-290° (WNW) with near vertical dip and dip slip displacements but which are very small in displacement and bedding

shows no significant drag at these faults with offset often dying out along strike over short distances. These faults, he notes, have little control on the geology but appear to influence of erosion along the escarpment margins.

- The second group recognised are faults with NE-SW strikes which show large amounts of drag and significant offset of geological units older than the intrusives. This group included a strongly faulted syncline in the centre of the area (Abu Ghannush) with bounding faults with strikes of 035-045° and significant dragging of the beds.
- A third group of NNW striking faults is discussed in passing but of which he actually records little beyond the fact that they too can show major drag.

ii) The Jafarah plain and the Al Aziziyah Fault System

The Al Aziziyah Fault, or fault system, also known as the Gafsa-Gafara Fault system as it passes westward into Tunisia, lies approximately half way between the Jabel Nafusah escarpment and the modern coastline (Figure 7.1). This fault (system) has been widely referred to in many papers but only vaguely represented on most maps (e.g. Figure 7.2). It is viewed by most authors as a near east-west (within Libya at least) trending, down to the north normal fault or fault system (Desio et al., 1963; Lipparini, 1965; Boote et al., 1998; Swire and Gashgesh, 2000; Klett, 2002; Pizzi et al., 1999).

The only published cross-sections that include the fault are at regional scales and are derived from borehole correlations, and in particular, the deeper boreholes from the western part of the Jafarah plain/Nafusah Escarpment in Libya. The main target is to better understand the stratigraphic setting of the petroleum reservoir systems of the Ghadamis basin to the south and the offshore Pelagian basin to the north (Fig.7.4). These cross-sections clearly show a major thickening of the Triassic-Jurassic sequence (Kurrush, Al Aziza and Abu Shaybah Formations) north of the Al Aziziyah normal fault, which at least in the case of one section (Fig. 7.4A, Klett, 2002, based on Boote et al.,

1998) is located immediately northward of a Palaeozoic and/or basement high known as the Jafarah Arch; although the evidence for this is not shown. Both sections show a marked thickening of the Mesozoic sequence under the escarpment itself. Regional cross-sections through the immediate area of Gharian are, based on shallower boreholes intended for hydrogeology purposes (Pizzi et al., 1999) but apparently based on Pizzi and Sartori, 1984), imply the Jabel Nafusah escarpment is a function of a horst block uplift or half-graben bounding system (Fig. 7.5, sections 1 and 3) which extends northward of the Jabel Nafusah toward the Al Aziziyah Fault.

In contrast to these studies, Anketell and Ghellali (1991) presented an extensive discussion of the surface expression of the Al Aziziyah fault system as an east-west trending belt of WNW-ESE trending sigmoidal (riedel) shear faults which were interpreted as having a complex history with an initially sinistral but later dextral strike-slip history (see Anketell and Ghellali, 1991; Fig. 3, 4 and 7) during the Late Cretaceous and Tertiary. The origin of the faults they ascribe loosely to be linked to African – European collision and to reactivation of the ‘Jafarah’ arch of Hercynian age. However little or nothing is said of their normal component effect in greatly thickening and down throwing to the north of the Mesozoic sequences.

Given that they acknowledge the paucity of data in terms of measured dip from subsurface studies, the clear absence of any kinematic data, the limited surface exposure, plus the absence of any detailed seismic reflection data. The lack of topographic expression to confirm these faults and ideas it is impossible to see how such a complex interpretation for this fault system could have been reliably derived from limited borehole data alone.

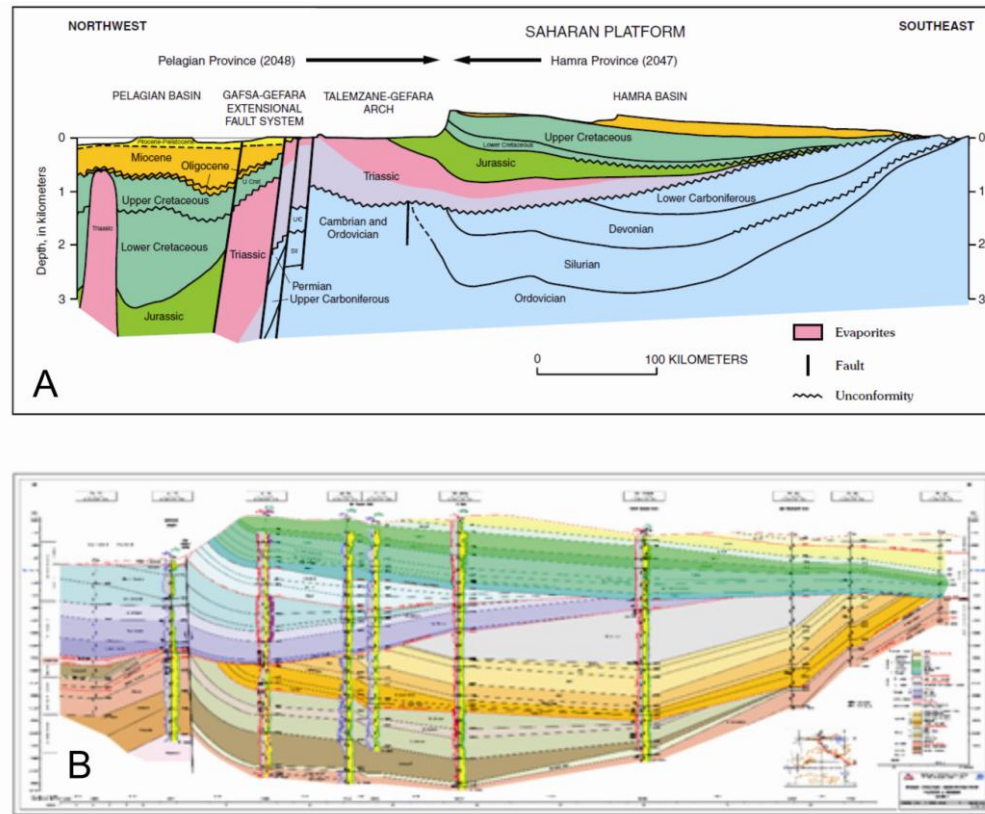


Figure 7.4 Illustrative cross-sections of the Jafarah Plain and the Jabel Nafusah escarpment from borehole data at the western end of the escarpment (see Fig. 7.1 for approximate location) based primarily on well depths only. A is from Klett, 2002 (after Boote et al., 1998 and others) and B from Letouzey al., (2005).

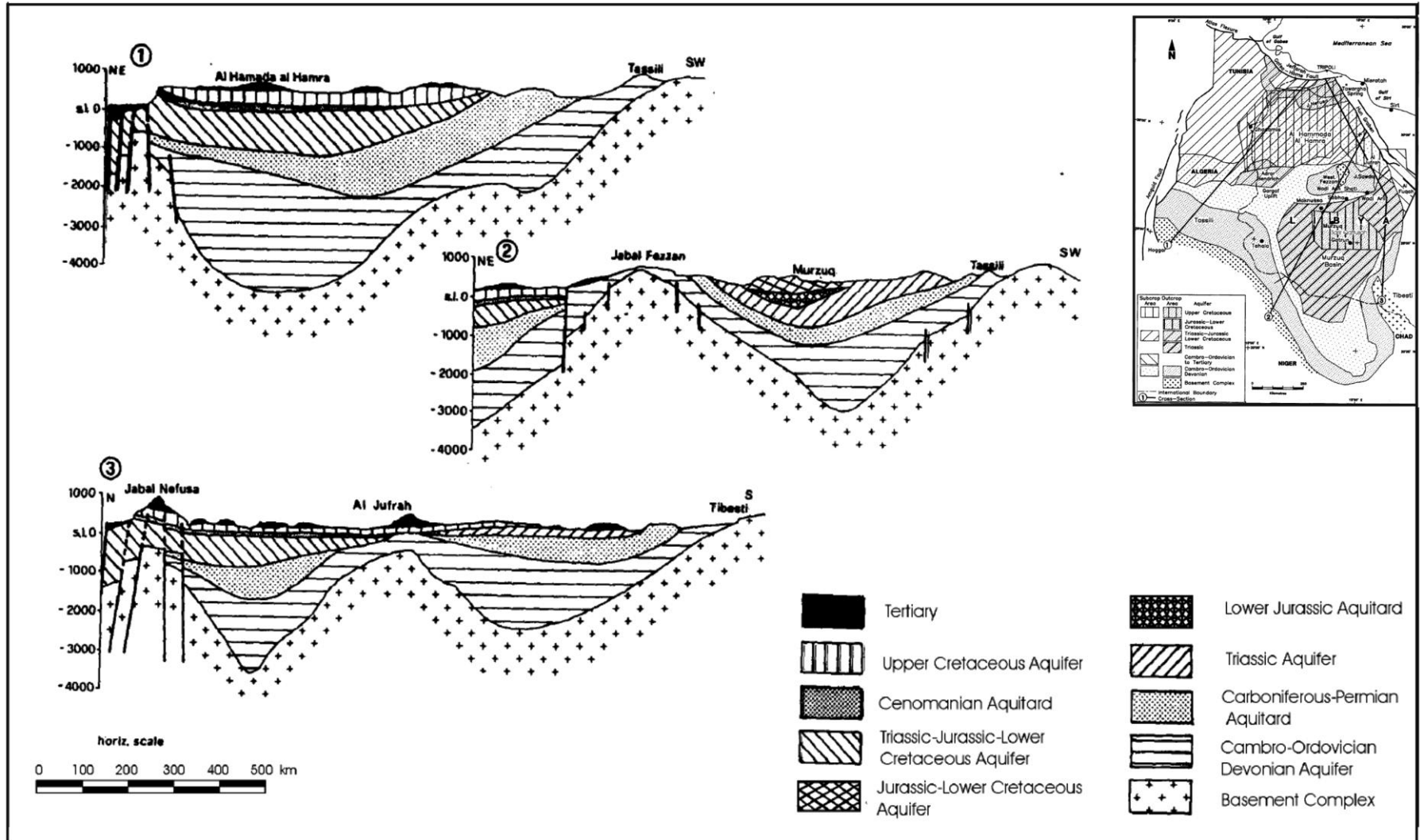


Figure 7.5 Illustrative cross-sections through Gharian from Pizzi et al., 1999.

iii) The Jebel Nafusah Escarpment

The escarpment was described in detail by Miller (1971) in terms of its topography. It is impact on the drainage systems in a series of contour and drainage maps. Miller subdivided the Jabel into western (from the border at Wazin to just east of Kabaw), central (Kabaw to midway between Yifran and Gharian) and eastern (which includes Gharian and Wadi Ghan) segments based primarily on the height of the scarp relative to the plain (see Fig. 7.1A for place names).

The western Jabel is dominated by a linear range front as a whole and the linearity of individual front segments. The central segment is the highest and coincided with the structural highest point of the underlying Cretaceous geology. The eastern segment he notes is lower again and declines in significance eastward to the coast as it becomes more and more dissected.

On larger scales he emphasised the more convoluted nature of the escarpment and in particular sharp changes in the range front strike from ENE- WSW to NW and back to ENE-WSW and noted the dissection of the range front by NW trending faults where these were known. In the eastern sector he particularly emphasised (Miller 1971, p 378) the impact of NW trending faults and the controls they exert on markedly linear stream drainage patterns and their occurrence in relation to the rapid decrease in height of the escarpment to the NE of Wadi Ghan. To summarise Miller raises several significant points about the escarpment:

- Its apparent youthfulness shown by its steep gradient and limited erosion by short, ephemeral, drainage systems which drain northward;
- It's E-W to ENE-WSW continuity and linearity at a number of scales;
- The disruption of this continuity by NW trending valleys and where, it could be established, NW trending faults;

- The lack of geological outliers to the north of the escarpment.

The problem Miller clearly posed (in contrast to others) is ‘what is the primary control on the topography of the escarpment?’ In fact he dismissed older suggestions that it was a “palaeo” sea cliff or the retreated erosional front of the Aziziyah Fault or some combination of these, all of which have been suggested at one time or another. He leaves only two possibilities;

- a monoclinal (or anticlinal) flexure located immediately northward of the present escarpment such that erosion has obscured the northward dipping limb (although this he then argues against as not being viable, as while it might explain some of the geological dips it fails to explain the geomorphology);
- a normal fault that downthrows to the north with the primary escarpment marking the fault trace which he believes to be very attractive but dismisses on the basis that there is no exposed Cretaceous strata lying to the north of the fault in the Southern Jafarah plain area. Such outliers would of course be simple proof of a normal sense downthrow across the escarpment.

iv) Summary of the problems

The lack of clarity of geological understanding therefore lies in a combination of

- lack of observational/kinematic data for the fault systems of the region;
- an explanation of the Nafusah escarpment itself;
- the pervading idea that the Gharian dome is a consequence of igneous doming;
- the limited sub-surface knowledge of the structure and stratigraphy, in particular, of the southern part of the Jafarah Plain.

While this study cannot address all of these problems in full it will seek to provide an improved geological context for the area based on an integration of field observations both past and present, with a logical explanation of some of the observed anomalies in light of modern geological understanding of structures and pluton emplacement.

7.3 Key Field Observations

7.3.1 Al Azizyah Fault and the exposed Aziza Formation in the Jafarah Plain

The Al Aziza Formation limestones are exposed in a series of low hills that extend NW (Fig. 7.2) from the foot of the escarpment toward the town of Al Aziziyah, these hills include Kaf Bates (aka Raz Mazul, see Fig. 6.1) which was studied previously by Muttoni et al, (2001) for palaeomagnetic purposes (see Chapter 6) and is included on the detailed geological map (Map 2).

From Aziziyah town itself south west for some 20 km toward the town of Bir Al Ghanam (Fig. 7.6) is a semi-continuous elevated ridge which comprises a series of small hills of Al Aziza Formation limestone that has been extensively quarried for decorative stone. In the quarries entered during fieldwork the limestones were repeatedly observed to dip shallowly ($<10^\circ$ to a maximum of 15°) in an overall south to south-south-eastward directly toward the Jabel Nafusah escarpment.

Although the Al Azizyah Fault itself is located some distance to the north of these quarried exposures they must lie within the gently southward tilted footwall of the main normal fault. The topography from here rises gently southward across the southern Jafarah plain toward the Jabel Nafusah escarpment and its major re-entrant in the form of Wadi Gabel directly northwest of Gharian.

In one quarry ($32^\circ 29' N$, $12^\circ 52' E$) it was possible to demonstrate a right way up context for the limestone (well developed ripple cross-lamination) of the Al Aziza Formation which in turn was in almost immediate conformable stratigraphic contact with green and purple mud and fine sands of the underlying Kurrush formation (also recognised on the map of Anketell and Ghellali 1991).

No exposures can be seen down dip between this point and where the Al Aziza/Abu Shaybah boundary first outcrops at the base of the Jabel Nafusah escarpment north of

Gharian (Fig. 7.6) in Wadi Abu Shaybah. Conservatively this is a distance of 21 km in the down dip direction. A simple calculation, assuming a constant dip would indicate that the Al Aziza/Kurrush stratigraphic boundary should be buried to a depth of between 1.8 km (assuming 5° of constant dip) and 5.6 km depth (if 15° of dip is assumed) over the distance to the base of the escarpment. That neglects the small topographic change which would add to these figures.

Likewise for the Al Aziza/Abu Shaybah boundary this should be buried to a minimum of 1.6 to 5.4 km assuming the same dips and a reasonably constant thickness for the stratigraphy. Obviously such assumptions are major but they clearly imply that a regionally significant step in the geology has to be accounted for south of the Al Aziziyah fault system. If these units are to be exposed at all in this area and logically this has to be located either within the southern Jafarah plain or, much more likely, at the base of the Nafusah escarpment itself as even the stratigraphically highest exposed Nalut Formation should in fact be buried to some considerable depth at the Jabel Nafusah front.

The implication of this is that these outcrops of Al Aziza and Kurrush Formations along the Aziziyah-Bir Al Ghanam road are indeed relatively simple outliers with respect to the outcrops of these units immediately north of Gharian. They provide one clear line of evidence for a major normal fault along the Jabel Nafusah escarpment. This does however then pose the question as to what is the nature of the outcrops of the Al Aziza Formation that lie directly between Aziziyah town and the escarpment and this will be returned to later in the chapter.

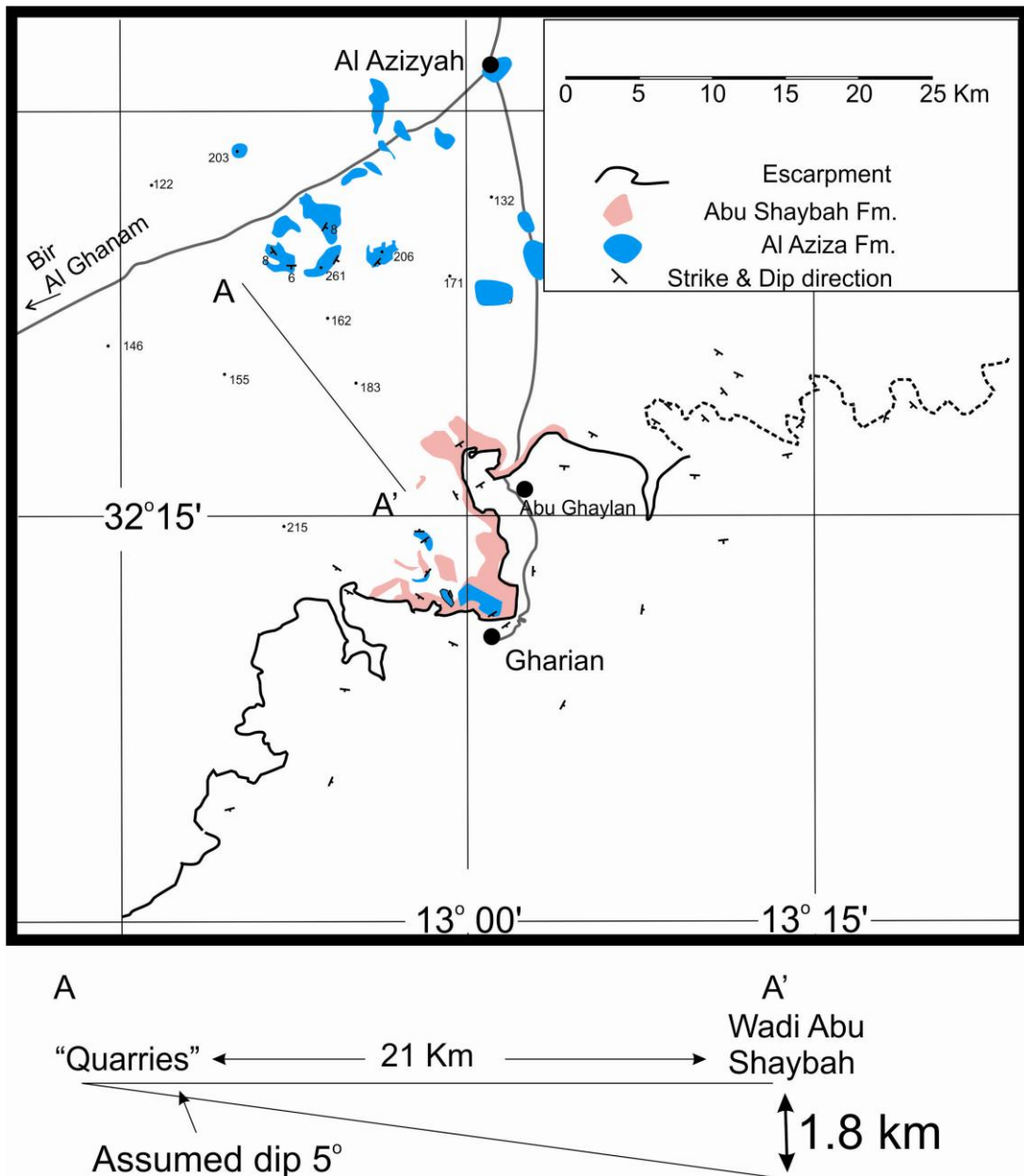


Figure 7.6 Sketch map of the distribution of Aziza limestone north of the Jabel Nafusah and illustrative calculation of the displacement at the Jabel Nafusah were it assumed to be a single simple normal fault.

7.3.2 Structural Analysis of Faults Around the Gharian Area

Fault analysis in the field area was undertaken by a series of traverses at nine principle localities (Table 7.1), primarily along road cuts which provide the best exposed sections (Map 2). Further data were also collected during normal fieldwork as and when possible. Standard field practice was adopted such that the orientation of the fault plane, slickenlines and/or other kinematic indicators, and observable offset were all recorded (Hardcastle, 1989; Price and Cosgrove, 1990). Unfortunately slickenlines and other kinematic indicators were found to be exceptionally rare in this area; so although simple bed displacement could often be measured the exact kinematic nature of this offset could not be readily established for the great majority of observations.

Therefore, the analysis that follows is based on a systematic analysis of the clustering of the data and relating this to the field observations in a direct manner where true offset could be established and or where cross-cutting relationships were observed (Table 7.2). A total only 17 sets of well-developed slickenlines are observed and all showed that the faults were of steeply dip-slip character while accompanying offsets indicated normal displacement. This was consistent with observed offset outcrop patterns which were, in all cases, of apparently normal displacement in relation to bedding dip and minor fractures regardless of fault strike and also consistent with other observations such as “Petit” steps (Petit, 1987). At 16 localities clear cross-cutting relationships are observed between different fault sets (Table 7.3).

| | Locality Name | Location | Stratigraphic Units sampled | Nature of outcrop |
|---|--|--|---|--|
| 1 | Old Gharian Tripoli highway | 32.264426°N 13.034324°E - 32.269034°N 13.031763°E | Kiklah to Sidi as Sid | Some 1.7 km of continuous road cut, fully exposed on one side with considerable vertical access due to repeated twists in road |
| 2 | Kabted Jamel | 32.208547°N 13.036625°E - 32.214372°N 13.018752°E | Abu Ghaylan- Abu Shaybah and close to the Kaf Tekut intrusion | 2.3 km of variable height (~3-15 m) and sporadic roadcuts but with hillsides above |
| 3 | Wadi Gabel | 32 12 4.573 °N 013 01.522°E | Abu Ghaylan- Abu Shaybah | Roadcut extending some 200 m |
| 4 | Gharian Tripoli highway | 32.183160°N 13.039265°E - 32.177834°N 13.034075°E | Ain Tobi mbr. carbonates of the Sidi as Sid | 0.8 km of continuous low (2- 4 m) recently exposed roadcuts |
| 5 | Abu Rashada road | 32.169429°N 13.007475°E - 32.181247°N 13.006922°E | Nalut to Abu Shaybah | Continuous 3 km long exposure in one or both road margins with extensive hillslopes above with extensive vertical coverage |
| 6 | Northern Abu Rashada road | 32.204125°N 12.985646°E | a low anticline exposing Aziza (and Kurrush?) Fms. | Roadcut extending some 400 m |
| 7 | Old Wadi Gabel road | 32.184863°N 13.037295°E 32.184544°N 13.028212°E | Ain Tobi – Abu-Shaybah and including basaltic dykes | 0.9 km traverse along roadcuts to a main track |
| 8 | Kaf Kalaya road (west of Abu Rashada road) | | Abu Ghaylan- Abu Shaybah | Continuous 2.5 km long exposure in one or both road |
| 9 | Wadi Abu Shaybah | 32 11 179°N 013 00.740°E | Al Aziza-Abu Shaybah to Abu Ghaylan | Wadi and roadcuts but with hillsides above |

Table 7.1 Locations of traverses undertaken primarily to collect structural data on faults.

i) Stereographic Analysis

A total of 170 fault/fracture observations were made and when plotted initially do not form an obvious clear pattern (Fig. 7.7a). However, contouring of the poles to planes reveals two distinct paired strong clusters (Fig. 7.7b). These two clusters were separated from the rest based on the strike of the fault plane and were re-plotted as planes and their corresponding poles (Fig. 7.8a and b).

This reveals a set of planes with NNE-SSW (000-030) strikes (n=39) with steep dips (generally in excess of 70°) to either WNW or ESE which are termed the Group A faults. A second and the most numerous set of isolated fault planes (n=71) strikes WNW to ESE (~265-305) with dips normally in excess of 70° but with some lower ones here termed the Group B faults. These two sets of fault planes were found widely throughout the area (Map 1 in Appendix 4) and found to be consistent from site to site in terms of orientation with respect to each other.

These were always near perpendicular to the normally gently south-south-eastward regional bedding dip. Field relations revealed an ambiguous cross-cutting relationship between these two groups which may suggest that they formed contemporaneously (i.e. in some cases an A Group fault is seen to cut a B Group while the opposite was also found to be true). However, only a total of 10 unequivocal such examples were observed, Table 7.2. These two sets of faults were primarily observed in the Sidi as Sid Formation and, in particular, in traverses close to or on the margin of the escarpment (localities 1, 4 and 5 of Table 7.1, Map 1).

Field relations for Group A faults show minor normal displacements (usually of the order of <0.5m) and in many cases virtually no displacement but with clear karstic fills that are well consolidated (Fig. 7.9 a and b) indicating these were once open fractures.

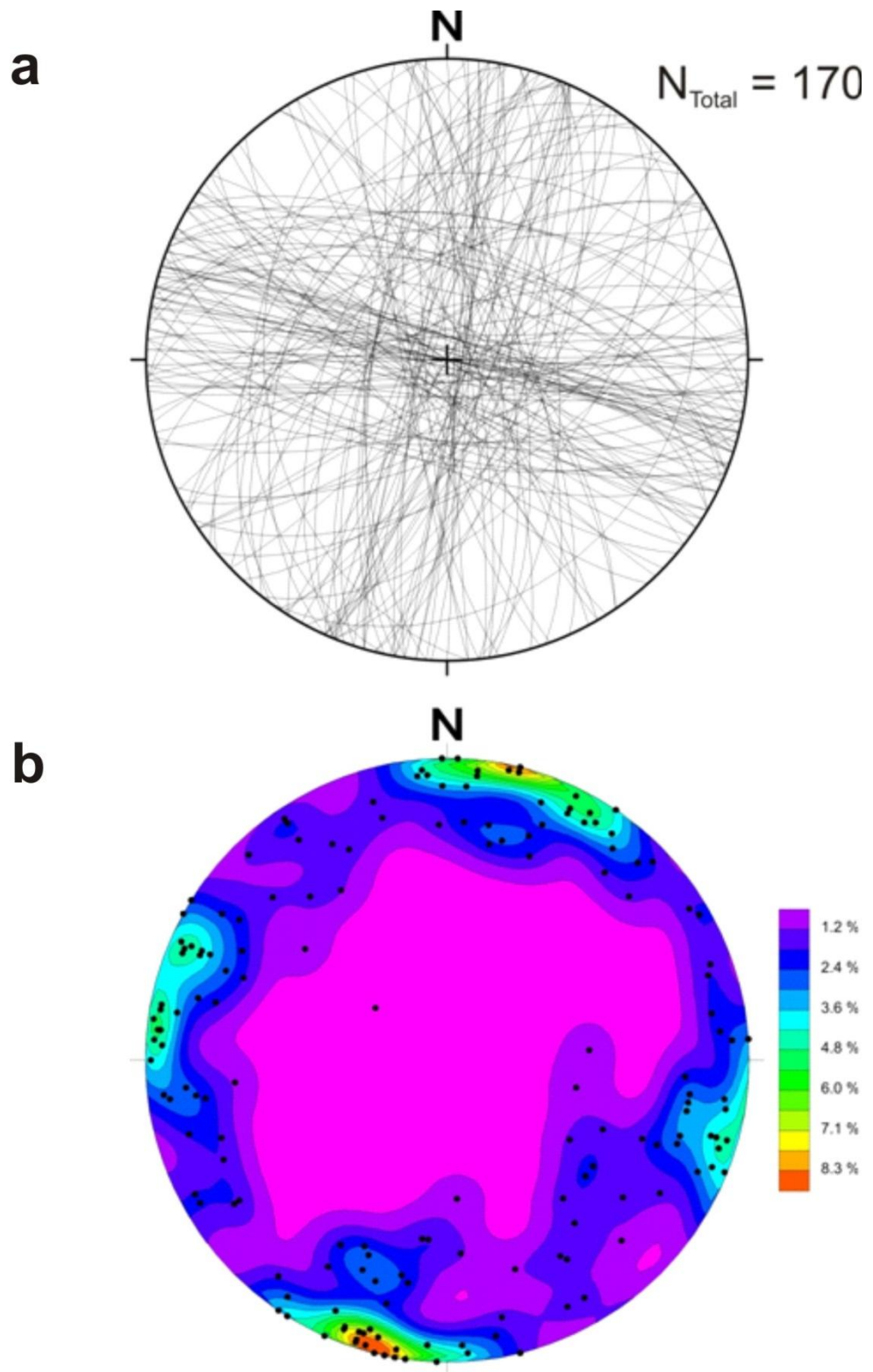


Figure 7.7 Stereonet projection of all faults recording during the fieldwork presented as **a)** planes and **b)** contoured poles to planes.

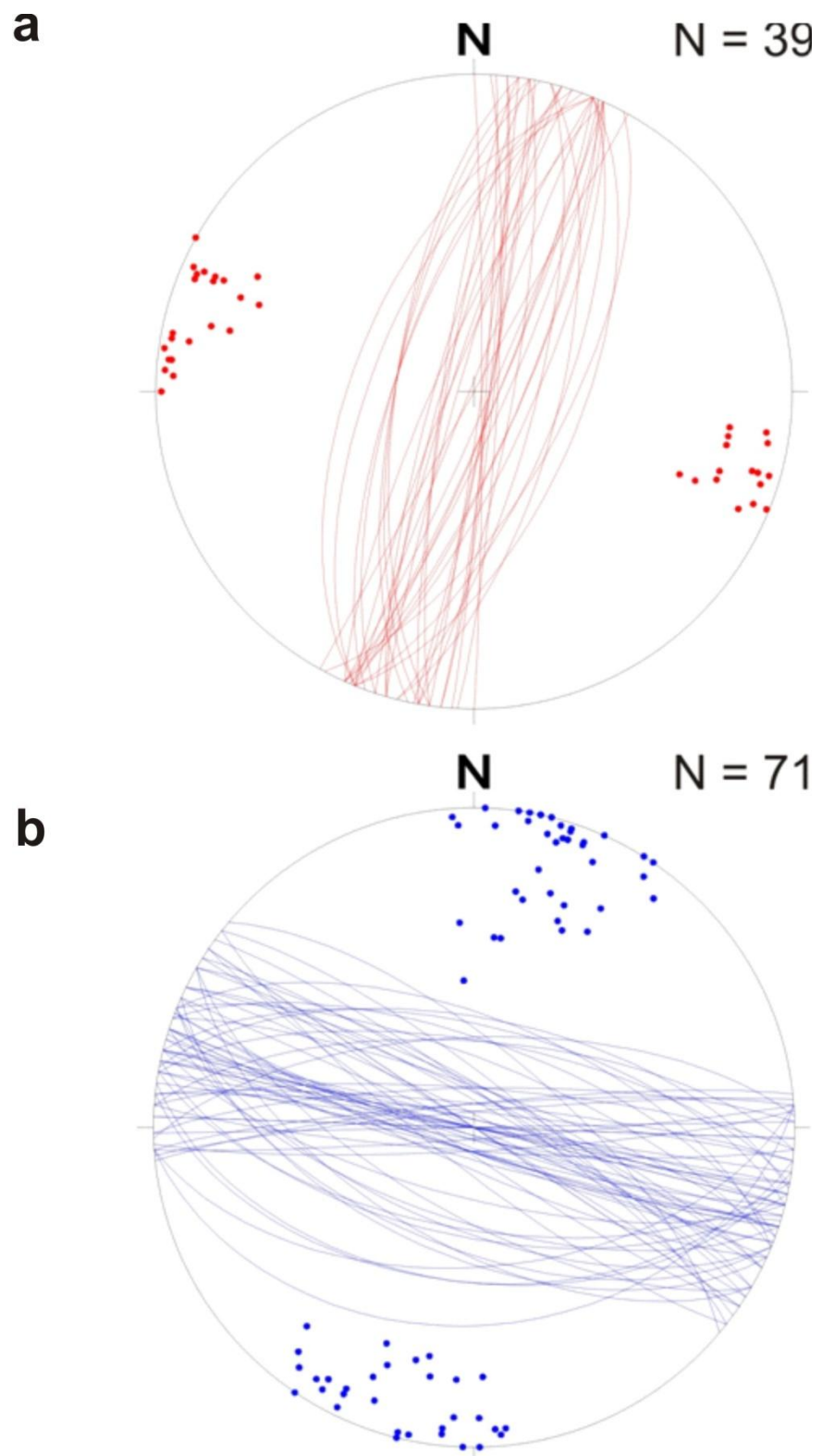


Figure 7.8 Stereonets of poles and planes for a) A group and b) B group faults.

| Location – name | GPS- Ref | Cross-cutting | Older | Younger |
|--------------------------------|-----------------------------|-----------------------------|-------|---------|
| Wadi Gabel Road | N 32 11 079 E013 02.133 | 203/84 W cut by 300/84NE | A | B |
| Wadi Gabel Road | N 32 11 079 E013 02.133 | 294/90 cut by 202/84 W | B | A |
| Wadi Gabel Road | N 32 11 079 E013 02.133 | 108/87S cut by 213/78W | B | A |
| Old Gharian-Tripoli highway | N32 15.965 E013 01.861 | 204 cut by 104/48 | A | B |
| Old Gharian-Tripoli highway | N32 15.965 E013 01.861 | 190/80W cut by 108/84S | A | B |
| Abu Rashada Road | N32 10.223 E013 00.434 | 124/84S cut by 22/64 | B | A |
| Abu Rashada Road | N32 10.223 E013 00.434 | 018/84E cut by 282/90 | A | B |
| Abu Rashada Road | N32 10.223 E013 00.434 | 202/62W cut by 128/18S | A | B |
| Abu Rashada | N32 10.223 E013 00.434 | 208/66W cut by 124/90 | A | B |
| Abu Rashada Road | N32 12.282 N01259.091 | 183/84 cut by 256/90 | A | B |
| Kabted Jamal | 32 12 891 013 00621 | 072/62N cut by 328/ 84 E | JN | B |
| Old Gharian-Tripoli highway | N32 15.965 E013 01.861 | 164/78w cut by 094/84S | HG | B |
| Abu Rashada Road | N32 10.223 E013 00.434 | 266/84N cut by 274/68NE | JN | B |
| Kabted Jamal | N32 012.891 E 013 00.621 | 68/38S cut by 190/86 | JN | A |
| Tripoli-Gharian Highway | N32.11051 E01302.450 | 265/86 cut by 04/68 | JN | A |

Table 7.2 Cross cutting relations data.

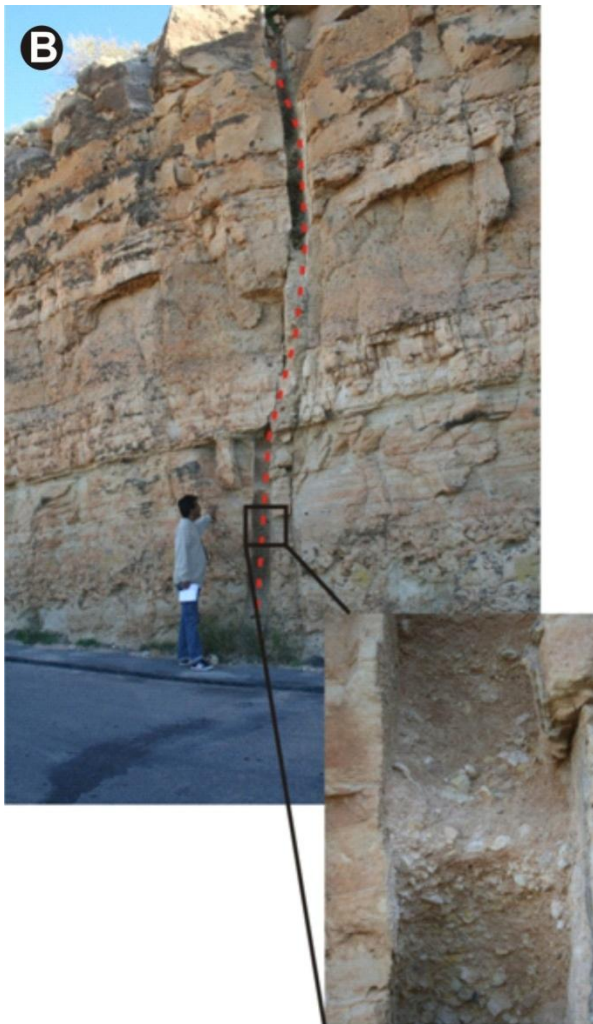


Figure 7.9A Group A faults displaying minor normal displacement in the form of mini horsts and grabens (Locality7 Old Wadi Gabel road). **B** Karstic fill and open voids in Group A faults (Locality 1 Old Gharian-Tripoli Highway).

Group B faults are particularly well represented on the Landsat images used in Google Earth where the fault plane is often picked out by vegetation along the fault (Fig. 7.10) but where offsets are virtually negligible. Like the Group A faults when Group B faults were well observed they were seen to be normal in character with again typically only minor displacements (<0.5 m) and often paired in such a way that they showed development of minor horst and graben structures (Fig. 7.11). Neither the A nor B faults show any significant drag in their hanging or footwalls. Gray (1971) noted the existence of the B faults and points out that they exert a significant control on the development of the escarpment west of Gharian where they do exhibit up to 40 m of displacement but no mention is made of the A group faults at all.

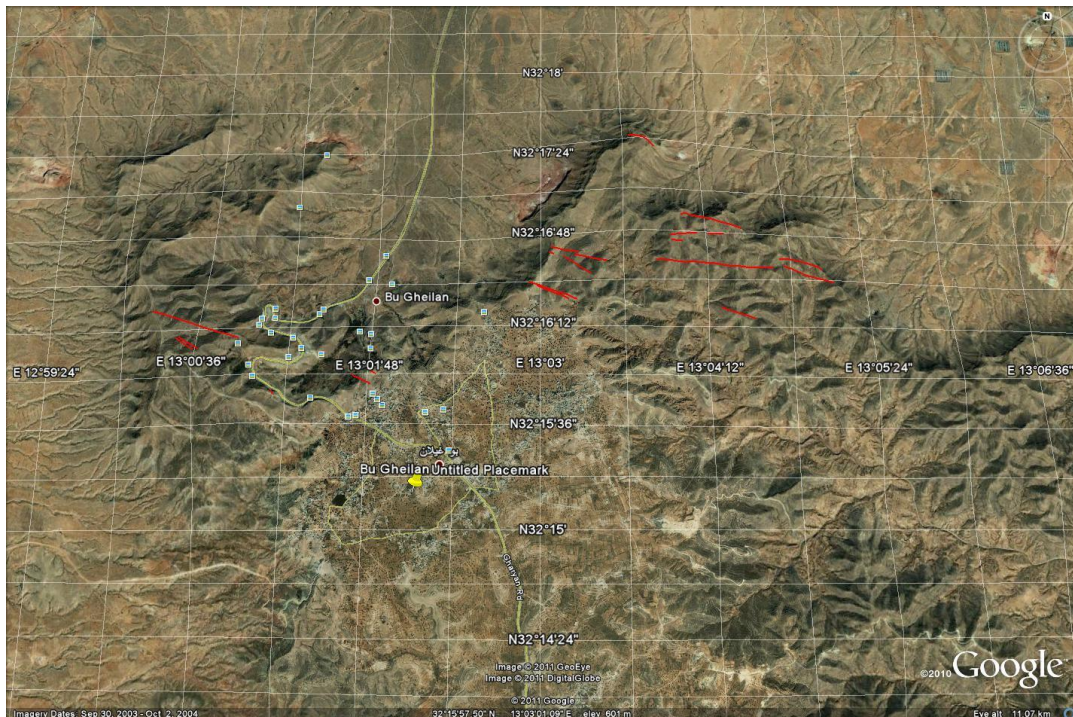


Figure 7.10 Google Earth image showing Group B orientated faults traversing the Wadi Ghan-Abu Ghaylan topographic plateau, where they show little or no displacement but are readily picked out by the growth of low shrubby vegetation associated with them.

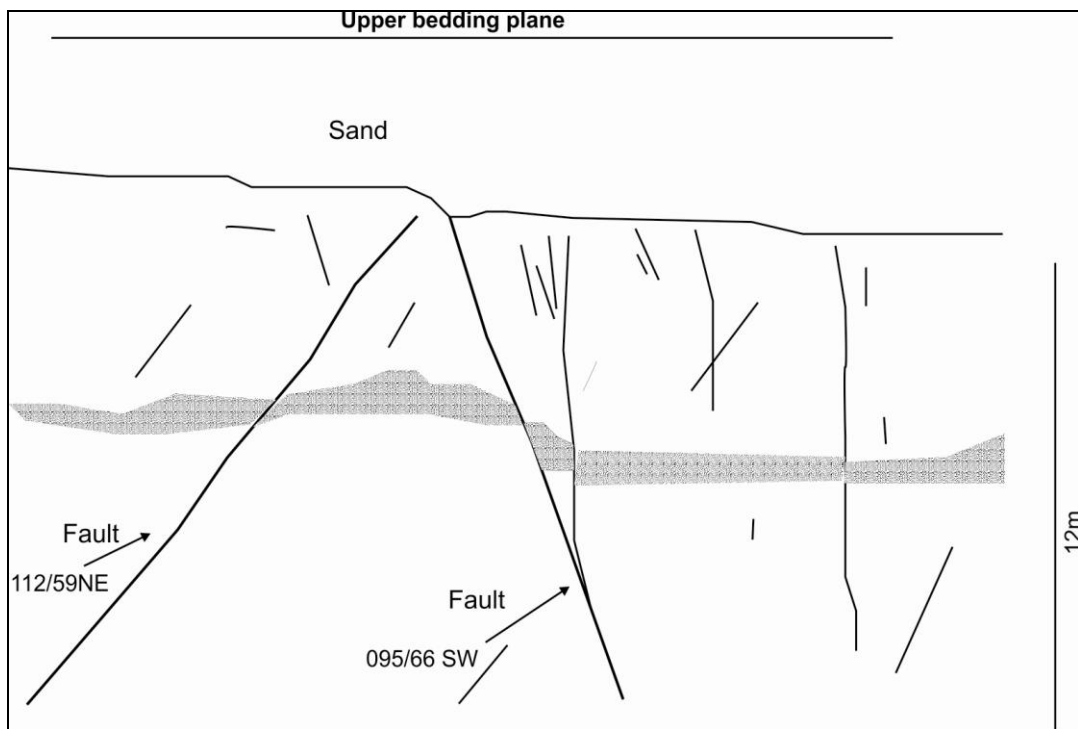


Figure 7.11 Horst and graben type structures with associated minor displacement of Group B normal faults.

Removal of both A and B group faults from the overall data set reveals two further distinct sets of planes that can again be readily separated (Fig. 7.12) on the basis of their orientations. The first of these clusters strikes NW to NNW with dips to either WSW or ENE and which vary between 60-80° of dip (Fig. 7.13a, n= 25). This group is termed the Hun Graben Faults (HG) in further discussions and were, as noted above, found to be of normal character where slickenlines could be observed with determinable bed offset.

In places these faults are often associated with significant normal drag of their hanging wall strata (Fig. 7.14). In places where the fault plane is not well exposed it is difficult to tell whether a NW fault is present or whether in fact it projects to surface as a monocline with a particularly steep middle limb. Gray (1971) noted both the drag and significant stratigraphic offset of across this group of faults.

The final and slightly more numerous (n=34) set of data, known as the Jabel Nafusah fault group (JN), has a variable NE-SW strike with dips that are generally lower than the other groups in the range 40-70° with occasional exceptional low and exceptionally high dips (Fig. 7.13b). These faults commonly form horst and graben structures (Fig. 7.15a), and or were overlain by warped strata forming breached or unbreached anticlines (Fig. 7.15 b).

Cross cutting relationships between the Hun Graben and Jabel Nafusah fault groups could not be satisfactorily established in an outcrop. However, both A and B group faults were found cutting Jabel Nafusah and a single example of a group B fault was found cutting the Hun Graben faults (Table 7.3). Groups A and B are therefore believed to post-date the Jabel Nafusah faults and there is tentative evidence that Group B cuts the Hun Graben faults.

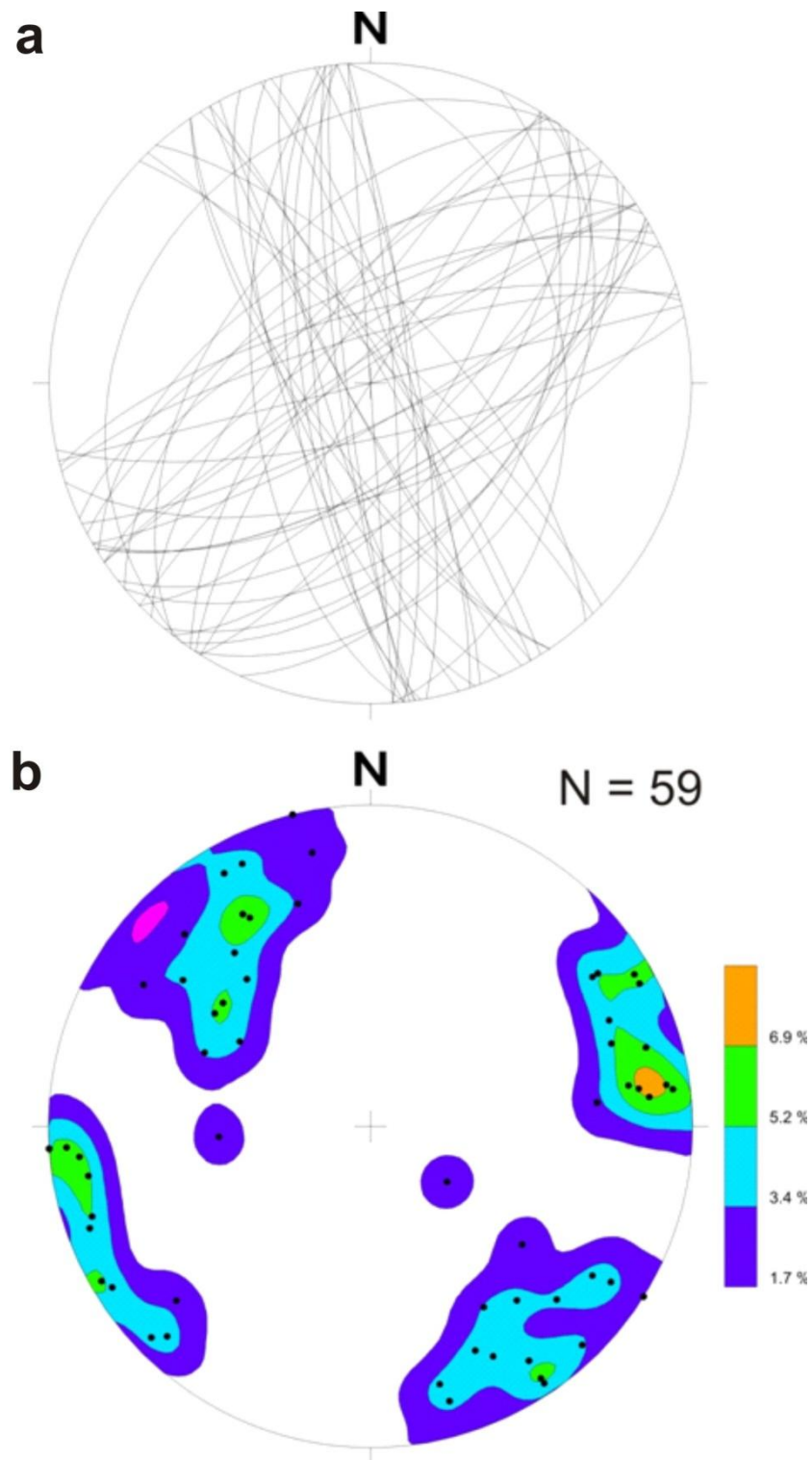


Figure 7.12 The fault population after removal of the A and B groups plotted as (a) planes and (b) contoured poles to planes.

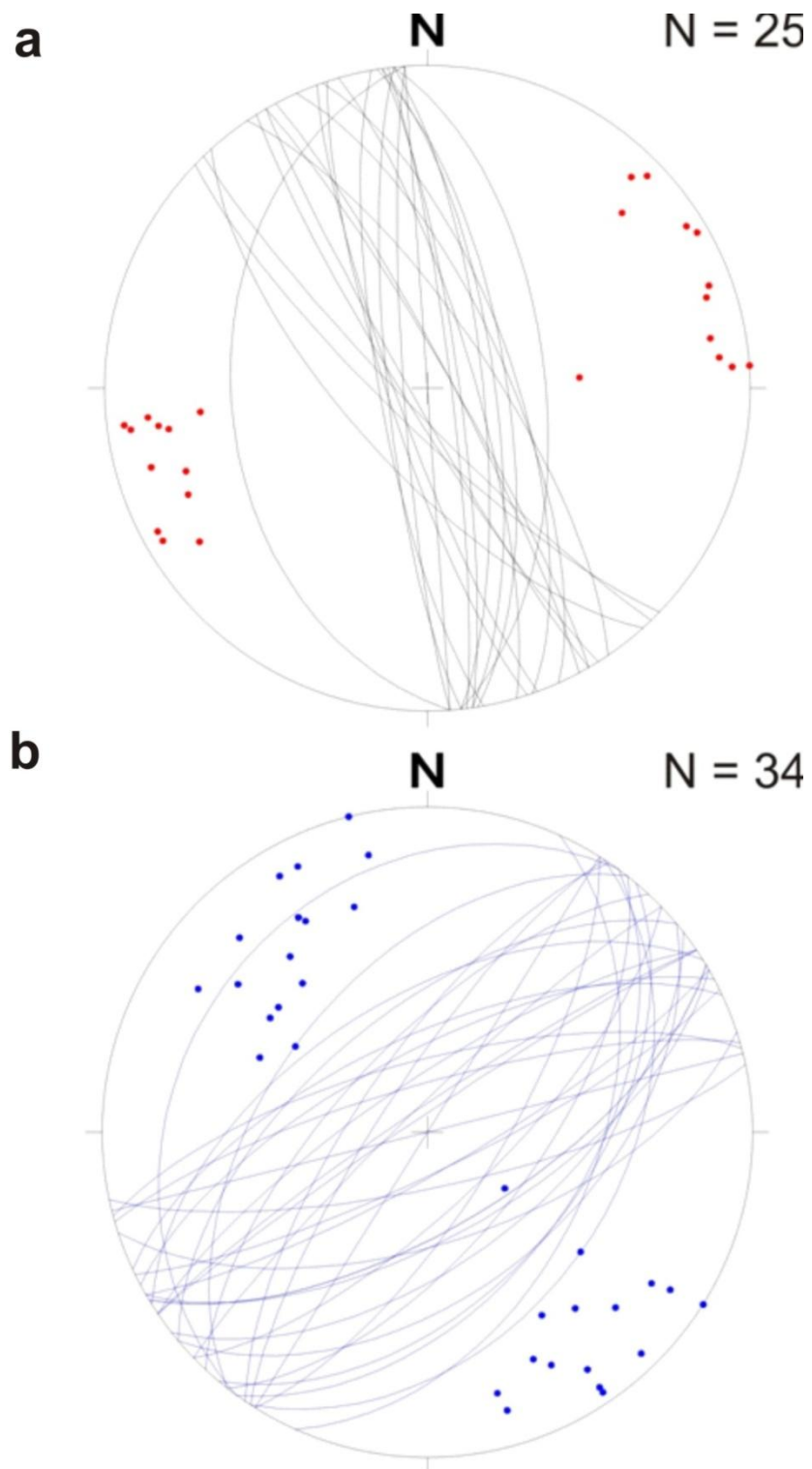


Figure 7.13 Stereonets of the remaining faults separated into a) a NW-NNW group ‘The Hun Graben’ faults and b) an NE – ENE ‘Jabel Nafusah’ group.



Figure 7.14 Hun Graben faults showing significant drag of their hanging walls, view from Wadi Ghan road.

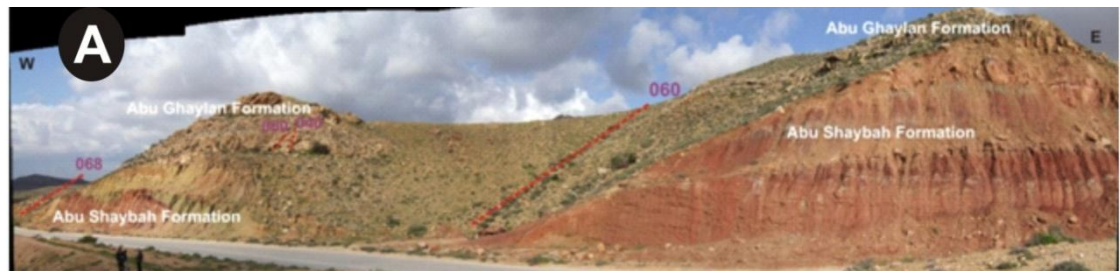


Figure 7.15 Jabel Nafusah faults showing **a)** significant offset of the Abu-Shaybah-Abu Ghaylan boundary on the Kabted Jamel road section and **b)** an unbreached anticline overlying JN faults in Wadi Gabel.

These findings are in good agreement with previous authors. In their recent analysis of lineament patterns from DEMs and existing geological maps Saadi et al. (2009) report the NW-SE trending, the Hun Graben faults, to be the most numerous in their data sets (see rose diagram in Fig. 7.2 and their separation into stratigraphic units in Figure 7.16). They also detected the NE-SW (to E-W) Jabel Nafusah trend as the second most common lineament. They don't however record the A and B groups already noted in this chapter.

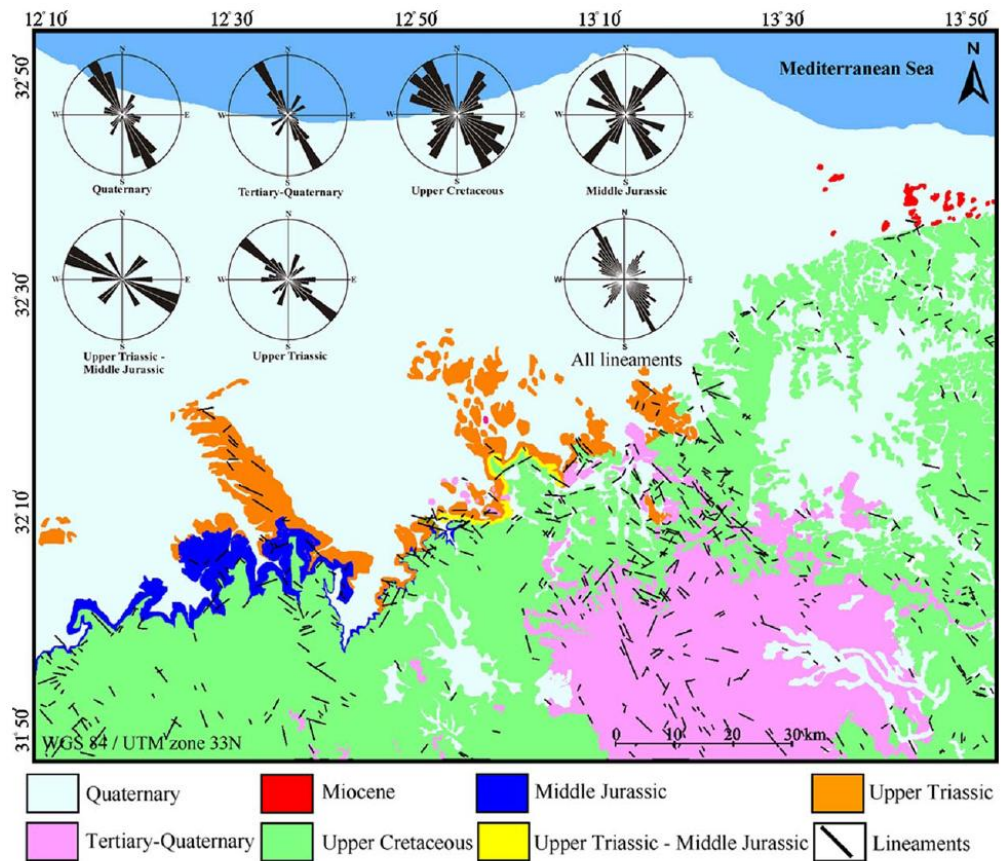


Figure 7.16 Geological map of the Jabel Nafusah area centred on Gharian showing lineaments from DEMs and geological maps as rose diagrams for individual stratigraphic units (Saadi et al., 2009).

7.3.3 The Jabel Nafusah Faults in Cross-section

Cross section A (Fig. 7.17), a NNW –SSE orientated through the Gharian area, reveals that the dips form a rollover type anticline with respect to the faulting in the escarpment immediately north of Gharian. This structure is quite clearly seen in the field defined by gently dipping strata in the core of the anticline, which rapidly steepens towards the controlling faults with the anticlinal hinge located in Wadi Abu Shaybah where at its lowest point, exposes the oldest Kurrush Formation in its core (Fig. 7.18).

Strata dips show repeated rapid steepening up toward a series of individual faults.

Between Gharian and Wadi Abu Shaybah the top of the Al Aziza Formation there is a net displacement across the fault zone of some 100 m across a series (at least 6 if not 7) significant normal faults.

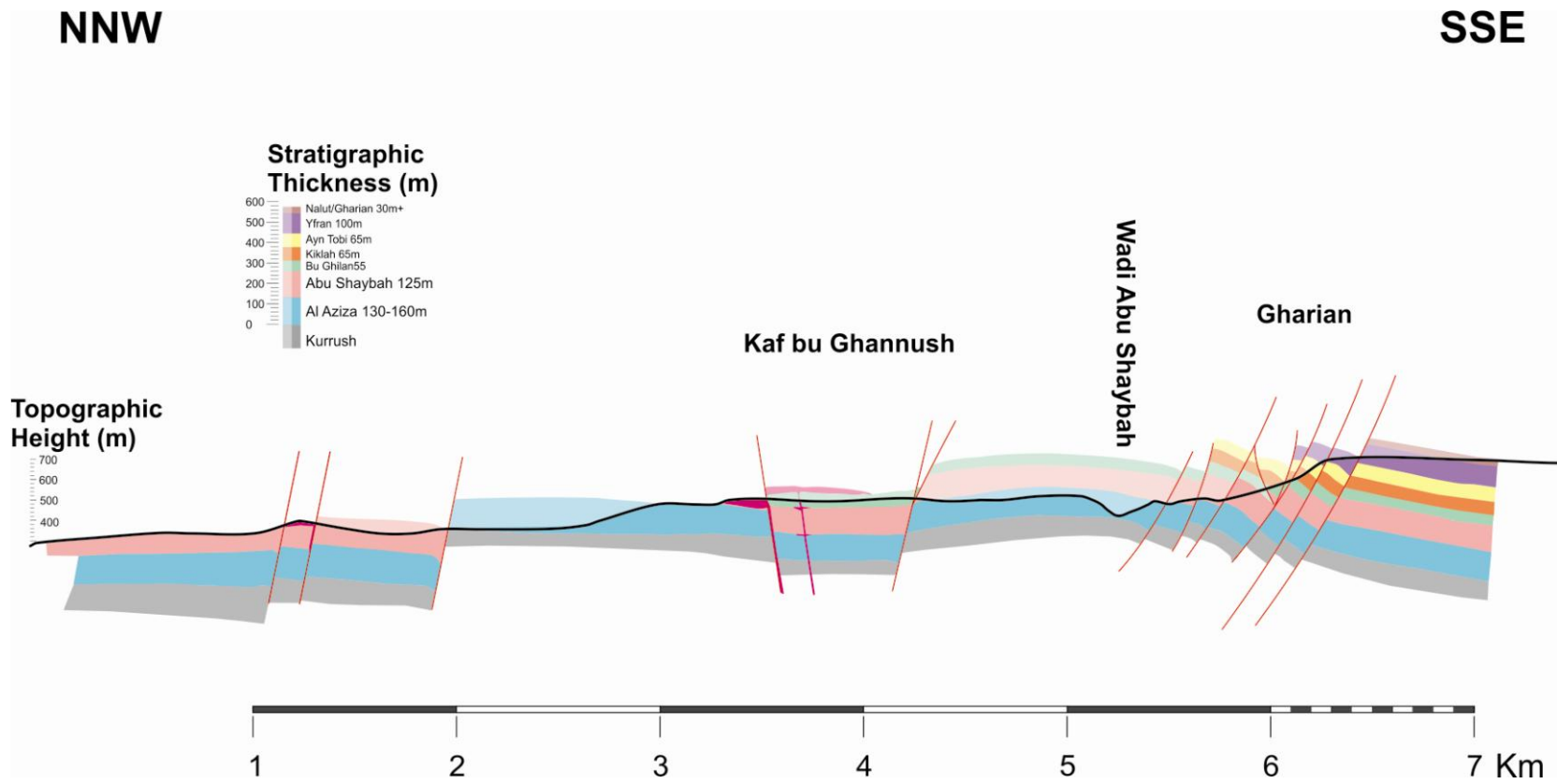


Figure 7.17 NW-SE cross section through Gharian.

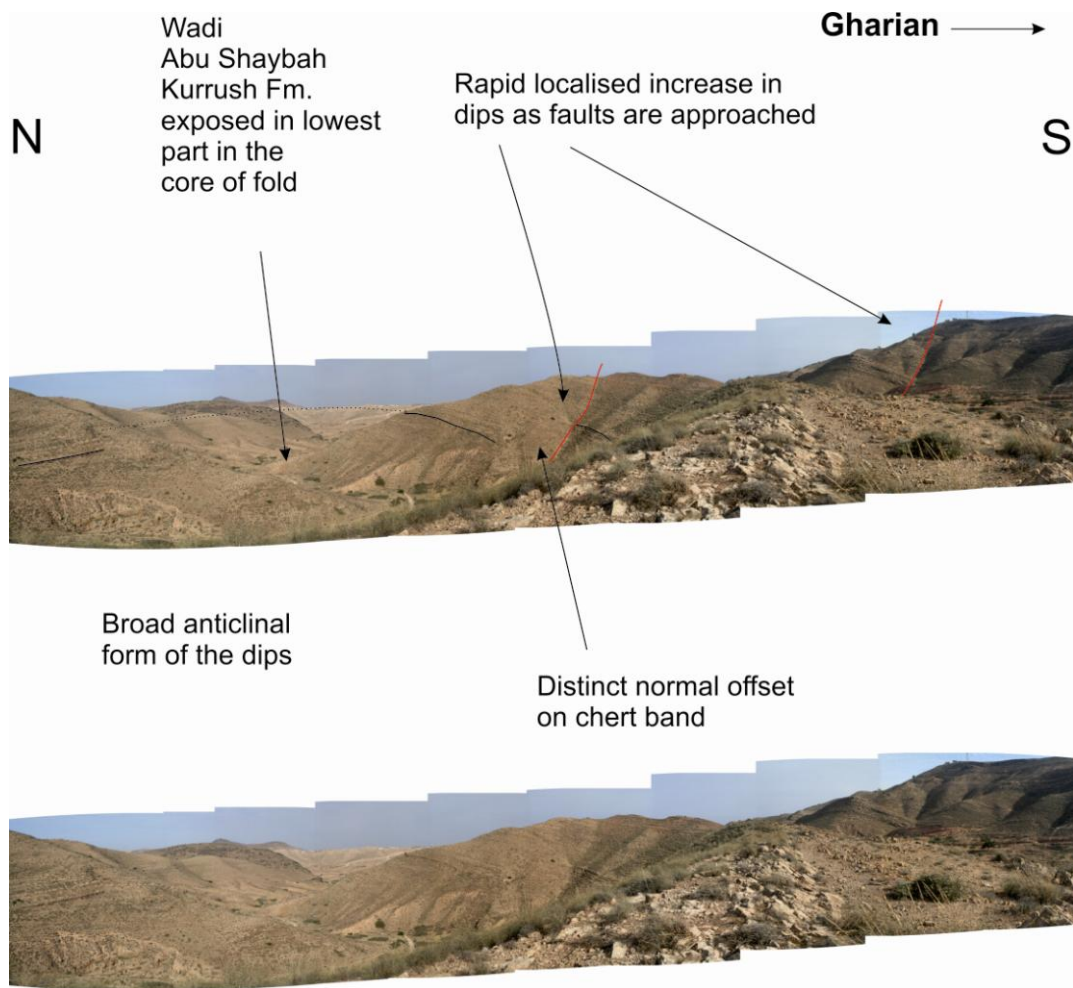


Figure 7.18 The Gharian rollover showing Al Aziza Formation in the core of the structure immediately north of Gharian viewed looking east.

The overall pattern is one of pronounced reverse drag on these faults and together they define a rollover anticline. The single largest fault, at least in terms of a damage zone, was that nearest the town of Gharian itself which was seen to be a 30+ m wide brecciated zone in Ain Tobi carbonates but across which we were unable to establish a simple throw (Fig. 7.19) in the field for this single fault. Given the width of the fault zone, its location as the first fault separating hanging wall from footwall and that it defines the edge of the escarpment it is believed likely that this is, locally at least, the “master fault” in the NW-SE orientated fault system and it exerts a strong and obvious control on the topography.



Figure 7.19 A ~30m wide brecciated fault zone closest to Gharian (N32 10.275 E013.00.488). Given the location, the substantial width and the proximity to very shallowly southward dipping strata in the footwall (some 35 m to right of the photograph) this fault zone is thought to be the master fault in the system.

Detailed mapping is required to truly establish the individual faults exact nature but some of the faults are seen to be highly cusped in shape (Fig. 7.20). The curving nature of the fault plane could reflect an original listric type geometry for this fault and or it has been subsequently modified to at least enhance this curvature. In at least one locality what appears to be a relay ramp linking individual fault strands was seen immediately north of Gharian itself (Fig. 7.21).

Overall the stratal dips and normal faults define a well-developed rollover anticline immediately north of Gharian which is here named the Gharian rollover anticline. The location and the nature of the complex faulted syncline at Kaf Bu Ghannush (Fig. 7.18), which is in part overlain by the intrusion, originally described by Gray (1971), is consistent with it being a crestal style syncline which is commonly found in association with rollover anticlines.

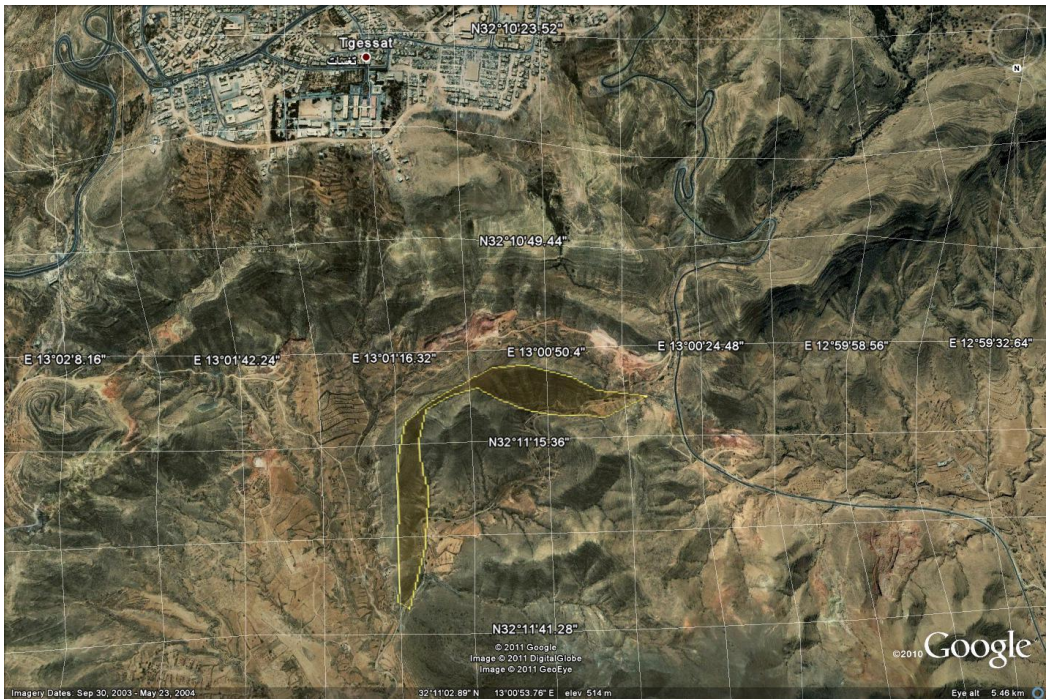
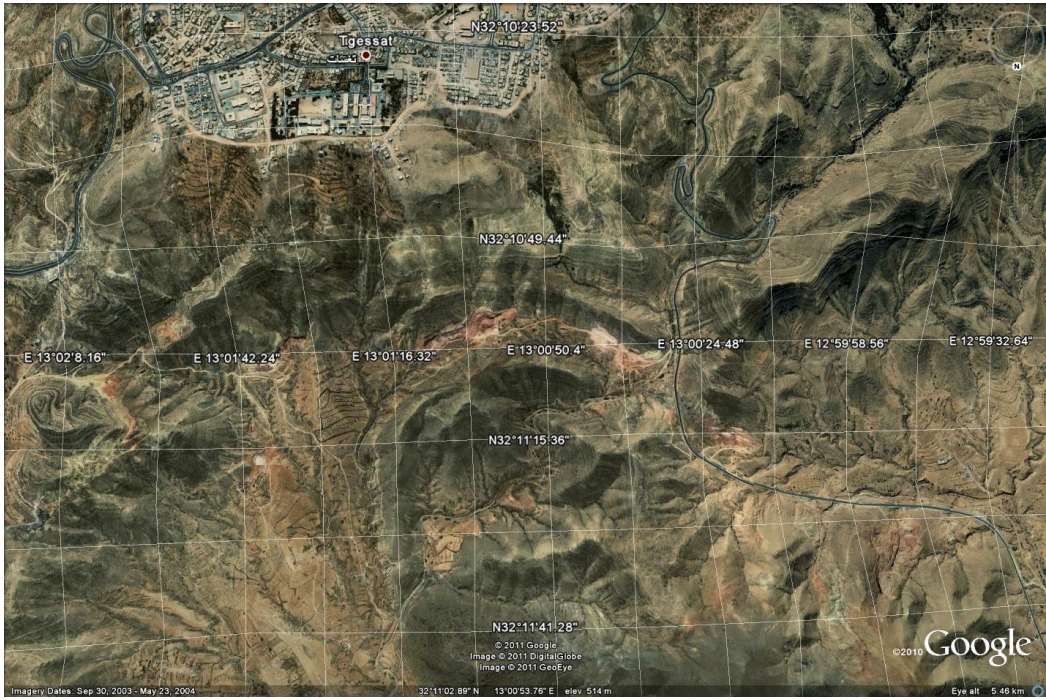


Figure 7.20 Highly cusped faults affecting the Al Aziza Formation in the Wadi Abu Shaybah. Gharian, to the south, is at the top of the image.



Figure 7.21 Possible relay ramps in the main escarpment immediately northeast of Gharian town, viewed from Old Wadi Gabel road.

The overall geometry of the strata and the faults define a rollover anticline and crestal syncline not unlike many seen elsewhere in seismic section normally for example the Lenita fault of the Bremer Basin, Australia (Fig. 7.22).

The fault structure here would appear to post-date much or all of the deposition at least up to and including the Sidi as Sid Formation as no clear evidence of growth to be seen. However this may be a function of erosion but in the Australian example cited only the uppermost part of the section shows any signs of growth strata after formation of much of the structure. At a larger scale cross section A (Fig. 7.18) confirms a very broad gentle anticlinal overall shape to the area in NW-SE section such that the northernmost outcrops of Abu Shaybah Formation, in the extreme NW of the area, dip very gently ($\sim 5^\circ$) northwestward toward the Azizyah Fault some 21 km to the north.

The NE-SW cross section shows that the thickness of the Al Aziza and Abu Shaybah Formations increases by 5% into the north of study area. This may provide evidence for faulting that could play a major role at a large scale. The net displacement of the top of the Al Aziza Formation in the footwall from immediately below Gharian to some 6.5

km NW of the presumed master fault indicates a total of 1.2 km of net normal displacement with downthrow to the north across this fault system.

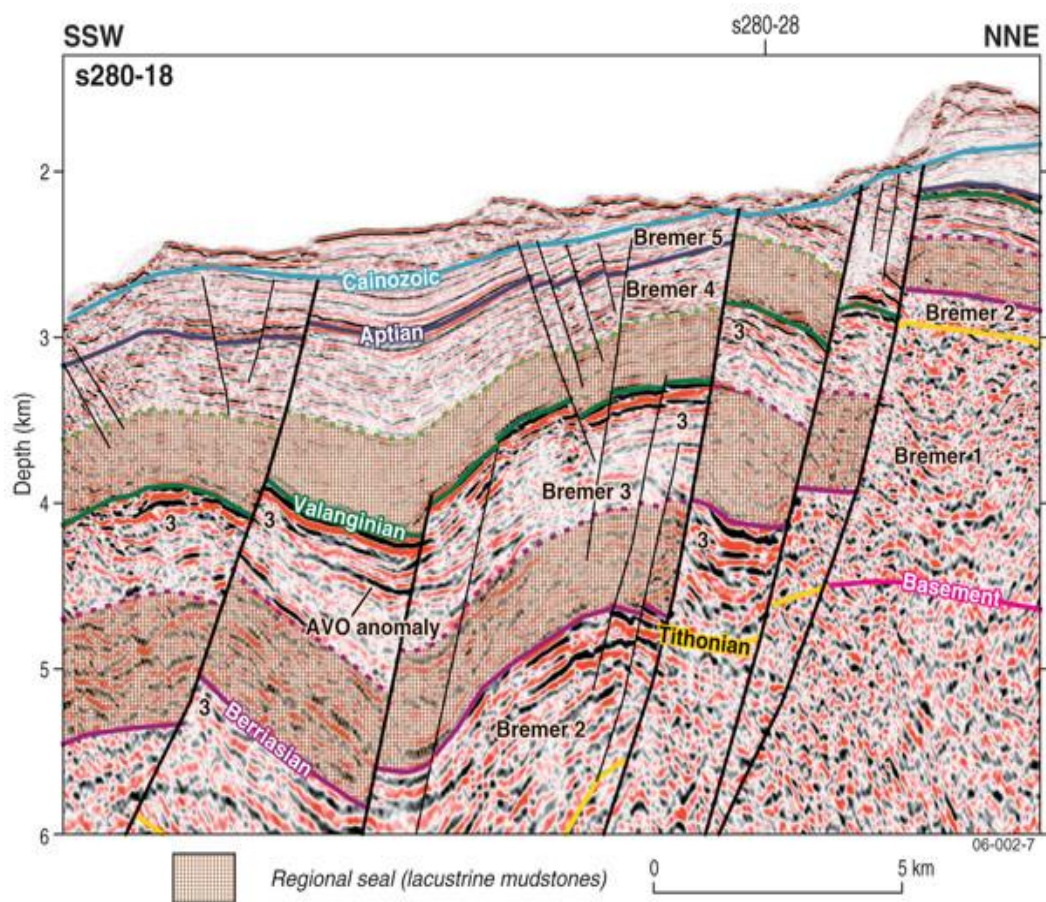


Figure 7.22 Large rollover structure adjacent to the Lenita fault of the Bremer Basin, Australia

(http://www.pesa.com.au/publications/pesa_news/feb_06/pesanews_8026.html accessed 28/11/2011). The seismic image shows the Lenita fault on the right with a rollover anticline and synclinal crestal collapses with similar geometries to that seen at Gharian. Growth sedimentation post dates the main part of the section and really occurs in the uppermost part of the section.

7.3.4 The Hun Graben Faults in Cross-section

A NE-SW orientated cross section (Fig. 7.23) reveals a slightly simpler overall structure in that strata have a component of dip such that they essentially dip gently (south) westward in the west and (south) eastward in the east defining an overall gentle anticline with a NW-SE axis. Parallel to the fold axis orientation are a series of minor normal faults which pass upward and or along strike into monoclines. This gives the overall structure a 'stepped' form.

The monoclines are a product of passive folding over the normal faults where they are buried (Fig. 7.24). These NW-SE faults and folds modify (steepening up strata) or when faults are actually present appear to cut the NE-SW structures. For example, the fault plane of Figure 7.20, which is a key element in the rollover structure, is markedly curved and appears to be greatly modified by a very steep monocline in the west where it interacts with a NW trending structure that runs close to the Abu Rashada road for some 5 km. It is therefore, named the Rashada monocline. It controls emplacement of a series of intrusions along it but more importantly and has a down to the west stratigraphic throw from mainly Al Aziza Formation to the east, forming high ground, to Abu Shaybah Formation in the west forming abroad expanse of low ground. To the east, the Al Aziza Formation outcrop forming a sharp ridge with gently dipping beds that ends abruptly against low lying ground occupied by gently dipping Abu Shaybah Formation sandstones; again clearly indicative of a fault or very tight monocline.

Likewise the floor of the main Wadi Gabel is formed by flat lying to gently dipping south or north red sandstones-siltstones. However, at the eastern margin of the Wadi/ the foot of the escarpment (below what will be described as the Wadi Qasam-Abu Ghaylan topographic plateau) the dips steepen to 15°, with a strong eastward component again indicating the presence of a monocline or normal fault.

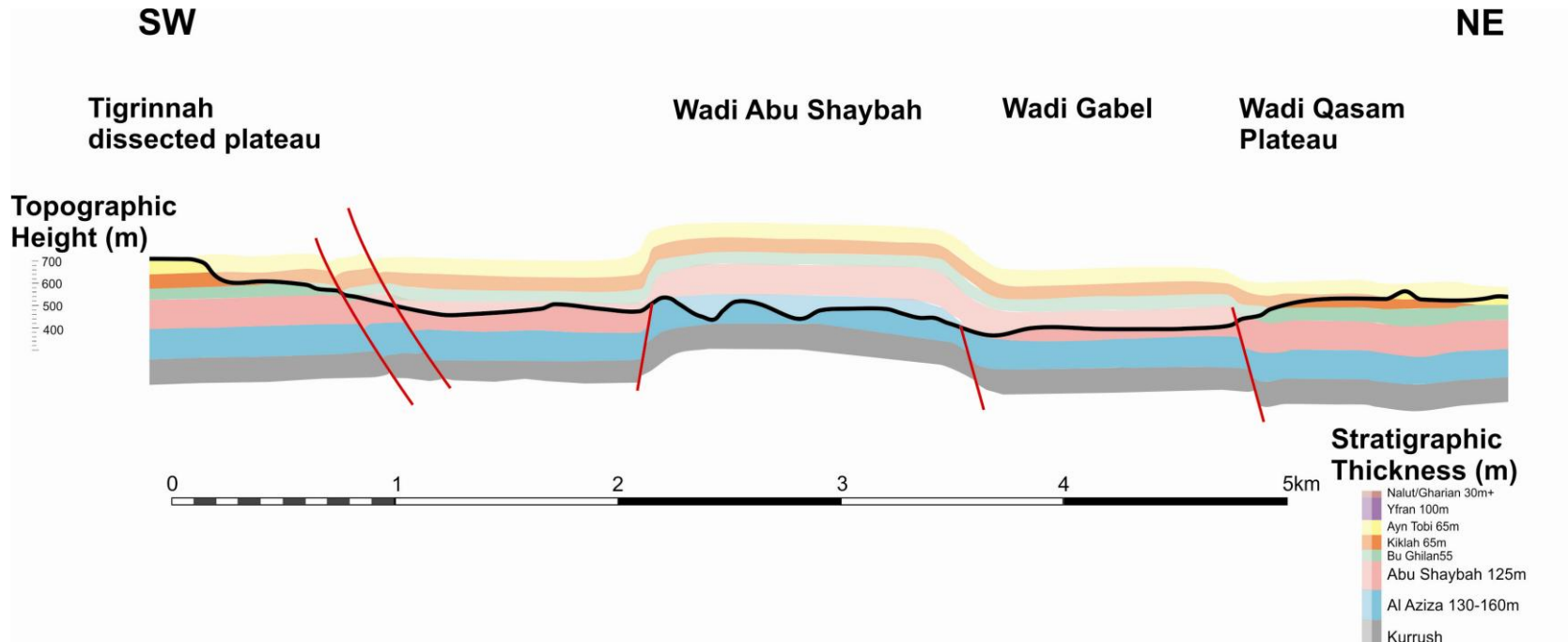


Figure 7.23 SW-NE section across the NW trending Hun Graben Faults.

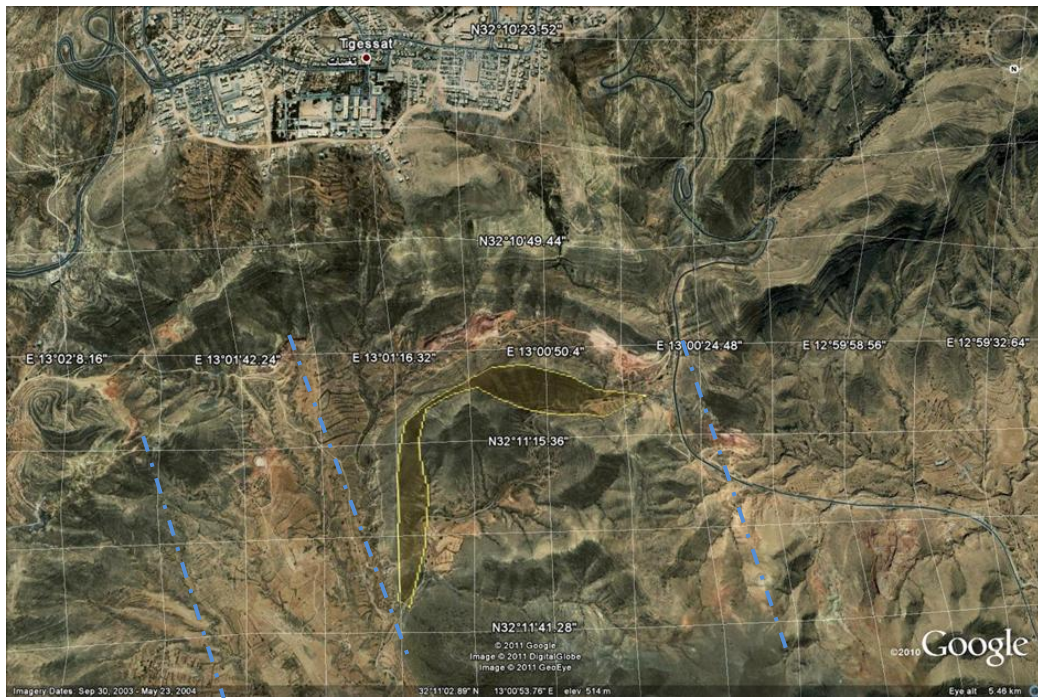


Figure 7.24 Interaction of the Al Aziza rollover anticline with the NW trending faults/monoclines.

In cross sections of the Hun Graben-Sirt Basin (Fig. 7.25), the geology of which is closely controlled from extensive drilling for hydrocarbons, these faults and their associated folds control structural and depositional highs and lows (Abadi et al., 2008).

This cross section and many other published sections like it (e.g. Ahlbrandt, 2001) have a gross vertical exaggeration, in this case of in excess of 30:1. This has been done because of the very large ground distance across the Hun-Graben and Sirt Basin and to emphasise the vertical displacement of the faults themselves. In reality at a 1:1 scale the vertical displacements of these normal faults is very small relative to the cross section length and the overall structure, is in reality, a gentle warping or corrugation of the strata in a NW–SE orientation. The major NW-SE structure controls of the area are summarised in Figure 7.26 and as follows.

The principle structure is a NW-SE trending anticlinal fold axis which plunges gently (5-10°) SE running directly through Gharian and is flanked by parallel normal faults and

/or monoclines and a pair of lesser amplitude synclines. One syncline forms the higher ground of the Abu Shaybah-Wadi Qasam plateau the other the Tigrinnah highlands north and east of Gharian. Although not investigated in detail, the Wadi Ghan fault zone which exposes relatively high stratigraphic levels, Ain Tobi member carbonates, at low topographic levels is interpreted as one flank of major rift NW –SE trending rift. This fault zone is readily visible on regional scale DEMs and is a zone of similar dimensions to the Hun Graben itself (Fig. 7.27) which it clearly parallels.

The lack of recognition of the significance of this large scale structure by previous authors is due in part to its relative remoteness but also that is partially masked by the Tertiary flood basalts field located southwest of Gharian (Fig. 7.1 and 7.3) and partly a function of the sheer scale of the Hun-Graben-Sirt Basin rift system (Fig. 7.28)

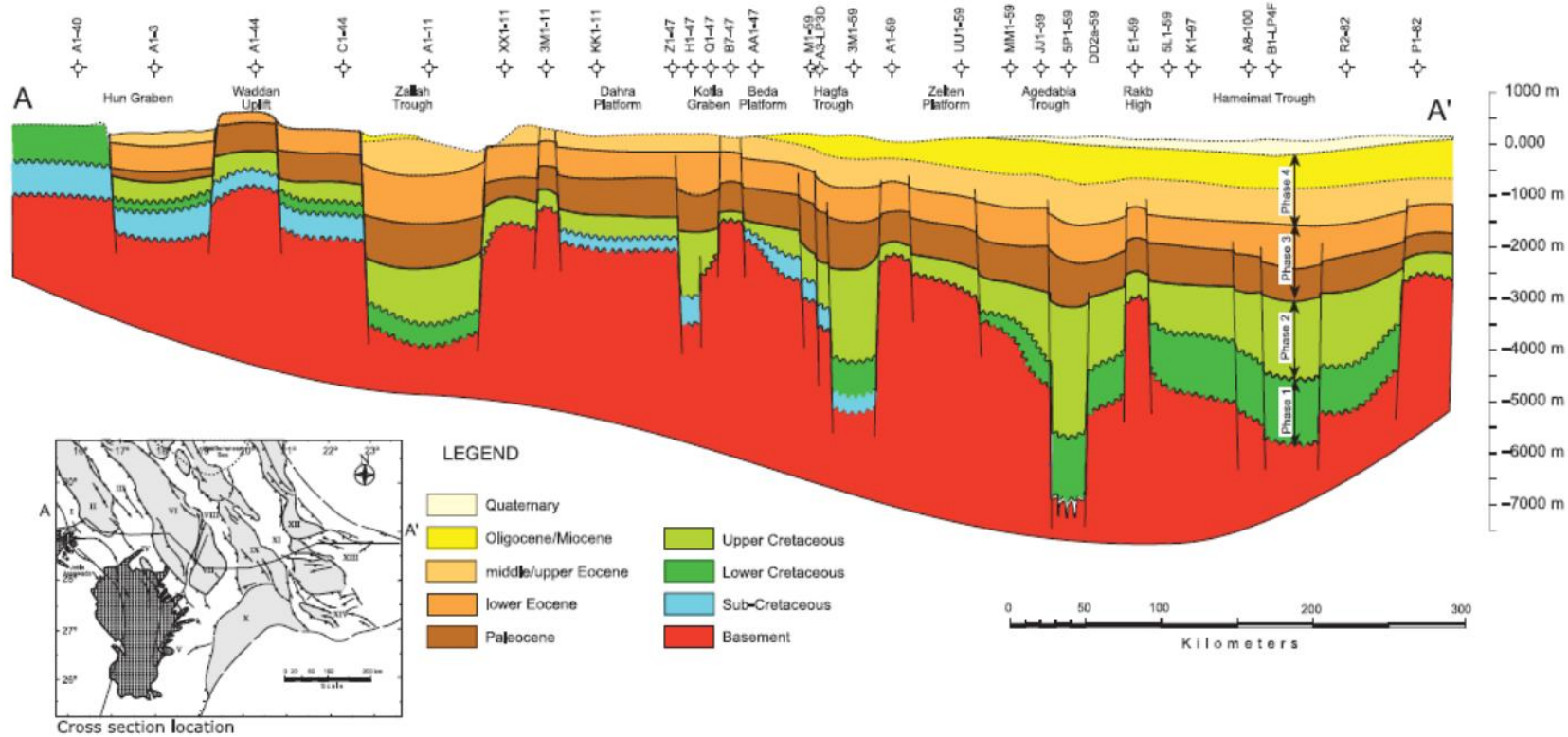


Figure 4. East-west structural cross section showing the major horsts and grabens across the Sirt Basin, leveled to present-day sea level. Note the major thickening of the Cretaceous and Paleocene sediments across the major faults bounding the main horst and graben structures.

Figure 7.25 E-W Cross section of the Hun Graben and Sirt basin showing the effect of NW trending faults (from Abadi et al., 2008).

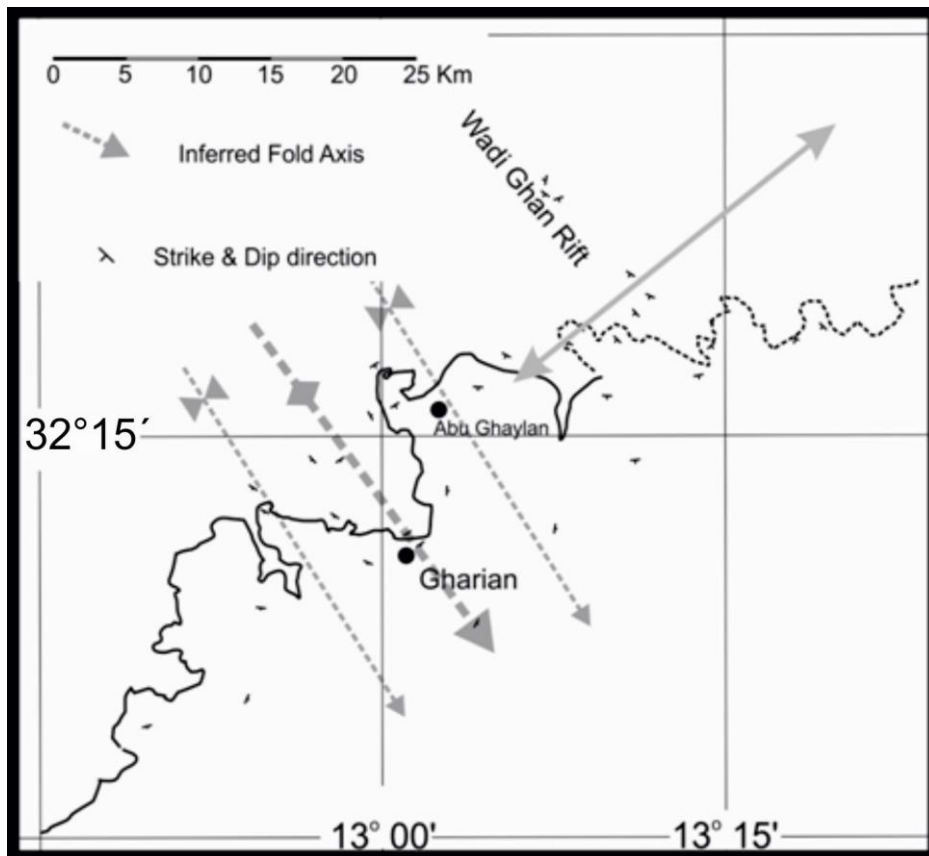


Figure 7.26 Summary of the major NW structures in the Gharian area.

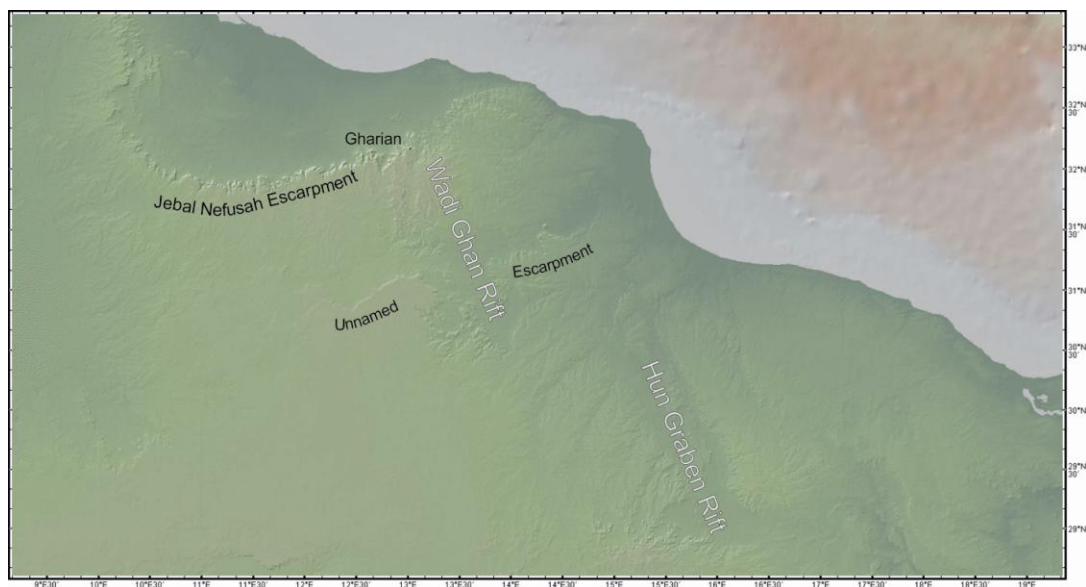


Figure 7.27 SRTM derived DEM image (<http://www.geomapapp.org> & Ryan et al., 2009) of northern Libya showing the parallelism of the Wadi Ghan / Hun Graben rifts.

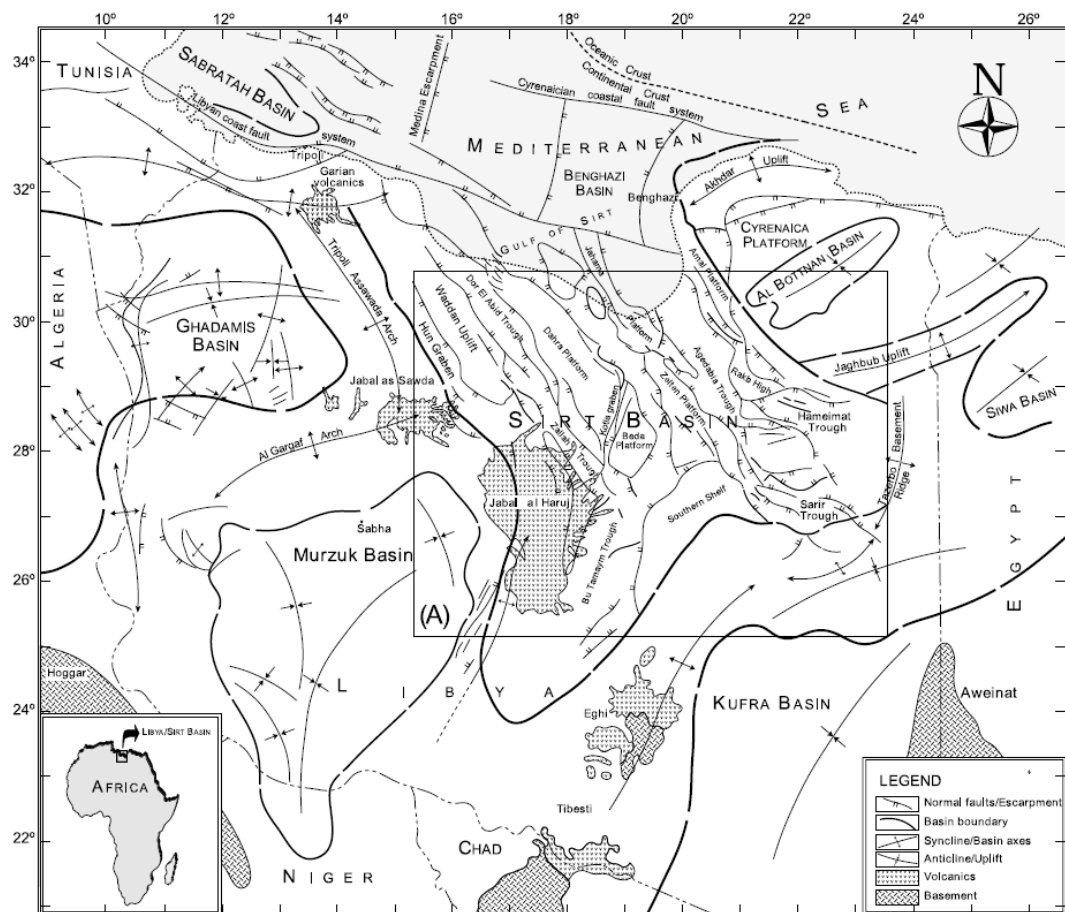


Figure 7.28 Tectonic map of Libya (from Abadi et al., 2008) to emphasise the scale of the NW-SE trending Hun Graben-Sirt Basin system in northern central Libya.

7.4 The Interaction between Topography, Stratigraphy and Structure

The structures as previously described, and the stratigraphy they control, have a slightly unusual interaction with the topography in that they can show partial and local strong topographic inversion. This is a consequence of the strongly contrasting physical properties of the units and the prevailing arid to semi-arid setting of the region throughout the Tertiary to present –day as Africa has drifted only slowly northward during that time. The most pertinent aspects of differential erosion are summarised by Simms (2004, p 477) as follows:

“Denudation mechanisms differ fundamentally between limestone and silicate rock types, which are subject to very different rate thresholds and enhancers/inhibitors.

Silicates are removed largely by erosion, the mechanical entrainment and transport of particles. This is a relatively high energy, and highly episodic, process which occurs only when a minimum threshold flow velocity is exceeded; it is inhibited by vegetation cover and favoured by strongly seasonal runoff. Limestone is removed largely by chemical dissolution at a rate directly proportional to runoff. Dissolution is a relatively low energy process that can occur at any flow velocity or in static water; in general it is enhanced by vegetation cover and non-seasonality of runoff. These contrasting factors in the denudation of silicates versus limestone can produce strikingly uneven rates of surface lowering across a landscape, sometimes akin to the well known ‘tortoise and hare race’, where the slow and steady denudation of limestones may in the long term exceed the sometimes rapid, but often localized and episodic, erosion of silicates. Prolonged exposure of limestone to a humid temperate climate in a tectonically stable environment produces low relief corrosion plains in which limestone uplands are anomalous and, in most instances, due to recent unroofing from beneath a siliciclastic cover. In a highly seasonal or semi-arid climate almost the exact inverse may develop, with ‘flashy’ runoff and sparse vegetation favouring erosion rather than dissolution.”

In the case of the Jabel Nafusah in the Gharian area, the physical contrasts are between the relatively robust and resistant carbonates of the Al Aziza, Abu Ghaylan Formations, the Ain Tobi member of the Sidi-as-Sid Formation and the Nalut Formation which contrast with the weak, easily eroded mudstones and poorly consolidated sandstones of the Kurrush, Abu Shaybah and Kiklah Formations and the variable marls and thin carbonates of the Yafran member of the Sidi- as-Sid Formation (Table 7.3). Added to this the mountainous terrain of the Jabel Nafusah although set in a semi-arid to arid region does attract very localised heavy rainfall which is concentrated upon the northern face of the main escarpment itself with relatively little runoff on the dip slope to the south.

| Unit | | Typical/dominant lithology | Occurrence and physical expression |
|-----------------------|-----------------|--|---|
| Nalut Formation | | Crystalline dolomite with rare chert horizons | Occasionally forms highest cliff in the main escarpment (westward to Kiklah) but more often a secondary escarpment to the south of the main escarpment |
| Sidi as Sid Formation | Yafran Member | Interbedded marls and laminated mudstones | Easily eroded, mostly found on south facing dip slopes or recessed in minor escarpment behind/southward of the main Jabel Nafusah |
| | Ain Tobi Member | Regularly bedded and dolomitised bioclastic crystalline carbonates | Normally forms the topmost cliff in the Jebal Nefusah escarpment and as an extensive upland plateau |
| Kiklah Formation | | Poorly lithified variably bedded sandstones to siltstones | Only ever preserved in vertical section where protected by Ain Tobi limestones above. Typically recessed in the escarpment face or forming a bench where exposed immediately above the Bu Ghelan Lstn. The biggest 'bench' is in the form of the Abu Ghaylan-Wadi Qasam plateau |
| Abu Ghaylan Formation | | Very variable limestones, with evidence of syn-sedimentary slumping and disturbance and post deposition dissolution and probable dissolution of original evaporites. | Cliff forming on escarpment but with highly irregular expression,. Forms a highly dissected ridge system north of Tigrinnah |
| Abu Shaybah Formation | | Poorly lithified cross bedded sandstones with some mudstones and clays | Generally forms the lowest topography in the major wadis or preserved in steep sections at the base of the escarpment when protected by Abu Ghaylan Limestone immediately above. In such sections it is typically quarried and easily processed for building sands and/or for clays |
| Al Aziza Formation | | Well bedded but relatively thinly (30-100 cm) bedded limestones, interbedded with thinner mud | Typically forms stepped low angle hillsides with each step representing a single bedding plane |
| Kurrush Formation | | Soft, poorly consolidated muds, silts and micaceous sands | Rarely exposed, only in lowest ground in the protected cores of folds dominated by Al Aziza Limestone |

Table 7.3 The Stratigraphic units and their topographic expressions.

This leads to a topography being a direct function of the exposed unit, be it siliciclastic which erodes rapidly and forms relatively low flat lying areas with subdued topography or the carbonates (and especially the Ain Tobi member and Abu Ghaylan formation) which form upstanding areas with distinct escarpments and low relief dip slopes.

The geomorphology of the area can be sub-divided and related to the principal underlying geological formations as follows (Fig. 7.29);

a) The Gharian escarpment and Plateau

Where the margins of the Ain Tobi member and Abu Ghaylan formation coincide the highest escarpments (250-300 m) form as seen immediately N and NW of Gharian town itself. To the south of Gharian erosion and the stratal dip from a gently south-south-eastward dipping plateau (max height 680-710 m) which is in fact a geological dip-slope of some 5-10°. The uppermost stratigraphic unit, the Nalut formation, adds a further but minor step to the plateau or escarpment but is normally weakly expressed while the intervening muds, silts and clays of the Yafran member are poorly exposed and form indistinct gentle slopes forming the area upon which the town itself is built.

This morphology and lithological pairing is repeated in a small area south and south – east of the village of Abu Ghaylan where a major outlier of the Sidi as-Sid carbonates dominates the topography forming a small plateau and narrow ridge. As consequence here is a very high escarpment and the topography in general is marked by strike parallel ridges capped by resistant carbonates of either the Ain Tobi member or lower ridges capped by Abu Ghaylan Formation carbonates.

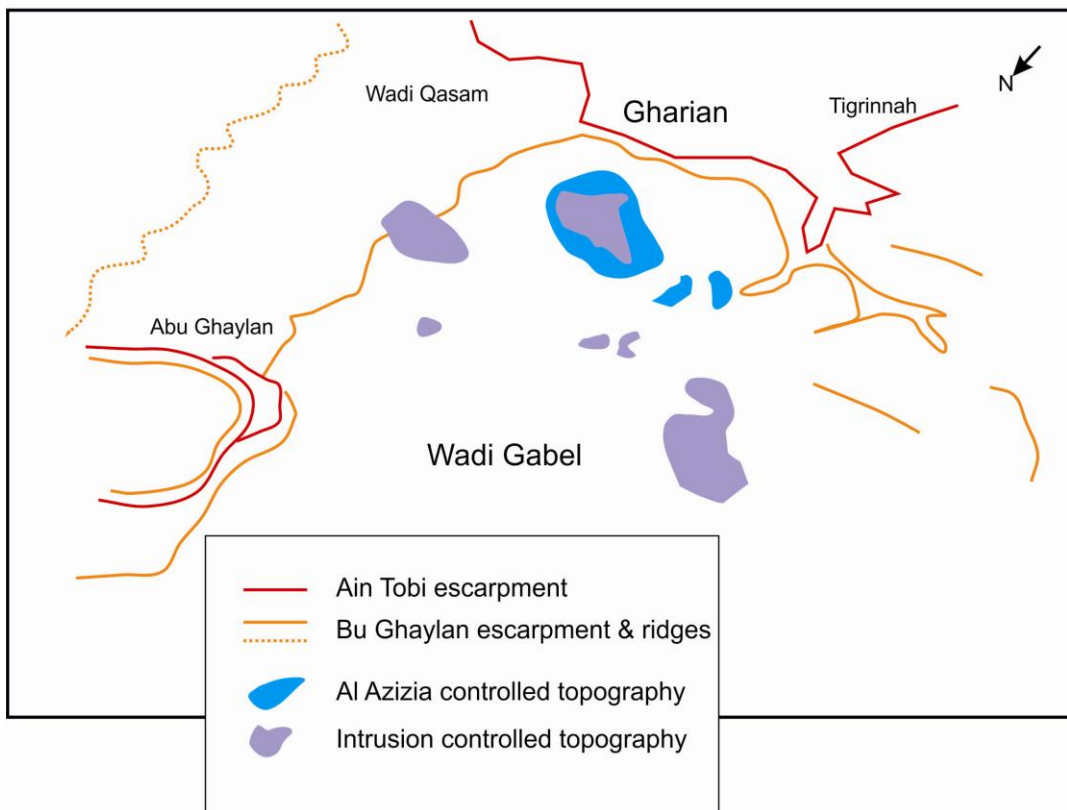
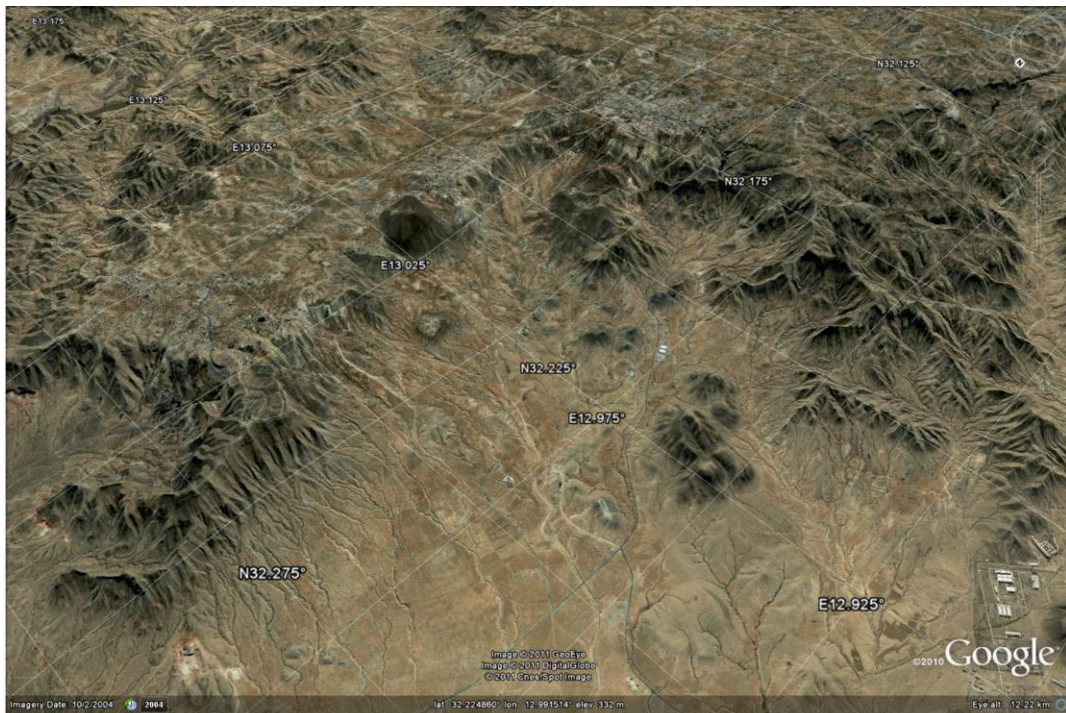


Figure 7.29 A) Google Earth image and B) sketch of the main geomorphology of Gharian.

The eastern margin of the Gharian plateau where it borders the next topographical unit, the Wadi Qasam-Abu Ghaylan Plateau, is sinuous to irregular in shape and in general has gradual slopes. Overall the topography reflects the effects of drainage systems cutting into the edge of the resistant Ain Tobi carbonate outcrop suggesting that, at the largest scale, there is no strong structural control in this area but a simple conformable normal erosive geological contact between the robust overlying carbonates and the softer underlying clastics of the Kiklah Formation.

b) The Wadi Qasam-Abu Ghaylan Plateau

To the north and east of Gharian a second plateau lies at a distinctly lower elevation (~550 m). This gently undulating surface comprises low rounded hills with thin veneers of flat lying to gently dipping Sidi as sid limestones (mostly Ain Tobi member) forming distinct outliers. These are surrounded by extremely poorly exposed flat lying terrane to broad low relief valleys between the outliers and floored by distinctly reddened soils. These areas are interpreted as being underlain by Kiklah Formation clastics which are preserved and exposed in the top of the escarpment (with Wadi Gable) on the west side of this plateau immediately above gently undulating Abu Ghaylan formation carbonates.

The eastern margin of this plateau ends abruptly along a NW trending line east of which the topography is much more rugged and marked by steep ridges and valleys cut, apparently, into Ain Tobi carbonates according to the regional geology map (Sheet NI 33.13R, Tarabulus, 1975). Given that the main part of the plateau is underlain by the Kiklah Formation and topped by minor outliers of Ain Tobi there is clear evidence of, in effect, stratigraphic downthrow to the east of this NW dividing line be it a fault or a monocline.

c) Wadi Gabel

Wadi Gabel is a broad low area lying between the Wadi Qasam-Abu Ghaylan Plateau to the east, the Gharian Plateau to the south and the high ground north of Tigrinnah. It is marked by broad open valleys with reddened soils and occasional low rounded hills exposing sandstones of the Abu Shaybah Formation. These sandstones which are also exposed both at the foot of the escarpments and in quarries where it is worked for sand. This topography is punctured by a series of hills which are formed by the igneous intrusions and or the more resistant Al Aziza Formation.

d) The Tigrinnah highlands

The rugged topography north of Tigrinnah is a function of the exposed carbonates of the Ain Tobi member and Abu Ghaylan Formation forming a series of strike parallel ridges which interconnect along NW trending spurs from the main ridges. The highest of the ridges are capped by Ain Tobi carbonates with a clear intervening step between them reflecting erosion of the Kiklah Formation which is exposed in escarpments between the two carbonates.

One can envisage the erosion of the area proceeding in a series of distinct stages (Fig. 7.30) such that when the erosion surface is cutting into carbonates it is topographically 'normal' as dissolution is very slow. However, when it reaches the intervening clastics it becomes readily 'inverted' as they are rapidly eroded by the highly seasonal nature of the run-off in flash events (Simms, 2004).

The gross effect is then a mix of inverted and normal topography with respect to structure; Wadi Gabel forms the majority of the lowest ground yet has developed over the core of the main anticline as erosion has reached the stratigraphic level of the Abu Shaybah formation, except in its very core where the south-eastward plunge of the fold brings the Al Aziza Formation into play which then forms upstanding rounded hills.

The relatively high ground of the Abu Ghaylan-Wadi Qasam plateau is underlain by a syncline preserved by a capping of Ain Tobi carbonates. In the near future this area will rapidly erode through the exposed Kiklah Formation and have a much rougher surface when the heterolithic Abu Ghaylan Formation carbonates are exposed as on its western flank as seen in the high ground north of Tigrinnah.

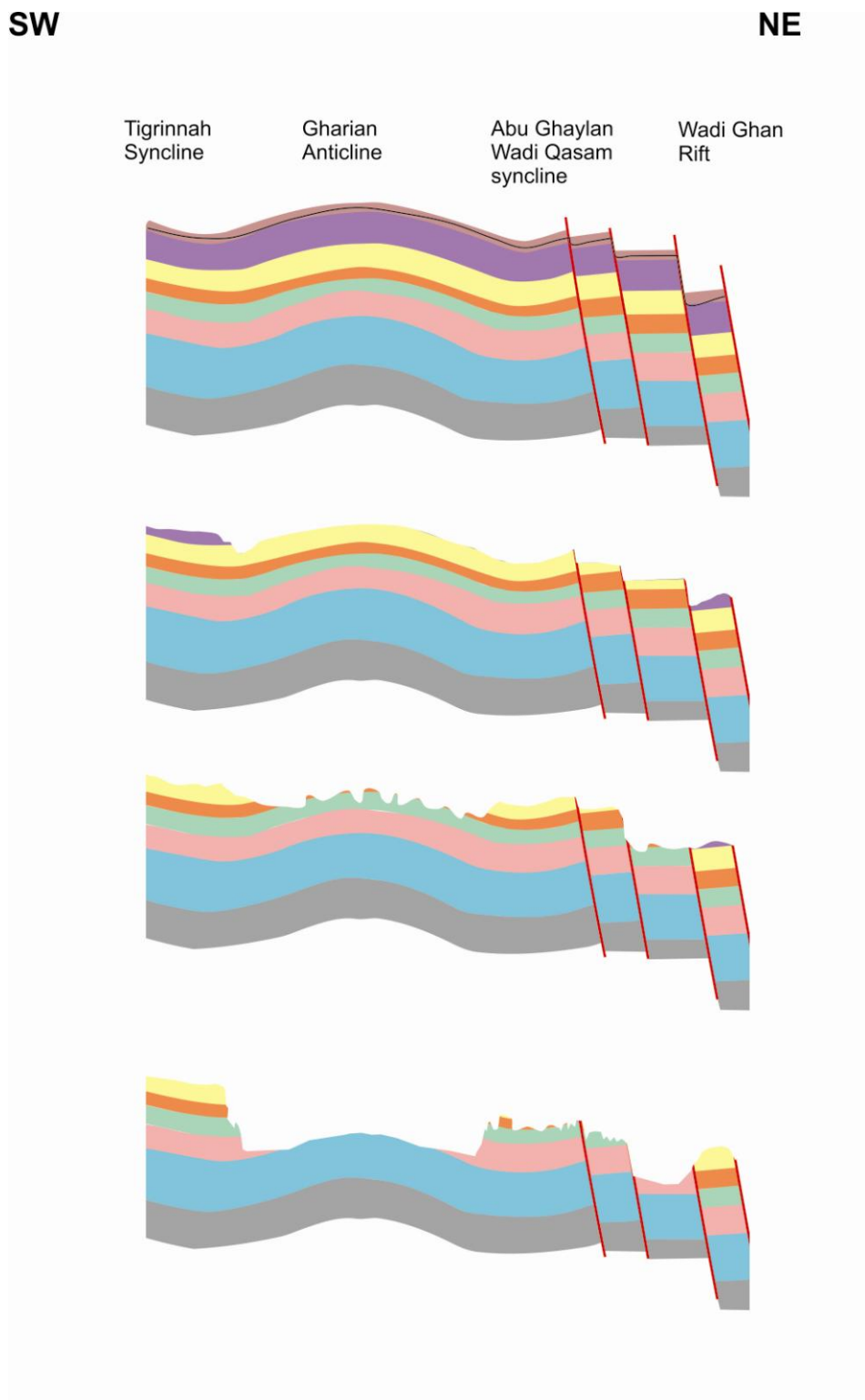


Figure 7.30 Differential erosion and its interplay with the main structures over time, oldest at the top, Stratigraphy as in cross sections (Fig. 7.17 and 7.25).

7.5 Structural Control of Intrusions

The accompanying geological map (Map 2), as previously noted, is an extended and ground truthed version of the Gray (1971) map. Gray's original map which is originally compiled from fieldwork carried out by undergraduate students is considered to be correct in all but minor respects. However, Gray's interpretation of the map was limited by the then lack of understanding of the structural geology of the area.

i) The intrusions and doming

The major intrusions in the Gharian area comprise phonolitic to trachy-phonolites and the minor dykes tend to be of a more basaltic composition (Gray, 1971; Piccoli, 1971). Radiometric ages (K-Ar) are scarce and rather old in terms of their execution but indicate that there has been sporadic igneous activity in the broader region during the Early Eocene (~50 Ma), Late Eocene (~40 Ma) and 12-1 Ma periods (Beccaluva et al., 2008). The intrusions form part of a wider igneous province which is dominated by flood basalts (Fig. 7.1B, 7.2, 7.30) some 20-80 km to the southwest of Gharian, which carry mantle derived lherzolite xenoliths (Beccaluva et al., 2008). This igneous activity is believed to be part of a much larger igneous province linked to African-European collision (Farahat et al., 2006; Azzouni-Sekkal et al., 2007).

The field relations of the intrusions in the broader area were investigated and described by Piccoli (1971) and in particular around Gharian by Gray (1971) who provides detailed descriptions. In the main body of the paper Gray describes and illustrates the passive emplacement nature of the intrusions emphasising their conformity with the strata into which they are intruded and overall describing them as sills or laccoliths (Gray, 1971 p 313 and 314 and his Figure 4 and 5). He further specifically notes that the intrusions caused no more than very localised over-steepening of the dips extremely close to their margins. He also clearly believed their emplacement was essentially as

simple passive stocks and sills fed in part by, locally stratigraphically discordant, dykes. While he notes in passing their close spatial relationship with faults of the Hun Graben (NW) and Jebel Nefusah (JN) trends he doesn't fully develop this. Our field observations entirely supports this previous work i.e. floors and roofs, where seen, clearly parallel local strata (e.g. Abu Ghannush) while presumed feeder dykes are clearly discordant and cross-cut strata in all formations at high angles.

In particular Grey (1971) shows very clearly that in the case of the largest intrusion (Abu Ghannush) that it exploited the NW trending faults, through which the magma ascended, but caps the NE trending faults that form the complex syncline which lies beneath the main planiform part of the intrusion. The most common faults that are linked to the intrusions are the Hun Graben group and Gray specifically regarded these as being unrelated to doming in an igneous context. The regional (1:250,000) geological map of the area shows a broad NW trending zone of intrusions that lie between the Wadi Ghan fault zone and a line running NW-SE immediately east of Gharian itself (Fig. 7.31a). Within this belt of intrusions one can further subdivide it into a series of NW and NE trending linears whose intersection is the most common locus of the intrusions (Fig. 7.31b). These correspond with the HG fault system, which clearly controls the regional ascent of the magma, while at a more localised scale the intersection of the HG structures with the JN faults acts as a strong control on the actual locus for the emplacement of the intrusions. At larger scales still the obvious spatial relations between igneous intrusives and extrusives and their controlling NW and E-W structures has previously been emphasised (e.g. Farahat et al., 2006; Fig. 7.32).

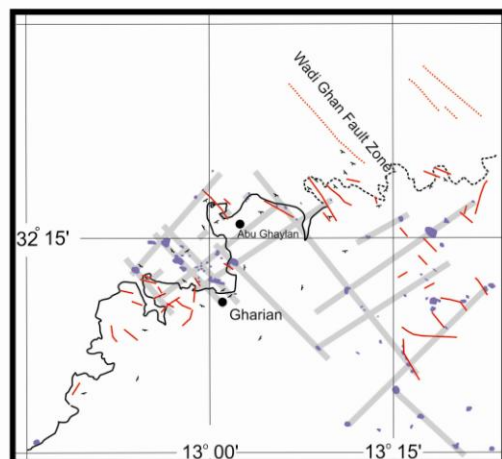
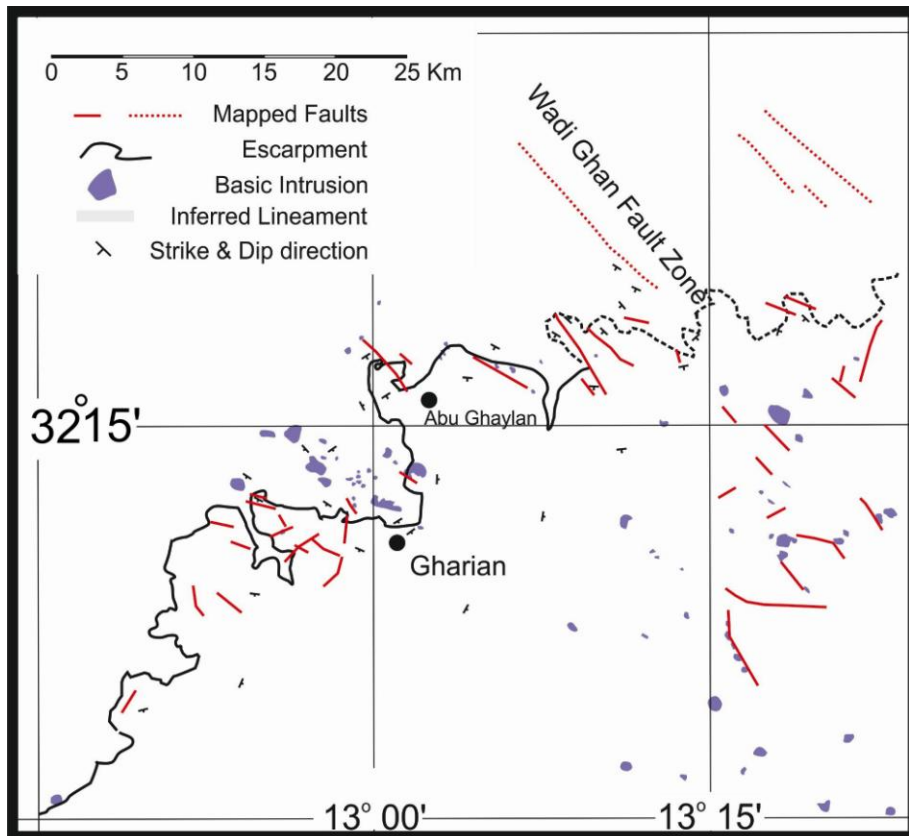


Figure 7.31 **A)** Location of igneous intrusions around Gharian from the 1:25, 00 scale geological maps (Sheet NI 33.13R, Tarabulus, 1975). **B)** Their interpretation as being located at the intersection of NW-SE Hun Graben faults and NW-SE Jabel Nafusah faults.

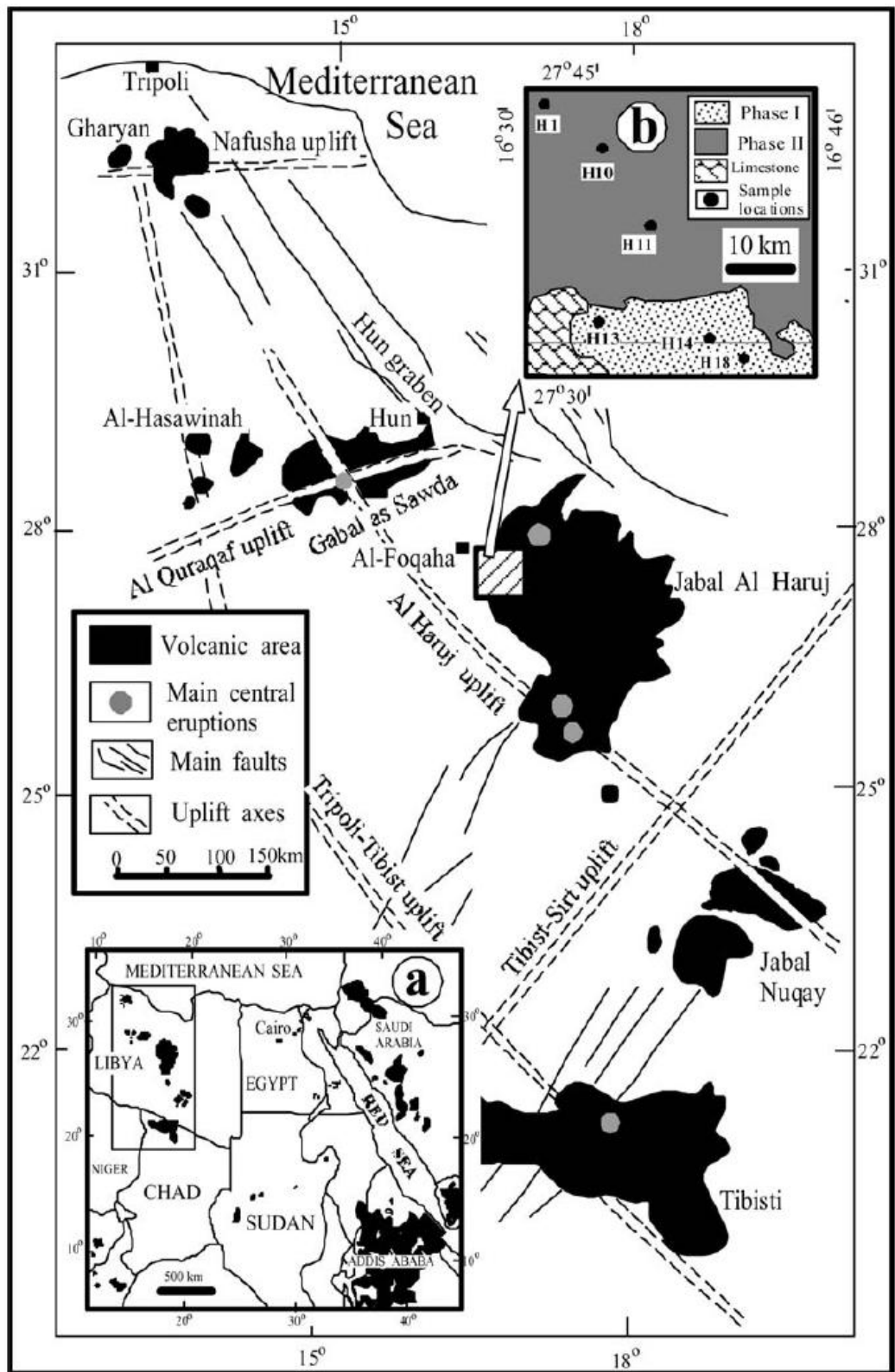


Figure 7.32 Regional map is showing the distribution of the main volcanic fields in northern Libya and inset there setting in northern Africa and Arabia as a whole (Farahat et al., 2006).

It is worth quoting Gray's (p 312 and 313) key statement in full as follows:

“While it is easy to assume that the close association of the phonolitic intrusives and the unique intensity of faulting associated with the Gharian Domes indicates that the domes and faults were formed as a result of the intrusion of the phonolite, a more complex history appears to be indicated. Except in the case of the Kaf Tekut dome, and in the local reversal of dip on the north side of the Wadi Abu Shaybah dome, arching of the sediments by the exposed intrusives cannot be demonstrated. Furthermore, some of the intrusives show remarkably little disturbance of the enclosing beds. It is my conclusion that most of the doming of the beds was caused by a deeper seated intrusives not now exposed, and possibly prior to the emplacement of the exposed intrusives.”

It is abundantly clear that Gray's interpretation, in essence, fundamentally contradicts itself and that those who have since referred to it have failed to see the subtlety of what was actually written. The above quote clearly indicates that:

- a) the doming is not related to the exposed intrusions at all;
- b) that the doming may well pre-date the intrusions;
- c) that he ascribes the doming to an unknown, unseen, deeper seated intrusion, for which he presents no evidence.

This study agrees with (a), (b) and (c) is an absurdity based on both Gray's own and our field observations which provide no support for such a conclusion. Instead it is concluded that arching of the strata is not a function of igneous emplacement but as will be further discussed is the interaction of NW-SE folds and NE-SW folds in response to faulting.

7.6 Structural Synthesis

There appear to be a number of reasons for the lack of clarity in understanding of the geological evolution of the region in the past. These are;

- the strong lithological and structural control exerted on the geomorphology including partial topographic inversion;
- the role of normal faults in producing folds at a range of scales has previously gone unrecognised;
- the lack of clarity of the principle structure of the Jabel Nafusah escarpment;
- a false requirement for folding to be a function of igneous doming and not as a result of normal faulting.

As is demonstrated in cross-section (Fig. 7.17) the principal structure of the escarpment at Gharian is a rollover anticline above a major normal fault zone. This fault and escarpment clearly parallel but lie behind the main escarpment. Field evidence from the main range front in the area north of Abu Ghaylan also revealed much evidence for the normal character of the Jabel Nafusah system faults. In this area, which would be the footwall to a major normal fault along the range front, low amplitude anticlines, much less conspicuous than that at Gharian, are observed (Fig. 7.33) associated with normal faults of the JN system. At smaller scales and further into the footwall block (within the Abu-Ghaylan-Wadi Qasam plateau) arrays of normal faults form southward tilted horst and graben type structures (e.g. Fig. 7.34, near Kaf Tekut section).

In short there is no obvious reason not to believe that the Jabel Nafusah escarpment is anything other than the product of erosion of a major normal master fault where the upthrown southern side is a backrotated southward tilted horst block and that the overall structure is in the style of many major half graben structures showing all the features one would expect of the footwall (e.g. Holdsworth and Turner, 2002).

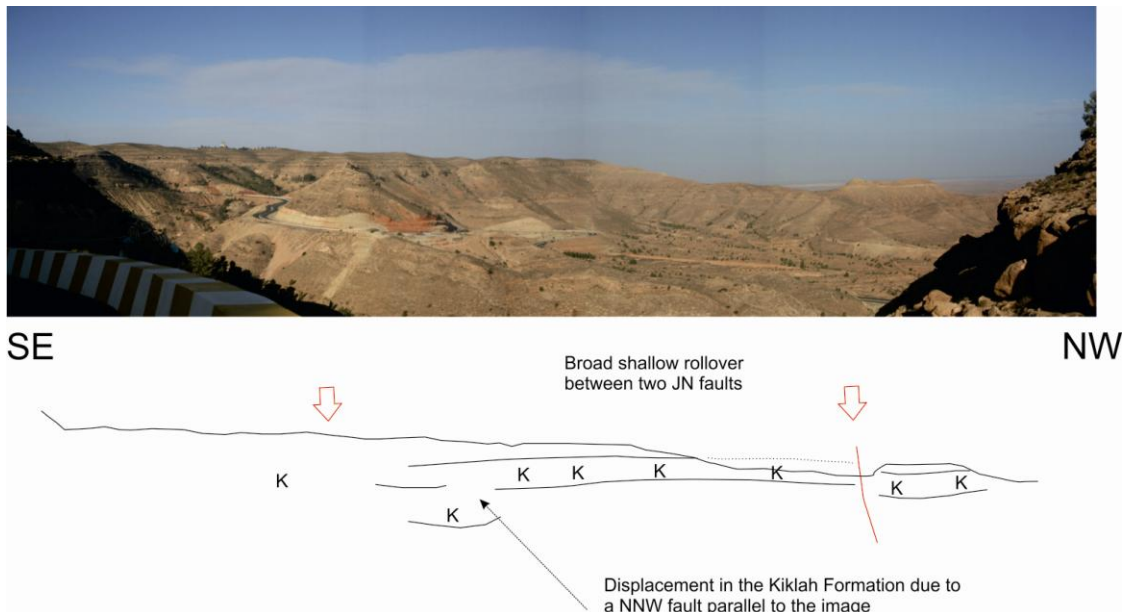


Figure 7.33 Nafusah escarpment north of the village of Abu Ghaylan viewed from the old Gharian-Tripoli highway looking across the new highway. On the right hand side of the image the Jafarah plain is visible in the distance. K marks the Kiklah Formation displaced by two major normal faults of the JN system and forming a broad, low amplitude anticline between them. The red arrows mark the position of the JN faults one being concealed in a major valley. The Kiklah Formation is also offset by NW trending faults of the Hun Graben system in the foreground.

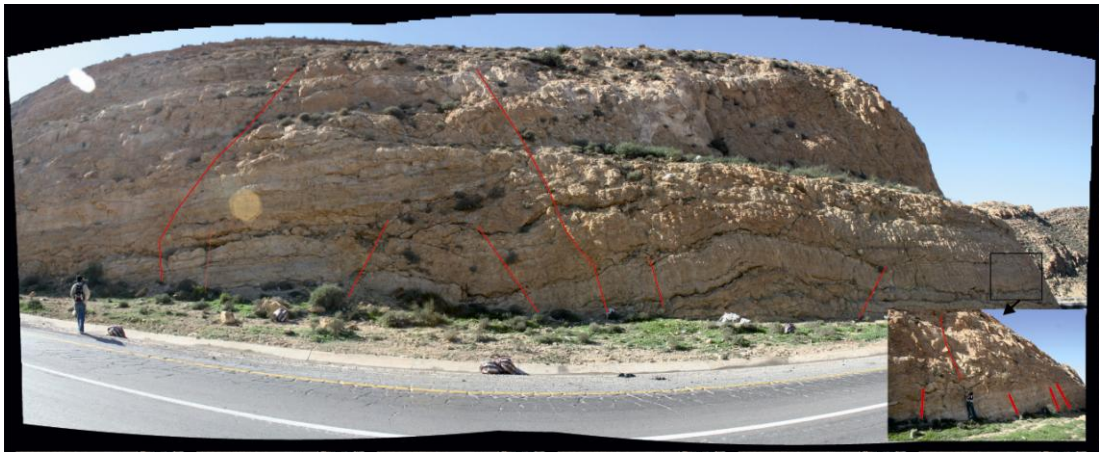


Figure 7.34 Horst block system -road sections.

The overall interpretation from this study is that both the Jabel Nafusah and the Gharian escarpments are the expression of major normal faults which form a small part of a large regional rift system of faults (Fig. 7.35). Given the large rollover anticline at Gharian (Fig. 7.17) plus recently published evidence from the continuation of the Nafusah escarpment into Southern Tunisia (Gabtni et al., 2009; Fig. 7.36) it is strongly suspected that the major master faults have a listric geometry and cut significantly down into the underlying Triassic and older units.

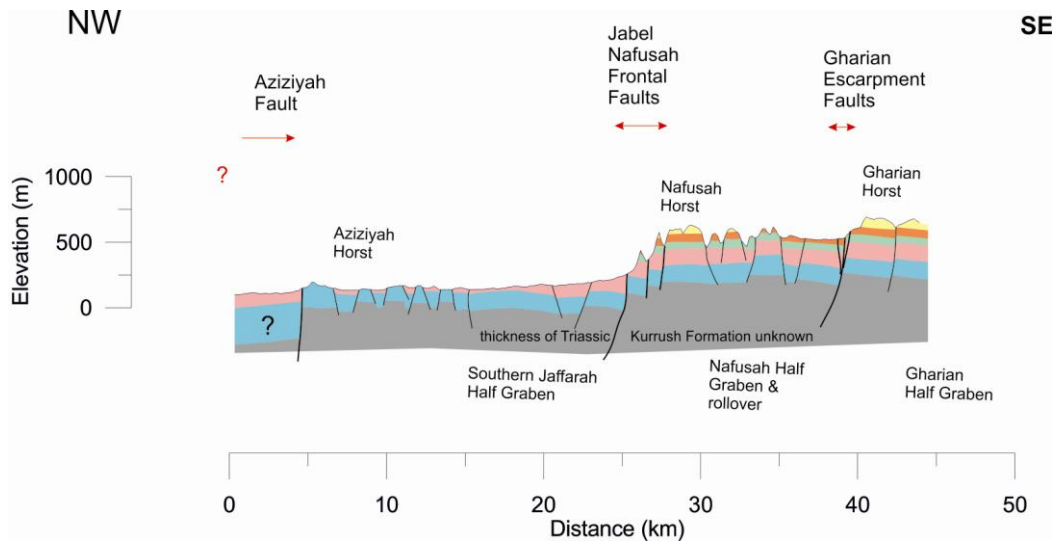


Figure 7.35 NW–SE Regional schematic cross section is showing the setting of the Nafusah Horst block in relation to the Jafarah Plain, the Nafusah escarpment and the Gharian Horst.

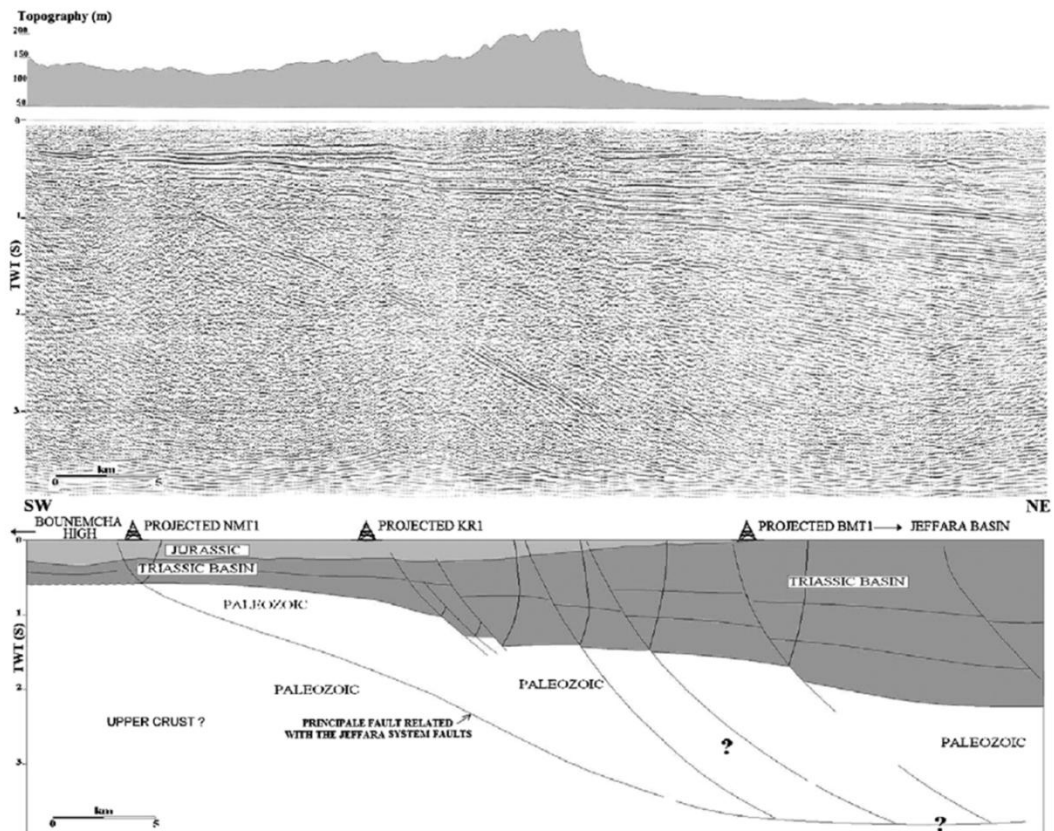


Figure 7.36 Seismic reflection profile and interpretation across the Jafarah fault system in southern Tunisia (from Gabtni et al., 2009).

The timing of the development of the Nafusah structures in the immediate Gharian area is clearly post Ain Tobi deposition and as far as can be currently determined post Nalut deposition in the Turonian or post c. 91 Ma. It is also believed that the southernmost major structure of this group has not been mapped at all but is visible on the DEM of Figure 7.27 as a distinct escarpment located some 30km southward of and parallel to the Nafusah escarpment which is traceable for in excess of 100km. Like the Nafusah escarpment it has a southward dipping plateau located to the south of it. In their study of the subsidence of the Hun Graben and Sirt Basin (Abadi et al., 2009) indicate that E-W to SE-NW faulting (Fig. 7.37 a and b) was most active in the Lower Cretaceous but continued sporadically in parts of the basin until at least Campanian times.

During the Upper Cretaceous and continuing into the Tertiary several rifting phases are identified with subsidence and normal faulting in a NW-SE orientation (Fig. 7.37 a and b). Hence, it is believed that in the main the NW trending 'HG' system faults and their associated folds post-date the Jabel Nafusah 'JN' fault system.

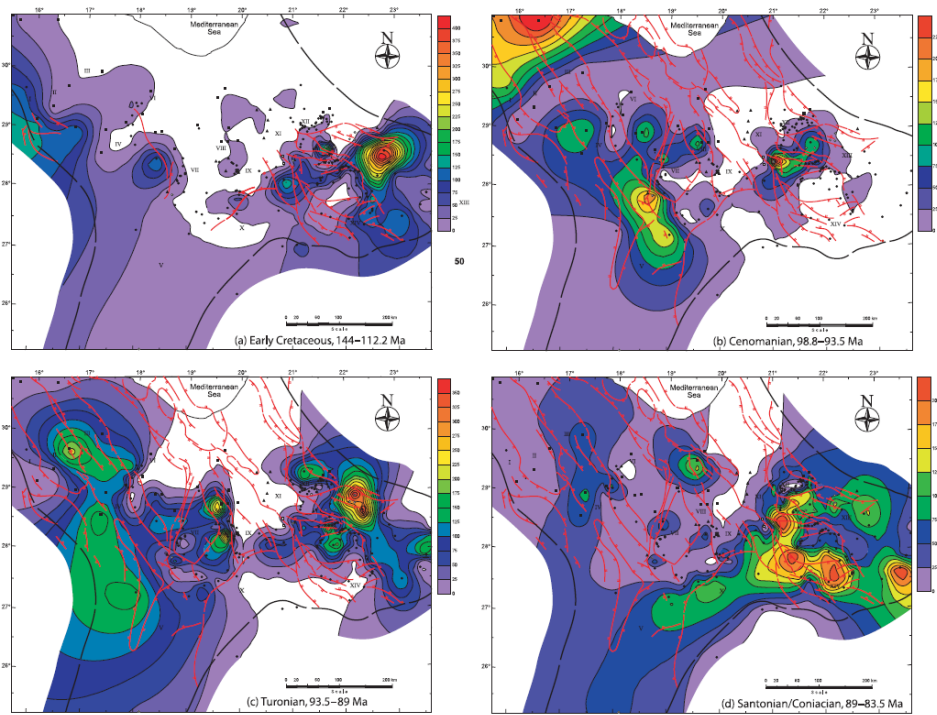


Figure 8. Contour maps of tectonic subsidence (m) of (a) Early Cretaceous, 144.0–112.2 Ma; (b) Cenomanian, 98.9–93.5 Ma; (c) Turonian, 93.5–89 Ma; (d) Santonian or Coniacian, 89–83.5 Ma; (e) Campanian, 83.5–71.3 Ma; (f) Maastrichtian, 71.3–65 Ma; (g) Danian–Ypresian, 65–49 Ma; and (h) Lutetian–Present, 49–0 Ma.

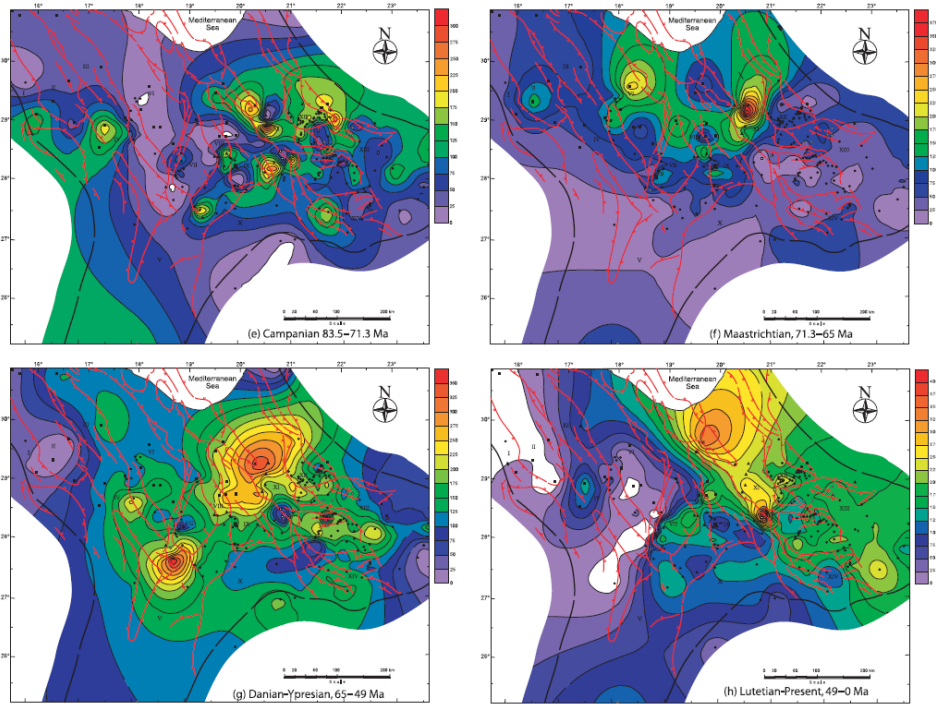


Figure 8. Continued.

Figure 7. 37 a & b Subsidence and fault history of the Hun Graben and Sirt basin (from Abadi et al., 2009).

The effect of both systems is to produce a series of structural highs and lows which in part at least manifest themselves as subtle extensional folds which overprint each other to produce a complex basin and dome interference pattern. The scale of the extension folds depends on the spacing of the master faults and the NW structures are perhaps best viewed as a gentle corrugation the previous normal fault system of the Jabel Nafusah. The “Gharian Dome” is simply the biggest and most obvious expression of this interference pattern. In the extreme NW of the mapped area, within the Wadi Ghan Rift, (map 2) Kaf Bates where Muttoni et al., (2001 – see Chapter 6) studied the Al Aziza Formation for palaeomagnetic purposes is locally known as the Raz Mazul dome at whose core the Triassic Kurrush Formation sediments are exposed as in the Gharian. This is separated on its SE side by a JN system fault from a narrow south-eastward plunging synclinal structure. During fieldwork domes and basins were also identified as far west as Kiklah on the Jabel Nafusah and it is suspected that this interference pattern continues for some considerable distance.

The A (NNE trending) and B (WNW trending) group faults are less obvious in their interpretation as they have little significant offset of geological markers across them. They are both clearly younger than the Jabel Nafusah ‘JN’ faults (Table 7.3), but only very limited evidence for their age relation with respect to the Hun Graben ‘HG’ faults was found. They are potentially synchronous with each other. In the main they have very little displacement across them and indeed in some cases appear to be little more than open fractures (Fig. 7.9B). Given their lack of displacement, possible synchronicity, and that they post-date the JN fault system. They are tentatively suggested to be the result of Tertiary movements related to the NW trending Hun Graben structures and the development of their associated folds. Our very limited observation of slickenlines, which suggested a steep dip slope component of movement, does not preclude that these fractures perhaps have an unrecognised strike slip

component to their motion which if this were the case it is conceivable that may be related to the south-easterly Hun Graben plunging folds in the form of partially dilatational shear fractures (Price and Cosgrove, 1990). Detailed analysis of these fractures is required to assess their true nature but they have no map scale effects.

7.7 Summary and Conclusions

The Jabel Nafusah escarpment is the eroded remains of a master normal fault in a system of southward tilted half-grabens which formed as part of the African extensional margin on the southern Tethyan margin in latest Early Cretaceous times.

It may be that the locus of extension was migrating northward through time from the Hun-Graben – Sirt basin where similar NE-SW extension dominated earlier in Early Cretaceous times with progressively younger periods of extension to the north of the Jabel Nafusah on the Azizyah fault, the main coastal scarp fault and Pelagian offshore areas (see Figure 7.4a and discussion in Klett, 2002).

The Jabel Nafusah system was later overprinted by the NW faults of the Hun Graben in the Late Cretaceous and Tertiary (Fig. 7.38). It is an echelon equivalent to the Wad Ghan rift. These NW structures gave rise to a gentle corrugation of the strata in low amplitude relatively long wavelength folds with a generally south easterly plunge. The interaction of these two extensional systems has given rise to a form of interference pattern of generally subtle domes and basins. The largest of these domes is the Gharian dome which is a consequence of this interference and not, as previously supposed, an unseen igneous intrusion. The Tertiary igneous intrusions and extrusions of the region are clearly structurally controlled in their emplacement but do not in any significant manner affect the geometry of the geology.

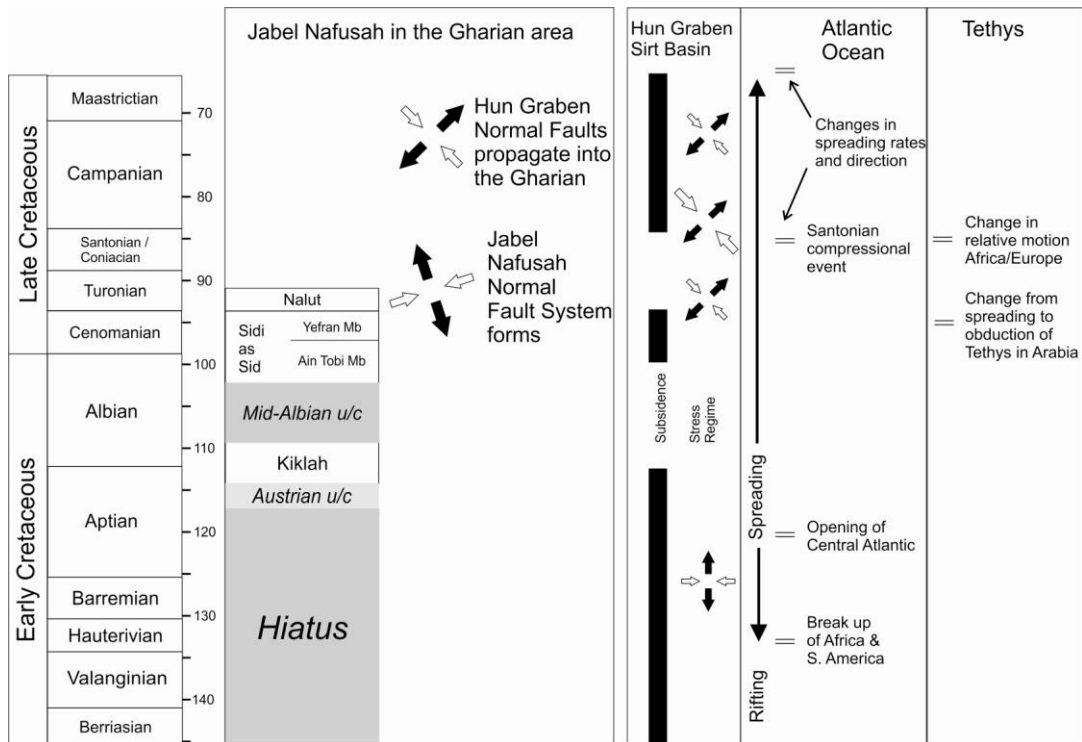


Figure 7.38 Synoptic Tectonostratigraphic column for the Jabel Nafusah and wider area (modified from Abadi et al., 2009).

Further study of the kinematics of the faults is clearly required to fully establish the above relations coupled with a wider mapping of the region as a whole to better understand the interference pattern at all scales.

The timing of the various vents needs to be more deeply understood and in particular many more strategically placed measured stratigraphic sections need to be undertaken to better understand the role of early fault activity.

Despite an expectation that there was likely to be clear signs of inversion, due to African-European collision, no clear markers (e.g. footwall) shortcuts of such inversion were encountered. Unlike much of North Africa to the west, northern Libya is, for the

most part, a very well preserved record of Tethyan and subsequent rifting that requires further in depth study (Fig. 7.39).

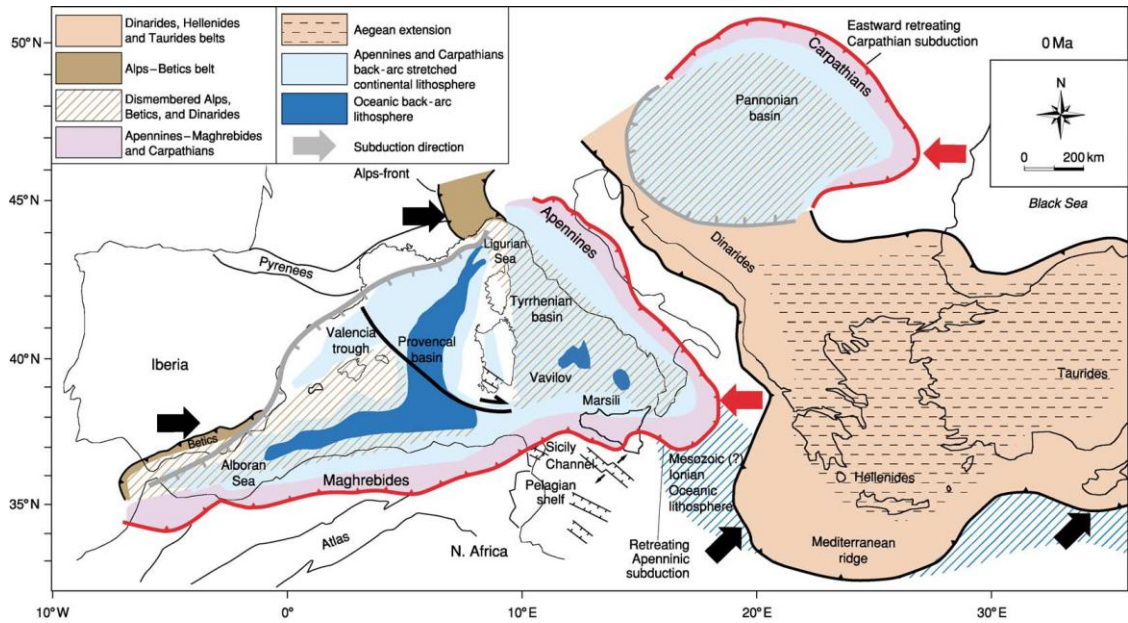


Figure 7.39 Geotectonic setting of the north African coast. The sharp northward deflection of the Maghebrides fold and thrust belt, through Sicily and into Italy, around the remains of the Ionian oceanic plate immediately north of Libya has meant that tectonic inversion of this part of the Tethyan margin is relatively limited (Carminati and Doglioni, 2005).

Chapter 8: Synthesis and Conclusions

8.1 Introduction

In this chapter the results from the previous chapters are integrated into a geological history for the Gharian area. During the course of geological investigation, an understanding of the sedimentary processes, environments, structure and age controls were developed and to improve the geological interpretations. The timing of structural and sedimentary events in the Gharian area and adjacent areas are summarised in Table 8.1.

8.2 Geological history of the Gharian area

In order to meet the objectives of this study (to describe and interpret the sedimentary processes and palaeoenvironments of the Kurrush and Al Aziza and Abu Shaybah Formations as addressed in Chapter1) and to reconstruct the Triassic palaeoenvironment history of the Gharian area, the three formations are summarised here as discussed in the preceding chapters:

8.2.1) Kurrush Formation

i) Environment

The Kurrush Formation is poorly exposed and it consists of red micaceous sandstone, mud and siltstone facies. However, the base is not exposed in the Gharian area. Within the limited outcrop exposure in the Gharian area and the sedimentological characteristics of red sandstone in the Wadi Abu Shaybah indicate deposition a continental environment (delta plain) (Fig. 8.1) but, this requires further in depth study using subsurface data from the Gharian area and Jafarah plain. In the latter part of middle Triassic shallow water marine conditions were well established in the area which resulted in the deposition of limestone and its micro facies (Al Aziza Formation).

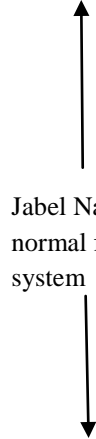
| Era | AGE (Ma) | PLATE TECTONIC EVENTS | LIBYA AND ADJACENT AREA | JABEL NAFUSAH |
|-----------------|-----------------|---|---|---|
| Mesozoic | 80-65 | Relative movement of the African plate changed from eastwards to north eastwards. End of seafloor spreading in Mediterranean. | Infill of grabens with marine shales and micrites. Shallow marine carbonates and clastics on horsts. Deposition of organic rich shales in Sirt Basin. | Hun Graben normal fault propagate into the Gharian |
| | 125-80 | Seafloor spreading axis switched to southern axis (south of Turkish, Balkan and Lombard terranes). | Major igneous flooding episode in Sirt Basin. End of rift phase. Subsidence in Sirt basin. Formation of horsts and grabens. |  Jabel Nafusah normal fault system |
| | 165-125 | Seafloor spreading in Tethys Ocean along northern axis (north of Sila, Lombard and Austrian Terranes). | Progressive collapse of Sirt Arch. Deposition of Nubian sands. | |
| | 165-125 | Establishment of the Tethys seaway. | Extensional regime in Libya. Continued rifting and deposition of continental clastics. | |
| | 240-155 | Break up of Pangaea along Caribbean-North Atlantic-Mediterranean axis. | Beginning of rift phases. Triassic continental clastics found in rift basins in Libya. | Kurrush, Al Aziza and Abu Shaybah Formations |

Table 8.1 Plate tectonic summary showing the main plate tectonic events which have shaped the development of North Africa, the reflection of these events can be observed in the structural and sedimentological history of Jabel Nafusah and adjacent areas (see Chapter 7) (modified from Boot et al., 1998; Vail, 1991; Hallett, 2002).

ii) Dating evidence

A total of 6 samples were collected at 2 sites from the Kurrush Formation and failed to yield useful information due to unstable demagnetisation (section 6.5). Therefore, age of the Kurrush Formation was assigned as the Fassnian and this is based upon the relative stratigraphic position of the Al Aziza Formation above and the Al Guider Formation below.

8.2.2) Al Aziza Formation

i) Environment

The full succession of the Al Aziza Formation is exposed in the Gharian area. The lower boundary is taken at the first appearance of limestone beds (Burrowed and laminated micrites and dolomites facies) overlying conformably the sandstone of the Kurrush Formation. A sedimentary analysis of the Al Aziza Formation allows the recognition of seven facies and then grouped into one facies association (a shallow shelf platform area). Therefore, facies association suggests that sedimentation probably occurred mostly within the inner ramp setting. Evaluation of the depositional environment of the Al Aziza Formation was attempted during this study and a more precise depositional setting was suggested. Based on the sedimentological and palaeontological features of the Al Aziza Formation an intertidal-subtidal carbonate flat to shelf lagoonal environment is proposed (Fig. 8.1) as opposed to the environment proposed by Asserto and Benelli (1971). In the latter part of middle Triassic (Carnian) shallow water marine conditions (siliciclastic setting) were well established in the area which resulted in the deposition of symmetrically rippled siltstone and fine-grained sandstone facies (Abu Shaybah Formation).

ii) Dating evidence

A total of 126 samples were collected from 2 sites in the Al Aziza Formation for dating purposes. The Al Aziza Formation in Gharian is latest Ladinian in age rather than latest Ladinian to earliest Carnian age as suggested by Muttoni et al., (2001). This is based upon the magnetostratigraphy study (Chapter 6).

8.2.3) Abu Shaybah Formation

i) Environment

The Abu Shaybah Formation consists of cross-bedded sandstone, red to yellow alternating with green and red of clays and pebble. Environment of the Abu Shaybah Formation divided into a shallow marine and fluvial system.

a) Shallow marine

The end of the Al Aziza Formation (Ladinian) the sea level trend is of a relative rise and lower Abu Shaybah Formation was deposited (Fig. 8.1). There was some terrigenous material in the basin. The lower Abu Shaybah is identified by the first appearance of symmetrically rippled siltstone and fine-grained sandstone (section 4.8.1), conformably overlying the last limestone bed of the Al Aziza Formation. This situation is consistent with the gradual transgression phase which probably took place at the end of the Al Aziza Formation (section 4.4). Facies analysis of the lower unit argues for intertidal flat environment (section 4.9.1, Chapter 4) which is consistent with Makhoul (2003), rather than the shallow water neritic to low intertidal or shallow subtidal environment of Asserto and Benelli (1971).

b) Fluvial system

The end of the lower of the Abu Shaybah is resulting in regression and followed by deposition of fluvial clastic facies of the Abu Shaybah Formation (Fig. 8.1). Therefore, middle and upper part of the Abu Shaybah Formation was deposited in a continental environment (low to a high energy sand fluvial) (Fig. 8.1), indicating the area was emergent during that time. Evaluation of the depositional environment of the upper and middle Abu Shaybah was carried out during this study allowing a more precise depositional setting to be suggested than by previous authors. Sedimentary structures and facies analysis of the mid and upper units argue for a fluvial system (section 4.9.2 and 4.9.3). This is in contrast to the aeolian to shallow low sinuosity or meandering stream, and arid lagoonal or coastal lacustrine depositional environments of Asserto and Benelli (1971).

ii) Dating evidence

A total of 91 samples were collected from 4 sites from the Abu Shaybah Formation for dating purposes. The Abu Shaybah Formation is earliest Carnian in age and this is based upon the magnetostratigraphy study which was carried out in the Chapter 6.

8.2.4) Palaeogeography of the Early Mesozoic

The Palaeogeography of the Early Mesozoic (the K-A-AS formations) is located on the edge of a marginal continental environment and the formations are diagrammatically represented by deposition diagram (Fig. 8.1). Changes in tectonic activity may have influenced local / regional relative sea-level fluctuations and climate also related change in sea level (section 4.11).

The palaeoenvironment for the deposition of the Kurrush Formation was quite varied. Within the lower Kurrush Formation of the Jafarah Basin a marine incursion is indicated by the presence of dolomitic limestone (Hammuda et al., 1985). Sedimentological analysis indicates that the Kurrush Formation is dominantly a marine environment in the Jafarah Plain and becomes marginal marine in the Gharian area. With reference to sequence stratigraphy, the deposition of the Kurrush Formation relates to facies changes and also reflects localised sea level oscillations.

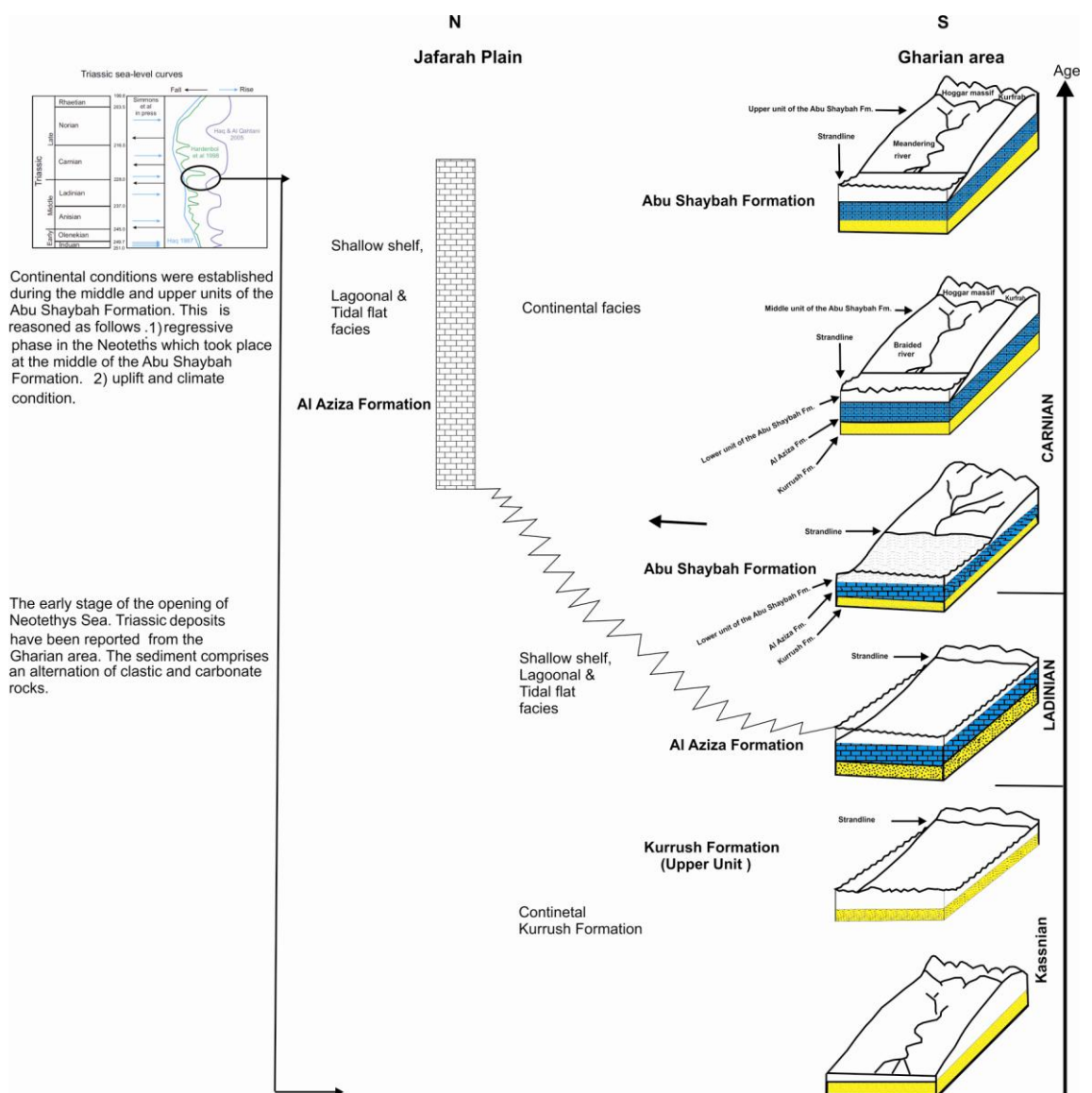


Figure 8.1 Palaeoenvironment model during the Early Mesozoic Kurrush, Al Aziza and Abu Shaybah Formations times, showing the overall of depositional facies.

The Al Aziza Formation relates to the low in eustatic sea level and a marine transgression and regression onto northern Gondwana (Fig. 8.2). The Triassic was generally a time of a low sea level and evidence for that is derived from the depositional model for the Al Aziza Formation, which comprises of a low energy, inner ramp setting (Chapter 4, section 4.6).

The Abu Shaybah Formation represents small sea level drop and evidence for that is derived from the lower part of the Abu Shaybah passing upward from shallow marine into a fluvial system. Sediments Middle to Late Triassic age were deposited in an continental environment (Abu Shaybah Formation) that gradually shifted to shallow water marine (Abu Ghaylan Formation) in the central Jabel Nafusah (Gharian area) to evaporite (lagoonal) environments in western Jabel Nafusah (Bir Al Ghanam member) in the Early Jurassic.

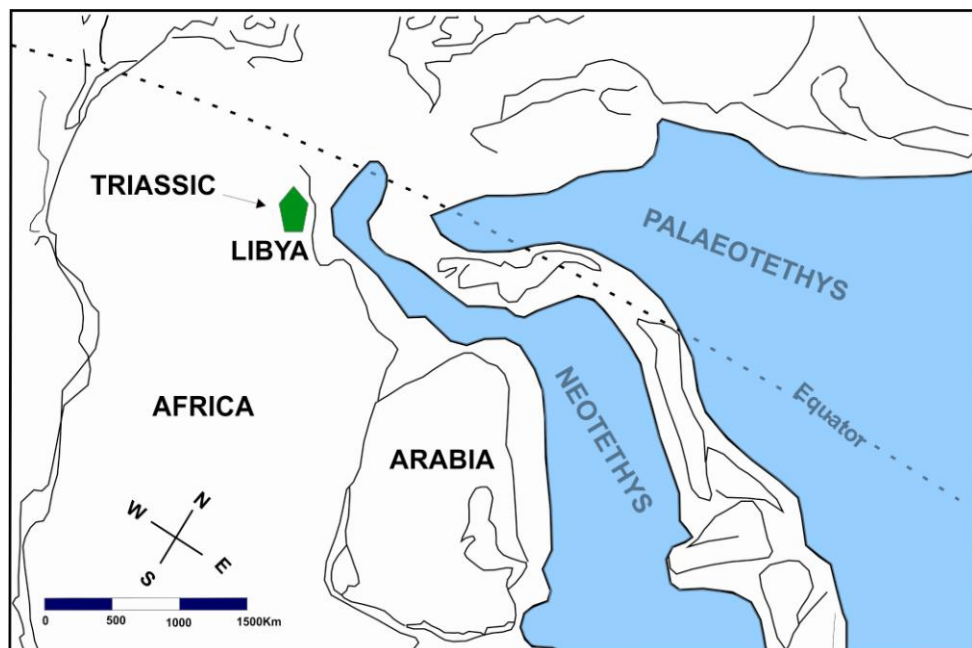


Figure 8.2 Triassic palaeogeographic reconstructions of palaeotethys and Neotethys at the northern Gondwana region (after Stampfi and Borel, 2002a; Makhlof, 2006).

8.2.5 Depositional controls during the Triassic

i) sea-level

During the Triassic a broad Tethys Ocean (palaeo-Tethys) existed in the northeast of Libya which is included the Gharian area. Furthermore, Middle Triassic time is sedimentation onto a very low gradient setting in the Gharian area. The palaeogeography during the Triassic period was controlled by sea level fluctuation which resulted in regression and followed by deposition of an intertidal-subtidal carbonate flat to shelf lagoonal environment (Al Aziza Formation). This is followed by transgression that gradually shifted to a shallow water marine (Lower of the Abu Shaybah Formation). During the late Triassic (Carnian) continental conditions were gradually established in the Gharian area by deposition of fluvial systems (section 4.11). Sea-level acts as base level in fluvial systems and sea-level is associated with climate. Therefore, sea-level during the Triassic history of the Gharian area related to icehouse and greenhouse period and this could correspond to the observed coarsening upwards and fining megasequences. This documents a withdrawal of marine conditions (Al Aziza and lower Abu Shaybah), the establishment of continental conditions and a change in fluvial style. Therefore, a sea-level lowering to occur to produce the initial coarsening upwards megasequence followed by a sea level rise to produce the fining upwards megasequence.

ii) Climate

Climate has controlled the rate of sedimentary supply to the Gharian area. The Triassic saw a relatively arid condition. The arid conditions are maintained into the Kurrush, Al Aziza and lower part of the Abu Shaybah Formation. Evidence for arid climatic conditions is derived from facies analysis, vegetation and soils (Chapter 4, section 4.11). However, a more humid climate begins to appear and become progressively more

dominant in the uppermost part of the Abu Shaybah Formation (meandering river system). Evidence for humid climate is derived from kaolinite however; the source of kaolinite is not considered to be the Gharian area and is likely to be derived from an area at some distance in the south of Libya where igneous rocks are located. The meandering river system in the upper part of the Abu Shaybah Formation carried the kaolinite into the Gharian area. Chapter 6 established that plate motions could have moved the landmass through different climate zones and therefore could account for a climate change. The magnetostratigraphy from this study (Chapter 6) and from existing stratigraphic schemes (Chapter 6, Fig 6.17 and 6.18) suggests that the K-A-AS formations span the Middle (Ladinian) to Late (Carnian) Triassic. Therefore, climate controls appear to have a major bearing on the coarsening and fining upwards megasequence. Climatic controls can explain the palaeogeographic changes that have affected the sediment supply in the fluvial system from the south of Libya. Therefore, changes in grain size and the changes in environment recorded in the coarsening and fining upwards megasequences observed in the Gharian area suggests that climatic changes may have altered weathering rates and sediment supply.

iii) Tectonics

The Triassic rift system affected the Gharian area as extensional faults have been observed within the study area. The data collected (Chapter 6 and 7) suggest that syn-tectonic sedimentation did not occur (at least in the Gharian area) and that faulting occurred after sedimentation of the K-A-AS formations. Chapter 6 and 7 established that the Gharian area was part of the African extensional margin on the southern Tethyan margin in latest Early Cretaceous times. Furthermore, this study shows that there is no direct evidence for fault activity within the Gharian area and it is possible that the initial coarsening upwards megasequence could be a function of the broader regional scale rifting process characterised by relative uplift and tilting towards the

south into, across and beyond the Jabel Nafusah fault. This suggests that the area may have been affected by regional uplift and this may have occurred much further to the south of the study area in the continental interior of the Gondwanan landmass.

Therefore, there is no strong structural control in the Gharian area, but topography does appear to be important in controlling when the erosion surface cut into the clastics and it becomes readily 'inverted' as they are rapidly eroded by the highly seasonal nature of the run-off in flash flood events.

8.3 Conclusions

A number of important conclusions can be drawn from this study:

- 1) During the lower Triassic the Gharian area is a very low continental margin setting.
- 2) The sedimentary facies and depositional systems were analysed to provide palaeoenvironmental and palaeogeographic reconstruction for the study area. A shallow shelf sea (Neotethys) existed to the north and allows a major regressive event, with development of:
 - i) The Kurrush Formation (marginal continental environment possibly delta plain).
 - ii) The Al Aziza Formation (inner ramp: an intertidal-subtidal carbonate flat to shelf lagoonal environment).
 - iii) During the early Triassic (Carnian) there was small sea level rise and some influx of material in the basin which allowed the shallow marine environment to be deposited (lower of the Abu Shaybah Formation).

- iv) The end of the lower of the Abu Shaybah resulted in regression followed by deposition of fluvial clastic facies of the Abu Shaybah Formation (the braided river system and higher sinuosity meandering river system)
- 3) The Triassic climate was relatively arid. Climate has controlled the rate of sedimentary supply to the Gharian area. Evidence for a humid climate is observed in the upper of the Abu Shaybah Formation but this is likely to be derived from an area at some distance in the south of Libya.
- 4) Most of the Al Aziza and Abu Shaybah samples convey a weak but stable remanent magnetization.
- 5) The Al Aziza Formation has yielded a primary remanence that has suffered a substantial post-acquisition clockwise rotation ($\sim 50^\circ$).
- 6) The Al Aziza Formation in the Gharian area is latest Ladinian in age whilst the Abu Shaybah Formation in the Gharian area is earliest Carnian in age.
- 7) The palaeomagnetic data from the Al Aziza and Abu Shaybah Formation yield a distinct series of polarity zones that provide clear local and regional correlation and are readily tied to a recently compiled global magnetostratigraphic time scale.
- 8) The Abu Shaybah Formation in the Gharian area is the stratigraphic equivalent of the Aziza Formation at Azizyah and Kaf Bates.
- 9) Faults in Gharian area indicate that tectonics were active from the Early Cretaceous and this is the period of the opening of the south and equatorial Atlantic during the Barremian and Albian, respectively.

10) The Jabel Nafusah escarpment is the eroded remains of a master normal fault in a system of southward tilted half-grabens that formed as part of the African extensional margin on the southern Tethyan margin in latest Early Cretaceous times.

11) Tertiary igneous intrusions and extrusions in the Gharian area are structurally controlled.

References

- ABADI, A. M., VAN WEES, J.D., VAN DIJK, P. M. & CLOETINGH, S. A. P. L. 2008. Tectonics and subsidence evolution of the Sirt Basin, Libya. *AAPG Bulletin*, 92, 993-1027.
- ABDUL AZIZ, H., SANZ-RUBIO, E., CALVO, J. P., HILGEN, F. J. & KRIJGSMAN, W. 2003. Palaeoenvironmental reconstruction of a middle Micene alluvial fan to cyclic shallow lacustrine depositional system in the Calatayud Basin (NE Spain). *Sedimentology*, 50, 211-236.
- AHLBRANDT, T. S. 2001. The Sirte Basin Province of Libya—Sirte-Zelten Total Petroleum System. *U.S. Geological Survey, Bulletin. L.M . Carter, U.S. Geological Survey Bulletin 2202–F:29*.
- AL-GHAMDI, N. M. 2006. *Facies sequence framework and evolution of rudist buildups, Shu aiba Formation, Saudi Arabia. Geological Sciences*. Master of Science, 77pp.
- ALI KALEFA EL-GHALI, M. 2005. Depositional environments and sequence stratigraphy of paralic glacial, paraglacial and postglacial Upper Ordovician siliciclastic deposits in the Murzuq Basin, SW Libya. *Sedimentary Geology*, 177, 145-173.
- ALLEN GURRAN, H. 1985. The trace fossil assemblage of A Cretaceous nearshore environment: Englishtown Formation of Delaware, U.S.A. *In: ALLEN GURRAN, H. (ed.) Biogenic structures: Their use in interpreting depositional environments*. Society of Economic Paleontologists and Mineralogists, No.35, 347.
- ALLEN, J. R. L. 1968. *Current ripple there relation to patterns of water and sediment motion* North-Holland Publishing Company/ Amsterdam, 433pp.

- ALLEN, J. R. L. 1970. Studies in fluvial sedimentation: a comparison of fining-upwards cyclothems, with special reference to coarse member composition and interpretation. *J. Sedim. Petrol.*, 40, 298–323.
- ALLEN, J. R. L. 1971. *Physical processes of sedimentation*, Fourth impression, London, Fakenham and Reading, 248 pp.
- ALLEN, P. A. & ALLEN, J., R 1990. *Basin Analysis principles and applications*, Blackwell Science LTD, 45pp.
- ALLEN, J. R., L 1965. A review of the origin and characteristics of recent alluvial sediments. *Sedimentary Geology*, 5, 89-191.
- ALONSO-ZARZA, A. M. 2003. Palaeoenvironmental significance of palustrine carbonates and calcretes in the geological record. *Earth-Science Reviews*, 60, 261-298.
- ALSHARHAN, A. S. 1993. Sedimentary facies analysis of the subsurface Triassic and hydrocarbon potential in the United Arab Emirates. *Facies*, 28, 97-108.
- ALYAGOUBI, N. A. 2007. *Geochemical Characterization of the Shale beds, Late Triassic Al AZIZYAH FORMATION, Jefara Basin, NW Libya*. Master Degree in Science, 37 pp.
- ANKETELL, J. M. 1996. Structural history of the Sirt Basin and its relationship to the Sabratah Basin and Cyrenaican Platform , Northern Libya. *In: SALEM, M. J., BUSREWILL, M. T., MISALLATI, A. A. & SOLA, M. A. (eds.) The Geology of the Sirt Basin*. Amsterdam: Elsevier, III, 57-87
- ANKETELL, J. M. & CHELLALI, S. M. 1991. A Palaeogeographic map of the Pre-Tertiary surface in the region of the Jafarrah Plain and its implication to the structural history of northern Libya. *In: SALEM, M. J., SBETA, A. M. & BAKBAK, M. R. (eds.) The Geology of Libya* Academic Press, London, VI, 381-2406.

- ARNDORFF, L. 1993. Lateral relations of deltaic palaeosols from the Lower Jurassic Rønne formation on the island of Bornholm, Denmark. *Palaeogeography, Palaeoclimatology, Palaeoecology*, 100, 235-250.
- ASSERETO, R. & BENELLI, F. 1971. Sedimentology of the Pre-Cenomanian formations of the Jabel Gharian *In: Symp. Geol. Libya (ed. Gary)*. Fac. Sci., Univ. Libya , Tripoli, 37-85pp.
- AZZOUNI-SEKKAL, A., BONIN, B., BENHALLOU, A., YAHIAOUI, R. & PAUL LIÉGEOIS, J. 2007. Cenozoic alkaline volcanism of the Atakor massif, Hoggar, Algeria. *Geological Society of America*, 418, 321-340
- BADALINI, G., REDFERN, J. & CARR, I. D. 2002. A SYNTHESIS OF CURRENT UNDERSTANDING OF THE STRUCTURAL EVOLUTION OF NORTH AFRICA. *Journal of Petroleum Geology*, 25, 249-258.
- BADENAS, B. & AURELL, M. 2010. Facies model of a shallow-water carbonate ramp based on distribution of non-skeletal grains (Kimmeridgian, Spain). *Facies*, 56, 89-110.
- BAEGI, M. B. & PERSKI, Z. 1996. The classification and genesis of the Granitoid intrusions of the eastern part of the Tibesti massif Libya based on remote sensing studies. 6 (182), 41-46.
- BANERJEE, S. 1980. Stratigraphic Lexicon of Libya. Ind. Res. Cent., Tripoli, Bull, 300 pp.
- BAUSCH, W. M. 1978. The central part of the Jabel Nefusa volcano (Libya) survey map, age relationship and preliminary results. *Seitc.*, 2, 389-400.
- BECCALUVA, L., BIANCHINI, G., ELLAM, R. M., MARZOLA, M., OUN, K. M., SIENA, F. & STUART, F. M. 2008. The role of HIMU metasomatic components in the North African lithospheric mantle: petrological evidence

- from the Gharyan lherzolite xenoliths, NW Libya. *Geological Society, London, Special Publications*, 293, 253-277
- BELLINI, E. & MASSA, D. 1980. A stratigraphic contribution on the Palaeozoic of southern Basin of Libya. *In: SALEM, M. J. & BUSREWIL, M. T. (eds.) The Geology of Libya*. Accademic Press, London, 463-499.
- BESSE, J. & COURTILOT, V. 1991. Revised and Synthetic Apparent Polar Wander Paths of the African, Eurasian, North American and Indian Plates, and True Polar Wander Since 200 Ma. *J. Geophys. Res.*, 96, 4029-4050.
- BIJU-DUVAL, B., DERCOURT, J. & LEPICHON, X. 1977. From the Tethys Ocean to the Mediterranean Sea: A plate tectonic model of the evolution of western Alpine system. *In: BIJU-DUVAL, B. & MONTADERT, L. (eds.) Structural history of the Mediterranean basins, International symposium, Editions Technip, Paris, 143-164.*
- BISHOP, W. F. 1975. Geology of Tunisia and adjacent parts of Algeria and Libya *Bulletin of the American Association of Petroleum Geologists*, 159, 413-450.
- BODIN, S., PETITPIERRE, L., WOOD, J., ELKANOUNI, I. & REDFERN, J. 2010. Timing of early to mid-cretaceous tectonic phases along North Africa: New insights from the Jeffara escarpment (Libya-Tunisia). *Journal of African Earth Sciences*, 58, 489-506.
- BOGGS, SAM 1995. *Principles of sedimentology and stratigraphy*, Prentice Hall, 774 pp.
- BOGGS, SAM, J. 1987. *Principles of sedimentology and stratigraphy* . A Bell and Howell Company, 784pp.
- BOOT, D. R. D., CLARK LOWES, D. D. & TRAUT, M. W. 1998. Palaeozoic petroleum systems of north Africa. *In: : MACGREGOR, D. S., MOODY, R.T.J*

- &CLARK-LOWES, D.D. PETROLEUM GEOLOGY OF NORTH AFRICA.
(ed.) *Geological Society of London*, 132.7-68.
- BOURQUIN, S., ESCHARD, R. & HAMOUCHE, B. 2010. High-resolution sequence stratigraphy of Upper Triassic succession (Carnian-Rhaetian) of the Zarzaitine outcrops (Algeria): A model of fluvio-lacustrine deposits. *Journal of African Earth Sciences*, 58, 365-386.
- BRACK, P. & MUTTONI, G. 2000. High-resolution magnetostratigraphic and lithostratigraphic correlations in Middle Triassic pelagic carbonates from the Dolomites (northern Italy). *Palaeogeography, Palaeoclimatology, Palaeoecology*, 161, 361-380.
- BRIDGE, J. S. 2003. *Rivers and Floodplains: Forms, processes, and sedimentary Record*, Blackwell Science Ltd a Blackwell publishing company, 491.
- BROMLEY, R. G. 1990. *Trace Fossils: Biology and Taphonomy.*, Chapman and Hall, 280 pp.
- BROMLEY, R. G. 1996. *Trace fossils : Biologu, taphonomy and application* Chapman and Hall, 361pp.
- BULL, W. B. 1991. *Geomorphic Response to Climatic Change*, Oxford, OUP, 326 pp.
- BURCHETTE, T. P. & WRIGHT 1992. Carbonate ramp depositional systems. *Sedimentary Geology*, 79, 3-57.
- BUROLLET, P. F. 1963. Field trip guidebook of the excursion to Jebel Nefus (Mesozoic/Tertiary section in Tripolitania). First Saharan symp., petrol. Explor.Soc. Libya, Tripoli, 17 pp.
- BUROLLET, P. F. & MAGNIER, P. 1960. Remarques sur la limite Cretace-Tertiaire en Tunisie et Libya. *Int. Gongr., Copenhagen, report*, 5, 136-144.
- BUSSON, G. 1967. Le Mesozioque Saharien, pt 1:L' extreme-sud tunisien: France, . *Gent. Rech. Zones Arides, Ser. Geol.*, 8, 194p. Summarized as Mesozioic of

southern Tunisia in Guidebook to geology and history of Tunisia: Petroleum Exp. Soc.Libya 9 Ann. Field Conf., 131-151.

BUSSON, G. 1970. Le Mesozoique saharien. 2e partie:essai de synthese des sondages algerotunisiens. *Publication du centre de Recherche sur les zones arides,CNRS,11(2).*

BUTLER, R. F. 1992. *paleomagnetism: Magnetic Domains to Geologic Terrans*, Cambridge, Mass, Blackwell Scientific, 223 pp.

CARMINATI, E. & DOGLIONI, C. 2005. Mediterranean Tectonics. *Encyclopedia of Geology, Elsevier: 135-146.*

CARR, I., D 2002. Second-Order sequence Stratigraphy of the palaeozoic of north Africa. *Petroleum Geology, 25, 259-280.*

CATUNEANU, O., KHALIFA, M. A. & WANAS, H. A. 2006. Sequence stratigraphy of the Lower Cenomanian Bahariya Formation, Bahariya Oasis, Western Desert, Egypt. *Sedimentary Geology, 190, 121-137.*

CHANNELL, J. E. T. 1996. Palaeomagnetism and palaeogeography of Adria, in: A. Morris, D.H. Tarling (Eds.), *Palaeomagnetism and Tectonics of the Mediterranean Region. Geol. Soc. Spec. Publ, 105, 119-132.*

CHRISTIE, W. 1966. *Geology of the Gharian area, Tripolitania,Libya, Ministry of Industry, Geo.Sec, Bulletin, No.5.*

COLLINSON, J., MOUNTNEY, N. & THOMPSON, D. 2006. *Sedimentary structures*, Third edition, Terra Publishing. 292 pp.

COLLINSON, J. D. 1996. Alluvial sediments. In: READING, H. G. (ed.) *Sedimentary environments : processes, facies and stratigraphy*. Blackwell Science Publication, Oxford, Kingdom, 37-82 pp.

COLLINSON, J. D. & THOMPSON, D. B. 1982. *sedimentary structures*, BNOC, University of Keele. London, 194 pp.

- COLLINSON, J. D. & THOMPSON, D. B. 1989. *Sedimentary structures*, Chapman and Hall, 2-6, London, 207pp.
- COLOUR CHAR, T. R. 2009. Rock Colour chart: with genuine Munsell color chips. *The Geological Society of America*.
- CONANT, L. C. & GOUDARZI, G. H. 1967. Stratigraphic and tectonic framework of Libya *Bull. Am. Assoc. Petrol. Geol.*, 51, 719-730.
- DAMBORENEA, S. E. & LANÉS, S. 2007. Early Jurassic shell beds from marginal marine environments in southern Mendoza, Argentina. *Palaeogeography, Palaeoclimatology, Palaeoecology*, 250, 68-88.
- DARDOUR, A. M., BOOTE, D. R. D. & BAIRD, A. W. 2004. STRATIGRAPHIC CONTROLS ON PALAEOZOIC PETROLEUM SYSTEMS, GHADAMES BASIN, LIBYA. *Journal of Petroleum Geology*, 27, 141-162.
- DE KOCK, M. O., EVANS, D. A. D., KIRSCHVINK, J. L., BEUKES, N. J., ROSE, E. & HILBURN, I. 2009. Paleomagnetism of a Neoproterozoic-Paleoproterozoic carbonate ramp and carbonate platform succession (Transvaal Supergroup) from surface outcrop and drill core, Griqualand West region, South Africa. *Precambrian Research*, 169, 80-99.
- DESIO, A. 1971. Outlines and problems in the geomorphological evolution of Libya from the Tertiary to the present day. In: GRAY, C. (ed.) *In : Symposium on the Geology of Libya*. Tripoli: University of Libya, 11-36.
- DESIO, A., RANCHETTI, C. R. & INVERNIZI, G. 1960. Sulla Stratigrafia del Trias in Tripolitania e nel sud-Tunisino, *Rev. ITAL-pALEONTAL. Stratigr.*, Vol .66, 273-322.
- DESIO, A., RONCHETTI, C. R., POZZI, R., CLERICI, F., INVERNIZZI, G., PISONI, C. & VIGANO, P. L. 1963. Stratigraphic studies in the Tripolitanian Jabel, Libya. *Rev.Ital. Paleontol. Stratigr. Mem.*, 9, 1-26.

- DILL, H. G., BOSSE, H. R., HENNING, K. H., FRICKE, A. & AHRENDT, H. 1997. Mineralogical and chemical variations in hypogene and supergene kaolin deposits in a mobile fold belt the Central Andes of northwestern Peru. *Mineralium Deposita*, 32, 149-163.
- DOLBIER, R., ANDERSON, T. & TEMPEL, R. N. 2010. Origin of Chert in Mississippian Monte Cristo Formation, Southern Nevada, and Its Relationship to the Antler Orogeny. *I.W.M. Keck Museum, University of Nevada, Reno, Reno, NV (rdolbier@unr.edu)*. Adapted from poster presentation at AAPG Convention, Denver, Colorado.
- DONOVAN, S. K. 2009. Trace Fossils, Mass Extinctions, and Event Boundaries. *Ichnos: An International Journal for Plant and Animal Traces*, 16, 177-178.
- DRIDI, M. 1998. Field trip guidebook to Triassic outcrops in Southern Tunisia. *Enterprise Tunisienne D' Activities*, 1-15.
- DUNHAM, R. J. 1962. Classification of carbonate rocks according to depositional texture. In: EDITOR), I. W. E. H. (ed.) *Classification of carbonate rocks*. American Association of Petroleum Geologists Memoir 1, 108-121.
- EL-ZOUKI, A. Y. 1980. Stratigraphy and lithofacies of the continental clastics (Upper Jurassic and Lower Cretaceous) of Jabel Nafusah, NW Libya. In: SALEM, M. J. & BUSREWILL, M. T. (eds.) *The geology of Libya*, . Academic press London, II, 294-418.
- EL HINNAWY, M. & CHESHITEV 1975. Geological map of Libya, Tarabulus (N133-13). Explanatory Booklet. Industrial Research Center, Tripoli.
- EZAKI, Y. 2009. Secular Fluctuations in Palaeozoic and Mesozoic Reef-Forming Organisms During Greenhouse Periods: Geobiological Interrelations and Consequences. *Paleontological Research*, 13, 23-38.

- FARAHAT, E. S., GHANI, M. S. A., ABOAZOM, A. S. & ASRAN, A. M. H. 2006. Mineral chemistry of Al Haruj low-volcanicity rift basalts, Libya: Implications for petrogenetic and geotectonic evolution. *Journal of African Earth Sciences*, 45, 198-212.
- FATMI, A. N., ELIAGOUBI, B. A. & HAMMUDA, O. S. 1980. Stratigraphic nomenclature of the Per-Upper Cretaceous Mesozoic rocks of Jabel Nafusah, NW Libya. *In: (SALEM, M. J. & BUSREWIL, M. T. (eds.) In: The Geology of Libya. Academic Press, London.*
- FATMI, A. N. & SBETA, A. M. 1991. The Significance of the occurrence of Abu Ghaylan and Kiklah Formation east of Wadi Ghan, Eastern Jabel Nafusah. *In: SALEM, M. J. & BUSREWILL, M. T. (eds.) The Geology of Libya. Academic Press, 1,57-65.*
- FATMI, A. N., SBETA, A. M. & ELIAGOUBI, B. A. 1978. Guide to the Mesozoic stratigraphy of Jabel Nefusa, Libya Jamahiriya. Arab. Dev. *INST .Publ.No.7, 35pp.*
- FIELDING, C. R. 2006. Upper flow regime sheets, lenses and scour fills: Extending the range of architectural elements for fluvial sediment bodies. *Sedimentary Geology*, 190, 227-240.
- FISHER, R., A. 1953. Dispersion on a shore. *Proceeding of the Royal Society of London, Series A*, 217, 295-305.
- FLETCHER, R. C., BUSS, H. L. & BRANTLEY, S. L. 2006. A spheroidal weathering model coupling porewater chemistry to soil thicknesses during steady-state denudation. *Earth and Planetary Science Letters*, 244, 444-457.
- FLUGEL, E. 2004. *Microfacies of Carbonate Rocks (Analysis, and Interpretation and Application)*, Springer-Verlag Berlin Heidelberg, 976 pp.

- FÖLLMI, K. B. 1996. The phosphorus cycle, phosphogenesis and marine phosphate-rich deposits. *Earth-Science Reviews*, 40, 55-124.
- FRIEND, P. F., SLATER, M. J. & WILLIAMS, R. C. 1979. Vertical and lateral building of river sandstone bodies, Ebro Basin, Spain. *Journal of the Geological Society*, 136, 39-46.
- GABTNI, H., JALLOULI, C., MICKUS, K. L., ZOUARI, H. & TURKI, M. M. 2006. The location and nature of the Telemzan High-Ghadames basin boundary in southern Tunisia based on gravity and magnetic anomalies. *Journal of African Earth Sciences*, 44, 303-313.
- GABTNI, H., JALLOULI, C., ZOUARI, H. & MICKI, M. M. 2009. Deep structure and crustal configuration of the Jeffarah basin (Southern Tunisia) based on regional gravity, seismic reflection and borehole data: How to explain a gravity maximum within a large sedimentary basin? *Journal of Geodynamics*, 47, 142-152.
- GAO, Y., SHI, G. R. & PENG, Y. 2009. A new bivalve fauna from the Permian-Triassic boundary section of southwestern China. *Alchering* 33, 33-47.
- GHOSH, P., SARKAR, S. & MAULIK, P. 2006. Sedimentology of a muddy alluvial deposit: Triassic Denwa Formation, India. *Sedimentary Geology*, 191, 3-36.
- GIBLING, M. R. 2006. Width and Thickness of Fluvial Channel Bodies and Valley Fills in the Geological Record: A Literature Compilation and Classification. *JOURNAL OF SEDIMENTARY RESEARCH*, 76, 731-770.
- GIRAUDI, C. 2005. Eolian sand in peridesert northwestern Libya and implications for Late Pleistocene and Holocene Sahara expansions. *Palaeogeography, Palaeoclimatology, Palaeoecology*, 218, 161-173.
- GLOVER, R. T. 1999. *Aspects of Intraplate Deformation in Saharan Cratonic Basins*. Ph D, University of Wales, Aberystwyth, 237 pp.

- GOUDARZI, G. H. 1980. Structures - Libya *In*: M.T, S. M. J. A. B. (ed.) *The Geology of Libya*. Academic Press, London ,III, 879-892.
- GRADSTEIN, F. M., OGG, J. G. & SMITH, A. 2004. *A geologic time scale 2004*, Cambridge University Press, Cambridge, 589 pp.
- GRAY, C. 1971. Structure and origin of the Gharian Domes. *In*: GRAY, C. (ed.) *In: Sympoisum on the Geology of Libya*. Faculty of Science, University of Libya, 307-319 pp.
- GRIGANI, D., LANZONI, E. & ELTRASH, H. 1991. Palaeozoic and Mesozic subsurface palynostratigraphy in the AL Kurfrah basin, Libya. *In*: SALEM, M. J., HAMMUDA, O. S. & ELIAGOUBI, B. A. (eds.) *The geology of Libya*. Academic press, London, IV,1159-1229.
- GRILL, B. & ZUSCHIN, M. 2001. Modern shallow- to deep-water bivalve death assemblages in the Red Sea -- ecology and biogeography. *Palaeogeography, Palaeoclimatology, Palaeoecology*, 168, 75-96.
- GUIRAUD, R. 1998. Mesozoic rifting and basin inversion along the northern African Tethyan margin: an overview. *Geological Society, London, Special Publications*, 132, 217-229.
- GUIRAUD, R., BINKS, R. M., FAIRHEAD, J. D. & WILSON, M. 1992. Chronology and geodynamic setting of Cretaceous-Cenozoic rifting in West and Central Africa. *Tectonophysics*, 213, 227-234.
- GUIRAUD, R. & MAURIN, J.-C. 1992. Early Cretaceous rifts of Western and Central Africa: an overview. *Tectonophysics*, 213, 153-168.
- GUMATI, Y. D. & NAIRN, E. M. 1991. Tectonic subsidence of the Sirte basin, Libya. *Petroleum geology*, 14, 93-102.
- HAGAN, G. M. & LOGAN, B. W. 1974. History of Hutchison Embayment tidal flat, shark bay, Western Australia. *AAPG Memoir*, 22, 283-315.

- HALLETT, D. 2002. *Petroleum Geology of Libya*. Elsevier Science B.V. Amsterdam , the Netherlands, 235pp.
- HAMMUDA, O. S., SBETA, A. M. & ELIAGOUBI, B. A. 1985. *Stratigraphic nomenclature of the Northwestern offshore of Libya* The Earth Society of Libya, 166 pp.
- HAQ, B. U. & AL-QAHTANI, A. M. 2005. Phanerozoic cycles of sea-level change on the Arabian Platform. *GeoArabia*, 10, 127-160.
- HAQ, B. U., HARDENBOL, J. & VAIL, P. R. 1987. Chronology of fluctuating sea-level since the Triassic. *Science*, 4793, 1156-1167.
- HARDCASTLE, K. C. 1989. Possible paleostress tensor configuration derived from fault-slip data in eastern Vermont and eastern New Hampshire. *Tectonics*, 8, 265-284.
- HARDENBOL, J., THIERRY, J., FARLEY, M. B., JACQUIN, T., DE GRACIANSKY, P.-C. & VAIL, P. R. 1998. Jurassic chronostratigraphy. In: IN: DE GRACIANSKY, P.-C., HARDENBOL, J., JACQUIN, T., VAIL, P.R. (EDS.) (ed.) *Mesozoic and Cenozoic Sequence Stratigraphy of European Basins. Society of Economic Paleontologists and Mineralogists Special Publication 60 (chart)*
- HARMS, J. C., SOUTHARD, J. B., SPEARING, D. R. & WALKER, R. G. 1975. *Depositional environments as interpreted from primary sedimentary structures and stratification sequences*, Soc. Econ. Palaont, 161.
- HASIOTIS, S. T. 2004. Using Trace fossils to differentiate between Alluvial, Lacustrine, Eolian and Marine Paleoenvironments. *AAPG Hedberg Conference*. Baku, Azerbaijan, 5pp.
- HASSAN, H. S. 2009. *Major tectonic elements of Libya*. <http://sepmstrata.org/Libya-Hassan/Regional-Geology-Libya.html> [Online]. Available:

<http://sepmstrata.org/Libya-Hassan/Regional-Geology-Libya.html> [Accessed 2011].

HAY, R. L. & REEDER, R. J. 1978. Calcretes of Olduvai Gorge and the Ndolanya beds. *Sedimentary Geology*, 25, 649-673.

HECHT, F., FURST, M. & KLITZSCH, E. 1964. Zur Geologie von Libyen (Contribution a la geologie de la Libye) *Geol. Rundschau Dtsch*, 53, No.2, 431-470.

HEIN, F. J. & WALKER, R. G. 1977. Bar evolution and development of stratification in the gravelly, braided, Kicking Horse River, British Columbia. *Canadian Journal of Earth Sciences*, 14, 562-570.

HERTWECK, G., WEHRMANN, A. & LIEBEZEIT, G. 2007. Bioturbation structures of polychaetes in modern shallow marine environments and their analogues to Chondrites group traces. *Palaeogeography, Palaeoclimatology, Palaeoecology*, 245, 382-389.

HEWARD, A. P. 1978. Alluvial fan sequence and megasequence models: with examples from Westphalian D - Stephanian B coalfields, northern Spain. In: MIALL, A. D. E. (ed.) *Fluvial sedimentology*. Canadian Society of Petroleum Geologists, Memoir, 5, 669-702.

HILDEBRANDT, C. & EGENHOFF, S. 2007. Shallow-marine massive sandstone sheets as indicators of palaeoseismic liquefaction -- An example from the Ordovician shelf of Central Bolivia. *Sedimentary Geology*, 202, 581-595.

HILLIER, R. D., MARRIOTT, S. B., WILLIAMS, B. P. J. & WRIGHT, V. P. 2007. Possible climate variability in the Lower Old Red Sandstone Conigar Pit Sandstone Member (early Devonian), South Wales, UK. *Sedimentary Geology*, 202, 35-57.

- HOLDSWORTH, R. J. & TURNER, J. P. 2002. *Extensional tectonics: Faulting and related processes.* , Key Issues in Earth Sciences. Bath , UK, The Geological Society, 328 pp.
- HOLMES, M. A. 1995. PEDOGENIC ALTERATION OF BASALTS RECOVERED DURING LEG 144. *Papers in the Earth and Atmospheric Sciences*, 144, 381-398.
- HOUNSLOW, M. W., HU, M., MØRK, A., WEITSCHAT, W., VIGRAN, J. O., KARLOUKOVSKI, V. & ORCHARD, M. J. 2008. Intercalibration of Boreal and Tethyan time scales: the magnetobiostratigraphy of the Middle Triassic and the latest Early Triassic from Spitsbergen, Arctic Norway. *Polar Research*, 27, 469-490.
- HOUNSLOW, M. W. & MUTTONI, G. 2010. The geomagnetic polarity timescale for the Triassic: linkage to stage boundary definitions. *Geological Society, London, Special Publications*, 334, 61-102.
- HUBERT, J. F. & HYDE, M. G. 1982. Sheet-flow deposits of graded beds and mudstone on an alluvial sandflat-playa system: Upper Triassic Blomidon redbeds, St Mary's Bay, Nova Scotia. *International Association of Sedimentologists*, 457-474.
- IMAGE, S. D. D. <http://www.geomapapp.org> & Ryan et al [Online]. [Accessed 2009].
- IRELAND, R. J., POLLARD, J. E., STEEL, R. J. & THOMPSON, D. B. 1978. INTERTIDAL SEDIMENTS AND TRACE FOSSILS FROM THE WATERSTONES (SCYTHIAN–ANISIAN?) AT DARES BURY, CHESHIRE. *Proceedings of the Yorkshire Geological and Polytechnic Society*, 41, 399-436.

- IRVING, E. & IRVING, G. A. 1982. Apparent polar wander paths carboniferous through cenozoic and the assembly of Gondwana. *Surveys in Geophysics*, 5, 141-188.
- KEARSEY, T. 2009. *Multi-proxy palaeoclimate reconstruction of the Permian-Triassic mass extinction event. PhD. Thesis, Plymouth University, UK, 285 pp.*
- KEY, R. M., SMITH, R. A., SMELROR, M., POWELL, J. H., THORSNES, T., NJANGE, F., SÆTHER, O. M. & ZANDAMELA, E. B. 2008. Revised lithostratigraphy of the Mesozoic-Cenozoic succession of the onshore Rovuma Basin, northern coastal Mozambique, 1-30 pp.
- KHADKIKAR, A. S., MERH, S. S., MALIK, J. N. & CHAMYAL, L. S. 1998. Calcretes in semi-arid alluvial systems: formative pathways and sinks. *Sedimentary Geology*, 116, 251-260.
- KHALAF, F. I. & GABER, A. S. 2008. Occurrence of cyclic palustrine and calcrete deposits within the lower Pliocene Hagul formation, East Cairo district, Egypt. *Journal of African Earth Sciences*, 51, 298-312.
- KILANI-MAZRAOUI, RAZGALLAH-GARGOURI, S. & RAZGALLAH-GARGOURI, B. 1990. Mannai-Tayech, The Permo-Triassic of Southern Tunisia ^ Biostratigraphy and palaeoenvironment. *Palaeobot. Palynol.* 66, 273,291.
- KIRSSCHVINK, J. L. 1980. The least-squares line and plane and the analysis of palaeomagnetic data. *Geophysical journal*, 62, 699-718.
- KLEIN, G. D. 1963. Bay of Fundy intertidal zone sediments. *sedimentary Petrology*, 33, 844-854.
- KLETT, T. R. 2002. Total Petroleum Systems of the Pelagian Province, Tunisia, Libya, Italy, and Malta—The Bou Dabbous– Tertiary and Jurassic-Cretaceous Composite. *U.S. Geological Survey Bulletin 2202-D.*

- KLITZSCH, E. 1970. Die strukturgeschichte der zentral-Sahara: Neue Erkenntnisse zum Bau und zur Palaeographie eines Tafellandes. *Geol.Rundsch*, 59 (2), 459-527.
- KLITZSCH, E. 1971. The structural development of the part of north Africa since Cambrian time *In: The Geology of Libya . Tripoli University, Faculty of Science, Tripoli, 253-262 pp.*
- KNIGHT, K. B., NOMADE, S., RENNE, P. R., MARZOLI, A., BERTRAND, H. & YOUNG, N. 2004. The Central Atlantic Magmatic Province at the Triassic-Jurassic boundary: paleomagnetic and $^{40}\text{Ar}/^{39}\text{Ar}$ evidence from Morocco for brief, episodic volcanism. *Earth and Planetary Science Letters*, 228, 143-160.
- KNUT, B. 1989. *Sedimentology and petroleum geology*. Springer-Verlag. 363p.
- KOMATSU, T., CHEN, J.-H., CAO, M.-Z., STILLER, F. & NARUSE, H. 2004. Middle Triassic (Anisian) diversified bivalves: depositional environments and bivalve assemblages in the Leidapo Member of the Qingyan Formation, southern China. *Palaeogeography, Palaeoclimatology, Palaeoecology*, 208, 207-223.
- KONO, M. 2006. Ships' Logs and Archeomagnetism. *American Association for the Advancement of Science*, 312, 865.
- KONRÁD, G., SEBE, K., HALÁSZ, A. & BABINSZKI, E. 2010. Sedimentology of a Permian playa lake: the Boda Claystone Formation, Hungary. *Geologos*, 16, 27-41.
- KROH, F. & WILLIAMSON, P. E. 2005. Preliminary AVO results from the Bremer Sub-basin, SW Australia. *Preview, Australian Society of Exploration Geophysicists* 118, 15-18.
- KRYNINE, P. D. 1948. The origin of red beds *Trans.N.y. Acad.Sci*, 11,60-68.

- KRYNINE, P. D. 1950. Petrology, stratigraphy and origin of the Triassic sedimentary rocks of connecticut. *Bull. Conn. Geol.Nat.Hist.Surv*, 73, 239 pp.
- KÜRSCHNER, W. M. & HERNGREEN, G. F. W. 2010. Triassic palynology of central and northwestern Europe: a review of palynofloral diversity patterns and biostratigraphic subdivisions. *Geological Society, London, Special Publications*, 334, 263-283.
- LABOURDETTE, R. & JONES, R. R. 2007. Characterization of fluvial architectural elements using a three-dimensional outcrop data set: Escanilla braided system, South-Central Pyrenees, Spain, *Geosphere*, 6, 422-434.
- LACHENBRUCH, A. H. 1962. Mechanics of thermal contraction cracks and ice-wedge polygon on permafrost. *Geo.Soc.AM* 70, 1-69.
- LAGHA, S. 1977. Petrography of the Triassic phosphorites in Gharyan area, NW Libya. *Petroleum research Journal (Libya)*, 9, 45-50.
- LEEDER, M. 1999. *Sedimentology and sedimentary basins from turbulence to tectonics*, Blackwell Science, 592 pp.
- LEHRMANN, D. J., PAYNE, J. L., FELIX, S. V., DILLETT, P. M. & YOUYI YU, H. W. 2003. Permian-Triassic boundary section from shallow-marine carbonate platforms of the Nanpanjiang basin, south China: Implications for oceanic conditions associated with the end -Permian extinction and its aftermath. *Palaios*, 18, 138-152.
- LETOUZEY, P. A., REYMOND, A., DARTOLS, F., DEBARRE, R. & GODART, Y. 2005. Petroleum potential of the Ghadamis basin, Libya. *AAPG International Conference and Exhibition. Paris*, 5 pp.
- LIPPARINI, T. 1940. Tectonics and Geomorphology, Tripolitania area, Libya. *Min of industry Geol. Soc. Bul.* 4, 222-301 pp.

- LIPPARINI, T. 1965. Tectonic and geomorphology of Tripolitania, Libya. *Ministry of Education, Kingdom of Libya, Bull. Italia, No. 4, 44 pp.*
- LOGAN, B. W., REZAK, R. & GINSBURG, R. N. 1964. Classification and Environmental Significance of Algal Stromatolites. *The Journal of Geology, 72, 68-83.*
- LOTTAROLI, F., CRAIG, J. & THUSU, B. 2009. Neoproterozoic-Early Cambrian (Infracambrian) hydrocarbon prospectivity of North Africa: a synthesis. *Geological Society, London, Special Publications, 326, 137-156.*
- LOUGHNAN, F. C., KO, M. K. & BAYLISS, P. 1964. The red-beds of the Triassic Narrabeen group. *Journal of the Geological Society of Australia, 11, 65 - 77.*
- LUCAS, S. G. 2010. The Triassic timescale: an introduction. *Geological Society, London, Special Publications, 334, 1-16.*
- MACGREGOR, D. S. & MOODY, R. T. J. 1998. Mesozoic and Cenozoic petroleum systems of North Africa. *Geological Society, London, Special Publications, 132, 201-216.*
- MACHETTE, M. N. 1985. Calcic soils of south-western United State. *Soc. Am Spec. Pap. No, 203, 1-21.*
- MAGNIER, P. 1963. Etude stratigraphique dans le Gebel Nefousa et le Gebel Garian (Tripolitaine, Libya). *Bulletine-Societe Geologique de, 5, 89-94.*
- MAHER, E. & HARVEY, A. M. 2008. Fluvial system response to tectonically induced base-level change during the late-Quaternary: The Rio Alias southeast Spain. *Geomorphology, 100, 180-192.*
- MAKHLOUF, I. M. 2003. Depositional Environments of the Late Triassic/Early Jurassic Abu Shaybah Formation along southern Neotethys. *Mu tah Lil-Buhuth wad-Dirasat, 18, 61-76.*

- MAKHLOUF, I. M. 2006. Late Triassic -Early Jurassic Neotethyan Evolution at Northern Gondwana. (Jordan and Libya, Mediterranean region). *Geologica Acta*, 4, 371-376.
- MARTIN, D., L., MUNROE, H. D. & NAIRN, A., EM. 1991. First results of the palaeomagnetic study of Libyan Mesozoic limestones: The Garnian Aziza Limestone Formation-preliminary data. In: SALEM, M., J & SBETA, A., M (eds.) *The Geology of Libya*. Elsevier, Amsterdam, 2433-2440 pp.
- MÁRTON, E. & NARDI, G. 1994. Cretaceous Palaeomagnetic Results From Murge (Apulia, Southern Italy): Tectonic Implications. *Geophysical Journal International*, 119, 842-856.
- MARZOUK, L. & YOUSSEF, M. B. 2008. Relative Sea-level changes of the Lower Cretaceous deposits in the chotts area of southern Tunisia. *Turkish J. Earth Sci*, 17, 835-845.
- MCCLAY, K. 1987. *The mapping of geological structures*, Open University Press.
- MCCLAY, K. R. 2002. Recent advances in analogue modelling: use in section interpretation and validation In: HOLDSWORTH, R. E. & TURNER, J. P. (eds.) *Extensional tectonics: Faulting and related processes*, 2, 185-209.
- MCFADDEN, P. L. & MCELHINNEY, M. W. 1988. The combined analysis of remagnetisation circle and direct observation in paleomagnetism. *Earth Planet.Sci.Lett*, 87, 161-172.
- MERNILD, S. H., HASHOLT, B. & LISTON, G. E. 2008. Climatic control on river discharge simulations, Zackenberg River drainage basin, northeast Greenland. *HYDROLOGICAL PROCESSES*, 22, 1932–1948.
- MERRILL, R. T. & MCEIHINNEY, M. W. 1983. *The Earth's magnetic field*, Academic press, London.

- MIALL, A. D. 1977. A review of the braided river depositional environment. *Earth Science Review*, 13, 1-62.
- MIALL, A. D. 1984. *Principles of sedimentary basin Analysis*, Springer-Verlage, 490 pp.
- MIALL, A. D. 1985. Architectural element analysis: a new methods of facies applied to fluvial deposits. *Earth Science Review*, 22, 261-308.
- MIALL, A. D. 1996. *The geology of fluvial deposits: Sedimentary facies, Basin Analysis, and Petroleum geology*, Springer-Verlage Berlin Heidelberg , 582.
- MICHALZIK, D. 2003. Facies sequence of Triassic-Jurassic red beds in the Sierra Mader Oriental (NE Mexico) and its relation to early of the Gulf of Mexico. *Sedimentary Geology*, 71, 243-259.
- MILLER, V. C. 1961. *Photogeology*, McGraw-Hill book company , INC. New York , 248 pp.
- MILLER, V. C. 1971. A preliminary investigation of the geomorphology of the Jebel Nefusa. In: GARY (ed.) *In: Symp. Geol Libya Univ. Libya, Tripoli*, 365-385 pp.
- MJØS, R. O., WALDERHAUG & PRESTHOLM, E. 1993. Crevasse splay sandstone geometries in the Middle Jurassic Ravenscrag Group of Yorkshire, UK. In: MAEZO, M. & PUIGDEFABREGAS (eds.) *Alluvial Sediment*. Blackwell Scientific Publications. 167-184.
- MONTY, C. L. V. 1966. Distribution and structure of recent stromatolitic algal, Eastern Andros Island, Bahams. *Ann.Soc. Geologique de Belgique*, 90, 55-100.
- MONTY, C. L. V. & HARDIE, L. A. 1976. The geological significance of the freshwater blue-green algal calcareous marsh. *Sedimentology*, 20, 447-477.
- MRIHEEL, I. Y. & ALHNAISH, A. S. 1995. Study of the Messinian carbonate-evaporite lithofacies offshore western Libya. *Terr Nova-Oxford*, 7, 213-220.

- MULLER, K. J. 1978. Conodonts and other phosphatic microfossils. *In*: HAQ, B. U. & BOERSMA, A. (eds.) *Introduction to Marine Micropaleontology*. Elsevier North-Holland, 376.
- MUTTONI, G., GAETANI, M., BUDUROV, K., ZAGORCHEV, I., TRIFONOVA, E., IVANOVA, D., PETROUNOVA, L. & LOWRIE, W. 2000a. Middle Triassic paleomagnetic data from northern Bulgaria: constraints on Tethyan magnetostratigraphy and paleogeography. *Palaeogeography, Palaeoclimatology, Palaeoecology*, 160, 223-237.
- MUTTONI, G., GAETANI, M., BUDUROV, K., ZAGORCHEV, I., TRIFONOVA, E., IVANOVA, D., PETROUNOVA, L. & LOWRIE, W. 2000b. Middle Triassic paleomagnetic data from northern Bulgaria: constraints on Tethyan megnetostigraphy and paleogeography. *Palaeogeography, Palaeoclimatology, Palaeoecology*, 160, 223-237.
- MUTTONI, G., GARZANTI, E., ALFONSI, L., CIRILLI, S., GERMANI, D. & LOWRIE, W. 2001. Motion of Africa and Adria since the Permian: paleomagnetic and paleoclimatic constraints from northern Libya. *Earth and Planetary Science Letters*, 192, 159-174.
- MUTTONI, G., KENT, D. V., BRACK, P., NICORA, A. & BALINI, M. 1997. Middle Triassic magnetostratigraphy and biostratigraphy from the Dolomites and Greece. *Earth and Planetary Science Letters*, 146, 107-120.
- MUTTONI, G., KENT, D. V. & CHANNELL, J. E. T. 1996. Evolution of Pangea: paleomagnetic constraints from the Southern Alps, Italy. *Earth and Planetary Science Letters*, 140, 97-112.
- MUTTONI, G., KENT, D. V., JADOUL, F., OLSEN, P. E., RIGO, M., GALLI, M. T. & NICORA, A. 2010. Rhaetian magneto-biostratigraphy from the Southern Alps

- (Italy): Constraints on Triassic chronology. *Palaeogeography, Palaeoclimatology, Palaeoecology*, 285, 1-16.
- MUTTONI, G., KENT, D. V., OLSEN, P. E., STEFANO, P. D., LOWRIE, W., BERNASCONI, S. M. & HERNÁNDEZ, F. M. 2004. Tethyan magnetostratigraphy from Pizzo Mondello (Sicily) and correlation to the Late Triassic Newark astrochronological polarity time scale. *GSA Bulletin*, 116, 1043–1058.
- NAKAJIM, T. 1982. Sedimentology and Uranium prospecting of the Siwliks in western Nepal, Geological Survey of Japan, 33, 593-612.
- NICHOLS, G. 1999. *Sedimentology and stratigraphy*, Blackwell Science Ltd, 355 pp.
- NICHOLS, G. 2009. *Sedimentology and Stratigraphy*, Wiley-Blackwell, A John Wiley and Sons, Ltd. 419 pp.
- NIELSEN, S. N. 2005. The Triassic Santa Juana Formation at the lower Biobío River, south central Chile. *Journal of South American Earth Sciences*, 19, 547-562p.
- NOAA. 2010. <http://www.ngdc.noaa.gov/geomagmodels/IGRFWMM.jsp> [Online]. [Accessed 2010].
- NOVOVIC, T. 1977b. *Geological map of Libya, 1:250,000 Sheet Nalut NH 32-4. Explanatory Booklet. Arabic sum. Industr. Res. Cent. Tripoli. 74.*
- OLSEN, H. & LARSEN, P. H. 1993. Structural and climatic controls on fluvial depositional system: Devonian, North-East Greenland. *Sediment*, 17, 401- 423 p.
- ÖZKAN, A. M. & ELMAS, A. 2009. Petrographic Characteristic of the Kızıloren Formation (Upper Triassic-Lower Jurassic) in the Akpınar (Konya - Turkey) Area. *Ozean Journal of Applied Sciences*, 4, 451-464.
- PAIK, I. S. & LEE, Y. I. 1998. Desiccation cracks in vertic palaeosols of the Cretaceous Hasandong Formation, Korea: genesis and palaeoenvironmental implications. *Sedimentary Geology*, 119, 161-179.

- PAREDES, J. M., FOIX, N., COLOMBO PIÑOL, F., NILLNI, A., ALLARD, J. O. & MARQUILLAS, R. A. 2007. Volcanic and climatic controls on fluvial style in a high-energy system: The Lower Cretaceous Matasiete Formation, Golfo San Jorge basin, Argentina. *Sedimentary Geology*, 202, 96-123.
- PEMBERTON, S. G., MACEACHERN, J. A. & FREY, R. W. 1992. Trace fossil facies models: environmental and allostratigraphic significance. *In: WALKER, R. G. & JAMES, N. P. (eds.) Facies models: response to sea level change* Geological Association of Canada, St Johns, Newfoundland, 47-72.
- PETIT, J. P. 1987. Criteria for the sense of movement on fault surfaces in brittle rocks. *Journal of Structural Geology*, 9, 597-608.
- PETTIJOHN, F. J., POTTER, P. E. & SIEVER, R. 1987. *Sand and Sandstone* Springer-Verlag New York, 553 pp.
- PICCOLI, G. 1971. *Outlines of Volcanism in Northern Tripolitania*, Symposium on the Geology of Libya. University of Libya, Tripoli, 232–331.
- PIZZI, G., C & GIUDICE, D. 1999. Modelling of the Western Jamahiriya aquifer system. *Managing Non-Renewable resource, Tripoli, Unesco/IHP-V TECHNICAL Documents in Hydrology*.
- PIZZI, G. & SARTORI, L. 1984. Groundwater management by means of a quasi-three-dimensional finite element flow model. *Challenges in African hydrology and water resources (Proceeding of the Harare Symposium)*, 144, 175-191.
- PLINT, A. G. 1983. Sandy fluvial point-bar sediments from the Middle Eocene of Dorset, England. *In: COLLINSON, J. D. & LEWIN, J. (eds.) Modern and Ancient fluvial system*. Oxford London: Black well Scientific Publications. 355-368.
- PLUMMER, P. S. & GOSTIN, V. A. 1981. Shrinkage cracks: Desiccation or syneresis? *Sedimentary Research*. 51, 1147-1156.

- POMONI-PAPAIOANNOU, F. & KARAKITSIOS, V. 2002. Facies analysis of the Trypali carbonate unit (Upper Triassic) in central-western Crete (Greece): an evaporite formation transformed into solution -collapse breccias. *Sedimentology* 49, 113-1132.
- POPE, M. C. 2004. Cherty carbonate facies of the Montoya Group, southern New Mexico and western Texas and its regional correlatives: a record of Late Ordovician paleoceanography on southern Laurentia. *Palaeogeography, Palaeoclimatology, Palaeoecology*, 210, 367-384.
- PRATT, D. 2000. Plate Tectonics: A Paradigm Under Threat. *Journal of Scientific Exploration*, Vol. 14, No. 3, 307–352.
- PRICE, N. J. & COSGROVE, J. W. 1990. *Analysis of Geological Structures*, Cambridge Univ. Press, 502 pp.
- PRONA, E. 1914. Per la geologia della Tripolitana. . *Atti R. Accad.Sci Torino*, 50, 26p.
- PYE, K. 1994. *Sediment transport and depositional processes*, Blackwell Scientific Publications, 397 pp.
- RAY, S. & CHAKRABORTY, T. 2002. Lower Gondwana fluvial succession of the Pench-Kanhan valley, India: stratigraphic architecture and depositional controls. *Sedimentary Geology*, 151, 243-271.
- READING, H. G. 1986. Sedimentary Environment and facies. In: READING, H. G. (ed.) *In Facies*. Second edition, Blackwell Science,
- READING.H.G 1996. *Sedimentary Environments and facies*, Blackwell Scientific, London, 688 pp..
- REINECK, H. E. & SINGH, I. B. 1975. *Depositional sedimentary environments* Springer Verlage Berlin Heidelberg New York, 439.

- RETALLACK, G. J. 1988. Field recognition of paleosols *In*: REINHART, J. & SIGLEO, W. R. (eds.) *Paleosols and weathering through time : Principle and Application*:. Geological Society of America Paper 216, 1.20.
- RETALLACK, G. J. 2001. *Soil of the past: An introduction to paleopedology*, Blackwell Science, Oxford, 404 pp.
- RICHTER, R. 1936. Marken und Spuren in Hunsruckschiefer. *I.Schichtung und Grundleben.Senckenbergiana*, 18, 215-244.
- RODRÍGUEZ-LÓPEZ, J. P., MELÉNDEZ, N., DE BOER, P. L. & SORIA, A. R. 2010. The action of wind and water in a mid-Cretaceous subtropical erg-margin system close to the Variscan Iberian Massif, Spain. *Sedimentology*, 57, 1315-1356.
- ROHL, U., RAS, V. U. & WIRSING, G. 1992. Microfacies, paleoenvironment, and facies-dependent carbonate diagenesis in upper Triassic platform carbonates off northwest Australia. *Proceedings of the Ocean drilling program, Scientific results*, 122, 129-147.
- RUFFELL, A., MCKINLEY, J. M. & WORDEN, R. H. 2002. Comparison of clay mineral stratigraphy to other proxy palaeoclimate indicators in the Mesozoic of NW Europe. *Phil. Trans. R. Soc. Lond*, 360, 675-693.
- RYAN, K. M. 2008. *Fluvial architecture of the Interval spanning the pttsburgh and fishpot limestones (Late pennsylvanian) southeastern Ohio*. Master of Science The college of Arts and Sciences of Ohio University, 124 pp.
- SAADI, N. M., ABOUD, E., SAIBI, H. & WATANABE, K. 2008. Integrating data from remote sensing and gravity for geological investigation in the Tarhunah area, Northwest Libya. *International Journal of Digital Earth*, 1, 347-366.

- SAADI, N. M., ABOUD, E. & WATANABE, K. 2009. Integration of DEM, ETM+, Geologic, and Magnetic Data for Geological Investigations in the Jifara Plain, Libya. *Geoscience and Remote Sensing, IEEE Transactions on*, 47, 3389-3398.
- SADALMELIK. 2007. *Topographic map of Libya. Created with GMT from public domain GLOBE data.* http://en.wikipedia.org/wiki/File:Libya_Topography.png [Online]. [Accessed 2010].
- SALTZMAN, M. R. 2003. Organic Carbon Burial and Phosphogenesis in the Antler Foreland Basin: An Out-of-Phase Relationship During the Lower Mississippian. *JOURNAL OF SEDIMENTARY RESEARCH*, 73, 844-855.
- SCHANDELMEIER, H. & REYNOLDS, P. O. 1997. Palaeogeographic-palaeotectonic atlas of the North-Eastern Africa, and adjacent areas. *Balkema, Rotterdam*, 160 pp.
- SCHMID, S., WORDEN, R. H. & FISHER, Q. J. 2006. Sedimentary facies and the context of dolocrete in the Lower Triassic Sherwood Sandstone group: Corrib Field west of Ireland. *Sedimentary Geology*, 187, 205-227.
- SCHNEIDER, D. A. & KENT, D. V. 1990. Paleomagnetism of Leg 115 sediments: Implications for Neogene magnetostratigraphy and paleolatitude of the Reunion hotspot. *Proc. ODP Sci. Results*, 115, 717-736.
- SCHÖNING, M. & BANDEL, K. 2004. A diverse assemblage of fossil hardwood from the Upper Tertiary (Miocene?) of the Arauco Peninsula, Chile. *Journal of South American Earth Sciences*, 17, 59-71.
- SCHUMM, S. A. 1972. Fluvial palaeochannels. In: RIGBY, J. K. & HAMBLIN, W. K. (eds.) *Recognition of ancient sedimentary environments*. Soc. Econ. Palaeontol. Mineral, Spec. Publ, 16.98-107.
- SCHUMM, S. A. 1977. *The Fluvial System*, New York, 338.
- SCHUMM, S. A. 1985. Patterns of alluvial rivers. *Ann. Rev. Earth Planet.Sci*, 13, 5-27.

- SEDDIQ, H. 2004. Libya: Exploration overview and future opportunities. *United Nations Conference Trade and development 8th Africa oil and gas, Tradw and Finance conference and exhibition*. Morocco, United Nations.1.
- SEILACHER, A. 1967. Bathymetry of trace fossils. *Marine Geology*, 5, 413-428.
- SELLEY, R. C. 1976. *An introduction to sedimentology*, Academic Press Inc. (London) Ltd, 408 pp.
- SELLEY, R. C. 1985. *Ancient Sedimentary Environments and their sub-surface diagnosis*, London, Chapman and Hall.
- SELLEY, R. C. 2000. *Applied sedimentology, Second edition*. Academic Press, 523.
- SENGOR, A. M. 1979. Mid-Mesozoic closure of Permo-Triassic Tethys and its implication. *Nature*, 279, 590-539.
- SENGOR, A. M. 1984. The Cimmeride orogenic system and the tectonic of Eurasia. *Geol.Soc. AM. Spec*, 195, 82.
- SENGOR, A. M. 1985. The Story of Tethys: How many wives did Okeanos have? *Episodes*, 8, 3-129.
- SHEMESH, A., KOLODNY, Y. & LUZ, B. 1983. Oxygen isotope variations in phosphate of biogenic apatites, II. Phosphorite rocks. *Earth and Planetary Science Letters*, 64, 405-416.
- SIMMS, M. J. 2004. TORTOISES AND HARES: DISSOLUTION, EROSION AND ISOSTASY IN LANDSCAPE EVOLUTION. *Earth Surface Processes and Landforms Earth Surf. Process. Landforms*, 29, 477-497.
- SIMPSON, E. L., HILBERT-WOLF, H. L., SIMPSON, W. S., TINDALL, S. E., BERNARD, J. J., JENESKY, T. A. & WIZEVICH, M. C. 2008. The interaction of aeolian and fluvial processes during deposition of the Upper Cretaceous capping sandstone member, Wahweap Formation, Kaiparowits Basin, Utah, U.S.A. *Palaeogeography, Palaeoclimatology, Palaeoecology*, 270, 19-28.

- SINCLAIR, H. D., SAYER, Z. R. & TUCKER, M. E. 1998. Carbonate sedimentation during early foreland basin subsidence: the Eocene succession of the French Alps. *Geological Society, London, Special Publications*, 149, 205-227.
- SMITH, N. D. 1970. The Braided Stream Depositional Environment: Comparison of the Platte River with Some Silurian Clastic Rocks, North-Central Appalachians. *Geological Society of America Bulletin*, 81, 2993-3014.
- SOUGNEZ, N. & VANACKER, V. 2011. The topographic signature of Quaternary tectonic uplift in the Ardennes massif (Western Europe). *Hydrol. Earth Syst. Sci.*, 15, 1095–1107.
- STAMPFLI, G. M. & BOREL, G. D. 2002. A plate tectonic model for the Paleozoic and Mesozoic constrained by dynamic plate boundaries and restored synthetic oceanic isochrons. *Earth and Planetary Science Letters*, 196, 17-33.
- STECKLER, M. S., BERTHELOT, F., LYBERIS, N. & LE PICHON, X. 1988. Subsidence in the gulf of suez: implications for rifting and plate kinematics. *Tectonophysics*, 153, 249-270.
- STRAATEN, L. M. U. V. 1950. Environment of formation and facies of the Wadden sea sediments. *Noninklyl. ned. Aardirjksde Genootschap*, 67, 354-368.
- STRAATEN, L. M. U. V. 1954. Sedimentology of recent tidal flat deposits and the psammities du condeoz (Devonian). *Geologie en Nijnbouw*, 2, 25-44.
- http://www.pesa.com.au/publications/pesa_news/feb_06/pesanews_8026.html .
- [Online]. [Accessed accessed 4/5/2009].
- SWIRE, P. H. & GASHGESH, T. M. 2000. Concession 9 and surround the bio-chrono- and lithostratigraphy and hydrocarbon prospectivity of the northwest Ghadames basin and Jafarah Plain. 52 pp.
- SWIRE, P. H. & GASHGESH, T. M. 2004. The Bio-Chrono and Lithostratigraphy and hydrocarbon prospectivity of the NW Ghadamis and Jifarah Trough. *In:*

- SALEM, J. & OUN, K., M (eds.) *Second Symposium The Geology of NW Libya*
I. Sedimentary Basin of Libya. Tripoli, 1: 173-215.
- TAKASHIMA, R. E. I. S. H. I., N ISHI, H. I., HUBER, T. & L E C K I E, M. 2006.
 Greenhouse world and the Mesozoic Ocean. *The Oceanography Society*, 19. No.
 4, 82-92.
- TARLING, D. H. 1971. *Principles and applications of palaeomagnetism*, Chapman and
 Hall.164 pp.
- TAUXE, L. 2007. [http/ earthref.org/ MAGIC/ books/ Tauxe](http://earthref.org/MAGIC/books/Tauxe) [Online]. [Accessed 2010].
- TAUXE, L., TUCKER, N. P., PETERSEN, J. L. & LABRECQUE 1983. The
 magnetostratigraphy of Leg 173 sediments, *Palaeogeogr. Palaeoclimatol.*
Palaeoecol, 42, 65-90.
- TAWADROS, T. 2001. *Geology of Egypt and Libya*. , Balkema, Rotterdam, 461p.
- THE ROCK COLOR CHART COMMITTEE, U. S. G. S. 2009. Rock Color Chart:
 With genuine Munsell color chips. *The Geological Society of America, Boulder,*
Colorado.
- TUCKER, M. E. 1982. *The field description of sedimentary rocks* Geological society of
 London hand book .
- TUCKER, M. E. 1985. Shallow-marine carbonate facies and facies models.
GEOLogical Society, London, Special publications, 18, 147-169.
- TUCKER, M. E. 2001. *Sedimentary petrology*, blackwell Science, Oxford, 272 pp.
- TUCKER, M. E. 2003. *Sedimentary rocks in the field.*, Wiley Blackwell Chichester.
 234 pp.
- TUCKER, M. E. & WRIGHT, V. P. 1990. *Carbonates Sedimentology.*, Blackwell
 Secientific Pubbblication, 482 pp.
- TURNER, B. R. 1980a. Palaeozoic Sedimentology of the southeastern part of Al
 Kufrah Basin, Libya: A model for oil exploration. *In: SELAM, M. J. &*

- BUSREWILL, M. T. (eds.) *The geology of Libya*, cademic press, London, 351-374.
- TURNER, P. 1980b. *Dvelopments in Sedimentology : Continental red bed*, Elsevier Scientific Publiishing company Amstrerdam - Oxford - New York. 562 pp.
- ULAK, P. D. 2009. Lithostratigraphy and late Cenozoic fluvial styles of Siwalik Group along Kankai River section, East Nepal Himalaya. *Nepal*, 12, 63–74.
- VAIL, J. R. 1991. The Percambrian teconic structures of north Africa. *In*: SALEM, M. J., SBETA, A. M. & BAKBAK, M. R. (eds.) *The geology of Libya*. Elsevier, Amsterdam,Vi, 2259-2268.
- VAN DER VOO, R. 1993. *Paleomagnetism of the Atlantic, Tethys and Iapetus Oceans* Cambridge University Press, 424 pp.
- VAN HOUTEN, F. B. 1948. Origin of red banded Early Cenozoic deposits in rocky mountain region. *Bull. Amer. Assoc. Petrol. Geol.*, 32, 2083-2126.
- VANDEGINSTE, V., SWENNEN, R., GLEESON, S. A., ELLAM, R. M., OSADETZ, K. & ROURE, F. 2006. Development of secondary porosity in the Fairholme carbonate complex (southwest Alberta, Canada). *Journal of Geochemical Exploration*, 89, 394-397.
- VAROL, B., ALTLNER, D. & OKAN, Y. 1988. Dasycladacean algae from the Mesozoic carbonate facies of the Sariz-Tufanbeyli autochthon (Kayseri,SE Turkey). *Mineral Res .Expl. Bull*, 108, 49-56p.
- VONEYNATTEN, H., KRAWINKEL, H. & WINSEMANN, J. 1993. Plio-Pleistocene outer arc basinss in southern central America (Osa Peninsula, Costa Rica). *Sedimentary Geology*, 20, 399-414.
- WALKER, R. G. 1992. Facies, facies models and modern stratigraphic concepts. *In*: IN WALKER, R. G. & JAMES, N. P. (eds.) *Facies model, Respons to Sea level change*. Geological Association, 1-14.

- WARD, P. D., MONTGOMERY, D. R. & SMITH, R. 2000. Altered River Morphology in South Africa Related to the Permian-Triassic Extinction. *Science*, 289, 1740-1743.
- WEAVER, R., ROBERTS, A. P. & BARKER, A. J. 2002. A late diagenetic (syn-folding) magnetization carried by pyrrhotite: implications for paleomagnetic studies from magnetic iron sulphide-bearing sediments. *Earth and Planetary Science Letters*, 200, 371-386.
- WEINBERGER, R. 1999. Initiation and growth of cracks during desiccation of stratified muddy sediments. *Journal of Structural Geology*, 21, 379-386.
- WILSON, M. & GUIRAUD, R. 1992. Magmatism and rifting in Western and Central Africa, from Late Jurassic to Recent times. *Tectonophysics*, 213, 203-225.
- WINSTANLEY, I. 1990. *Collins dictionary of geology*, Collins and Glasgow, 565.
- WOLELA, A. 2008. Sedimentation of the Triassic-Jurassic Adigrat Sandstone Formation, Blue Nile (Abay) Basin, Ethiopia. *Journal of African Earth Sciences*, 52, 30-42.
- WRAY, J. L. 1978. Calcareous algae. In: HAQ, B. U. & BOERSMA, A. (eds.) *Introduction to marine micropaleontology*. Elsevier North-Holland, 376 pp.
- WRIGHT, V. P. 1994. Losses and grains in weathering profiles and duripans. In: PARKER, A. & SELLWOOS, B. W. (eds.) *Quantitative diagenesis: Recent development and application to reservoir geology*. Mathematical and Physical Sciences, 453.95-123.
- WRIGHT, V. P. & TUCKER, M. E. 1991. Calcretes: An introduction. In: WRIGHT, V. P. & TUCKER, M. E. (eds.) *Calcretes. Introduction* Association Sedimentologists. Reprint Series 2, 1-22.

- YOURI, H. & GILLES, M. 2008. Facies architecture and cyclicity in a mosaic carbonate platform: effects of fault-block tectonics (Lower Lias, Causses platform, south-east France). *Sedimentology*, 55, 155-178.
- YU, Y. & TAUXE, L. 2006. Acquisition of viscous remanent magnetization. *Physics of the Earth and Planetary Interiors*, 159, 32-42.
- ZIEGLER, P. A., CLOETINGH, S., GUIRAUD, R. & STAMPFLI, G. M. 2001. Peri-Tethyan platform: constraints on dynamics of rifting and basin inversion. *In*: P.A.ZIEGLER, R, W. C., A.H.F. ROERTSON AND S. CRASQUIN-SOLEAU (ed.) *Pre-Tethys Memoir 6: Pre-Tethyan Rift / Wrench Basins and Passive Margins.*: Mem. Mus. Natn. Hist. Nat, 186.9-49.
- ZIJDERVELD, J. D. A. 1967. demagnetisation of rocks: Analysis of result. *In*: COLLINSON, D. W. A. R., S. K. (ed.) *Methods in Palaeomagnetism*, 254-286.

Appendix 1

X- Ray diffraction data

Code AB-22

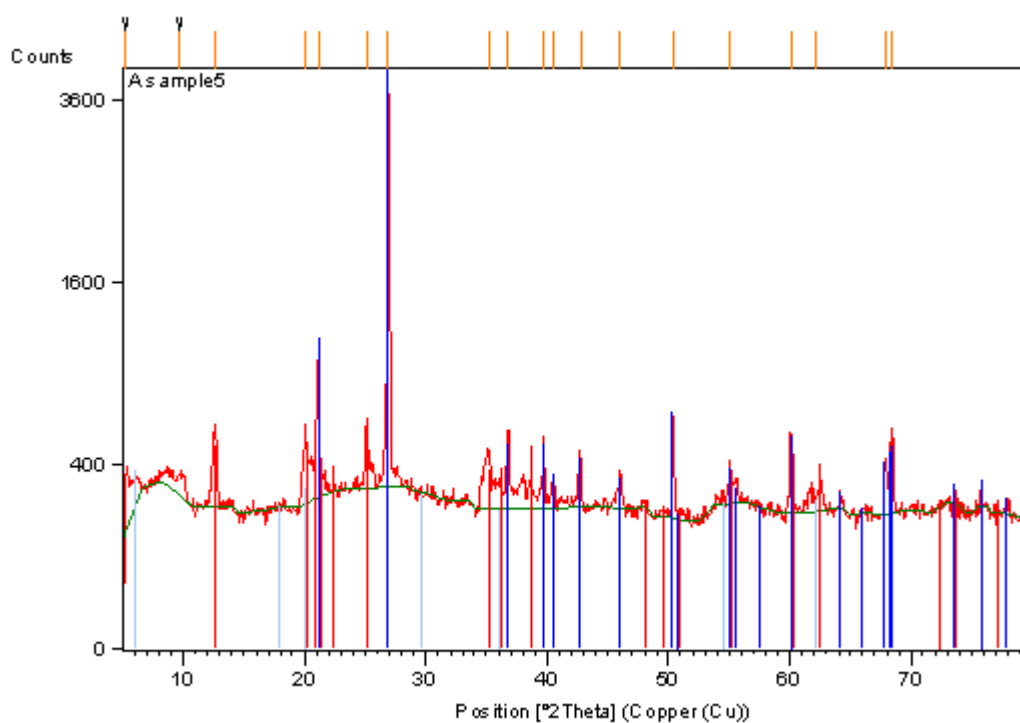
Peak List

| Pos. [°2Th.] | Height [cts] | FWHM [°2Th.] | d-spacing [Å] | Rel. Int. [%] |
|--------------|--------------|--------------|---------------|---------------|
| 5.2775 | 173.24 | 0.2362 | 16.74555 | 4.58 |
| 9.6318 | 72.10 | 0.9446 | 9.18284 | 1.91 |
| 12.5966 | 365.96 | 0.2362 | 7.02737 | 9.68 |
| 20.0759 | 354.89 | 0.3149 | 4.42304 | 9.38 |
| 21.0985 | 742.85 | 0.2362 | 4.21091 | 19.64 |
| 25.1458 | 338.71 | 0.2362 | 3.54159 | 8.96 |
| 26.8926 | 3781.78 | 0.2362 | 3.31538 | 100.00 |
| 35.1877 | 247.05 | 0.3936 | 2.55051 | 6.53 |
| 36.8343 | 246.69 | 0.4723 | 2.44019 | 6.52 |
| 39.6942 | 308.80 | 0.2362 | 2.27073 | 8.17 |
| 40.5151 | 121.22 | 0.2362 | 2.22659 | 3.21 |
| 42.7011 | 205.50 | 0.2362 | 2.11753 | 5.43 |
| 46.0392 | 138.44 | 0.3149 | 1.97148 | 3.66 |
| 50.3760 | 421.54 | 0.2362 | 1.81146 | 11.15 |
| 55.0528 | 177.28 | 0.2362 | 1.66813 | 4.69 |
| 60.1614 | 308.72 | 0.2362 | 1.53812 | 8.16 |
| 62.1358 | 54.22 | 0.9446 | 1.49391 | 1.43 |
| 67.8996 | 220.43 | 0.2362 | 1.38045 | 5.83 |
| 68.4066 | 232.13 | 0.3840 | 1.37032 | 6.14 |

Pattern List

| Visible | Ref. Code | Score | Compound Name | Displ. [°2Th] |
|------------|--|-------|---------------|---------------|
| Scale Fac. | Chem. Formula | | | |
| * | 00-001-0527 | 32 | Kaolinite | 0.315 |
| 0.079 | Al ₂ Si ₂ O ₅ (OH) ₄ | | | |
| * | 01-083-0539 | 78 | Quartz, syn | 0.267 |
| 1.003 | Si O ₂ | | | |

Graphics



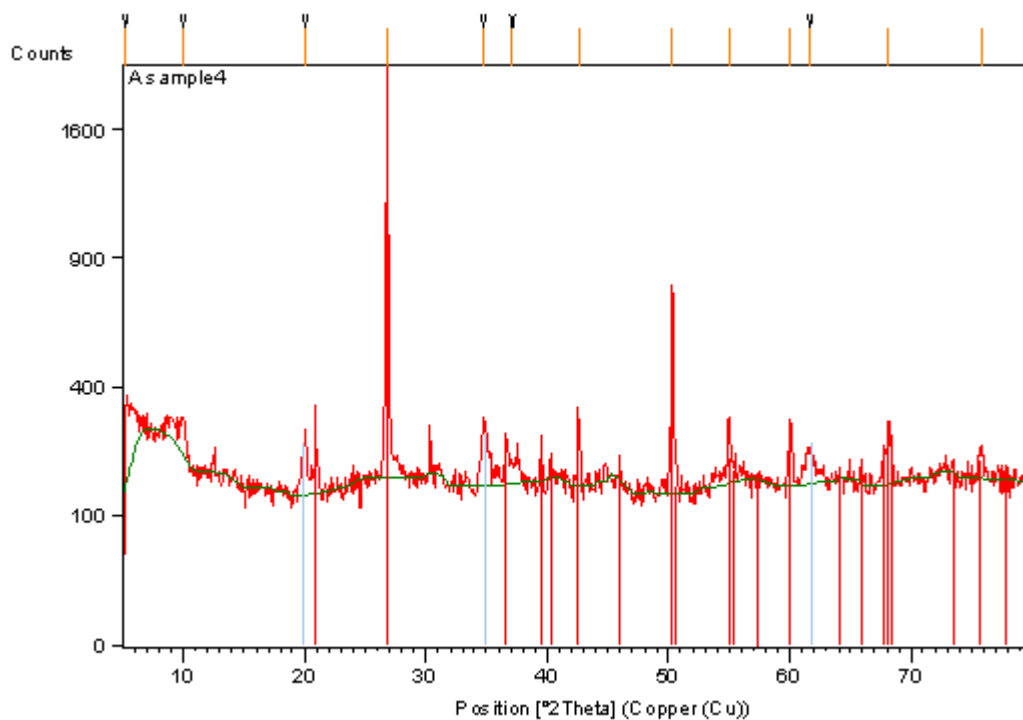
Code AB-23

Peak List

| Pos. [°2Th.] | Height [cts] | FWHM [°2Th.] | d-spacing [Å] | Rel. Int. [%] |
|--------------|--------------|--------------|---------------|---------------|
| 5.2759 | 170.08 | 0.2362 | 16.75045 | 9.12 |
| 10.0092 | 90.26 | 0.4723 | 8.83742 | 4.84 |
| 20.0565 | 108.90 | 0.3149 | 4.42726 | 5.84 |
| 26.8027 | 1865.37 | 0.1574 | 3.32629 | 100.00 |
| 34.7926 | 159.86 | 0.3149 | 2.57856 | 8.57 |
| 37.0980 | 42.14 | 0.9446 | 2.42345 | 2.26 |
| 42.6052 | 140.71 | 0.2362 | 2.12208 | 7.54 |
| 50.3170 | 651.33 | 0.2362 | 1.81344 | 34.92 |
| 55.0344 | 145.03 | 0.2362 | 1.66864 | 7.78 |
| 60.0612 | 158.08 | 0.2362 | 1.54045 | 8.47 |
| 61.6992 | 73.35 | 0.9446 | 1.50343 | 3.93 |
| 68.1094 | 99.23 | 0.6298 | 1.37671 | 5.32 |
| 75.8047 | 64.03 | 0.5760 | 1.25391 | 3.43 |

Pattern List

| Visible | Ref. Code | Score | Compound Name | Displ. [°2Th] |
|------------|---------------|-------|---------------|---------------|
| Scale Fac. | Chem. Formula | | | |
| * | 00-046-1045 | 54 | Quartz, syn | 0.064 |
| 0.653 | Si O2 | | | |



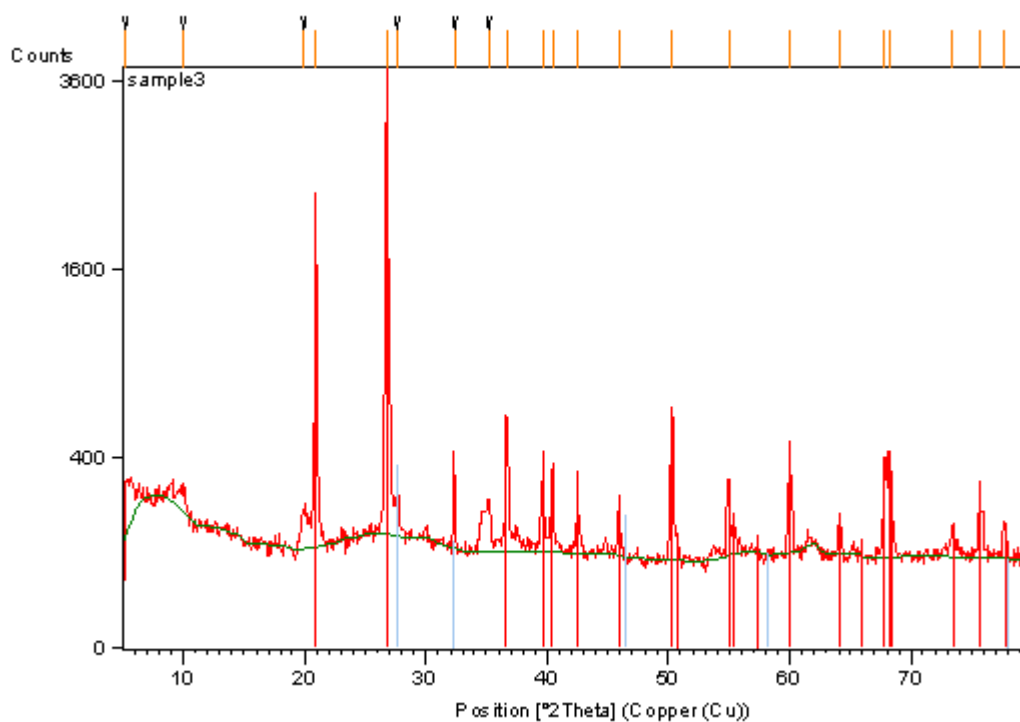
Code AB-24

| Pos. [°2Th.] | Height [cts] | FWHM [°2Th.] | d-spacing [Å] | Rel. Int. [%] |
|--------------|--------------|--------------|---------------|---------------|
| 5.2728 | 169.17 | 0.1574 | 16.76051 | 4.45 |
| 9.9651 | 83.62 | 0.4723 | 8.87645 | 2.20 |
| 19.9702 | 104.99 | 0.4723 | 4.44621 | 2.76 |
| 20.9295 | 2280.19 | 0.2362 | 4.24453 | 60.01 |
| 26.7774 | 3799.80 | 0.2362 | 3.32937 | 100.00 |
| 27.6531 | 200.12 | 0.2362 | 3.22590 | 5.27 |
| 32.3317 | 321.98 | 0.2362 | 2.76898 | 8.47 |
| 35.1501 | 136.86 | 0.2362 | 2.55315 | 3.60 |
| 36.6870 | 526.88 | 0.2362 | 2.44965 | 13.87 |
| 39.6274 | 204.38 | 0.2362 | 2.27440 | 5.38 |
| 40.4598 | 285.47 | 0.2362 | 2.22951 | 7.51 |
| 42.5216 | 135.84 | 0.2362 | 2.12606 | 3.57 |
| 45.8998 | 123.62 | 0.2362 | 1.97713 | 3.25 |
| 50.2769 | 582.64 | 0.2362 | 1.81479 | 15.33 |
| 54.9459 | 232.41 | 0.2362 | 1.67112 | 6.12 |
| 60.0184 | 305.51 | 0.3149 | 1.54145 | 8.04 |
| 64.0875 | 107.03 | 0.2362 | 1.45304 | 2.82 |
| 67.7786 | 313.84 | 0.2362 | 1.38262 | 8.26 |
| 68.2463 | 233.55 | 0.2362 | 1.37428 | 6.15 |
| 73.3368 | 37.65 | 0.9446 | 1.29096 | 0.99 |
| 75.7252 | 155.42 | 0.2362 | 1.25607 | 4.09 |
| 77.7118 | 91.60 | 0.3840 | 1.22783 | 2.41 |

Pattern List

| Visible | Ref.Code | Score | Compound Name | Displ. [°2Th] |
|---------|-------------|-------|---------------|---------------|
| | Scale Fac. | | Chem. Formula | |
| * | 00-046-1045 | 76 | Quartz, syn | 0.101 |
| 1.028 | Si O2 | | | |

Graphics



Appendix 2

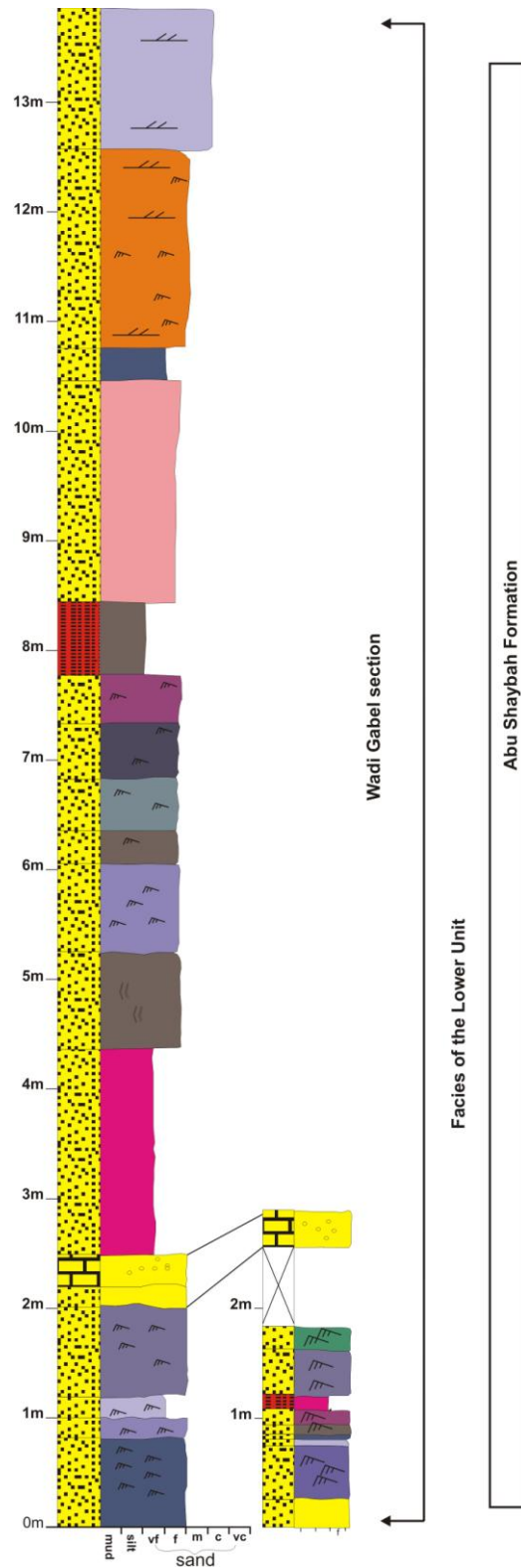


Figure 1.1 Sedimentary logs from east and west of the Wadi Gabel sections (location ③). The sections shows facies (F-VC) where is used as a marker horizontal between two sections.

Appendix 3 Sample orientation utilised both sun and magnetic compass for Kurrush, Al Aziza, Abu Shaybah and Abu Ghaylan Formations.

| Section | K1-1 | Location | Kabted Camel | | Abu Shaybah Fm. | | | |
|---------|---------|------------|--------------|-----|-----------------|--------|--------|---------|
| Sample | Comment | Date | Dip | Mag | Time | Shadow | Sun | sun-mag |
| K1-1 | | 5th Nov 08 | 58 | 130 | | | | 0 |
| K1-2 | | 5th Nov 08 | 61 | 128 | | | | 0 |
| K1-3 | | 5th Nov 08 | 60 | | | | | 0 |
| K1-4 | | 5th Nov 08 | 63 | | | | | 0 |
| K1-5 | | 5th Nov 08 | 68 | | | | | 0 |
| K1-6 | | 5th Nov 08 | 65 | | | | | 0 |
| K1-7 | | 5th Nov 08 | 76 | | | | | 0 |
| K1-8 | | 5th Nov 08 | 47 | | | | | 0 |
| K1-9 | | 5th Nov 08 | 59 | | | | | 0 |
| K1-10 | | 5th Nov 08 | 61 | | | | | 0 |
| K1-11 | | 5th Nov 08 | 64 | | | | | 0 |
| K1-12 | | 5th Nov 08 | 64 | | | | | 0 |
| K1-13 | | 5th Nov 08 | 67 | | | | | 0 |
| K1-14 | ** | 5th Nov 08 | 65 | | | | | 0 |
| K1-15 | | 5th Nov 08 | 49 | | | | | 0 |
| K1-16 | | 5th Nov 08 | 42 | | | | | 0 |
| K1-17 | | 5th Nov 08 | 59 | 179 | | | | 0 |
| K1-18 | | 5th Nov 08 | 51 | 249 | 11.48 | 274.5 | 254.54 | -5.54 |
| K1-19 | | 5th Nov 08 | 89 | 192 | 11.55 | 212 | 194.14 | -2.14 |
| K1-20 | | 5th Nov 08 | 36 | 135 | 11.58 | 150 | 133.05 | 1.95 |
| K1-21 | | 5th Nov 08 | 30 | 195 | 12.02 | 213 | 197.27 | -2.27 |

| Section | AR | Location | Abu Rashada-Road | | Abu Shaybah Fm | | | |
|---------|---------|------------|------------------|-----|----------------|--------|--------|---------|
| Sample | Comment | Date | Dip | Mag | Time | Shadow | Sun | sun-mag |
| AR1-1 | | 5th Nov 08 | 40 | 273 | | | | |
| AR1-2 | | 5th Nov 08 | 61 | 256 | | | | |
| AR1-3 | | 5th Nov 08 | 59 | 274 | 3.14 | 238 | 278.78 | -4.78 |
| AR1-4 | | 5th Nov 08 | 50 | 214 | 3.17 | 173 | 214.46 | -0.46 |
| AR1-5 | | 5th Nov 08 | 45 | 265 | 3.2 | 225 | 267.14 | -2.14 |
| AR1-6 | | 5th Nov 08 | 53 | 242 | | | | 0 |
| AR1-7 | | 5th Nov 08 | 56 | 246 | | | | 0 |
| AR1-8 | | 5th Nov 08 | 49 | 266 | | | | 0 |
| AR1-9 | | 5th Nov 08 | 46 | 279 | | | | 0 |
| AR1-10 | | 5th Nov 08 | 69 | 291 | | | | 0 |
| AR1-11 | | 5th Nov 08 | 44 | 284 | | | | 0 |
| AR1-12 | | 5th Nov 08 | 55 | 254 | | | | 0 |
| AR1-13 | | 5th Nov 08 | 75 | 295 | | | | 0 |
| AR1-14 | :* | 5th Nov 08 | 51 | 260 | | | | 0 |
| AR1-15 | | 5th Nov 08 | 82 | 277 | | | | 0 |
| AR1-16 | | 5th Nov 09 | 79 | 275 | | | | 0 |
| AR1-7 | | 5th Nov 08 | 71 | 260 | | | | 0 |
| AR1-18 | | 5th Nov 08 | 76 | 253 | | | | 0 |
| AR1-19 | | 5th Nov 08 | 71 | 271 | | | | 0 |
| AR1-20 | | 5th Nov 08 | 58 | 261 | | | | 0 |
| AR1-21 | | 5th Nov 08 | 61 | 271 | | | | 0 |
| AR1-22 | :* | 5th Nov 08 | 66 | 325 | | | | 0 |
| AR1-23 | | 5th Nov 08 | 78 | 274 | | | | 0 |
| AR1-24 | | 5th Nov 08 | 71 | 318 | | | | 0 |
| AR1-25 | | 5th Nov 08 | 74 | 99 | 4.27 | 45 | 100.43 | -1.43 |
| AR1-26 | ;* | 5th Nov 08 | 65 | 110 | | | | 0 |
| AR1-27 | | 5th Nov 08 | 37 | 106 | 4.33 | 52 | 108.47 | -2.47 |
| AR1-28 | | 5th Nov 08 | 35 | 106 | 4.36 | 53 | 109.98 | -3.98 |
| AR1-29 | | 5th Nov 08 | 72 | 64 | | | | 0 |
| AR1-30 | | 5th Nov 08 | 76 | 60 | | | | 0 |
| AR1-31 | | 5th Nov 08 | 63 | 76 | | | | 0 |
| AR1-32 | | 5th Nov 08 | 10 | 92 | | | | 0 |

| Section | AZ | Location | | Wadi Abu Shaybah | | Al Aziza Fm. | | 0 |
|---------|---------------|------------|-----|------------------|------|--------------|-----|---------|
| | | | | | | | | 0 |
| Sample | Comment | Date | Dip | Mag | Time | Shadow | Sun | Sun-mag |
| AZ1-1 | Al Aziz stone | 6th Nov 08 | 53 | 154 | | | | 0 |
| AZ1-2 | | 6th Nov 08 | 53 | 136 | | | | 0 |
| AZ1-3 | | 6th Nov 08 | 43 | 131 | | | | 0 |
| AZ1-4 | | 6th Nov 08 | 19 | 191 | | | | 0 |
| AZ1-5 | | 6th Nov 08 | 65 | 181 | | | | 0 |
| AZ1-6 | | 6th Nov 08 | 17 | 266 | | | | 0 |
| AZ1-7 | | 6th Nov 08 | 17 | 131 | | | | 0 |
| AZ1-8 | | 6th Nov 08 | 18 | 274 | | | | 0 |
| AZ1-9 | | 6th Nov 08 | 35 | 170 | | | | 0 |
| AZ1-10 | | 6th Nov 08 | 33 | 181 | | | | 0 |
| AZ1-11 | | 6th Nov 08 | 18 | 285 | | | | 0 |
| AZ1-12 | | 6th Nov 08 | 27 | 52 | | | | 0 |
| AZ1-13 | | 6th Nov 08 | 63 | 147 | | | | 0 |
| AZ1-14 | | 6th Nov 08 | 72 | 147 | | | | 0 |
| AZ1-15 | Chert | 6th Nov 08 | 78 | 143 | | | | 0 |
| AZ1-16 | | 6th Nov 08 | 30 | 251 | | | | 0 |
| AZ1-17 | | 6th Nov 08 | 35 | 167 | | | | 0 |
| AZ1-18 | | 6th Nov 08 | 48 | 186 | | | | 0 |
| AZ1-19 | | 6th Nov 08 | 20 | 217 | | | | 0 |
| AZ1-20 | | 6th Nov 08 | 42 | 152 | | | | 0 |
| AZ1-21 | | 6th Nov 08 | 28 | 52 | | | | 0 |
| AZ1-22 | | 6th Nov 08 | 27 | 87 | | | | 0 |
| AZ1-23 | | 6th Nov 08 | 29 | 62 | | | | 0 |
| AZ1-24 | | 6th Nov 08 | 18 | 80 | | | | 0 |

| | | | | | | | | |
|--------|--|------------|------|------|--|--|--|---|
| AZ1-25 | | 6th Nov 08 | 19 | 104 | | | | 0 |
| AZ1-26 | | 6th Nov 08 | 28 | 136 | | | | 0 |
| AZ1-27 | | 6th Nov 08 | 24 | 125 | | | | 0 |
| AZ1-28 | | 6th Nov 08 | 36 | 129 | | | | 0 |
| AZ1-29 | | 6th Nov 08 | 31 | 94 | | | | 0 |
| AZ1-30 | | 6th Nov 08 | 34.5 | 94 | | | | 0 |
| AZ1-31 | | 6th Nov 08 | 125 | 49.5 | | | | 0 |
| AZ1-32 | | 6th Nov 08 | 35 | 28 | | | | 0 |
| AZ1-33 | | 6th Nov 08 | 29 | 88 | | | | 0 |
| AZ1-34 | | 6th Nov 08 | 37 | 90 | | | | 0 |
| AZ1-35 | | 6th Nov 08 | 41 | 145 | | | | 0 |
| AZ1-36 | | 6th Nov 08 | 57.5 | 120 | | | | 0 |
| AZ1-37 | | 6th Nov 08 | 30 | 344 | | | | 0 |
| AZ1-38 | | 6th Nov 08 | 49 | 186 | | | | 0 |
| AZ1-39 | | 6th Nov 08 | 28 | 37 | | | | 0 |
| AZ1-40 | | 6th Nov 08 | 52.5 | 186 | | | | 0 |
| AZ1-41 | | 6th Nov 08 | 18 | 262 | | | | 0 |
| AZ1-42 | | 6th Nov 08 | 23 | 292 | | | | 0 |
| AZ1-43 | | 6th Nov 08 | 31 | 93 | | | | 0 |
| AZ1-44 | | 6th Nov 08 | 48.5 | 189 | | | | 0 |
| AZ1-45 | | 6th Nov 08 | 49.5 | 153 | | | | 0 |
| AZ1-46 | | 6th Nov 08 | 38.5 | 94 | | | | 0 |
| AZ1-47 | | 6th Nov 08 | 35.5 | 160 | | | | 0 |
| AZ1-48 | | 6th Nov 08 | 32 | 54 | | | | 0 |
| AZ1-49 | | 6th Nov 08 | 37 | 54 | | | | 0 |
| AZ1-50 | | 6th Nov 08 | 26 | 64 | | | | 0 |
| AZ1-51 | | 6th Nov 08 | 22 | 57 | | | | 0 |
| AZ1-52 | | 6th Nov 08 | 25 | 34 | | | | 0 |

| | | | | | | | |
|----------|---|------------|------|-----|--|--|---|
| AZ1-53 | | 6th Nov 08 | 56 | 219 | | | 0 |
| AZ1-54 | | 6th Nov 08 | 32 | 32 | | | 0 |
| AZ1-55 | | 6th Nov 08 | 16.5 | 77 | | | 0 |
| AZ1-56 | | 6th Nov 08 | 19.5 | 117 | | | 0 |
| AZ1-57 | | 6th Nov 08 | 22.5 | 43 | | | 0 |
| AZ1-58 | | 6th Nov 08 | 28 | 70 | | | 0 |
| AZ1-59 | | 6th Nov 08 | 63 | 73 | | | 0 |
| AZ1-59 B | B | 6th Nov 08 | 35 | 137 | | | 0 |
| AZ1-60 | | 6th Nov 08 | 61 | 106 | | | 0 |
| AZ1-61 | | 6th Nov 08 | 64 | 100 | | | 0 |
| AZ1-62 | | 6th Nov 08 | 48 | 86 | | | 0 |
| AZ1-63 | | 6th Nov 08 | 26 | 325 | | | 0 |
| AZ1-64 | | 6th Nov 08 | 25 | 30 | | | 0 |
| AZ1-65 | | 6th Nov 08 | 22 | 305 | | | 0 |
| AZ1-66 | | 6th Nov 08 | 37 | 147 | | | 0 |
| AZ1-67 | | 6th Nov 08 | 28 | 30 | | | 0 |
| AZ1-68 | | 6th Nov 08 | 22 | 16 | | | 0 |
| AZ1-69 | | 6th Nov 08 | 51 | 159 | | | 0 |
| AZ1-70 | | 6th Nov 08 | 49 | 117 | | | 0 |
| AZ1-71 | | 6th Nov 08 | 38 | 76 | | | 0 |
| AZ1-72 | | 6th Nov 08 | 68 | 83 | | | 0 |
| AZ1-73 | | 6th Nov 08 | 47 | 85 | | | 0 |
| AZ1-74 | | 6th Nov 08 | 15 | 37 | | | 0 |
| AZ1-75 | | 6th Nov 08 | 26.5 | 270 | | | 0 |
| AZ1-76 | | 6th Nov 08 | 30 | 279 | | | 0 |

Section AZ right side location

| Sample | Comment | Date | Dip | Mag | Time | Shadow | Sun | Sun-mag |
|--------|---------|------------|------|-----|-------|--------|--------|---------|
| AZ1-77 | | 7th Nov 08 | 45 | 91 | 10.16 | 144 | 100.64 | -9.64 |
| AZ1-78 | | 7th Nov 08 | 18 | 33 | 10.19 | 77 | 34.29 | -1.29 |
| AZ1-79 | | 7th Nov 08 | 49.5 | | 10.22 | 151 | 108.96 | -108.96 |
| AZ1-80 | | 7th Nov 08 | 21.5 | 74 | 10.25 | 119 | 77.63 | -3.63 |
| AZ1-81 | | 7th Nov 08 | 37 | 346 | 10.28 | 29 | 348.31 | -2.31 |
| AZ1-82 | | 7th Nov 08 | 30.5 | 1 | 10.31 | 47 | 6.99 | -5.99 |
| AZ1-83 | | 7th Nov 08 | 43 | 189 | 10.33 | 229 | 189.45 | -0.45 |
| AZ1-84 | | 7th Nov 08 | 31 | 352 | 10.38 | 30 | 351.39 | 0.61 |
| AZ1-85 | | 7th Nov 08 | 35 | 355 | 10.41 | 35 | 357.33 | -2.33 |
| AZ1-86 | | 7th Nov 08 | 32 | 339 | 10.44 | 21 | 344.05 | -5.05 |
| AZ1-87 | | 7th Nov 08 | 29 | 10 | 11.09 | 43 | 12.35 | -2.35 |
| AZ1-88 | | 7th Nov 08 | 31 | 340 | 11.16 | 13 | 344.21 | -4.21 |
| AZ1-89 | | 7th Nov 08 | 25 | 190 | 11.19 | 216 | 188.12 | 1.88 |
| AZ1-90 | | 7th Nov 08 | 38 | 336 | 11.23 | 5 | 381.12 | -45.12 |
| AZ1-91 | | 7th Nov 08 | 29 | 322 | 11.27 | 352 | 326.22 | -4.22 |
| AZ1-92 | | 7th Nov 08 | 24 | 308 | 11.31 | 334 | 309.34 | -1.34 |
| AZ1-93 | | 7th Nov 08 | 22 | 307 | 11.33 | 331 | 306.91 | 0.09 |
| AZ1-94 | | 7th Nov 08 | 30 | 344 | 11.37 | 10 | 347.04 | -3.04 |

Section AZ left side location

| Sample | Comment | Date | Dip | Mag | Time | Shadow | Sun | Sun-mag |
|--------|---------|------------|------|-----|-------|--------|--------|---------|
| AZ2-1 | | 7th Nov 08 | 22 | 238 | 4.03 | 189 | 239.58 | -1.58 |
| AZ2-2 | | 7th Nov 08 | 31 | 313 | 4.07 | 260 | 311.33 | 1.67 |
| AZ2-3 | | 7th Nov 08 | 19 | 292 | 4.12 | 242 | 294.26 | -2.26 |
| AZ2-4 | | 7th Nov 08 | 26 | 282 | 4.14 | 232 | 284.63 | -2.63 |
| AZ2-5 | | 7th Nov 08 | 31 | 304 | 4.17 | 252 | 305.18 | -1.18 |
| AZ2-6 | | 7th Nov 08 | 26 | 351 | | | | 0 |
| AZ2-7 | | 7th Nov 08 | 26.5 | 356 | 4.23 | 306 | 0.25 | 355.75 |
| AZ2-8 | | 7th Nov 08 | 31 | 266 | | | | 0 |
| AZ2-9 | | 7th Nov 08 | 27 | 292 | | | | 0 |
| AZ2-10 | *** | 7th Nov 08 | 25 | 338 | | | | 0 |
| AZ2-11 | | 7th Nov 08 | 48 | 240 | | | | 0 |
| AZ2-12 | | 7th Nov 08 | 25 | 206 | | | | 0 |
| AZ2-13 | | 7th Nov 08 | 23 | 209 | | | | 0 |
| AZ2-14 | | 7th Nov 08 | 35 | 272 | 4.42 | 223 | 280.52 | -8.52 |
| AZ2-15 | | 7th Nov 08 | 29 | 328 | | | | 0 |
| AZ2-16 | | 7th Nov 08 | 19 | 42 | | | | 0 |
| AZ2-17 | | 7th Nov 08 | 20 | 278 | | | | 0 |
| AZ2-18 | | 7th Nov 08 | 38 | 301 | 4.55 | 243 | 302.64 | -1.64 |
| AZ2-19 | | 7th Nov 08 | 47 | 334 | 4.57 | 277 | 336.96 | -2.96 |
| AZ-20 | | 7th Nov 08 | 64 | 331 | 5 | 273 | 333.43 | -2.43 |
| AZ2-21 | | 7th Nov 08 | 75 | 326 | 5.02 | 268 | 328.75 | -2.75 |
| AZ2-22 | | 7th Nov 08 | 34 | 32 | 5.05 | 336 | 37.21 | -5.21 |
| AZ2-23 | | 7th Nov 08 | 65 | 339 | 50.07 | 280 | 341.51 | -2.51 |
| AZ2-24 | | 7th Nov 08 | 27 | 112 | 5.11 | 53 | 115.14 | -3.14 |
| AZ2-25 | | 7th Nov 08 | 23 | 34 | 5.13 | 335 | 37.44 | -3.44 |
| AZ2-26 | | 7th Nov 08 | 20 | 65 | 5.17 | 5 | 68.4 | -3.4 |
| AZ2-27 | | 7th Nov 08 | 24 | 35 | | | | 0 |
| AZ2-28 | | 7th Nov 08 | 24 | 62 | | | | 0 |
| AZ2-29 | | 7th Nov 08 | 22 | 36 | | | | 0 |
| AZ2-30 | | 7th Nov 08 | 24 | 23 | | | | 0 |
| AZ2-31 | | 7th Nov 08 | 62 | 260 | | | | 0 |

Section ER

| Sample | Comment | Date | Dip | Mag | Time | Shadow | Sun | Sun-mag |
|--------|---------|-------------|-----|-----|-------|--------|-------|---------|
| ER1-1 | | 11th Nov 08 | 67 | 32 | 10.15 | 82 | 39.11 | -7.11 |
| ER1-2 | | 11th Nov 08 | 66 | 19 | 10.2 | 67 | 25.2 | -6.2 |
| ER1-3 | | 11th Nov 08 | 64 | 14 | 10.23 | 58 | 16.85 | -2.85 |
| ER1-4 | | 11th Nov 08 | 80 | 16 | 10.25 | 63 | 22.3 | -6.3 |
| ER1-5 | | 11th Nov 08 | 49 | 26 | 10.29 | 68 | 28.19 | -2.19 |
| ER1-6 | | 11th Nov 08 | 83 | 343 | | | | 0 |
| ER1-7 | | 11th Nov 08 | 79 | 59 | 10.38 | 101 | 63.25 | -4.25 |
| ER1-8 | | 11th Nov 08 | 70 | 66 | 10.42 | 110 | 73.19 | -7.19 |
| ER1-9 | | 11th Nov 08 | 89 | | 10.44 | 104 | 67.67 | -67.67 |
| ER1-10 | | 11th Nov 08 | 84 | | 10.46 | 133 | 97.14 | -97.14 |
| ER1-11 | | 11th Nov 08 | 71 | 70 | 10.49 | 112 | 76.86 | -6.86 |
| ER1-12 | | 11th Nov 08 | 77 | | 10.51 | 96 | 61.35 | -61.35 |
| ER1.13 | | 11th Nov 08 | 56 | 60 | 11.01 | 100 | 67.83 | -7.83 |
| ER1.14 | | 11th Nov 08 | 53 | 49 | 11.03 | 89 | 57.33 | -8.33 |
| ER1-15 | | 11th Nov 08 | 77 | 78 | 11.06 | 113 | 82.1 | -4.1 |
| ER1-16 | | 11th Nov 08 | 77 | 63 | 11.09 | 97 | 66.87 | -3.87 |
| ER1-17 | | 11th Nov 08 | 79 | | 11.11 | 117 | 87.39 | -87.39 |
| ER1-18 | | 11th Nov 08 | 74 | 37 | 11.15 | 71 | 42.44 | -5.44 |
| ER1-19 | | 11th Nov 08 | 83 | | 11.17 | 94 | 65.97 | -65.97 |

Section WG

| Sample | Comment | Date | Dip | Mag | Time | Shadow | Sun | Sun-mag |
|--------|---------------------|-------------|------|-----|------|--------|--------|---------|
| WG1-1 | | 11th Nov 08 | 35 | 70 | 1.26 | 63 | 73.51 | -3.51 |
| WG1-2 | | 11th Nov 08 | 36.5 | 77 | 1.3 | 68 | 79.72 | -2.72 |
| WG1-3 | | 11th Nov 08 | 37 | 98 | 1.32 | 90 | 102.32 | -4.32 |
| WG1-4 | | 11th Nov 08 | 51 | 35 | 1.34 | 28 | 40.93 | -5.93 |
| WG1-5 | | 11th Nov 08 | | | | | | 0 |
| WG1-6 | | 11th Nov 08 | 70 | 107 | 1.37 | 94 | 107.83 | -0.83 |
| WG1-7 | | 11th Nov 08 | 87 | 68 | 1.42 | 57 | 72.32 | -4.32 |
| WG1-8 | | 11th Nov 08 | 89 | | 1.44 | 58 | 73.91 | -73.91 |
| | Out of surface base | | | | | | | 0 |
| WG1-9 | | 11th Nov 08 | 23 | 320 | 1.47 | 307 | 323.8 | -3.8 |
| WG1-10 | | 11th Nov 08 | 27 | | 1.5 | 187.5 | 205.17 | -205.17 |
| WG1-11 | | 11th Nov 08 | 31 | | 1.51 | 199 | 216.97 | -216.97 |
| WG1-12 | Yellow sand | 11th Nov 08 | 77 | | 1.54 | 245 | 263.84 | -263.84 |
| WG1-13 | | 11th Nov 08 | 29 | 264 | 1.57 | 247 | 266.7 | -2.7 |
| WG1-14 | | 11th Nov 08 | 67 | 12 | 2.05 | 352 | 13.98 | -1.98 |
| WG1-15 | | 11th Nov 08 | 70.5 | | 2.07 | 347 | 9.59 | -9.59 |
| WG1-16 | | 11th Nov 08 | 70 | | 2.9 | 344 | 7.1 | -7.1 |
| WG1-17 | | 11th Nov 08 | 23 | | 2.12 | 161 | 184.94 | -184.94 |
| WG1-18 | | 11th Nov 08 | 29 | 223 | 2.15 | 198 | 222.76 | 0.24 |
| WG1-19 | | 11th Nov 08 | 31 | | 2.2 | 329 | 355.12 | -355.12 |

Section AG

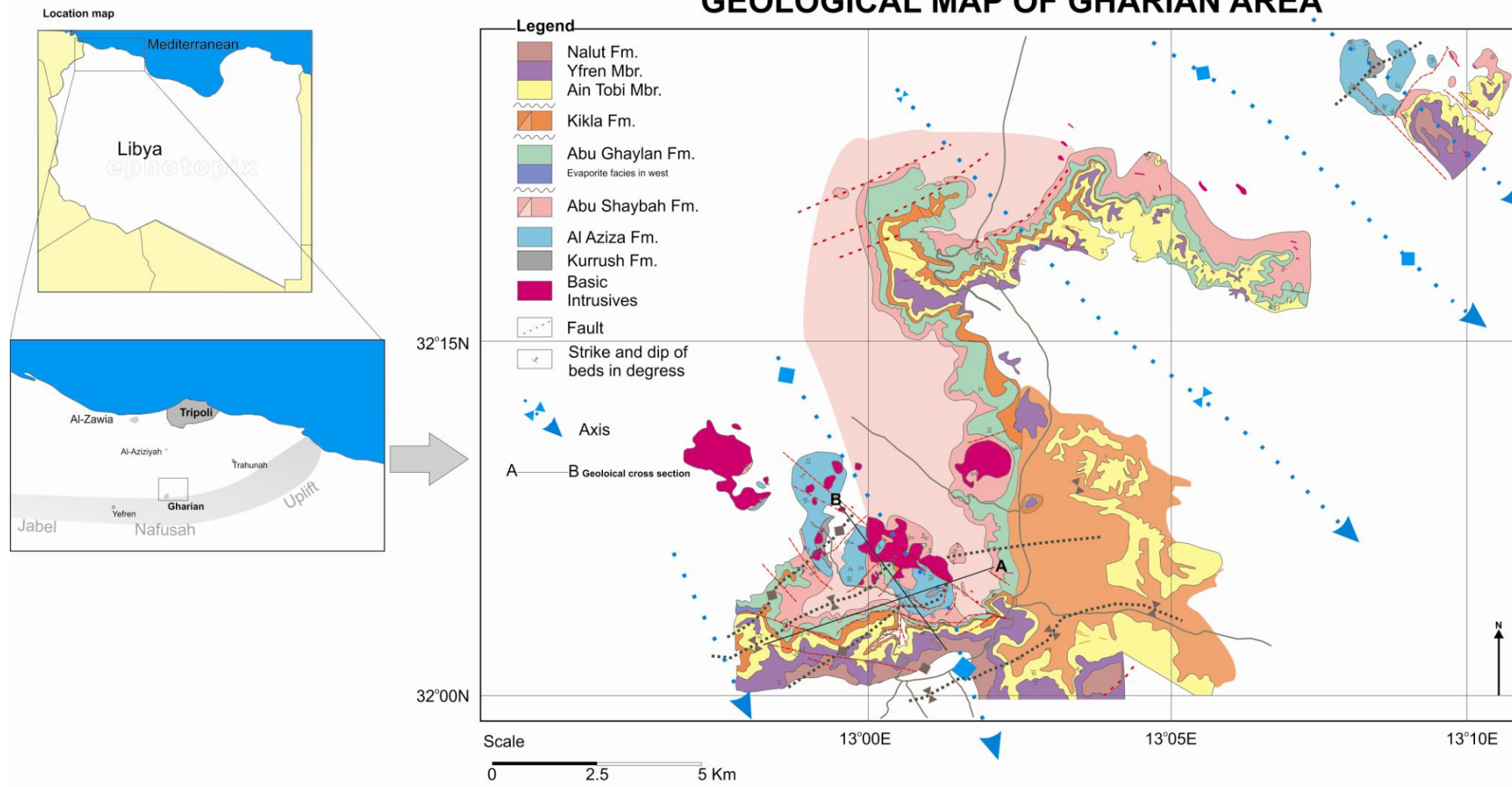
| Sample | Comment | Date | Dip | Mag | Time | Shadow | Sun | Sun-mag |
|--------|---------|-------------|------|-----|------|--------|-----|---------|
| AG1-1 | | 11th Nov 08 | 34 | 190 | | | | |
| AG1-2 | NO SUN | 11th Nov 08 | 36 | 42 | | | | |
| AG1-3 | | 11th Nov 08 | 42 | | | | | |
| AG1-4 | | 11th Nov 08 | 33 | 172 | | | | |
| AG1-5 | | 11th Nov 08 | 40 | 204 | | | | |
| AG1-6 | | 11th Nov 08 | 32 | 196 | | | | |
| AG1-7 | | 11th Nov 08 | 37 | 230 | | | | |
| AG1-8 | | 11th Nov 08 | 25 | 250 | | | | |
| AG1-9 | | 11th Nov 08 | 29 | 215 | | | | |
| AG1-10 | | 11th Nov 08 | 36.5 | 226 | | | | |
| AG1.11 | | 11th Nov 08 | 20 | 288 | | | | |

Section K1-2

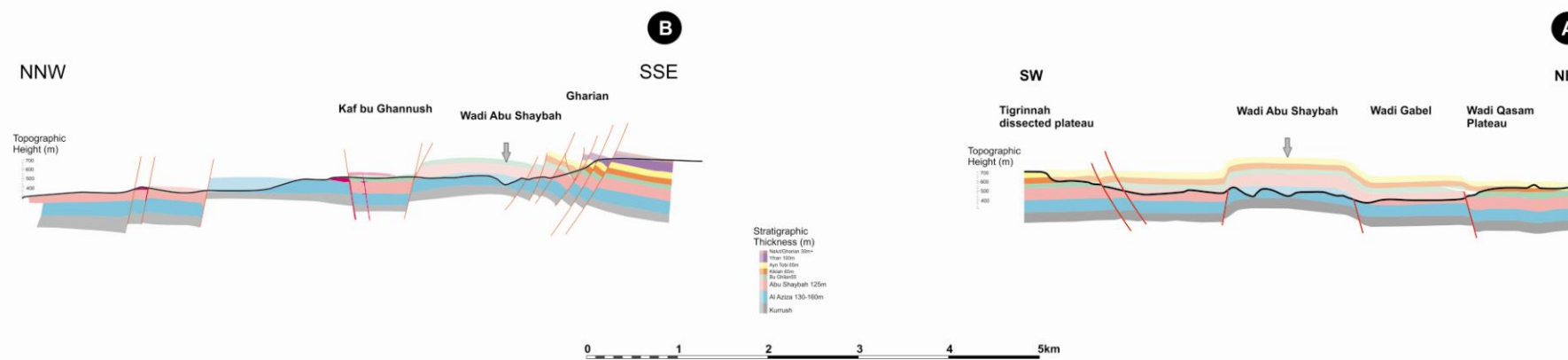
| Sample | Comment | Date | Dip | Mag | Time | Shadow |
|--------|-------------|------------|------|-----|------|--------|
| K1-1 | Yellow beds | 7th Nov 08 | 53.5 | 4 | 0 | 0 |
| K1-2 | 312853 | 7th Nov 08 | 63 | 15 | | 0 |
| K1-3 | 3563042 | 7th Nov 08 | 66 | 65 | | 0 |
| K1-4 | | 7th Nov 08 | 82 | 78 | | 0 |
| K2-1 | Red beds | 7th Nov 08 | 64 | 262 | | 0 |
| K2-2 | 312845 | 7th Nov 08 | 69.5 | 267 | | 0 |
| | 3561991 | | | | | |

MAP 1

GEOLOGICAL MAP OF GHARIAN AREA



Geological cross sections



MAP 2

